Book of Abstracts

EUROEM 2008
European Electromagnetics

Book of Abstracts

EUROEM 2008
European Electromagnetics

21-25 July 2008
Swiss Federal Institute of Technology
(EPFL)
Lausanne, Switzerland

Committees

Symposium Chair

Farhad Rachidi (EPFL)

Symposium co-Chairs

Markus Nyffeler (Armasuisse)
Marcos Rubinstein (HEIG-VD)

Honorary Past Chairmen

Juergen Nitsch (Univ. Magdeburg)
Donald McLemore (ITT Ind.)

Organizing Committee

Rachid Cherkaoui (Chair)
Andrée Moinat (Administration)
Bertrand Daout (Exhibition Chair)
Carl Baum, Alain Jaquier (International Liaison)
Pascal Leuchtman (National Liaison)
Davide Pavanello (Submission & Review)
Abraham Rubinstein (IT support, web site)
Keyhan Sheshyekani (Administration and Publishing Assistant)
Simon Cottier, Pooyan Manoochehrnia, Francesco Merli, Abbas
Mosaddeghi, Isabel Nzazi Andzouonou, Gabriela Quintero, Eden Sorolla,
Felix Vega, Ana Vukicevic, Pierre Zweiacker (local arrangements)

Technical Program Committee

Technical Program Chair

Armin W. Kaelin, Meteolabor AG

HPEM co-Chairs

Fred M. Tesche, William A. Radasky

UWB co-Chairs

Dave V. Giri, Frank Sabath

UXO-TID co-Chairs

Ira Kohlberg, Jan Rhebergen

Other Technical Program Committee Members

C. Baum, D. Nitsch, J. Mosig, A. Skrivervik, R. Vahldieck

Swiss National Committee

N. Ari, K.-D. Behnke, M. Bittner, G. Dürrenberger, D. Gautschi, J. Gut,
W. Hirschi, M. Ianoz, P. Krähenbühl, O. Martin, C. Monney, I. Rose,
H. Schär, E. Van Deventer, H. Wipf

International Steering Committee

Australia
K. Esselle
F. Schlagenhaufer
P.D. Smith

Austria
G. Diendorfer

Belgium
J. Catrysse

Brazil
A. Piantini, S. Visacro

Canada
B. Kordi, S. Loyka,
S. Mishra,
A. Podgorski,
L. Shafai, J. LoVetri

China
Y. Gao, L. Shi

Colombia
F. Roman

Croatia
D. Poljak, V. Roje

Czech Republic
L. Palisek

Finland
R. Pirjola

France
M. Drissi, J.P.
Parmantier, D. Serafin,
A. Zeddam

Georgia
R.S. Zaridze

Germany
H. Garbe, K.H.
Gonschorek, F. Heidler,
J.L. ter Haseborg, S.
Tkachenko, G. Wollenberg

India
D.C. Pande, J. Thomas

Iran
R. Moini, S.H.H. Sadeghi

Israel
E. B. Joffe, A. Tehori

Italy
F.G. Canavero, P. Corona,
M. D'Amore, F. Delfino,
M. Feliziani, F. Maradei,
C.A. Nucci, A. Orlandi,
M. Paolone, M.S. Sarto

Japan
M. Ishii, T. Shindo,
M. Hayakawa

Lithuania
M. Dagys

Macedonia
L. Grcev

Poland
A. Karwowski

Russia
A. Didenko, N. Korovkin,
V. Koshelev, Y.V. Parfenov,
L.L. Siny, V. Terekhin

Serbia
A. Djordjevic

Singapore
Z.N. Chen, See Kye Yak

South Korea
S. Nam

Spain
A. Rubio Bretones,
J. Montanya, F. Silva

Sweden
M. Bäckström, J. Carlsson,
V. Cooray, L. Jansson,
A. Larsson, N. Theethayi,
R. Thottappillil

The Netherlands
F. Leferink, A. Tijhuis,
A.P.J. Van Deursen,
A. Yarovoy, P. Zwamborn

Ukraine
I. Magda, V. Shostak

United Kingdom
N. Carter, C. Christopoulos,
R. Hoad, B.A. Kerr, A.
Marvin, D. Parkes, A.
Ruddle, A. Wraight

USA
T. Andreadis, V. Carboni,
K. A. Dighe, E.G. Farr,
R. Gardner, J.C. Giles,
S. Grzybowski, T. Hubing,
D.P. McLemore,
R.G. Olsen, W. Prather,
V.A. Rakov,
C. Rostam-zadeh,
E. Schamiloglu, A. Stone,
D.C. Stoudt,
M.A. Uman, T. Wieting

Table of Contents

HPEM - 07 – High-Power Microwaves (Invited)

HPEM - 08 – Intentional EMI #1 (Invited)

Table of Contents

HPEM - 09 – Susceptibility

HPEM - 13 – Susceptibility #1 (Invited)

HPEM - 14 – Intentional EMI #2 (Invited)

HPEM - 15 – Electromagnetic Compatibility in Power Systems

HPEM - 16 – Nonlinear Dynamics and Chaos (Invited)

HPEM - 19 – Measurements Techniques #3

Table of Contents

HPEM - 22 – Critical Infrastructure & Related Topics

HPEM - 23 – Biological Effects

HPEM - 27 – High-Power RF Source Technology (Invited)

HPEM - 28 – Lightning Characterization & Simulation (Invited)

HPEM - 29 – Biological Effects and Medical Applications (Invited)

HPEM - 41 – High-Power Microwaves

HPEM - 42 – Transmission Lines at Low and High Frequencies: Theory, Numerical and Experiments.
Part 2: Numerical Methods and Measurements (Invited)

HPEM - 43 – Pulsed Power

HPEM - 44 – Microstrip and Patch Antennas

UWB - 05 – Antennas for UWB Communications

UWB - 06 – UWB - Modeling & Simulation #1

UWB - 07 – Conformal Time Domain Numerical Methods (Invited)

UWB - 08 – UWB - Pulsed Power

UWB - 09 – UWB - Communications

UWB - 14 – UWB for Medical Imaging and Sensing (Invited)

UXO-TID - 1 – Underground & Subsurface

Table of Contents

POSTER SESSION 1

Table of Contents

Table of Contents

POSTER SESSION 2

POSTER SESSION 3

Table of Contents

Nature Inspired Optimization Techniques in Engineering:
Let Darwin and the bees help improve your designs

Yahya Rahmat-Samii

Northrop-Grumman Professor in Electromagnetics
Department of Electrical Engineering
University of California, Los Angeles, USA
E-mail: rahmat@ee.ucla.edu
Web: http://www.antlab.ee.ucla.edu

Engineers are constantly challenged with the temptation to search for optimum solutions for complex engineering system designs. The ever increasing advances in computational power have fueled this temptation. The well-known brute force design methodologies are systematically being replaced by the state-of-the-art Evolutionary Optimization (EO) techniques. In recent years, EO techniques are finding growing applications to the design of all kind of systems with increasing complexity. Among various EO's, nature inspired techniques such as Genetic Algorithms (GA) and Particle Swarm Optimization (PSO) have attracted considerable attention. GA utilizes an optimization methodology which allows a global search of the cost surface via the mechanism of the statistical random processes dictated by the Darwinian evolutionary concept (adaptation, selection, survivability and mutation). PSO is a robust stochastic evolutionary computation technique based on the movement and intelligence of swarms of bees looking for the most fertile feeding location applying their cognitive and social knowledge. This key-note presentation will focus on: **(a)** an engineering introduction to GA and PSO by describing in a unique fashion the underlying concepts and recent advances for those who have used these techniques and for those who have not had any experiences in these areas, **(b)** discussions on multi-objective optimizations with real, binary and hybrid parameterizations, **(c)** demonstration of the potential applications of GAs and PSO's to a variety of engineering designs including antennas for remote sensing and satellite communication applications, arrays for radio astronomy imaging, multi-band, wideband and UWB antenna designs in personal communications, design of electromagnetic and photonic bandgap (EBG & PBG) structures, etc, and **(d)** assessment of the advantages and the limitations of these techniques.

Biography:

Yahya Rahmat-Samii is a Distinguished Professor, holder of the Northrop-Grumman Chair in electromagnetics and the past chairman of the Electrical Engineering Department at the University of California, Los Angeles (UCLA). Before joining UCLA in 1989, he was a Senior Research Scientist at NASA's Jet Propulsion Laboratory. Dr. Rahmat-Samii was the 1995 President of IEEE Antennas and Propagation Society. Dr. Rahmat-Samii was elected as a Fellow of IEEE in 1985. Dr. Rahmat-Samii has received numerous awards, including the 1992 and 1995 IEEE AP-S Wheeler Best Application Prize Paper Award, 1999 University of Illinois ECE Distinguished Alumni Award, IEEE Third Millennium Medal, and AMTA'2000 Distinguished Achievement Award. In 2001, Rahmat-Samii was the recipient of an Honorary Doctorate in Physics from the University of Santiago de Compostela, Spain. In 2001, he was elected as a Foreign Member of the Royal Flemish Academy of Belgium for Science and the Arts. In 2002, he received the Technical Excellence Award from JPL and in 2005 he was the recipient of the URSI Booker Gold Medal. He is the recipient of the 2007 Chen-To Tai Distinguished Educator Award of the IEEE Antennas and Propagation Society. In 2008, Prof. Rahmat-Samii was elected to the membership of the US National Academy of Engineering. Prof. Rahmat-Samii is the designer of the IEEE AP-S logo which is displayed on all IEEE AP-S publications.

Electromagnetic Terrorism and Potential Infrastructure Failures

I. Kohlberg[1], C. E. Baum[2], and D. V. Giri[3]

[1]*Kohlberg Associates Inc, Reston, Virginia, USA*
[2]*University of New Mexico, Albuquerque, New Mexico, USA*
[3]*Pro-Tech, Alamo, California, USA and University of New Mexico, Albuquerque, New Mexico, USA*
E-mail: ira.kohlberg@gmail.com

In the 21st century much of the industrialized world will be faced with maintaining the health and welfare of its interconnected infrastructures against electromagnetic terrorism using High-Power Electromagnetic weapons and the electromagnetic field created by detonating a High Altitude Nuclear Weapon—the HEMP threat. Traditionally, we tend to think of HPM weapons being applied locally, and the HEMP threat being applied on a national or sub-national basis. The creation of large real-time information-dependent networks used by industrialized countries allows terrorists the opportunity to attack coupled infrastructure and also produce large scale cascading failures. New system level approaches, fortified with technology based on EMC techniques are required to meet these challenges. These issues have recently been studied in detail in the USA by a Congressionally Mandated EMP Commission chaired by Dr. William Graham. This commission addressed the consequences of a terrorist nuclear-induced high altitude electromagnetic pulse (HEMP) attack against the USA. Studies revealed that large systems can be susceptible to HEMP and that when infrastructures are coupled in such a way that the control of each one depends on the state of the other, new control paradigms may be necessary to insure survivability. Innovative operational policies combined with novel theoretical techniques that quantify the resilience of interacting infrastructure components in the ambient state and dynamically assess the situation and provide the allocation of resources to optimize the response in the perturbed states are required. In this paper we examine: (1) the use of system theory to assess the effect of coupling between the Electric Power Grid (EPG) and the Public Data Network (PDN) under a terrorist attack, and (2) propose a new paradigm for survivability—an infrastructure under attack be modeled as a random graph, and that connectedness—the ability to support a network spanning cluster, be a measure of its ability to resist insult. The consequences of these viewpoints are explored.

Plenary

Some Recent Work on Intentional EMI in Sweden

M. Bäckström[1], R. Thottappillil[2], D. Månsson[2], R. Montano[3], O. Lundén[4], T. Nilsson[1]

[1]*Saab Communication, SE-581 88 Linköping, Sweden*
[2]*Uppsala University, Division for Electricity, EMC Group, Box 534, SE-751 21 Uppsala, Sweden*
[3]*High Voltage Valley, Box 832, SE-771 28 Ludvika, Sweden*
[4]*Swedish defence Research agency FOI , Box1165, SE-581 11 Linköping, Sweden*

E-mail: mats.backstrom@saabgroup.com

Our society is rapidly becoming more and more dependent on electrical and electronic systems. This applies also to systems crucial for basic functions of the society, such as electric power transmission, medical care, telecommunications, transportation, banking and finance, food and water supply, emergency services and decision making. This heavy reliance on electronics, also in safety-critical applications, brings the question of its robustness against *Intentional Electromagnetic Interference* (IEMI) into focus. Of special interest is the rapidly spreading use of new types of wireless systems since these are easy to interfere with and difficult to protect.

One reason why the IEMI threat against civil systems has to be taken in all seriousness is that the perpetrator may come close to the system under attack. If so, the terrorist does not need access to military RF weapons; it will suffice to get hold of e.g. a radar transmitter or even simple "home-built" devices [1]. Another reason is that most civil equipment lack immunity requirements against these threat levels. There seems to be only one major exemption to this, namely civil aircraft, since these are built to withstand the harsh radar environment at airports.

While IEMI threats have been recognized for decades by the military, in later years also the threat against civil systems has got an increased attention. This is reflected also in Sweden where research into the civil aspects of IEMI has been carried out within the defence sector since the late 1990's. Quite recently, an area of research dealing with the threat of IEMI specifically directed against transmission and distribution of electric power has been established at a Swedish civilian research centre called *High Voltage Valley (HVV)*. This, and related initiatives, hopefully means that civil funding can compensate for reductions within the defence sector.

Activities at HVV started in 2006 with a pre-study for Vinnova [2]. It joined stakeholders in IEMI and in power transmission and distribution. Risk areas were identified and key research areas formulated for protecting vital power system facilities against IEMI. The project included seven work packages, such as *Likely response of Swedish power grid in the event of HEMP*, *Most critical facilities for HPEM/Jamming attack*, *Development of surveillance technologies for critical facilities* and *Contingency plan in the event of a successful attack* The first major research program is a 1.1 MEuro EU project *Assessment and mitigation of risk for disabling control centres of large power networks by intentional radiofrequency interference*, planned to start in spring 2008.

In the EMC group at the Division of Electricity, Uppsala University, research on IEMI has been carried out since 2004. The research has been supported in part by the Swedish Rail Administration (Banverket) and by the Swedish Emergency Management Agency (KBM). The research include EMC surveys of railway facilities, propagation of transients into facilities, susceptibility of systems of the European Rail Traffic Management System (ERTMS) [3], susceptibility of COTS equipment and classification of vulnerability of civilian facilities.

Within the defence sector substantial studies on EM effects, funded by the Swedish Armed Forces, have been carried out by FOI and FMV during many years, including also civil systems [1]. At FOI quite extensive studies on susceptibility of low noise amplifiers, as well as studies on GPS, WLAN and wireless camera have been published in later years [4]. The studies have included aspects of both interference and permanent damage.

References
1. M. G. Bäckström, K. G. Lövstrand, "Susceptibility of Electronic Systems to High-Power Microwaves: Summary of Test Experiences", IEEE Transactions on Electromagnetic Compatibility, Vol. 46, No. 3, August 2004, pp. 396 – 403.
2. "Electromagnetic Terrorism – Power Transmission and Distribution system Response and Immunity", June 2007, Vinnova grant 2006-02499, *High Voltage Valley*, Box 832, SE-771 28 Ludvika, Sweden. Restricted distribution.
3. D. Månsson, R. Thottappillil, M. Bäckström, O. Lundén "Vulnerability of European Rail Traffic Management System to Radiated Intentional EMI", accepted for publication in *IEEE Trans. on EMC,* February 2008.
4. M. Höijer et al., "Final Report: HPM–skyddsmetoder för NBF", FOI Report FOI-R—2127—SE, February 2007. Swedish Defence Research Agency FOI, Sensor Technology, Box 1165, SE-581 11 Linköping, Sweden, www.foi.se.

Plenary

HPEM Activities at the International Scientific and Technical Center (ISTC Moscow)

V.A. Terekhin[1], W.A. Radasky[2][1]

[1]*Russian Federal Nuclear Center – All-Russia Scientific Research Institute of Experimental Physics, Sarov, Russia*
[2]*Metatech Corporation, Goleta, USA*
E-mail: terekhin@vniief.ru

The paper contains a review of results of some International Scientific and Technical Center (ISTC) projects have been performed by VNIIEF EMP group with Metatech Corp collaboration and ISTC financial supporting. The projects dealing with HPEM problems have been carried out during 1996-2008. The list of considered topics is following:

1. Theoretical Study Generation and Propagation of Intense High-Power Electromagnetic Pulse in Atmosphere and Ionosphere Including Nonstationary, Nonlinear and Kinetic Effects (ISTC Projects #311 and 2210).
2. Generation Ultra-Wideband Electromagnetic Pulse from Faster-than-Light Sources (ISTC Project #1158)
3. Development of Mobile Simulator of Positive Lightning Current Effect on the Grounded Objects (ISTC Project #3161).
4. Theoretical Study of Super – Alfvenic Plasma Flow with Anisotropic Electron Velocity Distribution (ISTC Projects #310, 1704 and 2104).

Plenary

An Overview of the Research on High-power Electromagnetics in China

Lihua Shi

Nanjing Engineering Institute,Nanjing , China

E-mail: shilh@jlonline.com

The research on high-power electromagnetics(HPEM) has received great attention in China in resent years. Based on a brief survey of the published papers in academic journals in Chinese language, this paper gives an overview of the main research directions and some progresses of China in HPEM. High-power microwave(HPM), ultra wide-band(UWB) pulse, high-altitude nuclear electromagnetic pulse(HEMP) and lightning electromagnetic pulse(LEMP) are four types of HPEM environment mostly concerned with in the literatures. The coupling analysis method, interference effect, experiment facility and standardization aspects are summarized and introduced.

(1) Experimental research. The sensitivity experiment covers typical computer system, data acquisition board, individual circuit component, small personal electronic devices and some commonly used electro-explosive devices. One general result is that the faster the leading edge of the disturbance field, the serious the interference effect. Compared to radiation interference, conductive disturbance attracts more and more attention recently. Besides experiments on electronic equipments, biological effects of HPEM have also been tested.

(2) Computational simulation and verification. FDTD method is the commonly used method in analyzing the coupling of cables and structures for short pulses. Several native visualization software systems have been developed. Some methods to reduce the dimension, to save the memory or to enhance the accuracy in FDTD calculation are proposed. Transmission line model is also used as a simple method to evaluate cable coupling. Some experiments were carried to study the coupling of cables and the tested and calculated results verified each other.

(3) Test and measurement facilities. Several HEMP simulators and some other HPEM test methods are introduced. Artificially trigged lightning has also been carried each year to gather experimental data of LEMP and to verify protection effects. The present situation of the measurement systems is also overviewed.

(4) Standardization. Compared to IEC's standardization process, China's national standards on HPEM is not very completed. One main trend in resent years is that although there is no official compulsory request, it seems most of the test labs begin to pay attention on the measurement uncertainty. Some comparative calibration has been initiated between different labs.

References

1.   *High Power Laser and Particle Beams.1997-2007*
2.   *High Voltage Engineering.1997-2007*
3.   *Chinese Journal of Radio Science. 1997-2007*
4.   *Journal of Microwaves. 1997-2007.*

Plenary

Detection Technologies and Systems for Humanitarian Demining: An Overview Based on the GICHD Guidebook

C. Bruschini[1], H. Sahli[2]

[1]*CBR Scientific Consulting, Lausanne, Switzerland*
[2]*Vrije Universiteit Brussel, Dept. of Electronics and Information Processing, Brussels, Belgium*
E-mail: Claudio.Bruschini@epfl.ch

Over the last 10-15 years considerable funding and effort has been invested worldwide in order to develop new technologies for Humanitarian Demining (HD). Some of the most notable developments which have taken place in HD sensing related R&D during this period include: (i) a shift from a focus on the individual sensor as a solution towards the individual sensor as part of a set of tools, (ii) an increased emphasis on area reduction and the detection of minefield indicators rather than individual mines, (iii) an increased emphasis on trace explosive detection, (iv) the gaining of importance of systematic test and evaluation (in particular via ITEP).

A host of physical principles – electromagnetic-based systems (metal detectors, GPR), trace explosive detection, bulk detection systems, remote sensing, etc. – have been investigated for landmine detection as well as area reduction. They are described, for example, in the **GICHD Guidebook on Detection Technologies and Systems for Humanitarian Demining** [1,2], together with the corresponding technologies and systems and their *estimated technology readiness*. The *Guidebook* can be ordered free of charge from the GICHD Website.

It is however fair to say that the mine action community as a whole was often not satisfied with the situation. Indeed, "the delivery to deminers of new tools and equipment […] has not met early expectations" - not enough research results have been turned into successful commercial products which have made Mine Action faster, more cost effective or safer. Reasons for the lack of progress from R&D to field use include: (i) the complexity of the problem, including environmental and operational aspects; (ii) the mismatch between research ideas and application requirements in the field, and (iii) the significant non-technological problems in funding the resources to turn prototypes into fully tested commercial products ready to use in the field. The corresponding bottlenecks and lessons learned have been further analysed by the European DELVE project [3].

In addition, in a number of cases the ineffectiveness in bridging the gap between R&D and Deployment was due to the lack of an overall, coherent strategy (coordinated *end-to-end planning*), integrating RTD actors, mine action donors and field practitioners (deminers). For example, demonstrator systems developed using Earth Observation techniques have been sufficiently demonstrated, together with their cost/benefit potential; however, their take-up by end users has not been successful. In the end, only electromagnetic-based technologies, in particular enhanced metal detectors and ground penetrating radars, have seen significant advances and are being introduced into the field. Test results consistently confirm that some of these technologies can indeed increase the productivity of humanitarian demining, while at least maintaining the current high levels of safety. Several development groups have shown this is the case for the combination of a metal detector with ground penetrating radar. The first such combined system are now been fielded and others are expected to follow shortly [1].

The landmine problem remains far from solved. R&D of practical detection technologies and systems continues therefore to represent one of the most significant contributions to its solution.

References
1. C. Bruschini, H. Sahli, and A. Carruthers, Guidebook on Detection Technologies and Systems for Humanitarian Demining. Geneva: Geneva International Centre for Humanitarian Demining, ISBN 2-88487-045-8, 2006. www.gichd.ch and http://www.gichd.ch/1248.0.html.
2. C. Bruschini, H. Sahli, and A. Carruthers, "Detection Technologies and Systems for Humanitarian Demining: Overview of the GICHD Guidebook and Review of Conclusions", Proc. IAEA/INFN Technical Meeting on Combined Devices for Humanitarian Demining and Explosive Detection, Padova, Italy, Nov. 13–17, 2006.
3. DELVE CONSORTIUM, "Humanitarian Demining R&D Lessons Learned", DELVE Deliverable D4.2, v2.3.0, May 2007, 60 pp. http://www.delve.vub.ac.be/

Plenary

Documented Electromagnetic Effects (EME)

D. V. Giri[1,2]

[1]*Pro-Tech, 11- C Orchard Court Alamo, CA, 94507-1541 USA*
[2]*Dept. of Electrical Computer engineering, University of New Mexico, Albuquerque, NM 87131-0001 USA*
E-mail: Giri@DVGiri.com   URL: wwww.dvgiri.com

This presentation will begin with placing this subject of **EME** in the broader context of **E**lectromagnetic **E**nvironments, **E**ffects and **P**rotection or **E³P.** To begin with, the environments can be anti-electronics or anti-personnel. The anti-electronics environments can be nature-made such as a lightning discharge or man-made such as Intentional **E**lectro**M**agnetic **I**nterfering **S**ignals or **IEMIS**. Characterization and quantification of the EME comes from an understanding of the coupling and interaction between the environments and the system. Once the effects are understood, the goal then becomes one of achieving **E**lectro**M**agnetic **C**ompatibility or EMC, resulting in a protected system. These interrelationships are schematically shown in Figure 1.
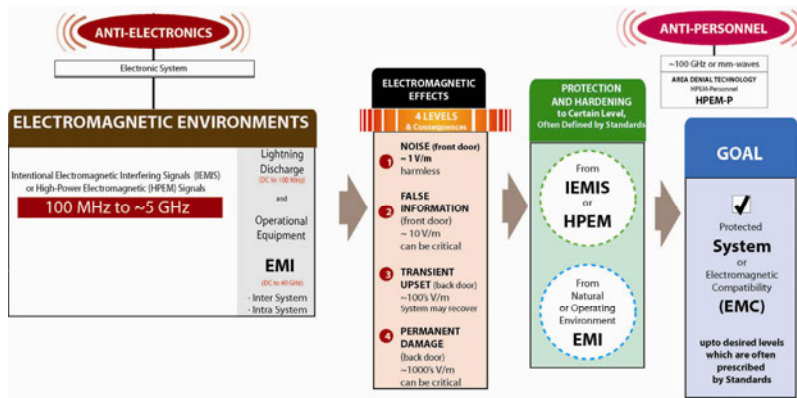
Fig. 1 - Electromagnetic Environments, Effects and Protection (E³P)

There are many examples of the generation of electromagnetic environments such as narrowband HPM, moderate band damped sinusoidal radiators and hyperband radiating systems in technical reports, journal articles and text books. In this presentation, we focus on documented EME. EME has been documented at many levels of electronics, such as component, circuit, sub-system and system level. We will review the documented effects data, which comes in different forms. The effects range from harmless noise in electronic equipment to a catastrophic effect in the US aircraft carrier *Forrestal* incident on July 29, 1967, off the coast of North Vietnam. In some High-Power Electromagnetics (HPE) laboratories, especially in Europe, source/antenna systems have been used in investigating and documenting the effects on micro-processors, and computers. In the civilian infrastructure, U.S. Federal Aviation Safety Reporting System (ASRS) has compiled reports of effects on navigational circuits from passenger electronic devices (PED). U.S.FDA has also documented medical equipment problems in hospitals, due to both conducted and radiated interferences, some resulting in loss of life. There have been at least seven incidents of aircraft falling out of the sky during 1959-1988 due to natural lightning. There are also other EMI incidents that have brought aircraft down such as the German Tornado fighter aircraft near the VoA station in Munich, Blackhawk helicopters and an F-111 crash during the U. S. air strike of Libya in 1986. The source of the incident EM environment may thus be *natural*, *accidental* or *intentional*. There have been reported cases of intentional cyber or software attacks and an incident where a huge area of Moscow had no phone communications for one day as a result of intentional electromagnetic effect [1]. The main point of this paper is that EME is real and it is prudent to be pro-active and preempt such RF threats to military and civilian infrastructure rather than react to it after the fact.

References

1.   L. Siniy, "Russian Research of Intentional Electromagnetic Disturbances over the Past Ten Years", Presented at AMEREM 2006.

Transient E.M. fields radiated by large earthing systems

M. Lefouili [1], B. Nekhoul[1],   K. Kerroum[2], K. El Khamlichi. Drissi[2]

[1] *LAMEL Laboratory, University of Jijel, BP 98 Ouled Aissa 18000 Jijel, Algeria*
Email: Lefouili_moussa@yahoo.fr
[2] *LASMEA Laboratory, Blaise Pascal University, 24 Avenue des Landais, 63177 Aubière, France*
Email: Kamal.KERROUM@lasmea.univ-bpclermont.fr

Introduction Electromagnetic field approach is the most rigorous method for modeling the transient behavior of grounding system, because it solves full Maxwell's equations with minimum approximations. This approach can be implemented either by Method of moment (MoM) or by Finite Element Method (FEM).

The model for the transient behavior of grounding system based on MoM was first developed by Grcev [1]. This model consists to transform the associated electric field Maxwell's equation to a system of linear algebraic equations with minimum assumptions; consequently, it is believed to be accurate. The higher is the frequency of input sources, the greater is the accuracy of the electromagnetic field approach

The electromagnetic field approach for the transient analysis of grounding based on finite element method was developed by Nekhoul & al [2]. The difficulty in this approach is to transform the open boundaries of both air and earth environment into a closed boundary problem using spatial transformation, which will reduce the size of the problem. The main advantage of this electromagnetic field approach based on FEM is that the descritization of the domain (geometry of the medium) of the problem can be highly flexible non-uniform patches or elements that can easily describe complex shapes.

Proposed Approach

In this work we propose a hybrid approach for transient analysis of grounding system [3].This approach is based on: Electrical dipole theory for determining EM fields' radiation in infinite conductive medium; Modified images theory for taking in account the interface in the half space instead Summerfield's integrals; Transmission line approach for determining the longitudinal and leakage current.   It has been shown that, the total radiated electromagnetic field is the sum of the contributions from each constituent dipole.
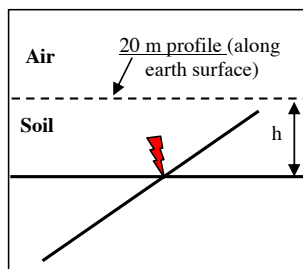
Fig.1. Two buried conductors   Fig, 2. Electric Field, our model   Fig, 3. Electric Field, NEC 4.1 code
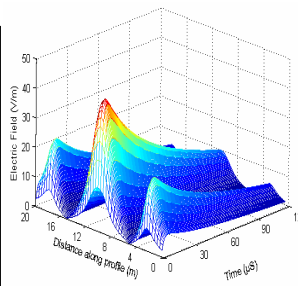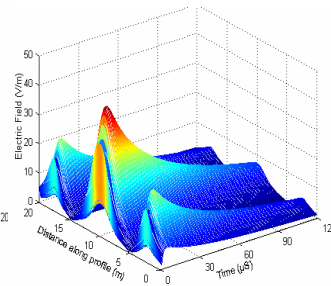
The physical situation is display in Figure 1. The conductors are 15 meters long, located one meter beneath air soil interface. Figure 2 and 3 illustrates the electric field (component Ex) along profile at the soil surface, radiated by this grounding systems, obtained by our model and NEC-4.1 code [4] respectively.

The comparison with NEC-4.1 code results for one buried conductor, two buried conductors and Buried grid shows that our computation model is in good agreement.

References

1. L.D. Grcev "Computer analysis of transient voltages in large grounding systems". IEEE Transactions on power delivery, Vol.11, N°2, April 1996.
2. B.Nekhoul, C. Guerin, P. Labie, G. Menier, R. Feuillet and Brunotte X. "A finite element method for calculating the electromagnetic fields generated by substation grounding systems" IEEE Trans on magnetic, Vol.11, No3, May 1995.
3. M. Lefouili, B. Nekhoul, B. Harrat, K.Kerroum and K. El Khamlichi Drissi "Transient EM fields generated by buried conductor",International Review of   Electrical Engineering (IREE). Praise Worthy Prise Vol.1 N°.1 Marsh April 2006
4. NEC- 4.1 , numerical Electromagnetic code January 1992.

Electromagnetic Pulse Generated by Pulsed Arc Electrohydraulic Discharge Water Treatment Reactors

Jen-Shih Chang[1], T. Ikeda [1, 2], H.O.L. Li [1] and K.Teii[2]
[1]*McMaster University,Hamilton,Canada*
[2]*Kyushu University, Fukuoka, Japan*
E-mail: changj@mcmaster.ca

The pulsed arc electrohydraulic discharge *(PAED)* is a direct plasma treatment technique for drinking and waste water treatments, where electrohydraulic discharge is defined as discharge inside water. Due to the nature of large pulse current (10 to 100 kA peak current) and short pulse (10 microseconds level) operations [1], an unwanted electromagnetic pulse (EMP) was experimentally observed. In this work, an experimental investigation has been conducted to study this EMP propagation in a PAED reactor. An experiment is conducted in 3 L volume eccentric electrode positioned PAED reactor for the charging voltage from 1.8 to 3.5 kV and electrode gap distance between two Ti made rod electrode from 0.5 to 3 mm. A spark gap controlled 0.5 kJ/ pulse power supply was used. Electromagnetic pulse wave from was measured by Piezo type pressure transducers placed several location inside reactor wall. Typical current, voltage and EMP induced pressure waveforms are shown in Figure 1. Since discharge volume is relatively smaller (discharge electrode gap distance with radius of less then few mm) by-compared with reactor volume, EMP propagation may acted as point source , hence observed EMP induced pressure waveform was not significantly depending on the position inside reactor:. The mechanism of EMP and induced pressure generation and propagation will be discussed in detail.
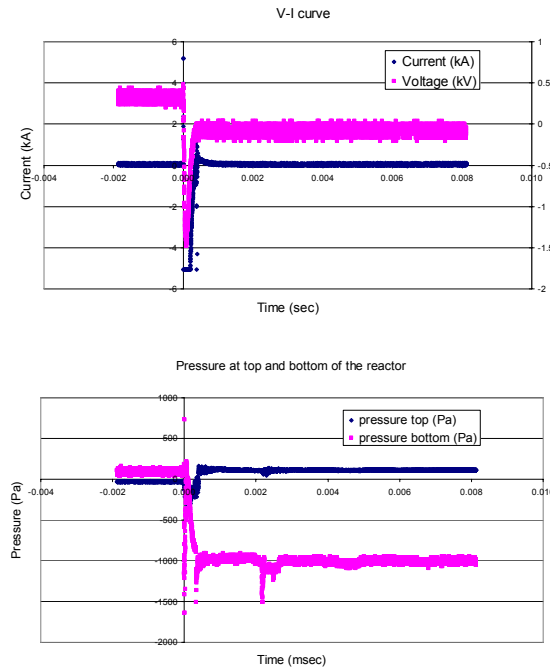
Fig. 1 – Typical current, voltage and EMP induced pressure waveforms

References
1.   B.R. Locke , M. Sato, P. Sunka, M.R. Hoffman, J.S. Chang , "Electrohydraulic Discharge and Nonthermal Plasma for Water Treatment", Ind Eng Chem Res. Vol. 45: pp. 882-905, 2005.

Measurement of Amplitude and Phase Fluctuation of Radiowave Propagation in Wireless Traffic Monitoring System

A. Intarapanich[1], R. Tongta[2] and C. Thongsopa[2]

[1]*National Electronics and Computer Technology Center, Pathumtani, Thailand*
[2] *Suranaree University of Technology, Nakon Ratsrima, Thailand*
E-mail: chan@sut.ac.th

Wireless sensor network for traffic monitoring is very attractive due to easiest installation and reconfiguration on the road. However, radio wave propagation under moving cars on the road introduces amplituse and phase fluctuation which may degrade the wireless sensor network performance. In this research, we collect amplitude and phase data of radio wave propagation under stationary and moving traffic. Some statistical properties are analyzed. The statistical properties of the received signal are important to the wireless sensor network performance. Moreover, the receiver performance can be improved by utilizing these statistical properties in receiver system design.

A channel sounder is built for study radio wave propagation at 2.4 GHz. The probing signal is Binary Phase Shift Keying (BPSK) with bitrate of 24 kpbs and modulated by a PN sequence. The transmitter is a direct conversion system. The receiver is a heterodyne system with an I-Q demodulator. The I-Q signal is sampling and store in a digital oscilloscope. The measured I-Q signal is then analyzed using MATLAB software. The measurement is performed on a road intersection as shown in Fig. 1. Three traffic conditions are investigated in the experiment. First, the measurement is performed without traffic, i.e. no vehicles on the road. Amplitude and phase fluctuation is investigated in other two scenarios where vehicles are on the road. The first scenario is stationary condition where all vehicles are stop at the intersection. In the second scenario, data is collected while all vehicles are moving. 10000 I-Q signal samples are acquired during the measurement in all scenarios.

Fig. 2 shows the histogram of the amplitude of received signal computed by measured I-Q signal in moving traffic condition. The moving vehicles generate random multipath signals which are combined at the receiver. It is well known that the amplitude of complex signal under multipath environment is Rayleigh distributed [1] when the number of multipath components is large enough. However, it can be seen from the histogram of measured signal that the amplitude distribution resembles Gaussian distribution. It is possible that the moving vehicles could not generate enough multipath components so that the condition for Rayleigh distributed amplitude is hold. To estimate the number of multipath components and statistical properties of each component, a sophisticate channel sounder is needed.
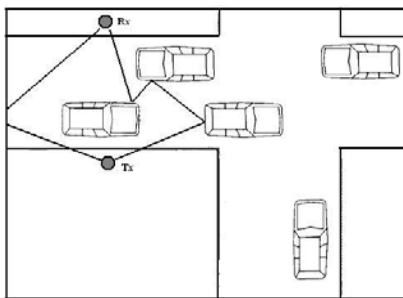
Fig. 1 – A measurement scenario   **Fig. 2 – Received amplitude histogram**
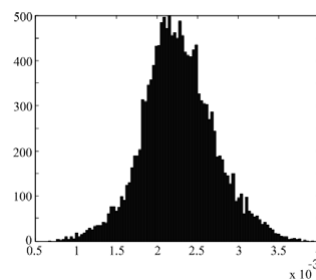
References
1. T. S. Rappaport , Wireless Communication: Principles & Practice, Upper Saddle River, NJ, Prentice Hall PTR, 2000.
2. A. A. M. Saleh and R. A. Valenzuela, "Statistical Model for Indoor Multipath Propagation," IEEE Journal on selected Areas in Communication, vol. SAC-5, pp. 128-137, 1987.
3. L. P. Kafle, A. Intarapanich, B. A. Sesay, J. R. Davies, J. McRory, and G. McGibney, "A Wideband MIMO Channel Measurement System for Indoor Office Environment," Proc of World Wireless Congress, pp. 95-100, 2004.

HPEM - 01
Electromagnetic Environments

Oral Presentations

Electromagnetic Threats to PCs

Libor Palisek, Jiri Kusala, Lubomir Vrana, Radislav Miksik
VOP-026 Sternberk, s.p., division VTUPV Vyskov,
V. Nejedleho 691, 682 03 Vyskov, Czech Republic,

E-mail: l.palisek@vtupv.cz

The results from many tests carried out in various testing facilities around the world show high sensitivity of electronic equipments to power electromagnetic fields. The most sensitive equipments to power electromagnetic fields are obviously personal computers (PCs). PCs are very important part of almost all today's systems and PCs are usually the most sensitive part of these systems therefore it is necessary to consider PCs as a crucial parts of the systems and it is necessary to find their vulnerabilities in critical systems like systems in the infrastructures, military systems etc. There are a lot of possible electromagnetic threats and the most of them are included in relevant Electromagnetic Compatibility (EMC) standards but there is possibility of intentional electromagnetic interference (IEMI) [2] which is not included in regular EMC standards. For critical systems it is necessary to consider these electromagnetic phenomena too. As IEMI will be considered HPM (High Power Microwave) [1], UWB (Ultra Wide Bandwidth) and NEMP (Nuclear Electromagnetic Pulse) too in this study.

The aim of this study is to present some results obtained during experimental measurements of PCs susceptibility to HPM, UWB and NEMP irradiation. As an equipment under test (EUT) will be chosen regular PCs setups with peripherals like monitors, keyboards and mice and without peripherals too. Setups for Ethernet, WIFI (Wireless Fidelity) and USB (Universal Serial Bus) communication will be used too. Susceptibility of regular PCs including notebooks to used HPM, UWB and NEMP irradiation will be presented as well as susceptibility of Ethernet, WIFI and USB communications. At the end of this presentation effectiveness of used testing signals HPM, UWB and NEMP to achieve typical effects on tested PCs setups will be compared and evaluated.

Fig. 1 – NEMP Testing of PCs setup   **Fig. 2 – HPM 9 GHz Testing of notebook**
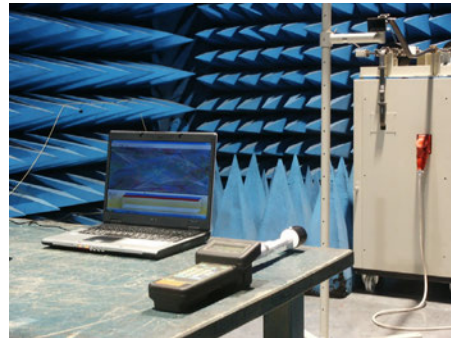
References
1.   D. Taylor, D.V. Giri, "High-Power Microwave Systems and Effects", Taylor & Francis, 1994.
2.   IEC 61000-2-13, First edition, 2005-03, Electromagnetic compatibility (EMC) – Part 2-13: Environment – High-power electromagnetic (HPEM) environments – Radiated and conducted.

Vulnerability of electronic equipment:
Coupling Paths and Component Vulnerability

M. Höijer[1], R. Jonsson[2], O. Lundén[3], L.-G. Huss[4], H. Frennberg[5] & L. Jansson[6]

[1,2,3,4,5]*Swedish Defence Research Agency FOI, SE-581 11 Linköping, Sweden*
[6]*Saab Bofors Dynamics, SE-691 80 Karlskoga, Sweden*

E-mail: magnus@foi.se

The vulnerability of electronic equipment against electromagnetic irradiation depends on many different parameters. These parameters include the pulse shape, the frequency content, the pulse repetition frequency, the polarisation and from which direction the electronic equipment is irradiated (directivity issue). In reality the situation is further complex than this list of parameters indicates. True high level test facilities does often, not to say always, only offer a limited number of possible test parameters. To that come that actual testing is limited by time and financial restrictions. One should also be very well aware of that testing is much more time consuming than to perform measurements, the accuracy in testing performed is often very limited. A typical test may e.g. have given that when irradiated by 1 kW electronic equipment is killed by the electromagnetic field. However, no knowledge is gained whether the equipment is killed already by 900 W. Often the uncertainty interval might be as big as 100 W to 1 kW. Hence very few true parameter studies of the vulnerability are actually performed.

To be able to somewhat improve the situation we propose the use of the in Fig.1 presented principal description of vulnerability. Vulnerability consists of two parts; First how efficient the incident electromagnetic field couples to the electronic components, and secondly the actual vulnerability of the components. The electromagnetic coupling can be described by antenna theory and is in Fig. 1 represented by the antenna. The electromagnetic coupling is in most cases a linear process and accurate measurements can be performed, though even those can be time-consuming.

Here we present results from both antenna coupling measurements and component vulnerability tests. We have performed extensive antenna coupling measurements. Theses are presented in several earlier papers, mainly concerning the directivity issue, e.g. [1]. Here we focus our presentation on the polarisation and inherent frequency dependencies. Concerning component vulnerability test, we show test results as well modelling results on the pulse length dependency.
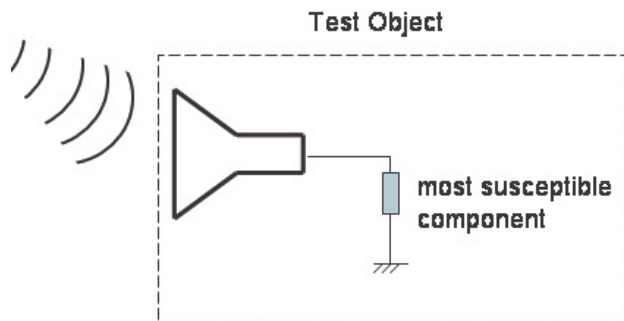
Fig. 1 – Vulnerability of electronic equipment depends on how efficient the electromagnetic field couples to the electromagnetic components and the vulnerability of the components themselves.

References
1. M. Höijer, M. Bäckström and J. Lorén "Angular Patterns in Low Level Coupling Measurements and in High Level Radiated Susceptibility Testing," IEEE Transactions on Electromagnetic Compatibility, Proceedings of the EMC Zurich '03, ETH Zentrum - IKT, CH-8092 Zurich, Switzerland, February 18-20, 2003.

HPEM - 03
Vulnerability of Systems & Components

Oral Presentations

Simulation of ESD Immunity Test by a Software Tool based on the Finite Integration Technique

S. Caniggia[1], F. Maradei[2]

[1]*EMC Consultant , Viale Moranti 7, 20010 Bareggio (MI), Italy*
[2] *Sapienza University of Rome,Dept. of Electrical Eng. Via Eudossiana 18, Rome, Italy*

E-mail: fr.maradei@ieee.org

The aim of this paper is to simulate by numerical software tools ESD conducted and radiated immunity tests in accord to the IEC 61 000-4-2 standard [1], and its second edition which is still under discussion. The possibility to have a reliable prediction tool suitable for ESD compliance is very appealing since in the recent years many standards are including numerical modeling as possible instrument to be used in the certification process.

The most important aspect to cope with when dealing with the simulation of ESD immunity tests, concerns the numerical modeling of commercial ESD generators which are widely used for testing the immunity of electronic equipment, and permit to reproduce typical human-metal ESD events. A numerical model of the ESD generator by the commercial numerical code Microwave Studio (MWS) based on the finite integration technique has been recently proposed [2]-[4]. The model accurately simulates the discharge current in contact-mode taking into account the geometry and the loading effect of the generator (see Fig. 1), and can be used to predict both conducted and radiated disturbances. An example of the ESD radiated field obtained by simulations is shown in Fig. 2. The developed model of the ESD generator is used to simulate ESD immunity tests on cables and circuits.
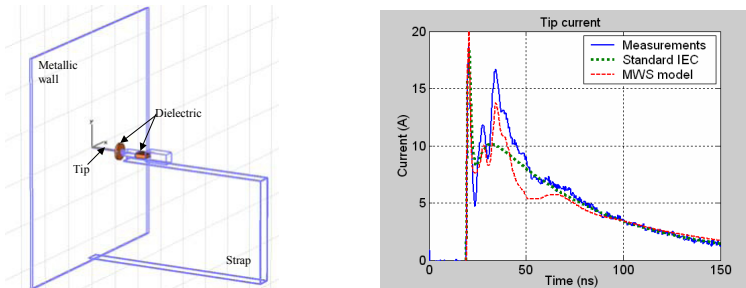
Fig. 1. MWS model of the test setup used for ESD current calibration (a) and tip current (b).

(a)   (b)
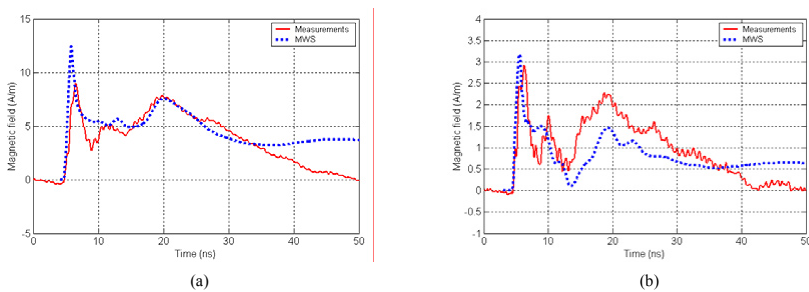
Fig. 2 Radiated magnetic field at a distance of 15 cm (a) and of 45 cm (b) from the ESD event: results obtained by the software tool MWS (dotted line) and by measurements (continuous line).

References
1. Electromagnetic Compatibility (EMC) Part 4-2: Testing and Measurement Techniques – Section 2: Electrostactic Discharge (ESD) Immunity Test*”*, IEC-EN 61000-4-2, 1996-09.
2. S. Caniggia, F. Maradei, "Circuital and numerical modeling of ESD coupling to shielded cables", European EMC Symposium, Eindhoven, Semptember, 2004.
3. S. Caniggia, F. Maradei, "Circuit and numerical modeling of electrostatic discharge generators", *IEEE Trans. Industry Applications*, vol.42, no.6, Nov./Dic. 2006.
4. S. Caniggia, F. Maradei, "Numerical Prediction and Measurement of ESD Radiated Fields", *IEEE Trans. on EMC*, Vol. 49, Aug. 2007, pp. 494-503.

Efficiency of electronic mode tuning with a two orthogonal LPDA antennas scanning system in a reverberation chamber

C. Tsigros[1], M. Piette[2]

[1,2]Royal Military Academy, Brussels, Belgium

E-mail : christo.tsigros@rma.ac.be

The method usually applied for mode tuning a reverberation chamber consists of placing a rotating stirrer that breaks the waves coming from a fixed source antenna, reflecting and scattering them in various time-dependent directions. Not conceived originally for reverberation purpose but rather as a Faraday cage, the cubic shape of the small LEMA chamber ($15m^3$) was a priori expected to be a penalty for obtaining good differentiation of the resonance frequencies. From the studies done the last years on this chamber [1][2][3][4], it turns out that the drawback of the cubic shape can be overcome in so far the mechanical stirrer is properly designed and if the "factor 6" rule of thumb usually considered as the minimum ratio of the operating frequency to the fundamental resonance frequency of the cavity to have enough modes in the chamber [5] is relaxed to a "factor 9" rule of thumb. Because the mechanical stirrer has to be electrically large to be efficient, it can be quite cumbersome and limits the working volume available for the EUT, especially in small reverberation chambers. In large chambers with low LUF (Lowest Usable Frequency), huge stirrers can cause stability and vibration problems.

The method of electronic mode tuning presented here could be an interesting alternative to the mechanical tuning. It is based on the use of a scanning system consisting of two orthogonal rails on which a transmitting LPDA (Log Periodic Dipole Array) is sequentially moved. The work has been made in the perspective of making immunity testing according the IEC 61000-4-21 [6] standard at HIRF (High Intensity Radiated Fields) in the frequency band of mobile phone and GPS systems (800-2500MHz). The three components of the E-field, the forward and reverse output powers and the displacement of the two transmitting LPDA have been measured for each of the 150 tuner positions, at eight locations of the working volume and at twenty two frequencies within the frequency range of interest. The results are oriented and analyzed in function of the requirements of the standard, i.e., the field uniformity. The results show that this source tuning method using scanning systems that is less cumbersome than the conventional mechanical mode stirrer is quite efficient. Indeed, for each of the three components of the E-field the uniformity, the normalized standard deviation given by (1) is less than the 3 dB limit over the whole frequency range of interest, i.e. 800 to 2500 MHz.

$$\sigma_{ij}(dB) = 20\,Log_{10}\,(\frac{\sigma_{ij} + \langle \overleftrightarrow{E_{ij}} \rangle_8}{\langle \overleftrightarrow{E_{ij}} \rangle_8}) \qquad (1)$$

References
1. M. PIETTE, "*From cubic Faraday Cage to HIRF Testing Reverberation Chamber*", IEEE & URSI Joint Symposium EuroElectromagnetics (EUROEM'04), 12-16 July 2004, Magdeburg, Germany, Paper HPEM 13-2.
2. M. PIETTE, K. MOESEN, S. MONTEZUMA, *"Experimental Field Statistics Validation in a Cubic Reverberation with Mechanical Mode Stirring & Bistatic Cross-Polarized Illumination"*, Progress In Electromagnetic Research Symposium, 22-26 Aug 2005, Hangzhou, China. Proc. pp.424-427.
3. M. PIETTE, "*Complete Space-Time Validation of a Single Mode Stirrer Reverberation Chamber for Immunity Testing*", Fourth IEEE Asia-Pacific Conf. on Environmental Electromagnetics (CEEM'06), Dalian, China, Proc. pp.449a-d.
4. M. PIETTE, "*Anisotropy & Polarization Analysis in a Cubic Mode Stirred Chamber*", Fourth IEEE Asia-Pacific Conf. on Environmental Electromagnetics (CEEM'06), Dalian, China, Proc. pp.448a-e.
5. Wu, Chang, "*The effect of an Electrically Large Stirrer in a Mode Stirred Chamber"* IEEE Trans. on EMC, Vol.31, No.2, 164-169, 1989.
6. IEC 61000-4-21 (2003) : Electromagnetic compatibility (EMC). Part 4-21: Testing and Measurements techniques – Reverberation Chamber methods

HPEM - 06
Electromagnetic Compatibility

Oral Presentations

Development of Countermeasure Device to Prevent Leakage of Information Caused by Unintentional PC Display Emanations

Yasunao Suzuki, Ryuichi Kobayashi, Masao Masugi, Kimihiro Tajima, and Hiroshi Yamane
NTT Energy and Environment Systems Laboratories, Tokyo, Japan
E-mail: suzuki.yasunao@lab.ntt.co.jp

1. Introduction

A working personal computer (PC) usually produces unintentional electromagnetic fields, and some of these emissions often carry significant information processed in the PC. In some cases, the information of the screen content of a video display unit could be reconstructed by intercepting such emissions at a distance. Such a threat of information leakage from compromising emanations has been pointed out by Win van Eck in 1985 [1], and that is known as "van Eck eavesdropping" or "TEMPEST" (a codename used by some military organizations) [1][2]. We have studied a countermeasure technique called "emanation security" for such a problem. This paper describes a protecting device we have developed to defend PC displayed information against eavesdropping.

2. Display signal interface and leakage emanations

Video signal interfaces for PC displays are standardized by the VESA (Video Electronics Standards Association). The video screen is constructed with pixels, which are drawn on the screen along with the scanning line. A pulse signal used for determining the draw timing of the pixels is called a "dot clock" and its frequency is about 30 to 200 megahertz. The video signals are synchronized with this dot clock, whose frequency spectrum extends to about 1 gigahertz. According to this high frequency, the video signal can easily be emitted as electromagnetic fields. The dark line in Fig. 1 shows an example of frequency spectrum of electric field emitted from a PC. An example of the original PC screen image is shown in Fig. 2(a), and the image reproduced from detected leakage emanations is shown in Fig. 2(b). This result suggests that the original image is regenerated, and the smallest character in the lowest row (in the case of 30 point font) can be discriminated clearly.

3. Effectiveness of developed device

We have developed a countermeasure device to prevent information leakage from PCs. The outward appearance of the device is shown in Fig. 3. The device is connected to the video display connector on a PC, and it picks up the video signal to regenerate the dot clock. This dot clock is modulated to generate a jamming signal that is fed to the PC and to the video display terminal in common mode. The jamming signal radiates from the PC and then obstructs eavesdropping to cover up the leakage signal. The frequency spectrum of the emanation from a PC when the countermeasure device is active is shown in Fig.1 by the light-colored solid line.

The intercepted image of the original image (Fig. 2(a)) when the countermeasure device is active is shown in Fig. 2(c). This result demonstrates that the device is effective; the original image disappears completely. We planned to display fixed vertical stripes on the eavesdropping display monitor to counteract the scheme of video-frame averaging used by eavesdroppers to improve image quality.

4. Conclusion

We have developed a device to counteract eavesdropping of PC displayed information from intercepted unintentional emission. We have shown that the device effectively protects the security of PCs. Future work is to establish an objective index that evaluates the ability to protect against information leakage.
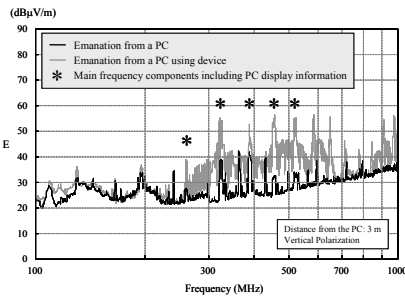
Fig. 1. Electric field strength of the emanations from a PC
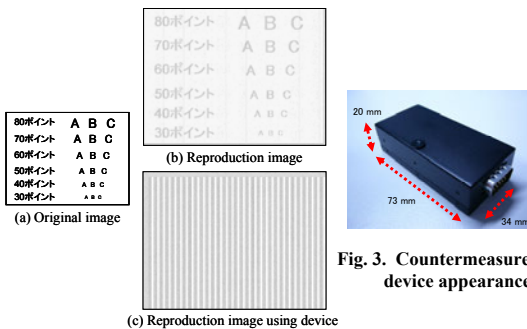
Fig. 2. Reproduced display image and effectiveness of device

Fig. 3. Countermeasure device appearance

References

1.   Wim van Eck, "Electromagnetic Radiation from Video Display Units: An Eavesdropping Risk?," Computers & Security Vol. 4 No. 4, pp. 269–286, (1985)
2.   National Security Agency, "NACSIM 5000 TEMPEST Fundamentals.," Fort George G. Meade, 1992, Md.

Improvement in Tuner Efficiency and Field Uniformity introduced by Multiple-Sources in Reverberation Chamber*

Y.M. Shen[1], D. Shi[1], Y.G. Gao[1], Y.M. Zhang[2]

[1]*School of Telecommunication Engineering, Beijing University of Posts and Telecommunications, Beijing, China*
[2] *The Fourth Survey & Design Institute of China Railway, Wuhan, China*
E-mail: shenyuanmao@bupt.edu.cn

Now mechanical stirrers or paddles are used as the most popular way to generate a statistically uniform, isotropic and randomly polarized field required by Reverberation Chamber (RC). Also, some alternative stirring techniques have been proposed to avoid the mechanical rotating elements, in which is the source-stirred RC (SSRC) [1]. Although, SSRC is just a preliminary technique and there still remain many problems such as the source structure design, its basic concept can be used in popular mechanical mode stirring RC for reference, for example multiple-sources. According to the theory of SSRC, the source location together with some other factors determines the field distribution in RC and the sources movement can stir the field distribution. So, if there are several available excitation sources (multiple-sources) at different locations in RC, we can get some additional stirring effect through changing the excitation sources location at every stirring step. Therefore multiple-sources RC can be looked as a conventional mechanical mode stirring RC which makes use of the source-stirring to get extra stirring effect, and obviously, multiple-sources will improve the RC performance.

Based on the simple planar model, the electric field expression has been figured out to simulate the field distribution, and then helps to reveal the influence introduced by multiple-sources in RC. The simulation results indicate the improvement in field uniformity (table 1) and tuner efficiency (fig.1) [2], that coincide with the theory analysis well. More details should be investigated further to help the multiple-sources as a method to improve RC performance and slower RC degradation in the low frequency range.
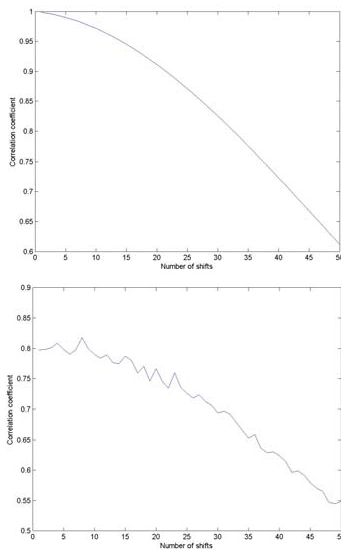
Fig. 1 correlation coefficient change with number of shifts (below: double sources up: single source)

Table 1: Standard deviation

Frequencies (MHz)	Standard deviation (dB)		
	Single source	Double sources	Four sources
100	-9.1	-8.4	-9.4
200	-11.5	-12.3	-11.8
300	-8.0	-12.1	-13.5
400	-9.2	-14.1	-14.9
500	-7.5	-12.1	-14.3
600	-8.2	-14.1	-15.0

Reference：

1. G. Cerri, V. M. Primiani, S. Pennesi, P. Russo, "Source Stirring Mode for Reverberation Chambers", IEEE Transactions On Electromagneitc Compatibility, Vol.47, No.4, pp.815-823, Nov. 2005.
2. IEC 61000-4-21, 2003. Reverberation Chamber Test Methods.

HPEM - 06
Electromagnetic Compatibility

Oral Presentations

Wireless Base Stations and Headsets efficiency and Radiation Effects

J. Gavan[1] and S. Tapuchi[2]
[1]*Holon Institute of Technology, Israel*
[2]*Sami Shimon Institute, Israel*
E-mail:gavan@hit.ac.il

Wireless Radio equipment and users are increasing tremendously and only for cellular communication exceed two thousands hundreds million. This tremendous increase in the number of wireless transmitters significantly increase the probability of harmful mutual interference and of people exposed to non ionized radiation from the transmitting equipments. The majority of the transmitted energy is wasted as interference and radiation sources to most operating receivers and numerous human being due to the low efficiency of mobile wireless energy transmission

The power density levels of radiation from most urban cellular base station are usually less than the stricter standard power density level thresholds due to distance and far field propagation conditions.

However radiation effects to mobile headsets users are significantly stronger than from base stations and unpredictable due to the reactive near field proximity distances from the radiation source, complexity and hot spots of the Electro-Magnetic (EM) reactive near field components reaching the users head.

In this paper will be analyzed radiation effects from far field propagation conditions base station antennas, techniques for enhancing the low efficiency of power and signal transmissions for cellular radio systems. This will be followed by describing the complex radiation field components absorbed from headsets by the individual users and the actual importance of the Specific Absorption Rate (SAR) expression, considering that power density levels are not well defined under EM near field conditions. Mitigation techniques will be discussed for increasing the efficiency of base stations and headsets, their batteries life-time and for decreasing significantly the radiation intensity effects in the users head and body.

Will also be described simulation methods to compute and compare the SAR of conventional mobile radio headsets with novel proposed headsets of reduced radiation to the users head

Oral Presentations

HPEM - 06
Electromagnetic Compatibility

Estimation of the Optimum Cell Sizes in the Cellular Communication System

Vladimir B. Trigubovich

Belarusian Medical Academy of Post-Graduate Education, Informatics dept.
220714, 3, P.Brovka str., Minsk, Belarus

E-mail: v_trigubovich@tut.by

One of the problems of the modern communication systems is the increasing of inter- and intrasystem radio interferences (RI). It may be explained by the limited volume of the electromagnetic (EM) resource. A solution of this problem lays in the sphere of the EMC theory methods.

Last time, cellular design of the communication systems is widely used to decrease level of RIs. It enables us reusing of similarly tuned signals in devises placed into adjacent clusters. But such design of communication systems leads to increasing of co-channel interferences (CCI) level. It is obviously, the less geometrical size of cells, the more value of CCI is. Therefore, it is possible to find optimum sell size in view of such suppositions.

So, in the paper we discuss approach to estimation of the optimum cell size. This one is mainly based on the technique for estimation of the CCI level [1, 2], as well as technique for estimation of signal losses due to propagation along trace transmitter-receiver [3, 4].

Let's consider a simple scheme for accounting of transmitter interfering influence on receiver. In view of the Friis formula, we can find power at the receiver input as

$$P_2 = P_1 A r^{-m} = P_1 r^{-m} \frac{G_{tr} S_{ef}}{4\pi}. \tag{1}$$

Here S_{ef} and G_{tr} are parameters of receiving and transmitting antennae, r is the distance between receiving and transmitting positions. For free-space EMW propagation conditions m is to be equal to 2. To receiver be operational, power P_2 must, at least, exceed sum of CCI power P_{CCI} plus power of other RIs P_{RI}, $P_2 > a(P_{CCI} + P_{RI})$. Here *a* is a multiplier, it may be calculated in view of type of signal to be used in the communication system.

Let us investigate one base station (BS) which is placed in the centre of the communication system. To our research not be very sophisticated, we suppose BSs, having the same signal tunings as "our" BS, are placed on the smooth surface with some intervals D, 2D,…, $[D_{LOS}/D]D$; here D is the distance between neighbor clusters. Number of CCI sources within the ring shape area defined by the distances iD and (i-1)D is equal to the number of clusters to be placed within ring area $\pi(i\text{D})^2 - \pi(i\text{-1})^2\text{D}^2$. By using technique known from [1], we may estimate CCI level by the formula

$$P_{CCI} = P_{BS} \sum_{i=1}^{[D_{LOS}/D]} \frac{(2i-1)}{1 + 4\left(\frac{iD}{\Delta D}\right)^2}. \tag{2}$$

Here distance D_{LOS} may be estimated as

$$D_{LOS} = 4.12\left(\sqrt{H_{tr}} + \sqrt{H_r}\right),$$

where H_{tr} and H_r are the effective antenna heights of some transmitter and "our" receiver. In the expression (2), ΔD is the parameter introduced temporary to simplify our calculations, P_{BS} is the BS transmitter power.

It is obviously, distance D depends on the cell radius R_c, therefore we may estimate cell size R_{copt} to sum $a(P_{CCI} + P_{RI})$ be minimum or optimal.

In the research we suppose to find dependences of the CCI normalized level as function on cell radius R_c. It may enable us to find optimum cell sizes if general level of other RIs in the communication system is known.

References
1. A. F. Aporovich, V. Trigubovich, "To signal separation by using frequency and distance," Electrosvyaz, №3, 2003.(in Russian).
2. V. Trigubovich, "To estimation of level of co-channel interferences in the communication systems," XVII Int. Zurich Symp. on EMC. 27 Feb.-3 March 2006. Symp. proc. on CD. 2006. – P. 116-119.
3. V. Trigubovich, "To estimation of RI appearance at the receiver input," – EUROEM-2004, Magdeburg, Book of abstracts, p.41, 2004.
4. A. F. Aporovich, V. Trigubovich, "To definition of selection by using distance at massive influence of radio interferences," Radiotekhnika, №7, 2007. (in Russian).

EMP Indirect Effects: Damped Sinusoidal Transients, Conducted Susceptibility Test, CS116 of MIL-STD-461E

Sandeep M. Satav, V.V. Rama Sarma, K. Rajeshwar Rao

Scientists, EMI-EMC Centre, RCI, Hyderabad, India

...

E-mail: sandeep_rci@rediffmail.com

Indirect effects of Electromagnetic Pulse (EMP) on structures, cables and systems are characterized by damped sinusoidal transients and can be simulated by conducted susceptibility test CS116 of MIL-STD-461E. It is important test for military equipment meant for surviving in EMP environment. In this paper a review on interpretation of the test requirement as per MIL-STD-461E and test set-up is presented. Need for automation of the test is necessary to save testing time and to maintain accuracy and precision. Specifications for design and development of an automated test system for carrying out CS116 test has been worked out meticulously. An automated test system is designed, fabricated and integrated at a competent supplier's end. Dedicated GUI based application software has been developed. The software has provision of accommodating correction factors for calibration probes, attenuators etc. Calibration and test results for a dummy load simulation are presented. At last, a model Equipment Under Test (EUT) has been tested and hardened for meeting the requirements of the test. Performance and functional test results are presented.

Calibration mode and test mode (bulk cable injection on cables and power leads) of Conducted susceptibility, damped sinusoidal transients test i.e. CS116 of MIL-STD-461E are shown in fig.1 (a) and (b) respectively. A photograph of the automated CS116 test system is shown in fig.2
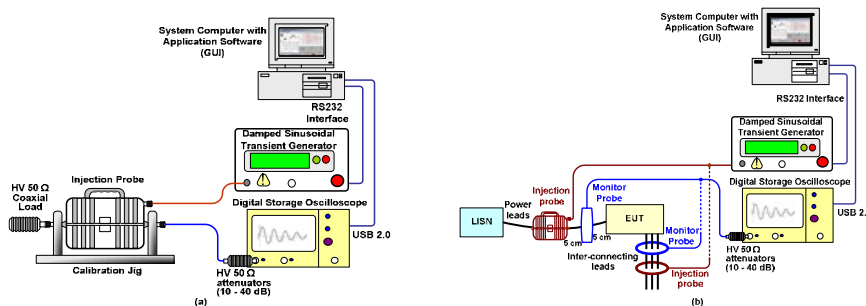
Fig. 1 – CS116 Test Set up – (a) Calibration Mode, (b) Bulk Cable Injection Test Mode

Fig. 2 – Photograph of Automated Test System for CS116 Test

References
1. J. Escalante *et.al*., "An Illustrative Experiments on Electromagnetic Oscillations". [Online]. Available: http://arxiv.org/ftp/physics/papers/0510/0510122.pdf
2. Oren Hartal, "Hardening of I/O Ports to EMP Susceptibility requirements of MIL-STD-461E", INCEMIC 2006.
3. "Requirements for the Control of Electromagnetic Interference Characteristics of Subsystems and Equipemnt", MIL-STD-461E, 20 August 1999.

HPEM - 06
Electromagnetic Compatibility

Oral Presentations

Recent Progress on Relativistic Magnetrons Driven by Transparent Cathodes

E. Schamiloglu, M. Fuks, C.J. Buchenauer, S. Prasad, and M. Roybal

University of New Mexico, Albuquerque, NM, USA

E-mail: edl@ece.unm.edu

The relativistic magnetron has been studied for nearly three decades and remains as one of the most sought-after high power microwave (HPM) source because of its simplicity and frequency tunability. Recently, researchers at the University of New Mexico proposed that a transparent cathode can significantly improve the output characteristics of this HPM source [1]. Since then, a comprehensive study using particle-in-cell simulations [2] has elaborated the many benefits of using this cathode, whose photograph is shown in Fig. 1. This talk will enumerate the various benefits of operating a relativistic magnetron using a transparent cathode. In addition, the initial results of experiments at the University of New Mexico on an A6 magnetron [3] driven by a short-pulse Sinus-6 accelerator will be presented. Planned experiments on an A6 magnetron using a longer pulse (50 ns) accelerator at UNM will also be described.
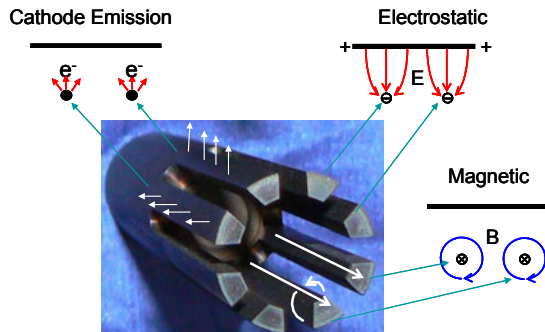
Fig. 1 – Photograph of a transparent cathode that self-consistently provides cathode priming, magnetic priming, and rf priming.

References

1. M. Fuks and E. Schamiloglu, "Rapid start of oscillations in a magnetron with a transparent cathode," Phys. Rev. Lett., vol. 95, pp. 205101-1–205101-4, 2005.
2. H.L. Bosman, M.I. Fuks, S. Prasad, and E. Schamiloglu, "Improvement of the output characteristic of magnetrons using the transparent cathode," IEEE Trans. Plasma Sci., vol. 34, pp. 606-619, 2006.
3. A. Palevsky and J. Bekefi, "Microwave emission from pulsed relativistic e-beam diodes II: The multiresonator magnetron," Phys. Fluids, vol. 22, pp. 986–990, 1979.

HPEM - 07
High-Power Microwaves (Invited)

Oral Presentations

Studies of Anode and Cathode Materials for use in
Repetitive Narrow-Band High-Power Microwave Sources

Anders Larsson, Mose Akyuz, Patrik Appelgren, Mattias Elfsberg,
Tomas Hurtig, Cecilia Möller and Sten E Nyholm
Swedish Defence Research Agency (FOI), Defence & Security, Systems and Technology
Grindsjön Research Centre, SE-147 25 TUMBA, Sweden

E-mail: Anders.Larsson@foi.se

High-power microwave (HPM) devices may be used in systems for disrupting or destroying electronic equipment. Two types of high peak-power narrow-band vacuum tubes are the virtual cathode oscillator (vircator) and the magnetically insulated line oscillator (MILO), but other alternatives exist. In many situations it may be advantageous to generate the microwave pulses repetitively in order to achieve the intended effect. The problem with repetitive operation is that it stresses the electrodes of the vacuum tube significantly more than single-shot operation due to material heating in the electrodes and degradation of the vacuum quality inside the cavity caused by material emission from the anode and the cathode.

To study electrode material endurance in a pulsed high-power microwave source, a series of experiments with an axial vircator powered by a repetitive Marx generator has been conducted [1, 2]. An axial vircator with side extraction was designed in which it is simple to exchange the anode and cathode for testing different anode-cathode configurations and different materials. The experiments performed include stress tests, where the anode and cathode materials are stressed for evaluating durability, and functionality tests, where the microwave generation capability of the different materials is investigated.

The Marx generator used had a pulse-repetition frequency of 10 Hz, and the vircator was subjected to 1-s-bursts. Different cathode materials (e.g., velvet and graphite emitters) show significant differences in voltage and current traces as well as differences in the time for the onset of microwave radiation and statistical variation in the time of microwave emission. Repetitive microwave pulse generation does put a lot of stress on the anode and the cathode materials of the vircator. Figure 1 shows an example of the effect on an anode grid which has been subjected to several repetitive electron beam bursts. This paper elaborates on differences seen in the behaviour of the vircator with different electrode material combinations.

Fig. 1 – Example of wear in a stainless steel anode mesh.
Left: Fresh anode mesh. Right: Anode mesh submitted to several bursts.

References
1. M. Elfsberg, T. Hurtig, A. Larsson, C. Möller and S. E. Nyholm, "Experimental studies of anode and cathode materials in a repetitive-driven axial vircator", 2007 IEEE Pulsed Power and Plasma Science Conference, Albuquerque, USA, 17-22 June 2007
2. M. Elfsberg, T. Hurtig, A. Larsson, C. Möller and S. E. Nyholm, "Experimental studies of anode and cathode materials in a repetitive-driven axial vircator", IEEE Transactions on Plasma Science (*accepted for publication*)

SPICE simulations and measurement techniques for protection circuits against UWB and HPM signals

F. Brauer[1], J. L. ter Haseborg[1]

[1]Hamburg University of Technology, Institute of Measurement Technology and EMC, Hamburg, Germany
E-mail: f.brauer@tu-harburg.de

The protection of complex electronic systems against high-power electromagnetics (HPEM) is inevitable nowadays. The disturbance or even destruction of civil or military systems by man-made intentional electromagnetic interferences (IEMI) can lead to high costs or endanger human life in the worst case. Nonlinear protection elements against signals with rise times above 1 ns, e.g. electrostatic discharge (ESD) or lightning electromagnetic pulses (LEMP), have been successfully developed and simulated in SPICE [1]. High-power electromagnetic pulses, like ultra wideband (UWB) pulses with rise times below 1 ns, exhibit a broad spectrum and a high amplitude. Therefore these pulses can couple into electronic systems with a specified resonant frequency band with a high probability. The traditional nonlinear protection concepts like spark gaps or varistors show no or merely a linear behavior against UWB pulses [2]. Only fast protection diodes with extremely small parasitic capacitances are capable against UWB signals. Different results of SPICE simulations and measurements show, that these diodes cause a reduction of the energy of the pulse. The limiting factor is the response time of the protection diode and the parasitic inductance of the feed line, which leads to a small residual energy in the transient response [3]. Another protection concept, which has been used in combination with nonlinear elements, is the use of interdigital bandpass filters in microstrip technique [4].

In addition there are high power microwave signals (HPM) with narrowband spectra, whereby the centre frequencies are in the GHz range. In a further investigation UWB protection circuits have been tested under CW conditions. For frequencies above 800 MHz the protection elements have only reacted in a linear way, because the parasitic effects and the limited response time impair the protective effect of these elements [5]. Even with linear filters high demands have to be made also in withstand voltage and in the high-frequency behavior. Therefore the protection of high frequency signal lines against HPM signals is very difficult.

In this contribution different protection concepts are considered under UWB and HPM conditions. SPICE models for nonlinear protection elements are simulated up to several GHz. As it is challenging to take all parasitic effects of the protection elements into account, the SPICE models and simulations are verified by improved measurements in time and frequency domain. The results are to facilitate the development and the prediction of the behavior of protection circuits in complex systems against any form of line-bounded HPEM disturbances.

References

1. K. Borgeest, "Optimierung und Simulation des transienten Ansprech- und Übertragungsverhaltens nichtlinearer Schutzschaltungen für HF-Systeme", PhD thesis, Hamburg University of Technology, Hamburg, 1998.
2. T. Weber, „Messverfahren und Schutzmaßnahmen für elektromagnetische Pulse im UWB - Bereich", PhD thesis, Hamburg University of Technology, VDI Verlag, Düsseldorf, 2004.
3. R. Krzikalla, J.L. ter Haseborg", SPICE Simulations of UWB pulse stressed protection elements against transient interferences", IEEE International EMC Symposium Chicago, August, 2005.
4. R. Krzikalla, J.L. ter Haseborg, "Practical design of protection circuits against extremely fast high power electromagnetics", EuroEM 2004, Magdeburg, Germany, July 2004.
5. F. Brauer, R. Krzikalla and J. L. ter Haseborg, "Investigation of the behaviour of UWB protection elements against HPM signals", Kleinheubacher Tagung 2007, Germany, September 2007.

HPEM - 07
High-Power Microwaves (Invited)

Oral Presentations

High Power Electromagnetic Pulse Protector and Microwave Limiter

Holger Karstensen[1], Frank Felbier[1], Uhland Goebel[1], Mischa Graeni[1], Roger Blake[1], Beat Herrmann[2]

[1]*HUBER+SUHNER AG, Pfäffikon, Switzerland*
[2]*HUBER+SUHNER AG, Herisau, Switzerland*

...
E-mail: holger.karstensen@hubersuhner.com

Wireless devices used in commercial or military applications are vulnerable to electrical interferences such as lightnings and High Power Electromagnetic pulses (HPEM), e.g. High Power Microwave (HPM) and Ultra Wide Band (UWB) pulses. Especially in electronic warfare systems the use of HPEM can be a threat for electronic systems, especially Radar. HPEM weapons usually transmit an extremely high energy microwave beam to the victim's radar antenna. When no or only insufficient protection is installed the received pulse can cause massive malfunction or even permanent damage of the receiver input stage making the enemy blind and an easy target for attack.

The goal of this work was to provide a full range protection unit for single- and multi-channel naval RF (ESM and communication) receivers. The application area of this protection device is of course not limited to this special case. As the requirements for the protection unit (very high power and very fast) cannot be met by a single element alone a combination of different limiter and protection elements had to be taken. Our concept was to combine gas discharge tube (GDT) and PIN limiter diode technology. GDTs are devices with high power ratings but slow response times. PIN diodes handle only medium power levels but are faster than GDTs. Therefore a multi-stage design has been chosen to combine a GDT stage at the input with following PIN diode stages. The approach is a 3-stage hybrid limiter surge protection unit as it is shown in the schematic in Fig. 1.

The first stage is a coaxial dual GDT construction that provides the standard EMP and HPM limiting function. It features low RF limiting speed but survives very high CW and peak power levels. The EMP feed-through voltage is very low. The second stage is a power PIN stage in grounded co-planar waveguide technology on AlN substrate with anti-parallel diodes providing a medium level limiting function. The third stage is the low level limiter consisting of fast low power PIN diodes.

Major requirements were a protection against peak power levels of 70dBm at the input within a frequency range of 30 – 3000MHz, a limiter threshold of < 23dBm, a low (< 1.5dB) insertion loss, and, in case of a multi-channel receiver, a channel phase tracking of ± 5° @ 3GHz.
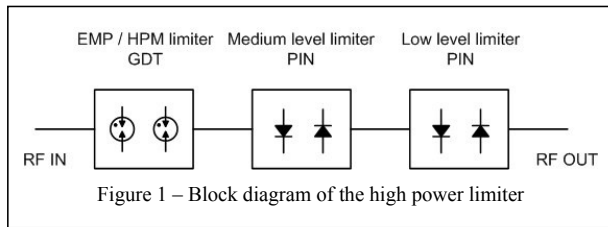
Figure 1 – Block diagram of the high power limiter

Figure 2 shows the measured transfer characteristics of the high power limiter. The frequency was 1.22GHz, the pulse width 10µs at a pulse rate of 500Hz. Up to input power levels of 67dBm (5kW, maximum available power), the output remained repeatable below 20dBm.

Details of the design including modeling results for the GDT and the PIN-stages will be given, the questions concerning the packaging of the components will be explained, the transient behaviour will be discussed, further measurement results and engineering samples will be shown.
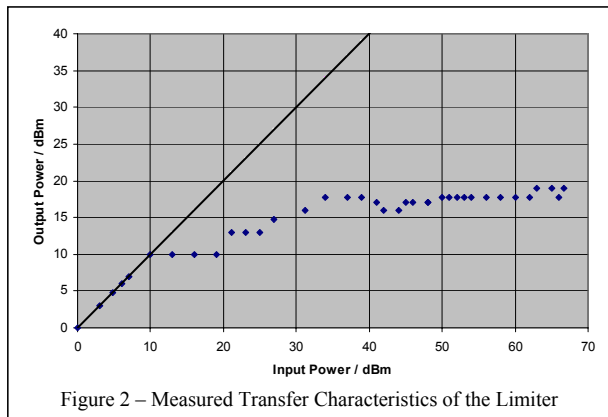
Figure 2 – Measured Transfer Characteristics of the Limiter

Stability of a TWT against Reflections Using the Large Signal Model

V. Kumar, V. Srivastava

[1]*Asia-Pacific Institute of Management, 3&4 Institutional Area, Jasola, Sarita Vihar, New Delhi – 110025, India*
[2]*Microwave Tubes Group, Central Electronics Engineering Research Institute, Pilani, Rajasthan – 333031,India*

Email: vk_aggarwal@rediffmail.com, vikas@asiapacific.edu

The travelling wave tube (TWT) is a high gain, broadband microwave amplifier, which is commonly used in a communication system. It works on the principle of continuous interaction between the electric field and the electron beam. A special type of RF circuit known as the slow - wave structure (SWS) is employed for this purpose. Helix is commonly used SWS for extremely wide-band applications. Stability of the traveling wave amplifier during the lifetime of operation is a highly critical aspect and becomes a highly dominant factor for use of the device in space applications. Factors responsible for the instability in the device include reflections, backward wave oscillations, band-edge oscillations and generation of higher order spurious modes. Reflections may be present in device due to any mismatch at the input or output ends in the tube and the presence of reflections can lead oscillations in the tube rendering the device unstable. Oscillations are produced in the presence of reflections when the following condition is satisfied. Where G is the gain, L is the circuit loss, ρ_L is the reflection coefficient at the output end and ρ_I is the reflection coefficient at the input

$$G - L - \rho_L - \rho_I > 0 \qquad (1)$$

end. In order to suppress the reflections and improve the stability of the device a TWT uses severs and attenuators (in the form of center loss and tip loss coatings). Also in order to improve the efficiency, a TWT is often designed in more than one section. Large signal analysis has been carried out for the design of C-band helix TWT to evaluate the effect of the using severs and attenuator coatings in a single and multi-section TWT. The following designs of the TWT have been analyzed using the large signal model:

(a) Single Section Tube
(b) Two Section Tube
(c) Two-section tube with sever loss
(d) Two-section tube without sever loss
(e) Input section with tip loss
(f) Output section with tip loss

SUNRAY-3D code has been used for the large signal analysis of helix TWT. The SUNRAY code employs 2.5-dimensional multi-signal analysis approach. In the 2.5-D large-signal analysis, the electron beam in one rf wavelength of the base frequency (the base wavelength) is represented by cylindrical charged discs, each one of which are sub-divided into up to four rings of equal cross-sectional area and axial thickness. The model is capable for the analysis of multiple input signals together with their higher order harmonics and inter-modulation products. The program analyses TWTs with arbitrary variation in the helix pitch and RF loss (including sever and tip loss) in the slow wave structure. Induced Backward voltage components and reflected voltage components due to mismatches at the terminations are also included in the program. The effect of the reflected voltage components caused by mismatches at ends of each section of the helix is also included. If the number of rings per disc is one, the 2.5D LSM is able to compute output power down to –250dBm for zero drive. The program can therefore be used to determine the conditions which provide finite output power for zero drive and it is supposed that the condition will lead to oscillation. The structures have been analyzed under different beam currents and the (a) Fundamental power (b) 2nd harmonic power (c) Gain (d) Phase have been calculated under different drive power levels. The obtained results have been discussed in context with the stability of the device.

Repetitively-Rated Plasma Relativistic Microwave Oscillator with Tunable Radiation Frequency in Every Pulse

**O. T. Loza[1], I. L. Bogdankevich[1], D. M. Grishin[2], A. V. Gunin[2], I. E. Ivanov[1], S. D. Korovin[2],
G. A. Mesyats[3], D. A. Pavlov[1], V. V. Rostov[2], P. S. Strelkov[1], D. K. Ulianov[1]**
[1] A. M. Prokhorov General Physics Institute RAS, Moscow, Russia
[2] Institute of High Current Electronics SB RAS, Tomsk, Russia
[3] Lebedev Phyisics Institute RAS, Moscow, Russia

loza@fpl.gpi.ru

First repetitively-rated microwave oscillator was created with the pulse power 10^8 W and the radiation frequency tunable electronically within two octaves from a pulse to a pulse according to any preset algorithm. The HPM oscillator is based on the Cherenkov interaction of relativistic electron beam with plasma preformed individually before every pulse in a sequence (bunch) with the rep-rate of 50 Hz. Such microwave oscillators are known as relativistic Cherenkov plasma masers [1] (CPM) which earlier were capable to generate only single HPM pulses. The present CPM was driven by an accelerator [2] with maximal electron energy of 550 keV, maximal current of 5 kA, pulse duration of 80 ns, maximal rep-rate of 50 Hz, the duration of a bunch of pulses up to 2 s, and the magnetic field up to 1.4 T. The geometry and parameters of the present CPM were close to those of [3] where the frequency was tuned from 4 to 28 GHz at 50-MW power level. This CPM differs substantially from [3] only by the output unit, which involves a mode converter so that the emitting horn radiates TE11 mode of a circular waveguide. The CPM used an electron beam with the current of 2 kA and electron energy of 500 keV, the beam power was 1 GW.

The microwave pulse power was registered by "hot-carrier" detectors. The total energy of a microwave pulse or a bunch of pulses was measured by a broadband calorimeter [4] which completely overlapped the emitting horn. Measurements of frequency intervals where radiation took place were carried out by a calorimetric spectrometer, comprising the above calorimeter and filters with cut-off frequencies of 5, 9, 12, 15 and 20 GHz. To distinguish the spectrum fine structure a heterodyne was used with the reference frequency varying from 8 to 12 GHz; the mixed signal was registered by an oscilloscope TDS 7404 with the band of 4 GHz.

The registered energies of HPM pulses throughout the frequency bands were from 1.5 to 2 J whereas the pulse duration did not exceed 30 to 40 ns, therefore, an average pulse energy was 50 MW. For a CPM the radiation frequency of a pulse is determined by the plasma density, namely, the frequency rises if the density is increased. With the lowest plasma density the radiation of bunches was registered by the calorimetric spectrometer only within the interval from 5 to 9 GHz, our earlier studies [5] showed that in this case the spectrum width is narrow. With the high plasma density all the HPM energy was registered above 12 GHz, where the spectrum width of any pulse is of the order of the mean frequency.

When the plasma density was changed from a pulse to a pulse in a bunch in turn from the lowest to the highest value then the radiation frequencies were registered by the calorimetric spectrometer in the bands below 9 GHz and above 12 GHz. This confirms the capability to "appoint" radiation frequencies individually for every pulse in a bunch.

Discreet changes of the radiation frequency with variations of plasma density were registered by heterodyne method in the band from 9 to 12 GHz, the interval between frequencies was ~ 0.5 GHz which corresponded to the changes of longitudinal modes of the oscillator [6].

References
1. M. V. Kuzelev, O. T.Loza, A. A. Rukhadze, et al., "Plasma Relativistic Microwave Electronics", Plasma Physics Reports, 2001, vol. 27, N. 8, pp. 669–691.
2. G. A Mesyats, S. D. Korovin, A. V. Gunin, et al., Laser and Particles Beams, 2003, v. 21, pp. 197-209.
3. P. S. Strelkov and D. K. Ulianov, "Emission Spectra of a Cherenkov Plasma Relativistic Maser", Plasma Physics Reports, 2000, v. 26, N. 4, pp. 303-307.
4. A. G. Shkvarunets, "A broadband microwave calorimeter of large cross section", Instruments and Experimental Techniques, 1996, v.39, N4, pp.535-538.
5. I. L. Bogdankevich, I. E. Ivanov, O. T. Loza, et al. "Narrow-band radiation regime of tunable relativistic Cherenkov plasma maser". AMEREM 2002 Symposium, 2-7 June 2002, Annapolis, Maryland, USA.
6. I. L. Bogdankevich, O. T.Loza, and D. A. Pavlov, "Frequency stability in plasma relativistic microwave oscillators", Technical Physics Letters, 2007, V. 33, N. 8, pp. 629–631.

New Developments in the Protection Against Intentional Electromagnetic Interference (IEMI) Since AMEREM 2006

W. A. Radasky, *Metatech Corporation, Goleta, California USA*
E-mail: wradasky@aol.com

Over the past two years since the last AMEREM Conference in Albuquerque, New Mexico in July 2006 there have been several conferences where significant information relating to the threat of Intentional Electromagnetic Interference (IEMI), the vulnerability of equipment and systems to IEMI, and the means to protect from the threat of IEMI have been presented.

In 2007 and in early 2008 there were several conferences in which the topic of IEMI was discussed. These included:
- EMC Europe Workshop in Paris, 14-15 June 2007
- International Conference on Electromagnetics in Advanced Applications in Torino, 17-21 September 2007
- 18th International Zurich Symposium on EMC in Munich, 24-28 September 2007
- 19th International Zurich Symposium on EMC in Singapore held jointly with the Asia-Pacific Symposium on EMC, 19-23 May 2008.

Of these four conferences, the EMC Europe Workshop and the EMC Zurich in Singapore Conference had the most significant participation from authors dealing with the subject of IEMI.

For EMC Europe, a special session on IEMI was held with 8 papers covering topics dealing with:
- Effects on communications and transportations systems
- IEMI scenarios dealing with railway systems
- IEMI impacts on computer networks
- IEMI detectors for safety and security
- The use of percolation theory to model the effects of IEMI on ad-hoc wireless networks

For EMC Zurich in Singapore a special session with 10 papers dealing with IEMI and HPEM covered:
- Propagation of UWB transients in cables
- Probabilistic analyses of the immunity of a data transmission channel when exposed to IEMI
- Pulse testing of network interface cables
- Response of electric railway systems to IEMI threats
- Study of the impact of IEMI on critical infrastructures
- Comparisons between HEMP and HPEM parameters
- Progress in the standardization of IEMI and HPEM

This review paper will discuss the highlights of these important papers with emphasis on how the state of the art regarding IEMI has been advanced.

After the review of these earlier papers, this EUROEM 2008 Special Session on IEMI will be introduced.

HPEM - 08
Intentional EMI #1 (Invited)

Oral Presentations

System of national standards on protection of the information against intentional electromagnetic influence

V.N. Bogdanov[1], Y.V. Parfenov[2], N.B. Safronov[1], L.L. Siniy[3], M.Y. Zhukovskij[1]

[1] *St.-Petersburg branch "Scientific and technological centre " Atlas ", St.-Petersburg, Russia*
[2] *"The incorporated institute of High Temperature of the Russian Academy of Science", Moscow, Russia*
[3]*JSC "Research Test Centre Electromagnetic Compatibility", Moscow, Russia*

E-mail: info@atlasnw.ru

Intentional electromagnetic influence [1] is the new factor of threats of information safety of crucial objects. This threat should be estimated as long-term, adequate protective measures demanding acceptance from the state.

Realization of threat of intentional electromagnetic influence is destruction, distortion and blocking of the information owing to an electromagnetic attack on basic elements of the vital objects:

–   the automated control systems of the core and auxiliary technological processes, and also processes of a safety of objects;

–   elements of systems of physical protection of objects - monitoring systems and management of access, systems of gathering and processing of the information, etc.;

–   systems of transfer of the information and communication of objects with federal controls.

With a view of revealing, counteraction and minimization of consequences of electromagnetic attacks the System of national standards on protection of the information from intentional electromagnetic influence is created in Russia.

The basic directions on creation of System are development of legal, normative, organizational and technical questions of protection of the information from electromagnetic attacks. Construction of System is based on principles of a priority of the preventive approach to a safety, adequacy of measures of protection, zonings of protection, a priority of application of means and the maximal integration with systems of protection of the information and physical protection of objects.

Per 2007 in basic standards (GOST R 50922 and GOST R 51275 [2-3]) are entered concepts and definitions «protection of the information against intentional electromagnetic influence ». GOST R 52863 «Protection of the information. The automated systems in the protected execution. Tests for stability to intentional electromagnetic influence. The general requirements» is prepared for introduction since July, 2008. The further development of System of national standards provides development of general provisions of the organization of works on protection of the information against intentional power electromagnetic influences, requirements to means of protection and means of detection of electromagnetic attacks.

In the report substantive provisions of the Russian standards on protection of the information against intentional electromagnetic influences are considered.

References
1.   IEC 61000-2-13: Electromagnetic compatibility (EMC) - Part 2-13: Environment – High-power electromagnetic (HPEM) environments – radiated and conducted.
2.   GOST R 50922-2007 Protection of the information. Terms and definitions.
3.   GOST R 51275-2007 Protection of the information. Objects of information. The factors influencing the information. General provisions.

HPEM - 08
Intentional EMI #1 (Invited)

Oral Presentations

Protection of Fixed Installations from Intentional Electromagnetic Interference (IEMI)

Richard Hoad[1]

[1] *QinetiQ Ltd., Cody Technology Park, Farnborough, Hampshire, UK, GU14 0LX*

...

E-mail: rhoad@qinetiq.com

All types of electronic infrastructures, systems, and equipment are potentially vulnerable to Intentional Electromagnetic Interference (IEMI) [1] and items which process sensitive data are potentially vulnerable to electronic eavesdropping. These electromagnetic threat forms are not new but are an emerging technical concern for information security because of the prevalence of electronics embedded into infrastructures.

Electronics within fixed information processing installations, such as data centres, office accommodation, data recovery/backup centres and telecommunications exchanges, may be particularly vulnerable especially where physical security is not adequate or well maintained. electromagnetic disruption can cause long term availability issues for processing facilities as a consequence of inadequate incident response planning. Electronic eavesdropping may cause breaches in confidentiality and integrity through untraceable losses of sensitive information.

Providing protection for each and every item of equipment can be costly. It is also difficult to justify costs where the magnitude of the risk posed by electromagnetic threats is not well understood. However, experience has shown that including electromagnetic protection as a requirement at the outset of a project is known to be cost effective.

This paper discusses assessment and detection methods which can be used to help to quantify the risk and assist with generating an appropriate response to an EM initiated incident. Other technical and non-technical means of providing EM protection for a fixed installation will also be discussed.

This paper references published guidance and practical experience, where available.

References
1. IEEE Transactions on Electromagnetic Compatibility, Volume 46, Number 3, August 2004, 'Special Issue on High-Power Electromagnetics (HPEM) and Intentional Electromagnetic Interference'.

HPEM - 08
Intentional EMI #1 (Invited)

Oral Presentations

Susceptibility of IT-Networks to HPM and UWB Threats

Frank Sabath[1], Berthold Römer[1]

[1] *Bundeswehr Research Institute for Protective Technologies and NBC-Protection, D-29623 Munster, Germany*

E-mail: FrankSabath@bwb.org

Studies indicate that while **H**igh **P**ower **E**lectro**m**agnetic (HPEM) sources are becoming more powerful, electronic equipment is becoming more susceptible to potential HPM attacks. With HPEM research being conducted worldwide, there is an increasing threat to NATO military equipment and critical infrastructure. Damaging terrorist attacks by low-cost, low-tech devices could disrupt or destroy the electronic circuitry of key nodes in an IT network, with potential catastrophic effects.

Due to its strong dependency on reliable network services, the implementation of the military doctrine of **n**etwork **c**entric **o**perations (NCO), or **n**etwork **e**nabled **c**apabilities (NEC), puts additional burden on electronic systems in IT infrastructure and communication equipment. NCO/NEC seek to translate an information advantage, enabled in part by information technology, into a competitive war fighting advantage through the robust networking of well informed geographically dispersed forces. The operative goal of NCO/NEC are to permit entities that are conducting military missions (commanding officers) to pull needed information from data bases and other repositories by employing modern information technology and sharing of information within operative forces. As NCO/NEC focuses so much on distributing and sharing of information, one has to be wary of the effect of false information entering the system, a major reduction of network performance of a total breakdown for a limited period. As those effects have the potential to erase the operational efficiency gained by NCO/NEC, the susceptibility of the communication network and especially of critical components of the IT-infrastructure is of vital interest.

One of the objectives of the research work performed at WIS has been investigation of the susceptibility of a complete military **C**ommand, **C**ontrol, **C**ommunication, **C**omputer and **I**ntelligence (C4I) network. This talk presents results of HPM and UWB investigations on a C4I system. The talk starts with results gained form exposure by the HPM simulator SUPRA [1]. The following second part focused on effects caused by UWB waveforms [2]. As a measure for the traffic through the C4I system the incoming traffic rate is depicted in figure 1. Other characteristic parameter, like outgoing traffic rate or retransmission rate, are in good correlation with the incoming traffic rate. Generally, all curves are showing the typical S-shaped progression. They differ in the location (repetition rate) and steepness of the falling edge, e.g. fading of system performance. In the closing third section general tendencies are derived by comparison of HPM results with those of the UWB investigations.

red: E=0,9 En, blue: E=0,6 En, green: E=0.48 En   red: E=1,6 En, blue: E=1,2 En, green: E=1.0 En
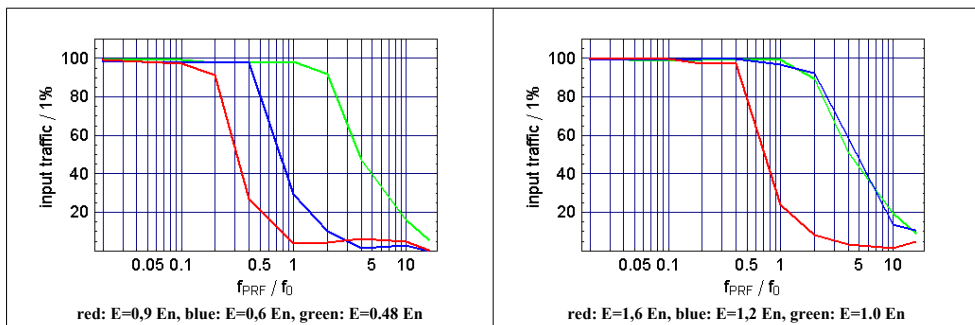
Fig. 1 – Input data traffic rate during exposure to vertical (left) and horizontal (right) polarized UWB field.

References
1. F. Sabath, M. Bäckström, B. Nordström, D. Sérafin, A. Kaiser, B. A. Kerr and D. Nitsch, Overview of Four European High-Power Microwave Narrow-Band Test Facilities, IEEE Trans. EMC, vol. 46 (3), pp. 329-334, August 2004.
2. W. D. Prather, C. E. Baum, R. J. Torres, F. Sabath and D. Nitsch, Survey of Worldwide Windband Capabilities , IEEE Trans. EMC, vol. 46 (3), pp. 335-344, August 2004

High Power Microwave effects on alarm systems and components

Jostein Godø[1], Odd H. Arnesen[2], Mats Bäckström[3], Brian A. Kerr[4], Ernst Krogager[5]

[1]*NorwegianDefence Estates Agency, Oslo,Norway*
[2]*Norwegian Defence Research Establishment, Kjeller,Norway*
[3]*Saab Communication, Linköping, Sweden*
[4]*QinetiQ, Malvern, UK*
[5]*Danish Defence Acquisition and Logistics Organization, Ballerup, Denmark*
...
E-mail: jostein.godo@forsvarsbygg.no

We present a compilation of results from a series of tests dealing with effects from HPM on alarm systems and components. Most important are joint Nordic (DK, FI, NO, SE) HPM susceptibility experiments using the Swedish Microwave Test Facility (MTF) and a Norwegian test series. The test objects entailed a multitude of technologies. Results from other objects in these tests have been presented elsewhere [1-5]. This presentation will focus on results from alarm and access control systems and components. Our investigation of electronic systems for alarm and access control is in an early phase and includes just a small number of systems and components. However it shows a great variety in robustness in alarm systems and components.

Tests have been done on some items on their own and on alarm centrals with detectors and card readers connected. The communication between the various components has in most systems been on wire, but some were wireless.

In some tests we have not been able to monitor the systems and components during radiation. In those cases we have checked the functions of the components and systems before and after radiation and looked for other signs of influence. For alarm centrals we have looked for malfunctions and error messages. We have seen PIR detectors which have been through destructive tests recovering to different states of function later on. PIR detectors which have been monitored during radiation have shown very different reactions to radiation.

References
1. T. Nilsson, O. Lunden, M. Bäckström,. HPM Susceptibility Measurements on WLAN and GPS Systems, EMC Europe Workshop, Rome, September 2005.
2. O.H. Arnesen et al., High Power Microwave Effects on Civilian Equipment, URSI General Assembly, New Delhi, October 2005.
3. O.H. Arnesen et al., IEMI against Modern Civillian electronic Technologies, EMC Zurich, Singapore 2006.
4. O.H. Arnesen et al., High Power Microwave Effects on Civilian Wireless Equipment, EMC Europe Workshop, Rome, September 2005.
5. O.H. Arnesen et al., IEMI susceptibility of data links in local area computer networks; wlan and fibre optics versus copper cable, EMC Europe Workshop 2007, Paris 2007.

HPEM - 08
Intentional EMI #1 (Invited)

Oral Presentations

Different Coupling Behavior of NEMP and UWB Pulses to PCB traces

S. Fisahn, H. Garbe

Institute for the Basics of Electrical Engineering and Measurement Science
Leibniz Universität Hannover, Hannover, Germany
E-mail: fisahn@ieee.org

UWB techniques are not only used in high speed communication systems, but also in the field of intentional electromagnetic interference (IEMI). While UWB pulses cover a large frequency range from 300 MHz to several GHz, an impact of modern electronic devices by these pulses could lead to malfunctions as well as destruction of the electronics. Investigations of the coupling effects of UWB pulses to complex electronic systems have shown, that increasing the system dimensions lead to an increased coupling efficiency [1]. This result seems to be universally applicable for all electronic systems, but susceptibility investigations on a generic microcontroller board (GMB) show surprisingly different results. Since measurement errors could be excluded, this effect has been investigated more detailed by additional measurements and numerical field calculations. The essential results of these investigations will be presented in this contribution.

As mentioned above, the susceptibility of a generic microcontroller board has been investigated. In contrast to the measurement setup in [1], the EUT was not placed in an open TEM waveguide, but on an open area test site (OATS). Thus, UWB pulses radiated by an impulse radiating antenna (IRA) illuminated the EUT. Furthermore, the whole circuitry was realized on a single PCB with signal tracks on the bottom layer and a ground plane on the back layer. In order to perform investigations with different coupling lengths (4, 6 and 8 cm), three versions of the GMB have been built up. The measurements point out, that the PCB with shortest coupling length is most sensitive, whereas the one with the longest coupling length showed the highest interference immunity. Additional measurements with another PCB that consists of only one signal track matched at both ends and a ground plane (according Fig .1) show similar results in time domain (TD). Further investigations performed with a numerical field calculation program deliver a possible answer for the unexpected results of the susceptibility tests. As shown in Fig. 2a, an increase of the coupling length effects higher voltages in the frequency range below 800 MHz. Above this frequency the coupling to the 6 cm track becomes larger than to the longest one, whereas the coupling to the shortest track is maximal in the frequency range from 1.3 to 3 GHz. Since UWB pulses cover a large frequency range up to several GHz, it becomes clear, that shorter coupling lengths do not increase the susceptibility of an electronic system against UWB in general. The time domain simulation results in Fig. 2b point out that the maximum voltage amplitude occurs in case of the shorted signal track. Since the signal track has been designed as a 50Ω-microstrip line that is terminated with its characteristic impedance at both ends, only small reflections appear. (In theory, there should not be any reflections, but the transition from the microstrip line to the resistor is not realized perfectly. Thus, this inhomogeneity causes reflections.) In practical use, signal tracks will be unmatched due to the input or output impedance of connected devices occasionally. Then, these signal tracks form line resonators that can be excited by transient field pulses. In summary it must been said the existence of substrate material and a ground plane has also an effect that must be taken in consideration, too.
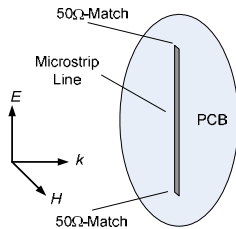
Fig. 1 - Simulation model
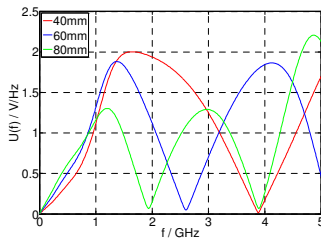
Fig. 2a – Calculated voltage in FD for different coupling lengths (at E=1kV/m)
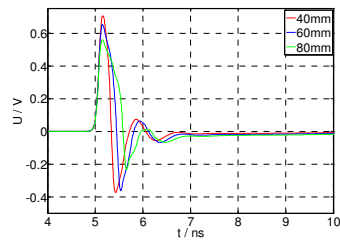
Fig. 2b – Calculated voltage in TD for different coupling lengths (at E=1kV/m)

References
1.　M. Camp, H. Garbe and F. Sabath, "Coupling of transient ultra wide band electromagnetic fields to complex electronic systems", Proceedings of the IEEE International Symposium on Electromagnetic Compatibility, vol. 2, pp.483-488, 2005.

Investigation of Stun Gun Effectiveness as Intentional Electromagnetic Interference (EMI) Sources

R. Tuttle, G. Baker, J. Rudmin

Institute for Infrastructure & Information Assurance, James Madison University, Harrisonburg, VA USA
BakerGH@JMU.edu

Determined malefactors have demonstrated the use of common systems as effective weapons against civilian infrastructures, e.g. commercial jetliners used as kinetic weapons and cell phones used to trigger explosive devices. This undergraduate research project investigated the possibility of using readily available stun gun devices for electro-magnetic interference with or disruption of personal computers. At present, the system effects of high power electromagnetic sources are well recognized by world scientific and military communities. Former CIA Director John Deutch has said that, "the electron is the ultimate precision-guided weapon" [1]. There has been much research on the deleterious effects of pulsed voltages and currents on electronic system operation. In the course of the investigation of nuclear electromagnetic pulse (EMP) effects on electronics during the Cold War period, it became evident that garden variety, unprotected electronics would malfunction, in some cases burn out, in the presence of externally induced pulsed currents in the milliampere range. EMP and high power microwave (HPM) research have demonstrated that these effects can have serious consequences in terms of interruption or termination of critical system operation. Although military systems have been the primary concern for EMP research, it is clear that the civilian infrastructure electronic communication, processing and control systems are at least as vulnerable to disruption from intense electromagnetic environments [2].

We conducted an experimental program using 50KV and 600KV hand-held stun guns to inject personal computers. The project involved fabrication of voltage divider circuits to measure stun gun output waveforms and direct-injection of personal computer ports to determine computer vulnerability to upset and damage. Results show that computers are highly susceptible to temporary and permanent debilitation from these devices. The results have implications for other types of data, communications, and control electronics. The project has been a successful learning experience on many aspects of high power electromagnetics and general research procedures including: familiarity with electromagnetic analysis techniques, experiment design, data gathering procedures and high power electromagnetic device safety practices.

References
1. Congressional Hearing, Intelligence and Security, Chairman Jim Saxton, Joint Economic Committee, June 17, 1997.
2. M. Backstrom et al., Preliminary Study Regarding the Resistance of Critical Societal Systems to High Intensity Electromagnetic Radiation, Royal Swedish Defense Research Agency, Report FOA-R-97-00538-612-SE, August 1997.

HPEM - 08
Intentional EMI #1 (Invited)

Oral Presentations

Evaluation of Pulse Testing of Network Interface Cards

E. B. Savage, W. A. Radasky, K. S. Smith, M. J. Madrid

Metatech Corporation, Goleta, California, USA
E-mail: savagee@cox.net

Ethernet networks are an important part of many modem systems, and a significant factor to be considered in any EM susceptibility assessment. Generally the coupling of threatening EM fields (such as ultrawideband) to cables can be calculated, at least in an idealized case, but it is more difficult to calculate the effects on the system of such coupled signals - generally laboratory measurements must be used instead. Because they are so prevalent, an important system to consider is the Ethernet interface for PCs – "NIC" cards (Network Interface Cards). It might be estimated that cards should be able to withstand pulses of at least a kilovolt, corresponding to the lower levels of pulses for international standards[1], and those standards provide guidelines for making pulse vulnerability tests. Here we will discuss how pulse susceptibility tests may be performed, and present some useful lessons we have learned from performing such tests.

The basic test approach is simple. A network is set up – usually two PC's networked together. An electric pulse is driven on the network cable, and any resulting adverse effect, upset or damage, is noted. There are two common ways to introduce the test pulse into the network: capacitive coupling (Figure 1), which uses field coupling to insert the test pulse into the system, and direct injection (Figure 2), with the pulser hardwired into the NIC. Below we introduce some issues concerning such tests:

Capacitive Coupling: This approach has advantages, such as allowing normal communication during the pulsing, but the drive level is about half that of direct drive. Often the direct injection approach gives very similar upset results, but without this loss, and so, essentially, direct drive has twice the upper drive level.

Effect Levels 0,1,2,3,4: Numbers are often used to denote system effects, for example, from 0 = no effect to 4 = permanent damage. It may be too simplistic. Usually upset levels are distinguished by the recovery needed, such as the file transfer needs to be re-started, or the PC needs a soft or hard reboot. However, for NIC, another recovery option is the need to unplug the PC before re-booting. Also we might want to distinguish between relatively benign communication corruptions and Windows upsets – random Windows commands sometimes occurred during the tests. Damage should not be a single level. The highest level should be complete permanent loss of the NIC, but it was found that often the "permanent damage" was to non-essential components on the NIC cards (interestingly, these components are thought to be there for EMC/EMI emission compliance – the cards may no longer meet specs, but they still work).

Retained heat: A shot that produces device breakdown can heat up the device (in damage cases, this is seen in "burnt" parts), and it should be allowed to cool before the next shot. If not, breakdown will be even easier, and a damage level may be found that is inaccurately too low.

Do a full postmortem: A NIC is declared dead if it no longer works, even after doing a full power-down re-boot. However, NIC cards still get some power even when the PC is off, so the AC power should be unplugged first. Also, because of retained heat, a re-boot should be tried again after a very long cool-down period.
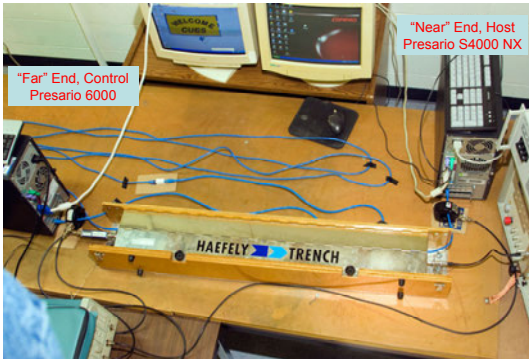
Fig. 1 – Capacitive trench testing.

Fig. 2 – Direct injection testing.

References

1.   IEC 61000-4: Electromagnetic compatibility (EMC) - Part 4: Testing and measurement technique*s.*

Infrared temperature and electrical power measurements in comparison with time-domain SPICE coupling models for bridgewire EED circuits at pulsed, wideband electromagnetic irradiation

F. Sonnemann

Diehl BGT Defence GmbH & Co. KG, D-90552 Roethenbach a.d. Pegnitz, Germany

E-mail: frank.sonnemann@diehl-bgt-defence.de

The susceptibility of EED against CW irradiation can be determined by observing the steady state temperature rise of the heating element, which in turn can be related to an equivalent DC current. According to the German VG 95379/20 and depending on the class of hazardousness this equivalent DC current must keep the safety margin which is defined either 7 dB / 17 dB off the DC-No-Fire current. However, at pulsed irradiation no safety margins are currently defined, because no established measurement technique to determine induced energy or peak temperature rise is available.

An (inert) EED test system for HPEM irradiation tests will be presented, which allows three different methods to determine the peak temperature of the inert EED device during HPEM irradiation. The first method uses an infrared quantum detector with a rise time of about 10 ns for direct observation of the heating element. The peak temperature is calculated from the measured emission (detector voltage) by solving the detector equation after the unknown emitter temperature. The result will be compared with a direct current measurement in combination with a bridgewire heating model based on a partial differential equation which includes the temperature dependence of the specific electrical resistivity, heat capacity and heat conductivity. The last method uses a power measurement in combination with the well known Rosenthal temperature model, which is often used for bridgewire EED. The peak temperature calculated with the proposed methods differs of about ± 20 %, which is due to the inaccuracy of the bridgewire geometry (length, diameter), the model parameters and measurement uncertainties.

The presentation describes the EED measurement set-up in a HPEM environment, the methods to determine the bridgewire peak temperature and discusses first results achieved from the DS effects testing which are compared with time-domain SPICE coupling models incorporating common- and differential mode coupling.

HPEM - 09
Susceptibility #2

Oral Presentations

Investigations and Simulation of Electromagnetic Behavior in 3D Hybrid Electronic Devices for Embedded Applications

J.M. Dienot [1] , E. Batista[2], L. Bouchelouk[2]
[1]University Institute of Technology, Tarbes, France
[2]Power Electronics Associated Research Laboratory, Séméac, France

E-mail: jm.dienot@iut-tarbes.fr

Works presented focus on investigations and simulations aspects to identify and reproduce new electromagnetic disturbances cases at device level. These behaviors can occur because of the impact and non-stop progress of integration of electronic hybrid systems, using mixed components and integrated circuits, especially for embedded and transport applications. The volume of these circuits trend to reduce, and coupling ways for example between on-PCB numerical PWM pattern and power converter chip (MOSPower, IGBT) becomes more and more problematic[1]. A new complete review of conventional EMC emissions or susceptibility behavior, applied on the electronics parts of an hybrid technology chip system is proposed. Starting with well-know established techniques of emission and immunity characterizations on electronic devices[2], new electromagnetic measurements have been developed, excited by a special directive warming set-up added to near-field scan table and TEM cell configuration[3]. Different canonical cases have been tested, using elementary and complex electronic configurations : copper wire tracks and couplings, digital programmable device, integrated circuits, power switches… The complete review of experimental results confirm the real impact of temperature on conventional emission and susceptibility behavior : near-field noise responses are very sensitive to increasing thermal environment(See fig.1). Phenomena is reproducible, and can show about ten dB of real shift on frequency repartition EM noise energy. Coupling factors and thresholds susceptibility levels have also a different behavior to hot heating. Modeling works, conducted to reproduce the effect of external temperature on electromagnetic emission and susceptibility, point on electrical mobility and technological parameters of chips and devices which are very sensitive to the temperature[4]. So, the electromagnetic responses of the PCB architecture is mainly driven by active device. But the electromagnetic coupling factors, inductive or capacitive types, are also identified as actors of these new electromagnetic coupling cases[5][6]. This global multi-physics approach wants to demonstrate and give confirmation of real impact of external temperature to complete library models works dedicated to EMC, and to realize efficiently future EMC investigations and previsions for electronics integrated chips with embedded hybrid technology.
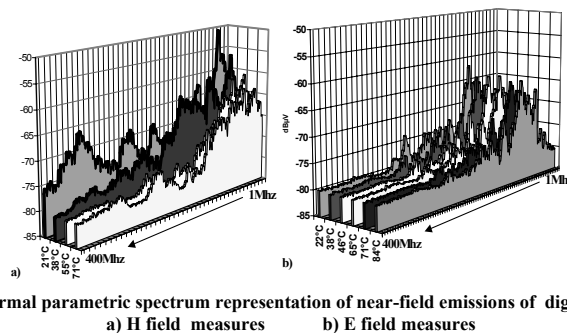
Fig. 1 - New 3D thermal parametric spectrum representation of near-field emissions of digital PWM PLA chips
a) H field measures   b) E field measures

References
1.   S. Weber, S. Guttowski, E. Hoene, W. John and H. Reichl, " EMI couplings from automotive traction systems", In Proc. IEEE EMC-S, , pp. 591-594 , May 2003.
2.   K.P. Slattery, J. Neal, and W. Cui, "Near-field measurements of VLSI devices", IEEE Transactions on Electromagnetic Compatibility, vol.41, n°4, pp 374-384, November 1999.
3.   J.M. Dienot, G. Lourdel, "Experimental study of thermal influence on EMC emissions of digital circuit on PCB", In Proc. of EMC Zurich'05, pp. 299-302, February 2005.
4.   E. Hoene, A. Lissner, S. Weber, S. Guttowski, W. John and H. Reichl, "Simulating electromagnetic interactions in high power density inverters", In Proc. IEEE 36th PESC Conf., Recife, pp. 1665-1670, 2005.
5.   J.M.Dienot, "Characterization and simulation of digital device electromagnetic noise under non-ambient temperature conditions.", Electronics Letters Volume 43, Issue 20, pp 1073-1074, September, 2007.
6.   P.S. Nelakanta, Handbook of Electromagnetic materials, monolithic and composite versions and their applications, Isbn 0-8493-2555-5, CRC press Ed., 1995.

HPEM - 09
Susceptibility #2

Oral Presentations

Measurement of EM Field inside a Cruising Aircraft
- Potential Problems for the Use of Mobile Phones on Board -

A. Kohmura[1], J. Picard[2], N. Yonemoto[1] and K. Yamamoto[1]

[1]*Electronic Navigation Research Institute(ENRI) , Tokyo, Japan*
[2]*Ecole Nationale de l'Aviation Civile, Toulouse, France*

E-mail: kohmura@enri.go.jp

It is well known that electromagnetic (EM) emissions from Portable Electronic Devices (PEDs) carried on board aircrafts can interfere with avionics systems. Use of PEDs including mobile phones is therefore limited in aircrafts. On the other hand, commercial services offering passengers to use GSM (Global System for Mobile Communications) mobile phones on aircrafts are set to start soon in the world. In this system, transmission power of these GSM phones in the cabin is controlled to be small by placing low power base stations (Pico-cells) that link the phones to terrestrial communications via satellites.

However, there are safety concerns about this service in Japan and countries that use transmission methods other than the GSM. PDC (Personal Digital Cellular) and CDMA (Code Division Multiple Access) are used with 800 MHz, 1500 MHz and 2000 MHz bands in Japan. Some handsets sold in Japan are also compatible with GSM for international roaming purpose. In these circumstances, when a passenger turns on his/her non-GSM mobile phone intentionally or unintentionally, it may radiate very strong signal because the phone tries to maintain its link with distant ground station, which can interfere with aircraft system. Though some countermeasures using jamming systems are planned, it is difficult to comply with the emission regulation for avionics equipments [1].

The purpose of this report is to investigate how much non-GSM transmission from the ground base stations reaches inside a cruising aircraft. The EM field in the above three bands is measured using a wideband antenna connected to a spectrum analyzer on a cruising Beachcraft Model 99 aircraft. The EM field over Yamagata airport is recorded at altitudes from 1500 feet to 7000 feet with a 500 feet interval in geographically identical positions.

Figure 1 describes the maximum observed E fields between 860 MHz and 887 MHz at each altitude. The band is allocated only for ground base stations. The figure shows that 56 to 64 dBµV/m has been observed inside the aircraft, and the same tendency is found also in other bands allocated for ground stations. The EM field at higher altitudes where general commercial jet planes cruise, 30000 – 40000 feet, is expected to be about 30 dBµV/m according to the free-space path loss calculation. Meanwhile, the lower limit of power reception of a typical CDMA phone is around 26 dBµV/m (-110 dBm) at 870 MHz. It means that the communication can be established between ground base stations and non-GSM phones on board even at cruising altitudes.

The potential problems of installing mobile phone systems on board have been discussed through the EM field measurement in the air. In order to install this Pico-cell system in non-GSM countries, mechanisms must be considered to cut direct links from non-GSM phones to ground stations such as shielding techniques for aircrafts. Finally, the flight safety when the system is installed in non-GSM countries can be ensured.

HPEM - 09
Susceptibility #2

Oral Presentations
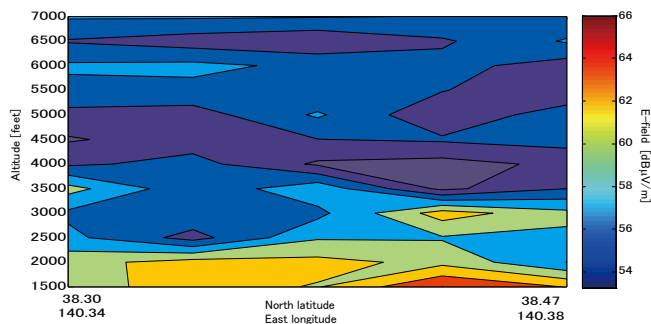
Fig. 1 – Maximum observed E-field from base stations in 800 MHz band over Yamagata airport

References
1. RTCA (Radio Technical Commission for Avionics) Document 160F Section 21 Category M, 2007 Dec.

Wunsch-Bell Criterial Dependence for Si and GaAs Schottky-Barrier Field-Effect Transistors

G.I. Churyumov[1], M.V. Glumova[2], V.V. Starostenko[2], V.Yr.Tereshenko[2], D.A. Unzhakov[2], S.A. Zuev[2]

[1]*Kharkov National University of Radio Electronics, Kharkov, Ukraine*
[2]*Taurida National Vernadsky University, Simferopol', Ukraine*

E-mail: g.churyumov@ieee.org

The reacting of powerful pulsed electromagnetic field with semiconductor devices (transistors, microcircuits) adversely affects their operation modes and, in some instances, it can lead to the complete loss of control by these devices. Traditionally, for determining resistance of the semiconductors devices to the external electromagnetic radiation the Wunsch-Bell criterion is used. However, for some devices this criterion is not executed, especially, with decreasing geometry of active region of these devices.

In present paper a numerical mathematical model of the Si and GaAs Schottky-barrier field-effect transistor is considered. This model permits current and thermal modes of these devices to be investigated when reacting of the powerful electromagnetic pulses takes place. In this case changing characteristics of semiconducting materials with increasing temperature is taken into account. Using of the mathematical model allows dynamics of the electrothermal processes to be studied including an outgrowth of avalanche process, forming current "cord", thermal breakdown of the devices and, etc.

The computer modeling results showed that in studies of the external reacting of the electromagnetic pulses with semiconductor devices as criterion of the resistance it is necessary to take into account the volume density of power instead its surface density.

Audit and analysis of the electromagnetic field exposure levels in the vicinity of telecommunication network base stations

C. P. Nicolaou[1,3], G. K. Demetriou[2], G. C. Makrides[1], A. P. Papadakis[3], P. A. Razis[3], G. E. Georghiou[1]

[1]*Department of Electrical and Computer Enginneering , University of Cyprus, Nicosia, Cyprus*
[2]*Department of Network Development, Radio Access Networks ,Cyprus Telecommunication Authority, Nicosia, Cyprus*
[3]*Department of Physics, University of Cyprus, Nicosia, Cyprus*
E-mail: ncharal@ucy .ac.cy

The growth of mobile telecommunications, in an attempt to satisfy the needs of modern society for mobile communications, wireless internet browsing and transferring of real time voice and video, has become an everyday life necessity, which is integrated to the lifestyle of people. In order to succeed in meeting this requirement, telecommunication companies are increasingly utilising a higher range of frequencies, so as to create sufficient numbers of broadcasting speech and data channels. On the other hand, the application of higher frequencies for communication purposes has the disadvantage of decreasing the coverage area, which results in the attenuation of the transmitted signal strength, especially in urban areas, where the presence of building structures is frequent. A practical solution to provide companies with greater coverage area and better quality of the provided services is to use multiple cellular base stations near houses. This unavoidably means that the cellular stations, which are sources of predominantly electromagnetic fields, are in close proximity to residences and offices, where people spend most of their time. As a result, there is great public concern and anxiety regarding the possible health effects caused by continuous long term exposure to electromagnetic fields. With this in mind, the current work began in an attempt to provide better insight into the electromagnetic field exposure levels near telecommunication base stations. In this work, measurements have been conducted in the whole of the telecommunication network in the vicinity of base stations for one of the two major mobile telecommunication providers in Cyprus. The obtained results are compared with the ICNIRP guidelines and a general picture of the cellular base emissions in the entire network is hence made possible which has thrown light into the possible limitations and problems within the network.

HPEM - 10 Measurements Techniques #1

Oral Presentations

Real-Time Monitoring System in Millimeter and Optical Ranges

Y. Savenko [1], V. Vodotovka [2] and F. Repa [1]

[1] *National Technical University of Ukraine "Kyiv Polytechnic Institute", Kyiv, Ukraine*
[2] *Kyiv National University of Technology and Design, Kyiv, Ukraine*

E-mail: yaroslav_savenko@ieee.org

The paper presents the results on investigation of real-time monitoring system in millimeter and optical ranges. It has been developed an original real-time monitoring system. This system investigates properties of biological objects in millimeter and optical range both in active and passive mode of scanning. It has been also used for remote sensing different biological object and geoscience task as well. In addition to the monitoring there have been investigated treatment technologies in millimeter and optical ranges are provided as correction of own properties of object as for medical, ecological and agricultural purposes.

It had been investigated the using of real-time monitoring system for environment monitoring in particular a growth and biophysical properties of crops. It had been chosen as a model for agricultural field rectangular with sides a and b. Inside it is a regular structure of crop's strips with period T_I, width of strip d and height of strip h At the development of scanning model there were defined tasks for determine a growth of crops and determine their biophysical properties in real-time on all agricultural field. Scanning model consists of model of spatial scanning of field; model of reflecting of millimeter and laser radiation from binary heterogeneity as soil-crop; model of multiangular scattering on crop and especially on their components and model of biological object self radiation.

Proposed real-time monitoring system consists of subsystem of multiangular scanning, subsystem of reflected or/and self radiation scanning and subsystem of hardware-software processing scanned data from agricultural field of crops

Subsystem of hardware-software scanned data processing consists of multichannel correlation receiver, receiver to PC junction and program of analyzing and indication of scanning results. Main part of hardware system is multichannel correlation receiver, where it is operated correlation comparison of test signals and signals obtained during scanning process. Test signals are obtained previously for certain conditions of crops (kind of crop, its age, contained components and parameters of planting), and they are saved as special test data.

There were also analyzed possible opportunities for realization of monitoring system on base of proposed system set up on aircraft. In this case it had been investigated specification of aircraft (such as altitude, velocity and carrying capacity), features of airborne set up of subsystems and flying route for crop monitoring on whole field.

Results of simulation and experimental researches show that system for real-time monitoring of growth and biophysical properties of crops can be used for industrial development and producing the airborne system in extended range (visible, IR and millimeter) for agricultural needs. It would be very useful to produce an airborne monitoring system that could be set up and used on small aircraft by farmers, for example. Results of investigations could be also used for creating program and system for monitoring other kind of objects scanned not only in optical range. In some cases it could be possible to obtain data about growth of crop from mapped satellite data. But this data have more integral characteristics and have less resolution than airborne monitoring system.

Dual Reverberation Chambers for High-Dynamic Range Shielding Effectiveness Measurements

J. Schipper[1], M. Melenhorst[1], F.B.J. Leferink[1,2]
[1]*THALES Netherlands, Hengelo, The Netherlands*
[2]*University of Twente, Enschede, the Netherlands*
E-mail: leferink@ieee.org

We describe a test setup using <u>two</u> reverberation chambers with a common wall. In the common wall a device under test (DUT) can be mounted. One of the rooms is a conventional chamber with a stirrer. The other room is a Vibrating Intrinsic Reverberation Chamber (VIRC), where the walls are used to stir the fields, such as shown in Figure 1. The walls are moved by means of a simple motor with a crankshaft and elastic strings. Stirring the field by means of a mode stirrer is also possible.
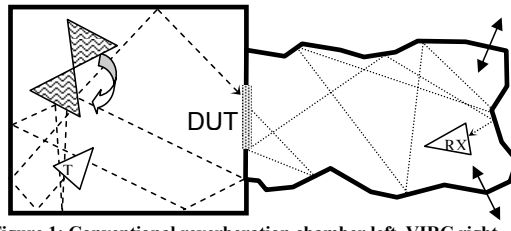
Figure 1: Conventional reverberation chamber left, VIRC right

An earlier setup was with one reverberation chamber and a simple conventional chamber, as described in [1]. Because a fire destroyed the laboratory, new chambers were built, and now two reverberation chambers, one of them being a VIRC, was used. The main advantage of a reverberation chamber is the high field strength while using only moderate power. On the reverse side, any small signal which enters the reverberation chamber through the DUT is intensified. As such, the dynamic range of the test setup is increased. Another advantage of using reverberation chambers is the high repeatability: In a conventional shielding effectiveness test the DUT creates lobes at high frequencies, such that static high and low field strength areas are fixed over the volume of the test setup. But in a reverberation chamber these lobes are dynamically distributed.

In [2] a nested reverberation chamber test procedure has been described. This method needs a much higher frequency for proper operation due to the limited size of the test fixture, compared to the method as described in this paper. The procedure we applied is described, and some test results are presented. A picture of the test setup is shown below.

Figure 2: Picture of the test setup

The test setup has been used to measure the shielding effectiveness of many samples, including
- Composite panels (Glass Reinforced Plastics) with woven metallic textile, carbon and metal fibres, paint etc.
- Various wire mesh and metalized fabrics
- Panels with multiple holes, honeycomb and joints
- and various other experiments

The test setup will be described and several test results will be shown.

References
1. Frank B.J. Leferink, Hans Bergsma, Wim C. van Etten, Shielding Effectiveness Measurements using a Reverberation Chamber, EMC-Zurich 2006
2. IEC 61000-4-21, Electromagnetic compatibility (EMC) - Part 4-21: Testing and measurement techniques - Reverberation chamber test methods, 2003

HPEM - 10
Measurements Techniques #1

Oral Presentations

High Power Millimetre Wave Pulse Sensor

Ž. Kancleris, M. Dagys, R. Simniškis and V. Tamošiūnas

Microwave laboratory, Semiconductor Physics Institute, A. Goštauto 11, Vilnius, Lithuania

E-mail: kancleris@pfi.lt

High power microwave (HPM) pulse generation techniques progressed rapidly towards higher frequencies in recent years [1]. This requires new sensors being able to measure HPM pulses in millimetre wave region. One of the possible solutions could be a resistive sensor (RS), the performance of which is based on electron heating effect in semiconductors. A sensing element of the RS is usually placed in the waveguide where HPM pulses propagate. Electric field of the pulse heats electrons in the sensing element, its resistance increases and by measuring this resistance change the power of the HPM pulse in the waveguide is determined. Experience gained using the RS in centimetre wave region highlighted their advantages over the diode. The RS measures HPM pulses directly, is resistant to large power overloads and demonstrates very good long-term stability. It can resolve nanosecond duration HPM pulses and can produce an output signal of the order of a few tens of volts without any amplification circuit. Since a stray pickup and electromagnetic interference are typical to the environment of HPM sources, the last feature of the RS is very useful performing measurements at such conditions. Unfortunately the most successful concept of the waveguide RS with a diaphragm [2] could not being directly downscaled to the millimetre wave region due to small dimensions of the waveguide.

In our previous paper [3] we proposed a new concept of the RS that is suitable for the millimetre wave region in 78-118 GHz range (W-band, waveguide window 2.4×1.2 mm^2). A three-dimensional finite difference time domain method has been applied to determine electrophysical parameters of the sensor providing nearly constant sensitivity of the RS in the waveguides frequency range. Here we present a practical realization of the ideas proposed in [3].

The proposed RS consists of two separate samples with ohmic contacts mounted in a close proximity to each other in the centre of the wide wall of the waveguide. Their upper contacts are shorted with a metal foil. The lower contact of one of the sensor is grounded while the other one is isolated. It is used for the RS feeding and the output signal measurement. Thus, the sensing elements are connected in series in respect to the DC circuit but in parallel in respect to the millimetre wave electric field. Characteristic dimensions of sensing elements (height h, width d and length l) and the specific resistance ρ of the sensing element are the parameters those have been varied to get the optimal frequency response of the RS [3]. Two groups of the RS with optimal dimensions $h \times d \times l = 0.1 \times 0.15 \times 0.6$ mm^3 made from $\rho = 1$ $\Omega \cdot$cm (first group) and 2 $\Omega \cdot$cm (second group) n-Si have been manufactured and tested.

It was observed that the reflection from the RS is independent of the specific resistance of the sensing elements and the VSWR < 1.25 within the frequency range. Measured insertion loss of the RS is practically independent of frequency. It is about 0.8 dB for both groups of the RS. Measurements of the sensitivity dependence on frequency have revealed that the largest sensitivity variation for the first group RS is roughly ±15% and ±8% for the second one in the frequency range 78-118 GHz. When the air gap between the samples and the finite thickness of the upper metal contact are taken into account, the reasonable agreement between measured and calculated sensitivity values has been obtained. The average sensitivity of the second group is almost 3 times larger than that of the first one. The manufactured RS have been tested using magnetron producing roughly 3 kW pulse power at 94 GHz. A pulsed current source is used for the RS feeding. It produces roughly 120 µs DC current pulse. The amplitude of current is adjusted to get 10 V DC voltage drop on the sensing elements. Using such DC supply, the output signal of the second group RS at a maximum pulse power exceeds 2 V whereas for the RS of the first group it is roughly 1.5 V.

The carried out investigations demonstrate that the manufactured sensors can be effectively used for the measurement of high power millimetre wave pulses.

References
1. M. Thumm, "High power gyro-devices for plasma heating and other applications", Int. J. Infrared Millim. Waves, vol. 26, p. 483, 2005.
2. M. Dagys, Ž. Kancleris, R. Simniškis, E. Schamiloglu and F. J. Agee, "The resistive sensor: a device for high-power microwave pulsed measurements, IEEE Antennas Propag. Mag., vol. 43, p. 64, Oct. 2001.
3. Ž. Kancleris, V. Tamošiūnas, M. Dagys, R. Simniškis, F. J. Agee, "Interaction of a semiconductor sample partly filling a waveguide's window with millimetre wave radiation" IEE Proc.-Microwaves Anten. Propag., vol. 152, p. 240, 2005.

Relativistic Cherenkov Microwave Oscillator without a Guiding Magnetic Field

E. M. Totmeninov, A. I. Klimov, V. V. Rostov

Institute of High Current Electronics, Siberian Branch, Russian Academy of Sciences
2/3 Akademichesky Ave., Tomsk 634055, Russia
E-mail: totm@lfe.hcei.tsc.ru

Research and development of relativistic microwave generators without an external magnetic field are of interest for some applications. Examples of such devices are, vircator [1] and MILO (Magnetically Insulated Transmission Line Oscillator) [2].

Another type of microwave device without an external magnetic field, the relativistic cherenkov microwave generator, is studied in this work. In this generator, a solid cylindrical relativistic electron beam is formed in a planar diode and propagates through a short ($L \approx 3\lambda$, λ – wavelength) resonant slow wave system without external magnetic field. Transportation of the electron beam in the drift tube uses the azimuthal component of the self magnetic field, which prevents the beam divergence under the action of the self space charge. Slowing down of the traveling wave to the light speed enables efficient interaction of the wave with the solid cylindrical relativistic electron beam. In this case the distribution of the electric field longitudinal component of the fundamental harmonic over the slow wave system cross-section is nearly uniform. Preliminary modulation of the electron beam at the entrance of the slow wave system provides the condition for efficient energy exchange at the phase velocity of synchronous wave a bit higher than the electron velocity. Well known PIC code KARAT [3] was used for the simulation. High simulated efficiency (30 – 40%) of the device was realized due to a double-humped shape of "cold" longitudinal distribution of z-component of RF electric field. Earlier, the possibility of generation at the condition of negative initial kinematic mismatch was shown in the theory for the relativistic monotron. However, this regime demonstrated a high start current.

In the experiment the solid cylindrical relativistic electron beam was formed in the planar diode that included the anode mesh and the metal-dielectric multi-blade cathode that was placed inside a focusing stainless steel electrode. The TM_{01} wave was generated with an efficiency of 10 ± 2 % (taking into account the total vacuum diode current) at a peak power of 1.3 ± 0.3 GW and the oscillation frequency of 4.03 GHz. The energy of the microwave pulse measured using aperture calorimeter was 13 ± 1 J. That corresponds to the power of 1.2 ± 0.1 GW. For some pulses the peak microwave power reached 1.5 ± 0.3 GW with 12 ± 2 % efficiency. The microwave pulse width (FWHM) was about 11 ns. The transmitted current measured just behind the anode mesh was ≈ 50% of the total diode current. Thus, the efficiency of the device was about 20 % taking into account the transmitted current. The difference between the efficiencies obtained in the numerical simulation and in the experiment was probably due to parasitic electron emission from the focusing electrode and changing the diode impedance during the driving pulse. May be additional optimization of slow wave system is needed.

References
1. S. A. Kitsanov, A. I. Klimov, S. D. Korovin, et al., "A vircator with electron beam premodulation based on high-current repetitively pulsed accelerator," IEEE Trans. Plasma. Sci., vol. 30, pp. 274-285, Feb. 2002.
2. M. D. Haworth, G. Baca, James N. Benford, et al., "Significant Pulse-Lengthening in a Multigigawatt Magnetically Insulated Transmission Line Oscillator," IEEE Trans. Plasma. Sci. Vol. 26. No. 3. June 1998. P. 312-319.
3. V. P. Tarakanov, "User's Manual for Code KARAT", Springfield: BRA, 1992.

HPEM - 11
High-Power Microwaves

Oral Presentations

One Method for Chiral and Metamaterial Strip Lines Determination

N. B. Raicevic[1] , S. S. Ilic[2]

[1,2]*Faculty of Electronic Engineering, Department of Electromagnetics, Nis, Serbia*
...
E-mail: nraicko@elfak.ni.ac.yu

The media where electric displacement and magnetic induction simultaneously depend on electric field and on magnetic field are biisotropic, or chiral and metamaterial media for special cases. The constitutive relations for this medium are:

$$\vec{D} = \varepsilon\vec{E} + \chi\vec{H} \; ; \; \vec{B} = \chi\vec{E} + \mu\vec{H} \; . \tag{1}$$

The aim of this paper is to investigate the influence of the strip conductor placed in infinite chiral media (when ratio $\chi/\sqrt{\varepsilon\mu} > 1$ this medium is metamaterial medium) between two grounded plate's position (Fig. 1) on effective dielectric permittivity and permeability, characteristic impedance of the system, and electric and magnetic field distribution. For numerical calculations, the conducting strips can be divided on many little parts (2N), replaced by infinite cylindrical conductors [1, 2]. Infinite linear electrodes are used as equivalent electrodes (EE). After the system of linear equations is solved, the unknown EE line charges, q_n', can be determined. Equivalent electrodes method (EEM) as very simple, powerful and accurate procedure is used.
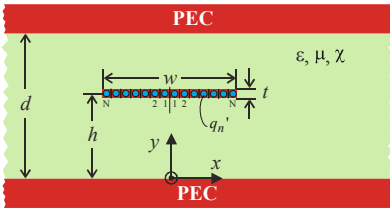
Fig. 1 – Strip line with chiral medium ε, μ, χ.
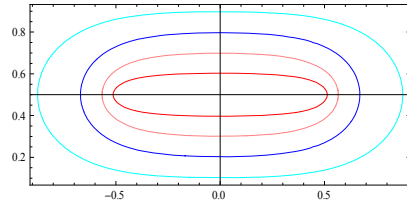
Fig. 2 – Equipotential curves.

It is necessary to know Green's function of uniform line charge placed in chiral dielectric medium, between two infinite perfectly conducting grounded plates. This function is determined in the closed form by using function of complex variable and conformal mapping. Also, TEM theoretical analysis of the strip line is used. The obtained numerical results for chiral media are compared with corresponding results determined by FEM.

Table 1 – Some electromagnetic values versus ratio $\frac{w}{d}$, **for** $w = 0.5d$, $\frac{t}{W} = 0.01$.

$\frac{w}{d}$	Electric Field V/m	Magnetic Field mA/m	$Z_c(\Omega)$	$C'(pF)$	$L'(\mu H)$
0.25	0.12099325	0.13642115	96.97941673	201.74404491	1.89740421
0.50	0.18778595	0.15226507	69.58217772	281.17860705	1.36137668
1.00	0.41640865	0.46950511	45.24330266	432.44013268	0.88518611
2.00	1.68967326	1.90512425	26.66668275	733.68780010	0.52173417

Results for electric and magnetic field strength in point $(x,y) = (d, 0.75d)$, characteristic impedance of the strip line (Z_c), capacitance (C') and inductance (L') per unit length, are presented in Table 1. Used numerical values are:

$\varepsilon_r = 9.2$, $\mu_r = 4.07$, $\chi_r = 1.73$, $U = 1V$, $h = 0.5d$, $t = 0.01w$, where $\chi_0 = \sqrt{\varepsilon_0 \mu_0} = \frac{10^{-8}}{3} \frac{s}{m}$.

References
1. N. B. Raicevic, S. S. Ilic, "One Hybrid Method Application on Anisotropic Strip Lines Determination", The 23rd Annual Review of Progress in Applied Computational Electromagnetics – ACES 2007 (on CD), pp. 8-13, Verona, Italy, March 19-23, 2007.
2. N. B. Raicevic, S. S. Ilic, "Equivalent Electrode Method Application on Anisotropic Micro Strip Lines Calculations", International Conference on Electromagnetics in Advanced Applications, ICEAA 07, paper 122 (CD), Torino, Italy, September 17-21, 2007.

Frequency-Agile High-Power Resonant Microwave Compressors

S. N. Artemenko, V. A. Avgustinovich, A. S. Shlapakovski, Yu. G. Yushkov
Nuclear Physics Institute, Tomsk, Russia
E-mail: shl@npi.tpu.ru

The problem of creating high-power resonant microwave compressors capable of wideband frequency tuning is considered. The resonant pulse compression technique based on the microwave energy storage in a cavity with its following fast release allows one to produce microwave pulses of nanosecond duration and megawatt-to-gigawatt peak power level from rather compact and relatively inexpensive devices. Frequency-agile resonant compressors could find application in short-pulse radars, for testing electronic hardware, or as RF drive sources in relativistic microwave amplifiers.

Results of the theoretical analysis are presented for the traditional compressor configuration including a storage cavity and output interference switch based on a waveguide H-tee and, also, for the configuration comprising a symmetric storage system and input-output coupler in the form of double waveguide tee. Conditions of realization and characteristics of frequency-agile compressors such as the cavity and compressor gains, pre-pulse amplitude, and output pulse duration have been determined. It has been shown that in the traditional configuration, the operating frequency hopping is possible at fixed cavity geometry and just a small change of the electric length of the H-tee short-circuited side arm (sub-opening the tee). This corresponds to the transition to neighbor cavity modes differing by axial indices, and the range of hopping can be as wide as the band of a single-mode waveguide. Moreover, at a certain degree of tee sub-opening, the switching over is possible between the two, or even three operating frequencies without any mechanical tuning at all, and with rather small reduction of the compressor gain. In the configuration with a symmetric storage system, the discrete variation of the operating frequency without any mechanical tuning is possible within the band of a single-mode waveguide, and, if the length of both arms of the storage system is slightly and identically changed, the operating frequency is varied continuously.

Also presented are the experimental results obtained with a first prototype of frequency-agile compressor, the two-frequency X-band megawatt compressor. This compressor demonstrated the same gain of ~16 dB at ~2 MW peak output power and ~4 ns FWHM pulse duration for two operating frequencies, 9.155 and 9.388 GHz. Input pulses of microsecond duration were produced by the tunable magnetron, which output power was up to 50 kW. The compressor was designed to operate in the $TE_{11(31)}$ and $TE_{11(32)}$ modes of the copper cylindrical cavity. The output H-tee was also made of circular waveguide sections. The diameter of the cavity differed from that of the tee arms (was larger) in order to provide higher Q-factor for the cavity and acceptable characteristics of the tee at the same time, so that the design included also the smooth Chebyshev transition. Switching over between the two operating modes was realized by means of ~ 2 mm displacement of the movable membrane in the side arm of the tee. In all experiments, commutation of the compressor operation regimes from energy storing to releasing stages occurred in air at the atmospheric pressure.

HPEM - 11
High-Power Microwaves

Oral Presentations

Electromagnetic Vehicles Immobilization System (ELVIS)

A. Tehori, J. Statlender, A.Tokarsky
Rafael Ltd, Haifa, Israel
E-mail: tehoria@rafael.co.il

The Electromagnetic Vehicle Immobilization System -ELVIS is a compact portable mesoband system. The system can be hand carried in a "trolley" case or be car-hosted. The system comprises of two HV power supplies one positive and one negative, a 500kV pulse generator, a switched oscillator (patent pending) and a transmitting antenna. The paper will give details of the characteristics of the system performance: pulse characteristics, repetition rate, field strength versus distance, etc…

Also, the paper will give details and results of immobilization tests, made on more than 15 types of commonly used cars.

The Impact of Phase Measurement toward the Total Radiated Power in A Gtem Cell

X Ngu[1], A Nothofer[2], D Thomas[3] and C Christopoulos[4]

[1,2,3 & 4]*University of Nottingham, Nottingham, United Kingdom*

E-mail: xavierngu@ieee.org

The Transverse Electromagnetic Cell (TEM) cell can be used to measure emissions from Equipment Under Test (EUT) with inclusion of phase measurement as reported in [1] and shown in Fig. 1(left). Due to the limitation of higher usable frequencies in TEM cell, a tapered TEM cell known as the Gigahertz Transverse Electromagnetic Cell (GTEM) Cell was introduced to accommodate higher frequencies. However, the GTEM cell has only one port. This restriction prohibits phase measurement because of the absence of the other port. This paper introduces a method where the phase measurement can also be performed with a GTEM cell. This method involves an additional rotation of 180° of the EUT to gain the power of P_2 shown in Fig. 1(right). This method also includes a way to establish a phase reference signal to gain the phase information of the dipole moments of the EUT. Using this technique, this work investigates the impact of the phase measurement toward the estimation of total radiated power by making a comparison between the total power radiated by a spherical dipole EUT at 200 MHz using (1) the GTEM cell that involve phase measurement [1], (2) the GTEM cell measurement according to IEC 61000-4-20 [2] and lastly (3) the value obtained from the Transmission Line Model (TLM) simulation [3]. The results are shown in Table 1. It is shown that the values of the total radiated power between the measurement that involves phase and the simulation are close within each other. Whereas the total radiated power obtained according to IEC 61000-4-20 differs by about 8 dB. This work provides an insight into the importance of the assumption that there is no phase difference between dipole moments. Here we have shown that by including the phase difference between dipole moments from the EUT in Electromagnetic Compatibility (EMC) test, the result has improved even for a single dominant radiator such as the spherical dipole antenna.

φ=45°; Primed axes are local EUT axes; non-primed axes are TEM/GTEM axes; $P_{1 \& 2}$ Measured magnitude & phase
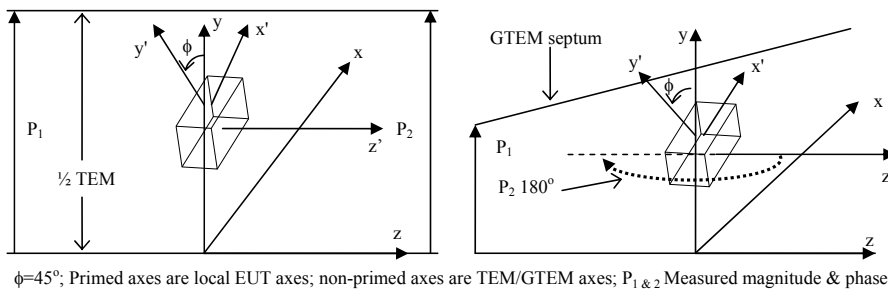
Fig. 1 – The total radiated power measured using the TEM (left) and the proposed method using the GTEM cell (right) for one EUT orientation. A method to establish a phase reference is included in GTEM cell measurement.

Table 1 - Comparison of total power radiated between three different methods

Method	Total power radiated (dBm)	Absolute difference against TLM simulation results (|dB|)
GTEM + phase	-98.815	0.613
GTEM + IEC 61000-4-20	-89.965	8.237
TLM simulation	-98.202	

References

1. Ma, M.T. and Koepke, G., A method to quantify the radiation characteristics of an unknown interference source. NBS Tech. Note 1059, Oct. 1982.
2. 61000-4-20, Electromagnetic Compatibility (EMC) – Part 4: Testing and measurement techniques. Section 20: Emission and immunity testing in transverse electromagnetic (TEM) waveguides. International Electrotechnical Commission, Geneva, Switzerland. 2003.
3. Christopoulos C., "The Transmission Line Modeling Method TLM", IEEE Press, Piscataway, NJ, 1995.

Oral Presentations

HPEM - 12 Measurements Techniques #2

A State of the Art Anechoic Chamber for Air vehicle Testing at Alenia Aeronautica

Gaetano Maurizio Ariano[1], Ilario Bertino[1], Marco Bozzetti[1], Paolo Galati [1]

[1]*Alenia Aeronautica, Italy*

E-mail: mbozzetti@aeronautica.alenia.it

A state of the art electromagnetic anechoic chamber has recently been built by Alenia Aeronautica at Caselle South Plant: this paper shows its main features and testing capabilities. It also describes a simulation analysis to predict the electromagnetic performance of the chamber and the typology of the acceptance tests.

The anechoic chamber is a full anechoic chamber, and it has been designed to carry out tests mainly on fighter and unmanned aircraft. Moreover, tests can be carried out on every SUT that is compatible with the dimensions of the main access door. A system to extract exhaust gas was installed in order to carry out tests on a wide variety of vehicles.

The anechoic chamber has been designed to carry out both HIRF/EMC and High Sensitivity tests: in particular HIRF/EMC tests in the frequency range 30MHz ÷ 18GHz with the capability of radiating a very high intensity electromagnetic field and High Sensitivity tests, such as installed (on SUT) antenna pattern measurement in the frequency range 500MHz ÷ 18GHz.

During the design phase and before construction of the full-scale chamber, a 1/12th scale model, metal-lined chamber had been manufactured to assess the desired electromagnetic performance. Moreover, during the construction phase, simulation campaigns were performed both to define the detailed internal layout and test acceptance methodology for particular cases not covered by the standards.

The size (shield to shield) of chamber is 30m wide, 30m long and 20m high, and the 18m wide by 8.5m high main door allows the SUT access. The shielded structure is a cube of 3mm-thick steel panels welded together, and it guarantees values of shielding effectiveness more than 100 dB in the frequency range 100kHz to 20GHz. The floor surface includes a 10 metre diameter turntable to rotate a 30 ton SUT with an angular accuracy of ± 0.02° and a pathway to allow SUT access. Both the pathway and the turntable are permanently covered by ferrite tiles. A hoist system permits lifting of the SUT (max 25 tons) up to 10 metres from the turntable centre enabling EMC testing on aircraft with the landing gear retracted.
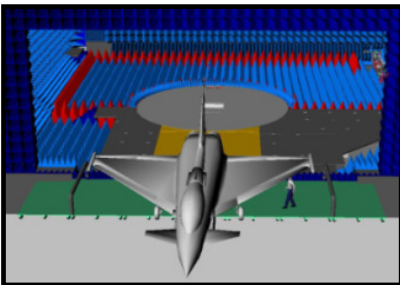
Figure 1 access of the aircraft through the main door
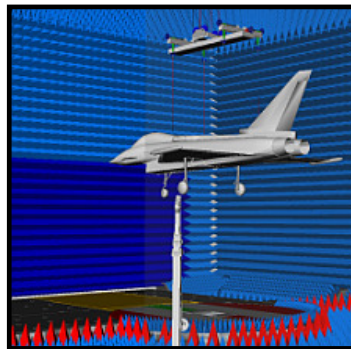
Figure 2 lifting of the aircraft for the execution of the test

This paper describes the anechoic chamber design and, in particular, the special ability to perform the test along the diagonal direction of the square base in order to increase distance between the test antenna and the SUT and also decrease the number of first and second order spurious reflections that reach the quiet zone.

Development of Logging System for High Power Electromagnetic Field

Ryuichi Kobayashi[1], Yasunao Suzuki[1], Mamoru Sato[2], Masao Masugi[1], and Kimihiro Tajima[1]

[1] *NTT Energy and Environment Systems Laboratories, Tokyo, Japan*
[2] *NTT Advanced ε echnology Corp., Tokyo, Japan*
E-mail: KOBAYASHI.RYUICHI<AT>lab.ntt.co.jp

1. Introduction

With the development of electronics technologies, telecommunication systems have the ability of high-speed processing and high-performance operation. Therefore, the influence on society becomes big when EMC trouble occurs. Moreover, a radio transmitter can easily be obtained from the market. Thus, malicious threats of exposure to High Power ElectroMagnetic (HPEM) pulses are increasing [1]. This paper describes development of a logging system for HPEM, which may affect telecommunication systems.

2. Configuration

Configuration of developed logging system for HPEM is shown in Fig. 1. This system is constructed with probes, band-pass filters, detectors, and a logging unit. The system monitors electromagnetic fields in a frequency range from the HF-band to the SHF-band, continuously. When an HPEM is coming, the probe, whose band matches the HPEM pulse, picks up the pulse. Output of the probe goes through a band-pass filter to a detector and the output level is converted into DC voltage. When the DC level is more than a threshold level determined beforehand, the logging unit records the level, frequency band, time, and date. Then, an alarm signal is sending to outside. An external view of the system and probes are shown in Fig. 2. The system is in a shielded box that has shielding performance of at least 100 V/m. Furthermore, to make the sensitivity of each band the same, a system uses six probes.

3. Specification and sensitivity

Specifications of the system are shown in Table. 1. We selected six bands, which can easily produce HPEM. In our system, six bands include amateur radio- and Radar bands. Moreover, to enlarge the dynamic range of the system, we use a logarithmic circuit for detectors. Measured characteristics in 2.45 GHz band are shown in Fig. 2. The probe factor is about 39 dB and total insertion loss is 14 dB. Measured results of the sensitivity in 2.45 GHz band when the signal generator is directly connected to the input terminal of the detector are shown in Fig.3. The result shows good linearity in the range from -50 to 10 dBm in a 50 Ω measurement system. Using this result, incident E-field strength E_{ins} is derived by

$$E_{ins} = P_{in} + (F_{probe} + L_{filt}) + 107 \ [dB\mu V/m].$$

Thus, this system has good linearity from 100 to 165 dBμV/m and may have sensitivity to 175 dBμV/m. According to Ref.[1], one possible level of HPEM in this band is about 173 dBμ/V@10 m. Therefore, this system is almost able to detect that level.
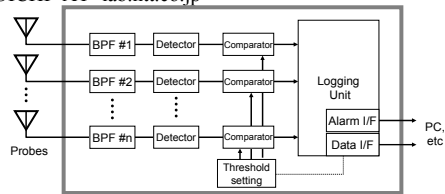
Fig. 1 Configuration of the system

(a) System   (b) Probes
Fig. 2 External view of system and probes

Table 1 Specification of the system

Item	value
No. of freq. band	6 (27M, 50-150M, 430M, 1-2G, 2.45G, 3-6G)
Dynamic range	40 dB
Output level of detector	0 – 2 V_{dc}
Max. E-field	100 V/m (at least)
Antenna directivity	Non directional
Recorded data	Level, time, date, and freq.

Table 2 Measured characteristics in 2.45 GHz band

Parameter	Probe factor F_{probe}	Insertion loss of filter L_{filt}
Values	39 dB	10 dB
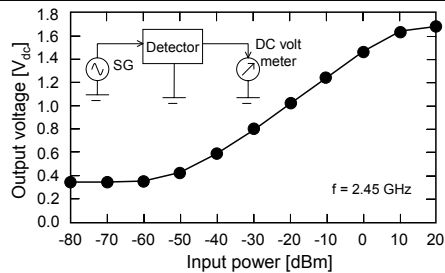
Fig. 3 Measured sensitivity of detector

4. Conclusion

We have developed a logging system for HPEM and evaluated its sensitivity. The results indicate that the system can detect possible HPEM. Future work will experimentally evaluate the validity of this system by applying HPEM.

References

[1] IEC 61000-2-13, (2005)

Generation and measurement of electromagnetic pulses with rise time down to 30 ps

L.L. Sinii, Yu.V. Dmitriev, V.F. Molochkov, and V.V. Neustruev

Research Institute of Pulse Technique, Luganskaya ul. 9, Moscow 115304, Russia

e-mail: cemc@niiit.ru

Currently, measurement instrumentation and test equipment for studying the susceptibility of various hardware to electromagnetic pulses (EMPs) are actively developed. Particular interest is the effect of EMP with the rise time less than 100 ps. In this case, of great importance is the accuracy of measured parameters of electric and magnetic fields. We developed field-generation cells CC577 and CC578 which generate rectangular electromagnetic pulses with ultrashort rise times in rather large test volumes. These calibration instruments are listed the public register of measurement instrumentation. The main parameters of cells are presented in Table 1. Cell's pulse edge waveforms are shown in Fig. 1.

Using these instruments, E- and H-field sensors for measuring of EMP components in the range of $3 \cdot 10^{-11}$-$3 \cdot 10^{-8}$ s were developed and calibrated with good accuracy. Sensors with cable communication lines 3 m long allow measurements of EMP components with rise time down to 30 ps with an accuracy of $\pm(15\text{-}20)$ %.

Sensors with fiber-optic communication lines 50 m long have the transient response rise time of 100 ps and operate in the range from 0.4 to 400 kV/m and from 1 to 1000 A/m. Now, works on increasing the rapidity of such sensors to 60-70 ps are doing.

Table 1. Main parameters of field-generation cells CC577 and CC578

Parameters	CC577	CC578
Calibration volume dimensions	130×130×25 mm	300×300×70 mm
Pulse rise time of generated pulses, no longer than, ps	30 ps	100 ps
Pulse width at the level of 0.9	130 ns	3 ns
Steady-state strength of EMP components:		
electric	250 V/m	73 кV/m
magnetic	0,66 A/m	194 A/m
Reproduction uncertainty of the steady-state strength of EMP components in the calibration volume	± 15 %	± 11 %
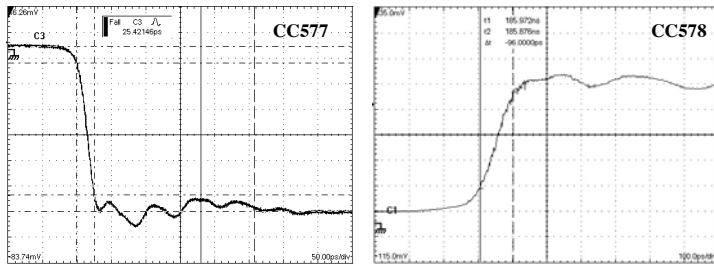
Fig. 1 - Pulse edge waveforms of CC577 (left) and CC578 (right).

Electro-optic sensors: Toward stable, sensitive and vectorial measurements of high power electromagnetic fields

M. Bernier[1], A. Warzecha[1], G.Gaborit[2], L. Duvillaret[1], J.-L. Lasserre[3]
[1]IMEP-LAHC, UMR CNRS 5130, Minatec-INPG,BP 257, 38016 Grenoble Cedex 1, FRANCE
[2]IMEP-LAHC, UMR CNRS 5130, Université de Savoie,73376 Le Bourget du Lac Cedex, FRANCE
[3]DGA/DET/CEG/LDP/CGN/EXC
E-mail: bernier@minatec.inpg.fr

This paper describes pigtaled electro-optic (EO) sensors based on Pöckels effect and used to characterize high power microwave (HPM). Firstly we present the developed sensors and some measurements obtained with our servo-controlled EO setup. Then we deal with remaining problems encountered with these kinds of probes before summarizing current skills and performances of the system and giving possible ways of improvement.

EO probes are particularly appropriate for free space electric (E) field characterization thanks to greater temporal and spatial resolutions (femtosecond and sub-millimetre, respectively) than the common sensors (antennas, bolometers, …). EO probes are based on the modification of a laser beam (either its polarization, phase or amplitude) crossing an EO crystal; its refractive indices depending linearly on the E field vector via the Pöckels effect. This property allows performing vectorial mapping of E-field [1]. However, this technique has been operated mainly in laboratories. The 1st problem, that was to carry the laser beam to the E-field sensitive crystal, has been solved using optical fibres. On the other hand, in order to make EO measurements as a widespread technique, two essential drawbacks still have to be overtaken. Measurement benches remained temporally unstable for outer measurements because of the dependence of refractive indices on the temperature. Moreover, even if EO sensors are completely suitable for high power E-field, the sensitivity has to be increased to reach EMC requirements.

Until now, our pigtailed probes (see Fig. 1a) have been based on polarization state modulation. Polarization of the laser beam crossing back and forth the sensor, depends mainly on the intrinsic anisotropies of both: crystal and PM-fibre (that are temperature dependent) but also, for a weaker part, on the E-field to be measured. It is essential to perfectly control the outcoming polarization to extract the E-field induced modulation. This control is achieved with our fully automated setup that includes servo–controlled half and quarter wave plates mounted on motorized rotation stages. Fig. 1b and 1c present examples of obtained results and Tab.1. summarizes the setup characteristics.
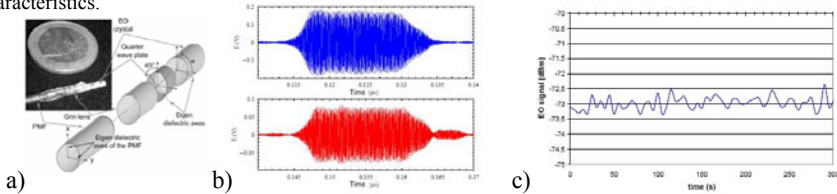
Fig. 1 – a) sketch of the EO sensor, b) 500kV/m - 9 GHz single shot pulse measured with horn antenna (top) and EO sensor (bottom), c) temporal stability of the measurement under outdoor conditions

Table 1 – EO sensor and associated measurements bench perfomances

Meas. characteristic	Bandwidth	Dynamic range	Spatial resolution	Invasiveness	Sensitivity	Selectivity E_x/E_y	Stability/temp. immunity
Current performances	kHz - 20 GHz	> 70 dB	10 μm	~ null (free space)	0.7 V.m^{-1}.Hz$^{-1/2}$	> 25 dB	>5 min (accuracy 1dB)

The next step consists in the improvement of the sensitivity $\mathbb{S}$, i.e. the ratio between modulated and mean parts of the laser beam. As the EO crystal is non-linear, the spectrum of the optical carrier ω_{opt} will be modified by the E field at angular frequency ω_{mod} (side peaks will appear at $\omega_{opt} \pm \omega_{mod}$). After modulation, ω_{opt} is rejected using high finesse Fabry-Pérot cavity (at least -20 dB is expected) and then whole signal is amplified by an optical amplifier (+ 30 dB). First experiments are in progress and we expect to improve our sensitivity $\mathbb{S}$ results by a 50 dB factor.

References
1. Yang K, David G, Yook JG, Papapolymerou I, Katehi LPB, Whitaker JF, "Electrooptic mapping and finite-element modeling of the near-field pattern of a microstrip patch antenna", *IEEE Trans. Microwave Theory Tech.*, vol. 48, pp. 288-294, 2000

Building the Capability to Perform Electromagnetic Effects Tests on Complex Systems

Dr. David C. Stoudt

Navy's Distinguished Engineer for Directed Energy
Naval Surface Warfare Center, Dahlgren, VA

...
E-mail: David.Stoudt@navy.mil

The interaction of electromagnetic waves with real systems is very complex and requires an extensive span of capabilities and facilities to perform experiments correctly and completely. Recent recognition of a variety of electromagnetic threats such as high-altitude electromagnetic pulse, lightning, high-power microwave weapons, as well as transmitters, in such commercial applications as communications, have made the understanding of the effects of these sources on electronics critical to the continued proper functioning of our infrastructure. Test facilities must represent a variety of interesting systems and must be located so that a variety of high-power electromagnetics sources can be applied. Available analytical tools should include a variety of statistical tools for data analysis and test planning, as well prediction and interpolation of test data. This paper describes the development of such a capability base at the Directed Energy Technology Office at the Naval Surface Warfare Center in Dahlgren, VA.

The first step in building the capability base was to build a series of test facilities. Those facilities include two multi-story buildings that use common commercial building construction techniques. These buildings are populated by electronic systems, such as computer networks, distributed control systems, communications switches, alarm systems, and SCADAs. The test facilities are located in an isolated part of NSWC-Dahlgren so that a variety of fields and impressed currents can be applied in realistic ways. A variety of test planning and data reduction techniques had to be developed to support the understanding of the causes of system and subsystem failure. These tools include statistical and neural net models of various types of system interactions. The point of the analysis is to develop the means to predict system and subsystem failure for a variety of illumination scenarios. Finally, numerical tools and analytical techniques are used to understand the coupling of the fields onto buildings, system cables, and other vulnerable parts of the system

This array of tools has been applied to good effect to a variety of tactical scenarios in both offensive military applications and applications for the protection of infrastructure from natural and intentional electromagnetic threats.

Methods to Determine the Effect of Pulse Width on Susceptibility Threshold Levels

Robert L. Gardner
Consultant, Alexandria, VA, USA

E-mail: Robert.L.Gardner@verizon.net

When measuring susceptibility levels in electromagnetic compatibility, intentional electromagnetic interference or high-power microwave testing the assumption is usually made that the peak electric field is the descriptor of the waveform that is the best predictor of failure of the system. In this paper, normalized test data is used to show that substantial differences in threshold are observed when the pulse width is varied in narrowband illumination of certain test objects. Statistical techniques are then used to help analyze the data. Often, when properly plotted, the difference in the thresholds due to different illumination conditions is apparent, we extend the study by using these data to demonstrate statistical techniques that are of use when the inference is not so obvious. Analysis of variance and covariance are the main tools used on these data sets to show the importance of pulse width in predicting the threshold failure level as compared to pulse repetition rate or number of pulses. Other predictors could also consider such comparisons as the current vice the peak incident electric field.

Neural net analysis represents another useful technique for analyzing this type of data. Published computer susceptibility data from Fang [1] is used to illustrate the technique. In this case, as well, there is clear dependence of the susceptibility threshold on the pulse width.

 [1] J. Y. Fang, Wang J-G, Qiao D-J, 2002, *High Power Laser and Particle Beams*, 14,2.

HPEM - 13
Susceptibility #1 (Invited)

Oral Presentations

Predicting EMI Effects on Complex, Distributed Electronic Systems Subjected to Wideband RF

Cynthia Ropiak, Ph.D.[1], and Frank Peterkin, Ph.D.[2]

[1]*SAQ Consulting Ltd., Chestertown, Maryland, U.S.A*
[2]*Directed Energy Technology Office, Naval Surface Warfare Center, Dhalgren, Virginia, U.S.A*

Cropiak@earthlink.net

Predicting electromagnetic interference (EMI) effects on electronic systems is challenging under the best of circumstances, but when the source of electromagnetic energy is a wideband radio frequency (RF) device and the test environment is complicated by having the electronics distributed over a significant area, the problem can become daunting. A promising statistical technique known as multivariate logistic regression (MLR) has been utilized in the analysis of problems such as these with varying degrees of success. Equation 1 contains the functional form for the probability of effect function (P) in the MLR format. The exponent in the equation is known as the Logit and contains the input parameters 'x_i' and fit variables 'a_i'. Reference [1] involves a successful application of the MLR technique to a data set associated with a distributed computer network.

$$P(x_1, x_2, \ldots) = \left[1 + e^{-\sum_i (a_0 + a_i f(x_i))} \right]^{-1}$$

(1)

Inherent limitations of the MLR technique are associated with the fact that it is a statistical technique wrought with the restrictions of statistical methods, combined with the fact that the fit parameters are often source descriptors (radiated power, distance from source, etc.) which innately connect the probability of effect fit with the test environment specifics. The second of these complications can be circumvented if the target is not distributed and the source of the energy is narrow band RF lying in the gigahertz frequency regime, because then it may be possible to specify electronic upset failure conditions in terms of the peak power density incident on the target. With the exception of the aforementioned restrictive condition, the traditional MLR technique does little to nothing to help with the problem of predicting electronic EMI effects for systems in untested settings. To be specific, for a target such as a distributed computer network, the traditional MLR technique cannot predict effects in building configurations that have not been tested.

In an effort to circumvent the inherent limitations associated with a traditional application of the MLR technique, a modified MLR method has been developed which combines empirical data gathered in an open air test environment with computational electromagnetic simulations. The fit parameters in the modified method are electromagnetic environment descriptors obtained via the simulations. Reference [2] discusses the modified MLR technique in the context of a purely simulated data set. The true power of the modified MLR method is realized when the empirical effects data set contains different building configurations for under these conditions it may be possible to use the resulting probability of effect fit to extrapolate to untested building configurations. A probability of effect fit is developed for a data set associated with three building configurations (concrete block, rebar, and rebar with wire mesh roof) and combined with a simulated data set in order to illustrate an application of the modified MLR method. The results will be discussed as well their applicability and limitations.

References
1. C. A. Ropiak, and P. R. Hayes, "Electromagnetic Susceptibility Data Analysis Using Multivariate Logistic Regression," Directed Energy Professional Society, November, 2002, Monterey, California.
2. C. A. Ropiak, P. R. Hayes, and D. C. Stoudt, "EMI Effects Analysis Techniques that Yield Exportable (Test Bed Independent) Results," EUROEM 2004, Magdeburg, Germany.

Transfer Function Measurements and Low Power Microwave Susceptibility Tests of a Complex Communication Network

Ch. Braun, P. Clemens, H.-U. Schmidt, M. Suhrke, and H.-J. Taenzer

Fraunhofer Institut Naturwissenschaftlich-Technische Trendanalysen INT,
P. O. Box 1491, 53864 Euskirchen, Germany
E-mail: michael.suhrke@int.fraunhofer.de

We report on microwave vulnerability tests of a configurable network communication system. The purpose of the measurements at Fraunhofer INT was twofold. First, transfer functions were determined in order to characterize the coupling of microwave fields into the equipment under test (EUT) including the investigation of shielding effectiveness of different boxes containing the network equipment. Second, susceptibility tests were performed at our facility for lower field levels. The INT test facility consists of a waveguide built as an open pyramidal asymmetric three-plate TEM transmission line which is located within a shielded hall. Inside the waveguide homogeneous microwave fields can be realized in a maximum test volume of approximately $2 \times 2 \times 3 \ m^3$. Transfer function measurements can be carried out by continuous wave (CW) illumination of the EUT using digital tunable sweep generators together with power amplifiers for frequencies between 1 and 8000 MHz and vector network analyzers as receivers. Susceptibility tests can be done with a pulse modulated generator in the frequency range from 150 to 3425 MHz for different pulse widths and repetition rates. The investigations focused on the vulnerability of the network components (commercial HUBs, switches, and routers) including media converters and uninterruptible power supply (UPS) units but not connected PCs and other peripherals as monitors or keyboards. To this end, several subsystems were set up and network traffic was generated involving the relevant network components. In order to detect malfunctions due to microwave illumination the traffic was monitored with network diagnostics software. In addition, the functioning of the components of interest was observed directly by watching the system LEDs with cameras. The setup also included different cabling ranging from fiber optic via SFTP (shielded) to UTP (unshielded) connections. Particularly the influence of the unshielded cables was tested in two different configurations.

A Perspective of Electromagnetic Susceptibility of Discrete Event Dynamic Systems and Hybrid Systems

I. Kohlberg[1] and R. L. Gardner[2]

[1]Kohlberg Associates Inc, Reston, Virginia, USA
*[2]Consultant, Alexandria, Virginia, USA*y
E-mail: Robert.L.Gardner@verizon.net

Predicting Intentional Electromagnetic Interference (IEMI) on large systems such as those used in infrastructures and on small systems such as Local Area Networks (LANs) has been elusive. Experimental programs to evaluate the susceptibility of these systems typically address the problem of determining the response of a particular system/subsystem against a limited suite of threat waveforms. This information is of great concern for the particular system in question but does not generally lend itself to identifying the root causes of system upset or permanent failure. This is not a new issue, and an extremely tough one to deal with on both a theoretical and experimental basis. Not dealing with it has tremendous negative consequences for the future since going down the same development path for next-generation software and hardware will only increase the susceptibility of these systems to IEMI. So what do we do? At the beginning of this decade the idea of mitigating systems against IEMI was synonymous with electromagnetic hardening and to a large extent married intellectually to an analogue (continuous time) viewpoint of networks. In the early 2000's Kohlberg and Gardner [1] introduced the notion that bit errors produced by unwanted electromagnetic fields could also cause system malfunctions and that the consequences of information breakdown was more relevant to Discrete Event Dynamic Systems (DEDS) and Hybrid Systems—typically comprised of continuous time and discrete time processes than analogue systems. Being able to mitigate DEDS and Hybrid systems against IEMI requires that we understand their susceptibility from a fundamental viewpoint. In this paper we examine our options. We begin with the idea that an ideal unperturbed system is characterized by the function, $F=(\{X\}, \{Y\})$, where $\{X\}$ is the set of all possible states and $\{Y\}$ is the set of all possible actions (events). Only a subset of actions applies to any state. Upset or failure of DEDS from IEMI occurs when the unwanted signal produces new states or actions, or changes the subset of actions associated with states. This latter case may be more difficult to detect since the sets $\{X\}$, $\{Y\}$ remain unchanged. EMC techniques strive to prevent any adverse actions from happening. However, future systems may operate on the principle that we can control adverse IEMI effects by developing systems characterized by the function, $F=(\{X\}, \{Y\}, \{Q\})$, where $\{Q\}$ is a set of control functions. These control theory approaches for mitigating IEMI will be discussed. Mitigating hybrid systems against IEMI requires a conceptually broader set of considerations than those for DEDS. These new features arise when a continuous normal phase of operation changes due to state changes. Examples of this are also discussed in this paper.

References

1.   Ira Kohlberg and R. L. Gardner, "Systems Topology for Electromagnetic Effects on Local Area Networks and Information Systems", Proceedings of the International Conference on Electromagnetics in Advanced Applications, Torino, Italy, 10-14 September 2001.

Inclusion of "Baum's Law" in Intentional Electromagnetic Interference Susceptibility Analysis

R. L. Gardner

Consultant, Alexandria, VA, USA

E-mail: Robert.L.Gardner@verizon.net

The sequence of events in testing an electronic system to intentional electromagnetic interference (IEMI) stress can be described as a series of transfer functions: source, antenna, propagation, external coupling, internal coupling and the effects on the electronics. All of these transfer functions are very sensitive to the frequency content of the waveform emitted by the source. Effects tests are designed to explore the sensitivity of the effects to various parameters describing the transmitted signal as well as those describing the test object.

The effects portion of this sequence is often difficult to handle analytically because the system effects are sensitive to frequency and waveform characteristics not just in the usual coupling sense but also manifest large and abrupt changes in state which represent upset and damage. The response curves are therefore not smooth functions. Since there is no useful theory for this part of the system response, it is usually handled empirically with the test operators exposing the target to different waveforms and observing the various state changes. This process links the source/antenna part of the transfer sequence directly with the effects end state giving information about the coupling part of the sequence only as a filter that is sampled in the process. The most transparent part of the coupling filter is in the resonant region of the system response, but requires very dense sampling to characterize in the resonant region unless one has additional information.

Baum's Law observes that all systems useful to people will have characteristic dimensions near that of the human hand. If that is true, the distribution of hand sizes and useful control sizes gives us a reasonable distribution of the useful pass band of the coupling part of the filter. If we concentrate our testing on a combination of the probability distribution of the source characteristics, the operating characteristics of the target system and that observed in coupling region then we can show a much more compressed test matrix.

Open Source Method for Integrated FDTD-SPICE Evaluation of Component/Circuit Response to Transient EM Fields

Dr. James R. Elliott

Electro Magnetic Applications, Inc., Denver, CO, USA

...
E-mail: JIM@EMADEN.COM

The assessment of vulnerability to HPM or EMP is a multi-level problem requiring efficient, accurate calculation of EM coupling to a system as well as evaluation of the interaction of the coupled energy with system components including possible non-linear terminal protection devices. As cheap computing has become wide-spread, the finite-difference time-domain technique [1] has proven itself ever more useful in performing high accuracy EM coupling even down to the circuit board level. Circuit simulation using SPICE [2] has also proven itself useful in evaluating details of the EM stresses experienced by components on a circuit board. The physical basis for integrating these two tools was outlined over ten years ago [2] and some commercial packages are now becoming available that accomplish this integration. However, a simple but general integration implementation unencumbered by proprietary constraints has much value in many circumstances. This paper will describe such an implementation.

The open source circuit simulation code used is based on the well-tested SPICE (3f5) from UC/Berkeley as modified by Georgia Tech to have the XSPICE code modeling capability [4]. Code modeling permits easy construction of new circuit elements that can be inserted into any SPICE circuit models. In the method developed in this effort, a new FDTD-SPICE connection circuit element acts as the portal for information exchange between the FDTD and SPICE codes:

FDTD	**Info Flow**	**SPICE**
H/E	$\int H \, dl \rightarrow I$	V/I
$\varepsilon \, (d\mathbf{E}/dt) + \mathbf{J}(\mathbf{E}) = \nabla \times H$	$E \leftarrow \int I \, dt$	$C \, (dV/dt) + I(V) = I$

The key features of the method are:

- FDTD code sets up the problem, starts the SPICE process and controls the time stepping
- FDTD and SPICE codes run as co-processes
- Inter-process communication is used to synchronize the processes
- FDTD and SPICE run independently except to exchange information twice per time step
- Interaction is symmetric; i.e., problem can be driven from either FDTD or SPICE codes
- FDTD-SPICE connection devices can be connected to any other SPICE devices or circuits
- Multiple connections are permitted between the FDTD and SPICE models
- Overhead for the FDTD-SPICE connection and inter-process communication is negligible

One illustration of the method will present results for a simple loaded antenna illuminated by a high intensity transient plane wave; the antenna input voltages will be compared for a passive load versus one protected by macro-modeled non-linear terminal protection device connected across the antenna terminals by a FDTD-SPICE connection device. A second example, looking at the voltage induced on a trace on a PCB illuminated by a plane-wave, will also be presented with and without diode protection.

References
1. For example,: A. Taflove and S. Hagness, ed.," "Computational Electrodynamics, The Finite-Difference Time-Domain Method", Boston Artech House, 2005
2. V. A. Thomas, M. E. Jones, M. Piket-May, A. Taflove & E. Harrigan, The Use of SPICE Circuits as Sub-grid Models for FDTD Analysis", IEEE Microwave and Guided Wave Letters, Vol. 4, May 1994
3. "NGSPICE User Manual", ngspice-rework-17, draft version 0.2, http:/ngspice.sourceforge.net/
4. F.L. Cox III, W.B. Kuhn, J.P. Murray and S.D. Tynor, "Code-level modeling in XSPICE", Proceedings IEEE International Symposium on Circuits and Systems, 1992

A New Method of Interference Evaluation between UWB System and Wireless LAN using a GTEM cell

S. Ishigami[1], M. Yamada[2], K. Gotoh[1], Y. Matsumoto[1], and M. Tokuda[2]

[1]*National Institute of Information and Communications Technology, Tokyo, Japan*
[2]*Musashi Institute of Technology, Tokyo, Japan*
E-mail: shinobu@nict.go.jp

Ultra Wide Band (UWB) technology is a wireless system that transmits the signal at high-speed transmission rate of 100 megabits per second (Mbps) – 480 Mbps with low power spectrum density in the distance within 10 m. The federal communications commission (FCC) has allocated the frequencies from 3.1 GHz to 10.6 GHz and from 22 GHz to 29 GHz for the unlicensed use of the UWB. And so a dedicated frequency band cannot be allocated for UWB system. We should consider carefully the interference problem between UWB and existing W-LAN or other wireless systems because the UWB system will be used over the frequencies that are allocated for the existing wireless systems.

The FCC [1] and the recommendation of ITU-R [2] defined the spectrum mask of UWB in terms of equivalent isotropic radiation power (EIRP). An EIRP is calculated by an electric field at the condition of a certain distance. An apparatus that can generate an intended electric field is required for interference evaluations. Moreover, the interference evaluations between wireless communications systems are usually performed in all measuring apparatuses connected. However, it is difficult to connect the communication system (receiver) of an antenna built-in type to the measuring apparatus. A transverse electromagnetic (TEM) waveguide can apply an intended field to the receiver of the antenna built-in type. A GTEM cell, which is applicable for several gigahertzes, is useful as a test fixture that can be carried out an interference evaluation of the UWB.

In this paper, we proposed a new method of the interference evaluation between the UWB and the wireless LAN by using the GTEM cell that can test the receiver with the antenna built-in type.

It was confirmed that the GTEM cell could be used in the frequency band of the direct-sequence spread-spectrum UWB (DS-UWB) up to 6 GHz by the evaluation of the frequency response. The interference evaluation was conducted between wireless LAN IEEE802.11a and DS-UWB. The amplitude probability density (APD) of the DS-UWB was also measured. As a result, even if the UWB signal is smaller than the receiver noise of wireless LAN, the throughput deteriorates than that in a case of the noninterference. Moreover, the signal of the DS-UWB was equivalent to the AWGN in a case of the throughput variation of 64QAM. We also evaluated the separation distances in regulation limits of US and EU/Japan as shown in Fig.1. As a result, since the separation distance in C/N that corresponds to the minimum receiver sensitivity of wireless LAN is 0.28 m, the UWB on practical use hardly influences wireless LANs. In contrast, the victim receiver needed the separation distance of 5.3 m or more to evade interference in a case of the FCC regulation limit in the minimum receiver sensitivity.
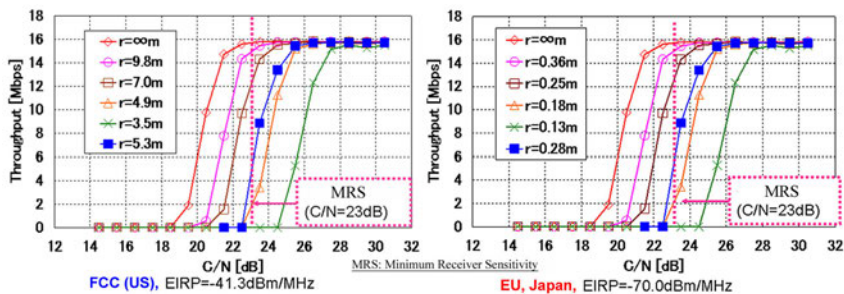
Fig. 1 – Separation distances in regulation limits of US (left figure) and EU/Japan (right figure).

References
1.   FCC CFR47 part 15, 2002.
2.   ITU-R Recommendations SM.1754 – SM.1757, 2006.

HPEM - 13
Susceptibility #1 (Invited)

Oral Presentations

Simulation of the effects of radiation on a LEO satellite memory & improve its fault tolerant ability, using SIHFT

Mahmood Nematollahzadeh[1], Ali Akbar Jamshidifar[2] , Shahrokh Jalilian[3]
[1]Faculty Member of Iran Telecommunication Research Center, Tehran, IRAN
[2]Faculty Member of Iran Research Organisation fo Science and Technoligy, Tehran, IRAN
[3]Iranian Space Agency, Tehran, IRAN
E-mail: nematz@itrc.ac.ir

Single Event Upsets (SEUs) are a major concern when computer systems are working in space environment [1]. SIHFT (Software Implemented Hardware Fault Tolerance) techniques provide low-cost solutions for online detection and correction of transient errors dues to the effects of the environment (radiation, EMC etc.). EDAC (Error Detection and Correction) is one of these techniques [2]. This approach is also well suited for COTS (Commercial Of-The-Shelf) parts, has been validated through fault injection experiments and radiation testing campaigns. Software-implemented fault injection (SWIFI) provides a low cost and easy-to-control fault injection technique for generating faults to the target system [3].

In this article a software environment has been developed based on VirSim tool [4], to simulate the effect of radiation on COTS memories and show the efficiency of the software EDAC. As a case study, a sample LEO satellite with 8 MB (Mega Byte) RAM (Random Access Memory) is considered, and a software EDAC for detecting and correcting the faults in the memory, is implemented. The software EDAC is responsible for reliability of data in this 8 MB RAM. The system has been implemented and simulated by VirSim, as a multi task software simulator tool. One separated task has been developed for injection SEUs to the 8MB memory of the satellite. The SEUs has been generated based on the ARGOS satellite reports [5]. According to these reports the average of SEUs is about 5.5 SEU/MB per day, where generates about 5 MBU (Multiple Bit Upset) out of any 100 SEU. About 4 of these MBUs are double events (2bit Upset) and 1 of them is triple. The software EDAC detects and corrects all 1 bit SEUs and detects all double MBUs but it dose not guarantee the detection of triple MBUs. The simulation results demonstrate the effectiveness of the approach in terms of fault detection and correction capabilities. The simulation results have been shown in the following tables. Table 1 shows the number of SEUs which have been injected to the memory in 2 individual tests, and table 2 depicts the effectiveness of software EDAC. As it can be seen from table 2, the software EDAC has detected more than 99 percent of errors caused by SEUs.

Table 1. SEUs has been injected to RAM

	Memory Size	Eradiation time [days]	Number of 1 bit SEU	Number of double MBU	Number of triple MBU	SEU / MB per Day
First Test	1 MB	20	101	5	1	5.35
Second Test	8 MB	40.5	1592	64	8	5.1

Table 2. Error Detection And Correction Coverage

	Memory Size	Total Errors	Error Detected	Error Corrected	Undetected Errors	Reliability
First Test	1 MB	107	106	101	1	~ 99%
Second Test	8 MB	1664	1659	1595	5	~ 99%

References:
[1]. P. Reyes et al, "New Protection Techniques Against SEUs for Moving Average Filters in a Radiation Environment", IEEE TRANSACTIONS ON NUCLEAR SCIENCE, VOL. 54, NO. 4, AUGUST 2007.
[2]. P.P. Shirvani et al, "Software-Implemented EDAC Protection Against SEUs," IEEE Trans. on Reliability, Special Section on Fault-Tolerant VLSI Systems, Vol. 49, No. 3, pp. 273-284, Sep. 2000.
[3]. Jean Arlat et al, "Comparison of Physical and Software-Implemented Fault Injection Techniques", IEEE TRANSACTIONS ON COMPUTERS, VOL. 52, NO. 9, SEPTEMBER 2003.
[4]. Jalilian, Jamshidifar, Nematollahzadeh, "VirSim, a Simulated Environment for Developing Multitask Software of Satellite", Third International Conference on Recent Advances in Space Technologies, TURKEY, June 2007.
[5]. P. P. Shirvani and E. J. McCluskey, "Fault-tolerant systems in a space environment: The CRC ARGOS project," Stanford Univ., CRC-TR 98-2, Dec. 1998.

Research of Means for Equipment Protection from Periodically Repeating Pulse Disturbances in Power Lines

Yu. Parfenov, B. Titov, L. Zdoukhov
AIHT, Moscow, Russia
parfenov@ihed.ras.ru

Research was carried out by means of the simulator of power supply network of a typical building. This simulator allows carrying out research of influence of pulse electric disturbances on working capacity of information systems depending on parameters of disturbances and ways of their injection into power cables. The protecting filter was used to prevent penetration of pulse disturbances into the general power network of a building. The experimental research has shown that the use of standard filters does not provide the decision of the given problem. The basic defect of standard filters is the use of voltage limiters. This circumstance attracts behind itself two inconveniences. First, the permanent control of working capacity of voltage limiters is required as their failure under the influence of high voltage pulses will result in penetration of these pulses into the next premises and failure of the equipment located in given premises. Secondly, as a result of their work the voltage acting on equipment under tests will be limited. Therefore results of tests will be deformed. For this reason there are no voltage limiters in the filter. The experiments have shown that entrance resistance of the protecting filter cannot be selected arbitrarily, and should correspond to the entrance impedance of an external power line. It allows to reproduce adequately influence of pulse disturbances to equipment under tests. For this reason the elements Z_0 and C_0 are mounted on a filter entrance. Elements Z_0 model the entrance impedances of an external power line, and capacitors C_0 prevent penetration of working 50 Hz voltage into these elements.

The local computer network was object of tests. For imitation of pulse disturbances the following nanosecond generators of periodically repeating high voltage pulses were used:

• GPRHVP-100: amplitude - 20…100 kV, rise time - 1 ns, pulse width - 50 ns, pulse repetition rate - 10…1000 Hz;

• GPRHVP-5: amplitude - 3.5…5 кВ, rise time - 1 ns, pulse width - 50 ns, pulse repetition rate - 1000…6000 Hz.

Two ways of pulse disturbances injection into power cable were used during tests:

• Inductive way by means of GPRHVP-100;

• Conducted way by means of GPRHVP-5.

A distance between computers and a place of pulse disturbances injection varied in a range from 10 to 40 meters. Sources of uninterrupted power supply, and also the devices intended for protection of the sensitive electronic equipment from high voltage pulse disturbances were used for protection of computers from pulses injected into power cable.

During tests data rate in the network was measured depending on amplitude of a voltage pulses and pulse repetition rate. Duration of influence of voltage pulses in each experiment was 60 seconds.

Results of experiments have allowed formulating following conclusions:

1. Inductive and conducted ways of injection of high-voltage nanosecond pulses into power lines entail serious threat for computer networks.

2. Decrease of data rate or denial of service and computers latch-up occurs at injection of nanosecond pulses into power cables.

3. The extent of decrease of data rate and the moment of computers latch-up depend on pulses amplitude and repetition rate, a way of injection and a distance between computers and an injection place.

4. Use of traditional protection devices does not entail increase of immunity of a local computer network to influence of the pulse disturbances injected into power cable.

HPEM - 14
Intentional EMI #2 (Invited)

Oral Presentations

Modal Decomposition of UWB Pulse in Power Cable Structures: Simple Experiment Showing Useful Possible Applications

T. R. Gazizov, A. M. Zabolotsky, I. E. Samotin

Television and Control Department, Tomsk State University of Control Systems and Radioelectronics
634050, Lenin Ave., 40, Tomsk, Russia

talgat@tu.tusur.ru

Details of ultra wide band (UWB) pulse propagation in power cables are of growing interest [1]. This abstract describes simple experiment on modal decomposition of the pulse in three-conductor flat cable structures. Two unusual facts must be noted. First one consists in that this experiment, despite of simplicity, shows a number of new and various applications. Second fact consists in that the investigation is partly relying on all themes of EUROEM 2008: particularly, for such topics as Intentional EMI, Hardening & Protection, UWB propagation, Sensor Technologies, Threats and Countermeasures for Critical Infrastructures.

Flat power cable (ПУГНП 3×1,5 type) widely used in various (domestic, medical, industrial, critical) low-voltage installations was used in experiment (Fig. 1*a*). Experimental setup was based on C9-11 oscilloscope. UWB pulse close to triangular form with total duration about 0.8 ns and magnitude 1.4 V on 50 Ohm load was used. The pulse was excited between conductors 1 and 2, while conductor 3 leaved open circuit at both sides. Resulting waveform between conductors 1 and 2 at the end of 15 m length cable was consisting of two pulses having about 97 and 100 mV magnitudes and 5.2 ns difference in time delay (Fig. 1*b*). Then, a small gap has been made in conductor 3 at the 5 m distance of cable. Thus, the structure became as two (5 m and 10 m) cable sections connected directly by conductors 1 and 2, while conductors 3 leaves disconnected (open circuit) at junction. Resulting waveform became consisting of four pulses having about 38, 62, 70 and 92 mV magnitudes and 1.3, 1.7 and 1.6 ns differences in time delay (Fig. 1*c*).
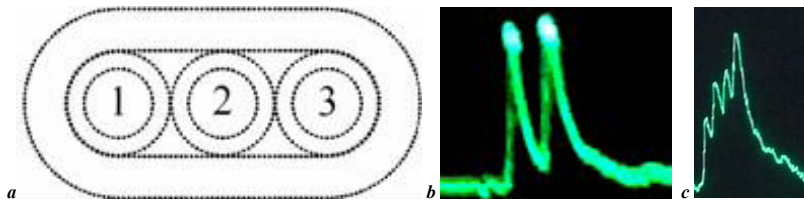
Fig. 1. – Cable cross-section with conductors numbered (*a*); decomposition of a pulse in two pulses at the end of 15 m cable (*b*) decomposition of a pulse in four pulses at the end of 15 m cable with a gap in conductor 3 at distance 5 m (*c*)

Some details of possible applications of the phenomena observed in the experiment (or their extensions) have been recently described by authors: (un)intentional decomposition and restoration of a pulse [2, 3]; decomposition of a pulse for protection [3, 4]. However, experimental confirmation of the phenomena for consequent decomposition of UWB pulse in cascaded sections of power cable into 2, 4, … pulses of smaller magnitudes has not been shown previously. This experiment has also highlighted the effect of losses and dispersion (hidden in lossless simulations). Moreover, other application of the modal phenomena has been revealed – to sense the presence (two pulses instead of one) and to diagnose a state (four pulses instead of two) of a conductor without electric contact with it.

References
1.   D. Mansson, T. Nilsson, R. Thottappillil, and M. Backstrom, "Propagation of UWB transients in low-voltage installation power cables," IEEE Trans. on Electromagn. Compat., vol. 49, Aug. 2007.
2.   A. M. Zabolotsky, T. R. Gazizov, A. G. Bova, W. A. Radasky, "Dangerous pulse excitation of coupled lines," in Proc. of the 17-th Int. Zurich Symp. on EMC, Singapore, February 27–March 3, 2006.
3.   T. R. Gazizov, A. M. Zabolotsky, A. O. Melkozerov, T. T. Gazizov, S.P. Kuksenko E. N. Gorin, I. G. Bevzenko, "Possibilities of new modal phenomena usage for aims of electromagnetic terrorism and for protection against it," in Proc. of the 7-th Int. Symp. on Electromagnetic Compatibility and Electromagnetic Ecology, St. Petersburg, Russia, June 26–29, 2007, (Russian).
4.   T. R. Gazizov, A. M. Zabolotsky, "New approach to EMC protection," in Proc. of the 18-th Int. Zurich Symp. on EMC, Munich, Germany, September 24–28, 2007.

Susceptibility of Network Interface Cards to High-Level Conducted Pulses

E. B. Savage, W. A. Radasky, K. S. Smith, M. J. Madrid

Metatech Corporation, Goleta, California, USA

E-mail: savagee@cox.net

Computers have become a very important part of many aspects of our lives, but there is also the valid worry of their susceptibility to upset or damage from electromagnetic attack, such as ultrawideband pulses (UWB)[1]. A significant vulnerability for modern systems is coupling to cables, especially network lines – because networks are ubiquitous and essential, but also can have significant cable lengths, while the associated electronics can be especially susceptible to conducted EM pulses. For example, a well designed power substation SCADA (Supervision Control And Data Acquisition) unit showed good immunity on its control ports, going out to the various sensors and controls in a power substation, but its Ethernet port was damaged by EM pulses[2]. Because they are so common, network interface cards (NICs) in personal computers (PCs), such as the sample shown in Figure 1, are of significant concern when considering EM vulnerability of many systems. It is important to know the EM susceptibility of NIC cards when doing a system assessment. This talk will discuss the results of EM pulse testing of several NIC cards, using pulses of various widths. Upsets and damage were produced during the pulse testing. The test used 20 samples cards, of seven different types, from 5 manufacturers.

Figure 2 shows a general circuit diagram for NIC cards, as deduced from inspection of the cards. The cards connect into an expansion slot on a PC, and have a network connector into which an Ethernet line is plugged. All cards tested had a high-frequency transformer and a large integrated circuit (IC), as seen in Figure 1. Typically there are also various components, such as resistors, capacitors, etc., between the transformer and IC, as indicated by the "Discretes" entry in Figure 2. Many cards also had the RC structure shown between the network connector and the transformer (one instead had a capacitor connected to the transformer, as symbolically shown in the circuit diagram). It is believed that this RC structure is there to help the NIC meet EMC emission specs, helping to short out common mode high frequencies.

The RC network has the first components seen by an incoming EM pulse, and so it is not surprising that these parts, both the resistors and the capacitors, were often damaged by EM pulses. However, it was surprising that usually the damage did not prevent the NIC card from continuing to function (i.e., communicate) properly. This reinforces the conclusion that these are EMC components. Thus, for a susceptibility evaluation, it would need to be determined if damage to these parts should be considered significant or not (and they were definitely damaged – including disintegration of the capacitor).

Some devices also had other damage, such that the card truly was incapacitated. In some cases physical damage was seen on the discrete components between the transformer and IC, and for one type of NIC the IC was destroyed – showing "bubbling" and "burning" from overheating.

Fig. 1 - Sample NIC card.   **Fig. 2 - General circuit diagram for a NIC.**
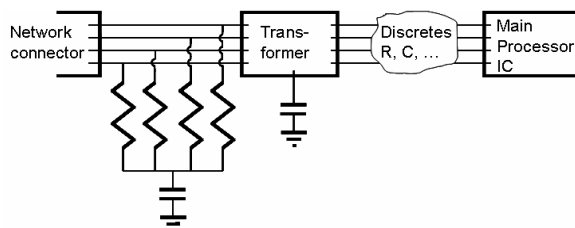
References
1. Wik, M. W., W. A. Radasky and R. L. Gardner, "Intentional Electromagnetic Interference (EMI) -- What is the Threat and What Can We Do About It?" Fifteenth International Wroclaw Symposium on EMC, June 27-30, 2000, pp. 896-897.
2. Savage, E. B., W. A. Radasky, J. G. Kappenman, J. L. Gilbert, K .S. Smith, and M. J. Madrid, "HEMP Impulse Injection Testing of Power System Electronics and Electrical Components", Meta-R-225, December 29, 2003.

HPEM - 14
Intentional EMI #2 (Invited)

Oral Presentations

The Prediction, Construction and Injection of Complex (Multi-frequency) Transient Waveforms

A. Wraight[1], P. Watkins[1]
[1]*QinetiQ, Farnborough, England*
E-mail: awraight@QinetiQ.com

This paper presents a novel method for the prediction of induced current from magnitude-only transfer functions. Magnitude-only transfer functions are used by the aircraft community to support flight clearances in high intensity radiated field (HIRF) environments [1, 2]. The availability of this type of transfer function makes it appealing to those conducting assessments against HEMP and HPEM environments as they provide a basis for the prediction of induced current in a transient environment. To compute the prediction, phase information is generated using minimum phase constraints that ensure an overestimation of the actual induced current in the majority of cases. For some applications, it is of interest to generate a range of predicted currents that bound a realistic induced current.

A novel algorithm for the prediction of induced currents will be presented that changes the phase component of a minimum-phase prediction by flipping zero-pairs outside of the unit circle on the z-plane [3]. The algorithm can be tailored to adjust the number of phase components that are changed thereby altering the structure of the predicted waveform. An example of the use of this algorithm will also be given.

The algorithm can also be used to de-convolve complex transients into their constituent frequency-amplitude-phase (relative) components. This information enables the re-construction of the predicted waveform for injection into cable bundles via an arbitrary waveform generator or similar equipment. Application of the techniques presented will be demonstrated via examples.

References
1. N. J. Carter, "The Revision of EMC Specifications for Military Aircraft Equipment," PhD Thesis, 1985, University of Surrey, England
2. EUROCAE ED107, "Guide to the Certification of Aircraft in a High Intensity Radiated Fields (HIRF) Environment", March 2001
3. A. Wraight, "Improvements in Electromagnetic Assessment Methodologies: Bounding the Errors in Prediction", PhD Thesis, 2007, Cranfield University, England

Calculating of the Transient Electromagnetic Field Emitted by Power Electronic Converters using the Hybrid Approach

M Melit[1], B Nekhoul[1], N Boudjerda[1], K Kerroum[2] and K El khamlichi Drissi[2]

[1]*LAMEL Laboratory, Jijel University, BP 98 Ouled Aissa, 18000 Jijel, Algeria.*
[2]*LASMEA Laboratory, Blaise Pascal University, 63177 Aubière, France.*
E-mail: melit@mail.univ-jijel.dz

The use of power electronics converters is in constant progresses in last years (power equipments, embarked equipments…). These devices are responsible of the increase of electromagnetic interference (EMI). During regular functioning of the switches (transistors, diodes…), transient currents and voltages flows in power circuit. For this reason, it's very important to quantify the electromagnetic field emitted by the converters in the transient domain and to know the perturbations source with its spectral contain.

Classically, numerical modeling in frequency domain is used and consists in the resolution of the integral equation by moment method [1]; the Fast Fourier Transform permits the study in time domain. This formalism is very rigorous, but it is of difficult implementation and requires an important calculation time.

Modeling this problem directly in the time domain, in the literature the approach consists on the resolution of the 3D Maxwell equations by FDTD [2]. In this objective a modeling approached by truncation is used. A more rigorous modeling requires taking into account of the open boundaries. The modeling by this approach requires tri-dimensional meshing which leads to more computations heaviness.

In our work, for study this problem directly in time domain, we propose the use of the analytic concept of the dipoles [3] associated to the modified images theory [4]. For the use of this analytic concept we calculate numerically in first step by FDTD the currents distribution in the converter's circuit. For this last objective we deduce a matrix equation after discretization of the equations of the transmission lines by FDTD. The use of the transmission lines theory requires a good knowledge of the per unit length parameters of the converter's traces; that we calculate while using the approach proposed by C. R. Paul [4]. Our proposition allows taking into account the non linearity introduced by real functioning of the switches (controlled transistor), and simple to implement and no time consuming. In order to validate our work we have implement the resolution of the Maxwell equations by FDTD while taking into account of open boundaries using absorbing boundary conditions, we confront the results that we get directly in time domain by the two approaches.

As application we propose to study the simple device presented in figure 1. We treat an ideal switch, and the turn-on process is modeled by taking a step signal with rise time $t_r = 0.5$ ns.
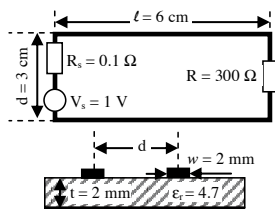
Fig. 1.a – Configuration of the circuit used for simulation
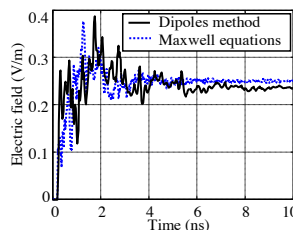
Fig. 1.b – Electric field
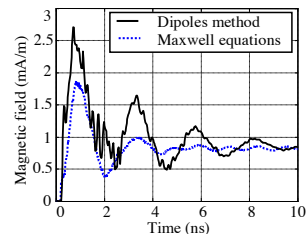
Fig. 1.c – Magnetic field

The figures 1.b and 1.c present the results of electric and magnetic field in the center of the circuit and at 5 cm above the circuit board. The two approaches give very close results in shape and amplitude. For the magnetic field we see a slight difference between the two methods; this difference shows that the method of modified images adapts especially for calculating of the electric field in the event that we have a perfectly ground plane.

References
1. R. F. Harrington, "Field computation by moment method", Malbar, FL: Krieger, 1968.
2. K. S. Yee, "Numerical Solution of Initial Boundary Value Problems Involving Maxwell's Equations in Isotropic Media", IEEE Trans. Antennas Propag., vol. 14, pp. 302-307, May 1966.
3. M. A. Uman, D. K. McCain, and E. P. Krider, "The Electromagnetic Radiation from a Finite Antenna", Am. J. Phys, vol. 43, pp. 33-38, 1975.
4. C. R. Paul, "Analysis of Multiconductor Transmission Lines", New York: Wiley Interscience, 1994.

HPEM - 15
Electromagnetic Compatibility in Power Systems

Oral Presentations

Influence of EM Field Induced by Generator Busbars on Control Cables

N.V. Korovkin, A.V. Smorgonskiy

St.-Petersburg State Polytechnical University, St.-Petersburg, Russia
E-mail: nikolay.korovkin@gmail.com

Reliability of automatic control systems at modern power plants greatly depends on transmission of control signals. At present, old unshielded cables are being replaced by modern shielded cables at many power plants. EM interferences induced in the control circuits can cause errors in electronic devices, breakdowns of equipment and power failures. That's why the estimation of these interferences is very important.

In this work we studied the influence of time-varying EM field of generator busbars. Generator busbar current induces magnetic flux that causes induction of EMF in cable shields. The shields of the cables are usually connected to the ground system. Therefore, the interferences are induced in large area circuits. After calculation of EMF and current in the cable shield, we can find the voltage induced in cable core by means of transfer impedance.

To simplify calculation of EMF induced in cable shields we have made several assumptions. We neglect:

- finite length and transverse sizes of conductors, assuming their essentially smaller than lengths of conductors. Therefore, expressions for the magnetic potential will be the same as for infinite line conductors;
- resistance of ground conductors in order to calculate the current induced in each contour separately, neglecting effects of other contours;
- inductive resistance of cable shields that is smaller than active resistance;
- interferences induced by high-voltage power lines connected to step-up transformer;
- interferences induced by the nearest generators;
- voltages induced in the conductors that are perpendicular to the generators busbars;
- anisotropic magnetic medium where EM field exists.

Accepted assumptions allow gaining estimations for induced EMF with an error 20-50% that is quite enough for the recommendations on necessity of interference decrement.

The method of estimation of interferences, induced in control system cables described earlier, was approved at Zhigulevskaya HPP, one of the largest power plants in Russia. Its installed capacity is 2300 MW.

The subjects of inquiry are the cables between central control panel of power plant, switchgear and generator control panel. The generator control panel is situated nearby each generator. The central control panel is located at the middle of the power plant building. The ground system has very extensive three-dimensional structure.
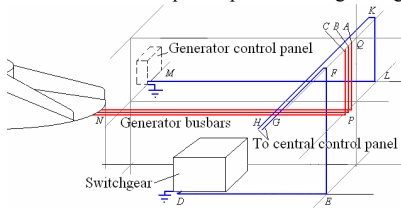
Fig. 1 – Generator busbars and control cable shields

We have studied the EM field formed by three-phase busbars between generators and step-up transformers. They can be approximately modeled by three parallel straight buses consist of the horizontal NP and vertical PQ parts (Fig. 1). Interferences are induced in the circuit formed by cable shields HKLM and DEFG. In view of the fact that ground conductors are interconnected in many different points, the resistance between points H-G as well as points M-D is near zero.

The value of EMF induced in the contour in normal mode is E=2.9 V. The total resistance of the contour is about 10 Ohms. In this contour there are four points of contact. Resistance of each of them can run up to 5 Ohms. Consequently, current in the cable shield is 100 mA. Such current by means of the mechanism of transfer impedance induces in the cable core voltage 500 mV.

At short-circuit conditions EMF and current induced in the cable increases in 5-10 times. So, voltage induced in the cable core will not exceed 2.5 V. Such voltage induced in cable core is dangerous only for coaxial cables. For twisted cables such voltages are not dangerous because voltage is induced in both conductors of the twisted pair, forming common mode.

We have also found that the most dangerous short-circuit for the control system of generator is not the failure on its own busbars, but the failure on the next nearest generator busbars.

Calculations carried out revealed that in general there are not so much problems with EMC of control cables at Zhigulevskaya hydroelectric power plant. Though, dimensions of the contour have great influence on the value of induced EMF. That's why such simple and rather cheap examination should be carried out at operating power plants.

References

1. K. S. Demirchjan, L. R. Neiman, N. V. Korovkin, V. L. Chechurin, Theoretical bases of the electrical engineering. St.-Petersburg: "Piter", 2003, vol. 3, 376 p.

Investigations of high-voltage power network, located in the regions with low soil conductivity

**B.V.Efimov[1], N.V.Korovkin[2], N.I.Gumerova[2],
A.N.Danilin[1], Yu.M.Nevretdinov[1], V.N.Selivanov[1]**

[1]*Applied-physics Center of the Energy Problems of the North - Subdivision of Kola Science Center
of Russia Academy of Sciences, Apatity, Murmansk reg., Russia*
[2]*Saint-Petersburg State Polytechnic University, Saint-Petersburg, Russia*

E-mail: Selivanov@ien.kolasc.net.ru, Nikolay.Korovkin@gmail.com

The analysis of power lines automatic opening statistics shows that the part of lightning outage in the regions with low soil conductivity is higher, then in other regions. The reason is high resistance of transmission tower grounding. The problem of substation equipment protection from the incoming power lines waves became aggravated. The effectiveness of lightning protection apparatus is reduced by the high series-connected ground mat impulse resistance.

Under conditions of rocky soils of North Russia have been measured input impulse resistances of hundreds of transmission tower and dozens of substation ground mats. The experiments have been carried out in operation power networks and on tasting grounds with impulse generators voltage up to 1000 kV. Based on the results of oscillogramms treatment are proposed calculation models of input ground resistance in micro-seconds range with taking into account influence of reactance and non-linear processes of spark formation in soil.

These models are included in new procedure of lightning outage rate and substations lightning guard reliability indexes calculations. Have been done lightning guard reliability calculations for dozens of power lines and substations. For nonstandard cases is proposed transition from standardization of specific design and electric factor to standardization of integral lightning guard reliability test.

HPEM - 15
Electromagnetic Compatibility in Power Systems

Oral Presentations

Troubleshooting EMC in designs with switching power supplies and fans

A. Mediano

Group of Power Electronics and Microelectronic (GEPM), I3A, University of Zaragoza, Zaragoza, SPAIN

E-mail: a.mediano@ieee.org

Many systems today like home appliances, communication equipments, medical instruments, etc. include a low power (6W-50W) switching power supply (SMPS). In addition, if the system includes some module with high dissipation (power converter, etc) a fan is usually used for cooling purposes.

That kind of systems must comply EMC regulations both conducted (9kHz to 30MHz) and radiated (30MHz to 1GHz) and both elements (SMPS and fan) are key elements to define the EMC profile of the product [1].

The power supply cord is a key element of the problem because: i) common mode EMI is radiated by that cable (typically in the 30-300Mhz range for that systems) and ii) conducted problems (9kHz-30MHz) goes to the LISN through the cable.

To minimize the problems, a lot of techniques have been published [2] including layout, mains filters (with X caps, Y caps, DM and CM chokes), ferrites, snubbers, shields in transformer, Y capacitors, etc.

The designer, based in experience, models, simulation and time, can obtain theoretically first prototypes with good results. But, in practice, it is usual to spend a lot of additional time ($\propto 1$/experience) with the prototype trying i) to reduce EMI to comply or ii) evaluating the real need of included EMI components to reduce cost.

This paper shows (first contribution) the experience of author in measuring common mode and differential mode currents in power supply cord: a) to fix EMC radiated and conducted problems, b) to find the source of a problem in the cable, c) to evaluate the need of a component (a ferrite, a cap, etc), d) to compare different values or configurations of a component/section and e) to analyze the SMPS EMI behavior with resistor load vs. fan load..

To illustrate the technique, a SMPS is used including mains filter, electronic load and a fan as explained before. The fan is included (second contribution) because the EMC profile of the system is not the same if we evaluate the SMPS with resistive load (same power as fan) or with the fan (figure 1). A picture of setup is shown in figure 2.

Fig. 1 – Fan current with linear vs. SMPS power supply.
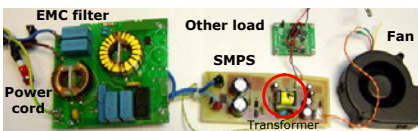
Fig. 2 – Complete setup for evaluation.

Figure 3 is an example of the technique for evaluation of two transformers (with/without shield winding) and influence of Y capacitor between primary and secondary (two well known design techniques [3]). The common mode current in cable is shown from 37,5MHz to 75MHz because that current is directly related to radiated profile of the system in that frequency range.
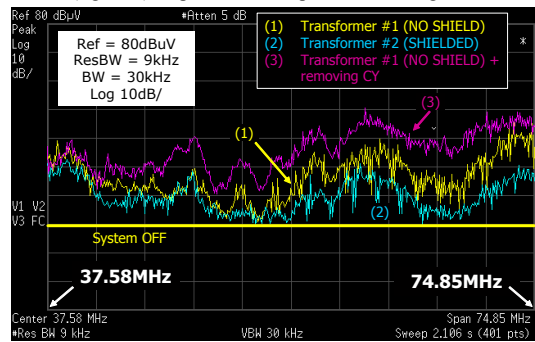
Fig. 3 – Example of transformer influence

References
1.   T. Williams · "EMC for Product Designers" · Ed. PARANINFO · 1997.
2.   Henry W. Ott · "Noise Reduction Techniques in Electronic Systems" · 2nd Edition · Ed. John Wiley & Sons · 1988.
3.   Power Integrations, AN-15 TOPSwitch Power Supply Design Techniques for EMI and Safety, April 2005

Reduction of Conducted EMI in Three Phase Inverter by a Dual Randomized Modulation Scheme

N. Boudjerda[1], M. Melit[1], B. Nekhoul[1], K. El khamlichi Drissi[2] and K. Kerroum[2]
[1] LAMEL, University of Jijel, BP 98 Ouled Aissa, 18000 Jijel, Algeria
[2] LASMEA, Blaise Pascal University, 24 Avenue des Landais, 63177 Aubière, France
E-mail: n_boudjerda@yahoo.fr

Several studies have shown that acoustic noise annoyances in Variable Speed Drive Systems (VSD) are strongly linked to the conducted EMI generated by the power converter [1]. Nowadays, it's well known that Randomized Pulse Width Modulation (RPWM) allows spreading the voltage/current spectrum in a large frequency band which allows meeting better the EMC standards and mitigates the noise annoyances in VSDs [2].

In DC-AC conversion the principal objective of RPWM is the reduction of the acoustic noise such as in naval propulsion, electric car and domestic apparatus [2-3].

In this paper, we propose a Dual RPWM scheme (DRPWM) for the three phase full bridge inverter. By use of a triangular carrier having two randomized parameters, the Power Spectral Density (PSD) of the voltage is better spread than the case of single randomized parameter schemes.

Each phase of the inverter requires one switching function, obtained by comparing three sine reference signals r_a, r_b and r_c to a single randomized triangular carrier. The classical simple RPWM schemes (only one randomized parameter) are RCF (Randomized carrier frequency) in which the switching period T is randomized and RPP (Randomized Pulse Position) in which the pulse position δ is randomized, this can be done by randomizing the fall time report β (Fig.1). We propose a randomization of both of the period T and the fall time report β giving a Dual RPWM scheme that we call DRPWM [4].

A rigorous spectral analysis of random signals uses the Power Spectral Density (PSD) noted W and given for a τ long RPWM pulse signal $u_\tau(t)$ by:

$$W(f) = \lim_{\tau \to \infty} \frac{1}{\tau} E\left\{ \left| F[u_\tau(t)] \right|^2 \right\}$$ (1)

$F[u_\tau(t)]$ is Fourier transform of signal $u_\tau(t)$ and $E\{.\}$ is the statistical expectation of the expression in brackets.

Based on the Wiener Khinchin Theorem, and by using the randomized parameters of the carrier, a general analytical model of PSD is established for phase to ground and phase to phase output voltages.

From Fig.2, the proposed dual RPWM scheme gives the best spread PSD, which is the EMC purpose of RPWM.
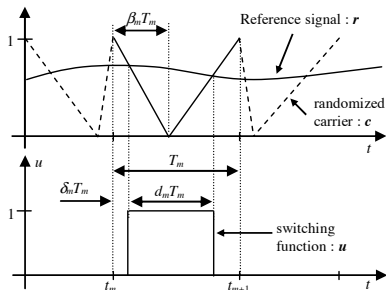
Fig. 1 – Modulating principle
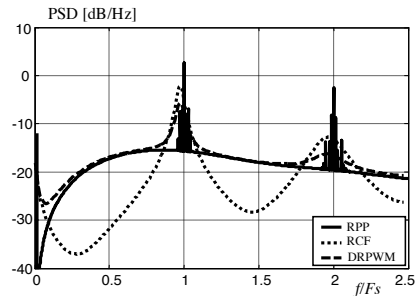
Fig. 2 – PSD of phase to ground voltage

References
1. Bech M. M., "Random pulse-width modulation techniques for power electronic converters", Ph.D. Thesis, Aalborg University, Aalborg East, Denmark, 2000.
2. Andrzej M. Trzynadlowski, "Active Attenuation of Electromagnetic Noise in an Inverter-Fed Automotive Electric Drive System", IEEE Trans. On Power Electronics, Vol. 21, N0. 3, May 2006, pp. 693-700.
3. K. Borisov, T. E. Calvert, J. A. Kleppe, E. M. and A. M. Trzynadlowski, "Experimental Investigation of a Naval Propulsion Drive Model With the PWM-Based Attenuation of the Accoustic and Electromagnetic Noise", IEEE Trans. On Ind. Electronics, Vol. 53, N0. 2, Apr. 2006, pp. 450-457.
4. N. Boudjerda, M. Melit, B. Nekhoul, K. El Khamlichi Drissi and K. Kerroum, "Reduction of Conducted Perturbations in DC-AC Converters by a Dual Randomization of Hybrid Space Vector Modulation", International Review of Electrical Engineering, Vol. 1, N0 1, March-April 2006, pp.154-161.

Analysis of wave processes in power lines subject to the frequency properties of the grounded electrode of the tower

Y.N.Bocharov[1], N.V.Korovkin[1], S.I.Krivosheev[1] T.G.Minevich[1], S.L.Shishigin[2]

[1]*Saint-Petersburg State Polytechnic University, Saint-Petersburg, Russia*
[2]*State Technical University, Vologda, Russia*

E-mail: Nikolay.Korovkin@gmail.com

In [1] we have presented a universal approach to the creation of mathematical models of linear electromagnetic devices with frequency-dependent equivalent parameters. Models are intended for use in time domain and can be used for calculations of wave processes in the system with nonlinear devices. The parameters definition of the models was proposed on the basis of the experimental frequency responses.

In this report we will present the results of set of full-scale experiments that were done for the grounded electrodes of power towers. These results were obtained with the help of the special high-voltage current source that injected short current pulses into the grounded electrodes. We did the measurements in the time domain and transformed the data to the frequency domain.

After that the mathematical models of the grounded electrodes of power towers were created and used for calculations of the propagation of the overvoltages along the lightning guard wire. The calculations of the transient processes taking into account the frequency properties of grounded electrode in different ranges: up to 10KHz, 100KHz and 1MHz were done. The results of simulations are in the good agreement with the experimental data.

References
1.   N. Korovkin, T. Minevich A universal method of setting up macromodels from frequency response of devices, Proceedings of the 16th International Zurich Symposium on Electromagnetic Compatibility, EMC Week 2005, Zurich, Switzerland, February 13-18, pp.307-312

HPEM - 15
Electromagnetic Compatibility in Power Systems

Oral Presentations

Experimental and Theoretical Study of Chaotic Wide-Band Microwave Generation in Non-relativistic Electron Beam with Virtual Cathode

E.N. Egorov, R.A. Filatov, A.E. Hramov, Yu.A. Kalinin, A.A. Koronovskii,
N.N. Kuznetsov, I.S. Rempen, D.I. Trubetskov
Saratov State University, Saratov, Russia
E-mail: aeh@nonlin.sgu.ru

The analysis of oscillatory processes in intensive beams of charged particles in regimes of virtual cathode (VC) formation is an important and actual problem. It is well-known [1–3] that the systems with VC are characterized by complex dynamics and can demonstrate a wide range of the nonlinear phenomena, including dynamical chaos. Researches of complex chaotic oscillations in such systems are very important both from the fundamental point of view (in order to investigate chaotic dynamics and pattern formation in the distributed active media) and for the practical applications (e.g., to create broadband chaotic microwave radiation sources). This report contains the results of experimental and theoretical study of low-voltage non-relativistic system with virtual cathode which is formed in electron beam with additional braking field. In such systems the VC may be formed in beams with low current and density [4]. In spite of that such systems may generate both periodic and wideband chaotic oscillations (WCO) of low power. At the same time the WCO-sources present considerable interest in practice for system of radiolocation, system electronic counter measure, communication systems, industrial and medicine application.

In our research we have investigated the oscillations in the electron beam with VC in different schemes. Firstly, the diode space with retarding field [4] has been discussed. Experimental research and numerical simulation have shown that in such system it is possible to achieve different oscillating regimes within the change of beam current, braking voltage and geometrical parameters. The complexity of the power spectral distribution increases with the growth of the retarding field value. As the retarding field grows, regular oscillations are replaced by the chaotic ones and then stationary VC take place in the system. At the same time, the output power increases, too. At the point where retarding potential value is equal to the half of the accelerating potential value, the output power and the oscillation's complexity reach their maximum value. After this point, the complexity and output power decreases slowly. Also, as the retarding potential value decreases the frequency bandwidth grows, too, and reaches its maximum in the chaotic regime. The second scheme we have investigated is the scheme with *multispeed* electron beam where VC is also formed due to additional braking of electrons. As the experimental and theoretical study has shown [5], in this case it is possible to enlarge the bandwidth of generated frequencies essentially and to lessen the irregularity of power spectrum (Fig. 1).
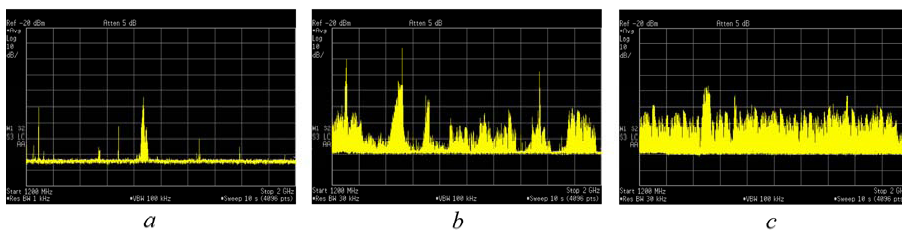
Fig. 1 – Experimental power spectra of microwave oscillations in the multispeed electron beam for different retarding potentials: (a) monoenergetic beam with small braking of electrons; (b) multispeed beam with 20% dispersion of electron velocities with small retarding potential; (c) multispeed beam with large retarding potential

References
1. Granatstein V.L., Alexeff I. High Power Microwave Sources. Artech House, 1987.
2. Dubinov A.E., Selemir V.D. *J. Communications Technology and Electronics*, 47 (2002) 575.
3. Egorov E.N., Hramov A.E. *Plasma Physics Reports*. 32 (2006) 683-694.
4. Kalinin A.Ju., Koronovskii A.A., Hramov A.E. et al *Plasma Phys. Rep*. 31 (2005) 938.
5. Kalinin Ju.A., Hramov A.E. *Technical Physics*. 51 (2006) 558-566

HPEM - 16
Nonlinear Dynamics and Chaos (Invited)

Oral Presentations

Effect of External Magnetic Field on Critical Current for the Onset of Virtual Cathode in Electron Beams

A.E. Hramov, S.A. Kurkin, A.A. Koronovskii

Saratov State University, Saratov, Russia

E-mail: aeh@nonlin.sgu.ru

The report is devoted to the numerical analysis of the effect of the focusing magnetic field on the critical value of electron beam current for the onset of virtual cathode oscillations. Recently, the generators with virtual cathode (vircators) being the sources of high power microwave radiation are the subject of intensive study [1]. The operating principle of vircators is based on oscillation of a virtual cathode in an electron beam with a supercritical value of the current. So, the determination of the critical current value is the real problem of high-power microwave electronics.

We considered a cylindrical waveguide bounded with the grid electrodes as a physical model in our report. The external magnetic field is applied along the longitudinal axis of the waveguide. An axially symmetrical beam without velocity and density modulation at the initial cross-section is injected to the drift tube. We consider two cases: a solid and an annular electron beam. It is shown that the focusing external magnetic field B, the filling factor of electron beam and its velocity, the geometrical parameters of the system and beam are the basic parameters having effect on the critical current. The particle-in-cell method has been used for numerical modeling of non-stationary processes in electron beam injected into drift tube. To simulate the processes the motion equation of any large particle and the Poisson equation have been solved self-consistently.

Fig. 1a shows the normalized critical current of solid electron beam versus the external focusing magnetic field. The values of static electron velocity have been used as parameters of the graphs. It is shown that there is the optimal value B_{opt} of magnetic field providing the minimal value of critical current. One can see that above the value B_{opt} the critical current increases monotonically and approaches the value which is obtained for infinite magnetic field in [2]. The optimal magnetic field B_{opt} depends on the electron beam velocity v/c, where c is the light velocity. The dependence of B_{opt} on v/c is shown in Fig. 1b from which we can see that the optimum external magnetic field increases linearly with the velocity v of the injected electron beam.

The similar results have been obtained from the study of tubular electron beam.

The analysis of the physical processes leads to the conclusion that the observable behavior of the critical current caused by competitive dynamics of longitudinal and transversal motion of electrons in the drift tube. When $B < B_{opt}$ the strength of magnetic field appears to be insufficient to compensate Coulomb repulsion in the electron beam. Therefore, most of the electrons exit the interaction space and land on the walls of the channel. On the other hand, when $B > B_{opt}$ electrons are oushed away from the virtual cathode and exit the drift tube through the injection cross-section. Thus two types of virtual cathode may be distinguished: the transversal virtual cathode ($B < B_{opt}$) and the longitudinal one ($B > B_{opt}$).
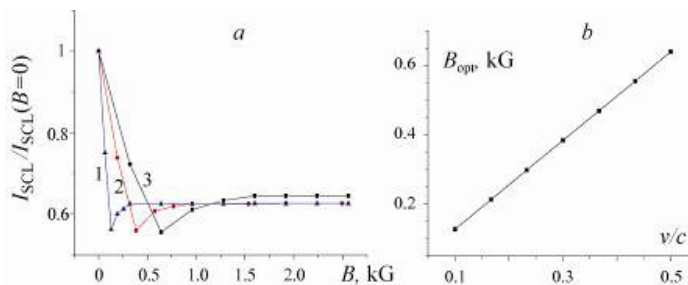
Fig. 1 – (a) The normalized critical current of solid electron beam via the external focusing magnetic field for different velocites v of electron beam in the input of the drift space: 1 – v/c=0.1, 2 – v/c=0.3, 3 – v/c=0.5 (b) the optimum external magnetic field B_{opt} vs electron velocity

References
1. D. Sullivan, J. Walsh, E. Coutsias, in: High Power Microwave Sources, Artech House Microwave Library, 1987, p.441.
2. L.A. Bogdankevich, A.A. Rukhadze, Sov. Phys. Uspekhi 14 (1971) 163.

Nonlinear Dynamics of Relativistic Electron Beam with Virtual Cathode in External Magnetic Field

A.E. Hramov, A.A. Koronovskii, S.A. Kurkin, I.S. Rempen
Saratov State University, Saratov, Russia

E-mail: aeh@nonlin.sgu.ru

The investigation of physical processes taking place in intense beams of charged particles with overcritical current in the regimes with a virtual cathode (VC) is currently of great interest [1-3]. As a number of experimental and theoretical investigations show, such systems with VC are characterized by complex non-stationary dynamics [2-4].

The basic regularities of nonlinear behaviour of VC were mostly analyzed in the context of one-dimensional models of electron beam dynamics with perfect magnetization. Thus the transverse movements of electrons was neglected and the beam motion accepted as one-dimensional [1,3,4].

The assumption of one-dimensional movement of the electron beam in the vircator is correct only when the external magnetic fields are rather strong which sometimes cannot be realized in physical experiment. Every so often the experimental models without any magnetic fields are used, or the magnetic fields are very weak [1-3]. It is well known that the generation power and the spectrum of the output radiation depend strongly from the value of external magnetic field [3,5,6]. Thus the investigation of the influence of external magnetic field upon the non-linear dynamics of electron beam with the virtual cathode seems a very important task.

The proposed report contains the results of numerical investigation of non-stationary non-linear dynamics and pattern forming processes in weakly relativistic electron beam with the virtual cathode. We used a 2D model where the dynamics of the electrons in interaction space was described with the help of particle-in-cell method and for calculation of self-consistent field the numerical integration of 2D Poisson equation by finite difference method was used. The special consideration was given to the influence of external magnetic field on the regimes of chaotic generation of the virtual cathode in the vircator system.

The studied system consists of a piece of waveguide in which we inject a weakly relativistic electron beam with the current exceeding the critical value (for the concrete geometry parameters). Along the axis the homogeneous finite-valued magnetic field is imposed which focuses the beam electrons.

In the framework of the research the regime maps of the vircator system have been calculated in the planes of controlling parameters "beam current – external magnetic field", "geometric parameters – magnetic field", "beam energy – magnetic field", etc. The dependence of the power generated by the vircator on different parameters has been analyzed. On the parameters' planes the regions of regular and chaotic dynamics of VC have been marked. The physical processes taking place in the electron beam that lead to chaos in the output signal have been analyzed. In the last case it is shown that the complication of VC oscillations is connected with the forming and interaction of electron structures in the drift space of electron beam.

References
1. D. Sullivan, J. Walsh, E. Coutsias, "Virtual Cathode Oscillator (Vircator) Theory", in: High Power Microwave Sources, Artech House Microwave Library, 1987, p.441.
2. A.E. Dubinov, V.D. Selemir. "Vircators (Review)" J. Communications Technology and Electronics, **47** (2002) 575.
3. D.I. Trubetskov, A.E. Hramov. "Lectures on Microwave Electronics for Physisists", vol. 2, Moscow, Fizmatlit, 2004.
4. V.G. Anfinogentov, A.E. Hramov, "On the Mechanism of Occurrence of Chaotic Dynamics in a Vacuum Microwave Generator with Virtual Cathode. Radiophysics and Quantum Electronics. **41** (1998) 764.
5. T.J.T. Kwan, H.A. Davis, "Numerical Simulations of the Reditron". IEEE Trans. Plasma Sci. **16** (1988) 185.
6. E.N. Egorov, A.E. Hramov, "Investigation of the Chaotic Dynamics of an Electron Beam with a Virtual Cathode in an External Magnetic Field". Plasma Physics Reports. **32** (2006) 683.

HPEM - 16
Nonlinear Dynamics and Chaos (Invited)

Oral Presentations

Synchronization of chaotic oscillations in microwave systems with overcritical beam current

Roman A. Filatov[1], Alexander E. Hramov[1], Alexey A. Koronovskii[1]
[1]*Faculty of Nonlinear Processes, Saratov State University, Saratov, Russia*

E-mail: alkor@nonlin.sgu.ru

The analysis of the chaotic synchronization phenomenon in various nature systems becomes an area of active research of nonlinear science [1]. The chaotic synchronization regime has been observed in a whole series of coupled physical, biological, physiological, chemical and other systems [2]. At present, several different types of chaotic synchronization are known such as generalized synchronization [3], phase synchronization [2], lag synchronization [4], complete synchronization [5] and time scale synchronization [6], which generalizes the above-listed types of chaotic synchronization.

Most research dealing with chaotic synchronization was performed on systems with low number of degrees of freedom and for the sample models of spatially extended systems (chains and networks of coupled nonlinear chaotic oscillators, coupled Ginsburg-Landau and Kuramoto-Sivashinsky equations and others). The study of chaotic synchronization in the spatially extended systems was experimentally and theoretically carried out for the nonlinear optical [7] and chemical [8] systems and for the low-frequency oscillations in plasma discharge tubes [9]. It was shown that while introducing the unidirectional or symmetric coupling in the distributed systems they demonstrate the various types of chaotic synchronization, namely the complete, lag and generalized synchronization. However, the chaotic synchronization in the locally coupled microwave beam-plasma systems is not examined in detail until now. At the same time research of chaotic synchronization regimes in spatially extended beam-plasma microwave systems seems to be important because of its applications dealing with data transmission and control of chaotic oscillations in microwave electronics systems.

The present work deals with research of chaotic synchronization in coupled beam-plasma microwave systems with overcritical current – Pierce diode fluid models [10], which seems to be interesting as an important model of beam-plasma systems showing various types of chaotic behavior.

In this work the fluid model of Pierce diode is briefly discussed, the complete synchronization and time scale synchronization of mutual coupled beam-plasma systems are described. We also discuss the generalized synchronization regime in unidirectionally coupled spatially extended beam-plasma systems and describe the method of modified system applied to the discussed model. In conclusion, we summarize the main obtained results.

References
1. S. Boccaletti, J. Kurths, G. Osipov, D.L. Valladares, C. Zhou, "The synchronization of chaotic systems", Physics Reports, vol. 366, 2002, p. 1.
2. A. Pikovsky, M. Rosenblum, J. Kurths, Synhronization: a universal concept in nonlinear sciences, Cambridge University Press, Cambridge, 2001.
3. N.F. Rulkov, M.M. Sushchik, L.S. Tsimring, H.D.I. Abarbanel, "Generalized synchronization of chaos in directionally coupled chaotic systems", Phys. Rev. E 51, vol. 2, 1995, p. 980.
4. M.G. Rosenblum, A.S. Pikovsky, J. Kurths, "From phase to lag synchronization in coupled chaotic oscillators", Phys. Rev. Lett., vol. 78, 1997, p. 4193.
5. L.M. Pecora, T.L. Carroll, G.A. Jonson, D.J. Mar, "Fundamentals of synchronization in chaotic systems, concepts, and applications", Chaos, vol. 7, 1997, p. 520.
6. A.E. Hramov, A.A. Koronovskii, "An approach to chaotic synchronization", Chaos, vol. 14, 2004, p. 603.
7. P. L. Ramazza, U. Bortolozzo and S. Boccaletti, "Experimental synchronization of spatiotemporal chaos in nonlinear optics", Phys. Rev. E, vol. 73, 2006, 036213.
8. M. Hildebrand, J. Cui, E. Mihaliuk, J. Wang and K. Showalter, "Synchronization of spatiotemporal patterns in locally coupled excitable media", Phys. Rev. E, vol. 68, 2003, 026205.
9. E. Rosa, W. Pardo, C. Ticos, J. Walkenstein, M. Monti, "Phase synchronization of chaos in a plasma discharge tube", Int. J. Bifurcation and Chaos, vol. 10, 2000, 2551.
10. J. Pierce, Limiting currents in electron beam in presence ions, J. Appl. Phys., vol. 15, 1944, p. 721.

Analytical and numerical study of chaotic generation in vircator with preliminary modulation of electron beam

I.S. Rempen, A.E. Hramov, A.A. Koronovskii

Saratov State University, Saratov, Russia
E-mail: aeh@nonlin.sgu.ru

This report is devoted to one of the vircator systems with controlled characteristics of output radiation – the scheme with input resonator system (vircator-klystron) which is suggested in [1]. The investigations have shown that this system gives opportunities of essential increase of efficiency and output power and narrowing of power spectrum of generated signal. The work [2] considers the scheme with the input resonator tuned to the frequency of virtual cathode (VC) oscillations and the circuit of external delaying feedback (vircator-klystron with external feedback). In our work we consider the problem of influence of initial modulation of the relativistic electron beam upon virtual cathode oscillations. The modulation is realized by setting a resonator at the input of vircator. The resonator is driven by external source of microwave signal (for example, relativistic magnetron). The possibility of modulation of relativistic electron beams is analysed in [3].

The following scheme is considered. The working chamber consists of a piece of cylindrical waveguide, into which the monoenergetic annular electron beam is injected through the input highly regenerative cavity. The beam current exceeds the limit vacuum current and thus VC is forming in the drift space. The beam reflected from the virtual cathode penetrates the resonator and drives it. The external harmonic signal coming from the low-power source (in comparison with microwave vircator) is also driving the resonator providing the necessary modulation depth of the initial electron beam. The resonance frequency of the input resonator is changed in wide scope from the autonomous frequency of the virtual cathode (near $f_{VC} \approx 8$ GHz in this case) up to double autonomous frequency $2f_{VC}$. The resonator has been modulated by resolving of non-stationary equation of stimulation of resonant system [4].

The numerical modeling shows that the increase of modulation depth with the frequency close to autonomous frequency f_{VC} of virtual cathode oscillation allows to improve the spectral characteristics of output radiation and to derive generation similar to single-frequency one. The prior modulation helps to shorten the duration of the transition process and to stabilize the frequency of current oscillations in the region of VC. We have also studied the influence of prior modulation (first of all, the influence of the frequency) on the different regimes of virtual cathode dynamics and spectral characteristics of the output signal of vircator with resonator. On Fig. 1 the power spectrums of vircator generation within different tuning of input resonator are shown. The most interesting effect is observed when the external resonator is tuned to the frequency $f_s=2f_{VC}$. In this case the system dynamics is similar to regular (it can be seen from the very low noise background in output power spectrum) and in the generation spectrum one can see low-powered frequencies f_{VC}, $4f_{VC}$ and a high-powered component $2f_{VC}$.

This means that the influence of external modulation at the frequency equal to the doubled autonomous frequency of the virtual cathode leads to synchronization of virtual cathode oscillations on the doubled frequency. This regime is very interesting in view of possibility of increase of frequency of microwave radiation generated by vircator system.
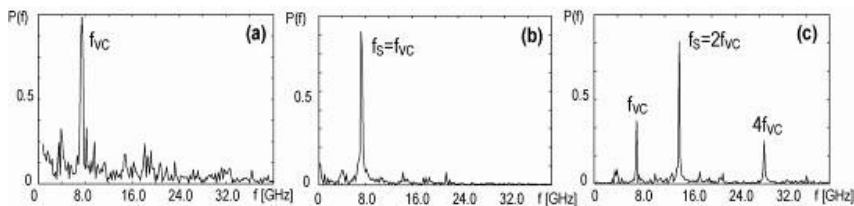
Fig.1: Output power spectra: (a) autonomous oscillations of VC; (b) $f_s = f_{VC}$ (c) $f_s = 2f_{VC}$

References
1. W. Jiang, K. Masugata, K. Yatsui "Mechanism of microwave generation by VC oscillation', Phys. Plasmas. vol.2, 1995
2. V. Anfinogentov, A. Hramov, "Oscillation Conditions of the Vircator Klystron with External Delayed Feedback: A Computer Simulation", J. Commun. Techn. Electron. Vol. 46, 2001
3. M. Friedman, V. Serlin, "Self-modulation of an intense relativistic electron beam", Phys. Rev. Lett.. vol.55, 1985
4. D. Trubetskov, A. Hramov. Lectures on microwave electronics for physicists. Vol. 1. Fizmatlit, Moscow, 2003.

HPEM - 16
Nonlinear Dynamics and Chaos (Invited)

Oral Presentations

Influence of Gas Ionization on Oscillations in Non-Relativistic Electron Beam with Virtual Cathode

R.A. Filatov, A.E. Hramov, Yu.A. Kalinin, A.A. Koronovskii
Saratov State University, Saratov, Russia

E-mail: filatov_ra@mail.ru

Microwave radiation sources using an electron beam with a virtual cathode as an active media are actively studied at present [1]. One important task in the investigation of the intensive electron beams with virtual cathode is consideration of the positive ion influence on the microwave oscillations in the electron beam. The positive ions appear due to the impact ionization of neutral gas by the electron beam with the virtual cathode. It is well known that electrons ionize most efficiently while its energy is sufficiently low (near 100 eV). This means that consideration of ionization processes in the electron beam with the virtual cathode is of great importance. Present report deals with the theoretical study of the positive ion influence on the oscillatory processes in the non-relativistic electron beam with the virtual cathode in a retarding field.

The investigation has been carried out in terms of PIC simulation [2]. The simulation shows that presence of neutral gas leads to the suppression of the virtual cathode oscillations and to the termination of the microwave generation. This is related with a neutralization of the virtual cathode space charge by the positive ions. Next the ions drift away, causing positive space charge to decrease and conditions for the virtual cathode formation arise again. Then this process repeats. As a result the output signal represents the sequence of the chaotic radiopulses. Fig. 1 shows the dependence of the output signal (curve 1) and the total positive space charge density in the working chamber (curve 2). It is easy to see than during the generation the density of the ion layer rises till the termination of the generation (maximums on the dependence). Then when the density reaches certain level (marked by the dashed line) the generation appears again in the system. This phenomenon has been investigated in terms of effective Pierce parameter modulation.

The results of numerical simulation are proved by the experimental research on the model of the non-relativistic vircator.
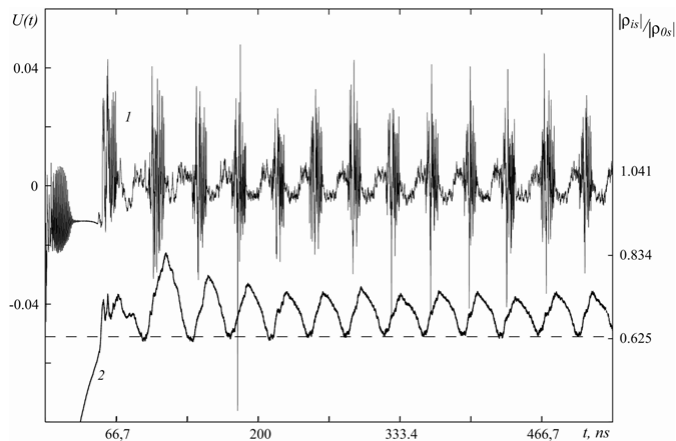
Fig. 1 – Output signal and total positive space charge in the gas-filed drift space

References
1.　V.L. Granatstein, I. Alexeff, High Power Microwave Sources, Artech House Microwave Library, 1987.
2.　R.A. Filatov, Yu. A. Kalinin, A.E. Hramov, D.I. Trubetskov. Radiophysics and Quantum Electronics. 2006, **49**(10) 769-778.

Pulsed Wakefield Excitation in Dielectric Waveguide by a Sequence of Short Bunches of Relativistic Electrons

V. A. Kiselev, A. F. Linnik, V. I. Mirnyj, I. N. Onishchenko, G. V .Sotnikov, V. V. Uskov
National Science Center "Kharkov Institute of Physics & Technology", Kharkov, Ukraine

E-mail: onish@kipt.kharkov.ua

Experimental investigations of intense wakefield impulses excitation in dielectric structures by a sequence of short bunches of relativistic electrons are presented. Experiments were performed using a sequence of bunches from the linac «Almaz-2» (energy 4MeV, number of bunches 6.10^3, diameter 1cm, duration 60 ps each, distance between bunches 350 ps, number of electrons in each bunch 10^9), injected into a dielectric structure of length 70 cm, made from Teflon ($\varepsilon=2.1$, tg$\delta=1.5\ 10^{-4}$), placed inside metal waveguide of round or rectangular cross-section. Researches on multibunch and multimode regimes have been carried out. For the semi-infinite case the restriction of a number of electron bunches, which wakefields are added up, was determined and explained as a result of wakefield removal from the injection plane with a group velocity. To increase the number of such bunches a resonator concept was proposed and explored that allowed to obtain higher peak amplitude. It was also shown that for the case of rectangular geometry the equispaced transversal modes were excited and due to their summation the amplitude of total excited wakefield increased greatly compared to the only principal mode excited. Energy losses of electron bunches up to 12% on wakefield excitation and corresponding RF power of excited radiation were measured. The measured frequency spectrum of the excited wakefield agreed with theoretically predicted spatial structure of wakefield in the form of a periodic sequence of opposite sign impulses.

HPEM - 16
Nonlinear Dynamics and Chaos (Invited)

Oral Presentations

Cellular Automata Model of Surface Discharge Dynamics

A.S.Adalev[1], N.V.Korovkin[1], M.Hayakawa[2], D.I.Iudin[3], V.Yu.Traktengerts[4]

[1]Saint-Petersburg State Polytechnic University, Saint-Petersburg, Russia
[2]The University of Electro-Communications, Tokyo, Japan
[3]Radiophysical Research Institute, Nizhniy Novgorod, Russia
[4]Institute of Applied Physics, Nizhniy Novgorod, Russia

E-mail: Alexei@Adalev.com, Nikolay.Korovkin@gmail.com

Despite the fact that the discharge over a dielectric surface is a widely observed and used phenomenon, the methods of its mathematical description and simulation are not sufficiently evolved. Rare papers related to creeping surface discharge use models which are similar to that proposed in [1] for modeling streamer evolution in gas. They treat just a single streamer stem and, moreover, all the attention is paid to the move of the streamer head. However, since streamer phase in the surface discharge development is rather short [2] and is replaced by the leader one very fast, a nonlinear conductance of a streamer channel behind the head plays the main role in the surface discharge.

In the present work the initially complex and nonlinear problem of creeping discharge modeling is divided into several problems of less complexity that may be solved separately at some time step. The discharge area (above a dielectric sheet separating a metal needle from a ground plain electrode)is presented as a system of gas sphere cells covering the dielectric. The discharge tree (conducting cluster) is represented by a nonlinear circuit consisting of capacitances, nonlinear conductances, and controlled sources. The latter simulate field potential of the needle electrode and of the free charge located in the neighboring cells. The coefficients for the controlled sources and cell capacitances are determined from the results of static field calculation.

In the model, cell conductance is strongly correlated to the density of electrons in the cell. The effects of electron drift, impact ionization, and photoionization are involved into the conductance model. The physical parameters of the latter two processes are deduced from the experimental data available in the literature. Further improvement of the conductance model is discussed in respect to plasma heating up to the temperatures that enough for the streamer-to-leader transition.

Cell initiation (attaching to the existing cluster) is performed if the initiation threshold of 26 kV/cm is reached in the cell. This ensures a gradual rise in the cell conductivity due to electron multiplication in air. Competition strategy is used for cell initiation when the probability of the latter depends not only on the potential of the cell but also on the potentials of the other candidates for initiation. Following the models of "irreversible growth" (e.g. [3]), the power law of probability dependence on electric field intensity was chosen.

In addition to discharge patterns which created to be very similar to experimental Lichtenberg figures, the model allows us to determine such local properties of the discharge as current, voltage drop, loss, field and charge distribution. This allows us to determine characteristics of electromagnetic radiation which is very important for EMC and also gives us an additional instrument for studying discharge physics. Moreover, the model may also easily take into consideration geometric features of electrodes and dielectric, so that we can examine their effect on the discharge as well.

References
1. I. Gallimberti, "A computer model for streamer propagation," J. Phys. D: Appl. Phys., vol. 5, pp.2179–2189, 1972.
2. E. M. Bazelyan and Y. P. Raizer, Spark discharge. New York: CRC Press LLC, 1998.
3. N. Femia, L. Niemeyer, and V. Tucci, "Fractal characteristics of electrical discharges: experiments and simulation," J. Phys. D: Appl. Phys., vol. 26, pp. 619–627, 1993.

Overview of HEMP and HPEM Standards

P. R. Barnes

Consultant for the
Metatech Corporation
Goleta, CA, USA

E-mail: barnespr@netcommander.com

This paper is intended to indicate the significant amount of standardization work that has been accomplished to protect electronic equipment and systems from high-power electromagnetic (HPEM) threats. HPEM threats include high-altitude electromagnetic pulse (HEMP), as well as intentional electromagnetic interference (IEMI) threats. Much of the earlier HEMP standardization work was performed for the protection of military systems such as the MIL-STD's used in the US, the German VG-Standards, and the STANAG standards created for NATO. These standards describe the HEMP environment, equipment tests, and installation practices. For example, the standard MIL-STD-188-125A specifies the design requirements for certain ground based installations. Many of the HEMP military standards are not available for open publication.

In the late 1980s, the International Electrotechnical Commission (IEC) began to development HEMP standards for commercial equipment. The HEMP standardization work was assigned to Subcommittee 77C (SC 77C) under the parent committee TC 77, Electromagnetic Compatibility (EMC). IEC standards have been published on the HEMP environment, protection methods, and tests to demonstrate HEMP immunity of commercial equipment. In June of 1999, after 10 years of intense activity, the scope of the work for SC 77C was expanded to include other HPEM man-made threats. SC77C's statement of work now covers standards in the field of electromagnetic compatibility to protect civilian equipment, systems and installations from threats by man-made high power phenomena including the electromagnetic fields produced by nuclear detonations at high altitude. The work by SC77C has followed the basic approach used to develop EMC standards by TC 77 and it has used existing IEC EMC standards wherever possible to minimize cost and duplication.

As of January 2008, SC 77C has published 17 documents: 13 International Standards and 4 IEC Technical Reports. Additional work is currently underway to standardize methods to protect distributed infrastructure systems against HEMP and to conduct HPEM system-level assessments. In addition, work on a HPEM simulator compendium similar to an earlier IEC HEMP simulator compendium is underway.

The electric power and communications infrastructures are important geographically large networks that are being addressed by the IEC as well as other standards organizations. The Telecommunication Standardization Sector of the International Telecommunication Union (ITU-T) has recently formed a working group to consider HEMP protection recommendations and standards for information and communications technologies. This group has a liaison with SC77C.

HEMP and HPEM standards have the potential of mitigating electromagnetic threats to the important civil infrastructure including power, communications, water, etc. These standards are also important for military procurement of commercial off the shelf equipment.

HPEM - 17
EM Standards & Specifications #1 (Invited)

Oral Presentations

NATO EMP Standards

R. A. Pfeffer[1], J. H. O'Kuma[2]

[1]*US Army Nuclear and Combating Weapons of Mass Destruction Agency*
Springfield, VA, USA
[2]*Survivability, Vulnerability and Assessment Directorate*
US Army White Sands Missile Range, NM, USA

E-mail: robert.pfeffer@us.army.mil

The North Atlantic Treaty Organization (NATO) continues to have a long-standing interest in nuclear-induced electromagnetic pulse (EMP) and its effects on platforms and systems. Since the end of World War II, considerable efforts were conducted to understand the governing physics and air chemistry that explained the electromagnetic environment now known as EMP. Additional efforts focused on predicting its coupling to platforms and systems, quantifying its potential effects on biological, mechanical and electrical elements of those platforms and systems, and finally developing cost-effective options that protect those operational platforms and systems against various EMP forms. Today, NATO EMP standards are used to establish protection criteria for the procurement of critical operational platforms and systems.

This unclassified paper will follow some of the important steps that led to the development of today's NATO military EMP standard. Two documents will be highlighted: NATO File No. 1460-3 EMP Engineering Practices Handbook, and NATO Standardization Agreement (STANAG) 4145, Nuclear Survivability Criteria for Armed Forces Material and Installations. Originally written in October 1977, the Handbook is intended to be used by Host Nations in the design, construction, and finally maintenance of important NATO facilities. STANAG 4145 followed the Handbook. It is the October 1979 coversheet for Allied Engineering Publication (AEP) 4 of the same title. AEP-4 Edition 4 now consists of three Annexes: ANNEX A (LAND), ANNEX B (NAVY), and ANNEX C (AIR). Edition 1 is dated April 1975.

The paper will conclude with comments on the unique challenges provided by the growing use of high-tech commercial-off-the-shelf (COTS) items in the procurement of NATO military platforms and systems. Additionally, several NATO initiatives are discussed that are intended to improve new equipment design, increase equipment protection from a wide range of electromagnetic environments (including EMP), and reduce overall acquisition costs.

Considerations for Deriving Standardized Box-Level EMP Conducted Pulse Immunity Requirements

W. J. Scott[1], M. R. Rooney[2]
[1]*Northrop Grumman Corporation, USA*
[2]*Defense Threat Reduction Agency, USA*
E-mail: walter.scott@ngc.com

This presentation discusses key technical and programmatic factors that need to be considered in deriving box-level conducted pulse immunity requirements for qualifying subsystems and equipment to withstand the effects of wideband pulses such as the nuclear high-altitude electromagnetic pulse (EMP). The factors to be discussed include system implications of the box-level spec; bulk vs. single wire current test considerations; wave shape considerations; pros and cons of multiple pulse testing; cable shield vs. core wire testing; equipment operational modes and configurations; ways to avoid excessive hardening; and programmatic considerations. Recommendations are provided for criteria for use in developing an affordable approach based on analysis of technical and programmatic factors discussed in the presentation.

The overall goal in deriving box-level EMP test specifications is to establish a lower bound on strength of each box in a system such that system designers can allocate EMP protection at the system level to ensure that the boxes in a system are survivable. Ideally, one is looking for the highest specification level that most equipment can withstand without the need for adding additional EMP protection at the box level. A further objective is to reduce system costs and hardening requirements while incurring minimum hardening costs.

Given these constraints, individual countries and international standards organizations have developed military and commercial standards that establish recommended test requirements and limits that may be used to determine lower-bound EMP strength of box-level equipment to be installed into military systems and platforms. In the U.S., MIL-STD-461F, Requirements for the Control of Electromagnetic Interference Characteristics of Subsystems and Equipment, is cited in military procurements to provide a uniform basis for establishing a lower-bound on immunity or susceptibility of electronic subsystems and equipment against conducted cable currents resulting from an EMP event. This presentation provides a technical basis for tailoring box-level conducted immunity requirements such as those in U.S. MIL-STD-461F, UK Defense Standard 59-41 and other commercial immunity standards to minimize the risk that the system-level protection design will result in equipment failures or negative strength vs. stress design margins during an EMP system-level validation test.

References
1.   G. Morgan et al, "Considerations for Preparing a Box-Level Specification," Rockwell International, January 5, 1984.

HPEM - 17
EM Standards & Specifications #1 (Invited)

Oral Presentations

Progress from 2006 to 2008 in the Development of HEMP and HPEM Standards by the International Electrotechnical Commission (IEC)

W. A. Radasky[1], R. Hoad[2]

[1]*Metatech Corporation, Goleta, California USA*
[2]*QinetiQ, Farnborough, UK*
E-mail: wradasky@aol.com

The International Electrotechnical Commission (IEC) headquartered in Geneva, Switzerland has been working since 1989 to produce standards and reports to describe the threats of and protection methods for the high-altitude electromagnetic pulse (HEMP) and other high power electromagnetic (HPEM) threats such as intentional electromagnetic interference (IEMI). This presentation will provide a short background for those not familiar with the IEC and will review the work that has been performed in the past two years in detail.

At the present time IEC Subcommittee 77C (SC 77C) has produced 17 publications covering both HEMP and HPEM. In addition, SC 77C is responsible for the maintenance of 2 additional standards dealing with protection methods. The HEMP work began in 1989 and has continued to the present time. In 1999 the work of SC 77C expanded to cover the threats of man-made high power electromagnetic fields with a focus on the protection from electromagnetic weapons designed to interfere with commercial equipment and systems. Three recent publications have dealt with these subjects:

- IEC 61000-1-5: High power electromagnetic (HPEM) effects on civil systems
- IEC 61000-2-13: High power electromagnetic (HPEM) environments – Radiated and conducted
- IEC 61000-4-33: Measurement methods for high power transient parameters.

The presentation will describe the organization, membership and operation of SC 77C and will emphasize the coordination of the HEMP and HPEM work with the normal EMC work of the IEC. The current work program, including the maintenance of published standards and new projects that have been approved by the National Committees of the IEC will also be discussed including:

- IEC 61000-4-35: High Power Electromagnetic (HPEM) Simulator Compendium
- IEC 61000-5-8: System-level Susceptibility Assessments for HEMP and HPEM
- IEC 61000-5-9: HEMP Protection Methods for the Distributed Civil Infrastructure

In addition to the documents under development, this presentation will discuss several new developments. One is the active liaison of IEC SC 77C with ITU-T. ITU-T is developing a new set of recommendations dealing with the protection of telephone central offices against the threats of HEMP and electromagnetic weapons. Another issue is the need to develop an approach to determine the measurement uncertainties for all IEC SC 77C test methods. There will also be discussion of the future plans for maintenance of existing IEC SC 77C publications.

In conclusion the presentation will provide information for those who may be interested in participating in the future work of IEC SC 77C.

The International HEMP Immunity Test Standard for Equipment and Systems – Development and Maintenance

P. R. Barnes

Consultant for the
Metatech Corporation
Goleta, CA, USA

E-mail: barnespr@netcommander.com

The International Electrotechnical Commission (IEC) is responsible for international standards that are used around the world and it is considered the authority for standards in electrical and electronics engineering. It is the worldwide leader in the development of commercial electromagnetic compatibility (EMC) standards. Many of these standards are used by the European Commission for the European market.

The IEC Technical Subcommittee SC77C is developing standards and technical reports for a wide range of electromagnetic transients including high-altitude electromagnetic pulse (HEMP) threats as well as many categories of Intentional Electromagnetic Interference (IEMI). This work resulted in a HEMP immunity test standard for equipment and systems which was published as an International Standard in 2001. This International Standard, IEC 61000-4-25, describes tests that are intended to demonstrate the immunity of electrical and electronic equipment when subjected to HEMP radiated and conducted electromagnetic disturbances.

HEMP radiated and conducted transient waveforms consist of a wide range of decaying exponential pulses and damped sinusoids. Prior to the development of the immunity test standard, the IEC published earlier HEMP standards that described the radiated and conducted electromagnetic environments. Another HEMP standard described the radiated and conducted waveforms for locations within structures with various shielding and surge protection. These interior standard HEMP waveform classifications were used as a guide for the development of the immunity tests. For civilian standards, it is important to minimize the cost of complying with the immunity requirements. Therefore, standard EMC tests have been specified, as appropriate, to demonstrate HEMP immunity. For some HEMP waveforms, standard tests were not available and specialized tests were developed. These tests included pulses with very large amplitudes and the late-time HEMP conducted environment.

IEC standards are revised as necessary during periodic maintenance cycles. In this manner, standards are kept up to date and are harmonized with other standards. The first revision of IEC 61000-4-25 is scheduled for 2010. This paper is intended to provide the background and rationale for the development of the immunity test standard and to discuss the possible revisions for this standard in the near future.

HPEM - 17
EM Standards & Specifications #1 (Invited)

Oral Presentations

Improvement process of an old standard: birth of the 61000-4-18

J. Delaballe[1], M. Ianoz[2] and W. Radasky[3]

[1]*Schneider Electric, Grenoble, France*
[2]*Honorary Professor, Swiss Federal Institute of Technology, Lausanne, Switzerland*
[3] *Metatech Corp., Goleta, CA, USA*
E-mail: michel.ianoz@epfl.ch

The immunity tests pertaining to transient phenomena have been developed in the 1990s and were written in the standard 61000-4-12, entitled "Oscillatory waves immunity tests". The standard described two tests : the ring wave and the oscillatory damped wave, shown in fig. 1.

A first amendment was suggested already in 1995, at the requirement of the IEC SC 17A & SC 17C, in order to increase the maximum frequency of the oscillatory wave up to 50 MHz needed for the tests of secondary systems of high-voltage switchgear and controlgear [1]. Discussions went on in WG3 and then in WG11 of SC77B, but nothing happened, until 1999, when the necessity for an amendment was again motivated now by:
- a request from SC77C, which needs the test at these frequencies for the HEMP;
- the need to provide a test which can reproduce induced currents in devices installed in GIS; the typical shape of such currents due to switches in GIS is that of a damped wave with frequencies up to 50 MHz (ref. [2] and fig. 2).
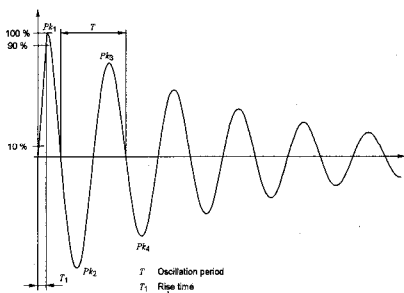
Fig. 1 - Damped oscillatory wave
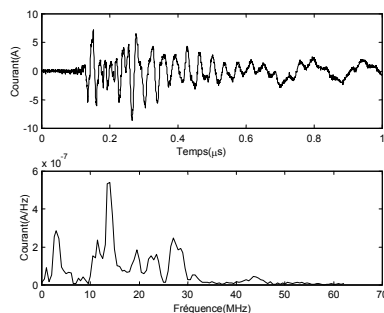
Fig. 2 - Current measured on the sheath of the voltage transformer cable on the LV side in a 125 kV GIS

In October 2000, the WG11 convener requested experts to deal with HEMP and GIS phenomena, as WG11 had only EMC experts. On September 3, 2004, a Questionnaire to the NCs was send asking them to decide between two possibilities:
1) maintain the old 4-12 standard, with two types of wave, but extending the frequency of the damped oscillatory wave to 30 or 50 MHz;
2) two separate standards, the old 61000-4-12, describing only the ring wave and a new one for the damped oscillatory wave.

The majority of the NCs choose the second option and a JWG 77B/77C was set up, which wrote a new 61000-4-18 standard, introducing a damped oscillatory wave with two wave types:
- a slow wave with two frequencies 100 kHz and 1 MHz;
- a fast wave with 3 frequencies: 3, 10 and 30 MHz.

In order to permit the manufacturers easier constraints for the generator the upper frequency was limited to 30 MHz. This new standard was issued in 2006.

The paper will present the main stages which led to the production of this new standard and its main technical parameters.

References
1. IEC 77B/WG3(Delaballe)09/95.
2. A. Eriksson et al., «Relay protection interference environment during normal operating conditions compared to IEC 1000-4-4/IEC 255-22-4», 1998 CIGRE Session, Paris, Group 36 «EMC in Power Networks», paper 36-301.
3. IEC 77B/425A/Q.

System-level Susceptibility Assessments for High-altitude Electromagnetic Pulse (HEMP) and High Power Electromagnetics (HPEM)

A. Wraight[1], M. Bäckström[2], R. Barnes[3], R. Hoad[1], W. Rasdasky[4],
W. Scott[5]

[1]*QinetiQ, Farnborough, England*
[2]*Saab Communication, Linköping, Sweden*
[3]*Consultant, Harrogate, TN, USA*
[4]*Metatech Corporation, Goleta, CA, USA*
[5]*Northrop Grumman Corporation, Lorton, VA, USA*
E-mail: awraight@QinetiQ.com

This paper discusses the content of a new document being developed by the International Electrotechnical Commission (IEC) Sub-committee 77C who are working on the development of civilian standards for the protection of infrastructure and systems to the effects of High-altitude Electromagnetic Pulse (HEMP) and High Power Electromagnetic (HPEM) environments. The document (to be published as IEC 61000-5-9 [1]) describes an assessment methodology for the assessment of equipment, sub-systems and systems to the effects of HEMP and HPEM and includes detailed information and guidance on the following phases:

• Sub-systems and equipment characterization
Critical aspects of the system are identified such that the impact of any HEMP or HPEM induced effect can be correctly assigned as either immunity or susceptibility during the susceptibility assessment phases. Also, areas of potential weakness are identified based upon information about similar systems or technology types. During this phase it is useful to gather immunity and/or susceptibility information that may be relevant.

• System analysis
The purpose of the system analysis phase is to identify critical sub-systems/equipment, system configurations and operational modes that should be assessed through a combination of low-level and high-level tests to estimate a system's susceptibility to the HEMP and HPEM environments.

• System test
This phase describes equipment and/or system level testing that can be used to provide information on the system's overall protection against a HEMP or HPEM environment. Detailed information and guidance on the application of low-level and high-level testing required to inform system-level susceptibility is also given.

• Susceptibility assessment
The purpose of this phase is to evaluate the test data including any observed effects such as equipment upset or damage that occurred during the testing to determine any degradation to normal system operational performance.

The document also includes a discussion on the use of reverberation chambers to characterize equipment susceptibility. This is a method that potentially reduces the time taken to identify frequencies at which systems are susceptible and seeks to focus high-level testing to environments that are likely to cause an effect.

The document will conclude with example system-level assessments for HEMP and HPEM separately.

References
1.   IEC 61000-5-9: System-level Susceptibility Assessments for HEMP and HPEM, CDV, June 2007

HPEM - 17
EM Standards & Specifications #1 (Invited)

Oral Presentations

Development of a New IEC Specification Dealing with HEMP Protection Methods for the Distributed Infrastructure

W. A. Radasky, *Metatech Corporation, Goleta, California USA*
E-mail: wradasky@aol.com

Following the important work of the U.S. Congressional EMP Commission [1] regarding the threat of HEMP to the United States and in particular to the electric power system, the International Electrotechnical Commission (IEC) decided to begin work within SC 77C to develop protection methods for the distributed infrastructure. The term "distributed" is intended to describe the problem of widespread connected civil systems that could be simultaneously illuminated by the electromagnetic pulse from a high-altitude (above 30 km) nuclear burst. This is a different problem than protecting a single facility against HEMP, as the impact of simultaneous "upsets" can create significant operational effects in many of the infrastructures. An example of the large area coverage due to the early-time HEMP is shown in Fig. 1. It is noted that the difference in time of arrival of the HEMP transient over the illuminated surface of the Earth is only 4.4 ms, which is much less than the time of a single power cycle (16.7 ms in the United States).

Fig. 1 – Area covered by the early-time HEMP from a 170-km burst over the United States

The draft specification, IEC 61000-5-8, is divided into 10 clauses including:
- Scope
- Normative references
- General introduction
- Definitions
- Description of the distributed infrastructure
- Spatial variation of HEMP environments
- Implications for HEMP coupling to long lines
- Relation of HEMP disturbances to natural EM environments
- Protection strategy
- Protection methods
- Bibliography

The presentation will review the status of the work thus far including the contributions of the members of the IEC project team: Mr. Richard Hoad (GB), Mr. Lars Hockstra (DE), Dr. Armin Kaelin (CH), Mr. John Kappenman (US), Dr. Eung Jo Lee (KR), Dr. Daniel Nitsch (DE), Dr. William Radasky (US), Dr. Frank Sabath (DE) and Mr. Atsushi Wada (JP).

References

1.   William R. Graham, Chairman, "Report of the Commission to Assess the Threat to the United States from Electromagnetic Pulse (EMP) Attack," Volume 1: Executive Report, 2004.

High-Power Electromagnetic (HPEM) Simulator Compendium

Frank Sabath[1], Mats Bäckström[2]

[1] *Bundeswehr Research Institute for Protective Technologies and NBC-Protection, D-29623 Munster, Germany*
[2] *Saab Communication, SE-58188 Linköping, Sweden*

...

E-mail: FrankSabath@bwb.org

The last decade has seen tremendous progress in the understanding of the threat of narrowband and ultrawideband environments. The theoretical and experimental investigations of effects caused by High-Power Electromagnetic (HPEM) fields resulted in the development of a set of environment waveforms of interest as described in IEC 61000-2-13. As HPEM, causing damage or failures in electronic parts of critical systems and devices, can result in technical or financial disasters as well as to injuries or the loss of life, there is a need for industry to test their equipment and systems to these IEMI threats.

Due to this development IEC TC 77C started to work on a technical compendium that provides information about existing simulators that could be used to simulate HPEM environments. In addition to characteristic parameters of various simulators the final document will indicate their applicability as test facilities and validation tools for IEC SC 77C immunity test requirements. In the sense of this specification, the group of HPEM simulators consists of narrowband microwave test facilities and ultrawideband simulators for radiated fields.

This talk briefs on the current status of this project. It starts with an introduction to the field of HPEM immunity testing and a presentation of the overall schedule of the IEC 61000-4-35 project. A general description scheme for simulators that can be used for HPEM radiating testing will be introduced in the main part of the talk. In addition to the technical characterization, the scheme addresses more commercial aspects such as availability, costs and operational status. The introduced scheme will be exemplified by a collection of datasheets describing narrowband, wideband and ultrawideband facilities and simulators that are operational or could be made available for use by the international community.

Protecting Telecommunications and Data Centres from Electromagnetic Attack: The Work of ITU-T SG5 Q15

D. J. Carpenter[1], H. Sekiguchi[2], T. Tominaga[3]
[1]*BT Design, Ipswich, United Kingdom*
[2]*NICT, Tokyo, Japan*
[3]*NTT, Tokyo, Japan*
...
E-mail: darren.carpenter@bt.com

The rapid adoption of services based upon the Internet Protocol (IP) has transformed many aspects of everyday life: we are all now used to using the internet to search for and purchase flights and rental cars; to shop for almost everything from DVDs to groceries; to organise our personal finances and investments; and to do many other things.

The adoption of IP has had many other impacts, equally transformative but perhaps less visible. One example is that currently underway within the telecommunications industry, where rapid technological convergence between 'traditional' telecoms and IP-based hardware is currently eroding the demarcation between the role of the traditional central office (with its switching and transmission functionality) and the data centre (with its IP routing functionality).

Almost every aspect of the speed of this transformation has taken many observers and planners by surprise. The development of broadband access services is a case in point, where customer adoption has consistently far exceeded supplier expectations in every market. IP services have become an essential part of the way that individuals organise and conduct their lives, that businesses attract and interact with customers; and that governments provide essential services. IP therefore has become of fundamental importance to the function of the world's most developed economies. As a result, the fundamental resilience of the telecommunications infrastructure that enables access to IP-based services has become a key issue to many policy makers.

In 2005, ITU-T Study Group 5 (SG5) started work on the preparation of guidelines designed to protect key telecommunications centres from disruption due to electromagnetic effects. This work was scoped to include protection from lightning damage, from normal Electromagnetic Compatibility (EMC) issues (both being within the sphere of expertise of SG5) and also the effects of High-Altitude Electromagnetic Pulse (HEMP) and High Power Electromagnetic (HPEM) attack. The desire was to produce a document set that presented the non-technical/non-expert reader with a guide to existing technical documentaion: these being, for lightning and EMC, documents from the ITU's K-Series of Recommendations (*Protection from Interference*); for HPEM and HPEM, documents from the IEC TC77 (*Electromagnetic Compatibility*) SC77C (*High Power Electromagnetic Transient Phenomena*).

This presentation shall introduce the ITU, the ITU-T and SG5 to the audience. It shall then describe the documentation set that this work will produce. The key learning points in the HPEM and HPEM domain shall then be presented, gained from applying the documents of IEC TC77 SC77C to the rapidly converging telecoms-IP domain.

Fast Current Impulse Test For Wind-Turbine Blades

J. Montanyà[1], P. Clapers[1], B. Hermoso[2], V. March[1], G. Solà[1], A. Illa[3], D. Romero[1], D. Aranguren[1] and J.R. Hermoso[1]

[1]*Technological University of Catalonia, Terrassa (Barcelona), SPAIN*
[2]*Public University of Navarre, Pamplona, SPAIN*
[3]*LABELEC, Terrassa (Barcelona), SPAIN*
E-mail: montanya@ee.upc.edu

Lightning protection level I according IEC 62305 [1] standards are usually adopted in the lightning protection system (LPS) of a wind-turbine blade. Nowadays, MW exceeding wind-turbines employs large blades that usually have carbon reinforced plastic (CRP) conductive materials as part of its structural beam. The typical lightning protection method is to have one or more air-terminals over the blade surface. However, one of the major problems regarding lightning protection of a blade is the close path between down conductor/s that connects the air-terminals to ground and CRP materials.

In other hand, the LPS of a blade should be verified by testing with a representative blade section. As requirement, the LPS level I adopts an impulse current with a rise time of 200 ns and a peak current of 50 kA. Such fast pulses are the major cause of lightning induced voltages to wiring. Testing a representative blade with this impulse characteristics results extremely difficult, however, such in aircraft experiences [2], low-level current tests are usually performed and employed to extrapolations.

In a wind-turbine blade due to the close path of down-conductors to CRP and the isolation between CRP components arise the question if subsequent strokes could produce internal arcs.

The paper describes the method and arrangement for injecting short rise-time impulse currents and presents experimental results of and experimental 5m blade tip.

Figure 1a presents the test arrangement composed by our experimental blade with a down-conductor and a CRP layers parallel to the down-conductor. In order to minimize the influence of the return path it was composed by several conductors placed in a coaxial form. The current injected to the tip and the current through the CRP are displayed in Figure 1b.
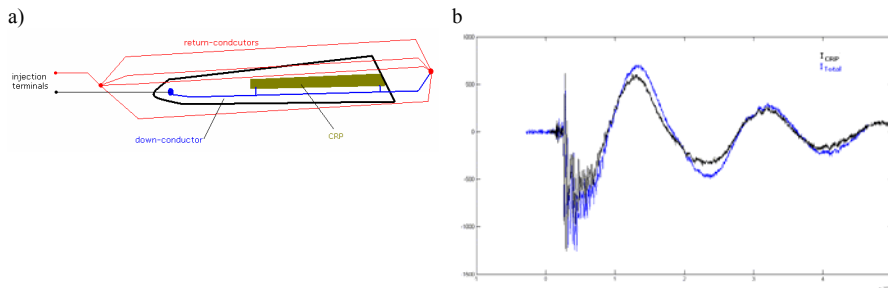
Fig 1 - a) Test arrangement and; b) obtained tip b) CRP currents

The paper discusses the method of extrapolation and the possibility of internal arcs originated by fast impulse currents.

References

1. EN-62305, Protection against lightning, 2006
2. J.A. Plumer, and E.J. Rupke, "Aircraft full vehicle testing with the defined pulse current waveforms: Methods of injection, measurements, and data interpretation", Int.l Conf. on Lightning and Static Electricity, 2003

HPEM - 18
Lightning Testing

Oral Presentations

Laboratory Study of Lightning Protection Devices' Performance

S. Grzybowski, T. Disyadej, and S. Mallick

High Voltage Laboratory, Mississippi State University, Mississippi State, USA

E-mail: stangrzy@ece.msstate.edu

Lightning performance of lightning protection devices depends on several factors. These factors include geometrical configuration of the devices, ground terrain, and polarity of lightning stroke. One of many concepts which has attracted some attention is an effect of the dissipation charge. The effectiveness of such devices has been the topic of discussion for many years. One particular experiment was performed in the High Voltage Laboratory and has been published in 2007 [4] but this study focused only on the magnitude of the emission current from the devices. The effectiveness of the devices on the lightning performance can be evaluated by measuring the critical flashover voltage (CFO) between the devices and a metal screen simulating cloud. The laboratory measurements under controlled condition for different devices may allow to compare the results and conclude on the lightning protection performance of the devices.

In this study, tested devices include Franklin Rod, spline ball ionizer, TerraStat® models TS 100, and TS 400. These four devices are totally different in dimension and configuration. The study focused on the CFO voltages of the air gap between the devices and a metal screen. The CFO voltage was evaluated using 250/2500 µs switching impulses with negative and positive polarity. Air gap spacing between the metal screen and the devices was 3 m. The metal screen was energized with switching impulse voltage generated by 3000 kV impulse generator.

Fig.1 Breakdown on the spline ball ionizer

The test results provide better understanding on the electrical phenomena of the lightning protection devices. This research helps to determine the improvement of lightning protection performance of the tested devices.

References
1. C. B. Moore, W. Rison, J. Mathis, G. Aulich, "Lightning rod improvement studies," Journal of Applied Meteorology, vol. 39, 2000.
2. G. Berger, " Determination of the inception electric field of the lightning upward leader," Proceeding of the 8th International Symposium on High Voltage Engineering, Yokohama, Japan, vol. 3, 1993.
3. S. Grzybowski, C.D. Taylor, "Effectiveness of dissipators used for lightning protection on 115 kV transmission and 13 kV distribution lines – long gap model test," Proceeding of the 23rd International Conference on Lightning Protection, Florence, Italy, 1996.
4. S. Grzybowski, C. D. Taylor, C, Bean, H. Gupta, and J. Grasty, "Experimental study of emission current from lightning protection devices under rain and wind conditions," IX International Symposium on Lightning Protection, Foz do Iguacu, Brazil, 2007.

Study of Spark Discharge in Soil at Reproduction of Lightning Current Pulse of Negative Polarity Using MCG

A.S. Kravchenko, Yu.V. Vilkov, M.M. Saitkulov, V.D. Selemir, V.A. Terekhin, A.A. Tutyaev
VNIIEF, Sarov, Russia
E-mail: kravchenko@ntc.vniief.ru

Energy sources based on magneto-cumulative generators (MCG) allow forming current pulses up to 90 kA amplitude and 200 μs length at half height on grounding rods. The current pulses simulate an effect of a current pulse of a positive polarity lightning on the grounding rod [1]. In connection with the fact that the majority of the thunderstorm dischargers have negative polarity with the current pulse front of several microseconds, VNIIEF developed and tested the MCG based energy source [2], in which the current pulse front formation of 2 μs is carried out with a current breaking unit, made of electrically exploding copper wires in an arc suppressing medium (Fig.1).

The paper presents experimental results of two energy sources – on the basis of one MCG-160 and on the basis of two generators MCG-160. A model of the active resistance change of the grounding rod that takes into account the current value and the rate of the spark channels distribution.

The current pulse of 50 kA amplitude and front length of 2 μs was formed on the grounding rod of 1 m length in the soil of 160 Ω·m specific resistance, using the energy source, based on one MCG-160 generator. Maximum length of the spark channels on the ground surface from the current input point was 3-4 m. The energy source, based on two MCG-160 generators, connected in serial, made it possible to increase the amplitude of the current pulse up to 90 kA having the same front length – 2 μs. In this experiment the maximum length of the spark channels on the ground surface from the current input point exceeded 8 m.

The figure 2 presents a pattern of the spark channels luminescence along the ground surface near the grounding rod obtained using a fast photo recorder. Bright vertical stripes inside a dielectric tower belong to the breaking unit, made of electrically exploding copper wires in a polyethylene covering. Фигура(Число) 2 представляет образец люминесценции каналов искры по поверхности основания(земли) около полученного прута основания, используя быстрый регистратор фотографии. Яркие вертикальные полосы в диэлектрической башне принадлежат ломающейся единице, сделанной из электрического взрыва медных проводов в покрытии полиэтилена.

The proposed model of the active resistance change of the grounding rod in the soil satisfactory describes the process of the current pulse formation in the current change range from 50 kA up to 90 kA.

Fig. 1 – The integral pattern of the energy source luminescence

Fig. 2 – The fragment of spark channel luminescence in the neighbourhood of the grounding rod

References
1. Yu.V. Vilkov, V.A. Zolotov, A.S. Kravchenko, et al., "Ultra-high current pulse formation on the high impedance load with the use of based on EMG energy source for lightning modeling," Elektrichestvo, no. 8, 2004.
2. Yu.V. Vilkov, A.S. Kravchenko, M.M. Saitkulov, et al., "Formation of a negative-polarity lightning current pulse using a magnetic explosion generator," Instruments and Experimental Techniques, vol. 50, no. 3, 2007.

HPEM - 18
Lightning Testing

Oral Presentations

Full Threat Level Transportable Lightning Simulation System

V.B. Carboni[1], H.J. Kishi[1], T.M. DaSilva[1], T.W. Tatman[1], I.D. Smith[1], C.C.R. Jones[2],
N.R.M. Ritchie[2], S.I. Richmond[2]
[1]L-3 Communications, Pulse Sciences Division, San Leandro, California, USA
[2]BAE Systems, Warton, United Kingdom

E-mail: vic.carboni@L-3com.com

The design of the Lightning Simulation System (LSS) shown in figure 1 is described in this paper. This system is a full threat level "Component A" lightning simulator designed primarily for aircraft testing and also suitable for component and materials testing. This system was recently used in the UK to successfully test the Typhoon Eurofighter and Nimrod aircraft.

The system uses an innovative design to achieve compactness and a wide operating range. The energy of the 750 kV Marx generators is stored in the inductance of the circuit comprised of the pulser and load and is then crowbared circuit at peak current through a series resistance to produce a pulse whose width is determined by the circuit's L/R time constant. The crowbar switch is SF6 gas insulated and laser triggered to provide the ability to switch at nearly zero volts with low jitter.

The LSS produces an output current which covers a range of 50 to 200 kA into an 8μH load with an action of up to 2×10^6 A^2-sec. with constant preset pulse shape throughout this entire range. The nominal pulse width (FWHM) is 69 μsec with a rise time to peak of 5.4 μsec and peak di/dt of 0.7×10^{11} A/sec.

Current amplitude and pulse width are remotely adjustable and controlling the operation is done via a computer using LabVIEW software that automatically sets the system parameters consistent with the desired current and then both controls the system and logs the resulting waveform data. The controls are isolated from the LSS by fiber optical links.

The system operates off standard power mains and occupies a space of approximately 20 feet (6 meters) long x 10 feet (3 meters) wide x 18 feet (5.5 meters) high and weighs about 90,000 lbs (41,000 Kg) full of oil and is trailer-mounted for mobility and towable about a test site by a standard aircraft tug. The system includes several shipping containers to enable transportation of the entire turnkey system, including the insulating oil, to sites anywhere in the world with only minimal disassembly and preparation.

Approximately 5,500 gallons (21,000 liters) of transformer oil insulate the high voltage components. Where SF6 gas is used for switching, a recirculation and reclamation system is provided that is capable of filling, recirculating and reclaiming the entire contents of the SF6 system.

The system is fully safety interlocked, fail safe and is CE-marked.
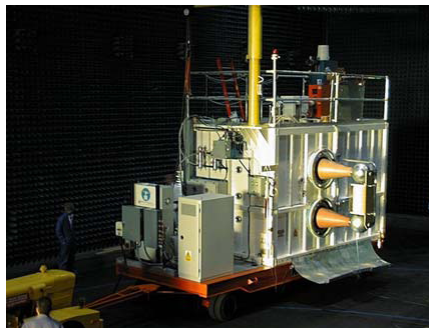
Fig. 1 - The Lightning Simulator

High Current Testing and Modelling of Aircraft for Lightning Clearance

C.C.R. Jones[1], C.J. Hardwick[2]
[1]*BAE Systems, Military Air Solutions, Warton, UK*
[2]*Culham Lightning Ltd, Abingdon, UK*

E-mail: chris.c.jones@baesystems.com

Many claims are made that high current whole aircraft testing of lightning clearance is impracticable, either because it is not possible to inject repeated high current pulses into a Carbon Fibre Composite structure without severe and expensive damage, or because of the size of a large transport aircraft. In this paper we will describe the experience of whole aircraft testing to the (almost) entirely CFC Eurofighter Typhoon aircraft (Figure 1) with current pulses ranging from 20kA up to 200kA, and to the metal Nimrod MRA4, Maritime Reconnaissance aircraft at levels from 15kA to 50kA. The tests carried out were part of the formal flight safety clearance programmes so this context also will be described, including the process applied and the complementary computer modeling work.

A number of conclusions will be drawn from the projects. First, providing lightning protection of structures and systems has been incorporated in the design, that testing of a CFC aircraft is quite a realistic proposition without incurring damage. That lightning whole aircraft testing to the full clearance threat of 200kA is feasible, also without expensive damage either to the aircraft structure or to the systems within. That the testing of a whole large transport aircraft to high currents in a proper return conductor rig designed to ensure a reasonable current distribution around the whole structure is practical. Some additional conclusions concerning the necessity to include appropriate safety margins or how to cover many more lightning attachment scenarios than the testing will allow, the significance of periodically grounded cable shields, and the importance of considering other waveform properties apart from peak amplitude will be discussed briefly.
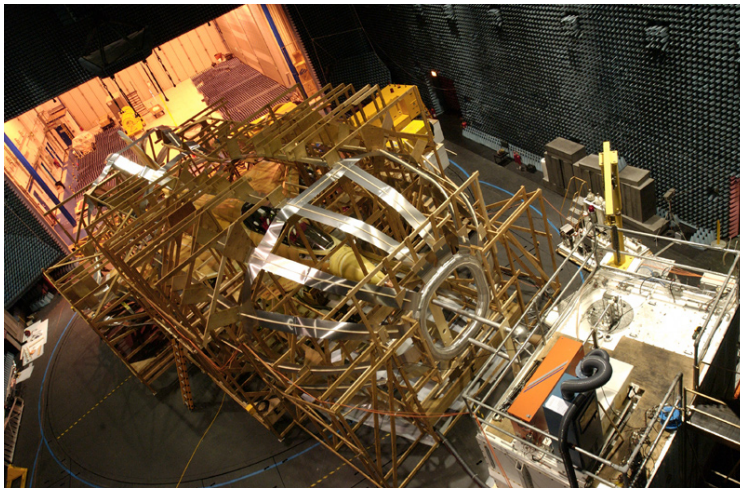
Fig. 1 – Eurofighter Typhoon Undergoing Whole Aircraft Lightning Testing to Full-threat.

HPEM - 18
Lightning Testing

Oral Presentations

Development and Evaluation of Two Reference Calibration Methods for Circular Loop Antenna in Low-Frequency Band

Masanori Ishii and Yozo Shimada

National Institute of Advanced Industrial Science and Technology, National Metrology Institute of Japan
E-mail: masanori-ishii@aist.go.jp

Recently, the low-frequency band (particularly below 30 MHz) is widely used in the induction heating (IH), the radio frequency identification (RF-ID) tag systems, and so on. In the fields of electromagnetic compatibility (EMC), it is important to measure the magnetic field strength accurately radiating from the electric devices. Therefore a magnetic antenna factor (MAF) of a receiving loop antenna must be accurately and simply calibrated.

In loop antenna calibration, the absolute calibration methods (ACMs) [1], [2] are popular. However they are not simple calibration methods. So antenna calibration laboratories or companies must make efforts to maintain the complicated calibration system and establish the traceability to the standards. Some of them are requesting that reference calibration methods (RCMs), which can be traceable to the standard of the MAF, are developed.

We propose the two RCMs for loop antenna calibration. One is the reference antenna method (RAM) with a correction factor for circular loop antennas (named Method 1). The other is the method combined the standard field method [1] with the RAM (named Method 2). Generally, in the RAM, the standard antenna is used as the receiving antenna [4]. However, in the Method 2, the standard loop antenna is used as the transmitting antenna.

In this study, we made a comparison and evaluated the two proposed method by the experiments. The ordinary shielded loop antennas [5] were used. They were 5.2 cm (named #A), 10.0 cm (named #S, #2, and #T), and 15.2 cm (named #B) in diameter. The #A and the #B were calibrated by the Method 1 and the Method 2 and the results were compared with each other. Before the two methods were carried out, the #S, the #2, and the #T had been calibrated by the three-antenna method [3]. In the Method 1, the #S is the standard antenna and the #T is the transmitting antenna. In the Method 2, the #S is used as the standard and the transmitting antenna at the same time.

The calibrated MAFs of the #A and the #B by the two methods and the differences between them are shown in Fig. 1 and Fig. 2, respectively. The frequency range is from 150 kHz to 30 MHz. In Fig. 1, it is found that the MAFs agree well. In Fig. 2, the differences are ± 0.5 dB, approximately. The large differences less than approximately 1 MHz are caused by the low sensitivity of the loop antennas. The differences in the range from 1 MHz to 30 MHz are within ± 0.25 dB, approximately. Therefore these results clearly show that the Method 2 is almost equivalent to the Method 1. The Method 2 can be performed more easily than the Method 1 because the only transmitting characteristic between the #S and the #A (or the #B) is measured. In the Method 1, the two transmitting characteristics between the #T and the #S and between the #T and the #A (or the #B) are needed. Thus it is expected that the uncertainty in the Method 2 is smaller than in the Method 1.

Using the proposed methods, the calibration service laboratories or companies can easily calibrate the MAF of the loop antennas as they can establish traceability to the standard of the MAF provided by national metrology institutes.
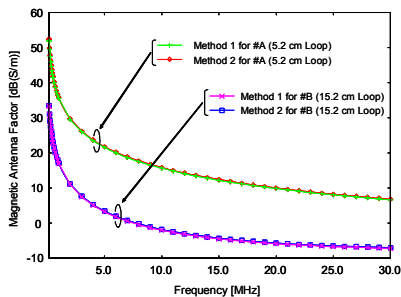
Fig. 1 Magnetic antenna factors obtained by experiment.
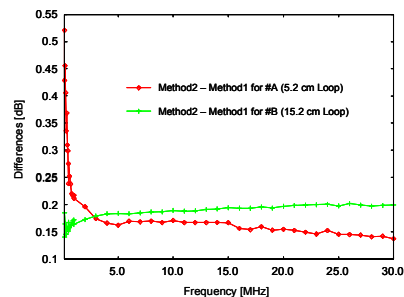
Fig. 2 Magnetic antenna factor: differences

References
1.   M. Kanda, "Methodology for electromagnetic interference measurements," IEICE Trans. Commun., vol. E78-B, no. 2, pp. 88–108, 1995.
2.   M J Alexander, M J Salter, D G Gentle, D A Knight, B G Loader and K P Holland, "Calibration and use of antennas, focusing on EMC applications," Measurement good practice guide No.73, National Physical Laboratory, Dec. 2004.
3.   M. Ishii and K. Komiyama, "Estimation of uncertainty of calibration for loop antennas by three-antenna method using automatic network analyzer," in Proc. Automatic RF Technique Group, June 2006, pp. 156–163.
4.   T. Morioka and K. Komiyama, "Uncertainty Analysis of Dipole Antenna Calibration Above a Ground Plane," IEEE Trans. Electromagn. Compat., vol. 48, no. 4, pp. 781–791, Nov. 2006.
5.   M. Ishii and K. Komiyama, "Impedance method for a shielded loop antenna," IEEE Trans. Instrum. and Meas., vol. 56, no. 2, pp. 422–425, Apr. 2007.

Methods and Resources of Near-Field Technology Available at LHFT

R. Chernobrovkin, I. Ivanchenko, M. Khruslov, N. Popenko, S. Radionov
Usikov Institute for Radiophysics and Electronics of the National Academy of Sciences of Ukraine,
Laboratory of High Frequency Technology, 12 Ak. Proskura St., Kharkov, 61085, Ukraine
E-mail: ireburan@yahoo.com

Near-field measurements allow one to get the information as the suitable field maps over and around various objects of interest. Such the maps are highly informative instrument to determine both the active areas of antennas and the areas with particularly low field concentration, to reveal the influence of edge effects and cross-talk coupling between adjacent elements in antenna array, to validate computer simulation software, to detect faults in penetrable materials, to determine the electromagnetic field created by electronic systems and components [1, 2]. In this paper the experimental set-up for near-field measurements in the inductive $(0<R<\lambda/2\pi)$ and radiating regions $(R<2D2/\lambda)$ at frequencies ranging from 6GHz to 150GHz are presented.

A computer-controlled *XYZ*- manipulator with maximal scanning area 200x200mm and point-to-point accuracy ±0.1mm is used. Depending on the aspect of experiments the measurements can be realized by moving either the probe or the object under study. The set of HF oscillators are applied to carry out the investigations in the frequency range of interest.

With reference to experiments in the inductive region both E-, and H-components are measured by a short electric monopole and a small loop antenna, respectively. In the latter, the effect of the parasitic electric field is removed by using the special metallic screen. The spatial resolution of these probes is practically equal to their physical sizes. However when the probe size reducing also decreases the amplitude of received signal, which may then became strongly affected by noise. In this respect, the probe design optimization has been carried out to achieve the maximal resolution and sensitivity. In our case the dynamic range and accuracy of the measurement are 30dB and 0.1dB, respectively.

For measurements in radiating region the probes as the open-ended waveguide filled with dielectric are used [3]. By working for reducing to an acceptable level the parasitic contributions produced by reflections and scattering on probe supports, transmission lines and leading-in cables, the absorbing materials are applied. The phase test signal is measured at the lower intermediate frequency to be different from the modulation frequency of the amplitude test signal so that the amplitude and phase field distributions are measured simultaneously with accuracy to within ±0.1dB and ±2^0, respectively. Dynamic range of the measurement is 30dB that allows observing a slower decrease in EM field amplitude, and low field areas appearing close to edge of the objects under study.

The scopes of presented facility are demonstrated by results of edge effects investigations with reference to the cylindrical dielectric grounded X-band monopole antenna. The near-field map in inductive region shows the EM field oscillations caused by the interference of EM waves reflected from the antenna edge.

In the millimeter range a set of experiments are performed to reveal the faults in dielectric matrix. For example, from the analysis of amplitude-phase EM field distributions in radiating region the space resolution in detecting two polyethylene threads (0.5λ)**,** as well as the resolvable faults size (0.3λ), and minimal contrast in permittivity of the matrix and faults (0.2) have been determined.

The most important information about interactions between the elements in multi-beam receiving array with elements as densely packed as possible can be obtained from the near-field measurement. This type of antenna array is used in the single-reflector radio telescopes allowing essentially to expand the field of view and to achieve the reception of multi-pixel radio images of some extent of the sky area without mechanical scanning. In our experiments the influence of edge effects on the radiation formation of individual element as the horn with dielectric insertion [4] has been determined from the near-field maps in radiating region.

In contrast to the well-known equipment for near-field measurements the presented facility provides the investigations in the wide frequency range both in the inductive and radiating regions with high resolution and sensitivity.

Referencies.
1. J.-C. Bolomey, F.E. Gardiol. Engineering application of the modulated scatterer technique. 2001 Artech House, Inc.
2. D. Baudry, et all. Applications of the Near-Field Techniques in EMC Investigations, Electromagnetic Compatibility, IEEE Transactions, v.49, N3, pp.485 – 493, 2007.
3. R. Chernobrovkin, I. Ivanchenko, N. Popenko. A novel V-band antenna for nondestructive testing techniques. Microwave and optical technology letters, v.49, N7, pp1732-1735, 2007.
4. V.B.Khaikin, et all. Tightly packed multibeam FPA at 30-38 GHz. In Proceed. of the 29-th ESA Antenna Workshop on Multiple Beams and Reconfigurable Antennas, pp.115-118, 2007.

HPEM - 19
Measurements Techniques #3

Oral Presentations

BCI Method applied to transfer impedance measurement

J. Rabaste, F. Desnoyers, M. Demko
EADS-NUCLETUDES, 91944 Les Ulis,France

E-mail: jrabaste@nucletudes.com

The Bulk Current Injection (**BCI**) method has been proposed to characterize the electromagnetic immunity of complex cables or harness. There are many ways to characterize this property in general: Shielding Effectiveness (**SE**) or Equivalent Surface Coupling (**ESC**) can be measured in an anechoid chamber or stripline but these parameters are very difficult to predict and in general are not specified as system requirement. The cable transfer impedance is related to the shield current and is very helpful for prediction and other specifications. For complex cables, methods using triaxial or quadraxial test benches are not suitable due to multiple forks and connections of such cables. In this case, it is necessary to use the **BCI** method and place the cable above a ground plane. The Direct Current Injection (**DCI**) method is destructive with anodic or organic protection. The **BCI** method of measurement previously described was implemented to design a test bench for an industrial application, and is based on a network analyzer to measure S_{21} parameters in voltage and in current (figure 1), assuming that transfer impedance is given by:

$$Zt(f) = 2 \frac{S_{21}v(f) * Fprobe(f)}{S_{21}i(f)}$$

(1)

The method was first validated on a reference test cable ([1]) and then applied to a complex cable with the following advantages: test concerns connectorized cables, and then validates technologies of shielding and selected connectors as well that the quality of assembly. The test bench allows point-to-point measurement of elementary cables, as well as complex ones. Tests of these complex cables are decomposed into elementary ones, and performed by successive sections. The contribution of each element is determined by software calculation. The section-by-section measurement allows the localization of a possible defect, and makes possible the correction or the improvement of the manufacturing processes. The design of the mechanical tools and the software has been studied in such a way that "non-expert operators" can use the bench with good reproducibility of measurement (<2dB typ).

Fig. 1 – BCI Test bench for complex cables

References
1.   Bureau de Normalisation de l'Aéronautique RE. Aéro 704 11: " Câblages à immunité spécifiée aux agressions. Méthodes de mesure de l'impédance de transfert (Zt) jusqu'à 100 MHz des connecteurs et raccordements".

Portable Wireless Transient Measurement System in Power Substations

K. Liu, W. H. Siew, R.W. Stewart

Department of Electronic and Electrical Engineering, University of Strathclyde, Glasgow, UK

E-mail:w.siew@eee.strath.ac.uk

Switching operations of power equipment such as disconnect switch and circuit breakers in high voltage substations generate significant electromagnetic fields, which constitute potential electromagnetic interference (EMI) to the equipments run in the substations.

To better characterize the transient electromagnetic fields distribution in power substations and to verify the theoretical models of transient generation, an effective and flexible transient measurement system is needed. One design option for this system is based on fiber-optical cables and oscilloscopes. By using optical signals to transfer signals from sensors located inside the power substation to outside oscilloscopes, where signals are acquired, this system works well in the harsh electromagnetic environment. However it has some limitations, like high cost, difficult to set up. Especially when a lot of sensors are used to get data from a complicated substation environment, it would become very time consuming and difficult to find spaces to lay out the 100 meter long heavy fiber cables. In the meantime the increased quantity of needed oscilloscopes will also make the system cost much more.

In recent years, electronic techniques advance rapidly. On one hand, some smart low cost wireless communication techniques like WIFI, Bluetooth, and ZIGBEE gradually go into maturity and get widespread application; on the other hand, programmable device's capability and density are consistently increasing. All these enable us to develop a portable wireless embedded system to do the transient measurement job without resorting to lengthy fiber cables and expensive oscilloscopes.

This paper presents a portable and cost effective wireless digital solution to the transient measurement, in which signal acquisition function realized by programmable devices provide high performance signal acquisition and processing capability and data transmission function by the application of flexible wireless communication protocol makes the system easy to use. Some design considerations to avoid the electromagnetic interference's impact on data transmission are also analyzed.

HPEM - 19
Measurements Techniques #3

Oral Presentations

A Novel Microwave-Photonic Device to Measure *S*-Parameters of DUT in Full 2-Port Calibration Without Coaxial Cables

Masanobu Hirose, Satoru Kurokawa

[1]*National Institute of Advanced Industrial Secience and Technology, AIST Central 3, Tsukuba-shi, Japan*
E-mail: masanobu-hirose@aist.go.jp

We have developed a novel microwave-photonic device that can measure *S*-parameters of two-port devices using a vector network analyzer (VNA) in full 2-port calibration. We call it a compact extended port shown in Fig. 1 (a), since it is a compact version of the previous extended port [1]. Because the novel device transmits and receives RF signals through optical fibers, the influences of the presence of coaxial cables can be removed completely in RF measurements. Another merit of using optical fibers is its low-loss characteristics (0.5 dB/km) compared to coaxial cables (0.5 dB/m at 1 GHz) because total cable length in antenna measurements is often more than 50 m.

The structure of the novel device is shown in Fig.1 (b). The device functions as the R and A channel receivers of a 4-ch receiver VNA. The PD is a photo diode to generate a RF signal that is converted into a modulated laser light at the source channel of the VNA and is transferred through an optical fiber. The EAM is an electro-absorption modulator of reflection type that converts a RF signal to a modulated laser light. The light is converted into the RF signal by a PD at each channel of the VNA. Therefore the compact extended port can replace a coaxial cable by optical fibers completely in any kinds of calibration methods using the VNA.
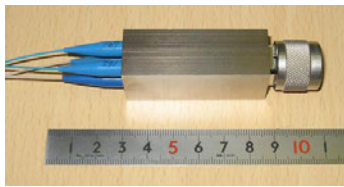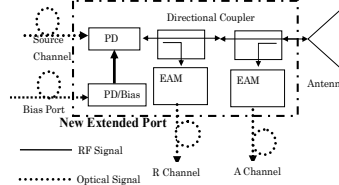
(a)   (b)

Fig. 1 – Compact Extended Port. (a) Picture. (b) Structure.
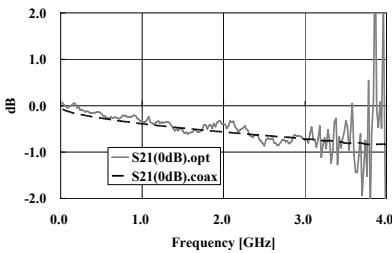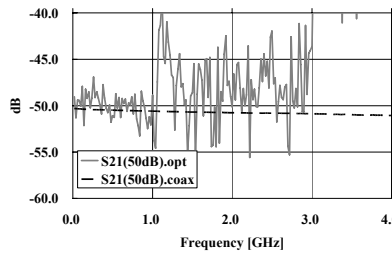
(a)   (b)

Fig. 2 – Calibrated S21 of a stepped attenuator. (a) 0 dB attenuation. (b) 50 dB attenuation.

Fig. 2 shows the calibrated S21 of a stepped attenuator, of which attenuations are 0 dB and 50 dB. Compared with the calibrated *S*-parameters measured by the compact extended ports and the conventional coaxial cables, we have found that the reflection coefficients agree within 0.1 and the transmission characteristic has the dynamic range of about 60 dB below 3 GHz.

We are now developing the improved version that will have the dynamic range over 80 dB, be able to measure the reflection coefficient within 0.02 deviation, and operate up to over 10 GHz.

References
M. Hirose, S. Kurokawa, and K. Komiyama, "Antenna Measurements by One-path Two-port Calibration Using Radio-on-fiber Extended Port Without Power Supply," IEEE Trans. Instrum. Meas., vol. 56(2), 2007.

Line-Series-Shunt Calibration with Transmission Lines in Arbitrary Characteristic Impedances for Broadband S-parameter Measurements

Chien-Chang Huang and Yuan-Hong Lin

Institute of Communication Engineering, Yuan Ze University
135, Yuan-Tung Road, Chung-Li, Taoyuan 320, Taiwan

E-mail: cch@saturn.yzu.edu.tw

The calibrations of non-coaxial test fixtures with vector network analyzers (VNAs) play an important role in device characterizations for microwave active/passive components. The thru-reflect-line (TRL) calibration has been reported as the most popular method due to its easy fabrication of the calibration standards. There are some TRL-variant techniques such as line-reflect-match (LRM) or line-reflect-reflect-match (LRRM) calibration methods for releasing the frequency band limitations by using the high quality match standards or additional calibration kits. Recently, a broadband calibration algorithm with total unknown standards has been proposed [1] to release the difficulties for acquiring the standard characteristics precisely, with the aids of nonlinear equation solving. This approach takes advantage of easy fabrications for the calibration standards. But the method is based on the matched (no reflection) transmission lines, that non-fifty ohm transmission lines may yield poor solutions for the nonlinear equations. This paper presents a calibration method based on the line-series-shunt (LST) calibration [1] for the arbitrary characteristic impedances of the transmission lines that may have advantages for some devices with lines not in 50 Ω. This algorithm is based on two assumptions. First, the planar transmission line is in the quasi-static operations that only the single-mode transmission exists. Second, the series and the shunt calibration standards behave like a serial-lumped element and a shunt-lumped element respectively. Meanwhile the lossy transmission lines and the complex impedance/admittance characteristics for the lumped components are allowed throughout the calibration procedure.

The characteristic impedance of the planar transmission is evaluated based on the low conductance loss condition [2]. Three different measured transmission matrix manipulations $[M_s]\cdot[M_\ell]^{-1}$, $[M_s]\cdot[M_T]^{-1}$ and $[M_T]\cdot[M_\ell]^{-1}$ can be constructed using the three calibrator data where $[M]$ is the similarity transformation of the actual calibrator matrixes. With the aid of the trace invariance for the similarity transformations, three nonlinear equations are obtained to find the propagation constant, the serial impedance and the shunt admittance with the Newton-Raphson solving scheme. The de-embedding procedure fully utilizes the measured data of the three standards in the least-square sense to minimize the measured uncertainties. To show the validity of the proposed calibration method, the CPW calibration standards are designed with the substrate of FR-4. To improve the contact repeatability of the calibration kits and the DUT to the VNA, the universal test fixture (Anritsu 3680-20) is used for the test-board connections. The final measured S-parameters for an inter-digit capacitor are verified by the TRL measured data as shown in Fig. 1, validating the line-series-shunt calibration results.
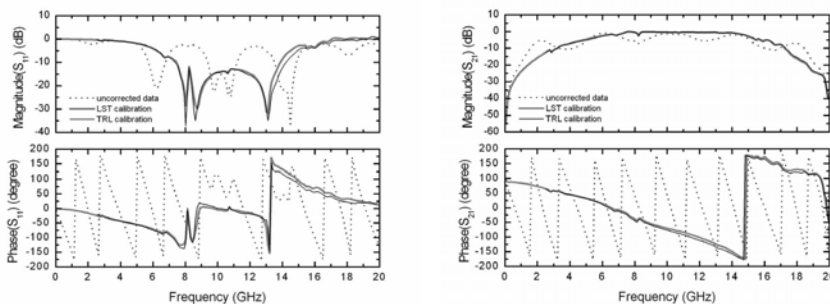
Fig. 1 –Measured results of the LST calibration for an inter-digit capacitor with comparisons of the TRL calibration.

References

1. C.-C. Huang and H.-C. Lin, "A novel calibration algorithm with unknown line-series-shunt standards for broadband S-parameter measurements," to appear in *IEEE Trans. Instrum. Meas.*
2. R. B. Marks and D. F. Williams, "Characteristic impedance determination using propagation constant measurement," *IEEE Microwave Guided Waves Lett.*, Vol. 1, pp. 141-143, June 1991.

HPEM - 19   Measurements Techniques #3

Oral Presentations

Hybrid Spiral with Loop Antenna

Neal Tesny[1], Stanley L. Henriquez[1], Marc S. Litz[1] , Robert Atkinson[1]
[1]*Army Research Laboratory, Adelphi, MD, USA*
E-mail: Litz@arl.army.mil

This paper describes the design, fabrication and evaluation of a logarithmic spiral antenna with a single loop (terminated in 200 Ω) surrounding the spiral. The broadband characteristics of this antenna combination are designed specifically as a sensor for the detection of EM noise. The frequencies of interest range from 50 MHz to 10 GHz. The low frequencies are detected by the loop antenna and the higher frequencies are detected by the spiral antenna. This style antenna can be located in buildings and passageways in inaccessible areas for the purpose of shielding integrity surveillance and life cycle shielding degradation monitoring. They can be used as permanent fixtures that detect critical threshold levels of unwanted EM radiation. The antenna structures have been modeled with the FEKO EM numerical code. Figure 1 depicts the patch model used in the numerical code analysis and figure 2 shows the results of the boresite gain predictions over the frequency range of 1 MHz to 10 GHz. The far-field gain has a peak gain of 6 dBi at approximately 473 MHz and has an input impedance of approximately 200 Ohms above 200 MHz. Measurements were performed in the laboratory. The paper will present the detailed results of the design and the FEKO analysis. The measured results of this 3' wide hybrid compare well with the predictions from the modeling.
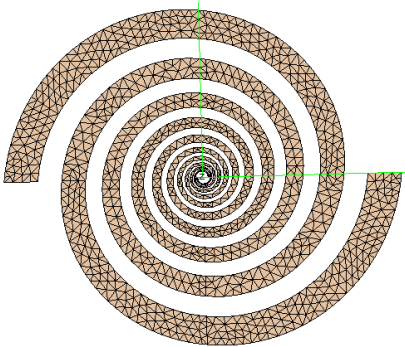
Figure 1. Spiral Antenna model without loop.
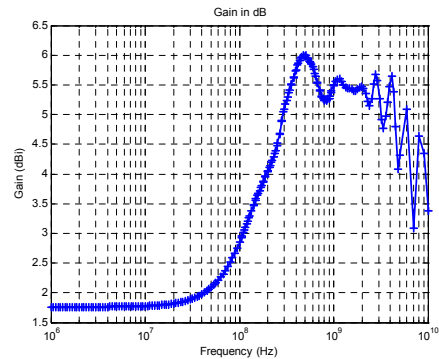
Figure 2. Predicted far-field gain.

References
1. K. Y. A. Lai, "A Novel Antenna for Ultra-Wideband Applications", PhD. Dissertation, Ohio State University, 1990.
2. J.D. Kraus, Antennas, New York: McGraw-Hill, 1950.
3. FEKO, EM Software & Systems (SA) Pty Ltd., 1998-2006.
4. M. Polun, "Feasibility Studies of New High Altitude Electromagnetic Pulse Test Materials", ARL-TR-3677, November 2005.

Insight into the Time-domain Response of a Top-Loaded Monopole Provided by a Rational Function Frequency Domain Model

J. McLean[1], H. Foltz[2], and R. Sutton[1]
[1]*TDK R&D Corp., Cedar Park, USA*
[2] *The University of Texas-Pan American, Edinburg, USA*

...
E-mail: jmclean@tdkrf.com

The top-loaded monopole shown in Fig. 1 can provide acceptable performance when size-limitations prevent the use of larger antennas such as conical antennas. A lumped-element, frequency-domain model also shown in Fig. 1 has previously been published which gives an accurate prediction of the monopole's performance up to the frequency of the first parallel resonance [1,2]. This model differs topologically from the one given in [3] and also consists of only lumped circuit elements. More than a rational function approximation, the model employs element values that are derived from physical phenomena. In the frequency domain the model has been useful to determine parametric relationships, such as the height to disk diameter ratio, which provide optimum performance, such as impedance bandwidth. The frequency domain model leads to an expression for the transfer function of the antenna which, using Laplace transform techniques, is used here to derive the time domain response. Because the frequency domain model is a rational function, much information about the time-domain response can be gleaned from the pole-zero constellation, a typical representation of which is given in Fig 1.
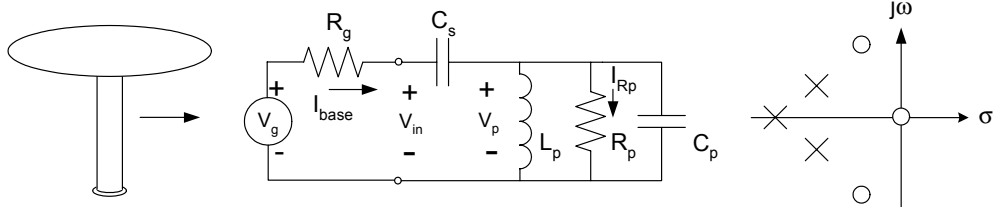
Figure 1: Broadband, lumped-element frequency-domain model and pole-zero constellation of the antenna transfer function showing three poles and three zeros.

A second-order approximation to this model is particularly useful. In practice, C_p is small and affects the behavior primarily in the vicinity of the parallel resonance. Thus, a good second-order approximation can be obtained by neglecting C_p. Using this approximation, the source resistance required for critical damping can be determined. Several practical cases are examined and, surprisingly, it is seen that relatively low source resistances (on the order of 200 Ohms) are typically required for critical damping. When such an approximation is valid (when the excitation function exhibits the necessary spectral characteristics), traditional second-order time domain parameters such as delay time, rise time, and settling time offer useful information about the antenna. Even when C_p is not negligible, these poles are dominant and the second-order model gives a good picture of the time domain behavior.

Time-domain step response measurements made with a sampling oscilloscope of the port-to-port transmission between three pairs of identical monopoles located in a single ground plane are used to verify the model. A TDR head is used to generate the step source function. Frequency-domain scattering parameter measurements are also made and a scattering matrix renormalization is used to effectively vary the source and load impedances. The renormalized frequency domain data is then transformed to the time domain to show the variation of the step response with source impedance and thus verify the predictions for critical damping.

References

1.　H.Foltz, J.S.McLean, L.Bodner, "Closed-Form Lumped Element Models for Folded, Disk-Loaded Monopoles," *2002 IEEE Antennas and Propagation International Symposium Digest*, pp.576-579, June 2002.
2.　H.Foltz, J.McLean, G.Crook, "Disk-Loaded Monopoles with Parallel Strip Elements," *IEEE Transactions on Antennas and Propagation,* vol. 46, no.12, December 1998, pp. 1894-1896.
3.　M. A. Morgan and F. K. Schwering, "Eigenmode Analysis of Dielectric Loaded Top-hat Monopole Antennas," *IEEE Transactions on Antennas and Propagation,* vol. 42, no.1, January 1994, pp. 54-61.

Oral Presentations

Analysis of Antennas and Scatterers with Nonlinear Loads: A MoM-AOM Approach

H.R. Karami[1], R. Moini[1], S.H.H. Sadeghi[1], S.M. Azimi[2]

[1]*Amirkabir University of Technology, Iran*
[2]*Hamedan University of Technology, Iran*

E-mail: hamidr.karami@gmail.com

A frequency-domain spectral balance technique is utilized in this paper to analyze the non-linearly loaded wire antenna located over a lossy dielectric half-space. The technique involves two stages. First, the problem is transformed to a nonlinear microwave equivalent circuit with the circuit parameters of antenna extracted by the method of moment (MoM) solution of the electric field integral equation [1]. Then, the arithmetic operator method (AOM) [2] is applied to solve the nonlinear microwave equivalent circuit. The main feature of the proposed technique is its efficiency in analyzing the transient response of the antenna with strong nonlinear loads over a lossy dielectric half-space. The technique works purely in the frequency domain, so the effects of lossy dielectric half-space can be considered properly by using method of moment in conjunction with Sommerfeld asymptotic method. The AOM is now used to the analysis of a centre nonlinearly loaded thin wire scatterer illuminated by Gaussian pulse. It is well known that the frequency domain behavior of scatterer excited by a Gaussian pulse can be represented by the Norton equivalent circuit obtained by the use of MOM. Applying the kirchhoff's circuit law to Norton equivalent circuit gives

$$I_{NL} = Y_{in}\,V_L - I_{SC} \tag{1}$$

where V_L is the terminal voltage, and the current of nonlinear subcircuits is I_{NL} corresponding to nonlinear load part. I_{SC} is the short circuit current of the antenna input and Y_{in} is the input admittance of the antenna for different frequency components, both being defined as a function of the frequency. Using the AOM transform matrix [2], T_V, the current-voltage nonlinear relationship can be represented in the frequency domain as

$$-I_{NL} = \sum_{n=0}^{N} a_n T_V^{n-1} V_L \tag{2}$$

One can substitute (2) into (1) and obtains V_L by an iterative numerical method such as Newton-Raphson method. The other parameters can be easily calculated by using V_L. In order to evaluate the performance of the proposed method, the midpoint transient current of the nonlinearly loaded antenna oriented at an angle of 45 degree over a lossy dielectric half-space with length of 1 m and radius of 6.74mm, excited by a Gaussian pulse voltage source at its midpoint is shown in Fig. 1. The *i-v* characteristic of nonlinear load used in this example is similar to [3].
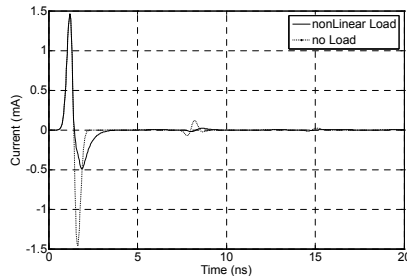
Fig. 1 – The midpoint transient current of the nonlinearly loaded antenna oriented at an angle of 45 degree over a lossy dielectric half-space with L=1m, a= 6.74mm, excited by a Gaussian pulse voltage source at its midpoint.

References
1. T. K. Liu and F. M. Tesche, "Analysis of antennas and scatterers with nonlinear loads," *IEEE Trans. Antennas Propagat*. Vol. AP-24, pp. 131-139, Mar. 1976.
2. C.R. Chang and M.B. Steer, Frequency-domain nonlinear microwave circuit simulation using the Arithmetic Operator Method, IEEE Trans Microwave Theory Tech 38 (1990), 1139–1143.
3. J. A. Landt, E. K. Miller, and F. J. Deadrick, "Time domain modeling of nonlinear loads," *IEEE Trans. Antennas Propagat*, vol. AP-31, pp. 121-126, Jan. 1983.

Sinusoidal Helix Antenna

Joseph R. Miletta[1], Marc Litz[2], Neal Tesny[2], Stanley L. Henriquez[2]
[1]*DE Technologies,Sumerduck, VA, USA*
[2]*Army Research Laboratory, Adelphi, MD, USA*

...
E-mail: Litz@arl.army.mil

The objective of the study is the design of a compact broad band antenna with moderate gain. The design goals are 1.2 GHz center frequency with a gain of 10dB or greater, and a reduction in antenna length of a factor of 2 or more, when compared to a standard antenna. A helix design was chosen for the study inspired by the results presented in earlier work. [1,2] The reduction in size is achieved by employing a slow-wave sinusoidal structure to the helix winding. Figure 1 compares the size of the compact antenna to the standard helix. The pitch chosen for the standard helix, shown in the Figure, was 15 degrees with a cross-sectional circumference of 1.25λ (λ is 9.84 inches).[3] The length and diameter of the compact antenna are ½ those of the standard helix. The amplitude of the sinusoid applied to the winding is 35% of the turn separation with 5 cycles per turn for the structure of Figure 1. Figure 2 compares the bore sight gain between the two antennas as calculated with the NEC code. The results show comparable gain over a broad frequency range. Additional modeling was conducted on the FEKO code. The report will present the results of parameter studies that address antenna pitch, sinusoid structure (amplitude and cycles per turn), input impedance and bandwidth. A prototype model was fabricated and tested. Modeling results are compared to the measurements. The measurements were performed in a 50 x 30 x 25' anechoic chamber.
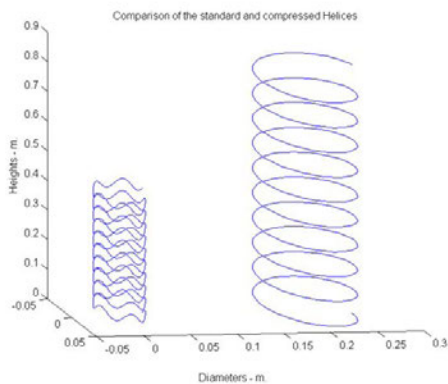
Figure 1 Standard helix antenna shown next to a helix with a sinusoidal slow-wave structure.
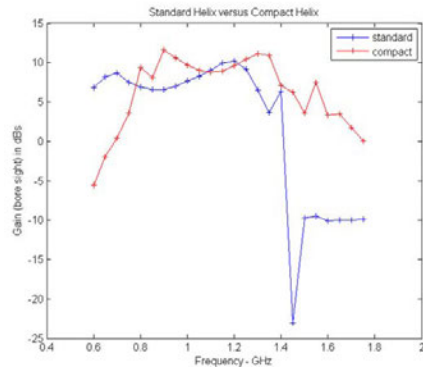
Figure 2 Comparison of bore sight gain between the standard helix and the compressed sinusoidal helix.

References:
1.   Joseph R. Jahoda, Compact High Power Microwave Antenna (HPMA), Final Report, Contract No. DAAD17-01-C-0010, ASTRON Wireless Technologies, 15 May 2004.
2.   Barts, R.M.; Stutzman, W.L., "A reduced size helical antenna," *Antennas and Propagation Society International Symposium, 1997. IEEE., 1997 Digest* , vol.3, no., pp.1588-1591 vol.3, 13-18 Jul 1997
3.   Richard C. Johnson, Antenna Engineering Handbook, 3rd Ed., Chapter 13, McGraw-Hill Inc., New York, 1993.

HPEM - 20
Wire, Plate and Aperture Antennas

Oral Presentations

Free-Space Antenna Factor Evaluation of Biconical Antenna Using Time-domain and Pulse Compression

Satoru Kurokawa, Masanobu Hirose

National Institute of Advanced Industrial Secience and Technology, AIST Central 3, Tsukuba-shi, Japan

E-mail: satoru-kurokawa@aist.go.jp

We have proposed a new method for evaluating a free-space antenna factor of a LPDA on the open area test site (OATS) [1] [2]. The proposed method is based on the techniques of a time domain analysis and a pulse compression technique for the reduction of the influence by the reflected waves, which cause the error of the evaluation of free-space antenna factor. In this paper, we show the results obtained by the new method for evaluating a free-space antenna factor of a Biconical antenna.

Biconical antennas are used H=6 m high on the masts. Frequency domain $S_{21}(\omega)$ is measured by the system with a VNA after the unknown-through full two-port calibration. The time domain $S_{21}(t)$ is calculated by inverse Fourier transform with a Hamming-type frequency-domain window. Fig. 1 and 2 show the time domain $S_{21}(t)$ and the frequency domain $S_{21}(\omega)$ respectively. [D=3m] and [D=20m] indicate the measured results at antenna distance 3 m and 20 m, respectively.

In $S_{21}(t)$ at D=3 m, the reflection path is 9 m longer than the direct transmission path and the path difference is long enough to separate the direct and reflected waves. In the time domain data at D=3 m, the direct wave is received after 16 nsec delay, and the undesired reflected wave from the ground plane appears at about 49 nsec. Therefore it is easy to eliminate the reflected wave by time gating. On the contrary, the data at D=20 m shows the direct and reflected waves are overlapped because the path difference is short. Therefore it is difficult to separate these two waves by a simple time-gate.

In order to calculate the free-space antenna factor of Biconical antenna, we need to obtain the direct transmission wave at D=20 m. Following the method in [1, 2], we separate $S_{21}(t)$ at D=3 m into the direct and reflected waves and the direct wave is used as a standard sample. We construct the Wiener filter that is expressed in the frequency-domain Fourier transform of the direct wave. Then, we calculate the compressed time-domain waveform by the inverse Fourier transform.

Fig. 3 shows the compressed time-domain waveforms (η=0.99) for D=3 m and D=20 m. Even in the case at D=20 m, it is found that the peaks are separated due to the pulse compression. It is enough for the case at D=20 m to be applied by a rectangular time-gate.

Finally we estimate the free-space antenna factor from the improved direct wave by using a three antenna method as shown in Fig. 4. [Proposed Method] shows the evaluated antenna factor by our method. [Catalog(D=4m)] indicates the antenna factor from the catalog data. The difference [diff] shows good agreement between them within about from +0.8 dB to -0.8 dB over the frequency range from 80 MHz to 300 MHz.

As is demonstrated here, the proposed method can be also used to estimate free-space antenna factors of biconical antennas.
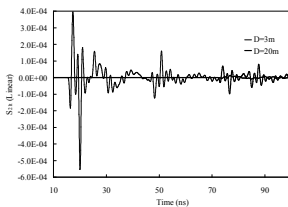
Fig. 1 S_{21} in the time domain
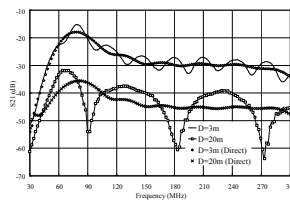
Fig. 2 S_{21} in the frequency domain
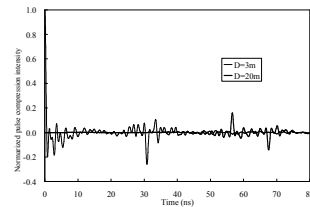
Fig. 3 Pulse compression result
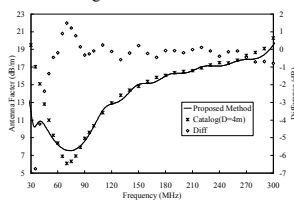
Fig. 4 Free-space antenna factor by our proposed method

References
1. S. Kurokawa, K. Komiyama, T. Sato, ``Experimental Study of Antenna Factor Measurement for Log periodic Antenna with the Time Domain Method,'' Proceeding of CPEM2004, Tu4c23, pp.196-197, 2004.
2. S. Kurokawa, M. Hirose, K. Komiyama, ``Time-domain Three Antenna Method for Evaluation of Antenna factors of Log-periodic Antenna,'' Proceeding of EUMW2007.

Using Numerical Methods to Validate the Analysis of Pyramidal Horn Antennas through Improved Diffraction Theory

Gordon Mayhew-Ridgers[1], Johann W. Odendaal[2], and Johan Joubert[2]

[1]*Vodacom (Pty) Ltd., Midrand, South Africa*
[2]*University of Pretoria, Pretoria, South Africa*

E-mail: gordon.mayhew-ridgers@vodacom.co.za

Diffraction theory has been used successfully in the past to analyse pyramidal horn antennas, especially for on-axis gain calculations [1-3]. The method is very fast, but relies on accurate expressions for the fields in the aperture plane of the horn. In this study, the expressions for the aperture fields have been refined to more accurately reflect the astigmatic nature of the wave that emanates from the throat of the horn. Up until now, measurements have mainly been used to illustrate the accuracy of such analytical methods. However, the general availability of accurate wideband measurement results for horns with varying dimensions is very limited. With the increasing availability of powerful numerical methods and computational power, another option is to use numerical methods as a benchmark. As such, the method of moments, employing the multilevel fast multipole method, is used here to validate the improved diffraction theory for pyramidal horn antennas with widely varying flare sizes and angles. As an example, Fig. 1 shows the agreement between the methods when calculating the electric field in the *E*-plane aperture of a standard Scientific-Atlanta Model 12-8.2 horn antenna. Fig. 2 shows the corresponding on-axis gain, including accurate measurement data. Fig. 3 depicts the on-axis gain for a similar antenna, but where the length of the flare section has been halved. These results illustrate the capabilities of the improved diffraction theory and also the possibility of using numerical methods as benchmark.
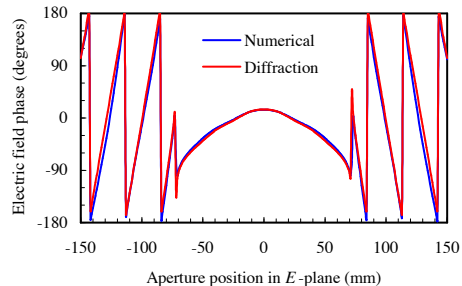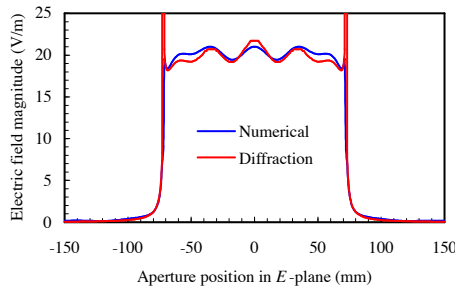
Fig. 1 – Magnitude and phase at 10 GHz of the electric field in the *E*-plane aperture of the standard horn antenna.
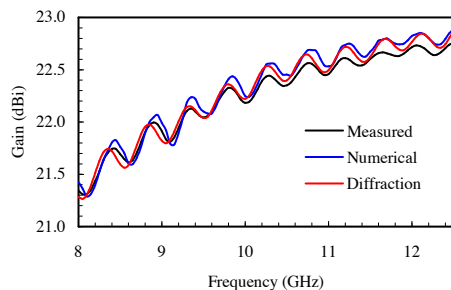
Fig. 2 – Gain of the standard horn antenna.
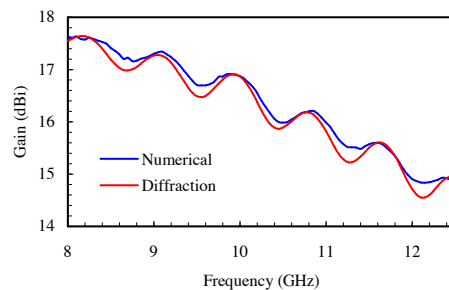
Fig. 3 – Gain of the shortened horn antenna.

References

1. J. F. Nye and W. Liang, "Theory and measurement of the field of a pyramidal horn," IEEE Transactions on Antennas and Propagation, vol. AP-44, no. 11, Nov. 1996, pp. 1488-1498.
2. G. Mayhew-Ridgers, J. W. Odendaal, and J. Joubert, "On primary incident wave models for pyramidal horn gain calculations," IEEE Transactions on Antennas and Propagation, vol. AP-48, no. 8, Aug. 2000, pp. 1246-1252.
3. J. W. Odendaal, "Predicting directivity of standard-gain pyramidal-horn antennas," IEEE Antennas and Propagation Magazine, vol. 46, no. 4, Aug. 2004, pp. 93-98.

Compact Antenna Design for High Power Microwave Applications

Haijing Zhou[1], Daibing Chen[2], Fukai Xu[1]

[1]*Institute of Applied Physics and Computational Mathematics,Beijing, P. R. China*
[2]*Institute of Applied Electronics, China Acedamy of Engineering Physics, Mianyang, P. R. China*

.
E-mail: zhou_haijing@iapcm.ac.cn

In the area of high power microwave (HPM), most of the HPM sources generate modes with circular symmetry, such as TM01 mode in circular waveguide and TEM mode in coaxial waveguide. The output waveguides are typically highly-oversized to handle higher peak power of GW level. It is well known that HPM systems are often required to produce directional beam. Therefore, novel microwave component and antenna designs are needed to make proper mode conversion and radiation.

As we know, high power mode converters can convert modes from TM01 or TEM to TE11 or HE11 [1]. But it is quite difficult for a mode converter design to reach high efficiency, high power capability, wide bandwith and compactness simultaneously. Vlasov antenna and COBRA (Coaxial Beam Rotating Antenna) were reported for HPM radiation [2-3]. For both of them, mode conversion and radiation occurred in the antenna apertures. Without mode converters needed, the antennas can be directly connected to HPM source, but they both have bad aperture efficiency and far-field patterns.

In this paper, we introduce our recent works on compact antenna design with axial maximum. The basic principle used in our designs is called "zoned phase shifting". Firstly, we use metal plates to divide the waveguide into several sub-waveguides or zones. Secondly, we use phase shifter in the different sub-waveguides or zones to make different phase velocity. For example, when a circular waveguide is divided into two half-circular waveguide, a propagating TM01 mode can be transformed to 2 propagating TE11-like modes with same polarization but 180 degree phase difference. One can add a half-circular dielectric cylinder in one half-circular waveguide to get lower phase velocity. One can also add some metal septum in the other half-circular waveguide to get higher phase velocity. By this means, we can finally make these 2 TE11-like modes in phase. Two TE11-like modes in half-circular waveguides in phase will produce a TE11 mode in circular waveguide.

Based on the above idea, we designed, simulated and fabricated several kinds of antenna for HPM applications in recent years. The results verify our design idea, and indicate the excellent radiation characteristics. This paper will give these designs, with both simulation results and experimental results.

References
1. R. A. Koslover etc., "Compact, Broadband High Power Circular TM01 to TE11 Mode Converter", U.S. Patent No.4999591.
2. M. Haworth etc., "Recent Progress in the Hard-Tube MILO Experiment", SPIE Vol.3158, 1997.
3. Clifton C. Courtney etc., "The Coaxial Beam-Rotating Antenna (COBRA): Theory of Operation and Measured Performance", IEEE Transaction on Antenna and Propagation, Vol.48, No.2, 2000.

The Design Of A Nearby Lightning Simulator

J.T. Naff[1], V.B. Carboni[1]
[1]*L-3 Communications, Pulse Sciences Division, San Leandro, California, USA*

E-mail: john.naff@L-3com.com

MIL-STD-464A describes waveform parameters of lightning indirect effects. The Lightning Simulator concept described here simulates the magnetic field 10 meters from a severe stroke (Current Waveform A). MIL-STD-464A also specifies the peak time rate of change of the electric field associated with the closure of the lightning stroke.

Some nearby lightning simulators try to create the required magnetic field with current in a spark or in a wire. It is very difficult to simulate the proper temporal behavior of the current over a sufficiently large volume to test objects of interest using the single current type of simulator.

The simulator concept described here separately creates the specified magnetic field and the specified electric field in both peak amplitude and time history. For this concept, the design parameters for a system capable of testing large vehicles or similarly sized test objects will be given. The simulator provides an environment that matches the MIL-STD-464A requirements for both magnetic and electric fields. To date, two implementations of the concept have been made and these will be described. Electrical waveforms from these implementations will be presented and comparisons with specifications will be made.

HPEM - 21
Lightning Analysis and Protection

Oral Presentations

Optimization of the Protection of a buried Telecommunication Cable against Lightning effects

Yannick Bourgeois[1], Ahmed Zeddam[1], Alain Reineix[2]
[1]*Orange Labs, 2, Avenue P. Marzin 22307 Lannion, France*
[2]*Xlim, 123 Avenue Albert Thomes 87100 Limoges, France*

...
E-mail: ahmed.zeddam@orange-ftgroup.com

The physics of lightning, as well as its interaction with power and telecommunication systems need research activities that require theoretical tools and also experimental studies in order to validate the different models and protective schemes. The most effective tool for studying both the direct and indirect effects of lightning on power and telecommunication networks is constituted by artificially triggered lightning. The aim of this paper is to assess the level and the waveshape of the voltages and currents generated on a buried telecommunication cable associated to a shielding cable used as protective measure. The results of simulation are validated using a comparison with measurements obtained during a campaign of triggered lightning carried out on 2006 in Cachoeira Paulista – Brazil [1]. Once validated, the model is then used in order to optimize the lightning protection of buried cable entering in the exposed sites such as a Radio Base Station.

In order to prevent lightning damage of buried cable, a common practice is the use of a shielding wire installed just above the cable in the ground. The physical and geometrical characteristics of the shield wire are of course depending of the conductivity and permittivity of the soil but also of the parameters of the lightning current. From an economic point of view it is convenient to optimize the cost of the installation by assessing the exact length of the shield wire required by an efficient protection accordingly to characteristics of soil and lightning. Such study is carried out by using a computer code based on the transmission lines theory associated to a topological approach [2]. It allows the evaluation of the currents and voltages generated, by an external electromagnetic wave and external sources located, on a complex telecommunication network composed of multiconductors lines interconnected by a network of linear loads.

The first step of our study leads to the validation of the computer code by using the results of experiments where a telecommunication buried cable was subjected to rocket-triggered lightning flashes obtained on the test site of Cachoeira Paulista - Brazil. The experimental telecommunications network is constituted by a 1000 m buried section connected to an overhead cable of 2000m long. The rocket launcher is connected to earth through a cooper electrode 1 m long which is buried horizontally close to the surface of the soil (figure 1).

Figure 2 shows the comparison between the measured and calculated current on the screen of the telecommunication cable measured 95m faraway from the injection point. On the same figure we have also reported the contribution to the signal due respectively to the radiated field and to the direct coupling.
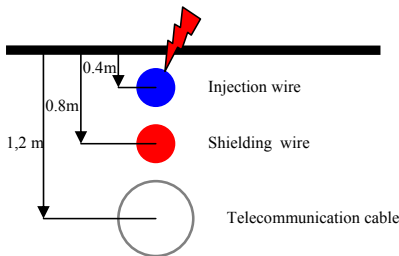
Fig. 1 – Protection of an exposed site
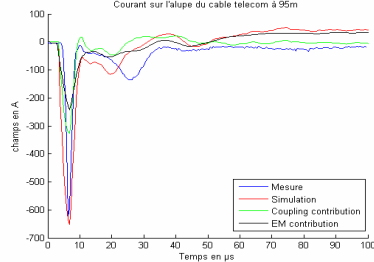
Fig. 2 Comparison: current on telecom cable

The good agreement between the theoretical and measured results validated our simulation code and allows us to perform a parametric study of a real installation in order to optimize the protection of an exposed site. The final paper will particularly focus on the evolution of the generated surges on the buried structures by taking into account the various physical parameters of the ground and of the shield wire.

References

[1] C.F. Barbosa, F.E. Nallin, S. Person, A. Zeddam, *"The effect of protection procedures applied to telecommunication lines on the lightning induced surges"*, ICPL 2004, Versailles, 2004.

[2] K. Kerroum, F.Paladian, J. Fontaine, M. Vautier, A. Zeddam, *"Approche globale du couplage d'une onde EM avec un système de câbles multifilaires"EMC Symposium,*CEM94, Toulouse, 1994.

Simulation of Lightning Current Pulse Effect Using MCG Based Energy Sources

Yu.V. Vilkov[1], A.S. Kravchenko[1], V.D. Selemir[1], V.A. Terekhin[1], W.A. Radasky[2]

[1]VNIIEF, Sarov, Russia
[2]Metatech Corporation, Coleta, USA
E-mail: kravchenko@ntc.vniief.ru

Magneto-cumulative generators (MCG), proposed and tested in VNIIEF, are nowadays sources of electromagnetic energy with the highest specific power, reaching 10 GW/kg. In these generators a chemical energy of high-power explosive substances (HE-charge) is transferred into the energy of a magnetic field of high (up to 100 T) inductance with an efficiency factor up to 20%. The generated power could be used to reproduce effects of electromagnetic pulses of natural (thunderstorm discharges) and artificial (electromagnetic pulse of nuclear explosion) origin.

Works on a lightning current pulse reproduction with maximum possible amplitudes (in nature) are being carried out in VNIIEF for a number of years. Effects of such pulses on typical grounding systems are being studied. The paper presents results of some varieties of energy sources tests, based on magneto-cumulative generators, at the lightning current pulse simulation on the grounding rod. In the experiments with the current pulse of the 70-90 kA amplitude for the first time we:

- recorded appearance and development of multiple high-power spark discharges along the ground surface up to 30 m length;
- detected significant asymmetry of electric potentials distribution, correlating with distribution of the high-power spark channels, near the grounding rod;
- measured volt-ampere characteristic of the grounding rod in a soil with a specific resistance of 160 $\Omega \cdot m$;
- recorded a decrease of an active resistance of the grounding rod in more than 12 times at the current pulse amplitude of 70 kA [1, 2].

Numerical code of the helical MCG with a transformer unit operation was developed for the MCG based energy sources and the typical grounding system efficient matching [3]. The current pulse front formation of 2 μs length was carried out with a breaking unit, made of electrically exploding copper wires in an arc suppressing medium, at reproduction of the current pulse of the lightning of the negative polarity.

Two models of a pulsed active resistance of the grounding rod that satisfactory describe the obtained experimental results are proposed.

An integral pattern of luminescence of the MCG based energy source and high-power spark discharges near the grounding rod is presented in the figures.

Fig. 1 – The integral pattern of the energy source luminescence   **Fig. 2 – The fragment of spark channel luminescence in the neighbourhood of the grounding rod**

References
1. Yu.V. Vilkov, V.A. Zolotov, A.S. Kravchenko, et al., "Ultra-high current pulse formation on the high impedance load with the use of based on EMG energy source for lightning modeling," Elektrichestvo, no. 8, 2004.
2. Yu.V. Vilkov, A.S. Kravchenko, V.D. Selemir, and V.A. Terekhin, "Studies of spark discharge appearance and propagation at lightning current pulse reproduction using a power source, based on EMG," Elektrichestvo, no. 8, 2005.
3. A.S. Kravchenko, and Yu.V. Vilkov, " A power supply for simulating lightning-current pulses," Instruments and Experimental Techniques, no. 4, 2006.

HPEM - 21
Lightning Analysis and Protection

Oral Presentations

Full Wave Analysis of Vertical Ground Rod Penetrating Two-Layer Soil

Vesna Arnautovski-Toseva[1], Leonid Grcev[1] and Khalil El Khamlichi Drissi[2]

[1] *Ss. Cyril & Methodius University, Faculty of Electrical Engineering and IT, 1000 Skopje, Macedonia*
[2] *University Blaise Pascal, LASMEA UMR 6602, 63177 Aubière, France*
E-mail: atvesna@feit.ukim.edu.mk

The research of high frequency grounding system's performance is increasingly important in different applications, such as, for example, EMC, lightning and fault protection in industrial and power plants, and in emerging technologies such as power line communications. In EMC studies, usually required quantities include longitudinal and leakage current, induced voltages and electromagnetic fields in the vicinity. Traditional analysis of grounding systems is generally based on static and quasi-static theory concepts of images [1] that take the soil as either homogeneous or inhomogeneous conducting medium with multiple horizontal layers. A comparison study of exact electromagnetic model vs. quasi-static models for ground rod in uniform soil [2], has suggested that applicability domain of the quasi-static models is restricted to some upper frequency limit. However, the electromagnetic model of grounding systems [3], considers homogenous soil only. The recently developed electromagnetic model for two-layer soil treats only horizontal grounding conductors [4].

This paper presents rigorous electromagnetic field approach for full wave analysis of the grounding performance of vertical ground rod penetrating two-layer soil. Mathematically, the model is formulated by mixed potential integral equation with exact Green's functions of stratified medium that involves Sommerfeld type integrals. Computationally, the model is based on the Galerkin approach in the method of moments and direct numerical integration of Sommerfeld integrals. For excitation by injection of current in the rod upper end, this solution gives current distribution, impedance to ground, electric field and potential distributions. Paper investigates the frequency domain response of a vertical ground rod penetrating two-layer soil with respect to the parameters of both layers and the rod geometry.

To analyze the grounding performance, Fig.1 presents a comparison of the leakage current density modulus along a 10-m vertical rod in two-layer soil, with the layer depth of 3-m in frequency range up to 10 MHz. Two alternative situations are analyzed, with upper layer soil reisistivity of 100-Ωm and bottom layer with higher resistivity 300-Ωm (K = +0.5) and with lower resistivity 33-Ωm (K = –0.5). (Here K is the reflection coefficient.) The results show that the rod generally behaves quite differently at low and high frequencies. At lower frequencies, the leakage current is almost uniform in each layer and depends on its resistivity, while at high frequencies the current distribution depends also on the frequency and the position in relation to the injection point. Presented method enables detailed parametric analysis of the grounding performance of parts of vertical ground rods in soil layers with different electrical characteristics in a wide frequency range.
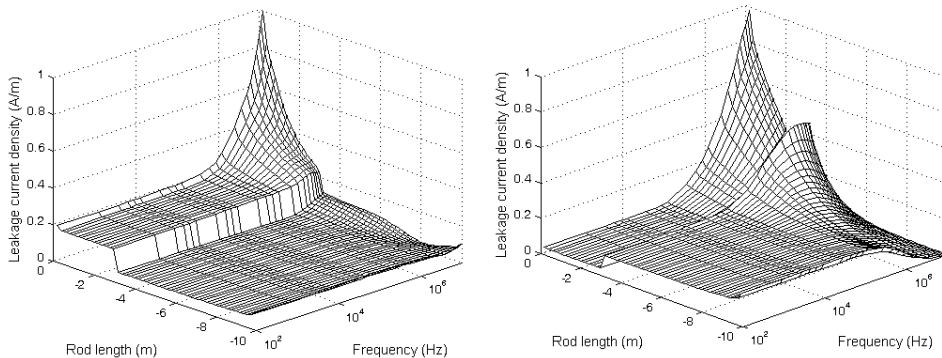
Fig. 1 – Leakage current density with respect to rod length and frequency: K = +0.5 (left), K = –0.5 (right)

References
1. T. Takashima, T. Nakae, R. Ishibashi, "High frequency characteristics of impedances to ground and field distributions of ground electrodes," IEEE Trans. Power Apparatus Syst. 100 (1980) 1893-1900.
2. R. Olsen, M. C. Willis, "A comparison of exact and quasi-static methods for evaluating grounding systems at high frequencies," IEEE Trans. Power Delivery 11 (1996) 1071-1081.
3. L.Grcev, F.Dawalibi, "An electromagnetic model for transients in grounding systems," IEEE Trans. Power Delivery, 5 (1990) 1773-1781.
4. V. Arnautovski-Toseva, L. Grcev, "Electromagnetic analysis of horizontal wire in two-layered soil", J. Computational Appl. Math., 168 (2004) 21-29.

The Effects of the Upward Leaders on the Collection Area of a Structure

S. Ait-Amar[1], G. Berger[2]

[1]ABB France, Pôle Foudre Soulé-Hélita, Persan, France
[2]Laboratoire de Physique des Gaz et des Plasmas, Gif-sur-Yvette, France
E-mail: sonia.ait_amar@fr.abb.com

The collection area for direct strikes to a structure is an important component in the risk assessment. The International Standard [1] describes the evaluation method of this surface. In the case of a complex structure, the analytical collection area is not obvious.

A 3D numerical model has been introduced in the last years [2] [3]. This model considers the structure geometry, the downward and upward leaders' propagation. It was demonstrated that the numerical model goes farther than the EGM and exhibits the effect of competing upward leader launched from the lightning protection system and from vulnerable zones on the structure.

The present paper aims to revisit the attractive area of structure by introducing the upward leaders' contribution. Using simple assumptions on the conditions for upward leader inception and downward-upward leader junction, the position of the downward and upward leader tips, just before the final jump, are firstly computed.

Afterwards, the extreme position of upward leader's tips determines the attractive radius. Finally, the collection areas for elevated and complex structures are evaluated and compared to those deduced from the International Standard [1].

References

1. G. Murtaza Hashmi and Matti Lehtonen, Modeling of Rogowski Coil for On-line PD Monitoring in Covered-Conductor Overhead Distribution Networks, Helsinki University of Technology (TKK), 2006.

On the Relationship between Lighting Channel Conductance and Flattening Effect of Electric Field at Close Range

A. De Conti[1], N. Theethayi[2], S. Visacro[1], V. Cooray[2]

[1]*Lightning Research Center, Federal University of Minas Gerais, Belo Horizonte, Brazil*
[2]*Division of Electricity, Uppsala University, Uppsala, Sweden*

E-mail: conti@cpdee.ufmg.br

According to Braginskii's theory [1], the radial expansion of spark gaps as a function of the input current versus time is given by $r \approx \sqrt{\left(4/\rho_0\pi^2\right)^{1/3} \int_0^t (\sigma\xi)^{-1/3} i^{2/3} dt + r_i^2}$, where r is the spark gap radius (m), i is the current (A), r_i is the initial radius (m), σ is the channel conductivity (S/m), ρ_0=1.29 kg/m^3 is the atmospheric density, and ξ is a dimensionless factor describing the rate of radial expansion of the arc channel. Assuming that this equation is also valid for representing the radial expansion of the lightning channel and considering a constant channel conductivity, the per-unit-length channel resistance $R(t)$ can be found from $R(t)=1/(\sigma\pi r^2)$. If the return stroke channel is represented as a nonuniform transmission line whose per-unit-length parameters (L and C) vary with height according to Jordan's formula, and if a typical lightning current is injected at the lower end of the channel by a lumped current source, the channel currents obtained with the use of the equations above with typical channel conductivities and different values of r_i and ξ lead to a flattening of electric field waveforms calculated at the near range (50 m) that is consistent with experimental data (see [2] for details). Note however that the transverse conductance and the nonlinear channel capacitance associated to the corona sheath surrounding the channel core were neglected in [2]. Theoretically, both parameters should be included in a more rigorous return stroke representation, and for this reason it is important to identify to what extent the E-field flattening shown in [2] is preserved with the inclusion of such transversal effects. Here, as in [3], we only consider the effect of a shunt conductance G per unit length, assuming a total conductance from the lightning channel to ground. Note that this is from the outset an important simplification since in actual lightning the shunt conductance should refer to losses confined to the corona sheath volume. In the performed analysis, we assumed σ=1×10^4 S/m, r_i=0.1 cm, and ξ=4.5, which are typical parameters representing the lightning channel, and G was either assumed constant or decayed exponentially with time from an initial value G_i with a time constant T_G. It was found that, for the assumed channel conductivity, the E-field flattening in the close range is still obtained if either (i) a constant, uniformly distributed conductance up to about 0.05 μS/m is added to the channel or (ii) a channel conductance exponentially decaying with time from a uniformly distributed value of the order of 10^{-6} S/m with T_G up to about 1 μs is added to the channel (see some of the evaluated cases in Fig. 1). Larger decay constants or larger values of G were found to lead to a continuous increase with time of electric fields calculated at 50 m. Note that the values above should be viewed simply as validity limits for the results presented in [2] since the inclusion of the channel shunt conductance is based solely on theoretical assumptions that need further experimental evidences.
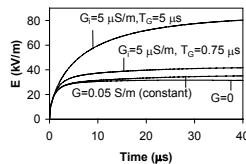
Fig. 1 –Electric fields calculated at 50 m from the channel base with the nonlinear return stroke model of [2].

References
1. S. I. Barannik, S. B. Vasserman, and A. N. Lukin, "Resistance and inductance of a gas arc", Sov. Phys. Tech. Phys., vol. 19, no. 11, 1449-1453, 1975.
2. A. De Conti, S. Visacro, N. Theethayi, and V. Cooray, "A comparison of different approaches to simulate a nonlinear channel resistance in lightning return stroke models", accepted for publication in the J. of Geophysical Research, 2008.
3. N. Theethayi and V. Cooray, "Representation of the return stroke as a transmission line – the apparent return stroke velocity", In Proc. of the 27th International Conference on Lightning Protection, Avignon, France, 2004.

A Preliminary Assessment of Radio Frequency Threats to Airports

D. V. Giri[1], F. M. Tesche[2], M.Nyffeler[3], P. Bertholet[4], H. Gusset[5] and H. Wipf[6]

[1]*Pro-Tech, Alamo, CA, USA*
[2]*EM Consultant, Saluda, NC, USA*
[3]*armasuisse, Spiez, Switzerland*
[4] *armasuisse, Spiez, Switzerland*
[5]*Swiss Army, Bern, Switzerland*
[6]*Skyguide, Zurich Airport, Switzerland*

E-mail: Giri@DVGiri.com

Civil aviation has become an integral component of present day society. It promotes an economic base for a community, assists and encourages trade, and is vital for the health, safety and welfare of the general public. Yet, we all know some of its vulnerabilities even from very low-level electromagnetic emitters. For example, cell phone use is prohibited in all phases of a flight, due to its potential adverse effects on navigational electronics on-board the aircraft. Other passenger electronic devices (PED) such as lap-top computers, DVD players etc., have been known to cause interference and are prohibited during the take-off and landing phase of a commercial flight. In addition to these low-level emitters, both military and civilian aircrafts are routinely required to operate under adverse electromagnetic environments (EME), such as

- Natural- lightning electromagnetic pulse (N-LEMP),

- Electrostatic discharge (ESD),

- Electromagnetic environment in and around airports,

- Intra-system electromagnetic interference (EMI), and

- Inter-system EMI.

In this paper, we present the results of a preliminary assessment of an Intentional Electromagnetic Interference (IEMI) threat in the context of an airport. We look at the airport as an electromagnetic systems with three distinct components; a) the physical airport including the air navigation services, the aircraft and the passenger terminal. Out of all the operations carried out at an airport, from an electromagnetic viewpoint, the systems of interest to us are: a) RF interfaces, b) Power utility, c) Communication, Navigation and Surveillance, d) Air Traffic Management and e) Other Sensors (e.g., meteorological). The results of our site survey of an airport in Switzerland (shown in Fig.1) will be presented

Fig. 1. A view of an airport in Switzerland

We discuss the potential RF threats in relation to the applicable MIL-STD-464 on aircraft and the FAA and JAA prescribed HIRF Environments.

Electromagnetic Interference Studies with an Air Defence System

D. Weixelbaum, E. Mutzbauer, R.H. Stark

Diehl BGT Defence GmbH & Co. KG, D-90552 Roethenbach a.d. Pegnitz, Germany

E-mail: Dieter.Weixelbaum@diehl-bgt-defence.de

Modern electronic systems are susceptible to intense electromagnetic fields. Coupling of electromagnetic (EM) waves mainly depends on target size, geometry, material properties and characteristics of the incident electromagnetic radiation. Usually coupling paths are very complex. Besides front door coupling, where the EM wave couples to the system through active antennas and sensors, most systems are very sensible to back door coupling. Here coupling paths are mainly unknown, hard to determine and hardening of the system is difficult. The EM-wave penetrates through small slits, holes and feed throughs or even parasitic antennas into the interior of the system. The field amplitude is then converted into currents and voltages on the signal and power lines. Dependent on the amplitude of the induced signals disruption or even destruction of electronic systems and components occur. In both cases the system loses the functionality it was designed for.

Complex and large systems like this Air Defence System usually consist of several sub-systems and components which are separated from each other, distributed and connected via data transfer cables and power lines. Breakdown of a single component or sub-system often causes a failure of the entire system. In addition data cables and power lines are excellent antennas for EM coupling. Hence EM Interference studies with such a complex weapon system are of growing interest. Systematic studies are required in order to determine coupling paths and error mechanisms of such systems in order to develop hardening concepts.

The paper presents EMI studies performed with an air defence system. The studies have been conducted at the EM-test facility WTD81 (Wehrtechnischen Dienststelle für Informationstechnologie und Elektronik) in Greding. Systematic studies were performed with continuous and pulsed low power microwave sources in a frequency range from several ten MHz up to the giga hertz regime and with ultra-wideband sources. Furthermore novel pulsed HPEM-DS sources which had been developed at Diehl BGT Defence, Roethenbach a.d Pegnitz were used to evaluate the system's sensitivities.

Requirements regarding support, infrastructure and test procedure are discussed. The irradiation tests were performed with systematic variation of parameters like fieldstrength, polarisation, angle of incidence, modulation-frequency and pulse repetition rate respectively. Test results and comparison of the system's susceptibility dependent on the source respectively and the irradiation parameters are presented.

HPEM - 22
Critical Infrastructure & Related Topics

Oral Presentations

The Security Assessment
of Critical Energy Infrastructures: an Evaluation Approach

F. Delfino[1], G. B. Denegri[1], S. Guido[1], M. Invernizzi[1], M. Masera[2], I. Nai Fovino[2] and S. Olivero[3]

1: Department of Electrical Engineering, University of Genoa
Via Opera Pia 11a, I-16145 Genova, Italy
2: Institute for the Protection and the Security of the Citizen, European Commission Joint Research Centre
Via E. Fermi 1, I-21020, Ispra, Italy
3: SiTI – Higher Institute on Innovation Territorial Systems,
Via Pier Carlo Boggio 61, I-10138 Torino, Italy
E-mail of the corresponding author: igor.nai@jrc.it

Risk assessment of critical infrastructures (transportation, communication, energy production and distribution, water distribution) have a relevant role today , due to the increasing number of threats, both of natural and of intentional action, which could affect the life of a country and the security of its citizens [1]. Power plants generating electric energy and the grid upon which it is transmitted and distributed are examples of "hybrid" critical energy infrastructures; in such systems typical process and ICT components are combined with power devices to setup real-time control functions [2]. In the latest years, these hybrid infrastructures started to be connected to internal and external communication networks, and ICT security has become a subject of primary concern, especially because such systems are prone to failures and vulnerabilities can be exploited by malicious software and agents.

This paper addresses the issue of the security of critical energy infrastructures and aims at merging the typical aspects of traditional risk assessment, based on reliability, safety and detailed identification of all the possible technical weaknesses, with the new concepts of ICT security. In particular, the attention is focused on the application of a risk assessment methodology, conceived to carry out a comprehensive security analysis of a generic industrial systems [3, 4, 5], in order to perform the security assessment of an energy production infrastructure, namely a combined cycle power plant. The methodology basically consists of five phases, pre-assessment (system modeling), vulnerability assessment, threat analysis, attack assessment and risk assessment. As far as the possible attack scenario is concerned, new attack patterns have been developed including together safety and security aspects with the creation of "macro-attack" tree templates, taking into account the failure rates of all the power plant components. The output of the analysis, namely the vulnerability, threat and attack indexes, and the final risk indexes for each service provided by the power plant (Fig. 1) and their dependence on the input values of vulnerability and threat plausibility has been investigated. Finally, the effect of the application of suitable countermeasures to mitigate the identified vulnerabilities has been studied and its beneficial action on the global risk index highlighted. The results of such analysis show how such methodology can be applied to perform comprehensive risk evaluations of other critical energy infrastructures, (e.g., the interconnected electric power grid and transformation substations).
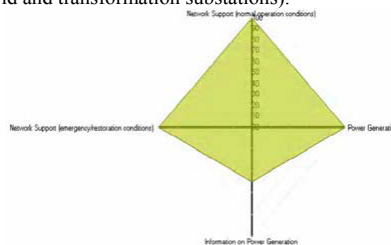
Fig. 1 – Risk radar chart for the high level services provided by the power plant.

References

1.   Commission of the European Communities, "Green Paper: on a European Programme for Critical Infrastructure Protection", Brussels, COM 576 (2005).
2.   A. Avizienis, J. Laprie, B. Randell, "Fundamental Concepts of Dependability", Res. Rep. n. 1145, LAAS-CNRS, 2001.
3.   I. Nai Fovino and M. Masera, "Emergent disservices in interdependent systems and system-of-systems", *Proceedings of the IEEE Conference on Systems, Man and Cybernetics*, Taipei, 2006.
4.   M. Masera and I. Nai Fovino, "Models for security assessment and management", *Proceedings of the International Workshop on Complex Network and Infrastructure Protection*, 2006.
5.   I. Nai Fovino and M. Masera, "A service oriented approach to the assessment of Infrastructure Security", *Proceeding of the First Annual IFIP International Conference on Critical Infrastructure Protection*, Dartmouth College, Hanover, New Hampshire, USA, March 19 - 21, 2007.

HPEM - 22
Critical Infrastructure & Related Topics

Oral Presentations

Interaction of Concrete based Buildings with Electromagnetic Waves

M. Sallin[1], B. Daout[1], M. D. Vo[1], H. Wipf[2]
[1]*Montena emc, Rossens, Switzerland*
[2]*Skyguide, Wangen b. Dübendorf, Switzerland*

E-mail: marc.sallin@montena.com

A detailed knowledge of electromagnetic wave interaction for building grade concrete is of interest in many safety critical environments like airports, power stations and civil defense facilities.

The work consists of a theoretical explanation of the processes leading to reflection at the interface air-concrete and to the attenuation inside the concrete wall. Focus lies in properly estimating the pertinent material parameters, especially with regard to the water content and the temperature inside the concrete.

The material complex permittivity is the important parameter that is dependant on the concrete's components: cement, gravel and water. It is of interest to compare different concrete mixtures in respect to their permittivity.

A special measurement system was developed to study this relationship. In use is an open-ended coaxial line probe, a network analyzer, temperature and humidity recording system and a climatic chamber with a controlled atmosphere. This allows continuous measurements during the hydration process of the concrete. The open-ended coaxial line probe is using a reflection method and was specially developed to adapt to materials, whose state of aggregation is non-stationary. For instance concrete going from a liquid to a solid state. The advantages of this method are the relatively large sample size and the reusable sensor structure.

Fig. 1 – Open-Ended Coaxial Line Probe

Present and Future Challenges of Aircraft Electromagnetic Certification

R. Hoad and A. Wraight

QinetiQ Ltd., Cody Technology Park, Farnborough, Hampshire, UK, GU14 0LX

E-mail: rhoad@qinetiq.com

The clearance of aircraft and aircraft systems to High Intensity Radiated Fields (HIRF) and for other aspects of EM certification is a challenging discipline. The HIRF radiated environment encompasses high power broadcast transmitters at HF (100 MHz) through to very high power Radar sources up to 18 GHz. Modern civil standards for HIRF such as RTCA DO160E/EUROCAE ED 14E [1] require testing of equipment and whole aircraft platforms up to peak electric field strengths of 7 kV/m (pulse modulation). The Electromagnetic environment is onerous and this is compounded by the greater integration of digital electronics onto modern air platforms. These challenges lead to greater emphasis on electromagnetic protection design for modern aircraft architectures and place stringent demands on the clearance and certification process which can encompass computational electromagnetic modelling and thorough susceptibility testing.

The aircraft on-board environment is also increasing in complexity due to increasing pressure for airlines to allow the use of passenger 'carry on' electronic devices such as laptops, known as Portable Electronic Devices (PEDs) and Transmitting PEDs (T-PEDs) such as mobile or cellular communications devices. Regulatory authorities are also keen to let market forces decide on the use of T-PEDs on aircraft [2]. There is evidence [3, 4] that these devices have caused interference to aircraft systems.

This paper discusses the trends in the civil and military external and internal environment, discusses the challenges that these changes represent. Insight is also provided into how the aircraft design influences the system response to electromagnetic disturbances and also how these challenges are being solved.

References

1. RTCA DO160E/EUROCAE ED 14 E.
2. UK Office for Communications (OFCOM) consultative document 'Mobile Services on Aircraft - Discussion paper on the introduction of mobile services on aircraft', 10th April 2006
3. Ross E., 'Personal Electronic Devices and Their Interference With Aircraft Systems', National Aeronautics and Space Administration, Langley Research, NASA / CR-2001-210866, June 2001
4. 'Effects of Interference from Cellular Telephones on Aircraft Avionic Equipment', UK Civil Aviation Authority (CAA), Report 2003/3, 30 April 2003

HPEM - 22
Critical Infrastructure & Related Topics

Oral Presentations

Damage Factors Estimation for Global Distributed High-Voltage Grids under the Influence of the Electromagnetic Disturbances

Y.A. Kholodov[1], A.K. Bordonos, A.S. Kholodov, N.E. Lavrinenko, I.I. Morozov, E.L. Stupitsky

[1]*Moscow Institute of Phycics and Technology, Moscow, Russia*

E-mail: kholodov@crec.mipt.ru

When the parameters of the external electromagnetic disturbance are the same as for the powerful geomagnetic storms, the technique of the estimation their influence on the high-voltage grids should contain the following basic phases:

the estimation of the induced currents in the transmission facilities induced by the electromagnetic disturbance and nonlinear transient processes arising;

the influence of the induced currents on the operation of the protection automatics for high-voltage grids elements;

the stability estimation for the whole power supply system in case of separate disconnection some elements of the network.

To estimate the induced currents it was chosen the equivalent circuit with two grounded transformers. By the comprehensive analysis of the working current protection system for high-voltage lines and the mechanisms of their operation it is shown, that the electromagnetic disturbance, continuing 30–60 s leads to the assured disconnection for the lines in spite of the automatic inclusion devices. Here the most sensitive to the influence of the electromagnetic disturbance will be electric mains with tension 500–1000 kV.

In this work in addition to the conventional algebraic and statistical models for the extreme cases investigations as well as for the network design and optimization problems it is suggested the simulation model which is based on the solution of the correspondent boundary-value problem on the graphs for the partial differential equations. Though, the circuit theory is developed for a long time the questions concerned with the non-harmonic dynamics and nonlinear processes in the global distributed networks are still not practically solved. Moreover, the existing methods require solving the high dimensionality equation systems even for the linear networks with the lumped parameters. This can be done more efficiently if we will be start our calculations directly from the dynamic equations without the assumption that all network process have the harmonic character and that is to suggest in this work. Thus, the proposed model has the set of the essential distinctions from the existing:

it takes into account the time dynamics all network processes and well enough simulates work of the global distributed high-voltage grids with given topology.

it can compute possible effects from the impact of the arbitrary external factors as well as investigate a possibility of the extreme case origination in the power grids.

it can be used for the network testing in the different operating modes before putting them into operation as well as on the system design phase.

it also can be used in the searching of the optimal energy-saving operating modes for the power grids with given topology.

Critical Infrastructure Protection and IT Warfare

Stefan Burschka

Swisscom AG, Bern, Switzerland

...

E-mail: stefan.burschka@swisscom.com

With the rise of the IP network a new quality of threat arose when real infrastructures such as telecom, electrical, transport and even the banking system were connected. The pace of this development is ever increasing not only promoting our economy but also giving rise to a new kind of criminal activity and warfare. Targeted IT Warfare complementing E-Warfare as stealth and very effective weapon against individuals, groups, businesses and countries is already common practise. In this context so called Bot Networks earned a dubious fame as distributed, invincible and up to now stealthy weapons responsible for 90% of criminal on-line activity such as Identity Theft, Corporate Espionage, Phishing and DDoS attacks. The next generation of Artificial Intelligence based Malware being stealthy circumventing nowadays IP security protection mechanisms and inventing new kinds of attacks by themselves is already technological possible. It only requires a criminal or political motivated business case, hackers with a research background and a financier.

Nevertheless, we allowed and promoted the evolution of this kind of E-Warfare by violating the most basic principles of reliable design, survivability and inappropriate product selection in favour of economic and political factors. Our trust in SW technology to cope with unwanted underlying complexity in lower layers by introducing even more complexity on higher layers produced even more havoc. Dependable principles of mechanic and electronic engineering were replaced by tool religion, doctrines, and ever complicated programming styles. By adding human error the present situation is definitely in favour of malicious elements.

Recent efforts in Critical Infrastructure Protection (CIP) aim at the understanding and prevention of outages and control faults in Critical Infrastructures (CI) by SW simulations. But assumptions are made about the attack or the fault scenarios, underestimating the system complexity or ingenuity of humans. Although being useful research, little support for our frontline troops the human administrator and security analyst is delivered. Therefore a special group at Swisscom in cooperation with armasuisse, IBM research, FUB and Fed Pol are now trying to address certain shortcomings in our IT defense lines. In order to achieve this, decent progress and cooperation between Industry, Institutions and Government is necessary in the area of technical law enforcement support, SW weapons research, code and protocol reverse engineering, troubleshooting support of CIs and Decision Support tailored for IP controlled Infrastructures. We constantly look for partners to accelerate progress.

HPEM - 22
Critical Infrastructure & Related Topics

Oral Presentations

Influence of SAR Averaging Schemes on the Correlation with Temperature Rise in the 30-800 MHz Range

R. Zaridze[1*], A. Razmadze[1], L. Shoshiashvili[1], D. Kakulia[1], G.Bit-Babik[2], A.Faraone[2]

[1]*Tbilisi State University, Tbilisi, 0128, Georgia*
[2]*Corporate EME Research Laboratory, Motorola Labs, Fort Lauderdale, FL, USA*
E-mail: rzaridze@laetsu.org

The dependence of the spatial correlation between the volume-averaged SAR and the corresponding steady-state temperature rise in the model, based on voxelized by researchers at the Air Force Research Laboratory, Brooks AFB, Visible Human Project data sets exposed to plane waves at 30MHz, 75MHz, 450MHz, and 800MHz, considering 4 cases for each frequency (frontal, lateral exposures with both E and H polarizations), on the SAR-averaging scheme is investigated. The model features 40 different tissues with frequency dependent electrical properties defined according to the Cole-Cole dispersion model, while the thermal properties including metabolic heat production rates and blood perfusion parameters for each tissue were compiled from different sources (P. Bernardi et al, J.Lagendijk et al, O. Gandhi et al, A. Hirata et al). The electrical and thermal numerical simulations were performed using proprietary software package FDTDLab, a Finite-Difference Time-Domain based electromagnetic and thermal computational suite. Relative to each exposure condition, averaged-SAR distributions were computed for a wide range of cubic SAR averaging masses: 0.1, 0.5, 1, 5, 10, 20, 50, 100, and 200 grams. The averaged-SAR was computed using the IEEE standard SAR-averaging procedure, employing different averaging tissue masses and various air-inclusion factors: 20%, 50% and 75%. Depending on the maximum allowable percentage of air in the averaging volume, the resulting averaged-SAR may feature a smooth distribution within the body or a markedly discontinuous distribution near the body surface (Fig.1).
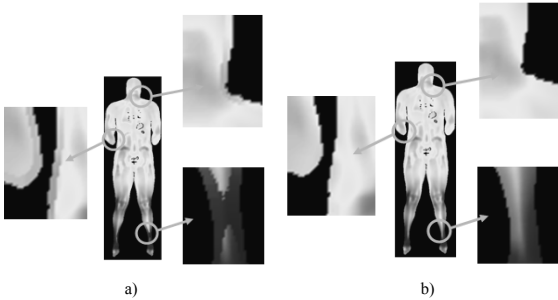
Fig. 1. 10-g average SAR distributions for (a) 20%, and (b) 75% air inclusion. The latter features a much smoother behavior near the body surface.

One of the distinctive aspects of the approach used in this study is that a global correlation coefficient is estimated using the temperature rise and mass-averaged SAR distributions across the whole body model, not just their peak values irrespective of the geometrical proximity, for each exposure condition. This approach leads to a global assessment of how well correlated averaged-SAR and temperature rise distributions are. The global correlation coefficient is here defined also for the case where several exposure conditions are considered together for its determination. Indicating with the index n the generic exposure condition and with m the specific averaging mass considered, the following formula is employed to derive the corresponding global correlation coefficient:

$$R^{(m)} = \frac{\sum_n \sum_{ijk} \left(SAR_{ijk,n}^{(m)} - \overline{SAR}^{(m)}\right)\left(\Delta T_{ijk,n} - \overline{\Delta T}\right)}{\sqrt{\sum_n \sum_{ijk} \left(SAR_{ijk,n}^{(m)} - \overline{SAR}^{(m)}\right)^2 \cdot \sum_n \sum_{ijk} \left(\Delta T_{ijk,n} - \overline{\Delta T}\right)^2}}$$

where $SAR^{(m)}_{ijk,n}$ and $\Delta T_{ijk,n}$ are the locally-averaged SAR, derived from the normalized SAR distributions for a cubic volume of mass m, and the temperature rise, respectively, at voxel (i, j, k) of the Visible Human model in the n-th exposure condition, while $\overline{SAR}^{(m)}$ and $\overline{\Delta T}$ are the ensemble SAR and temperature rise average values in the cumulative data set relative to the four plane-wave exposure conditions.

The impact of this distinctive behavior on the aforementioned correlation is shown to be only marginally significant. Most importantly, the proposed analysis indicates that the SAR averaged over 5 and 10 grams of tissue provides a better global correlation with the RF-induced temperature rise distribution for the considered plane-wave exposures.

Measurements of Induced Currents in Human Bodies Exposed to a Cellular Phone Base Station

H. Y. Chen and C. Y. Chuang

Department of Communications Engineering, Yuan Ze University
135, Yuan-Tung Road, Nei-Li, Chung-Li, Taoyuan Shian, Taiwan 320

E-mail: eehychen@saturn.yzu.edu.tw

Currents induced in human bodies near a cellular phone base station were measured by a parallel plate meter at 1869 MHz.   The geometrical structure of the parallel plate meter was made of two aluminum plates, wood, copper foils, and a resistor.   The upper and lower plates having a size of 900 and 2500 cm^2 with a thick of 2 mm are separated by a short distance of 4 cm, respectively.   The copper foils with a thick of 0.13 mm were pasted on the aluminum plates.   The resistor of 50 Ohms was connected between the two aluminum plates for measuring the induced currents by an Anritsu spectrum analyzer MS2721A.   For measurements of induced currents, the lower plate was connected to the ground.   Before measuring, the calibration of the parallel plate meter was checked using an Anritsu signal generator MG 3694B and an Anritsu spectrum analyzer MS2721A as shown in Fig. 1.   There are 6 measurement points for measuring induced currents on the roof-floor of a seven-story building.   The induced currents were measured when a man was standing on the parallel plate meter for wearing shoes and standing barefoot conditions.   The induced currents measured at these 6 measurement points are presented as shown in Table 1.   It is clear that the maximum induced current of 20.73 mA was found when a man stands barefoot near the cellular phone base station.   It is also found that a current reduction factor of 0.72~0.91 was occurred when the condition is changed from standing barefoot to wearing shoes.

Fig. 1 - Picture of calibration system

Table 1 - Induced currents measured at 6 locations when a man wearing shoes and standing barefoot. The unit of induced currents is in mA.

Location	1	2	3	4	5	6
Wearing Shoes	9.37	16.58	10.59	10.38	8.00	4.15
Standing Barefoot	10.10	20.73	12.76	11.43	11.16	5.32

HPEM - 23
Biological Effects

Oral Presentations

Magnetic Stimulation of Peripheral Nerves: Induced Electric Field in a Semi-Infinite Conducting Medium

Mihaela Plesa[1], Laura Darabant[1], Radu Ciupa[1], Catalin Curta[1], Adina Racasan[1]

[1]*TechnicalUniversityof Cluj-Napoca, Cluj-Napoca,Romania*

E-mail: Mihaela.Plesa@et.utcluj.ro

The great importance that the men's health has, led to the extension of the research areas from the modern medicine. So the investigation direction, named functional stimulation, is developed. This is based on the study of electric and magnetic stimulation of the nervous fibers. Magnetic stimulation offers some advantages compared to electrical stimulation, such as its non-contact, non-invasive nature and a lack of or minimal discomfort to the patient. The interest for the magnetic stimulation considerable increased in the last few years, due to its utility and applicability. This technique has been successfully used to diagnose a number of disorders of the neuro-muscular system and to map the motor cortex. Some of the limitations of the technique have been attributed to the poor focusing of the interacting electric field.

In this contribution, we present a model that combines elementary circuit analysis with the electromagnetic field theory to explain the action of the induced electric field upon nerve fibers. Maxwell's equations predict the induced electric field distribution that is produced when a capacitor is discharged through a stimulating coil. The current source and stimulating coil are modeled as a series RLC circuit. The induced electric field distribution within the tissue is calculated from the geometry of the stimulating coil [1-2] and the time course of the current [3]. The tissue is approximated by a semi-infinite conducting medium, considered homogeneous.
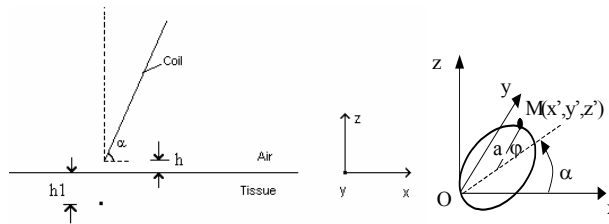
Fig. 1 – Stimulating coil placed over the tissue (conductive semi space)

The effect of the induced electric field upon the nerve is determined with a cable model. Neuronal structures can be modeled in the form of a cable and the membrane response can be computed by solving the equations describing the transmembrane potential of the cable in the presence of induced electric fields:

$$\tau \frac{\partial V}{\partial t} + V - \lambda^2 \frac{\partial^2 V}{\partial x^2} = \underbrace{- \lambda^2 \frac{\partial E_x}{\partial x}}_{=f(x)} \tag{1}$$

In our simulations we use different forms for magnetic coils (simple circular, elliptical and rectangular coils, figure of eight, slinky-coils); designed to improve focality of the electric field induced in the tissue during magnetic stimulation. The coils have the same number of turns (30), but these turns are differently positioned in space (different number of turns on each leaf). The radius of the leaf is 25mm. Then, we considered that each of these coils is a part of the RLC series circuit that represents the magnetic stimulator. The derivative of the transient current generated by the discharge of the capacitor is maximum at the beginning of the transient regime. The electric field and the transmembrane potential, generated by these coils, are computed and the obtained results are compared. All the computations are performed in a Matlab routine.

The model proposed allows a precise knowledge of the moment when the stimulation appears and of its duration and is useful for the design of optimized coils for stimulating peripheral nerves and neurons in the cortex.

References

1.   L. Cret, M. Plesa, D. D. Micu and R. V. Ciupa, "Magnetic Coils Design for Focal Stimulation of the Nervous System", EUROCON2007, Varsovia, Polonia, IEEE Catalogue Number: 07EX1617C, ISBN: 1-4244-0813-X, pp. 1998-2003.
2.   L. Cret, M. Plesa, D. Duma, R. V. Ciupa, "Magnetic Coils Design for Localized Stimulation", MEDICON 2007, Ljubljana, Slovenia, ISSN 1727-1983, ISBN 978-3-540-73043-9, Springer Berlin, pp. 665-668.
3.   Mihaela Plesa, Laura Cret, R. V. Ciupa, "Remarks on the electric field induced in the nerve fibers by magnetic stimulation", Acta Electrotehnica, Vol. 46, Nr. 4/2005, ISSN 1841-3323, pp. 225-231

Ultra Short Ultra Wideband Impulse Irradiation Effects on Human Cells

Y.G. Shckorbatov,[1] N.N. Kolchigin,[2] V.N, Pasiuga [1] O.V. Kazansky [2]

[1]*Kharkov National University, Institute of Biology, Kharkov, Ukraine,*
E-mail:Yury.G.Shckorbatov@univer.kharkov.ua
[2]*Kharkov National University, Dep. of Theoretic Radiopysics, Kharkov, Ukraine,*
E-mail:Nicolay.N.Kolchigin@univer.kharkov.ua

The effects of ultra short ultra wideband impulse irradiation on human cells are presented. We investigated the influence of this factor on the state of interphase nucleus of human buccal epithelium cell. Some of the earlier results of this work were presented in (Kolchigin, 2006). The buccal epithelium cells are the cells of the inner surface of the cheek. Due to their large size and easy availability these cells serve as an excellent model for cytophysiological research. These cells do not divide therefore their nuclei are constantly in the interphase state. Major nuclear content is chromatin which can be divided into two components: transcriptionally active euchromatin and transcriptionally silent heterochromatin. The balance between these two forms of chromatin determines functional state of the nucleus. In order to study this parameter cytologically the original method of evaluation of heterochromatin granule quantity has been developed (Shckorbatov, 1999).

Cells of human bucccal epithelium were obtained from the inner cheek surface by light scrapping with blunt spatula. Cells were suspended in 25 µl of solution containing 2.89 mM calcium chloride, and 3.03 mM phosphate buffer, pH = 7.0.

For irradiation of cell samples we developed a special device consisting of generator of short impulses, antenna and a set of attenuators. The short impulse generator formed the sequence of impulses with amplitude 25 V, wave resistance 50 O and width of the impulse 500 ps at the half of impulse height. Impulses were emitted at the frequency 1 MHz. We investigated the irradiation within the power density ranged from 10^{-6} to 10^{-2} W/cm^2. The irradiation time in all experiments was 10, 20, 40, and 60 s.

The irradiation in the range of 10^{-5} - 10^{-2} W/cm^2 induced significant increase in heterochromatin granule quantity. The effect was rising in the diapason 10^{-5} - 10^{-3} W/cm^2 and plateaued or even decreased at 10^{-2} W/cm^2. Effect was observed immediately after the irradiation. It was vanishing after 2 h of recovery at power densities 10^{-5} - 10^{-3} W/cm^2 but remained constant during 4 h of recovery after irradiation at intensity 10^{-2} W/cm^2. We assume that high intensity irradiation (10^{-2} W/cm^2) induces irreparable cell damage and cell death therefore cells do not recover.

Our results can be interpreted in the following way. The irradiation causes conformational changes of the chromatin which corresponds to its functional inactivation. Such effects are observed during various stress-related processes. It may serve as a primary mechanism of the electromagnetic factor action. Besides, we believe that electromagnetic fields cause direct changes in gene transcription as proposed by Blank and Goodman (2004).

References

1. Kolchigin N.N., Batrakov D.O., Shckorbatov Y.G., Pasiuga V.N, Kazansky O.V. "The effects of short exposition to low-energy impulse irradiation on human cells" Third International Conference on Ultrawideband and Ultrashort Impulse Signals, Sevastopol, p.151-152, 2006.
2. Shckorbatov Y.G. "He-Ne laser light induced changes in the state of chromatin in human cells" Naturwissenschaften, vol. 86, N9, p. 452-453, 1999.
3. Blank M, Goodman R. "Initial interactions in electromagnetic field-induced biosynthesis" Journal of cellular physiology, vol. 199, p. 359-363, 2004.

HPEM - 23
Biological Effects

Oral Presentations

Study on the Antenna Radiations and SAR Reduction by Varying Handset Box Materials

Hsi-Tseng Chou, Hsing-Yi Chen Da-Jen Wu, Wei-Yi Chiou and Kun-Han Liu

Department of Communications Engineering, Yuan Ze University, Taiwan
E-mail: hchou@saturn.yzu.edu.tw

The SAR induced by the radiation of handset antennas needs fulfill international standards in the commercial production. In order to achieve this, many efforts may be found in the literatures including external shielding techniques and utilization of directional antennas to prevent the energy from penetrating into the head. However, those techniques exhibit shortcomings of either uneasy use or degrading the reception due to the directional pattern.

This paper investigates potential reduction of SAR by properly selecting handset box structures and their materials without significantly impacting the antenna performances. The handset boxes are considered for the following two reasons. First, it is more nature to consider handset itself and allows the system optimally designed at the time of manufacture. Secondly, an increasing trend of using flip-type foldable handsets or embedded antennas has significantly decreased the chances of antenna's radiation to directly illuminate the humane heads in normal uses. In this case, the handset box becomes the primary interface to touch the head, which should be properly considered in the next stage of efforts to reduce SAR.

It is thus conducted in this paper to study their influences on SAR and antenna radiation performances with respect to the changes of materials and sizes of the handsets by using numerical simulations, which is further examined by experimental measurements. The goal is to conclude the characteristics of box structures and materials that may reduce SAR while, in the mean time, impacting the antenna radiations in a minimum extent. In the simulation, a monopole antenna mounted on a handset is assumed since it provides distinguished radiation characteristics that are well understood as it is used in a free space. Materials with their variations on the conductivity, permeability and permittivity are considered to provide useful information in serving as references in a realistic implementation. Two models (referred as Model A and B, respectively hereafter) are considered with Model A focusing on the examination of SAR influences while Model B focusing on the examination of antenna radiation. Thus Model A employs more accurate and realistic structures to model a humane head with distinguishable organs and a hand palm as the handset is held in a realistic use. Based on a conclusion in Model A, Model B simplifies those structures in order to accelerate the intensive computations in the simulation. Both models' results seem to agree very well.

In the experimental measurement, the SAR is measured using handsets attached on the side facing the head with resistive substrates that are formed by dielectric but conductive materials. The resistive substrates equivalently model the handsets' box shell in some extent. In particular, two types of handset configurations are considered, which includes a regular handset with embedded antennas and a flip handset with monopole antennas. The resistive substrates are obtained from markets, which exhibit the resistance varying from a good conductor to an isolator in a circuit point of view, and may exhibit the characteristics of box materials that are needed to reduce SAR.

The studies have shown that the handset box structure does influence significantly on the SAR induction and the utilization of magnetic plate, which can be considered for shielding purposes, can indeed reduce the SAR induction. Some graph curves and tables regarding to the variations of SAR with respect to the electrical properties of handset box materials will be presented, which can be employed as useful references for the realistic design of handset box. In particular, our studies indicate that smaller conductivity and relative dielectric constant, as well as large relative permeability, of the materials tend to induce smaller SAR inside human head at the cost of antenna performance degradation. Also slightly lossy material performs better than lossless material. Experimental studies are also show their effects. Tradeoff between SAR reduction and antenna performance needs to be considered. In this case, synthesis procedure might be employed for an optimized design.

Trapezoidal Envelope Pulse Propagation in Dispersive Attenuative Media with Applications to Biological Systems

K. E. Oughstun

College of Engineering & Mathematical Sciences, University of Vermont, USA
E-mail: oughstun @cems.uvm.edu

The dynamical evolution of a trapezoidal envelope pulse as it penetrates into a dispersive attenuative half-space is considered. Both asymptotic methods of analysis [1-4] and FFT based numerical results are used to explain the complicated dynamical pulse evolution. The material dispersion for microwave pulses is described by the Rocard-Powles extension of the Debye model of orientational polarization [5] with relative permittivity given by

$$\varepsilon(\omega) = \varepsilon_\infty + \frac{\varepsilon_s - \varepsilon_\infty}{(1 - i\omega\tau)(1 - i\omega\tau_f)}, \tag{1}$$

where $\varepsilon_s \equiv \varepsilon(0)$ is the static relative permittivity, τ is the relaxation time, τ_f is the frictional relaxation time, and where ε_∞ denotes the high-frequency limit of the relative dielectric permittivity described by this low-frequency model. Because of its central importance in both radar and telecommunication systems, the analysis is focused on the trapezoidal envelope pulse $f(t) = u(t) \sin(\omega_c t + \psi)$ with fixed angular carrier frequency $\omega_c > 0$. This pulse envelope function may be described by the time-delayed difference between a pair of trapezoidal envelope functions given by

$$u_j(t) \equiv \begin{cases} 0, & t \leq 0 \\ \dfrac{t}{T_j}, & 0 \leq t \leq 0T_j \\ 1, & T_j \leq t \end{cases} \tag{2}$$

for $j = r, f$. Both the asymptotic theory and numerical results show that when the initial pulse rise-time T_r or fall-time T_f of a trapezoidal envelope pulse exceeds a well-defined critical value that is independent of the material relaxation time, the propagated pulse dynamics become dominated by a set of Brillouin precursors whose peak values decay algebraically with propagation distance $z > 0$ as $1/\sqrt{z}$. In that case the pulse will penetrate much farther into the dispersive material than that described by the exponential penetration distance for a time-harmonic wave, carrying a significant fraction of the incident energy. For example, after propagating ten absorption depths in triply-distilled water at the input pulse carrier frequency, the signal amplitude of an input $1 V/m$ ten cycle rectangular envelope pulse with $f_c = 3.0 GHz$ carrier frequency is reduced by the factor e^{-10} to the value $4.54 \times 10^{-5} V/m$, while the peak amplitude of the Brillouin precursor is $9.4 \times 10^{-2} V/m$, over three orders of magnitude larger that that predicted by Beer's law. Application of these effects to biological systems are manifold. For example, each Brillouin precursor carries a nonzero quasistatic component into the tissue for the duration of the pulse. For a long ultrawideband pulse that induces a leading-edge Brillouin precursor, this small quasistatic component can persist for a long time before being cancelled by the trailing-edge precursor. Since cell membranes respond to induced DC levels, the health of the tissue may then be adversely effected.

References
1. A. Sommerfeld, "Über die fortpflanzung des lichtes in disperdierenden medien," Ann. Phys., Vol. 44, 177-202, 1914.
2. L. Brillouin, "Über die Fortpflanzung des Licht in disperdierenden Medien," Ann. Phys., Vol. 44, 203-240, 1914.
3. L. Brillouin, Wave Propagation and Group Velocity. New York: Academic Press, 1960.
4. K. E. Oughstun and G. C. Sherman, Electromagnetic Pulse Propagation in Causal Dielectrics, Berlin-Heidelberg: Springer-Verlag, 1994.
5. K. E. Oughstun, "Dynamical evolution of the Brillouin precursor in Rocard-Powles-Debye model dielectrics," IEEE Trans. Antennas & Propagation, Vol. 53, 1582-1590 (2005).

HPEM - 23
Biological Effects

Oral Presentations

Nanosecond Continuous and Pulsed Electric Field Test Setup for Biological Effect Study using a TEM cell

N. Boriraksantikul[1], P. Kirawanich[1], B. Camps-Raga[1], D. Sleper[2], M. S. Pathan[2], and N. E. Islam[1]

[1]*Dept. of Electrical and Computer Engineering, University of Missouri, Columbia, MO, USA*
[2]*Division of Plant Sciences, University of Missouri, Columbia, Missouri, USA*

E-mail: IslamN@missouri.edu

Effects from potential exposures to electromagnetic pulse (EMP) radiation due to high power pulse generators, cellular phones and other modern electronic accessories employing high frequency signals are of very concern to many. Studies of the biological effects from such sources are therefore an emerging research topic. However since the biological sample or the area under exposure is relatively small, the use of large test areas for measurements such as anechoic chambers or large open spaces does not provide an efficient experimental setup. A transverse electromagnetic (TEM) cell, on the other hand, which consists of a rectangular coaxial transmission section tapered with coaxial connectors on both ends, is a better choice and offers a uniform EM field in a shielded environment [1].

We propose to report on the development and the application of a scaled version of a TEM cell used in the study the germination rate studies of bio-energy sources (corn, soybean) using the cell in both CW and pulsed mode. Specifically the development of the test setup and results from the germination studies of wheat, corn and soy bean will be presented. The interactions of the TEM cell and nanosecond pulsed electric fields (nsPEFs) were preliminarily studied using a full-wave analysis technique. For experimental validation, the TEM cell was assembled and characterized experimentally for optimum operating frequency range. In order to apply the TEM cell with nsPEFs, a single-ended pulse forming line (SPFL) was used as a pulse generator [2]. The SPFLs in our facility can produce pulses with pulsewidths of 60 and 300 nanoseconds, maximum amplitude of upto 60 kV, and pulse risetimes of the order of 10 ns that are appropriate to operate in the uniform field region of the TEM cell.

Fig. 1 – TEM cell used in this study

References
1. M. L. Crawford, "Generation of standard EM fields using TEM transmission cells", IEEE Trans. Electromagn. Compat., vol. EMC-16, no. 4, Nov. 1974, pp. 189-195.
2. F. Belloni, D. Doria, A. Lorusso and V. Nassisi, "Novel pulse amplifying circuits based on transmission lines of different characteristic impedance," Nucl. Instr. and Meth. A, vol. 556, no. 1, Jan. 2006, pp. 296-301.

Conducting Oblate Ellipsoid Analysis in ELF Electromagnetic Field

M. T. Perić, S. R. Aleksić
Faculty of Electronic Engineering of Niš, Niš, Serbia
E-mail: mirjana.peric@elfak.ni.ac.yu

Exposure to external electromagnetic fields at extremely low frequencies (ELF) induces electric fields and currents inside bodies. At those frequencies the electric and magnetic fields are effectively decoupled, since quasistatic approximation can be assumed.

In this paper such analysis has done with an aim to determine simple and useful expressions in practice for calculation of penetrated ELF electromagnetic fields into bodies of oblate ellipsoid shape. The body is modelled as a half-oblate conducting ellipsoid placed at the perfectly conducting plane in the ELF electromagnetic field. Applying image theorem, this problem can be considered as an oblate ellipsoid placed in an axial electric field, E_0, Fig. 1. The model is homogeneous diamagnetic semiconducting material with relative permittivity ε_r and conductivity σ. The wave equation (1) can be formed using the Maxwell's equations. Solving this equation in ellipsoidal coordinate system [1] using the separation of variables procedure and satisfying boundary conditions at the body surface, the electromagnetic field components inside and outside the body can be determined.

$$\frac{\partial}{\partial u}\left[\frac{1}{h_w}\frac{\partial(h_w H)}{\partial u}\right] + \frac{\partial}{\partial v}\left[\frac{1}{h_w}\frac{\partial(h_w H)}{\partial v}\right] - j\omega\mu_0 h^2 H = 0 \tag{1}$$

A similar analysis can be done for an ellipsoid placed in an axial magnetic field. In that case, it can be assumed that the magnetic field inside the body has the same values as the external magnetic field.

In Fig. 2 some of the obtain results are shown. It can be concluded that the penetrated electric field is homogeneous and has only axial component. The penetrated magnetic field has only angular component which intensity linearly increases from the model axis to its surface. Through the model flows total current in axial direction.
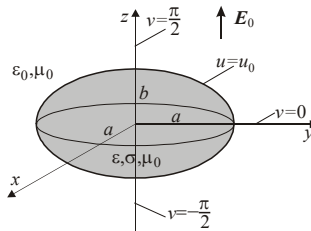
Fig. 1 – Conducting oblate spheroid

a)

b)
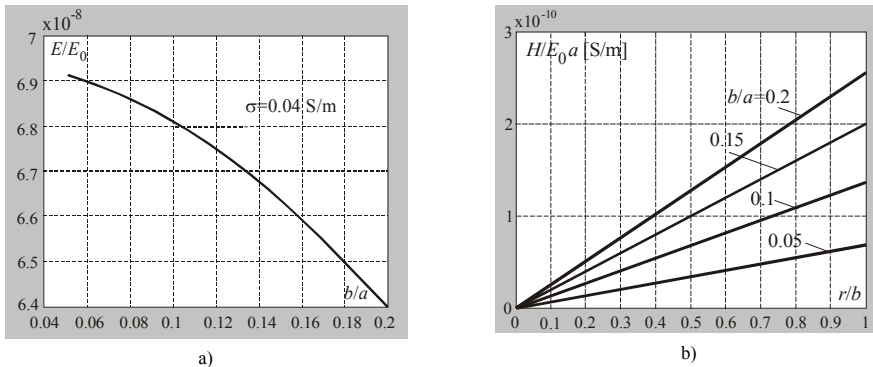
Fig. 2 – a) Penetrated electric field for different values of parameter *b/a* and σ=0.04 S/m;
b) Magnetic field distribution inside the body for different values of parameter *b/a*

References
1. M. Abramowitz and I. Stegun, Handbook of Mathematical Functions. Dover Publications, 1965.
2. L. Li, X. Kang, M. Leong, Spheroidal Wave Functions in Electromagnetic Theory. John Wiley & Sons, 2002.

HPEM - 23
Biological Effects

Oral Presentations

Health Effects of EMF Exposure in the TV Band

Elias A. Rachid and Michel W. Moughabghab

ESIB - St Joseph University, Campus des Sciences et Technologies B.P.11-0514 Beirut, Lebanon
Email: elias.rachid@fi.usj.edu.lb , michel_moughabghab@yahoo.fr

Introduction- With the very rapid development of the wireless communication system and propagation equipments, many questions are posed: Electromagnetic field values doorsteps are respected in installation of electromagnetic equipments? Many researchers have been performed over the last decades on the biological and health effects of ElectroMagnetic Fields (EMF). The researches have covered epidemiological surveys, exposure assessment, dosimetry, and analysis of sources… The evaluation of possible risks of EMF exposure requires a multidisciplinary approach, with expert groups in multi sciences: physics, biology, medicine, engineering, and epidemiology, and at the international and local levels supported by the national governments and health authorities. The assessment of health effects associated with exposure to electric, magnetic, and electromagnetic field had been performed by the World Health Organization (WHO) [1], jointly with the International Committee on Non-Ionizing Radiation of the International Radiation Protection Association (IRPA/INIRC) and the United Nation Environmental Program (UNEP) [2-4]. The outcome of such analyses consisted of comprehensive reports, published by WHO in the series of Environmental Health Criteria (EHC) documents [5].

Works and results- Our work consist to the measurements and statistical study of EM radiation fields in the TV band (300MHz to 800MHz), in a Lebanese city where they are more than eight TV stations towers and microwave links installed under the building after 1992 (see Fig. 1). Each TV station antenna is installed to a tower with a mean altitude level about 40 m, and 2 to 5 KW of power. The city contains about 10000 persons and around 3 Km^2 areas. An elevated relative risk of infantile leukemia has been raised for levels of superior or equal calculated magnetic fields to 0,2 µT, what lowers the value of norm of the magnetic field again to an intensity of 0,2 µT. With regard to the EMF the Environmental Protection Agency (EPA) proposes that in the ten years come fields magnetic alternative undergo by the population don't pass 2 µT anymore and that the E-fields don't pass 3 $V.m^{-1}$ and electromagnetic power density 0,1 $\mu W.cm^{-2}$ anymore and to all electromagnetic field type whatever as is the frequency. The measurements are taken into 300 meters of diameter area around the station and along 3 years. The measured values of average E-component respectively M-component vary from (1 to $10V.m^{-1}$, 0.8 to $8V.m^{-1}$ and 0.6 to $7V.m^{-1}$) respectively (6 to 15µT, 4 to 10µT, and 2.5 to 5.5µT) at (75m, 100m, and 150m) distance to the station. The risk of leukemia and cancers increases more than 500 % in the last 15 years (fig. 2) and it is variable from station to anther (Local area is a pertinent factor to reduce or increase the risk), incase the population growth increases about 20% in this last 15 years.

Conclusion- The electromagnetic field values doorsteps are not respected in installation these antennas. The risk of cancers increases, the greater part of this risk is coming from the EMF radiation. To respect to the health assessment, the minimum distance to the TV station antenna must be bigger than half kilometer.

Fig. 1 – Part of the City view and some TV antennas
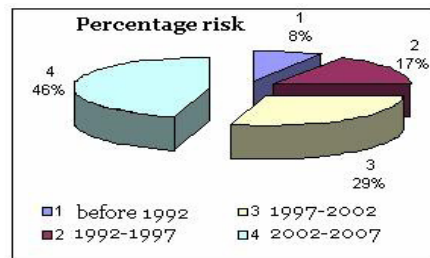
Fig. 2 - Percentage risk of Cancers and leukemia

References
1. WHO, The International EMF Project,http :llwww.who.int/docstore/peh-emf/ publications/facts_pres/efact/efs181.html.
2. ICNIRP, Guidelines on Limits of Exposure to Static Magnetic Fields, Health Phys., 66, pp. 540-548 1994.
3. WHO,. Magnetic Fields, Environmental Health Criteria Document, Geneva, World Health Organization, 1987.
4. R. Matthes, A.F. McKinlay, J.H. Bernhardt, P. Vecchia and B. Veyret, "Exposure to Static and Low Frequency Electromagnetic Fields, Biological Effects and Health consequences (0-100KHz)", Munich,   International Commission in Non Ionizing Radiation Protection, 2003.
5. WHO, EMF (300 MHz to 300 GHz), Environmental Health Criteria Document 137, Geneva, WHO, 1993.

*HPEM - 23
Biological Effects*

Oral Presentations

Estimation and Validation of Micro-Gap Breakdown Field from Discharge Current due to Human ESD

Yoshinori Taka and Osamu Fujiwara

Nagoya Institute of Technology, Nagoya, Japan E-mail: taka.yoshinori@nitech.ac.jp

Micro-gap electrostatic discharges (ESDs) due to an electrified human with voltages below 1000 V is known to cause a serious malfunction of high-tech information devices. In order to elucidate the generation mechanism of such human ESDs, we previously measured discharge currents due to the approach of a hand-held metal piece using a 6-GHz digital oscilloscope with a sampling frequency of 20 GHz, and then proposed an equivalent circuit model to calculate the discharge voltage across a spark gap, which cannot basically be measured [1]. From the discharge current and discharge voltage, gap breakdown fields can be estimated via a spark resistance formula. The experimental setup and its equivalent circuit are shown in Figs. 1(a) and 1(b), respectively. The results showed that at charge voltages bellow 600 V the estimated breakdown field from the discharge voltage is almost kept constant (2×10^7 [V/m]) regardless of the different approach speeds of the metal piece. In calculating the discharge voltage, however, inverse Fourier transform is required for the discrete data of the discharge current and human-body impedance measured in the time domain and in the frequency domain, respectively. In the previous paper [1], in lieu of the inverse Fourier transform, convolution integral in the time domain was used to calculate the discharge voltage, while the numerical artifact was not well investigated. In this study, we have calculated the discharge voltages from both of the inverse Fourier transform and convolution integral from, which are mathematically identical, and have examined how their artifact affects the calculated waveform. With a 12-GHz digital oscilloscope (sampling-frequency: 40 GHz) measurement of the discharge current has also been made, and discharge voltage waveforms have newly been derived

Fig. 1. (a) Measurement setup for discharge current and (b) its equivalent circuit.
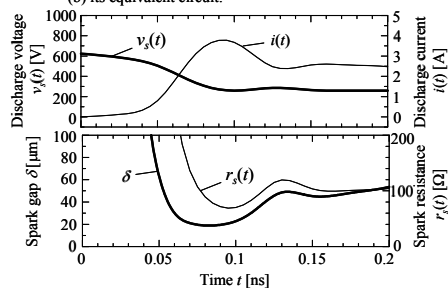
Fig. 2. Time changes in spark resistance $r_s(t)$ and spark gap δ calculated from measured discharge current $i(t)$ and the corresponding discharge voltage $v_s(t)$.

through the inverse Fourier transform and convolution integral. As a result, we have found that although the calculated results obtained by the both methods were rigorously different, there was in good agreement between the waveforms of the discharge voltages just after the spark, which has shown that arc discharges follow the spark. Figure 2 shows time changes in spark resistance and spark gap calculated from the discharge current and discharge voltage. Since it is difficult to identify from the measured discharge current waveform the time when a spark occurs, we have determined three types of spark length: δ_s at the time when the discharge current has a maximum gradient, minimum value δ_{min} of spark length and δ_p at the time when the discharge current reaches peak. The results have shown that the estimated spark length is 20-30 [μm] and the breakdown field is $(2\text{-}3) \times 10^7$ [V/m] at a charge voltage of 600V, which has been validated in comparison with other researcher's results including our previously published paper [1].

References

1. Y. Taka and O. Fujiwara, "Derivation of Breakdown Field from Discharge Current due to Collision of Hand-Held Metal Piece from Charged Human Body," Proc. of The XVI International Conference on Electromagnetic Disturbances 27-29 September, 2006 Kaunas Lithuania, pp.54-57, 2006.

HPEM - 23
Biological Effects

Oral Presentations

Estimating the Maximum Radiated Electromagnetic Emissions from Complex Systems

Todd H. Hubing

Clemson University, Clemson, SC, USA

...

E-mail: hubing@clemson.edu

Electromagnetic modeling software that uses numerical techniques to solve Maxwell's equations can be an important tool for engineers who need to analyze specific source-antenna configurations. However, very often it is more important to know how much a system is capable of radiating rather than how much a specific implementation of that system radiates. For example when designing an electronic product with several circuit boards, connectors, and cables that must comply with FCC, CISPR or military radiated emissions standards; it is usually not very helpful to know exactly how much a particular implementation of this system radiates. This is because small changes in any of the many system variables such as cable orientation, dielectric constants, source orientation or signal waveforms can (and often do) have a large effect on the radiated field strength at any given frequency.

Fig. 1 shows a circuit board being driven by 1-volt common-mode source relative to an attached cable. The board is one-meter above a ground plane. The radiated electric field strength 3 meters away is also shown in the figure for several cable lengths and positions. Note that at any given frequency the amplitude of the radiated field varies as much as 30 dB. The calculated radiation from a system like this would be highly dependent on the specific source frequencies and the length and position of the attached cable.
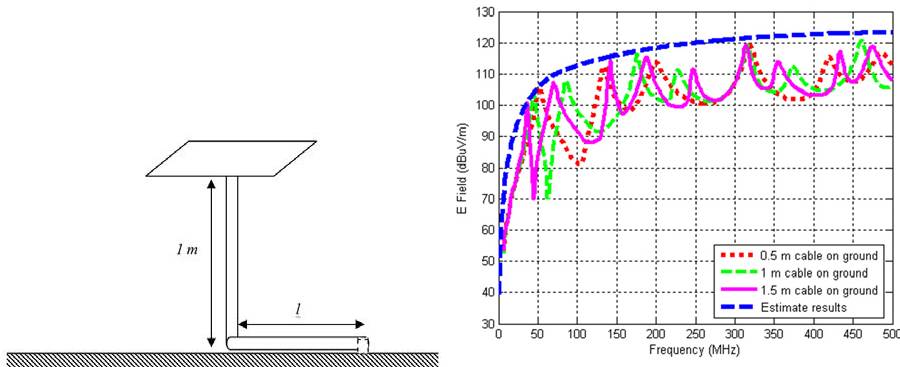
Fig. 1 – Circuit board with an attached cable and the calculated field strength 3 meters away for different cable geometries.

The dotted line in the figure is the estimated maximum possible radiated field from this configuration obtained using a relatively simple closed form expression [1]. Algorithms for several possible configurations have been developed [2]. Altogether, these algorithms enable engineers to estimate the maximum possible radiated electromagnetic emissions from relatively complex circuit-board/cable/enclosure configurations. This presentation describes these algorithms and demonstrates how they can be implemented in math modeling software such as Matlab and used to locate potentially significant radiation sources during the design phase of a system. Examples will be provided that also demonstrate how these algorithms can be used to troubleshoot existing designs.

References
1. S. Deng, T. Hubing and D. Beetner, "Using TEM Cell Measurements to Estimate the Maximum Radiation from PCBs with Attached Cables due to Magnetic Field Coupling," to be published in the *IEEE Transactions on Electromagnetic Compatibility*, May 2008.
2. Y. Fu and T. Hubing, "Analysis of radiated emissions from a printed circuit board using expert system algorithms," *IEEE Trans. on Electromagnetic Compatibility*, vol. 49, no. 1, Feb. 2007, pp. 68-75.

EMI Improvement by Adopting an Exposed-Pad LQFP Package

Nan-Cheng Chen, Sheng-Ming Chang, Ching-Chih Li

MediaTek Inc., HsinChu, Taiwan

charles.chen@mediatek.com

The EMI solution embedded in chip design is more and more important due to the popularity of high-speed circuits. One of the approaches to achieve better EMI solution is to adopt a good package design. However, good package designs always mean high design complexity and high cost, such as PBGA or FC-BGA [1]. Due to low cost and easier fabrication on PCB assembly, LQFP (Low-profile plastic Quad Flat Package) is commonly adopted on low-cost electronic devices, especially for consuming products. However, the electrical performance of such package is much worse than BGA-based packages, especially on EMI issue. Here, we tried to come up with a design methodology to improve the EMI issue by adopting E-pad LQFP (Exposed-pad LQFP) on our chip design. An E-pad LQFP means to have the die pad exposed and mounted on PCB directly by soldering. We could have a ground ring with bridges connected to the grounded exposed die pad, shown as Fig. 1(a), and make all the ground pads of the die down-boned to this ground ring. The 3D models of LQFP and E-pad LQFP were built up for 3D EM simulation, shown as Fig. 1(b) and Fig. 1(c), respectively. We implemented two PIFA antennas to act as a transmitter and a receiver on the die pad and outside the lead-frame, respectively. The simulation results for these two different models were done by HFSS, shown as Fig. 2(a) and Fig. 2(b). One could see that, the chip with all the ground pads down-bonded to ground ring of E-pad LQFP shows mush less noises coupled on both lead-frame and PCB, compared with the chip packaged by normal LQFP. The near-field measurement on real chips with these two different packages was also done by the EMI tester, EMV-200 of Hitachi, shown as Fig. 3(a) and Fig. 3(b). The measurement results also show the same trend of EMI improvement by adopting E-pad LQFP on our chip design.
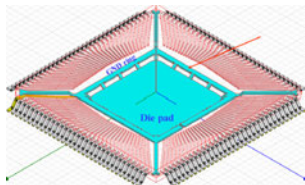
Fig. 1(a) – Lead-frame of E-pad LQFP,   **Fig. 1(b) – 3D model of E-pad LQFP,**   **Fig. 1(c) – 3D model of LQFP.**
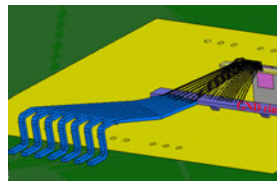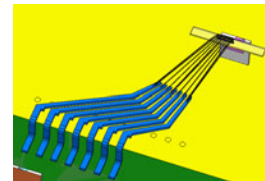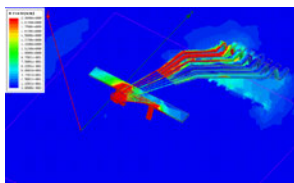
Fig. 2(a) – The H-field simulation result with E-pad LQFP,   **Fig. 2(b) – The H-field simulation result with LQFP.**
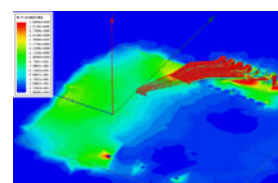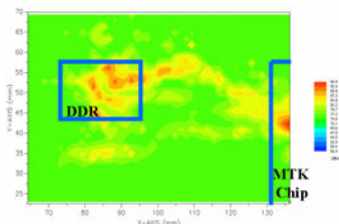
Fig. 3(a) – Near-field measurement result on the PCBA with the chip packaged by E-pad LQFP,   **Fig. 3(b) –Near-field measurement result on the PCBA with the chip packaged by normal LQFP.**
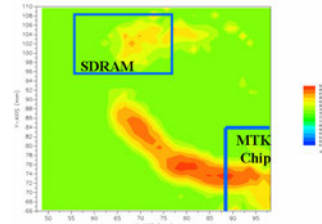
References
1. Diaz-Alvarez, E.; Krusius, J.P., "Design, simulation, fabrication, and characterization of package level micro shielding for EMI/EMC management in BGA environment," IEEE Electronic Components and Technology Conference, 2000. 2000 Proceedings. 50th.

HPEM - 24
Electromagnetic Compatibility in Microcircuits

Oral Presentations

Emission Measurement from Active RFID Tags in Boeing 747-400 Freighter

K. Yamamoto, N. Yonemoto, A. Kohmura and K. Yamamda

Electronic Navigation Research Institute, Independent Administrative Institution, Tokyo, Japan

E-mail: yamamoto@enri.go.jp

Introduction of active RFID tags is now under study for air cargo control and aircraft maintenance. However, electromagnetic emission from tags in aircraft has the risk to interfere with aircraft navigation systems [1]. Then, the possibility of interference must be investigated for flight safety. Emission from the tag, sensitivities of aircraft systems and propagation path loss in aircraft must be taken into account for the investigation.

This paper describes emission measurement from 433MHz active RFID tags. Since the tag emits FSK signal with very low duty factor, a conventional method recommended by RTCA (Radio Technical Commission on Aeronautics) [2] often fails to collect real emitted signal. Then, we have developed an accurate but fast measurement algorithm covering 2MHz - 6GHz range. The algorithm is employed to measure signal strength from the tag in anechoic chamber. The results have shown that the signal strength exceeds the limit recommended in RTCA DO-160E Section 21 (Emission of Radio Frequency Energy) at fundamental frequency 433.92MHz. However there are no spurious emissions exceeding the RTCA limit.

19 containers, each of which an active tag is pasted on are installed on Boeing 747-400 freighter. **Fig. 1** shows a configuration of the measurement in the upper cargo deck. Variations of signal strength and polarization from the tags have been measured at 9 different observation points such as cockpit, electronic bay or cargo decks in the freighter. This measurement is new and very important to analyze the effect of the freighter body and containers upon 433MHz propagation. Measured data are now under analysis and detailed propagation characteristics will be published soon. However, a preliminary analysis based on cumulative distribution of measured signal strength has shown that the signal strength in aircraft is 70dBμV/m or less at 95% probability and 78.7dBμV/m at the highest. Unusual high intensity signals, which may be caused by signal accumulation from multiple tags, have not been obvious. According to DO-160E Section 20 (Radio Frequency Susceptibility), this signal strength is about 55dB lower than the susceptibility level. Therefore, the possibility of direct interference with aircraft systems by emitted signals from the tags is very low. Another possibility of interference must also be considered between spurious emissions from the tags in air band and aircraft radio systems. Necessary information as propagation path losses between tags and aircraft systems through aircraft antennas will be presented in another paper.

Emission from 433MHz active RFID tags has been discussed in two different electromagnetic environments as in anechoic chamber and in Boeing 747-400 freighter. The results will be employed to estimate the possibility of electromagnetic interference with aircraft systems.

Fig. 1 – Configuration of Emission Measurement in Boeing 747-400 Freighter

References

1. N. Yonemoto, K.Yamamoto, K.Yamada and T.Hirata, "RF Emission Measurement of 433MHz RFID Tags for EMI Evaluation to Onboard Instruments of Aircrafts," Proc. of 7-th Int. Symposium on Electromagnetic Compatibility and Electromagnetic Ecology, ISBN 1-4244-1269-2, June 2007.
2. RTCA Inc., "Environmental Conditions and Test Procedures for Airborne Equipment," RTCA DO-160E, Dec. 2004.

Interference Pass Loss Measurement in Cargo Jet for EMI Evaluation by Active RFID Tags

Naruto YONEMOTO, Akiko KOHMURA, Kazuo YAMAMOTO, Kimio YAMADA

[1]*Electronic Navigation Research Institute (ENRI), Tokyo, Japan*

E-mail: yonemoto@enri.go.jp

Airlines or the civil aviation bureau in Japan are also interested in the installation of active RFID tags in their applications on cargo jets. However, aircrafts have some limitations of usage of the Transmitting Portable Electronic Devices (T-PEDs) during the flight even if they emit quite low power. That is the reason that the some EMI reports were indicated the probability of interference between onboard equipments and T-PEDs such as portable phones [1]. Therefore, ENRI started to study on the electromagnetic compatibility between RFID tags and onboard equipments   because there is no report focused on the characteristics of cargo jets.

This paper describes a new protocol to evaluate the potential interference in air applications. In previous time, all of the possibilities were tested under the procedure to validate to install high power devices even if the power is relatively small. According to the DO-307[2] published by Radio Technical Commission for Aeronautics (RTCA), the certification process for low-power T-PEDs was greatly simplified to evaluated the potential interference using RF emission of T-PEDs and its coupling path between T-PEDs and onboard equipments.

We measured RF emission from the active RFID tags based on the protocol written in RTCA DO-160F [3] in order to clarify the intentional or unintentional emission because some devices sometimes have many multiple or fractal harmonics or components from the internal circuits [4]. We observed the peak emission of RFID tags exceeds the limit of DO-160F at the intentional signals.

Coupling paths are divided into two paths, Back Door Coupling and Front Door Coupling. Back Door Coupling means that RF energy couples directly into the aircraft electrical and electronic equipment or into the wiring. In this case, the potential interference is evaluated by the peak emission from the RFID tags. And we confirmed the peak emission does not exceed the limit of aircrafts system qualification.

On the other hands, Front Door Coupling to aircrafts radio receivers must be considered in case by case basis because of the difference of the aircraft configuration such as seats, galleys or lavatories. In this case, we must consider the sensitivity of aircraft radio receivers and Interference Pass Loss (IPL) which is the RF attenuation between signal sources in cabin to the RF port of aircraft radio receiver shown in **Fig. 1**. The IPLs must be treated statistically by changing the place of the emission.

We measure the IPLs to 8 aircraft radio receiver in cargo jet to clarify the difference between cargo jet and passenger jet because most of reports measured in the passenger jets. Some measured results such as VHF communication system agreed with the references of passenger jets in spite of the windows covered with grounded metallic plates. Each IPL is measured at a frequency in the air band and at 433.92 MHz. Some worst cases of IPL were 70.35dB to the VHF communication system at 433 MHz, and 45.58 dB to ILS Localizer at 110 MHz.

Finally, we conclude that the IPLs are sufficient large to attenuate unintentional RF signals of active RFID tags below the sensitivity of aircraft radio receivers.

References
1. K. Yamamoto at al., "PED interference reporting system in Japan," Proceedings of the EMC 2007 symposium, pp.220-223, June26-29, St. Petersburg, 2007.
2. RTCA, "Aircraft Design and Certification for Portable Electronic Device (PED) Tolerance," DO-307, 2007.
3. RTCA, "Environmental Conditions and Test Procedures," DO-160F, 2007.
4. N. Yonemoto at al., "RF Emission measurement of 433 MHz RFID tags for EMI evaluation to onboard instruments of aircrafts," Proceedings of the EMC 2007 symposium,pp.232-235, June 26-29, St. Petersburg, 2007.
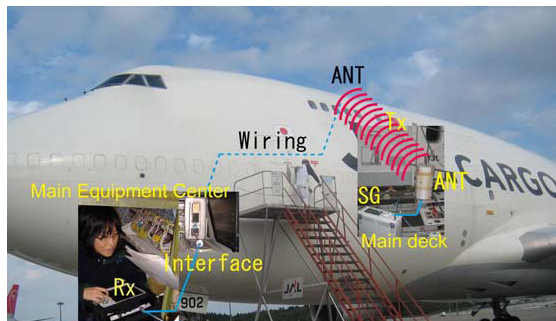
Fig.1 Typical IPL measurement setup

Coplanar Waveguide-Fed Slot-Coupled Hemispherical Dielectric Resonator Antenna

P. Abdulla, Y.K. Singh and A. Chakrabarty

Department of Electronics and Electrical Communication Engineering, Indian Institute of Technology, Kharagpur, W.B. India 721 302
E-mail: abdulla@ece.iitkgp.ernet.in

Dielectric resonator antennas (DRA) are increasingly popular [1] as they share many of the advantageous of microstrip antennas, such as small size, and light weight. In addition DRA exhibit relatively large bandwidth than that of microstrip antennas[2]. Moreover DRAs avoid the inherent disadvantage of microstrip patch antennas, including high conduction loss, and low efficiency due to surface wave excitation. It has been shown that DRA can be excited by a coaxial probe[3], a microstrip transmission line, aperture coupling[4]or a co-planar waveguide (CPW) feed [5]. However, to avoid via holes and for ease of fabrication and compatibility with solid-state devices, the uniplanar configuration could be advantageous. Despite that, the coplanar waveguide (CPW), feed to hemispherical dielectric resonator antenna (HDRA) didn't receive much attention. DRAs of cylindrical, hemispherical, and rectangular shapes are the most widely used and investigated. Hemispherical DRA has additional advantageous over the other shapes. The hemispherical shape is much easier to fabricate, and easy to analyze due to the absence of edges. In this paper an experimental study was undertaken in order to investigate the coupling from CPW to HDRA through capacitive slots. The capacitive coupling to HDRA has been studied experimentally and theoretically (using Ansoft HFSS simulation software [6]). An hemispherical DRA of radius 12.7 mm and $\varepsilon_r = 10$ was used for the simulations and measurement. The DRA is excited at its fundamental mode, TE_{111}. FR-4 substrate of $\varepsilon_r = 4.3$ and thickness 1.58 mm were used for the fabrication of coplanar waveguide feed. Very good matching is observed in the return loss, S_{11} and radiation patterns, of the simulated and measured results.

References
1. K.M. luk and K.W. Leung, Eds., *Dielectric resonator antennas*, London, U.K.; Research Press, 2003.
2. Kishk, A.A., M.R. Zonoubi, and D. Kajfez, "A numerical study of a dielectric disc antenna above grounded dielectric substrate", IEEE Trans. on Antenna Propagation. vol. 41, No.6, 1993, pp. 813-821.
3. K . W. Leung-, K. M. Luk, K. Y. *A.* Lai, and D. Lin, "Theory and experiment of a coaxial probe-fed hemispherical dielectric resonator antenna," IEEE Trans. Antennas Propagat*.,* vol. 41, , Oct. 1993. pp. 1390-1398
4. K. W. Leung, K. Y**.** A. Lai, K. M. Luk, and D.Lin, "Input impedance of aperture coupled hemispherical dielectric resonator antenna," Electron. Lett. *,* vol. 29, June 1993, pp. 1165-116.
5. Yong-Xin.G and K.M. Luk, "On improving coupling between a coplanar waveguide feed and a dielectric resonator antenna", IEEE Trans. on Antenna Propagation. vol. 51, No.8, Aug. 2003, pp. 2144-2146
6. Ansoft High Frequency Structures Simulator (HFSS), version 11.0, Ansoft Corporate**.** USA.

Sierpinski-carpet monopole antenna for multiband and wideband applications

Mahdi Naghshvarian Jahromi, Nader Komjani

Iran University of sicience&Technoloy (IUST), Tehran, IRAN

E-mail: m.naghshvarian@ee.iust.ac.ir

Three fractal monopole antennas using the Sierpinski-carpet geometry is described in this paper. The idea for these designs is gotten from semi-log-periodic behavior of fractal antenna. In this paper, we noted input impedance matching of antennas throughout the passband of them. In point of view, we will apply the wideband, broadband and multiband for these antennas. However, the phase reflection coefficients for these antennas even for wideband matching have multiband behavior. Our first wide-band design is named antenna1. This has a good input impedance match throughout the passband 2-20GHz. Second antenna is named antenna2. This antenna has an interesting behavior while has a multi-band behavior from 1-7GHz and has broad-band behavior from 7-20 GHz. However, for this antenna, because of two slots in ground plane of this antenna, the 6-7GHz band is eliminated. Third of antennas is named antenna3. It has a multi-band behavior from 0.5-17GHz. On average, we could match input impedance of antenna, for three desired behavior. The dimension of main- square for antenna1, antenna2 and antenna3 is 45, 60 and 132mm respectively. These antennas are suitable for the operating bands of GSM, ICMS, UMTS, Bluetooth, WLAN and HIPERLAN systems.

(a)	**(b)**	**(c)**
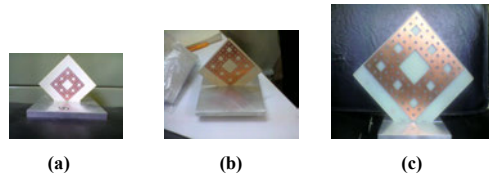
Fig. 3 The pictures of proposed antennas (a) Antenna1, (b) Antenna2, (c) Antenna3
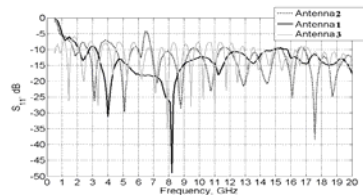
Fig. 1 Measurement input return loss of proposed antennas in dB.

————— **Antenna1** ············· **Antenna2** ————— **Antenna3**
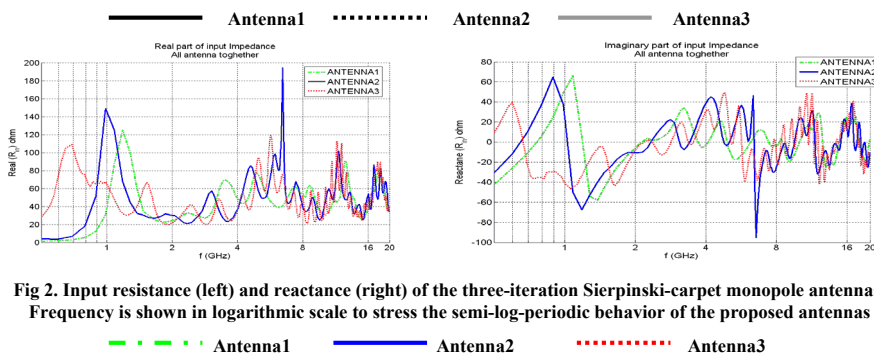
Fig 2. Input resistance (left) and reactance (right) of the three-iteration Sierpinski-carpet monopole antennas. Frequency is shown in logarithmic scale to stress the semi-log-periodic behavior of the proposed antennas

—·—·— **Antenna1** ————— **Antenna2** ············· **Antenna3**

HPEM - 25
Dielectric Antennas and Arrays

Oral Presentations

Tournament Selection Particle Swarm Optimization Algorithm Applied to EM Problems

Ružica M. Golubović[1], Dragan I. Olćan[2] and Juan R. Mosig[1]

[1]*Ecole Politechnique Fédérale de Lausanne, Lausanne, Switzerland*
[2]*School of Electrical Engineering, University of Belgrade, Belgrade, Serbia*
E-mail: ruzica.golubovic@epfl.ch, olcan@etf.bg.ac.yu, juan.mosig@epfl.ch

The canonical Particle Swarm Optimization (PSO) algorithm has been shown to be very effective for optimizing EM problems [1]. In this work, tournament selection strategy is incorporated into the PSO algorithm. After the whole swarm is moved, we apply p tournaments (where p is the total number of particles in the swarm) to build a new swarm [2]. The EM solutions found with the canonical PSO are compared to those found with PSO algorithm with tournament selection in order to compare efficiency of these two algorithms.

The optimization problem is a broadside antenna array with 42-point sources located along the *y*-axis with a constant inter-element distance of one half of a wavelength at the operating frequency. The optimization of excitation magnitudes is done to find the minimal side lobe levels. The solution is required to have symmetry of the excitation amplitudes, and therefore only one half of the excitations are optimized. To avoid an infinite number of solutions due to scaling, one coefficient is predefined. Thus, we have a 20-dimensional optimization problem. The criterion for the optimization is that the side-lobe levels should be lower then –80 dB for $\theta < 65°$, where θ is the angle between the array axis and the radiation direction. The cost-function is:

$$f_{cost} = \sqrt{\frac{1}{n}\sum_{i=0}^{n-1}\{max[0,\ 80 - F_{max} - F(\theta_i)]\}^2} \qquad (1)$$

where F_{max} is in the direction $\theta = 90°$, $\theta_i = i[°]$, $n = 65$, and $F(\theta_i)$ is given in dB. The theoretical result exists in the form of the binomial distribution of the amplitudes. The ratio of the highest and the lowest amplitude is of the order of 10^{11}, which is inconvenient from the standpoint of the numerical optimization. Hence, each coefficient is represented as $s_k = \ln(a_k)$, $k = 1,2,…,20$, so that the maximal ratio of the coefficients is less than 30. Each optimized parameter, s_k, has the lower bound equal to zero and the upper bound equal to the largest (21st).

For the comparison we used canonical PSO algorithm and PSO algorithm with tournament selection with following parameters: inertia coefficient $w = 0.73$, cognitive coefficient (controls the pull to personal best position) $c_1 = 1.496$, social-rate coefficient (controls the pull to the global best position) $c_2 = 1.496$, the maximal velocity $V_{max} = 0.2$. For the tournament selection PSO algorithm, asynchronous update of g_{best} is used (information about g_{best} is updated after each individual has moved), while for the canonical PSO algorithm synchronous update of g_{best} is used (information about g_{best} is not updated until the whole swarm has moved). The total number of iterations per one run is 300000. Both algorithms are run for 100 times, in order to get the good estimation of the average outcome of the optimization. For this problem the preferred value of the number of particles in the swarm, p, for the canonical PSO is empirically found to be $p = 3000$ and for the tournament selection PSO algorithm it is found to be $p = 100$. The averaged best-found solution results as a function of the number of iterations (EM solver calls), for both algorithms, are presented in the Fig 1. It can be seen that the tournament selection PSO outperformed the classical PSO algorithm. Further comparisons between these algorithms are being made on more optimization problems in order to be able to draw more general conclusions.
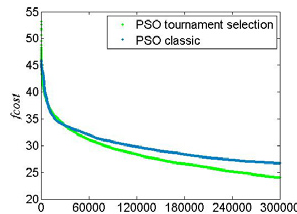
Fig. 1 – Broadside Antenna Array

References
1. J. Robinson and Y. Rahmat-Samii, "Particle Swarm Optimization in Electromagnetics," IEEE Transactions on Antennas and Propagation, vol. 52, no. 2, Feb. 2004, pp.397-407.
2. J. R. Pérez Lopez and J. Basterrechea "A Modified Particle Swarm Optimizer Applied to Linear Array Synthesis," EuCAP 2007 Proceedings, Edinburgh, UK, 11-16 Nov. 2007.

A Comb-shaped DVB-H antenna Covered Magneto-dielectric Material

Ya Deng and Qing Xin Chu, *Member, IEEE*
School of Electronic and Information Engineering, South China University of Technology
Guangzhou, Guangdong 510640, China
Email: qxchu@scut.edu.cn

Recently, there is a tremendous growth in demand for mobile terminal systems in application such as Digital video broadcasting for handheld terminals (DVB-H). It is an emerging technology providing high down link data rates for streaming audio, video and data files to portable devices. For the reception of terrestrial television, traditionally Yagi or whip antennas are used, however, these antennas must be too large to be assembled in handheld devices. Concerning the antenna implementation in small sized portable terminals, as the required frequency band, which is from 470MHz to 702MHz, corresponds to a relative bandwidth of about 40% and a free space wavelength from 42cm~64cm, the wide bandwidth and long wavelength presents a challenging combination. Although miniaturization can be achieved by using high permittivity materials as substrates, high dielectric constant material has two disadvantages. One is that the field remains highly concentrated around the high permittivity region and the field confinement results in low antenna efficiency and narrowband characteristics. The other problem stems from the fact that the characteristic impedance in a high permittivity medium is rather low which creates difficulties in impedance matching of the antenna relative to feed networks and free space. The adoption of magneto-dielectric material can solve both aforementioned problems. By using moderate values of permittivity and permeability, magneto-dielectric material can miniaturize the antenna by the same factor as high permittivity material. Furthermore, since the characteristic impedance of magneto-dielectric medium is close to that of the surrounding medium, it allows the ease of impedance matching over a much wider bandwidth. There are very few effective small internal antenna solutions which could be universally applicable to various kinds of DVB handsets. In [1], by using the upper and lower ground planes of a folder-type mobile phone, a shorted dipole antenna for DTV reception was presented, but the configuration used was only suitable for clamshell mobile phone. An earpiece cord antenna was proposed in [2], it used a matching network to get a better performance. One of the disadvantages of this technique is that an external earpiece cord must be used for the reception of DVB-H signals. In [3], meander conductive metal pattern and magneto-dielectric material were used to miniaturize the antenna size. However, a relative bandwidth of less than 5% made it unable to cover the required bandwidth of DVB systems. Although the comb-shaped antenna with a dimension of 200mm*42.5mm shown in [4] is particularly useful for DVB application, considering the large volume consumption, it is not suitable for handheld devices. In this paper, an improved comb-shaped antenna covered magneto-dielectric material is proposed for DVB-H application as shown in Fig.1, which can reduce the antenna size in [4] by 48%. It is sufficient to cover all DVB-H channels from 470MHz to 702MHz with $|S_{11}|<$-5dB and Gain>-7dB .

(a) Top view   (b) Side View
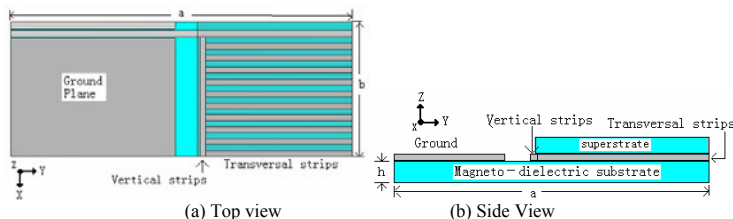
Fig.1 Schematic layout of the proposed antenna

References
1. K.L. Wong, Y.W. Chi, B. Chen, and S. Yang, "Internal DTV antenna for folder-type mobile phone," Microwave Opt Technol Lett, Vol. 48, pp. 1015-1019, 2006.
2. P. Lindberg, and A. Kaikkonen, "Earpiece cord antenna for DVB-H reception in wireless terminals," Electron. Lett., Vol. 42, No. 11, pp. 609–610, 2006.
3. Y. Mano and S. Bae, "A small meander antenna by magneto-dielectric material," Proc. IEEE. Int. Symp. Microwave Antenna Propagat. & EMC Tech. for Wireless Comm., Vol. 1, pp. 63-66, 2005.
4. T.L. Chen, C.W. Hsieh, "Comb-Shaped Dipole Antenna on Transparent Substrate," Electorn. Lett., Vol. 10, pp. 359-361, 2000

Fast Calculation of the Diffraction Operator Kernel used by the Wave Concept Iterative Process (WCIP) for problems of Scattering and Radiation by Planar Circuits in Free Space.

T.Bdour[1], N.Ammar [1], T.Aguili [1], and H.Baudrand[2]

(1) Communications Systems Laboratory in Tunis Engineering School, Belvedere, BP 37 Tunis, 1002 Tunisia
(2) Electronics laboratory LEN7, ENSEEIHT, 2 rue Camichel, 31071, Toulouse, France

E-mail: bdour_tarek@yahoo.com

Commonly, the computation of scattering and radiation by planar open circuits can be performed using the method of moments MoM [1]. Nevertheless, such analysis is difficult because of the singular behavior of the Green operator and the poor condition number of the reaction matrix when increasing the discretization fineness [2] .Furthermore; the MoM matrix size is proportional to the meshing cell number. This can severely penalize the CPU run time while performing the MoM matrix fill in and inversion tasks. To overcome these difficulties, an original integral method based on transverse wave formulation WCIP [3]-[5] has been proposed. The difference between the WCIP method and the previous integral methods is twofold .Firstly; the formulation is not based only on electric fields or magnetic fields equations but on their linear combination which permits us to handle diffraction operators instead of manipulating unbounded impedance or admittance operators. Secondly, as the WCIP distinguishes the topological characteristics of circuits from their embedding environment, a medium representation in the modal domain coexists simultaneously with a surface description in the spatial domain. To each representation is associated an integral matrix equation. These two equations are related by an iterative scheme.

The WCIP algorithm has been firstly designed to treat planar circuits that operate inside a rectangular wall [4]. Therefore, the extension to free space radiation problems is not obvious. However, satisfactory results, involving open structures simulation, have been obtained by an appropriate modeling of the free space environment in the modal domain. The major drawback of such modal approach lies in the fact that the involved spectral expansion double series of the diffraction operator are slowly convergent.

This paper proposes a novel rapid method of calculation of the dyadic diffraction operator kernel for open planar structures. In this method, the spectral expansion double series of the diffraction operator are divided into convergent and divergent parts to be converted separately in next step from modal to spatial domain into integral forms. An analytical form of the diffraction kernel is mathematically determined. As a result, the proposed technique greatly accelerates the calculation of the diffraction operator kernel compared with the spectral summation. The modeling assumptions of this technique are described in detail. Some numerical examples are performed to demonstrate rapidity and accuracy of the proposed method.

References
1. R.F. Harrington, Field Computation by Moment Methods. New. York : Macmillan, 1968.F. M. Tesche, M. Ianoz, and T. Karlsson, EMC Analysis methods and computational models. New York: Wiley Interscience, 1997.
2. K. F.Warnick and W. C. Chew, "Error analysis of the moment method," *IEEE Antennas Propag. Mag.*, vol. 52, pp. 38–53, Dec. 2004.
3. S.Wane,D.Dajon, H. Baudrand and P.Gamand "A new Full- Wave Hybrid Differential –Integral Approach for the Investigation of Multilayer Struccture Including Non uniformly Doped Diffusion", *IEEE Tansactions on Microwave theory and technique*,Vol.53,No.1,pp.200-214,January 2005
4. R.S. N'Gongo and H. Baudrand, "Application of Wave Concept Iterative Procedure in Planar Circuits,"Recent Res. Devel. Microwave Theory and Technique, vol. 1,pp. 187-197, 1999.
5. T.Bdour,N.Ammar,T.Aguili and H. Baudrand:" Modeling of Wave Penetration through CylindricalAperture using an Iterative Method Based on Transverse Wave Concept", *IEEE Microwave Conference KJMW*, pp.45-48 , November 2007.

A Full-Space Unbounded Conformal Mapping Technique for Multiconductor Transmission Line Parameter Extraction

Siamak Bonyadi-ram, Behzad Kordi, and Greg E. Bridges

Department of Electrical & Computer Engineering, University of Manitoba, Winnipeg, MB, Canada
E-mail: bkordi@ee.umanitoba.ca

Finite Element Method (FEM) based electromagnetic simulation software offers many useful capabilities for parameter extraction in modeling of power transmission lines. One of the difficulties in this class of problems is the handling of the open boundaries. A review of finite element open boundary techniques for static and quasi-static electromagnetic field problems is presented in [1]. Conformal mapping is one of the spatial transformation schemes mainly used for the calculation of two-dimensional static unbounded field problems. The important feature of conformal transformation is that the governing equation (Poison's equation in static electric and magnetic problems) remains unchanged, including the field energy equations which are usually used to calculate the per unit length (PUL) parameters [2]. However, in quasi-static cases, a scaling factor should be applied to governing equations [3] and energy relations. Bilinear transformation is one of the conformal mapping schemes that has been used to extract the parameters of transmission lines over an infinite ground plane [2]. This scheme maps the half space $y > 0$ into the interior of a unit circle and is useful for half-space problems such as microstrip and other planar transmission lines.

In this paper, a new generalization of the bilinear transformation is introduced in order to apply the mentioned conformal mapping scheme to full-space power line problems. The introduced transformation maps the upper ($y > 0$) and lower ($y < 0$) half-spaces into two unit circles. The air-ground interface ($y = 0$) is the common boundary of the two regions and is mapped to the circumferences of the two unit circles. The electromagnetic boundary condition on both unit circles is identical, which is known as a periodic boundary condition (PBC) in FEM literature. Although these circles coincide mathematically, they should be separated for numerical solution.

An example of an over-head three-wire transmission line with arbitrary cross section is shown in Fig. 1. The left-hand side circle in this figure shows the mapped air region, $y > 0$, with $\sigma = 0$ and $\varepsilon_r = 1$. The over-head wires ($\sigma = 10^6$ S/m) are also included in this region. The right-hand side circle is the mapped lower space, $y < 0$, which is the lossy ground with $\sigma = 0.01$ S/m and $\varepsilon_r = 4$. Using a proper scaling factor for the new mapping scheme, the quasi-static magnetic and electric problems are solved for the transformed structure using FEM and the scalar potentials and electromagnetic fields are calculated. An example of the A_z distribution is also presented in Fig. 1 (wire W_1 is excited). The PUL parameters are also derived using the energy relations. The calculated results for different cases of over-head lines are compared with those obtained by well-known Carson's formulation. The effect of mesh size on the accuracy of the results is also investigated.
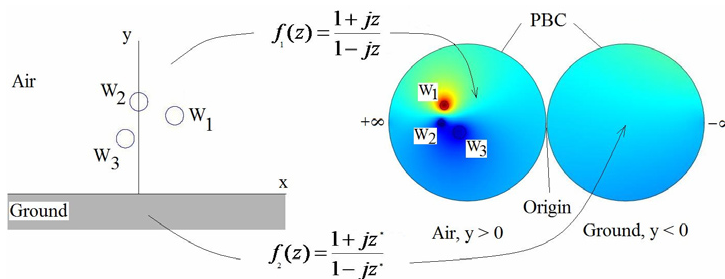
Fig. 1 – Cross section of a 3-wire transmission line above lossy ground (left) and its mapped geometry (right).

References
1.   Q. Chen and A. Konrad, "A review of finite element open boundary techniques for static and quasi-static electromagnetic field problems," IEEE Transactions on Magnetics, Vol. 33, No. 1, January 1997.
2.   L. Rubin, "Efficient conformal mapping technique for general transmission line parameter extraction", IEEE Transaction on Magnetics, Vol. 29, No 2, March 1993.
3.   S. Ramo, J. R. Whinnery and T. Van Duzer, Fields and waves in communication electronics. 3rd ed. New York: Wiley, 1994.

HPEM - 26
Numerical Methods #1

Oral Presentations

Investigation of Moment Method Solutions Based on Expansion Functions Defined in an Infinite Domain

D.Malka, H.Matzner and M.Haridim

HIT- Holon Institute of Technology, Golomb St. 52 Holon, 58102, Israel

*Abstract –*The efficiency of the Moment Method (MM) when the expansion functions are defined in an infinite domain is checked. It is shown that an efficient solution can be obtained   if the expansion functions contain the physical behavior of the field near the edges and at infinity.

*Index Terms —*Moment Method, Expansion functions, Infinite domain.

Moment Method is used frequently in solving electromagnetic problems [1]. Different expansion and test functions are chosen in order to have more accurate and fast converging solutions. Here we investigate the possibility to apply expansion functions defined in an infinite domain. This choice of expansion functions can increase the variety of electromagnetic problems that can be efficiently solved by the MM.

In order to do this we choose a simple electromagnetic problem, the thin, charged circular disc (Fig. 1) for which the analytic solution is known [2], and compare the analytic solution to our MM solution based on expansion functions defined in infinite domain. We analyze the behavior of E_ρ ($\rho, z = 0$) near the disc edge for $\rho > R$ and at infinity, and choose expansion functions which correctly obey this behavior. It can be shown that

(1) $E_\rho (\rho, z = 0) \sim a_1 (\rho - R)^{-1/2} + a_2 (\rho - R)^{1/2} + \ldots, \rho \to R$ (2) $E_\rho (\rho, z = 0) \sim b_1 / \rho^2 + b_2 / \rho^4 + \ldots, \rho \to \infty$

where $a_1, a_2, a_3, b_1, b_2, b_3$ are constants. Suitable expansion functions for E_ρ are, for example

(3) $1 / \rho (\rho^2 - R^2)^{1/2}, \ 1 / \rho^3 (\rho^2 - R^2)^{1/2}, \ 1 / \rho^5 (\rho^2 - R^2)^{1/2}, \ldots$ (4) $(\rho^2 - R^2)^{1/2} / \rho^3, \ (\rho^2 - R^2)^{1/2} / \rho^5, (\rho^2 - R^2)^{1/2} / \rho^7, \ldots$

Note that the first function in (3) is proportional to the analytic solution. We chose the linearly independent functions (5)

(5) $1 / \rho^5 (\rho^2 - R^2)^{1/2}, \ (\rho^2 - R^2)^{1/2} / \rho^3$ (6) $\sigma (\rho) = q / 2 \pi R (R^2 - \rho^2)^{1/2}$

in order to exclude the analytic solution (6), and used MM Galerkin method. The results for the surface charge density on the disc for one and two expansion functions are shown in fig. 2 and compared to the analytic solution.
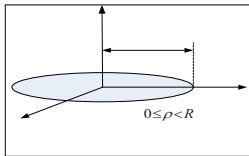
Fig.1. Isolated, infinitely thin, flat, circular, conducting disc of radius R with a total charge q placed on it.
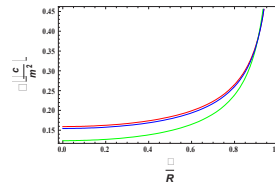
Fig.2. Charge distribution as a function of a point ρ/R on the disk for $0 \le \rho / R < 1$. Green line is for one expansion function blue line for two expansion functions, and red line is for the analytic solution.

It is seen that two expansion functions are enough for excellent convergence of the solution. Note that when taking 3 or more expansion functions from (3) or (4) – the analytic solution will appear. We conclude that efficient MM solutions based on expansion functions defined in an infinite domain is possible.

REFERENCES

[1] Roger F. .Harrington, *Field Computation Moment Methods*, IEEE Press Series on Electromagnetic Wave Theory, April 21, 1993.
[2] J.D. Jackson, *Classical Electrodynamics*, John Wiley & Sons, pp. 89-93

Improved Subgridding FDTD Method with Second-Order Accuracy at Magnetic Media Interface

Hai Ding and Qing Xin Chu, *Member, IEEE*
School of Electronic and Information Engineering, South China University of Technology
Guangzhou, Guangdong 510640, China
Email: qxchu@scut.edu.cn

The subgridding method is a robust and flexible tool in FDTD code because it could dramatically reduce the memory and CPU time requirements and improve the total computational efficiency, by the reasonable arrangement of grids with different sizes and the corresponding time step set for each mesh within the regions that need different investigation. In [1], the subgridding algorithm was achieved through the resolution increased fourfold in the subregion by the linear interpolation of the electric field and time and space averaging of the electric and magnetic field. However, a relative large error was indicated by a test of rectangular cavity with a thin metal plate. K. K. Mei introduced an expansion technique [2] that improved the accuracy by the quadratic calculation in the subregion. This subgridding algorithm introduced no extra numerical dispersion and numerical stable, and the second-order accuracy of the numerical solutions could be achieved readily in the inner regions with standard FDTD method, but the field components on the boundary between the fine and coarse grids were just obtained by the spatial and time interpolations, only the first order accuracy. The modification to the calculation for the fields on the boundary has been proposed [3], and a wave equation was employed to compute these missing field values. The solutions obtained could have the second-order (2nd) accuracy under the condition for the uniformity of the material in the whole computational domain. However, such a 2nd accuracy can not be preserved, in the case that the regions with different mesh division were filled with different medium material. The second-order accurate FDTD method at magnetic media interface in two dimensional cases with nonuniform grids has been reported in [4], and the 2nd accuracy of the derived equations has been verified by the calculation of the relative error of the numerical results of the magnetic field. In this paper, the 2nd accuracy FDTD technique at the magnetic media interface is employed to analyze the field components on the boundary between the fine and coarse grids in a subgridding FDTD modeling that is filled with different material medium. The 2nd accuracy of the numerical solution of the tangential magnetic field components at the junction of the meshes with the different sizes is obtained by the establishment of the nonuniform grids at the interface and the introduction of the auxiliary electric fields calculated by the neighboring field components, and the entire computational accuracy of the subgridding algorithm can be improved effectively. The numerical simulation results for a rectangular resonator partially filled with a magnetic material as shown in Fig.1 validate the better accuracy of the proposed method than the previous subgridding method without the additional computational capacity.
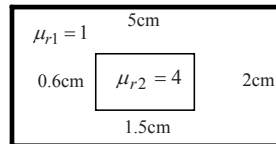
Fig.1 The Rectangular Resonator partially filled with a magnetic material

References
1. I. Kim and J. R. Hoefer, "A local mesh refinement algorithm for the time-domain finite difference method using maxwell's curl equations," IEEE Trans. Microwave Theory Tech, (38) 1990, 812~815.
2. S. S. Zivanovic, K. S. Yee, and K. K. Mei, "A subgridding method for the time-domain finite difference method to solve Maxwell's equation," IEEE Trans. Microwave Theory Tech, (39) 1991, 471~479.
3. D.T. Prescott and N. V. Shuley, "A method for incorporating different sized cells into the finite-difference time-domain analysis technique," IEEE Microwave guided wave lett, (11) 1992, 433~436.
4. Q.X. Chu and H. Ding, "Second-order accurate FDTD equations at magnetic media interfaces," IEEE Trans. Magn., 27 (2006), 3141-3143.

HPEM - 26
Numerical Methods #1

Oral Presentations

EMF Backscattered from an S-Shaped Inlet Cavity Calculated by Spectral Rays Tracking method

Elias A. Rachid

ESIB - St Joseph University, Campus des Sciences et Technologies B.P.11-0514 Beirut, Lebanon
Email: elias.rachid@fi.usj.edu.lb

Introduction- The EM backscattered from a S-Shaped inlet cavity is analyzed generally using different techniques such: integral equation method, hybrid combination of asymptotic high frequency and modal methods, and the geometrical optics ray method. A new ray tube launching and tracking method based in discretized Plane-Wave Spectrum (PWS) of source field is proposed. Fields at any observation point are expressed as a discrete sum of all contributions from ray tubes tracked backward within the propagation environment, each ray tube representing a sample of the source PWS. We have already applied this method with high accuracy in the context of multiple reflections and refraction in dielectric lens antenna analysis, open cavity and waveguide analysis (rectangular circular and dielectric)[1-3]. We propose here to demonstrate its potential in the context of S-Shaped inlet cavity analysis and compare the obtained results with the solutions and measured values figured in [4]. The formulation of the method was explained very clearly in [1, 2].

Principle of the method- To find the field at an observation point M, we sweep the directions of arrival to that point with ray tubes launched backwards from M. In a multi-reflecting and/or refracting environment, it is possible to track a ray launched from M through successive local refractions and reflections. For a given ``tube'' of directions of arrival, the ray path is found and saved after this backward launching step. When the four rays' tube reaches the source plane, the directions of the rays, projected on the transverse plane of the wave vectors space, define a transverse differential surface in the spectral domain. With the knowledge of both this spectral surface and the aperture distribution PWS, we calculate the field associated to the ray tube. This field is then transformed along the ray path previously saved, following the usual Geometrical Optics rules: in multi-reflecting and/or refracting environments, propagation of the field along a ray tube not only changes the phase of the field, but also its amplitude and direction, through reflection and transmission operators, and through phase front transformations at curved interfaces.

Validation and Conclusion- Figure 1 shows the two inlet geometries. The inlets are rectangular of the same planar dimensions and perfectly conducting and will be analyzed in 3D at 10 GHz with all propagating modes in the waveguide sections (6 modes). Figure 2 shows the backscatter vs. aspect angle (θ) for the inlets of figure 1 using SRT method and the Asymptotic Modal (AM). The results agree quite well. The maximum normalized absolute error between the two methods is small than 3% for the straight inlet and 5% for the S-bend inlet. More applications of the SRT compared to the Asymptotic Modal for another S-form give accurate results.
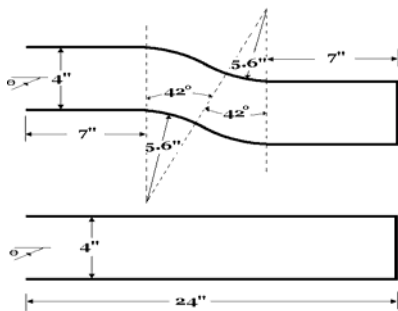
Fig. 1- Straight and S-bend inlet planar geometries
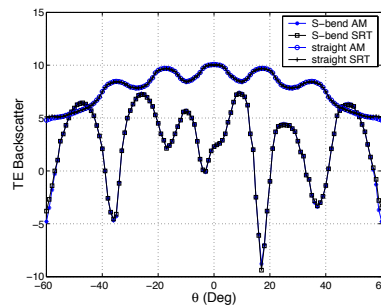
Fig. 2- TE Backscatter vs. aspect angle for S-bend and Straight inlets at 10 GHz

References
1. I.A. Ehtezazi and C. Letrou, "A spectral domain ray tracing method for quasi-optical device modelling", Antennas Propagat. Soc. Int. Symp. Dig , pp.1086-1089, 1998.
2. E. Rchid and C. Letrou, "A spectral domain ray: An Alternative method for devices modeling", 27th General Assembly of   Radio Science {URSI.}, no 1827, August 2002, The Netherland.
3. E. Rachid, and C. . Letrou, Spectral Ray Tracking: An Alternative Method for Guided Propagation Modeling, EIT2006, 6th conference, Michigan, USA, May 2006.
4. R.J. Burkholder , C.W. Chuang and P.H. Pathak, "Electromagnetic Fields Backscattered from an S-Shaped Inlet Cavity with an Absorber Coating on its Inner Walls" Final report No 715723-2, Ohio State University, USA, July 1987.

Towards the Development of Uncertainty Analyses in FDTD Simulations

R S Edwards, A C Marvin and S J Porter

University of York, York, England

E-mail: rse101@york.ac.uk

Standards exist that require an estimate of the uncertainty in measurements obtained from laboratory Electromagnetic Compatibility (EMC) measurements [1]. Currently no such requirements exist for the measurements obtained by Computational Electromagnetic (CEM) simulations. Uncertainty Analyses would provide a quantitative level of confidence in the results of the CEM simulations. Uncertainty can be defined as [2] a potential deficiency in any phase or activity of the modeling process that is due to lack of knowledge. Often when performing CEM simulations there is a lack of precise knowledge in some or all of the input parameters. If there are uncertainties in the input parameter data, then there will be uncertainties in the output. This type of uncertainty is often known as parameter uncertainty [2]. This paper investigates the effect of parameter uncertainty on the output of Finite Difference Time Domain (FDTD) simulations.

Three probabilistic methods that may be applied to FDTD simulations are the Monte Carlo Method (MCM), the Method of Moments (MoM) and Polynomial Chaos (PC). The MoM is similar to the method outlined in UKAS [1] for estimating the uncertainties in laboratory EMC measurements. This method requires fewer simulations to estimate the uncertainty than the more rigorous MCM, which is slow to converge. PC has been applied to one area of CEM [3], but has never before been implemented in FDTD. This method can be used to provide a first order estimate of the uncertainty, but with greater computational requirements than the MoM. Once the uncertainty has been estimated, using these three methods, it can be used to form 95% confidence intervals (CI) for the output of the simulations.

These three methods were applied to the simulation of a box with an aperture, illuminated with a 1V/m plane wave excitation. Inside this box was a daughterboard, the components of which were modeled by giving the board a reflection coefficient. There was an uncertainty in the value of the reflection coefficient, which was uniformly distributed between –0.91 and –0.97 at 1.8GHz. The three methods were used to calculate the *z*-component of the Electric field at the centre of the box, and the uncertainty (standard deviation) in this field.

Figure 1(a) shows the uncertainty in the field predicted by the three methods. The uncertainties predicted by the MCM and the MoM are in good agreement, the uncertainty predicted by PC agrees less well. The simulations were performed on a computer with a Pentium 4 processor at 3.0GHz. The more rigorous MCM took 55 hours to converge and used 36MB of memory. PC took 16 hours and used 970MB of memory. The MoM was by far the computationally cheapest method taking only 44 minutes and using 36MB of memory. The MoM is also in agreement with the more rigorous MCM, and is therefore the best method to use in this case. Figure 1(b) shows the mean field, along with its 95% confidence intervals. The mean field and the confidence intervals shown in this figure were calculated using the MCM with 150 simulations. The confidence intervals appear to be small around 1.8GHz. At this frequency the field is 0.466±0.0156 V/m with 95% confidence.
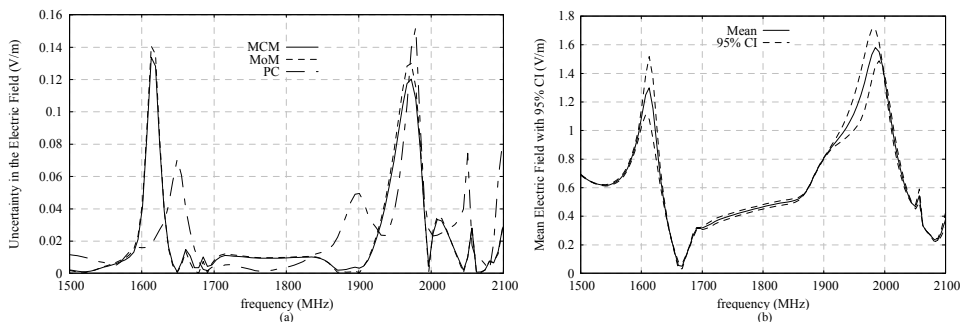
Fig. 1 – (a) Uncertainty in the Electric field predicted by the three UA methods, (b) Mean Electric field with 95% confidence intervals estimated using the MCM with 150 simulations.

References
1. "The Expression of Uncertainty in EMC Testing," UKAS publication LAB 34, Edition 1, 2002.
2. AIAA, "Guide for the verification and validation of computational fluid dynamics simulations," AIAA G-077-1998.
3. C. Chauviere, J.S. Hesthaven and L. Lurati, "Computational modeling of uncertainty in time-domain electromagnetics," SIAM Journal on Scientific Computing, vol. 28, issue 2, 2006.

HPEM - 26
Numerical Methods #1

Oral Presentations

A Closed Form Representation for Sommerfeld Integrals of the Electric Field Integral Equation

A. Shoory, R. Moini, and S. H. Hesamedin Sadeghi

Department of Electrical Engineering, Amirkabir University of Technology, Tehran, Iran

E-mail: shoory@aut.ac.ir

Sommerfeld integrals are generally involved in electric field integral equation (EFIE) representation of an electromagnetic boundary value problem in planar stratified media. The problems include a variety of applications in geophysical prospecting, target identification, microstrip antennas, micro wave integrated circuits, and etc. The integrals are semi infinite integrals of Bessel function with highly oscillatory and weakly damping kernels [1]. These integrals do not have analytical expressions and the time consuming process of numerical integration is the most convenient and reliable choice.

Since the Sommerfeld integrals of electric field expressions are naturally more singular than those in the corresponding potential functions, it is usually preferred to first evaluate the potential functions and then derive filed expressions as spatial derivatives of these functions [1]. A considerable body of research has been devoted to evaluate Sommerfeld integrals of potential functions using the numerical integration techniques, the so called discrete image method (DCIM) [3], and the rational function fitting method (RFFM) [3]. The latter two techniques give analytical representations of potential functions. DCIM and RFFM expand the Sommerfeld integral kernels respectively in the form of exponential and rational functions. This is done respectively using the numerical matrix pencil method (MPM) and the vector fitting (VECTFIT) method giving rise to respectively spherical and cylindrical wave representation of potential functions.

To the best of authors' knowledge, such expressions have been not reported for the electric field expressions. Therefore to accelerate the Sommerfeld integral evaluation we provide new closed form expressions for the electric field components. The nth order Sommerfeld integrals of the electric field expressions, S_n, can be generally represented as

$$S_n = \int_0^\infty f\left(k_\rho\right) J_n\left(k_\rho \rho\right) k_\rho^{n+1} dk_\rho \tag{1}$$

where J_n is the Bessel function of order n (=0,1,2), k_ρ is the radial wave number, $f(k_\rho)$ is the Sommerfeld integral kernel or namely the spectral electric field, and ρ is the radial distance in the cylindrical coordinates system of (ρ, φ, z).

To derive closed form expressions for the integrals of the form in (1) we first use the MPM to expand $k_\rho^n f(k_\rho)$ as

$$k_\rho^n f\left(k_\rho\right) = \sum_{i=1}^M a_i e^{-b_i k_\rho} \tag{2}$$

where a_i and b_i are the poles and residues of the exponential approximation.

Using Bessel function identities, we then arrive at the following expression e.g., for S_0 Sommerfeld integral,

$$S_0 = 2 \sum_{i=1}^M \frac{a_i b_i}{\left(b_i^2 + \rho^2\right)^{(3/2)}} \tag{3}$$

It is see n that the Sommerfeld integrals are calculated for any source-to-field separation distances at a single execution of the numerical MPM. Therefore, the proposed technique can provide a faster replacement to the numerical integration of Sommerfeld integrals in the EFIE representation of the problem.

References
1. K. A. Michalski and J.R. Mosig, "Multilayered media Green's functions in integral equation formulations," IEEE Trans. Antennas Propagat., vol. 45, no. 3, pp. 508–519, Mar. 1997.
2. Y. L. Chow, J. J. Yang, D. G. Fang, and G. E. Howard, "A closed-form spatial Green's function for the thick micro strip substrate," IEEE Trans. Microw. Theory Tech., vol. 39, no. 3, pp. 588-592, Mar. 1991.
3. V. N. Kourkoulos and A. C. Cangellaris, "Accurate approximation of Green's functions in planar stratified media in terms of a finite sum of spherical and cylindrical waves," IEEE Trans. Antennas Propagat., vol. 54, no. 5, pp. 1568-1576, May 2006.

An Accurate and Robust Approach for Evaluating VIE Impedance Matrix Elements Using SWG Basis Functions

Li Hu[1], Le-Wei Li[1,2], Tat Soon Yeo[1], and Ruediger Vahldieck[2]
[1]National University of Singapore, Kent Ridge, Singapore
[2]Swiss Federal Institute of Technology Zurich (ETH), Zurich, Switzerland
E-mail: lwli@nus.edu.sg

The volume integral equation (VIE) approach is one of the most popular methods used to solve the Maxwell's equations and to analyze various complicated electromagnetic problems involving inhomogeneous magneto-dielectric materials. Depending upon the formulations of the problems, the electric-field VIE (EF-VIE) [1], magnetic-field VIE (MF-VIE) [2], and combined-field VIE (CF-VIE) [3] have been separately used to solve pure dielectric, pure magnetic and magnetodielectric problems with the help of the method of moments (MoM) procedure. The Schaubert-Wilton-Glisson (SWG) functions [1] are usually chosen as the basis and testing functions in the MoM Galerkin's procedure. The integrals of VIE involve, however, $1/R$ and $1/R^2$ kinds of singularities caused by free space Green's function and its gradient, respectively. We cannot achieve a highly satisfied accuracy by using only the standard Gaussian quadrature. To overcome the problem of singular integrals, the most popular approach is the singularity subtraction method. However, to the authors' best knowledge, most of the previous focused issues in the mathematical and numerical treatments have been on the singularity over planar triangles, e.g. [4, 5, 6] and few has been done on tetrahedrons. Although non-planar case has been considered in [7], only $1/R$ singularity over polyhedral domains was discussed and only one singular term was subtracted. Even though the singular term can be subtracted and calculated analytically, the remaining function is not necessarily continuously differentiable; thus a standard Gaussian quadrature may lead to an inaccurate solution in general. In this paper, we present *an iterative, efficient and accurate method* for calculating *singularities of both order $1/R$ and order $1/R^2$ involved in the MoM solution of VIE*. In our method, a sufficient number of terms from Green's functions is subtracted so that the remainder is at least once continuously differentiable so as to enable the standard Gaussian quadrature method to be applicable. Similar ideas have been applied for surface integration problems in e.g. [4, 5, 6], here it is a further extension. Compared to the usual singularity extraction method which only extracts one term, the present method could significantly improve the accuracy of singular integral calculations. Compact iterative formulas are also derived and given here so that arbitrary terms of singularities can be subtracted and calculated analytically, which greatly facilitates its numerical implementation in the MoM procedure and also extendable to integral equation fast solvers.

References

1. D. H. Schaubert, D. R. Wilton, and A. W. Glisson, "A tetrahedral modeling method for electromagnetic scattering by arbitrarily shaped inhomogeneous dielectric bodies," *IEEE Trans. Antennas Propagat.*, vol. 32, pp. 77-85, Jan 1984.
2. J. L. Volakis, "Alternative field representations and integral equations for modeling inhomogeneous dielectrics," *IEEE Trans. Microwave Theory Tech.*, vol. 40, pp. 604-608, March 1992.
3. M. M. Botha, "Solving the volume integral equations of electromagnetic scattering," *J. Comput. Phys.*, vol. 218, no. 1, pp. 141-158, October 2006.
4. R. D. Graglia, "On the numerical integration of the linear shape functions times the 3-D Greens function or its gradient on a plane triangle," *IEEE Trans. Antennas Propagat.*, vol. 41, pp. 1448-1455, October 1993.
5. R. E. Hodges and Y. Rahmat-Samii, "The evaluation of MFIE integrals with the use of vector triangle basis functions," *Microwave Opt. Technol. Lett.*, vol. 14, pp. 9-14, January 1997.
6. P. Yla-Oijala and M. Taskinen, "Calculation of CFIE impedance matrix elements with RWG and NXRWG functions," *IEEE Trans. Antennas Propagat.*, vol. 51, no. 8, pp. 1837-1845, August 2003.
7. D. R. Wilton, S. M. Rao, A. W. Glisson, D. H. Schaubert, O. M. Al-Bundak, and C. M. Butler, "Potential integrals for uniform and linear source distributions on polygonal and polyhedral domains," *IEEE Trans. Antennas Propagat.*, vol. 32, pp. 276-281, March 1984.

Oral Presentations

Tuning of High-Power Antenna Resonances
by Appropriately Reactive Sources

C. E. Baum
University of New Mexico
Department of Electrical and Computer Engineering
Albuquerque New Mexico 87131
E-mail: cebaum@ece.unm.edu

In designing small high-power electromagnetic radiators (of the order of a half wavelength or so in size) based on switched resonant circuits, there are questions concerning the control of the resonance frequencies. This paper explores some techniques for tuning these frequencies based on the reactive properties of the source.

Consider the influence of the source impedance. This might be a simple capacitance C_s . However, at high frequencies $\tilde{Y}_s(s)$ (source admittance) may have more complex structure. This nonzero $\tilde{Z}_s(s)$ (source impedance) then combines with $\tilde{Z}_a(s)$ to shift the resonance frequencies. For present purposes we need a model for the source impedance. Let us choose an open-circuited transmission line. This has zeros (short-circuit resonances) at odd multiples of a quarter wavelength. One might choose the source as having zero impedance at an antenna resonance so as to deliver a large voltage to the antenna. Alternately, one can use the source characteristics to shift the resonance frequency.

One type of electrically small antenna is a loop of some kind producing a magnetic-dipole moment. When operating in resonance condition there may be some appreciable fraction of a wavelength across the structure. Let us model the antenna impedance (up to first resonance of current) as the parallel combination of an inductance and a capacitance. This is driven by a capacitive source; appropriate choice of the capacitance adjusts the resonance frequency.

Another type of electrically small antenna is an electric dipole of some kind, i.e., two separate conductors driven by some source between them, produding an electric dipole moment. Operated in resonance condition there may be some appreciable fraction of a wavelength across the structure. Let us model the antenna impedance (up to first resonance of current) as the series combination of a capacitance and an inductance. Again appropriate choice of the source capacitance adjusts the resonance frequency.

As we can see, judicious choice of the frequency dependence of the source impedance can alter the resonance frequency and resonance strength of the antenna, whether of loop or electric-dipole type. Here we have chosen some simple forms of the source impedance for illustration. More elaborate forms can also be pursued.

Switched Oscillator into a Helical Antenna at 500 MHz

D. V. Giri[1], F. M. Tesche[2], M. C. Skipper[3], M.Nyffeler[4] and P. Bertholet[4]

[1]*Pro-Tech, Alamo, CA, USA*
[2]*EM Consultant, Saluda, NC, USA*
[3]*ASR Corporation, Albuquerque, NM, USA*
[4]*armasuisse, Spiez, Switzerland*
Email: Giri@DVGiri.com

The switched oscillator topology has been described in [1,2]. We have investigated using this fundamental configuration to generate four separate oscillator modules; 200 MHz, 300 MHz, 400 MHz and 500 MHz. This system is designed as a fairly optimized configuration in several regards and can be used as a starting point for the present investigations. One of the primary constraints is that the electric fields must be the highest at the switch and must gradually decline from the switch section to the coaxial section. This is to ensure the correct position for switch closure. The ratio of electric fields in the coaxial section to the electric fields in the switch section is a fine balance between minimizing the length of the radial transmission line (RTL) and maximizing the probability that switching events will occur at the switch. In this presentation, we will describe the following aspects: a) preliminary oscillator layouts for four different frequencies, b) PSpice simulations of chosen layouts, c) Fabrication of two oscillators at 200 MHz and 500 MHz. and d) testing of these two oscillators in a dummy load consisting of a 100 Ohm transmission line. In addition to the design and fabrication of this switched oscillator, we have also integrated this switched oscillator source at 500 MHz into a helical antenna that has bandwidth of 400-600 MHz, as shown in Fig. 1. Fig. 2 shows the measured oscillator output into a 100 Ohm dummy load and Fig. 3 compares the measured and calculated transfer function. The measured transient responses of both components of the circularly polarized radiation are shown in Fig. 4.

Fig. 1 - Osc/antenna system   Fig. 2 - Measured output voltage   Fig. 3 - Calculated and measured transfer function
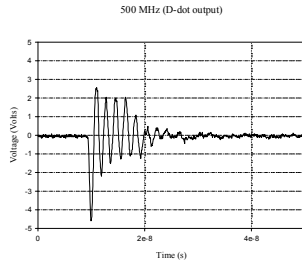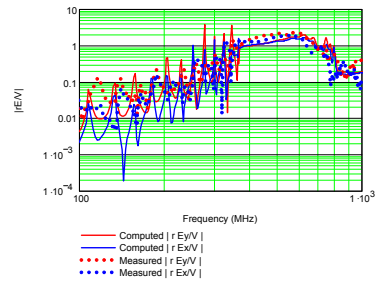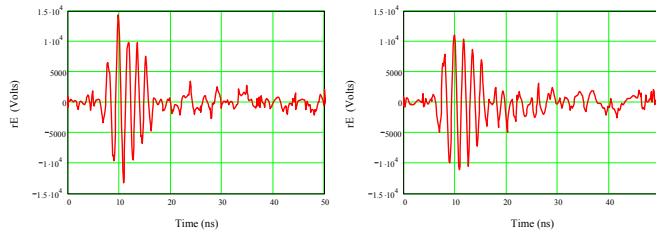
Fig. 4 - Transient radiated field components

References
1. C. E. Baum, "Switched Oscillators," Circuit and Electromagnetic System Design Note 45, 10, September 2000.
2. J. W. Burger, C. E. Baum, W. D. Prather, R. Torres, D. V. Giri, M. D. Abdalla, M. C. Skipper, B. C. Cockreham, J. Demarest, K. Lee and D. McLemore, "Modular Low Frequency High Power Microwave Generator," presented at AMEREM 2002, Naval Academy, Annapolis, MD.

Radiation Energy Losses in a Parametric Oscillator Formed by a Flux-Compression Generator with a Capacitive Load

V. G. Baryshevsky, A. A. Gurinovich

Research Institute for Nuclear Problems, Belarussian State University, Minsk, Belarus

E-mail: gur@inp.minsk.by

A.D. Saharov [1] demonstrated that fast explosive deformation of current-carrying circuits allows one to convert the energy of explosion to the energy of ultrahigh magnetic field and proposed a concept of the dedicated device, which was called flux-compression generator (FCG).

Now FCGs are widely used for production of very strong magnetic fields (150 megagauss) and high power X-ray pulses, for accelerator supplying and other purposes. From the electrodynamical point of view FCG can be considered as a time-dependant inductance. In this respect a connected to an accelerator FCG forms the circuit with time-dependant inductance and capacitance. A changing in time inductance produces time-dependant magnetic field and, therefore, electromagnetic radiation.

A radiative reaction force, which accompanies radiative process, is induced by the time-dependant electromotive difference in this circuit. As a result radiation losses and oscillation damping arise and influence on current and voltage generation in such a system.

Theoretical consideration of radiation losses in FCG made in [2] was based on representation of an FCG coil as a helical antenna. According to [2], energy losses in the FCG coil can be described by the sum of diffusion losses, which include diffusion of the compressed magnetic field into wires and isolation, and energy dissipation from the compressed volume by means of radiation from loops of the FCG coil.

In present report is shown that besides radiation from the FCG coil the system «FCG with a capacitive load» radiates also due to charge oscillation in the capacitive load. The equations describing electromagnetic radiation in such a system are obtained. Expansion of radiation field over multipoles is used. Influence of dipole radiation, which principal source is the capacitor, on operation of the system «FCG with a capacitive load» is analyzed. Multipole expansion allows us to describe influence of dipole electric and dipole magnetic radiation on behavior of the system «FCG with a capacitive load». In the framework of multipole approximation explicit expressions for radiation losses in this system are obtained. Radiation from capacitive load is shown to be important and even determining.

References
1.   A.D. Saharov, Uspekhi Fizicheskikh Nauk v.88 (1966) no.4.
2.   A.B.Prishchepenko and M.V.Shchelkachev, Electrichesvo 8 (1993) 31.

Application of Volume Free Electron Laser for development of High Power Microwave Sources

V. G. Baryshevsky, A. A. Gurinovich

Research Institute for Nuclear Problems, Belarussian State University, Minsk, Belarus

E-mail: gur@inp.minsk.by

Generators using radiation from an electron beam (traveling wave tubes [1,2], backward wave oscillators, free electron lasers) are now widespread [3]. All the above devices use one-dimensional distributed feedback, which is formed by either two parallel mirrors placed on the both sides of working area or a diffraction grating.

Electrical endurance of resonator limits radiation power and current of acceptable electron beam. Conventional waveguide systems are essentially restricted by the requirement for transverse dimensions of resonator, which should not significantly exceed radiation wavelength. The indicated problems can be overcome by the aid of volume (two or three-dimensional) multi-wave distributed feedback [4-9]. Use of volume distributed feedback makes also available effective modes selection in oversize systems, in which the radiation wavelength is significantly smaller then the resonator dimensions. New type of radiation generators using volume multi-wave distributed feedback was called Volume Free Electron Laser (VFEL).

In the present paper operation principles and specific features of VFEL are considered in view of its application for development of High Power Microwave source. The properties of a "grid" photonic crystal built from metallic threads are considered along with its frequency characteristics in view of their importance for VFEL lasing. VFEL prototypes operating in millimeter and centimeter wavelength ranges are discussed (see Fig.1). Experimental studies of generation threshold dependence on the resonator length for different "grid" photonic crystals are reported. Advantages of use of "grid" photonic crystal with changing in space parameters for VFEL lasing are demontrated. Possibility to develop VFEL operating in TeraHerz range is also considered.
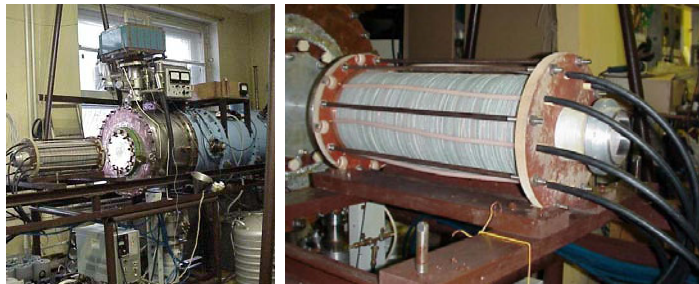
Fig. 1 – VFEL prototype

References
1. R. Kompfner "The traveling wave valve" *Wireless World,* **52**, pp. 369-372 (1946).
2. R.Pierce "Theory of the beam-type traveling-wave tube" *Proc. IRE*, **35**, pp.111-123 (1947).
3. V.L.Granatstein, R.K.Parker and C.M.Armstrong "Vacuum electronics at the dawn of the twenty-first century," *Proceedings of the IEEE*, **87**, no.5, pp.702-716, (1999).
4. V.G.Baryshevsky "Volume Free Electron Lasers"   *NIMfA*, **445**, pp.281-282 (2000); LANL e-print archive physics/9806039.
5. V.G.Baryshevsky, K.G.Batrakov, A.A.Gurinovich, I. Ilienko, A. Lobko, V. Moroz, P. Sofronov, and V. Stolyarsky "First Lasing of Volume FEL (VFEL) at Wavelength Range $\lambda \sim 4-6$ mm" *NIM A*, **483**, pp.21-24 (2002).
6. V.G.Baryshevsky, K.G.Batrakov, A.A.Gurinovich, I. Ilienko, A. Lobko, V. Moroz, P. Sofronov, and V. Stolyarsky "Progress of the Volume FEL (VFEL) experiments in millimeter range" *NIM A*, **507**, pp.137-140 (2003).
7. V.G.Baryshevsky, K.G.Batrakov, V.Mihalchik, V.P.Peftiev, V.I.Stolyarsky "A process for generating electromagnetic radiation and volume free electron laser apparatus for carrying out the process" Eurasian patent EA 004665B1.
8. V.G.Baryshevsky and I.D.Feranchuk "Parametric beam instability of relativistic charged particles in a crystal" Phys.Lett. A, **102**, pp.141-144 (1984).
9. Sher Alam, M.O.Rahman, C.Bentley and M.Ando "Basics of surface and volume FEL's" Proceedings of the APAC'01 pp.277-280 (2001)

Integration of a Compact RF Generator with an FCG Simulator

R. D. Curry[1], K. O'Connor[1], and L. Altgilbers[2]
[1]*University of Missouri-Columbia, Department of Electrical and Computer Engineering*
Center for Physical and Power Electronics, Columbia, MO, USA
[2]*US Army Space and Missile Defense Command, Huntsville Alabama, USA*
.E-mail: curryrd@missouri.edu

The University of Missouri-Columbia is developing a compact power conditioning system to transform the high current signal from a flux compression generator (FCG) to the high voltage, high frequency signal required for any pulsed power applications. The system consists of an air core, spiral-wound transformer, series exploding wire fuse, and an oscillating mesoband source.

The power conditioning transformer consists of a 1 μH primary winding inductance and a turns ratio of 1:3 with a coupling factor of between .75 and .85. Use of the transformer and a crowbar switch to minimize the peak voltage across the fuse allows the fuse length to be reduced without risk of arc breakdown. The fuse was designed to interrupt a peak current of between 25kA and 40kA in less than 300 ns. The multiple stage fuse is constructed using two sections with an effective length of less than 25 cm. A capacitance of about .275 nF connected to the transformer secondary is charged to a voltage of approximately 200-450 kV. The capacitor is then switched into an underdamped resonant circuit to generate RF oscillations. Using a two stage flux compressor built by TTU, we have demonstrated over 125 MW of RF using a simple tri-plate capacitor.

The low inductance, high voltage capacitor has been redesigned from a tri-plate geometry to a cylindrical geometry. The diameter of the capacitor was designed to be 15-16 cm in order to match the diameter of the pulse transformer and exploding wire fuse. The length was designed to be 15.24 cm to ensure compactness of the complete system. The capacitance of the new high voltage capacitor is designed to be approximately 650 nF. This capacitance is more than a factor of two greater than that of the original low inductance capacitor to increase the energy of the high voltage energy storage. The increased capacitance and dramatically reduced capacitor volume result in an overall energy density increase of a factor of 8 for the same charge voltage. However, with this higher energy density, there are higher electric fields, increasing the risk of dielectric failure. The capacitor design and construction was therefore adapted from the methods used for the spiral-strip pulse transformer, which have previously been charged to well over 450 kV. Although the capacitance is greatly increased, the resonant frequency range of the oscillator was optimized to be the same as the original prototype. Lowering the inductance of the secondary closing switch and shunt inductor corresponds to a frequency band of 60 MHz to 250 MHz.

This paper describes the design and construction methods of the new RF load oscillator. Details of the integration of this load with the pulse transformer and exploding wire fuse components are also included along with the FCG simulator design.

Pulsed Power Technology for HPEM Application

R.H. Stark, J. Urban, C. Bickes, V. Kadetov, D. Weixelbaum, E. Mutzbauer
Diehl BGT Defence GmbH & Co. KG, D-90552 Roethenbach a.d. Pegnitz, Germany

e-mail: robert.stark@diehl-bgt-defence.de)

High power microwave (HPEM) sources are designed to generate short, high power electromagnetic pulses. The high power electromagnetic radiation is able to disrupt or destroy electronic targets including the control and computer electronics of modern weapon systems. After coupling to the target system, the electromagnetic radiation is converted into current and voltage transients on signal and power lines. Dependent on the amplitude of the signals induced, components may be disrupted or even destroyed. In both cases the system looses its intended functionality.

HPM sources offer a novel and unique capability to attack electronic systems used in command posts, for surveillance and in information infrastructure at minimum collateral damage. Short-pulse HPM sources do not cause undesirable biological effects on personnel in the target area.

A range of high power electromagnetic sources have been developed by Diehl BGT Defence in cooperation with Rheinmetall Waffe&Munition. Those sources range from small, autonomous, man-portable systems to larger high power devices and multi-antenna array systems. Various technological approaches have been used to demonstrate potential of HPM technology.

Pulsed Power (PP) is the basic technology used for development of high power microwave sources. An overview on various PP technologies used for high power electromagnetic pulse generation will presented. Various applications of HPEM systems will be emphasized.

HPEM - 27
High-Power RF Source Technology (Invited)

Oral Presentations

Gigawatt Magnetron Gun in Secondary Electron Emission Mode and Prospects of its Application

S.A. Cherenshchykov

National Science Centre "Kharkov Institute of Physics and Technology", Kharkov, Ukraine,

E-mail cherench@kipt.kharkov.ua

The Secondary Emission Magnetron Injection Gun (SEMIG) is a novel universal electron source with a cold cathode. Unconventional principle of the gun is the self-excitation secondary-emission multiplication in crossed-fields. The SEMIG may have higher current density and lifetime much longer (up to 100,000 hours) than conventional thermionic guns. High power SEMIG with voltage up 1000 kV and current more 1 kA was calculated, designed and manufactured. The gun was tested in nanosecond pulse operating modes. The application of voltage pulses with amplitude up to 600 kV permitted to obtain the secondary-emission current amplitude up to 4 kA. The secondary emission nature of the cathode current up to 4 kA was established. The identification was held basing on considered features of the exciting and on the maintenance of the secondary emission current. The large amount of criterion gives the high validity of the identification. However, there is the probability of the parasitic explosive emission at extremely high voltage values since 800 k V.

The gun may be used in all types of high power microwave sources. Moreover due to possibility emission modulation and its ultra fast control the gun may be base for creation novel microwave and ultra-wideband short-pulse devices.

HPEM - 27
High-Power RF Source Technology (Invited)

Oral Presentations

Current and Voltage Distribution along Communication Towers Hit by Direct Lightning

V. Hedge[1], U. Kumar[2]

[1]*Department of Electrical Engineering, Malnad College of Engineering Hassan 573201, India,*
[2]*Department of Electrical Engineering, Indian Institute of Science, Bangalore 560012, India,*
e-mail: hegde_mce@ rediffmail.com

In order to answer a practically important question that whether the down conductors of lightning protection system to tall towers and buildings can be electrically isolated from the structure itself, this work is taken up. As a first step in this regard, it is presumed that the down conductor placed on metallic tower will be a pessimistic representation of the actual problem. This opinion was based on the fact that the proximity of heavy metallic structure will be having large damping effect. The post-stroke current distributions along the down conductors and towers, which can be quite different from that in the lightning channel, govern the post-stroke near field and the resulting gradient in the soil [1]. Also, for a reliable estimation of the actual stroke current from the measured down conductor currents, it is very essential to know the current and voltage distribution characteristics along the down conductors [2]. In view of these, the present work attempts to deduce the post-stroke current (Fig. 1) and voltage distribution (Fig. 2) along typical down conductors and towers. Solution of the governing field equations on an electromagnetic model of the system is sought for the investigation. Simulations are carried out using NEC-2 [3] and MATLAB. Simulation results providing the spatio-temporal distribution of the post-stroke current and voltage has provided very inquiring results. It is concluded that it is almost impossible to achieve electrical isolation between the structure and the down conductor. Further there will be significant induction into the steel matrix of the supporting structure.
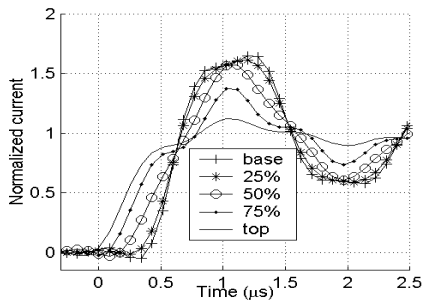
Fig. 1 - Current distribution along tower of 120 m height
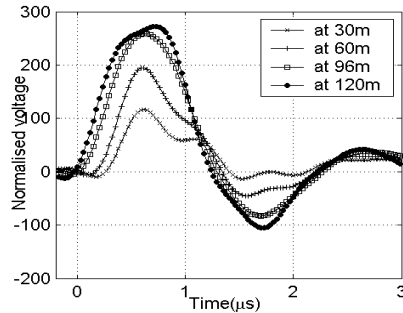
Fig.2 - Voltage difference between 120 m tower and electrically isolated vertical conductor running at the centre

References

1. Paresh Kumar Nayak , Experimental Investigations on The Lightning Surge Response of some Lightning protection Systems",   M.Sc. Thesis, IISc, Bangalore Sept. 2003.
2. Vishwanath Hegde, "Lightning Protection System to Indian Satellite Launch Pads: Stroke Classification and Evaluation of the Currents in the Intercepted Strokes," Ph.D. Thesis, High voltage Lab., Dept. of Electrical Engineering, IISc, Bangalore, Nov. 2006.
3. Pranav Darji, "Studies on post stroke characteristics of Lightning Protection System to Indian Satellite Launch Pads," M.E. Thesis, Dept. of High Voltage Engineering, IISc, Bangalore, Jun. 2004.

Currents in Buried Grounding Strips Connected to Communication Tower Legs during Lightning Strikes

N. Theethayi[1], R. Thottappillil[1], G. Diendorfer[2], M. Mair[3] and H. Pichler[3]

[1]*Division for Electricity, Uppsala University, Uppsala, Sweden.*

[2]*Austrian Electrotechnical Association (OVE) Dept. ALDIS (Austrian Lightning Detection & Information System), Vienna, Austria.*

[3]*Institute of Electrical Power Systems and Energy Economics, Vienna University of Technology, Vienna, Austria.*

E-mail: Rajeev.Thottappillil@angstrom.uu.se

Lightning strike to communication towers is a usual phenomenon. Communication towers and its associated electronics require lightning protection. Grounding of towers is an integral part of the overall lightning protection design. Communication towers are not isolated systems. Usually transmitting and receiving electronics are kept in a building adjacent to the towers and different types of cables run from the tower to the building. During a lightning strike to communication tower stroke currents are shared by the tower and by the shields of the cables along the tower. The currents in the tower proceed towards the grounding system (possibly a combination of counterpoises or ring conductors or ground rods or grounding grids) connected to tower legs' foundation. Here we examine lightning strike to communication tower on mount Gaisberg in Austria and measured currents at the tower top and those shared by an instrumented grounding strip connected to one of the tower leg's is presented. The measured currents at different locations along the 70-m long ground strip are compared with the predictions of a frequency dependant lossy transmission line (TL) model and reasonably good agreement was found. From this validation it is claimed that the TL models are appropriate for lightning transient analysis of grounding systems.

The tower top current is measured using a current sensor and analog data is transmitted using a fiber optic link to the digitizer system housed in the building next to the tower. The lightning current is measured just below the air termination on the tower top using a 0.25 mΩ current shunt. The shunt output signal is recorded by an 8 bit digitizer. The digitizing board has a memory of 16 MB/channel and is operated with a sampling rate of 20 MSamples/s to give record length of 800 ms [1]. Later, the tower current is offset corrected and filtered with 250 kHz. To reduce the data size for the analysis of this paper, it was resampled to 2 MS/s. There are buried grounding strips connected to each of the tower legs. The grounding strips are expected to carry some part of the total lightning currents measured at the tower and dissipates them into the soil. This mechanism is not clear. The authors wish to acknowledge the lack of information on the details of any complex grounding system under and nearby the tower other than the grounding strips taking off from the tower legs and down conductors of lightning protection system of the nearby buildings. The currents were measured at the grounding strip's take off point from the tower or the current injection point, 40 m from the injection point and 60 m from the injection point. The grounding strip was at a depth of 0.5 m. The strip had a rectangular cross section with an approximate dimension 30 mm × 3 mm, (overall conductor area of 9×10^{-5} m^2). The currents at injection point and at 40 m away from injection point were measured using Pearson current monitor (Model 301X). This current monitor has a bandwidth of 5 Hz – 2 MHz. Current at 60 m from injection point was measured using a Rogowski coil (LEMflex RR3000-SD/24) with a bandwidth of 8 Hz to 100 kHz. Fibre optic systems with a bandwidth of 0,2 Hz to 5 MHz were used for data transmission from all three sensors to the data acquisition system (Yokogawa DSO 708E operated with a sample rate of 10MS/s, 10 bit vertical resolution) located in the building.

References
1. G. Diendorfer, W. Schulz and M. Mair, "Evaluation of a LLS based on lightning strikes to an instrumented tower", Proc. of International Lightning Detection Conference (ILDC), Tuscon, Arizona, 2000.

Electromagnetic Fields Very Near to a Tall Tower Struck by Lightning: Influence of the Ground Conductivity

A. Mimouni[1,2], A. Mosaddeghi[1], F. Rachidi[1], M. Rubinstein[3]
[1]*Swiss Federal Institute of Technology, EMC Group, Lausanne, Switzerland*
[2]*Ibn Khaldoun University,Tiaret, Algeria*
[3]*University of Applied Sciences of Western Switzerland, Yverdon, Switzerland*

E-mail: a_mimouni@mail.univ-tiaret.dz

We present an analysis of the electromagnetic fields in the immediate vicinity of a tower struck by lightning. The electromagnetic fields are evaluated for observation points above, on the surface and below the ground plane characterized by a finite conductivity. The computations are obtained using two different approaches.

First, the so-called engineering models [1,2] are adopted for the description of the spatial and temporal distribution of the current along the lightning channel and the struck tower. The resulting electromagnetic fields are computed using the Finite-Difference Time-Domain (FDTD) technique, in which the engineering models are appropriately incorporated [3].

The second approach is based on the so-called Antenna Theory (AT) models (e.g. [4]) in which both the lightning channel and the struck object are represented by conducting wires and the lightning return-stroke current is injected by a voltage source at the tip of the tower. In this analysis, use is made of the Numerical Electromagnetics Code NEC-4 [5], a well-known and widely used computer code based on the Method of Moments for analyzing the electromagnetic response of antennas and scatterers.

Simulation results are performed considering two cases, namely (i) a lightning strike to ground, and (ii) a lightning strike to a 100-m tall tower. The effect of the presence of the tower as well as the effect of finite ground conductivity on the generated electromagnetic fields are illustrated and discussed.

It is shown that the underground electric fields, predominantly horizontal, are markedly affected by the ground conductivity. Above the ground and on the ground surface, the vertical electric field and the azimuthal magnetic field generated by a lightning return stroke initiated at ground level are nearly insensitive to the height of the observation point above ground. The magnetic field above the ground at such close distance is essentially unaffected by the ground conductivity. The presence of a tower results in a significant decrease of the electric fields in the immediate vicinity of the tower. Unlike the case of a ground-initiated return stroke, the above-ground vertical electric field associated with a return stroke to tall tower is very much affected by the ground conductivity. Both approaches predict that this component could, depending on the value of this parameter, exhibit an inversion of polarity [6].

References
1. F. Rachidi, V. A. Rakov, C. A. Nucci, and J.L. Bermudez, "Effect of vertically-extended strike object on the distribution of current along the lightning channel", J. Geophys. Res., 107 (D23) (2002) 4699, 2002.
2. Y. Baba and V. A. Rakov, "On the use of lumped sources in lightning return stroke models," Journal of Geophysical Research, vol. 110, 2005.
3. A. Mimouni, F. Rachidi and Z. Azzouz, "Electromagnetic environment in the immediate vicinity of a lightning return stroke", Journal of Lightning Research, Vol.2, 64-75, 2007.
4. Y. Baba, and M. Ishii, "Numerical electromagnetic field analysis of lightning current in tall structures", IEEE Trans. Power Delivery, 16(2), 324-328, 2001.
5. G. J. Burke, "Numerical Electromagnetics Code NEC-4 Method of Moments," Lawrence Livermore National Laboratory UCRL-MA-109338, 1992.
6. A. Mosaddeghi, D. Pavanello, F. Rachidi, M. Rubinstein, "On the Inversion of Polarity of the Electric Field at Very Close Range from a Tower Struck by Lightning", Journal of Geophysical Research, 112, D19113, doi:10.1029/2006JD008350, 2007.

HPEM - 28
Lightning Characterization & Simulation (Invited)

Oral Presentations

Numerical Electromagnetic Analysis of Lightning Surge Inside of 600-m class Independent Tower

S. Miyazaki[1], A. Tatematsu[1], H. Motoyama[1], and M. Ishii[2]
[1]*Central Research Institute of Electric Power Industory, Kanagawa, Japan*
[2]*The University of Tokyo, Tokyo,Japan*

E-mail: m-satoru@criepi.denken.or.jp

When lightning strikes a tall structure such as a tower or an intelligent building, the lightning current flowing through the structure generates overvoltages and transient electromagnetic fields inside of the structure. To evaluate the risk of faults and malfunctions of installed electronic equipments influenced by the electromagnetic interference from the lightning current, prediction of overvoltages on the power lines and of the characteristics of electromagnetic fields inside of the structures is indispensable.

A new 600-m class truss-structured independent tower is planned in Tokyo, which will be struck by lightning several tens of times a year. Thus, lightning surges on this tower have been calculated employing numerical electromangetic analyses, namely the method of moments (MoM) and the finite difference time domain (FDTD) method.

Induced voltage on a power line inside of the tower is investigated by using Numerical Electromagnetics Code (NEC-4), which is based on MoM. It has been found that the induced voltages on a power line are sensitive to the configuration of the tower and/or the grounding system. Fig. 1 shows calculated induced voltage at the upper part and at the bottom of the tower when a lightning current is injected from the top of the tower. The 10-90% virtual front time of the injected lightning current is 0.25 μs, taking account of a subsequent return stroke. The spike of the induced voltage at the bottom appears at about 4 μs is generated because there are lightning-current paths of different lengths.

Fig. 2 shows the magnetic field distribution on the vertical cross section of the observatory, when the upper corner of the observatory, located at the height of 375 m, is struck by lightning, calculated by the FDTD method. Although the lightning current generates magnetic field higher than 10 A/m/kA near the striking point, it decreases to below 2 A/m/kA at a point inside of the observatory, 2 m away from the wall close to the striking point.
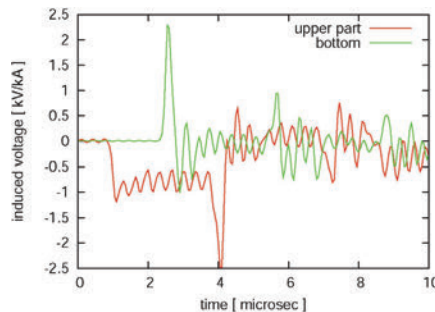
Fig. 1 – Calculated induced voltage on powe line inside of 600-m class independent tower.
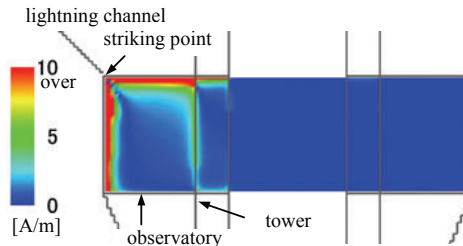
Fig. 2 - Magnetic field distribution inside of observatory for lightning current of 1 kA.

Evaluation of Lightning-Induced Disturbances in Buried Cables

F. Delfino[1], M. Paolone[2], R. Procopio[1], F. Rachidi[3], and M. Rossi[1]

[1] *Department of Electrical Engineering, University of Genoa, Italy*
[2] *Department of Electrical Engineering, University of Bologna, Italy*
[3] *EMC Group, Swiss Federal Institute of Technology (EPFL), Lausanne, Switzerland*

E-mail of the corresponding author: federico.delfino@die.unige.it

In the last years, the scientific community has paid particular attention to the development of formulations that can adequately describe the phenomenon of lightning electromagnetic field coupling to buried cables. The reason of such interest is mainly due to the fact that the number of power installations lying underground has been rapidly increasing in the recent past. Furthermore, such devices are much more sensitive to the effect of the lightning electromagnetic fields, due to the massive presence of power electronics.

The procedure for the coupling analysis basically consists of the following main steps: 1) Selection of an adequate return-stroke current model; 2) Evaluation of the lightning underground fields (E_r, E_z, H_ϕ); 3) Insertion of such fields as inputs for a field-to-buried line coupling model, which allows to compute induced voltages and currents. As far as the first step is concerned, we adopted in this study the so-called engineering models [1]..The field computation can be performed in two ways: one can resort to the exact method, developed by Sommerfeld [3] and implemented into a numerical code for lightning calculations in [4], or to use some approximate formulas, like the ones presented by Cooray in [5]. Concerning the third step, the transmission line theory has been adopted to describe the field-to-buried line cable and can implemented by means of a classical FDTD algorithm [6].

In this paper, the authors aim at highlighting how the differences between the results in the computation of the fields obtained by the application of the two aforementioned methods [4, 5] would affect the evaluation of the induced voltages and currents. As a first result, here the shield current on a buried cable has been considered and a comparison between simulated results (obtained with the two field calculation methods) and the measured ones [7] is presented. As can be seen, there are not significant differences between the two methods and both are in good agreement with measured data.
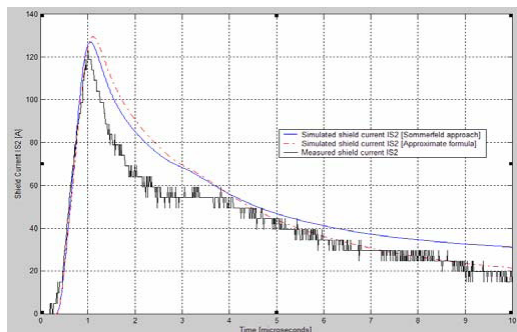
Fig. 1 – Induced currents on a buried cable. Comparison between measurements [7] and simulations.

References

1. V.A. Rakov, M.A. Uman, "Review and evaluation of lightning return stroke models including some aspects of their application", *IEEE Trans. Electromagn. Compat.,* vol. 40, no. 4, pp. 403-426, November 1998.
2. F. Heidler, "Analytische Blitzstromfunktion zur LEMP-Berechnung," *Proc. 18th Int. Conf. on Lightn. Protect.*, 1985.
3. A. Sommerfeld, *Partial differential equations in physics*, Academic Press, New York, 1949.
4. F. Delfino, R. Procopio, M. Rossi, F. Rachidi and C.A. Nucci, "An Algorithm for the Exact Evaluation of the Underground Lightning Electromagnetic Fields", *IEEE Trans. on EMC*, vol. 49, n. 2, pp. 401-411, May 2007.
5. V. Cooray, "Underground electromagnetic fields generated by the return stroke of lightning flashes", *IEEE Trans. on EMC*, vol. 43, no. 1, pp. 75-84, February 2001.
6. E. Petrache, F. Rachidi M. Paolone, C.A. Nucci V.A. Rakov, M.A. Uman, "Lightning-induced disturbances in buried cables", Part I: Theory, *IEEE Transactions on Electromagnetic Compatibility*, Vol. 47, No. 3, pp. 498-508, August 2005.
7. M. Paolone, E. Petrache, F. Rachidi, , C.A. Nucci, V. Rakov, M. Uman, D. Jordan, K. Rambo, J. Jerauld, M. Nyffeler, J. Schoene, "Lightning-induced disturbances in buried cables part II: experiment and model validation", *IEEE Trans. on EMC.*, vol. 47, no. 3, pp. 509-520, August 2005.

HPEM - 28
Lightning Characterization & Simulation (Invited)

Oral Presentations

HPEM - 28
Lightning Characterization & Simulation (Invited)

Oral Presentations

Calculation of Lightning-Induced Voltages on Distribution Networks: a New Interface Between the LIOV code and EMTP-RV

Alberto Borghetti[1], Carlo Alberto Nucci[1], Fabio Napolitano[1], Mario Paolone[1], Farhad Rachidi[2]

[1]*University of Bologna, Bologna, Italy*
[2]*Swiss Federal Institute of Technology, Lausanne, Switzerland*
E-mail: mario.paolone@unibo.it

Lightning-induced voltages are important sources of power quality problems: indeed, they can cause short interruptions and voltages sags on distribution systems. The analysis of these disturbances induced on distribution networks by lightning electromagnetic pulses (LEMP) radiated by nearby lightning, requires the availability of accurate models and relevant computer programs of LEMP-illuminated lines [1,2]. These should be able to reproduce the complex configuration of distribution systems including the presence of multi-branched lines, shielding wires and their complex groundings models, as well as that of surge arresters and distribution transformers.

In order to extend the analysis of the lightning performance of a single straight overhead line [3,4,5] to more complex distribution systems [6], the lightning-induced overvoltage code, henceforth called LIOV code, has been interfaced with the electromagnetic transient program (EMTP96) [7,8]. In view of the recent improvement of the EMTP implementing the augmented nodal analysis (EMTP-RV) [9-11], this paper proposes a new interface between the LIOV code and the EMTP-RV as well as the relevant validation based on experimental results obtained by means of triggered lightning technique [12-14].

The proposed interface represents an improvement of the one described in [7,8] considering that proposes a new treatment of the boundary conditions that allows to overcome the presence of a time step delay in correspondence of the LEMP-coupled lines terminations.

References

1. A.K. Agrawal, H.J. Price, S.H. Gurbaxani, "Tran-sient response of a multiconductor transmission line excited by a nonuniform electromagnetic field", IEEE Trans. on EMC, Vol. 22, No. 2, pp. 119-129, May 1980.
2. C.A. Nucci, F. Rachidi, "Interaction of electromagnetic fields with electrical networks generated by lightning", Chapter 8 of 'The Lightning Flash: Physical and Engineering Aspects', IEE Power and Energy series 34, IEE Press, 2003.
3. IEEE Working Group on the lightning performance of distribution lines, "Guide for improving the lightning performance of electric power overhead distribution lines", IEEE Std 1410, 2004.
4. Joint Cigré-Cired WG C4.4.02, "Protection of MV and LV networks against lightning. Part I: common topics", Cigré technical brochure, Nr. 287, February 2006.
5. A. Borghetti, C.A. Nucci, M. Paolone, "An Improved Procedure for the Assessment of Overhead Line Indirect Lightning Performance and its Comparison with the IEEE Std. 1410 Method", IEEE Trans. on Power Delivery, vol. 22, no. 1, pp. 684-692, January 2007.
6. A. Borghetti, C.A. Nucci, M. Paolone, "A Method for the Assessment of the Indirect Lightning Performance of Distribution Networks", Proc. of the Cigre Symposium Transient Phenomena in Large Electric Power Systems, April 18-21, 2007, Zagreb, Croatia.
7. C.A. Nucci, V. Bardazzi, R. Iorio, A. Mansoldo, A. Porrino, "A code for the calculation of Lightning-Induced Overvoltages and its interface with the Electromagnetic Transient Program", Proc. of the 22nd Int. Conf. on Lightning Protection, Budapest, Hungary, 19-23 September, 1994.
8. A. Borghetti, J.A. Gutierrez, C.A. Nucci, M. Paolone, E. Petrache, F. Rachidi, "Lightning-induced voltages on complex distribution systems: models, advanced software tools and experimental validation", Journal of Electrostatics, Vol. 60/2-4, pp. 163-174, Elsevier, 2004.
9. J. Mahseredjian, S. Lefebvre and X.-D. Do, "A new method for time-domain modelling of nonlinear circuits in large linear networks", Proc. of 11th Power Systems Computation Conference PSCC, August 1993.
10. J. Mahseredjian, L. Dubé, L. Gérin-Lajoie, "New Advances in the Simulation of Transients with EMTP: Computation and Visualization Techniques", Proc. of 7th International Conference on Modeling and Simulation of Electric Machines, Converters and Systems, Montreal, August 2002.
11. J. Mahseredjian, S. Dennetière, L. Dubé, B. Khodabakhchian "On a new approach for the simulation of transients in power systems" Proc. of the International Conference on Power Systems Transients IPST'2005, Montreal, June 2005.
12. V.A. Rakov, "Lightning discharges triggered using rocket-and-wire techniques", Recent Res. Devel. Geophysics, 2, Research Signpost, 1999, pp. 141–171.
13. V.A. Rakov, "Lightning properties from triggered-lightning experiments at Camp-Blanding, Florida (1997–1999)", Proc. 26th 26th International Conference on Lightning Protection, Rhodes, Greece, Vol. I, pp. 54–59.
14. V.A. Rakov, M.A. Uman, K.J. Rambo, M.I. Fernandez, R.J. Fisher, G.H. Schnetzer, R. Thottappillil, A. Eybert-Berard, J.P. Berlandis, P. Lalande, A. Bonamy, P. Laroche, A. Bondiou-Clergerie, "New insights into lightning processes gained from triggered-lightning experiments in Florida and Alabama", Journal of Geophysical Research 103 (D12) (1998) pp. 14117–14130.

Lightning Striking Characteristics to Wind Turbine Blade with a 3-Dimensional Leader Development Model

Takatoshi Shindo

Central Research Institute of Electric Power Industry (CRIEPI), Tokyo, Japan
shindo@criepi.denken.or.jp

Damages of wind turbine blades caused by lightning are one of important problems. Historically, the electro-geometric model such as A-W model [1] has been used to evaluate shielding performance of transmission lines. Recently, new models that take dynamic leader development into consideration have been also proposed [2]. These analyses are, however, 2-dimensional and it is difficult to apply the results to a non-symmetrical freestanding object such as wind turbines. In order to clarify the lightning striking characteristics to wind turbine blades, a three-dimensional leader development model has been constructed. In the model, it is assumed that a downward leader from a thundercloud develops to a direction of the maximum electric field and if the distance between the tip of the downward leader and earthed objects or upward leaders from the earthed objects becomes less than a critical distance, which is called striking distance, the final jump occurs.

A wind turbine of which height is 116 m is considered and the charge simulation method is used to simulate its blades. Figure 1 shows the arrangement of simulated charges inside the blade, which is set on the x-z plane (y=0) and the center is set as x=0.

a)   Arrangement of the blades   b) Charge arrangement to simulate the blade
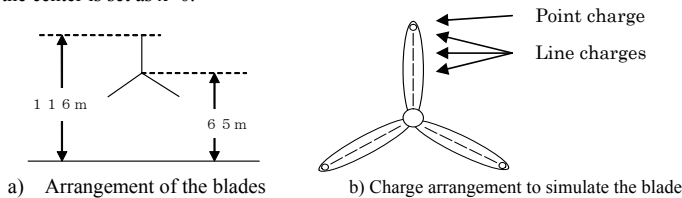
Fig. 1 Modeling of blades

Positive and negative charges of 20C in a thundercloud are set at the height of 8 km and 5 km from the ground. Downward leader is modeled by a uniform line charge and length of each step is 10 m. Furthermore, following relations are assumed.

1) Leader charge density λ (C/m) and lightning current I(kA): $\lambda = 38 \cdot I^{0.68}$

2) Striking distance Rs(m) and lightning current I(kA): Rs=6.72 $\cdot$ I$^{0.8}$

For simplicity, upward leader development from the blade is not considered in this analysis.

An example of the calculated results is shown in Fig. 2. When a downward leader starts in each region, the final striking point is determined as shown in Fig. 2. The analysis suggests that if lightning current is small, there is possibility that lightning strokes to lower blades occur.

Fig. 2 Relationship between starting point of a downward leader and the final striking point. (I=10kA)

References

1. H.R.Armstrong, E.R.Whitehead, "Field and Analytical Studies of Transmission Line Shielding", IEEE Trans. on PAS, Vol.87, pp.270-281, 1968.

2. L.Dellera, E.Garbagnati, "Lightning Stroke Simulation by means of the Leader Progression Model, Part I: Description of the Model and Evaluation of Exposure of Free-standing Structures", IEEE Trans. on Power Delivery, Vol.5, pp.2009-2022, 1990.

HPEM - 28
Lightning Characterization & Simulation (Invited)

Oral Presentations

The Impulse Coefficient of Horizontal Grounding Electrodes

S. Visacro, G. Rosado, A. L. Senna F.

LRC – Lightning Research Center – Federal University of Minas Gerais, Belo Horizonte, Brazil
E-mail: Lrc@cpdee.ufmg.br

It is known that the response of grounding electrodes to lightning current is usually quite different from the one presented to low frequency currents. This behavior comprises different aspects, being the response to impulsive currents and the ionization process the most relevant ones. This abstract presents some results of an experimental research that is specifically dedicated to evaluating the response of horizontal electrodes submitted to low intensity impulsive currents.

The response of grounding electrodes to low frequency phenomena is given by the grounding resistance R_{LF}. When impulsive currents are concerned, it is usual to consider such response by means of the transient impedance $Z(t)$, given by the ratio of the instantaneous values of the potential (developed in relation to remote earth) to the current applied to the electrode: $Z(t) = v(t)/i(t)$.

In lightning protection, the impulsive grounding impedance is frequently used to represent a simplified an objective response of grounding electrodes to lightning currents, being this impedance given by the ratio between the peaks of developed voltage and current waves: $Z_P=V_P/I_P$.

Since the measurement of Z_P is not a feasible task in most practical conditions, it is common to estimate this impedance from the measured low frequency resistance by means of the so-called impulse coefficient I_C that is given by the ratio Z_P/R_{LF}.

Two main aspects motivate developing this experimental evaluation. First, in the lightning protection community it is very disseminated the idea that the impulsive impedance is always larger than the low frequency resistance. On the other hand, the results of some works based in numerical simulation indicate that the impulse coefficient is basically equal to or larger than unity.

In order to develop this evaluation, the experimental setup represented in Fig. 1 was implanted. Horizontal electrodes (0.5 cm radius) with 3 different lengths (3, 6 and 12 m) were buried 0.5m deep in a high resistivity soil and in a low one (around 100 Ω.m and 3.5 kΩ.m). Low amplitude impulsive current waves were applied to represent the current of typical first and subsequent lightning strokes (respectively around: 3.5/60 μs and 0.5/60 μs). Typical results are indicated in Fig. 2 and the impulse coefficients I_C found from experiments are indicated in the graphic of Fig. 3. The figures are adapted from [1].
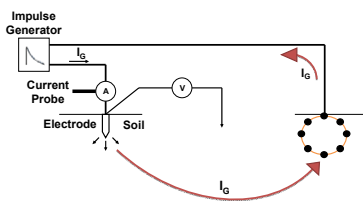
Fig. 1. Experimental setup: Impulsive current waves impressed by an impulse generator from an electrode under test to an auxiliary grid.
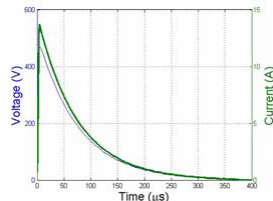
Fig. 2. The current and the developed grounding potential rise are measured using a two channel oscilloscope.
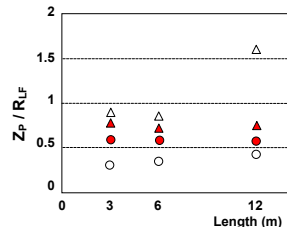
Fig. 3. Measured I_C - Triangle (high), circle (low) resistivity soil. Empty (front time T_F:~0.5 μs), in shadow (T_F:~3.5 μs).

The results presented above show some interesting features. First, all cases in the high resistivity soil show a coefficient I_C quite small, around or below 0.5. Considering the low resistivity soil and longer front time, this coefficient is around 0.7 for all electrode lengths, while for the shorter front time it is around 0.8 for length of 3 and 6 m and around 1.6 for a 12m length. This indicates that the effective length of the electrode fro a front time around 0.5 μs is significantly shorter than 12 m. Another interesting feature is that in the high resistivity soil, the coefficient I_C for waves with long front time is smaller than for short front time waves. The opposite happens in the low resistivity soil.

The final conclusion is that the ratio of the impulsive impedance to the low frequency resistance is significantly smaller than reported by results derived from numerical simulation. This leads to the recommendation of reevaluating the assumptions adopted for soil parameters, mainly the value of soil permittivity and the frequency dependence of soil parameters.

References

1. S. Visacro, G. Rosado, "Response of Grounding Electrodes to Impulsive Currents: an Experimental Evaluation", submitted to IEEE Transactions on Electromagnetic Compatibility, Aug. 2007.

Determining Voltage Source for
Lightning Return Stroke Electromagnetic Modeling

V. Javor, P. D. Rancic

Faculty of Electronic Engineering of Nis, Nis, Serbia
E-mail: vjavor@elfak.ni.ac.yu

Electromagnetic model is one of the classes of models [1-2] recently applied for determining lightning electromagnetic field of a lightning return stroke. These models can use either voltage or current source at the base of the channel. Current source is more adequate [3] for including measured or analytically defined characteristics of the channel base current [4], but most of antenna program codes commonly imply voltage source.

Determining voltage source involves a few necessary steps: implementation of Fourier transform to a time given current channel-base source, calculation of the antenna input impedance in frequency domain and obtaining adequate voltage source in frequency domain or in time domain (Fig. 1) by using inverse Fourier transform. These calculations are carried out and presented in this paper for the new proposed channel-base current function [5] and the new approximation of Sommerfeld integral [6]. As these calculations can be time consuming depending on FFT parameters choice the results for different FFT parameters are very interesting. These results are going to be presented in the full paper.
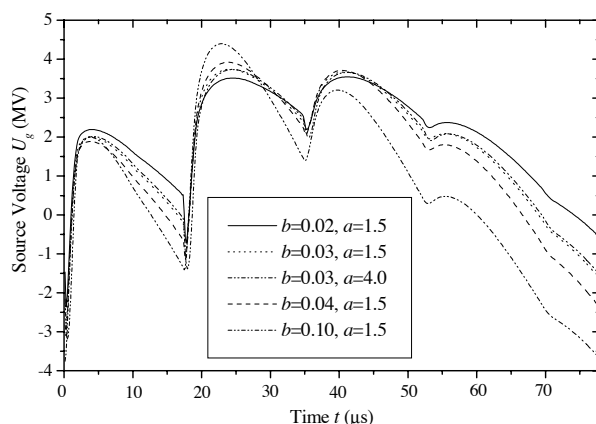
Fig. 1 - Voltage source for the lightning channel of h=2600m, a=5cm, and $Z'=0.1\,\Omega\,\mathrm{m}^{-1}$;
ground parameters $\varepsilon_{r1}=10$ and $\sigma=0.01\,\mathrm{Sm}^{-1}$; FFT of N=512 and $\Delta f=12.85\,\mathrm{kHz}$;
and parameters a and b of the channel-base current function.

References:
1. V. A. Rakov, "Review and evaluation of lightning return strokes including some aspects of their application," IEEE Trans. on EMC, vol. 40, no. 4, pp. 403-426, Nov. 1998.
2. R. Moini, B. Kordi, G. Z. Rafi, and V. A. Rakov, "A new lightning return stroke model based on antenna theory," Journal of Geophysical research, vol. 105, no. D24, pp. 29693-29702, Dec. 2000.
3. L. Grcev, F. Rachidi, and V. Rakov, "Comparison of electromagnetic models of lightning return strokes using current and voltage sources," in the Proc. of 12th Int. Conference Atmospheric Electricity, Versailles, France, pp. 593-596, 2003.
4. Y. Baba and M. Ishii, "Characteristics of electromagnetic return-stroke models," IEEE Trans. on EMC, vol. 45, no. 1, pp. 129-135, Feb. 2003.
5. V. Javor and P.D. Rancic, "Application of one suitable lightning return-stroke current model," in the Proc. of Int. Symposium on Electromagnetic Compatibility EMC Europe 2006, pp.941-946, Barcelona, Spain, September 2006.
6. V. Javor and P. D. Rancic, "Vertical monopole antenna model of the lightning discharge current: Two-image approximation of Sommerefeld's integral kernel," in the CD Proc. of 16th Conference on Computation of Electromagnetic Fields COMPUMAG 2007, Aachen, Germany, June 2007.

Use of the Five-Section CN Tower Model
in Computation of the Electric and Magnetic Field

I. K. Boev, W. Janischewskyj
University of Toronto, Toronto, Canada

E-mail: ivan.boev@utoronto.ca

As the number of special electronic devices sensitive to Electric (EF) and Magnetic fields (MF) increases, accurate modeling of the processes involved when lightning strikes a structure such as the CN Tower (CNT) is important for ensuring that the safety and electromagnetic compatibility of such devices are not compromised.

In this work, an engineering model based on the transmission line theory is developed and used to simulate a lightning strike to the tip of the CNT. The model represents the CNT as a series of Five Transmission Line (TL) sections with constant parameters and uses another TL section to model the Lightning Channel (LC). A current source producing a Heidler waveshape is assumed to inject current at the tip of the tower. This source creates two initial current waves, which have identical shapes but their amplitudes are inversely proportional to the wave impedances of the LC and the top section of the CNT. Each wave travels in opposite direction with different propagation velocities (with "v" upwards in the not yet ionized LC; with "c" downwards in the CNT). As the downward wave encounters mismatches of surge impedances at junctions of CNT sections, reflections and refractions take place. When these waves are reflected from the CNT into the now ionized portion of the channel, they travel there with "c" and are reflected and refracted at the front of the original LC wave travelling with "v". The "Lattice Diagram" is used to follow the interactions of all reflected and refracted components. These reflections and refractions influence the total current waveshape and in turn the EF and MF at a distance.

Assumptions have been made to model a strike to the CNT – a perfect ground is assumed; the LC is vertical with respect to ground and is attached to the tip of the CNT; the speed of propagation inside the CNT and inside the ionized part of the LC is "c" ($3.0*10^8$m/s); the speed of the return stroke current in the non-ionized part of the LC is equal to "v" ($1.9*10^8$m/s); the decay constant in the non-ionized part of the LC is Ψ= 2000m; the series of TL sections representing the CNT is terminated at a resistance of 21Ω to account for grounding; impedances of different CNT sections are shown in Table 1; impedance of the ionized part of the LC Z_{ch} = 300Ω; impedance of the non-ionized part of the LC Z_{tch} = 1.5*Z_{ch}; total Length of the Lightning Path (LC+CNT) = 8000m.

The described model was used to calculate the current along the tower structure and inside the lightning channel as well as the EF and MF at a distance of 2km away from the CNT. One of the strokes recorded on August 19, 2005 was used for comparison with calculated results and will be discussed during presentation.
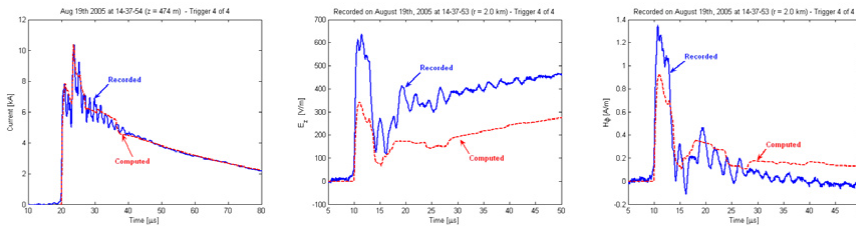
Fig. 1 – Recorded and Calculated Values for Current, E_Z, and H_Φ on August 19, 05 at 14:37:53h

Table 1 – Impedances of different CNT sections

Section	Impedance	Unit
L1, L2, L3, L4, L5	160, 105, 140, 86, 120	Ω

References
1. Ivan Boev, "Development of a Five-Section Model for Computing Lightning Current in the CN Tower", 2006, MASc Thesis, University of Toronto.
2. Farhad Rachidi et al, "Current and Electromagnetic Field Associated With Lightning – Return Strokes to Tall Towers" IEEE Transactions on Electromagnetic Compatibility, vol. 43, NO. 3, August 2001.
3. V. Shostak et al, "Return-Stroke Current Modeling of Lightning Striking a Tall Tower Accounting for Reflections within the Growing Channel and for Upward-Connecting Discharges," 11th International Conference of the International Commission on Atmosphere Electricity (ICAE'99), Huntsville, Alabama, USA, June 7-11, 1999.

Link between Lightning Activity and Temperature:
A Regional Study in Switzerland

P. Manoochehrnia[1], C. Price[2], F. Rachidi[1], M. Rubinstein[3], W. Schulz[4]
[1]*Swiss Federal Institute of Technology (EPFL), Lausanne, Switzerland*
[2]*Tel Aviv University, Tel Aviv, Israel*
[3]*University of Applied Sciences of Eastern Switzerland, Yverdon, Switzerland*
[4]*ALDIS, Vienna, Austria*
E-mail: Pooyan.Manoochehrnia@epfl.ch

Considering the importance of global warming and climate change, the problem of possible relationships between climate and lightning activity has recently attracted the attention of researchers (e.g. [1]). Positive correlations between global lightning activity and global temperature variations have been already confirmed in several studies (e.g. [1,2]) where it has been shown that a 1-degree Celsius variation in the temperature would result in an increase of lightning activity, ranging from 10% to 100% [2].

In this paper, we present a preliminary regional study of the link between temperature and lightning activity in Switzerland. Lightning statistics were obtained from the lightning database of the EUCLID (European Cooperation of Lightning Detection) network, recently presented in [3]. Any unknown time variations in the performance of the system are necessarily neglected. Data for the temperature are obtained from the terrestrial meteorology stations in the national network of the Swiss Federal Office of Meteorology and Climatology [4].

Fig. 1a presents the monthly negative cloud-to-ground flash count and the monthly mean maximum daily temperature in Switzerland for the months of August, 1999-2006, where the linear correlation factor is 75%.

A similar analysis has been done in the region of the Säntis in northeastern Switzerland, characterized by the highest lightning activity in that country. Fig. 1b shows the monthly mean of maximum daily temperature and the monthly number of the negative cloud-to-ground flashes within 100 km of the Säntis Mountain. The results show an 83% linear correlation.

(a)   (b)
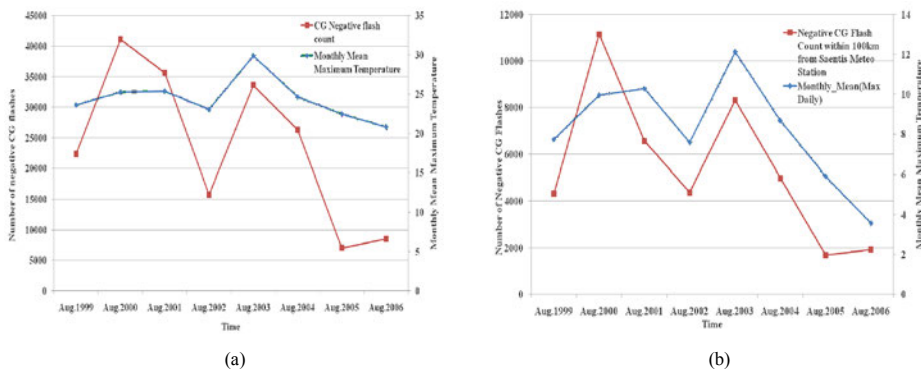
Fig. 1 –Monthly negative cloud-to-ground flash count and the monthly mean maximum temperature during the months of August, 1999 to 2006.
(a) The whole Switzerland, (b) within 100 km of the Säntis Mountain

References
1. C. Price, Global surface temperatures and the atmospheric electric circuit, Geophys. Res. Lett. 20, 1363, 1993.
2. E.R. Williams, Lightning and climate: A review, Atmospheric Research, 76, pp. 272-287, 2005
3. P. Manoochehrnia, F. Rachidi, M. Rubinstein, W. Schulz, Lightning statistics in Switzerland, 9th International Symposium on Lightning Protection, SIPDA, Foz do Iguaçu, Brazil, November 2007.
4. M. Begert, T. Schlegel, and W. Kirchhofer, Homogeneous Temperature and Precipitation Series of Switzerland from 1864 to 2000, International Journal of Climatology, vol. 25, pp. 65-80, 2005.

HPEM - 28
Lightning Characterization & Simulation (Invited)

Oral Presentations

Time Domain Dosimetry in Planar Layered Media

J. E. Page, J. Esteban

Dpto. de Electromagnetismo y Teoría de Circuitos. Universidad Politécnica de Madrid, Madrid, España

jep@etc.upm.es

The interaction of electromagnetic fields and biological tissues (in-vitro or in-vivo) is described in terms of the fields inside the tissue. The critical points of the phenomenon are the peak values of the E and H fields and the energy transferred to the tissue, which produces a temperature growing. A lot of work has been devoted to the cases of monochromatic electromagnetic fields, and some magnitudes, as the Specific Absorption Rate, are currently used as dosimetry indicators. But for arbitrary time varying fields, and in particular for short-pulse amplitude-modulated signals, the behaviour of the phenomenon is not fully understood yet. This work presents some results concerning the interaction of a pulse modulated plane wave impinging normally on a lossy layered media. This canonical problem can be used to obtain basic information about the expected peak fields and the energy transfer process in much more complex situations.

Let us consider an homogeneous plane wave propagating in z direction. For arbitrary time variation, the fields in some z constant plane are given by

$$\vec{E}(t) = \int_{-\infty}^{\infty} \vec{E}(f)\, e^{-\gamma(f)z} e^{2\pi f t}\, df \qquad \vec{H}(t) = \int_{-\infty}^{\infty} \frac{\hat{z} \times \vec{E}(f)}{\eta(f)}\, e^{-\gamma(f)z} e^{2\pi f t}\, df \tag{1}$$

where $\gamma(f) = \sqrt{-\omega^2 \mu(f)\varepsilon(f)}$ is the propagation constant and $\eta(f) = \sqrt{\mu(f)/\varepsilon(f)}$ the intrinsic impedance of the medium (the possible conduction phenomena are included in ε).

Let us consider now a plane layered structure transverse to the z axis and formed by N+1 lossy media. In the frequency domain, the field at any plane z constant in the structure can be written as

$$\vec{E}_i(z,f) = \vec{E}_{0I,i}\, e^{-\gamma_i(f)z} + \vec{E}_{0R,i}\, e^{\gamma_i(f)z} \qquad \vec{H}_i(z,f) = \frac{\hat{z}}{\eta_i(f)} \times \left[\vec{E}_{0I,i}\, e^{-\gamma_i(f)z} - \vec{E}_{0R,i}\, e^{\gamma_i(f)z} \right] \tag{2}$$

where the wave amplitudes $\vec{E}_{0I,i}$ and $\vec{E}_{0R,i}$ can be obtained in terms of the field value of the incident wave in a plane z constant of the first medium [1] using the relation

$$[E_0] = \left[M(\varepsilon_i, \mu_i, \sigma_i, d_i, f) \right] [U] E_{0I,1}\, e^{-\gamma_1(f)z_1} \tag{3}$$

were $[E_0] = (E_{0R,1}\ E_{0I,2}\ E_{0R,2}\ \text{---}\ E_{0I,N+1})^T$ and $[U] = (1\ 1\ 0\ \text{---}\ 0)^T$ and being $\left[M(\varepsilon_i, \mu_i, \sigma_i, d_i, f) \right]$ the transfer matrix of the system, of dimension $(2N)^2$

Let us consider finally the plane wave impinging on this structure. We can suppose without loss of generality that the plane where the wave data are known is used as origin of z´s. The time domain values of the fields using the expression (1) are

$$\vec{E}_i(z,t) = \int_{-\infty}^{\infty} \left[\vec{E}_{0I,i}\, e^{-\gamma_i(f)z} + \vec{E}_{0R,i}\, e^{\gamma_i(f)z} \right] e^{2\pi f t}\, df \qquad \vec{H}_i(z,t) = \int_{-\infty}^{\infty} \frac{1}{\eta_i(f)} \hat{z} \times \left[\vec{E}_{0I,i}\, e^{-\gamma_i(f)z} - \vec{E}_{0R,i}\, e^{\gamma_i(f)z} \right] e^{2\pi f t}\, df \tag{4}$$

and from this values we can calculate the peak value of the fields at any z plane. Some results for typical biological tissues will be presented during the conference.

A different issue is the one concerning to the distribution of the energy transferred to the media. Energy balance obeys the well known Poynting-Heaviside relation

$$-\vec{j}(z,t) \cdot \vec{E}(z,t) = \nabla \cdot \vec{E}(z,t) \times \vec{H}(z,t) + \vec{E}(z,t) \cdot \frac{\partial \vec{D}(z,t)}{\partial z} + \vec{H}(z,t) \cdot \frac{\partial \vec{B}(z,t)}{\partial z} \tag{5}$$

but there is not a simple way to establish the value of energy transferred to the material [2], so concepts as instantaneous Specific Absorption and Specific Absorption Rate have to be used with extreme care. Some discussion will be introduced during the presentation.

References
1.   R. E. Collin, Field Theory of Guided Waves. New York: McGraw-Hill, 1960.
2.   L. Landau, E. Lifchitz, Électrodinamique des Milieux Continus. Moscú: Mir, 1969.

Thermal Effects in Brain Slices Exposed to Radiofrequency Fields

N.C.D, Mifsud, I.R. Scott, A.C. Green, J.E.H Tattersall
Biomedical Sciences Department, Dstl Porton Down, Salisbury, SP4 0JQ, UK

E-mail: JTattersall@dstl.gov.uk

Previous studies have suggested that *in vitro* exposure to 700MHz radiofrequency (RF) fields at tissue specific absorption rates (SARs) up to 4.5mW.kg^{-1} can affect both evoked and spontaneous electrical activity in rat hippocampal slices [1]. More recent experiments have found that exposure to 380MHz RF fields at a tissue SAR of 400mW.kg^{-1} rapidly and irreversibly abolishes electrical activity in slices, apparently due to localised heating produced by the interaction of the RF field with the recording and stimulating electrodes [2]. The aim of this study was to determine whether smaller localised temperature rises could be responsible for the effects reported at much lower field intensities by Tattersall et al [1].

Extracellular field potential responses were recorded in hippocampal slices prepared from adult rats. The slices were exposed to RF fields in a new parallel plate exposure system [3], in which the E-field component was parallel to the slice. This produced better coupling of the field into the tissue than the older system used in [1] and thus required a lower field intensity to produce a given tissue SAR. This orientation of the E-field also reduced coupling of the RF into the stimulating and recording electrodes [2]. To determine the effect of localised heating on field potential responses, miniature resistive heating elements were constructed from 25µm diameter Teflon®-coated Pt/Ir wire supported by a 1.5mm diameter glass capillary. These were placed within 100µm of the recording or stimulating electrode and heated by constant electric currents passed through the wires. The heating elements were calibrated using an infrared camera (Jade, Cedip Infrared Systems).

In the system used in [1], exposure to 700MHz RF at a field intensity to produce a tissue SAR of 4.5mW.kg^{-1} resulted in changes in the population spike amplitude similar to those previously reported. In contrast, exposure in the new system with the same input power, which produced a higher tissue SAR of 29mW.kg^{-1}, had no effect on the population spike amplitude (Figure). Measurements with the infrared camera confirmed there was no detectable electrode heating in the new system at this SAR. Heating produced by the resistive elements near the recording or stimulating electrodes produced changes in the field potential which were similar to those seen during RF exposure in the older system.

The results indicate that the effects reported by Tattersall et al [1] may be explained by localised heating produced by interaction of the RF fields with the recording and stimulating electrodes.
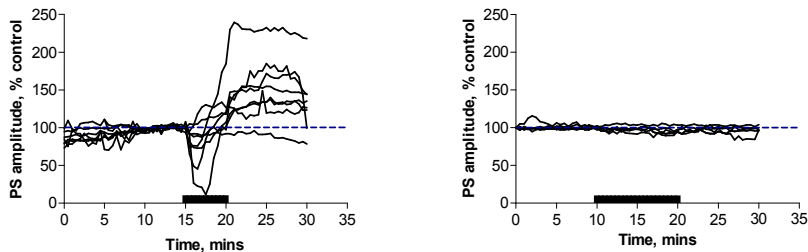
Fig 1 - Effect of exposure to 700MHz RF field (solid bar) on population spike amplitude in the older system (left, 4.5mW.kg^{-1}) and the new system (right, 29mW.kg^{-1})

References
1.   J.E.H. Tattersall, I.R. Scott, S.J. Wood, J.J. Nettell, M.K. Bevir, Z. Wang, N.P. Somasiri, and X. Chen. Effects of low intensity radiofrequency electromagnetic fields on electrical activity in rat hippocampal slices. Brain Res. Vol. 904, 43-53, 2001.
2.   A.C. Green, B. Truscott, N.C.D. Mifsud, Y. Alfadhl, X. Chen, and J.E.H. Tattersall. Thermal imaging and modelling of microelectrodes in a radiofrequency field. Bioelectromagnetics Soc. Abstr. Vol. 27, 305-306, 2005.
3.   R.I. Grose, R.G. Montague, A.C. Green, N.C.D. Mifsud, Y. Alfadhl, X. Chen, and J.E.H. Tattersall. A new transmission line system for exposure of brain slices to RF fields. Bioelectromagnetics Soc. Abstr., vol. 27, 319-320, 2005.

HPEM - 29
Biological Effects and Medical Applications (Invited)

Oral Presentations

Vascular Structure Construction in Human Model for Consideration of Blood Flow in Heat Exchange during EM Exposure

D. Kakulia[1], L. Manukyan[1], M Prishvin[1], V. Jeladze[1], R. Zaridze[1*], Bit-Babik[2], A. Faraone[2]

[1]*Department of Physics, Tbilisi State University, Laboratory of Applied Electrodynamics, Tbilisi, Georgia*
Corporate EME Research Laboratory, Motorola, Inc., Fort Lauderdale, FL, USA
rzaridze@laetsu.org

The goal of our study is to advance the method of complex thermal modeling based on detailed vascular structure implementation in the FDTD EM-Thermal simulation software [1]. The emphasis in this work is on the development of software tool capable of generating relatively complex vasculature based on both the available known geometries of human organs and the possibility of manual definition of particular vascular segments. The important steps are to build the vascular network for a human eye model which conforms with the existing human head geometry and mesh, define the data format to store the information on generated vascular structure including the coordinates, diameter, type (vain or artery) and tree structure in the vascular network. In the past several months we have implementing the algorithm for reconstruction and regeneration of vascular structure, based on the Discrete Vasculature (DIVA) algorithm, suggested by Van Leeuewen et al., [2]. We have described our implementation of this algorithm and results obtained from its application to several human organs (e.g., eye and liver) [1]. We further investigated the algorithm capabilities and developed the methodology to consider the detailed vascular structure in thermal calculations, particularly, modifying the bio-heat equation and computing blood flow vector in each voxel tissue. In addition, we are developing a new and more flexible methods for constructing the tissue vasculature. One of those alternative approaches is described in the paper. To solve the bio-heat equation first we need to generate the vascular structure with sufficient details and then based on vessels diameters and estimated blood velocity in capillaries compute the blood velocity vector in each cell of the discrete FDTD model. The new algorithm of constricting the vascular structure and blood velocity vector distribution in the tissue considering the blood flow conservation law has been developed.

In our algorithm the simulation domain is described by set of points on its boundary. The vessel construction starts from several root points, i.e., the points where arteries are allowed to enter the domain, also taking into consideration the existing vessels as input parameters. The construction further progresses from the root points advancing the vessels within the tissue and branching them recursively, so that branches of the same depth grow simultaneously. The direction of each particular vessel and its branching is controlled by the potential field. This vector field is
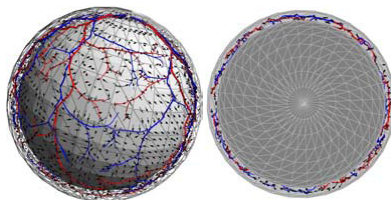
Fig1. Vasculature and velocity vector distribution

defined in each point of the simulation domain and represent the superposition of random smooth gradient fields created by the end points of already constructed vessels as well as domain boundary. Each boundary point and each point of the already generated vessel creates repulsive vector field within certain range of action around itself. At every step, the still empty areas (which eventually should contain the vessels end points), correspondingly, create attractive force. When constructing vascular structure we distribute the end points of arterial and venous networks uniformly in the tissue, with density sufficient to represent the main vascular structure of the relatively large vessels and the end points of venous network are displaced relative to the arterial ones. At the end the portion of the domain will remain without any vessel or end point. To account for blood perfusion in remaining vessels during thermal modeling the blood velocity vector in the tissue area is approximated by specific model which takes into account the conservation law of blood flow. The effective force, i.e., the force that moves blood in the capillaries is caused by pressure difference at end points of arteries and veins (high-arterial and low-venous cordial pressures). If we assume that in the tissue blood flows does not change with time, then blood velocity in each point is proportional to the effective force which can be determined based on defined pressure at each end point and assuming that it changes inversely with distance. According to this algorithm the blood velocity vector field can be built in the entire simulation domain, with fulfillment of blood flow continuity. The example blood velocity distribution based on this work is presented on Fig 1.

References:
1. L. Manukyan, D. Mazmanov, V. Labadze, D. Kakulia, R. Zaridze. Toolkit for regeneration of vascular structure for precise numerical study of thermal processes in electromagnetic human exposure and its implementation in FDTDLab. Direct and Inverse Problems of Electromagnetic and Acoustic Wave Theory, September 17-20, 2007, Tbilisi, Georgia. pp. 113-117.
2. Van Leeuwen G.M.J., Kotte A.N.T.J. and Lagendijk J.J.W. "A Flexible Algorithm for Construction of 3-D Vessel Networks for Use in Thermal Modeling" *IEEE Transactions on Biomedical Engineering*, vol. 45, no. 5, 1998, pp. 596-604.

SAR Calculations for Pregnant Woman with her Fetus and Placenta in Various Positions Exposed to EM Waves from Wireless Terminal

S. AKIMOTO[1], T. NAGAOKA[2], S. KIKUCHI[1], K. SAITO[1], S. WATANABE[2], M. TAKAHASHI[1], K. ITO[1]

[1]*Chiba University, Chiba, Japan*
[2]*National Institute of Information and Communications Technology, Tokyo, Japan*
E-mail: s.akimoto@graduate.chiba-u.jp

Radio frequency (RF) devices in the vicinity of the human body are increasing; therefore, evaluating the specific absorption rate (SAR) of fetuses in pregnant woman has become an important research topic. For example, when a commercial wireless terminal is used in the vicinity of the abdomen of a pregnant woman, the electromagnetic (EM) waves from the device penetrate her body and the fetus. This is because the wavelength of the EM waves of the device operating in VHF band are longer than those of a cellular phone operating in the GHz band. To evaluate the SAR of a pregnant woman and her fetus when the pregnant woman is wearing a wireless terminal on her abdomen, we used as a numerical model a 26th-gestational-week pregnant Japanese woman [1] being exposed to the near-field of a normal mode helical antenna (NHA) with a metallic case at 150 MHz [2]. In this numerical model, the fetus was positioned in the left occiput anterior (LOA) of the model's pelvis, i.e., the fetal occiput was directed toward the model's left anterior side. However, fetal presentation varies frequently at this stage of pregnancy and the placenta forms at various locations on the uterine wall. Therefore, we calculated the SARs of a fetus exposed to EM waves from an NHA with a metallic case using several pregnant-woman models with each model representing a different position of the fetus and placenta. Figure 1 shows four different pregnant-woman models (only abdomen shown): Model 1, LOA fetal presentation and anterior placenta; Model 2, LOA fetal presentation and posterior placenta; Model 3, right sacro anterior (RSA) fetal presentation and anterior placenta; and Model 4, RSA fetal presentation and anterior placenta. The SAR was calculated using the finite difference time domain (FDTD) method. The distances between the antenna and the surface of each model were kept at 40.0 mm in order to create a realistic situation. In addition, the position of each feeding point is the same height in the center of each fetal head.
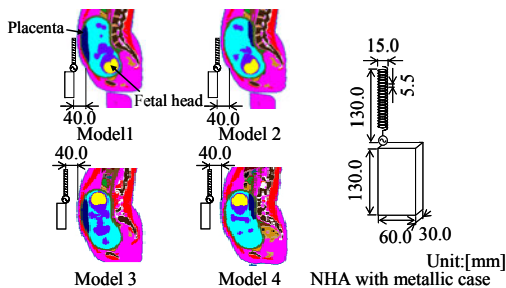
Fig. 1 – Calculation model
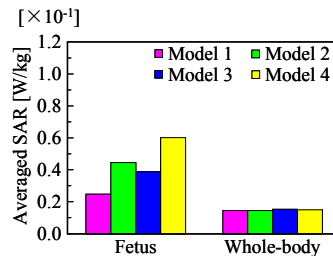
Fig. 2 – Averaged SAR

Figure2 shows the fetus-averaged SARs and the whole-body-averaged SARs for the four pregnant-woman models. Here, the radiated power of the antenna is normalized to 1 W. The whole-body-averaged SARs for these models agree well with each other (approximately 0.015 W/kg). This result demonstrated that the positions of the fetus and the placenta have no effect on whole-body-averaged SAR. For the fetus-averaged SAR, the values of Models 2 and 4 (when the placenta is in the anterior) are higher than those of Models 1 and 3 (when the placenta is in the posterior). This result confirmed that the EM energy from the NHA is attenuated by the placenta. In addition, the fetus-averaged SARs of Models 3 and 4 (when the fetus head is in the superior) are higher than those of Models 1 and 2 (when the fetus head is in the inferior). The distance between the antenna feeding point and the fetal body surface of Models 3 and 4 is approximately 40 mm shorter than that of Models 1 and 2. This result suggests that the fetus-averaged SAR depends on the distance between the feeding point and the fetus.

References

1.   T. Nagaoka *et al*., Phys. Med. Biol., vol.52, pp.6731–6745, 2007.
2.   S. Akimoto *et al*., The 2007 IEICE Society Conference, Japan, p.291, Sep. 2007.

HPEM - 30
Transmission Lines at Low and High Frequencies: Theory,
Numerical and Experiments. Part 1: Analytical Approaches (Invited)

Oral Presentations

Representation and Product Integration of 2 x 2 Matrices

Carl E. Baum
University of New Mexico
Department of Electrical and Computer Engineering
Albuquerque New Mexico 87131
E-mail: cebaum@ece.unm.edu

A previous paper [C.E. Baum, "The Combined Field in Quaternion Form," Physics Note 13, 2003] has considered the decomposition of 2 x 2 matrices using the four quaternion units. This gives a convenient way to represent such matrices for product integration, as we shall see. Such matrices are also useful for casting a second-order linear differential equation as a first-order vector/matrix differential equation, the solution of which is representable (and calculable) by a product integral.

The properties of the product integral can then be explored to understand the possible solutions of second-order linear differential equations. Only in special cases can the solution of the product integral be expressed in terms of one or a few of the usual sum (Riemann) integrals. In effect, this gives conditions on the "sum integrability" of such equations. As a special case we consider the solution of the telegrapher equations for a single-conductor (plus reference) transmission line.

A previous paper [C.E. Baum, "Construction of 2x2 Product Integrals from Solutions of Second Order Linear Ordinary Differential Equations," Mathematics Note 96, 2004] shows how product integrals of 2 x 2 matrices can be constructed in special cases. Basically one can take known solutions of second-order linear differential equations and manipulate them into product-integral form, obtaining functions such as Bessel functions in the solutions. Such cases are found in the solutions for nonuniform transmission lines (impedance and admittance per-unit-length matrices varying along the line). One should not expect that, in general, such known solutions should be found in the form of Riemann (sum) integrals over the transmission-line parameters.

This paper considers the product integration of 2 x 2 matrices by using the quaternion decomposition of such matrices. This gives conditions for the solution in terms of sum integrals. This is applied to the solution of second-order linear differential equations, including the telegrapher equations. The product integral, together with quaternion decomposition, of 2 x 2 matrices gives us some insight into the solution of second-order linear differential equations. In particular this shows when solutions can be expressed in terms of one or a few sum integrals. This in turn applies to the solution of the telegrapher equations for transmission lines.

Analytic Methods for Coupling to Cables with Large Numbers of Component Wires

J. L. Gilbert

Metatech Corporation, Goleta, USA

...
quantum_mechanic@alum.mit.edu

In this presentation, we discuss an analytic method for calculating coupling to the wires in a cable containing a large number of individual wires. We first examine the situation where the wire insulator thickness is small compared to the wire radius, so that the capacitance matrix is dominated by nearest neighbor interactions. In this case, it can be shown that the capacitance matrix is proportional to the transverse Laplacian operator

$$C = -6b^2 C_{od} \nabla_\perp^2 \tag{1}$$

where C_{od} is the capacitance per unit length between nearest neighbor wires in a hexagonal array, and $2b$ is the spacing between nearest neighbor wires. The equation for forward propagating modes along the line is, ignoring backwards propagating modes,

$$\frac{\partial F}{\partial z} = 3vb^2 RC_{od} \nabla_\perp^2 F \tag{2}$$

where R is the resistance of an individual line, v is the propagation velocity in the dielectric (which is assumed to be uniform) and $F=I+vQ$, where I is the wire current and Q is the charge per unit length on the wire. This is a simple parabolic diffusion equation and easily solvable for many geometric configurations of interest. It can be used to calculate how an incident electric field diffuses into the interior of the cable bundle as well as used to calculate the impedance looking back into a single line or group of lines.

We will give examples of the use of this technique as well as modifications to the technique to include situations where the wires further away than the nearest neighbors contribute substantially to the capacitance matrix. We will also show numerical examples of the calculation of the capacitance matrix including non-nearest neighbors by successive over-relaxation and compare them to the asymptotic form that results when small wire diameters are assumed.

Oral Presentations

Comments on the Excitation of a Shielded Multiconductor Cable

Frederick M. Tesche

Clemson University, Clemson, SC USA

...
E-mail: Fred@Tesche.com

The coupling of electromagnetic fields to shielded cables has been discussed in a variety of references, including [1, 2, 3, and 4]. Virtually all of the models assume that the cable shield is nearly perfect, with the result that the internal voltage and current inside the shielded cable are assumed to have no influence on the current and charge on the outside of the shield. Under this "good shielding approximation", the internal conductor of the cable is found to be excited by the external current and charge through the transfer impedance and admittance (or an alternate charge coupling parameter) of the cable shield.

In most of the past applications of these shielding models, the shield is assumed to have a right circular cylinder geometry, and a single inner conductor is coaxially located within the shield. This geometry provides simple expressions for the cable shield transfer parameters. It is possible, however, that some cables might not be coaxial, and there may also be more than one internal conductor within the shield. For these more complex cables, a question arises as to how to model the internal excitation of the cable. This is the subject of the present paper.

In this paper, the commonly-accepted Vance cable shielding model for a coaxial cable is first summarized. Then, some early work by Latham [5 and 6] is described, in which a model for the shielding of an offset conductor inside a braid shield is developed. Finally, this work of Latham is applied to the case of a shielded multiconductor cable, which is shown in Figure 1.
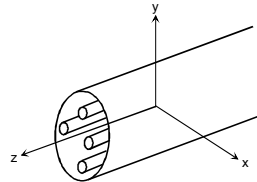
Fig. 1 – Illustration of a shielded multiconductor cable.

For the shielded multiconductor line, it is determined that the per-unit-length voltage source vector $\bar{V}'_s(z)$ is *independent* of the internal wire position and depends only on the shield transfer impedance parameters Z'_d and M'_d and the external shield current I_s. For the per-unit-length current source vector $\bar{I}'_s(z)$, it turns out that this source *does* depend on the multiconductor wire location within the shield through the per-unit-length capacitance matrix $\bar{\bar{C}}'$. This current source vector depends on the external shield charge Q′s and the charge transfer properties of the shield. Equation (1) summarizes these results.

$$\bar{V}'_s(z) = \begin{bmatrix} 1 \\ 1 \\ \vdots \\ 1 \end{bmatrix} \left(Z'_d + j\omega M'_t \right) I_s(z) \quad \text{and} \quad \bar{I}'_s(z) = -j\omega\bar{\bar{C}}' \begin{bmatrix} 1 \\ 1 \\ \vdots \\ 1 \end{bmatrix} \frac{1}{\varepsilon} \frac{\alpha_e \upsilon}{(2\pi b)^2} Q'_s(z) \qquad (1)$$

References
1. Vance, E. F., **Coupling to Shielded Cables**, Krieger Publishing, 1987.
2. Tesche, F. M., M. Ianoz and T. Karlsson **EMC Analysis Methods and Computational Models**, John Wiley and Sons, New York, 1996.
3. Degauque, P. and J. Hamelin, **Compatibilité Electromagnétique**, Dunod, Paris, 1990.
4. Hoeft, L. O., and J. S. Hostra, "Measured Electromagnetic Shielding Performance of Commonly-Used Cables and Connectors", *IEEE Trans. EMC*, vol. 30, No. 3, Aug. 1988, pp. 260-275.
5. Latham, R. W., "An Approach to Certain Cable Shielding Calculations", *Interaction Notes*, Note 90, January 1972.
6. Latham, R. W., "Small Holes in Cable Shields", *Interaction Notes*, Note 118, September 1972.

High-frequency Analysis of Radiated Emission from PCB Microstrips Through a Full-wave Transmission Line Model

A. G. Chiariello[1], A.Maffucci[2], G. Miano[1], F.Villone[2]

[1]*DIEL, Università di Napoli "Federico II", Napoli, Italy*
[2]*DAEIMI, Università di Cassino, Cassino (FR), Italy.*

E-mail: maffucci@unicas.it

In modern high-speed printed circuit boards (PCB) a relevant source of unwanted radiated emission is given by any signal trace routed on the outer layers. This paper addresses the problem of evaluating the far-field emissions from a PCB microstrip in high frequency ranges. From a theoretical point of view the electrical field emitted by a current distribution $\mathbf{J}_s(\mathbf{r}')$ over the surface S of the microstrip traces is given by:

$$E(\mathbf{r}) = \iint_S G(\mathbf{r},\mathbf{r}') \cdot \mathbf{J}_s(\mathbf{r}') dS , \qquad (1)$$

where G is the Green function, which should include in this case the effects of the dielectric slab and the reference plane. To solve (1) the proper current distributions along the traces is needed. For the past PCB generations this problem has been deeply studied and many practical indications have been provided to the designers [1]. For those generations the trace lengths were electrically short and very simple formulas could be derived from (1), providing upper bounds for the emissions due to the differential mode (DM) and common mode (CM) currents [2]. With increasing frequency, electrically long traces had to be considered and hence the transmission line (TL) model had been used to evaluate the current distribution [3]. Nowadays typical dimensions of trace widths and dielectric thickness are below 1 mm, hence the TL model is adequate up to some GHz. The next PCB generation foresees a further increase of frequency, leading to the need for a full-wave analysis, whose drawbacks are the high computational cost and the low qualitative insight on the solution.

In this paper we use the enhanced transmission line (ETL) model proposed in [4-5] to describe the full-wave distribution of DM and CM currents along a coupled microstrip. This model extends the validity limits of the standard TL model (STL) to higher frequencies and allows performing qualitative analysis on the solution. Preliminary results have been obtained with reference to a 50 mm-long coupled microstrip in homogeneous dielectric, with trace spacing of 2.5 mm. Figs.1a and 1b show the radiation diagram along the directions of maximum emission at 1m, computed at 1.7 and 2.5 GHz respectively. The case refers to a line fed at one end with a DM current of 1mA, with the far end open. The ETL results show an excellent agreement with the full-wave solution, whereas for high frequency the STL solution is clearly inadequate.
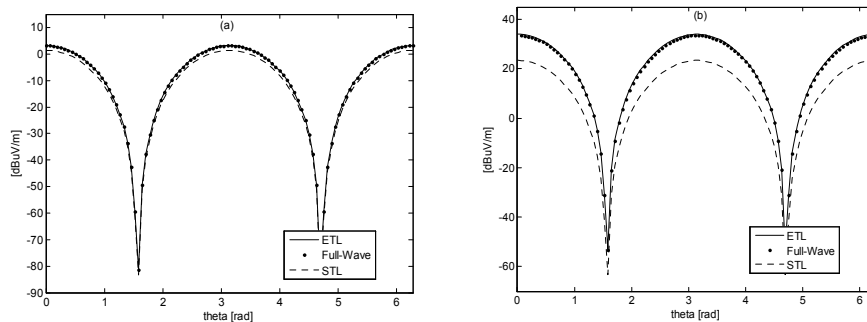
Figure 1: Radiation diagrams for emission of DM currents of a microstrip at 1.7 GHZ (a) and 2.5 GHz (b).

References
1.   L.B. Gravelle and P.F.Wilson, "EMI/EMC in printed circuit boards – A literature review", IEEE Transactions on Electromagnetic Compatibility, vol. 34, pp.109-116, 1992.
2.   C. R. Paul, "A Comparison of the Contributions of Common-Mode Currents and Differential-Mode currents in Radiated Emissions", IEEE Transactions on Electromagnetic Compatibility, Volume 31, Issue 2, pp.189 – 193, 1989.
3.   M.Leone, "Closed-form Expressions for the Electromagnetic Radiation of Microstrip Signal Traces", IEEE Transactions on Electromagnetic Compatibility, vol. 49, pp.322-328, 2007.
4.   A. Maffucci, G. Miano, F. Villone, *"*An Enhanced Transmission Line Model for Conductors with Arbitrary Cross-Sections", IEEE Transactions on Advanced Packaging, Vol.28, n.2, pp.174-188, May 2005.
5.   A. G. Chiariello, A. Maffucci, G. Miano, F. Villone, W. Zamboni, "A Transmission-line Model for Full-wave Analysis of Mixed-mode Propagation", in press on *IEEE Transactions on Advanced Packaging.*

Oral Presentations

Test Facilities of KhIPT to Study Objects Exposed to Ultra-Short Pulse Electromagnetics

I. I. Magda

National Science Center "Kharkov Institute of Physics and Technology NAS Ukraine;
1 Academicheskaya Str., Kharkov 61108, Ukraine; magda@kipt.kharkov.ua

Stands of NSC KhIPT are intended for testing the radio- and electronic equipment and components to impact of ultra-short pulses (USP) of microwaves with narrowband (NB) and ultra-wideband (UWB) frequency ranges.

MW NB stands TF-1, TF-2, TF-3, and TF-4 integrate half-open anechoic chamber (AC) and high-power MW source of ns/us pulse duration based on high-current relativistic electron beam (REB) coupling to various electrodynamic structures: vircator/virtode, BWO, ubitron, magnetron. Stands TF-3 and TF-4 use REB accelerators with the energy supply up to 40 kJ. Except HPM these facilities are capable to generate intense X-rays with the energy of several hundreds keV.

MW UWB stands TF-1M, TF-5, TF-6, and TF-7 are designed for USP tests. TF-1M and TF-6 matched to transmission lines provide operation in video-pulse mode, while TF-5 and TF-7 loaded to UBW antennas create an emissive EMI. TF-5 test facility incorporates TEM-cell designed as a 4 m nonuniform strip-line with the impedance of ~77 Ohm, operational area volume of ~1 m^3, and E-field strength of 1-190 kV/m. The emissive stand TF-7 is used for polygon tests. It consists of a pulse-power source (~1.6 GW, 70-75 Ohm) coupled to a half-circular parabolic reflector (R=0.9 m) IRA that is induced by two nonuniform conical/cylindrical lines. The FOM of the IRA exceeds 1.2 GW, and E-field strength at 10 m distance is as high as 120 kV/m.

Test facilities are equipped with the electric and optic transmission lines, probes and UWB oscilloscopes to register the parameters of EMI and test objects. Designed methods and infrastructure of test facilities provide studying the response of digital and analog electronics and components exposed to single-pulse and repetitive HPEM.

Test facilities generating NB and UWB microwaves and video pulses. [*] under reconstruction

Title (Type) Start Date	Frequency, GHz	Impulse Power, MW	Pulse Width, ns	Pulse Rise Time, ns	E-field Strength, κV/cm	Operation Area, m^3	Operation Mode
TF-1 (NB MW) 1986	3-10 (38*)	100-500 (10*)	20-30	5-6	0.2-15 (~0,2*)	~ 1 half-open AC	single pulse
TF-2 (NB MW) 1986	3-10	6-10	200-600	20-150	0.1-1.0	~ 1 half-open AC	single pulse
TF-3 (NB MW) 1991[*]	2.5-40	50-2000	30-50	5-6	0.2-30	~ 3 half-open AC	single pulse
TF-4 (NB MW) 1991[*]	2.5-40	0.3-10	600-1000	50-150	0.2-1.0	~ 3 half-open AC	single pulse
TF-1M (UWB VP) 1989	0.02-0.4	3000	10-40	2-6	0.4 – 2.5	0.3 coaxial line	single pulse
TF-5 (UWB MW) 1993	0.15-1.2	6	~1	0.3-0.5	0.03-0.4	~ 1 laboratory hall	single pulse / periodic 100Hz
TF-6 (UWB VP) 2005	0.08-2	210	1-5	0.2-0.25	0.01-2	0.7-1.2 strip line	single pulse / periodic 100Hz
TF-7 (UWB MW) 2006	0.15-3	1600	0.7-1.5	0.1-0.3	0.01-10	polygon	single pulse / periodic 1 Hz

Designs and Analyses of Some Cylindrical CPW Discontinuities

[1]**Volkan Akan,** [2]**Mehmet Duyar,** [3]**Erdem Yazgan, and** [4]**Mehmet Bayrak**

[1]*Senior Researcher, TUBITAK Space Technologies Research Institute, Ankara, TURKIYE*
[2]*Dr., Nigde Industry and Trade Governer Department , Nigde, TURKIYE*
[3]*Prof. Dr.,Department of Electrical and Electronics Eng., Hacettepe University, Ankara, TURKIYE,*
[4]*Prof. Dr., Department of Electrical and Electronics Eng., Selcuk University, Konya, TURKIYE,*

E-mail: volkan.akan@uzay.tubitak.gov.tr

In this article, designs and analyses of several CCPW (Cylindrical CPW) discontinuities as microwave reactive elements have been realized. The quasi-TEM characteristic parameters of CCPWs have been obtained by CMT (Conformal Mapping Techniques) which provide satisfactory accuracy at microwave frequencies and lead to closed-form analytical solutions suitable for CAD software packages. Designed discontinuities then simulated in CST Microwave Studio 2006B. The obtained results have been demonstrated as inductance, capacitance and also input impedance versus frequency and physical dimensions of the elements. The results show that CCPW discontinuities can be used successfully as passive elements for related applications.

In Fig.1, cross sectional view of the transmission line used to form CCPW discontinuities are seen with defined physical parameters.
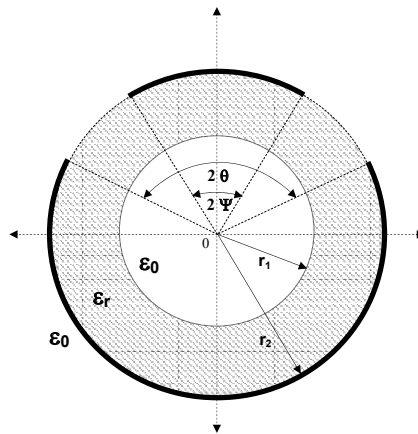
Fig. 1 – Cross-sectional view of CCPW for construction of related discontinuities.

Briefly, in this article it is shown that microwave reactive elements can be realized on CCPW type transmission lines. For the time being the experimental studies on these elements are going on and as future work they will be used for matching and feeding cylindrical type antennas.

References

1. N. Dib and A. Omar, "Dispersion analysis of multilayer cylindrical transmission lines containing magnetized ferrite substrates," IEEE Trans. Microwave Tech., vol. 50, No.7, pp.1730-1736, July 2002.
2. M. Duyar, V. Akan, E. Yazgan and M. Bayrak, "Analyses of Elliptical Coplanar Coupled Waveguides and Coplanar Coupled Waveguides with Finite Ground Width," IEEE Trans. Microwave Tech., vol. 54, No.4, pp.1388-1395, June 2006.
3. V. Akan and E. Yazgan, "Quasistatic TEM Characteristics of Multilayer Elliptical and Cylindrical Coplanar Waveguides", Microwave Opt. Tech. Lett., Vol. 42, No.4 pp.317-322., Aug. 2004.
4. E. Yazgan and V. Akan, "Conformal Mapping Techniques", Encyclopedia of Rf and Microwave Engineering, Vol. 1, John Wiley & Sons, 2005.

HPEM - 31
Simulators & Simulation Techniques

Oral Presentations

Modeling of a Current Transformer for Electromagnetic Transient Simulation in a Power Station

A. Ametani[1], N. Nagaoka[1], S. Tasaki[1], K. Nishimura[1], S. Okaba[2]

[1]*Doshisha University, Kyoto 610-0321, Japan*
[2]*Tokyo Electric Power Co., Yokohama 230-8510, Japan.*
E-mail: aametani@mail.doshisha.ac.jp

A number of mechanical and electronic (analog) elements in control circuits in generator stations and substations have been and are being replaced by digital elements. Since those digital elements are far more sensitive and fragile to an electromagnetic environment than the analog ones, the electromagnetic immunity (EMI) becomes more significant. In fact, a few disturbances and failures of control equipments have been experienced in generator stations and substations in Japan.

Japanese Electrotechnical Research Association has carried out overall and very deep investigations of disturbances and failure experiences, the mechanisms of the disturbances and failures, the strength of control equipments against the disturbances and the countermeasures in field which were collected from ten utilities in Japan for about 10 years to the year of 2001. It is found in the investigation that one of the dominant causes of electromagnetic disturbances against control circuits in a gas-insulated substation (GIS) is a swicthing surge due to a disconnector (occasionally a circuit breaker) operation. Because of a complex combination of short gas-insulated buses and lines in the GIS, multiple reflection and refraction of traveling waves at the boundaries of the buses and the lines generate a high frequency surge, which invades via a voltage tansformer (VT, CVT) and a current transformer (CT) into a low-voltage control circuit and results in malfunction and occasionally insulation failure of the digital elements of the control.

In a voltage-frequency characteristic of switching surges at CT secondary circuits measured in 15 different gas-insulated substations in Japan, it is observed that the frequency of the switching surges ranges from 2MHz to 80MHz and the peak-to-peak voltage from 10V to 600V. It is distinctive that no frequency component from 20MHz up to 40MHz is observed. Thus, there exist average values of the frequency, about 10MHz and 60MHz. Also, the peak-to-peak voltage is generator in the CT than in a VT, and transfer voltages via the CT result in more disturbances than those via the VT.

The disturbances due to switching surges are often malfunction and freeze of a digital circuit and are recovered by reset of the circuit. Thus, it is very hard to repeat the disturbances and find the cause. For this, a numerical simulation of a transient is very powerful. A simulation model of a VT has been established. However, there exists no useful CT model.

This paper has developed a model circuit of a CT for a transient simulation based on experiments of transient characteristics if various CTs. A transient response of the CT secondary circuit is measured, and its frequency response is numerically evaluated by Fourier transform. From the frequency response, a CT model similar to that of a Rogoski coil is synthesized. A transient simulation is carried out by the EMTP using the developed CT model, and the simulation results are compared with the measured results to investigate the accuracy of the CT model.

References

1.   G. Murtaza Hashmi and Matti Lehtonen, Modeling of Rogowski Coil for On-line PD Monitoring in Covered-Conductor Overhead Distribution Networks, Helsinki University of Technology (TKK), 2006.

Revitalization Report and Roadmap for the United State's Department of the Navy's Full-Scale Electromagnetic Pulse Test Facility.

K. Sebacher, C.Miller, A. Mazuc

United States Navy, Lexington Park, Maryland, United States

Kurt.Sebacher@Navy.Mil

The United State's Navy's premier aircraft Test and Evaluation facility at Patuxent River, Maryland, operates the U.S. DoD's sole remaining large-scale Electromagnetic Pulse (EMP) test stimulator This system tests aircraft and other systems up to and including Boeing 747 size aircraft. This EMP simulator test facility was recently extensively upgraded to meet the requirements of United States Military Standards, specifically MIL-STD-464A and MIL-STD-2169B. The upgrades include a complete reconstruction of the existing 5.9 Megavolt Horizontally Polarized Dipole (HPD) source, the integration of a new source simulator into the current Vertically Polarized Dipole (VPD) antenna, and the addition of a bounded wave antenna array that takes advantage of the same source. The HPD upgrades included re-engineering the MARX output switch technology, a change from an air to an oil-isolation system, rebuilding MARX stacks, changes to output peaker capacitors, changes to internal MARX stage interconnections and new rigging for the HPD antenna support structure. The VPD system incorporated the Defense Threat Reduction Agency (DTRA) Fast Electromagnetic Pulse Simulator (FEMPS), which required significant modifications to the transfer switch and transfer switch peaker capacitors and increasing the charging capacitors to meet specification requirements. This new VPD system can be de-convolved with a newly installed bounded wave antenna design. The development of a new instrumentation system that can adequately capture the high frequency components will also be discussed. The new instrumentation system with an expanded bandwidth of 1.4 GHz was the result of collaboration between U.S. Government, U.S. Industry and European Industry. This paper will present data taken from test firings from before and after the upgrades, and include frank discussions of the issues encountered. Planned future upgrades and the overall facility roadmap will be presented, along with discussion concerning the choices made. The paper will conclude with the UNCLASSIFIED results of a comprehensive facility characterization performed by the Defense Threat Reduction Agency on the newly upgraded system.

HPEM - 31
Simulators & Simulation Techniques

Oral Presentations

Characteristics of Combined Inductive-Capacitive Simulators

J. L. Gilbert, E. B. Savage and K. S. Smith

Metatech Corporation, Goleta, USA

...

quantum_mechanic@alum.mit.edu

During a series of tests of the susceptibility of computers to pulses injected on a 10baseT Ethernet connection, an unexpected result in the distribution of currents was obtained. The pulses were coupled to the connecting cable using The Electrical Fast Transient/Burst Immunity Test specified in IEC 61000-4-4 where a section of the cable was laid in a capacitive coupling clamp and fast current pulses were injected on the clamp which was terminated with a matched impedance. The injection produced a current pulse on the clamp that propagated away from the pulser from the injection ("upstream") end to the termination ("downstream") end, and the configuration is preferable to direct injection in that the perturbation of the electrical characteristics of the Ethernet connection is small.

The unexpected result was that the current injected into the Ethernet port on the upstream computer was approximately three times the current injected into the corresponding port on the downstream computer. We had naïvely believed that the downstream computer would be subjected to the greater current because the phasing of the current along the clamp would produce a buildup of current in the Ethernet cable in the forward direction. An analysis of the behavior of the clamp was performed using the multiline transmission line equations

$$\vec{L} \cdot \frac{\partial \vec{I}}{\partial t} + \vec{R} \cdot \vec{I} + \frac{\partial \vec{V}}{\partial z} = E_{inc} \tag{1}$$

and

$$\vec{C} \cdot \frac{\partial \vec{V}}{\partial t} + \vec{G} \cdot \vec{V} + \frac{\partial \vec{I}}{\partial z} = 0 \tag{2}$$

It was noted during the course of the analysis that the signs of the capacitive coupling and inductive coupling terms were additive for pulses propagating upstream and subtractive for pulses propagating downstream, and this accounted for the observed behavior. Confirmation of this analysis was obtained by varying the value of the terminating resistor on the clamp, which changed the ratio of the voltage to the current on the clamp and thus varied the ratio of the capacitive to the inductive coupling. The sign of the peak of the current injected into the downstream Ethernet port could be reversed and the magnitude substantially increased, albeit at the cost of degradation of other pulse characteristics. In the presentation, we will discuss the results obtained and the trade-offs encountered between pulse magnitude and characteristics such as rise time, pulse width and monopolar behavior.

We then extended this analysis to a class of simulators for high-altitude EMP (HEMP) coupling to long lines where a current is injected onto an elevated line parallel and proximate to a power or communications line connected to ports under test. The presentation will show coupling characteristics as a function of line configuration in both the frequency and time domains.

CAD Performance Modeling and Synthesis of Microstrip Dipole Array Antenna

P. J Soh[1], R. A. J. A Amir[1], M.M Aiza[1], A.A.H Azremi[1], M.Z.A Abdul Aziz[2]

[1]*School of Computer & Communication Engineering, Universiti Malaysia Perlis, Perlis, MALAYSIA*
[2]*Faculty of Electronic & Computer Engineering, Universiti Teknikal Malaysia Melaka, Melaka, MALAYSIA*

E-mail: pjsoh@unimap.edu.my

Performance simulation of antennas are commonly done using two different simulation techniques, the circuit model (CM) derived from the Transmission Line Model (TLM), and the other, using the Method of Moments (MoM).. However, previous works has failed to emphasize the importance of using a Computer Aided Design (CAD) using circuit model in simplifying synthesis of designed antenna structure, especially when multiplication of the antenna is done in a form of an array. In this work, two element units of microstrip dipole array antennas is simulated, presented and compared to prove the importance and accuracy of this technique. Both methods are simulated using Microwave Office. The basic microstrip dipole antenna is accurately modeled and the linear array structure is done by combining two basic element units. Both simulation sets of MoM and CM are evaluated to determine their level of variation in terms of return loss (S_{11}), bandwidth and resonant frequency (f_{res}). The MoM simulated structure is then fabricated on an FR4 board with a relative permittivity (ε_r) of 4.7 and measured to determine the degree of distinction between hardware and the two simulation sets. Antenna designed and simulated for each technique achieved the best return loss at WLAN frequency, with S_{11} values lower than -10 dB. CM presented in this work is observed to have less than 5% difference compared to MoM counterpart in terms of S_{11}. The frequency resonant shows a different of 2.4% between measurement and simulated results. A set of parametric study is also done to determine the level of variation of using this CAD model in terms of dipole length and its two width sizes, W1 and W2, against the antenna performance indicators.
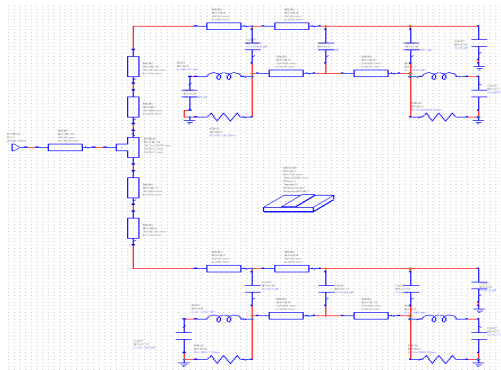
Fig. 1 – CAD Model for the Microstrip Dipole Array

Table 1 – Details of Simulated and Measured Result for the Dipole Array

	BW (MHz)	*S11* (dB)	*f*res (GHz)	*BW* Range	*BW* (%)
MoM (Sim)	60	-23.54	2.45	2.42-2.48	2.42
CM (Sim)	20	-24.84	2.45	2.44 -2.46	0.81
MoM (Meas)	100	-22.21	2.51	2.48-2.58	3.88

References
1. B. G. Duffley, G. A. Morin, M. Mikavica, Y. M. M. Antar, "A Wideband Printed Double Sided Dipole Array," IEEE Transactions of Antenna & Propagation, Vol. 2, No. 2, Feb 2004, pp 628 – 631
2. Jhin-Fang Huang, Mao-Hsiu Hsu, Jia-Wei Liang, "Wideband Printed and Double-Sided Dipole Pair Antennas with a Parallel Reflector," IEEE International Symposium on Microwave, Antenna, Propagation and EMC Technologies for Wireless Communications, Proc of the, 2005, pp 1635 - 1638

Design Study of a High Pressure Spark Gap Switch

S.H. Nam[1], H. Heo[1], S.S. Park[1], J.W. Shin[2], J.H. So[2], W. Jang[2]

[1]*Pohang Accelerator Laboratory/POSTECH, Pohang, KyungBuk, South Korea*
[2]*ADD, Daejeon, South Korea*

E-mail: nsh@postech.ac.kr

As a high voltage output switch of a triple resonance charging pulse generator, we designed a high pressure SF_6 gas filled spark gap switch. The triple resonance charging circuit has an air core step-up pulse transformer. The total voltage step up ratio of the generator, which is resulted from resonance as well as the transformer step-up ratio is about eleven. The total voltage step-up ratio is higher than the transformer ratio alone. There is a distributed pulse forming network (PFN) as an intermediate charging component. The charging voltage at this stage is above 500 kV. The output load impedance is about 100 ohm. Between the PFN and the load, the output spark gap switch is located. This switch is self-triggered with over-voltage developed on the PFN. The switch is designed to fill high pressure SF_6 gas to hold high voltage while maintaining its compactness. To design the pressure, we developed an analytical tool to predict the SF_6 gas breakdown strength at extremely high pressure range. The whole pulse generator components are immersed in a transformer oil filled stainless steel tank. We will present the design procedure of the output spark gap switch, and the preliminary performance of the triple resonance charging pulse generator with the switch.

HPEM - 33
Pulsed Power (Invited)

Oral Presentations

Conduction in Wide Band Gap Photo Conductive Power Switches Operated in Linear, Extrinsic Mode

S. R. Gyawali[1], C. Fessler, [1] W. C. Nunnally[1], and N. E. Islam[1]
University of Missouri, Columbia, Missouri, USA

E-mail: IslamN@missouri.edu

Photoconductive semiconductor switch (PCSS) made from high resistivity, wideband gap semiconductors such as Gallium Arsenide (GaAs), Silicon Carbide (SiC) and Gallium Nitride (GaN), among others, have potential applications in compact pulse power switching systems. In such switch types the external laser and optical delivery systems controls the resistive transition time, the switch inductance, and the switch temporal closure are nearly independent of applied voltage. Also, in a particular operation mode (when the photon energy less than the band gap energy) one can utilize small laser systems to control the optical absorption depth and limit the switch current density.

In this paper we discuss and compare the design and application of compact power PCSSs that are fabricated from compensated SiC and GaN materials, for pulsed power applications. Specifically, we analyze the role of the compensation mechanisms in GaN a compared with that of a similar SiC, structure which was fabricated and tested in the laboratory [2]. We also present the physical design of the switch for low inductance which is intimately associated with the pulse discharge system and the optical illumination system. Recent experimental results of prototype switches and the on and off-state transport mechanisms in the high resistivity material with traps and donor/acceptor sites in the materials are also included in our presentation [1].

The experimental setup for the SiC PCSS is shown in Fig. 1, which comprises of a T&M high frequency current viewing resistor (CVR) that measures the switch current, while the voltage across the switch is measured with a calibrated capacitive voltage divider. The transient waveforms are recorded on a Tektronix DP8446, digital phosphor oscilloscope and the discharge energy store is one or more 50 Ohm cables in parallel which is used to set the peak current for a given charge voltage. The coaxial cable length determines the switch current pulse length and the cable energy store is charged in several microseconds with a pulse charge system up to the desired experimental voltage. When the voltage across the switch reaches the maximum value, a 5 – 10 ns optical pulse from a Continuum Surelite II Nd:YAG laser is injected into the switch via an optical fiber ribbon cable or a cylindrical lens focused on the edge of the SiC slab. The switch closure discharges the energy stored in the cable source in the resistive load. The resistive load can be matched to the cable impedance or mismatched to evaluate the switch conduction resistance. Since the conduction resistance of the switch is proportional to the optical energy absorbed in the SiC, the resistive transition time is determined by the optical power applied through the optical fiber ribbon cable.

The simulation study focuses on trap occupancy and recombination terms required in the solution of the basic semiconductor continuity and Poisson's equations. The generation and recombination terms account for the changes in carrier statistics due to the trap levels and some of the parameters associated with it.
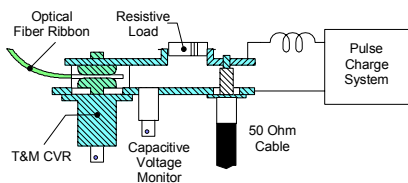
Fig 1 – Experimental setup for studying the PCSS
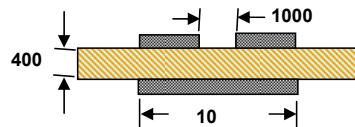
Fig 2 – PCSS design used in simulations

References

1. K. S. Kelkar, N. E. Islam, C. M. Fessler, and W. C. Nunnally, "Silicon carbide (6H) photoconductive switch for high power, linear mode operations through sub bandgap triggering", Journal of Applied Physics, pp. 093102, Nov. 2005.

A Model of Pulse Power Storage and Release via Pulse Forming Lines

P. D. Smith[1], C. Qu[1] and K. D. Hong[2]
[1]*Department of Mathematics, Macquarie University, Sydney, Australia*
[2]*Defence Science and Technology Organisation, Edinburgh, Australia*
E-mail: pdsmith@maths.mq.edu.au

The design of nanosecond high-current generators is usually one of three schemes: a high voltage microsecond pulse voltage generator and pulse forming line; a relatively low-voltage pulse voltage generator and inductive energy storage in vacuum; or the switching of energy into a load with the help of a plasma-erosion opening switch. The use of an inductive storage (IS) of energy with an electro-explosive opening switch (EEOS) allows the charging of a pulse forming line in about 100 ns; this ensures insulation of high electrical strength and reduces overall dimensions and weight of the line. The optimisation of various designs that include an EEOS is usually performed by examination of a large amount of experimental data for RLC circuit models. We consider a theoretical RLC-circuit model of a particular device, the magnetic-flux compression generator (MCG).

The energy conversion in the IS circuit occurs in two stages. Initially, the energy that is partially lost for fuse heating is stored in the inductance; this stage is simultaneously one of heating and of accumulation of magnetic energy. At the second stage, the fuse resistance is determined mainly by the density of expanding metal and grows by a few orders of magnitude in a short time (explosion stage), when magnetic field energy of increasing power is released into the fast-rising resistance of the fuse. We discuss the detonation phase of the MCG, how the energy efficiency varies with respect to inductance and the EEOS parameters, and how the energy is released optimally to the load; we discuss available experimental measurements.

Piezo based High Energy, High Voltage Generator

B. Schuenemann, F. Schoetzig, J. Schmitz, M. Jung

Rheinmetall Waffe Munition GmbH, Heinrich-Erhardt-Strasse 2, D-29345 Unterluess, Germany

E-mail: juergen.schmitz@rheinmetall.com

The design and initial experiments of a piezo based high voltage generator with high energy for high power electromagnetic (HPEM) sources are discussed. The intention is to describe the general layout and some results of conducted tests.

Piezo elements convert mechanical pressure directly into high voltage. Therefore, no intermediate matching and pulse shaping is necessary. It is possible with a few ten grams of explosive to generate pressures sufficient for high voltage pulses of many hundreds of kilovolt. The possibility to build compact energy sources with a volume of about 25 liters and a stored energy of a few hundreds of joule makes accessible a new way in the design of a very compact high power energy source as a cheap and strictly non lethal alternative to small magnetic flux compression generators (MCGs) for several pulsed power applications.

Main advantages of this generator are the compact size, high voltage output, nearly unlimited storage time and relatively low costs per experiment.

HPEM - 33
Pulsed Power (Invited)

Oral Presentations

First Trials of a 45 GW Pulsed-Power Generator

Adam Lindblom[a], Mattias Elfsberg[a], Tomas Hurtig[a], Anders Larsson[a,b] and Sten E Nyholm[a]

[a] *Swedish Defence Research Agency (FOI), Defence & Security, Systems and Technology, SE-147 25 TUMBA*
[b] *Uppsala University, Division for Electricity, Box 534, SE-751 21 UPPSALA, Sweden*

E-mail: Anders.Larsson@foi.se

The output from narrow-band high-power microwave (HPM) sources, such as the virtual cathode oscillator (vircator) and the magnetically insulated line oscillator (MILO), is strongly dependent on the voltage pulse feed. For proper operation of these radiation sources, the applied voltage should have a rectangular, flat-top shape. This can be achieved by the use of a transmission line as a pulse-forming unit. Up to now, mainly water-based transmission lines have bee used as high voltage and high power units. However, the development in high-voltage cable technology has made them useful as parts of high-voltage and high-power generator systems. The idea of the design of the generator presented here is the outcome of a PhD Thesis [1] and the generator design has been presented earlier [2]. The presentation here includes the first trials with the pulsed-power generator. The generator is designed to deliver a 200 ns voltage pulse of 500 kV into a 10 Ω unmatched load with an electric power of 25 GW. The generator has an impedance of 2 Ω and can deliver a rectangular pulse of 300 kV with duration 200 ns and power 45 GW across a matched load. The electrical design of the generator is shown in Figure 1. The primary energy storage of the generator consists of a 50 kV, 20 kJ capacitor bank. The 50 kV is discharged into a 1:12 transformer that charges a pulse-forming line to 600 kV. When charged, the pulse-forming line is discharged into the load via a spark gap. The total length, height and width of the pulse generator are 4 m, 2 m and 1.2 m respectively.
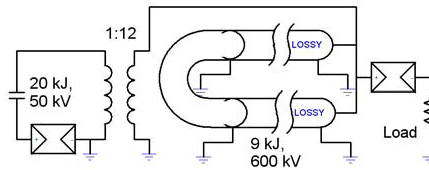
Fig. 1 – The electrical design of the generator.

The measurement results from a first trial are shown in Figure 2. The figure shows the measured load current. The primary capacitor bank was charged to 10 kJ (35 kV, 16 µF) and the load was 12 Ω at the trial.
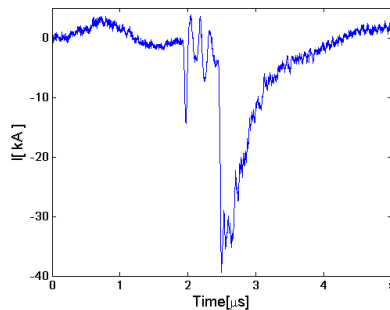
Fig. 2 – The measured current into the 12 Ω load.

References
1.   A Lindblom, *Inductive Pulse Generation*, Doctoral Thesis, Uppsala University (2006)
2.   A Lindblom, A Larsson, H Bernhoff and M Leijon, "45 GW pulsed-power generator", 2007 IEEE Pulsed Power and Plasma Science Conference, Albuquerque, USA, 17-22 June 2007

Differential Marx Generators

C. E. Baum

University of New Mexico
Department of Electrical and Computer Engineering
Albuquerque New Mexico 87131
E-mail: cebaum@ece.unm.edu

Marx generators are a commonly used type of high-power pulse source. They come in various forms (triggered or untriggered gaps). They can have fast-rising outputs through the use of peaking or transfer capacitors. Their usual configuration is, however, single ended, i.e., producing a voltage (positive or negative) with respect to some local "ground."

Some loads of interest are differential in form. In particular some antennas, such as loops, take this form. Even reflector antennas can use a differential feed. Thus one needs differential sources to drive such loads. Here we suggest the possibility of differential Marx generators.

One can have a differential Marx generator by simply taking two such generators, one operating plus and the other minus. One can have a symmetry plane between the two "halves." The electromagnetic fields then take the antisymmetric form. If the generators produce ±V, then the voltage delivered to the load (differential) is 2V. At the same time the peak voltage with respect to local "ground" (including the symmetry plane) is only ±V, thereby allowing larger voltages in the differential mode.

Other symmetries for a differential Marx generator are also possible. One can envision spirals and various kinds of screw symmetry (translation and rotation). For example, one might have a double helix like the DNA molecule, with the cross-triggers taking the place of the A, G, C, and T molecules. We then have many possibilties for the design of differential Marx generators. Different applications may suggest different forms. There also are many complexities such as various parasitic impedances which need to be considered in arriving at optimal designs.

HPEM - 33
Pulsed Power (Invited)

Oral Presentations

A Simplified Full EM Model for a MATRIX System

M. Armanious[1] and J. S. Tyo[1]

[1]The College of Optical Sciences, The University of Arizona, Tucson, AZ 85732, USA.
E-mail: tyo@ieee.org

A switched oscillator is a quarter-wave resonant length of transmission line of very low impedance. One end is terminated with a closing switch while the other end feeds a wideband antenna of relatively high input impedance. An implementation of such system, known as MATRIX, is still in its early development stages. In this work an electromagnetic "EM" model for the MATRIX system, based on the PDE solver provided by MATLAB, is presented. The system is 2-dimensional in that we enforce azimuthal symmetry on the geometry, but are able to compute the full three-dimensional EM fields in the structure. By invoking symmetry, $\partial/\partial\phi\{\bullet\}=0$, the geometry can be reduced to a 2D structure as shown in figure 1. Our simplified model consists of three cascaded sections of transmission lines: a radial transmission line "RTL," a conical transmission line "CTL," and a coaxial transmission line "COAX."

For simulation purposes, we modeled the load as an extension to the COAX with a permeability μ_{load}, bounded by radiation condition, with

$$\mu_{load} = \left(Z_L / Z_{c,COAX} \right)^2 . \tag{1}$$

The voltages, at the input and output terminals of the equivalent transmission line circuit, are related to electric calculated fields as follows

$$V_{in} = -\int_0^d E_z dz, \; V_{out} = -\int_{\rho_{o,COAX}}^{\rho_{i,COAX}} E_\rho d\rho, \tag{2}$$

where d is the RTL gap, $\rho_{i,COAX}$ and $\rho_{o,COAX}$ are the inner and outer radii of the COAX, respectively. Figure 2 shows the transfer function $T_{dB} = 20\log\left(|V_{out}|/|V_{in}|\right)$ versus frequency for a given MATRIX. The numerical analysis of the system showed an increase in the quality factor $Q = f/\Delta f$ due to reduction of the gap spacing d. Another observation was that the system resonates at a frequency lower than a λ/4 resonant length of transmission line. The RTL section has variable characteristic impedance, which makes the effective length of the resonating circuit shorter than that of a pure COAX line.
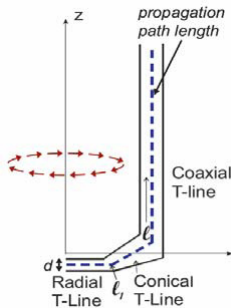
Fig. 1 - A Simplified model for the MATRIX.   Fig. 2 - Transfer functions verses frequency
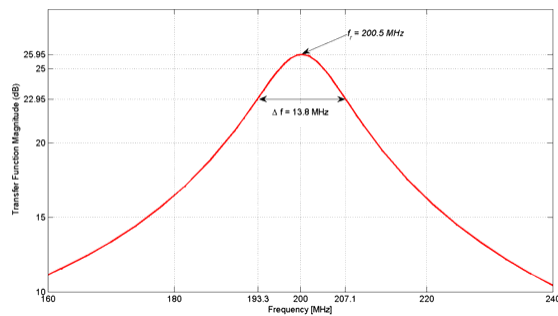
References
1. C. E. Baum, "A transmission-line transformer for matching the switched oscillator to a higher-impedance resistive load," in *Circuit and Electromagnetic System Design Notes #46* (C. E. Baum, ed.), Albuquerque, NM: Air Force Research Laboratory, 2001.
2. J. S. Tyo, M. C. Skipper, M. D. Abdalla, S. P. Romero, and D. V. Giri, "Performance limitations of transmission line oscillators for high power mesoband sources," in *15th IEEE Pulsed Power Conference*, 2007. In Press.

Electromagnetic Shielding of Composite Materials Using Electrochemical Discharge Nanoparticles

M. Jalali[1], R. Wuthrich[2]

[1,2]*Concordia University, Montreal, Canada*

E-mail: wuthrich@encs.concordia.ca

Cost and environmental issues are the factors that push the aeronautic industry to replace the heavy metallic pieces of airplanes by composites. Increasing the Electromagnetic (EM) shielding property of composite has been a goal since long time ago and several solutions (e.g. Metal mesh, Electroless coating, Conductive paint, Vacume metalizing …) have been proposed to reach it [1]. Based on new developments of science in the field of nanotechnology, many solutions (e.g. CVD, PVD, Aerosol, Mechanical milling, Sol-gel…) have been proposed as well. But only a few of them have been considered to be used in industry. Here for the first time, we propose a new method based on electrochemical discharge which will be integrated very easily to the traditional technique of composite fabrication. Comparing to the conventional techniques of improving the EM shielding, our technique will have the advantage of light-weighting and corrosion resisting. Comparing to unconventional techniques, it will have the great advantages of low-costing and simplicity. Based on researches which have been done by Wuthrich et al [2, 3], through electrochemical discharge, we could observe the creation of metallic nano-particle with the possibility of having the control on the concentration.

Uncomplicated system contains an electrode, counter electrode, aqueous electrolyte containing salt of desired nanoparticle and DC power supply provider of (1A/mm^2 at 20V). Electrical discharges occur between the cathode electrode which rotated (over 1000rpm) and the electrolyte and causes formation of gas film which has a key role in process by avoiding the metallic ions from setting down on electrode. Metal nanoparticles (typically 10-150nm) are formed in solution which could be separated by drying and deposited on HOPG [2, 3]. The deposition could be realized as well directly on carbon mesh which is going to be used in traditional composite fabrication. Increasing (by 4 times more) the electromagnetic shielding effectiveness (for range of 1-2 GHz) of transition metallic of Nickel particles by decreasing the size (10 times less) encouraged us to focus our research on fabricating of this type of nanoparticles [4].

$$M^+ + e^- \rightarrow M$$
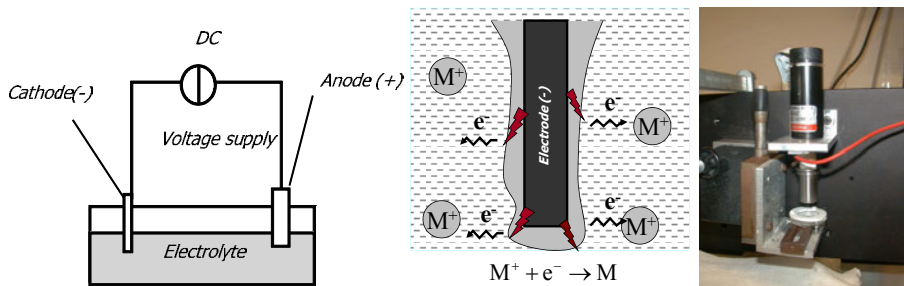
Fig. 1 – Left: Principles of Discharge, Centre: Creation of Nanoparticles in Solution, Right: Setup

References
1. S.Rea, D.Lintone, E.Orr, J.McConnel, "Electromagnetic Shielding Properties of Carbon Fiber Composites in Avionic Systems." Microwave Rev. 2005
2. A. Lal, R. Wüthrich, H. Bleuler: "Fabrication of nanoparticles for spectroscopic investigations by an STM", Electrochemical Micro and Nano Systems Technology, 23th-25th August 2006,Bad Godesberg, Germany
3. R. Wüthrich, A. Lal, H. Bleuler: "A table-top set-up for nano-particles production with electrochemical discharges", 5th International Workshop on Microfactories, 25-27th October 2006, Besençon, France
4. D.D.L. Chung, Review, "Electromagnetic interference shielding effectiveness of carbon Materials", Carbon 39 (2001) 279–285

HPEM - 34
Grounding and Shielding

Oral Presentations

Transparent Electromagnetic Shielding of Enclosures Against EMP Penetration

M. D'Amore, S. Greco, M. S. Sarto

Department of Electrical Engineering, Sapienza University of Rome, Rome, Italy
E-mail: marcello.damore@uniroma1.it

The EMP-interaction with an aluminum enclosure having a wall of carbon-fiber reinforced composite (CFRC) material was characterized by means of theoretical and experimental approaches: the simulated results were compared with measured data obtained by using a full-scale EMP generator [1]. In this paper the CFRC panel is replaced with two different types of transparent shields. The first shield consists of a commercial 175 μm-thick polycarbonate sheet, coated on one surface with an indium-titanium-oxide (ITO) film having thickness of 0.5 μm, and measured sheet resistance of 13.35 Ω/□. The second screen is realized with a nanostructured transparent metallo-dielectric thin film deposited on the panel surface. Titanium dioxide (TiO_2) is used as target material for the dielectric layers in transparent metals; the conductive layers are made of silver (Ag). The use of blocking layers, made of Titanium (Ti), is necessary to avoid silver oxidation. The structure of the resulting coating, which is constituted by 17 layers, is $(TiO_2/Ti/Ag/Ti/TiO_2)^4$ [2]. The thickness of the TiO_2 films is 32 nm, of the Ag layers is 17 nm and of the Ti interlayers 1 nm. The total metal content is 68 nm. The overall thickness of the coating is 332 nm. Fig.1 shows the considered 3 mm-thick aluminum box of dimensions 70 cm × 70 cm × 70 cm. The incident electric field is simulated by a double exponential function with time constants τ_1=5 ns, τ_2=200 ns and E_0=50 kV/m. The numerical simulation is implemented by a three-dimensional finite-difference time domain (FDTD) procedure and the thin layer model described in [1] and [3],

Fig.1 - The excited box.

respectively. The electric and magnetic transient fields are computed at positions (x=9.5 cm, y=34 cm, z=17.5 cm) and (x=2.5 cm, y=53.5 cm, z=27.8 cm), respectively, for comparison with measured data [1]. Figures 2(a) and 2(b) represent the obtained transient waveforms inside the enclosure without and with the Ag- or the ITO-transparent shield, respectively.
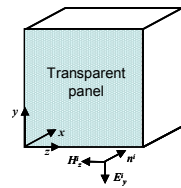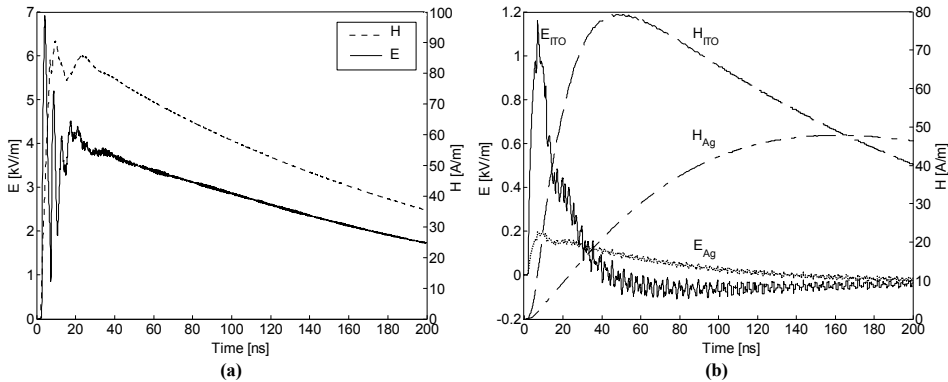
Fig. 2 - Transient electric and magnetic fields in the enclosure without (a) and with (b) the ITO- or Ag-shield.

It should be noted the better shielding performance of the nanostructured thin film: the E-peak value is reduced of factor 34 and the H-rise time is increased of factor 20. The optical transmittance in the visible range reaches the value of 70% for normal incidence.

References
1.   M. D'Amore, M. S. Sarto, "Theoretical and experimental characterization of the EMP-interaction with composite-metallic enclosures", IEEE Transactions on EMC, May 2000.
2.   M. S. Sarto, R. Li Voti, F. Sarto, M. C. Larciprete, "Nanolayered lightweight flexible shields with multidirectional optical transparency", IEEE Transactions on EMC, August 2005.
3.   M.S. Sarto, "Electromagnetic shielding of thermoformed lightweight plastic screens", IEEE Transactions on EMC, November 2004.

Direct Time Domain Analysis of a Grounding Electrode Based on the Antenna Theory

Vicko Doric, Dragan Poljak, Vesna Roje

Department of Electronics, University of Split, Split, Croatia

E-mail: vicko.doric@fesb.hr

The grounding electrodes play important role in protection of telecommunication systems and electrical power systems against overvoltages and fault currents. Thus, the analysis of the transient behavior of grounding electrodes is necessary for an efficient design of the protection system.

In general, the transient response of any linear system could be obtained directly, by solving the time domain equations, or by frequency domain approach and inverse Fourier transform. Previously used models can be classified as circuit approach [1], transmission-line approach [2] and antenna theory approach [3], [4]. Antenna theory approach is most accurate one, but also the most demanding and, until now, limited to the frequency domain analysis.

In this work a novel time domain model of the grounding electrode based on the wire antenna theory is proposed. Grounding electrode is modelled as a thin wire antenna excited with the current source at the wire end as shown in Fig 1a. The formulation is based on the correspondig homogeneus time domain Pocklington integro-differential equation for thin wire in infinite lossy medium. Rather demanding Green function containing convolution and the Bessel function is simplified assuming the low conductivity of the soil. Thus obtained equation is numerically handled via the time domain Galerkin-Bubnov scheme of the Indirect Boundary Element Method (GB-IBEM) [5]. Current distribution along the wire for each time step is obtained using the adequate marching on in time procedure. Validity of the proposed model is tested using antenna theory approach in frequency domain and inverse Fourier transform [4].

Computational example is related to the grounding electrode in a lossy ground with $\sigma=0.001 \text{S/m}$, $\varepsilon_r=10$. The length of the wire is 10m and the radius is 5mm. Grounding electrode is excited by the double exponential current pulse with parameters $I_0=1.1043\text{A}$, $\alpha=0.07924\cdot10^7\text{s}^{-1}$, $\beta=4.0011\cdot10^7\text{s}^{-1}$.
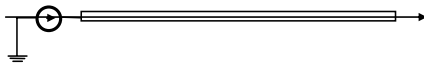
Fig.1 - a) geometry of the grounding electrode   b) current induced at the centre of the wire
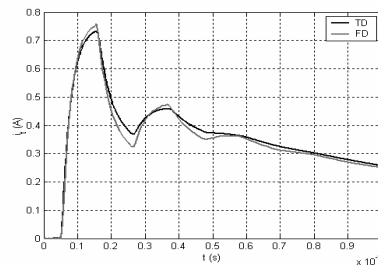
Figure 1b shows the current induced at the centre of the wire obtained using the proposed approach and frequency domain approach combined with IFFT. The results obtained via both approaches are in rather good agreement. Future work will aim to take into account the influence of the earth-air interface.

References

1. A. Geri, "Behavior of grounding systems excited by high impulse currents: the model and its validation," *IEEE Trans. Power Del.*, vol. 14, no. 3, pp. 1008–1017, Jul. 1999.
2. M. I. Lorentzou, N. D. Hatziargyriou, and B. C. Papadias, "Time domain analysis of grounding electrodes impulse response," *IEEE Trans. Power Del.*, vol. 18, no. 2, pp. 517–524, Apr. 2003.
3. L. Grcev and F. Dawalibi, "An electromagnetic model for transients in grounding system," *IEEE Trans. Power Del.*, vol. 5, no. 4, pp. 1773–1781, Oct. 1990.
4. D. Poljak, V. Dorić, Wire antenna model for transient analysis of simple grounding systems, part II: the horizontal grounding electrode, Progres in Electromagnetics Research, PIER 64, EMW Publishing , Cambridge, Massachusetts, 2006, pp 167-189.
5. D.Poljak, EMC Advanced Modelling in Computational electromagnetic Compatibility, John Wiley and Sons, New York 2007.

HPEM - 34
Grounding and Shielding

Oral Presentations

Design and Construction of a Shielded Cabinet for Laboratory Tests

F. Santamaría, A. Alarcón, O. Díaz and F. Román

Electromagnetic Compatibility Group Research of the National University of Colombia EMC-UN, Bogotá D.C., Colombia

E-mail: fsantamariap@unal.edu.co

During the last years the Electromagnetic Compatibility Group Research (EMC-UN) has developed laboratory tests on high voltage and Electromagnetic Compatibility (EMC). For EMC tests we designed and built shielded cabinets to guarantee the measurement quality and also to protect the measuring system.

Currently, it is possible to buy shielded cabinets with customized characteristics. However, price might be very high and the cabinet design and build process gave us knowledge about different materials EMC properties and construction techniques.

The general design required to achieve a shielding effectiveness above -60 dB and to store an oscilloscope and an Uninterrupted Power Supply (UPS). Additionally, the cabinet should have signal inputs with different kinds of coaxial cables.

First, the possible materials that could be used for the cabinet construction were analyzed. From this analysis, it was established that the better material is the cold-rolled galvanized steel, which has a high relative permeability (μ_r = 2000), for magnetic wave attenuation, a good relative electrical conductivity (σ_r = 0.2) and also has higher mechanical strength, which guarantees the cabinet durability.

Finally, we decided to build a double isolated shielded cabinet. With this configuration it is possible to improve the cabinet shielding effectiveness.

The built cabinets can be seen in Fig. 1. The pictures show the most critical parts of the construction, which are the wave guides for the signal inputs and the door. Note the proper closing of the door.

Fig. 1 – Shielded Cabinet. Note the door and the waveguides for input signals

Metallic and Magnetic Materials Used as Magnetic Field Shielding

A. Sánchez[1], M. Rodríguez[2]

[1]*M.Sc. (C) Universidad Nacional de Colombia, Bogotá, Colombia*
[2]*EMC research group, Universidad Distrital Francisco José de Caldas, Bogotá, Colombia*
E-mail: [1]asanchezsa@unal.edu.co, [2]marodriguezb@udistrital.edu.co

Academic and military research by industrialized countries has developed various shielding techniques against electromagnetic fields. With knowledge appropriation the industry has developed new materials and shielding techniques. In Colombia there are no many experimental studies about electromagnetic interference shielding techniques. The present study has been performed in order to determine near–magnetic field shielding effectiveness for two low–cost metallic and magnetic materials easily found in Colombian market: aluminum and iron (cold-rolled).

The experimental setup consist of two parts: 1) An air–core solenoid (length 0.98m, 487 turns and diameter 0.46m). The solenoid was connected to a 100Hz to 100kHz frequency range AC source, 2) Six cubical shields (10cm x 10cm x 10cm) in aluminum and cold rolled iron. Three shielding thicknesses were determined for both materials: 0.5mm, 1mm and 1.5mm. Experimental setup sketch and photos are shown in Fig. 1.
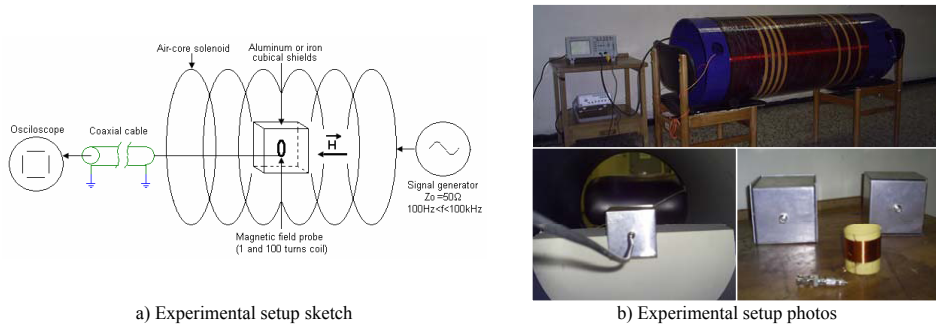
a) Experimental setup sketch   b) Experimental setup photos

Fig. 1 – Experimental setup: a) Sketch, b) Photos

Experimental results of shielding effectiveness offered by aluminum and iron shields as a function of frequency and shielding thickness are shown in Table 1.

Table 1 – Shielding effectiveness (S) measured for cubical shields: a) aluminum, b) iron (cold-rolled)

f [Hz]	a) S [dB] – Aluminum			f [Hz]	b) S [dB] – Iron (Cold-Rolled)		
	0.5mm	1mm	1.5mm		0.5mm	1mm	1.5mm
100	0,28	0,58	1,53	100	4,72	6,31	7,89
1000	3,33	6,34	9,54	1000	6,07	9,54	11,00
10000	12,75	16,22	19,01	10000	8,64	8,09	8,93
100000	19,53	21,58	24,28	100000	11,57	11,48	12,54

In aluminum case, there is a significant difference between results of Table 1.a) and theoretical equations proposed by Miller [1] (50% approximately). In iron case, there is the same situation between results of Table 1.b) and curves presented by Hemming [2] (50% approximately). It can be explained because used shields were closed by mean of screws. Therefore, used shields were not perfectly sealed. A study for aluminum and iron cubical shields perfectly sealed with frequencies above 100kHz will be performed, in order to compare differences between experimental shielding effectiveness results shown in Table 1 and shielding experimental effectiveness results for perfectly sealed shields.

References
1. D.A. Miller and J.E. Bridges, "Review of circuit approach to calculate shielding effectiveness" IEEE Transactions on Electromagnetic Compatibility, vol. 10, 1968. p.57-61
2. L. Hemming, Architectural Electromagnetic Shielding Handbook. New York: IEEE Press, 1992. p.21-23

Estimation of Electro-Magnetic Pulses Penetrating into Shielded Constructions

N. Shapovalova[1], O. Serkov[2]

[1] *National Technical University „Kharkiv Polytechnical Institute", M IEEE, Kharkiv, Ukraine*
[2] *National Technical University „Kharkiv Polytechnical Institute", M IEEE, Kharkiv, Ukraine*

E-mail: nat_ii@mail.ru

Nowadays radio-electronic systems situated in shielded constructions are expected to operate reliably under influence of different electromagnetic pulses. The parameters of these potential penetrated pulses should be estimated during all the stages of the shielded construction design. However, theoretical solutions of these problems face noticeable mathematical difficulties because it is necessary to deal with many different factors that influence electromagnetic pulses penetration. These factors include various heterogeneities such as apertures, chinks, docking assemblies, etc. that are widely used in real shielded constructions. That is why the *experimental approach* has been used to estimate parameters of the penetrated electromagnetic field (1). According to this approach, results of statistical manipulation of experimental data are presented in a form of simplified analytical equations, which are convenient in engineering calculations. The analytical equations have been used to develop ***software for estimation of parameters of electromagnetic pulses penetrating into shielded construction*** (2).

The designed software provides ***bidirectional transmission*** of parameters of construction model between the software and ***SolidWorks***. This interactive connection allows to use the model at every stage of its design, checking and validating engineering solution according to requirements of electromagnetic compatibility. In order to increase the model conformity, it is possible to adjust form of the construction, electro-technical parameters of used materials and also types, sizes and quantity of heterogeneities. After specifying construction parameters and parameters of external electromagnetic pulse, the parameters of ***penetrated electromagnetic pulse*** are estimated and ***visualised***. The influence of individual components (electrical and magnetic) of the electromagnetic pulse can be analysed. As the penetrated electromagnetic pulse is a superposition of two individual components – diffused one (penetrated through walls of the body) and aperture one (penetrated through heterogeneities), there is also possibility to estimate contribution of each individual component.

The influence of a wide range of external electromagnetic pulses can be simulated in order to verify and validate construction reliability during all the stages of its design ***without conducting real-life experiments***. At Fig. 1 the example of created model in SolidWorks and results of estimation of penetrated electromagnetic pulse are presented.
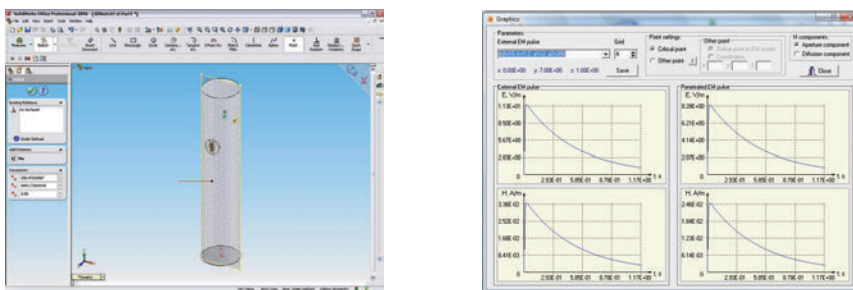
Fig. 1 – SolidWorks model (left) and electromagnetic pulse (external and penetrated) (right)

References
1. V. I. Kravchenko, V.V. Knyazev, G.V. Kravchenko, Y. S. Nemchenko, O. A. Serkov, Estimation of protective properties of space-system engineering objects under influence of natural and artificial electromagnetic fields. Kharkov: NTU "KhPI", 2007.
2. N. Y. Shapovalova, O. A. Serkov, V. O. Kravets "Software for Estimation of Electromagnetic Field Structure inside Shielded Constructions (Diffusion)," Certificate of Authorship 19268, January 19, 2007.

Oral Presentations

HPEM - 34
Grounding and Shielding

Electromagnetic shielding with metal thin film deposition

O. Alilou[1, 2], J-L. Lefebvre[1], P. Descamps[2]
[1] NXP Semiconductors, 2 rue de la girafe, BP5120, 14079 Caen Cedex 5 France
[2] Laboratoire de Microélectronique ENSI Caen-NXP (LAMIPS), 2 rue de la girafe, BP5120, 14079 Caen Cedex 5, France
E-mail: oussama.alilou@nxp.com

System-in-Package (SiP) is a growing trend of the electronic industry consisting in integrating one or several integrated circuits (ICs) together with discrete components of various technologies in a single package, resulting in one or several electronic systems. SiP allows for higher system miniaturization, performance and offers higher system integration.

However, new electromagnetic compatibility challenges occur with: on the one hand, the constitutive sub-elements of the SiP within the package are closer than ever to one another. Circuits of heterogeneous technologies originally designed to function in their own packages are now placed together in a same confined environment separated by distances as small as a few tens of microns only. On the other hand, because of their smaller size, complete SiP systems are also closer to one another in the end equipment. Thus, they can suffer from significant noise from the neighboring sub-systems. Each SiP may therefore need to be protected from external electromagnetic disturbances.

This paper first addresses the need for electromagnetic shielding of sub-systems in a mobile phone [1]. It will be shown that integration of electromagnetic shields within the SiPs against external incident disturbances not only offer more compliance to all types of electromagnetic environments, but also place SiP solutions higher in the system value chain.

Then, the SiP-specific boundary conditions are applied to the Maxwell equations for simplification, and a definition of shielding effectiveness formula applicable to SiP is proposed.

Tri-dimensional electromagnetic simulations of simplified shielding schemes are then presented. In order to assess the shielding effectiveness from thin-film deposited shields in SiP [Fig 1], and its influent variables, simulation results bench-test shown that a 60dB isolation from DC until 1.5GHz, and a 30dB from 1.5 GHz until 10GHz can be fitted.

Various parameters of this shielding technique are then considered and their relative performances influences compared.

Last, measurements of shielding effectiveness of a shielded SiP demonstrator are presented and compared to the initial simulations.
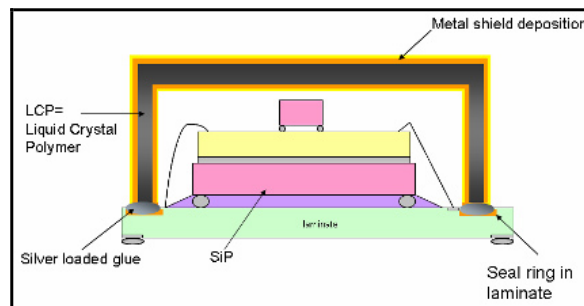
Fig. 1 – SiP shielding with thin film metal deposition

References
1.   N. Martin and H. Pohjonen, "System-in-Package (SiP) Modules for Wireless Multiradio", 2006 Electronic Components and Technology Conference.

Health and Safety Standards for Electromagnetic Energy: Development and Importance

Michael R. Murphy

Air Force Research Laboratory, Directed Energy Bioeffects Division, Brooks City-Base, TX, US

Michael.Murphy@Brooks.AF.mil

Concomitant with the ever increasing use of electromagnetic (EM) energy, there is also an increase in the opportunity, even certainty, for human exposure to EM emissions. Such exposures occur in three main categories: (a) Low-level, repeated, or chronic exposure to employees in certain occupations, users of certain technologies, and to the general public; (b) Accidental high level, acute exposure during development, maintenance, repair and operation of EM emitting systems, and (c) Intended low or high hevel exposures during medical procedures, security screening, and the application of EM-based police and military weaponry. Human exposures to EM are not only becoming more common, but the nature of the exposures are entering new regimes of frequency, power, and pulse characteristics, which may not have been adequately studied for potential health effects. Furthermore three civilian health concerns: (a) emissions form masts and phones used during wireless communications; (b) emissions from electricial transmission; and, to a lesser extent, (c) emissions from radar sites, have increased the anxiety of the general public and their governing organizations over the increased, so-called „electropolution" in the workplace, home, and general environment.

In the context of the increasing amount and complexity of EM exposure, the usefulness of EM technology, and public concern, scientifically-based health and safety standards have never been more important, yet the means by which they are developed are complicated and often misunderstood. This presentation will review the international organizations that conduct and support the research and other considerations (e.g., The World Health Organization EMF Project (1), the Bioelectromagnetics Society (2), and the European Bioelectromagnetics Association (3)) that provide the information for recognized international standard setting bodies (e.g., the IEEE International Committee on Electromagnetic Safety (4) and the International Commission for Non-Ionization Radiation Protection (5)), to recommend human exposure limits for EM radiation. The state of the current consensus as well as continuing controversies over appropriate levels of safe human exposure to EM will be discussed.

References

1.   http://www.who.int/peh-emf/en/
2.   http://www.bioelectromagnetics.org/
3.   http://www.ebea.org/Default.htm
4.   http://www.ICES-EMFSAFETY.org
5.   http://www.icnirp.de/

A Dynamic Model of the Cardiac Ventricular Action Potential. Simulations of Ionic Currents and Concentration Changes

A. I. Nicu[1], R. V. Ciupa[1], D. V. Rafiroiu[1], M. Voinicu[2]
[1]*Technical University of Cluj-Napoca, Cluj-Napoca, Romania*
[2]*University of Pitesti, Pitesti, Romania*
E-mail: anca.nicu@et.utcluj.ro

A parallel conductance model of the cardiac ventricular action potential is presented. The model is based on the Hodgkin – Huxley formalism, the same that we have used in our previous work to model the nerve cell action potential [1]. The present article focuses on processes that regulate intracellular Ca2+ ion concentration. The model presented here for the mammalian ventricular action potential is based mostly on guinea pig data. However, it provides the modelling frame for other types of ventricular cells.

Mathematical models of the **cardiac action potential** emerged from the necessity of modelling the heart and it's electrical conduction system. It has proven to be a powerful tool for clearing up some aspects of the cardiac function. The reason for this modelling action was drug treatment simulation, ment for minimising the pharmaceutical industry costs [2]. In 1991 Luo and Rudy presented an ionic model (LR-I) for the cardiac **action potential** (AP) in guinea pig ventricular cells, based on the Beeler – Reuter (BR) model but updated to include more recent experimental results [3]. However, they allowed for the possibility of changing the extra-cellular potassium concentration. In total, phase one of the Luo-Rudy model (LR-I) describes six different currents and uses nine variables, one of which is approximated by its steady state and replaced by a function, so that only eight variables are needed in the calculation. Later, Luo and Rudy updated their model further to produce the LR-II model.

For simulating the cardiac AP the Luo-Rudy model was implemented in Matlab. This model uses the Hodgkin-Huxley formalism and the differential equations that reproduce the responsable currents which produce the AP. The main objective of the simulation is the study of the electric behaviour of a patch membrane which is crossed by seven current components: one capacitive and six ionic.
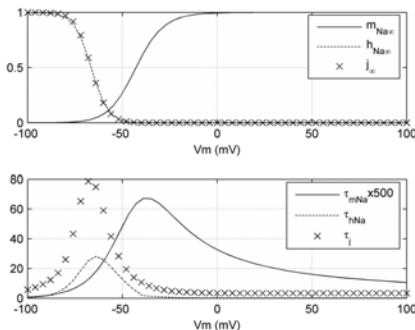
Fig. 1a - Natrium channels parameters   **Fig. 1b - Calcium chanels parameters**
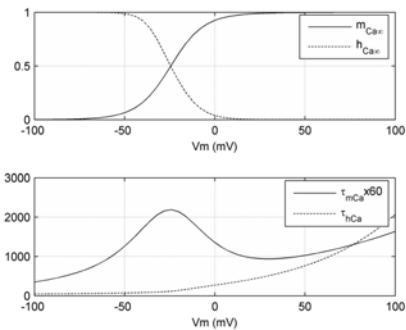
All of the current components were calculated, and also the action potential was determined and visualised. The program allows for changing the simulation conditions, making it possible to alter the action potential shape. The user can also see the effects that the current components have over the action potential's shape. We were able to observe that the results obtained are similar to the one published in the literature and to study some physiological aspects of the cells function.

References
1. Anca-Iulia Nicu, M. Plesa, L. CRET, C. Curta, D. V. Rafiroiu, "Electric circuit representation and numerical simulation of the nerve cells' active behaviour", EPCN 2006-Maribor, Slovenia, ISBN 83-921340-1-X, 2006.
2. DiMasi, J. A., Hansen, R. W., Grabowski, H. G. „The price of innovation: new estimates of drug development costs". Journal of Health Economics 22 (2003), 151-185.
3. Ch. Luo and Y. Rudy, "A model of the ventricular cardiac action potential", Circ. Res. 68, 1501-1526 (1991).

HPEM - 35
Biological Standards and Medical Applications

Oral Presentations

Energy Efficient Coils for Transcranial Magnetic Stimulation (TMS)

Laura DARABANT[1], Mihaela PLESA[1], Radu CIUPA[1], Octavian Cret[1], Adrian S. DARABANT[2]

[1]*Technical University of Cluj-Napoca, Cluj-Napoca, Romania*
[2]*Babes-Bolyai University, Cluj-Napoca, Romania*

E-mail: Laura.Darabant@et.utcluj.ro

The preoccupation for improving the quality of life, for persons with different handicaps, led to extended research in the area of functional stimulation. Due to its advantages compared to electrical stimulation, magnetic stimulation of the human nervous system is now a common technique in modern medicine. A difficulty of this technique is the need for accurate focal stimulation. Another one is the low efficiency of power transfer from the coil to the tissue. To address these difficulties, coils with special geometries must be designed.

One of the major problems that appear in the design phase is the computation of the inductivity of the stimulating coil and the electric field induced inside the human tissue. For simple shapes of the coils (circular), one can determine analytical computation formulas. When, however, the shape and the spatial distribution of the coil's turns do not belong to one of the known structures, a numerical method needs to be used for determining the inductivity and the electric field. The idea is to divide the coils in small portions. Starting from this method, two computation systems were already designed by the authors of this paper: the first one is classical and it just consists of a software implementation (Matlab) [1]; the second one consists of realizing a hardware architecture. The physical support is a FPGA device [3].

The problem with the software implementation is its running time. Coils are designed by trial-and-error, and this approach is impractical if each trial requires half a day of computation. Besides, as this time grows with the complexity of the coil, it prevents designing complex coils. FPGA-based hardware however provides the necessary acceleration and is, therefore, able to solve this bottleneck.

An adequate geometry of the stimulation coil can solve the main drawbacks of magnetic stimulation. The form and size of the turns, their position inside the coil, the insulation gap between turns are all important parameters that should be considered when designing a magnetic coil [2]. In [1] we analyzed the influence that space distribution of the magnetic coils' turns has on the efficiency of energy transfer from the stimulator to the target tissue, but the analysis was performed for a Slinky_3 coil of only 18 turns, with applications on transcranial magnetic stimulation (TMS). This estimation was based on the software inductivity calculus. Since a less time consuming technique is available (hardware implementation), now we can analyze larger coils of various shapes and different inner structure. An example is plotted in figure 1, showing a Slinky_4 coil with 70 turns, and one can observe the special inner structure of this coil. It turned out that the electrical energy dissipated in the circuit of the stimulator – required in order to achieve the activation threshold – is 25% lower for the most efficient configuration than for the less efficient one, and the coil heating per pulse is also 35% smaller!
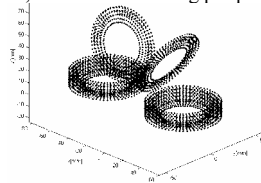
Fig. 1 – The inner structure of a Slinky_4 coil designed for improved focality during magnetic stimulation

The three quantities evaluated to establish the efficiency of energy transfer from the coil to the target tissue are: the energy dissipated in the circuit during one pulse of duration Δt, the peak magnetic energy in the coil required to induce a given electric field and the temperature rise in the coil after one pulse [2].

Since every medical application requires its own optimal structure of the magnetic coil, the results emphasized in this paper can play an important role for future work on coil design.

REFERENCES

1. L. Creț, M. Pleşa, D. D. Micu and R. Ciupa, "Magnetic Coils Design for Focal Stimulation of the Nervous System", Proceedings of EUROCON 2007.
2. J. Ruohonen, J. Virtanen and R. Ilmoniemi, "Coil Optimization for Magnetic Brain Stimulation", Annals of Biomedical Engineering, Vol 25, 1997.
3. I. Trestian, O. Creț, L. Creț and R. Tudoran, "FPGA-based computation of the inductance of coils used for the magnetic stimulation of the nervous system", Biodevices 2008, 28-31 January 2008, Funchal, Madeira, Portugal, pg.151-154.

HPEM - 35
Biological Standards and Medical Applications

Oral Presentations

On-Body UWB Channel Modeling for Two Representative Applications under Various Postures

Q. Wang, J. Wang, Member, *IEEE*

Department of Computer Science and Communications, Nagoya Institute of Technology, Nagoya, Japan
E-mail: wang.qiong@nitech.ac.jp, wang@nitech.ac.jp

The objective of this study is to derive an on-body UWB channel model with an emphasis on the statistical variation of the body posture. The channel modeling is mainly aimed at the entertainment and medical check-up application situations, which correspond to chest-ear link and chest-waist link respectively. For the entertainment application, extreme activity postures such as running as well as normal activity postures such as standing, sitting and walking are taken into account, while for medical check-up, extreme postures are eliminated. To derive such a complete on-body UWB channel model, we employ a high-precision human body model based on a statistical average of Asian adult males and the frequency-dependent finite difference time domain $((FD)^2TD)$ method [1].

First, based on the average power delay profile of all postures, it is concluded that one cluster is sufficient to describe the power delay profiles in these two transmission links. Moreover, as expected, the average power delay profile decays exponentially with arrival time. Second, assume that all of the obvious peaks in the power delay profile correspond to the multi-path rays. Those peaks, of which amplitudes are 30 dB lower than the maximum peak value, are taken into account to extract the channel parameters. Based on the Akaike information criterion, the Lognormal distribution provides a superior fit to the amplitudes contribution. Third, the arriving time of the first multi-path ray could be induced at the fixed mean value because of the tiny standard deviation. Forth, the inter-ray delay, which means the interval time delay between two successive rays, is fitted to the inverse Gaussian distribution according to the Akaike information criterion.

Based on the modified Saleh-Valenzuela (S-V) model [2][3] and the channel characterization, a discrete time impulse response function is brought forward applying to these two representative transmission links. All of the parameters required for the modeling of this impulse response function are summarized in Table 1. Comparison is carried out between the FDTD-derived data and statistically implemented model using the distribution of the rms delay spread and good agreement has been obtained.

Table 1 –Model parameters for two representative transmission links

Parameters	Description	Characteristics	Chest-ear	Chest-waist
γ [ns]	Ray-power-decay time constant	Exponential law	0.22	0.56
σ [dB]	Standard deviation of amplitude distribution	Lognormal	14.9	8.49
τ_0 [ns]	First ray average arrival time	Constant	1.19	1.96
$\tau_k - \tau_{k-1}$ [ns]	Distribution of inter-ray delay	Inverse Gaussian	μ_τ=0.35 λ_τ=0.26	μ_τ=0.28 λ_τ=0.95
Ω_0 [dB]	Mean power gain of the first ray*	$\Omega_0 = \mu_\tau G / \gamma$	-58.2	-74.0

*The mean power gain of the first ray Ω_0 is related to G (the reciprocal of the path loss) by $\Omega_0 = \mu_\tau G / \gamma$ where μ_τ is the mean time interval between two rays.

References
1. K.S. Kunz and R. Luebbers, "The Finite Difference Time Domain Method for Electromagnetics," CRC Press, Boca Raton, 1993.
2. A.A.M. Saleh and R.A. Valenzuela, "A statistical model for indoor multipath propagation," IEEE J. Selected Areas in Commun., vol.5, no.2, pp. 128-137, Feb., 1987.
3. A.F. Molisch (ed.), "IEEE 802.15.4a Channel Model Subgroup Final Report," IEEE P802.15 Study Group for WPAN, September 2004.

HPEM - 35
Biological Standards and Medical Applications

Oral Presentations

A Method for Harmonizing the Limits of Human Exposure to Magnetic Fields: Static versus Extremely Low Frequency Fields

C. Goiceanu, R. Danulescu

Institute of Public Health, Iasi, Romania

Email: cristig3@yahoo.co.uk

To protect human health, exposure to electromagnetic fields is limited according to provisions of standards and regulations. Given that the electromagnetic spectrum starting from static fields up to infrared radiation is very wide, exposure limits are set on domains of frequency: static fields, low-frequency fields, radiofrequency and microwave radiation. When assembling the parts of the standard, the continuity of exposure limit values for the entire spectrum has to be achieved. In some cases, at the transition between adjacent domains discontinuities in limit values occur.

Such a discontinuity in the frequency variation of the permissible level of magnetic flux density is observed at the transition from static to time-varying fields. For static magnetic fields [1] only, derived limits are provided in terms of both ceiling values and time-weighted average (TWA) values. On the contrary, for varying fields [2] it is provided only one single type of values that has to be regarded as a ceiling value that should not be exceeded in any moment of exposure.

The consequence of suppressing one type of derived limit value is that the maximum allowed level, even in the case of short-time exposure, suddenly falls down to the limit for the whole working day. Therefore, there is a discontinuity in limit values that leads to an abrupt reduction of permitted exposure level and, consequently, to some uncertainties and confusions in the process of checking compliance of measured field levels with limit values and reference levels provided by exposure standards.

To surpass these deficiencies, we searched for a way to harmonize the limit values for static fields with the ones for extremely low frequency fields. A buffer frequency range was considered to make the transition between the two regions with dual and, respectively, single limitation. Within the transition frequency range, dual limit criterion in terms of ceiling and TWA values was considered. We calculated frequency-dependent ceiling values to connect with the ceiling limits of static fields at the low end of transition frequency range and with the single limit value for varying fields at the high end.

The calculated frequency-dependent limit values for short-time exposures are based on the allowed relaxation of restrictions for the low end of extremely low frequency spectrum. We took into account the low values of tissular sensitivity for electric stimulation and the decrease of induced current in the body as frequency decreases. In the case of local exposure of limbs, given the lower maximum radius of limbs comparing to trunk and the fact there are no critical organs or tissues in limbs, higher values of magnetic flux density are permitted. Consequently, two transition functions were calculated for whole-body exposure and local exposure of limbs, respectively. Both of them have the generic form:

$$B_L = \frac{a}{f^b} \tag{1}$$

The coefficients a and b as well as the lower and upper limits of the buffer frequency range were calculated taking into account that the frequency variation of proposed limits should be in quite good agreement with the ideal frequency variation required by the biophysical grounds briefly presented above.

Therefore, we propose a manner of calculating frequency-dependent ceiling limit values that could be used to improve human exposure standards. Adding frequency-dependent limits at the low end of electromagnetic spectrum can contribute to achieve exposure standards that have continuity on the entire frequency spectrum. As far as discontinuities are eliminated, the method will also help the implementation of regulations by avoiding some uncertainties related to the relevant value of exposure limit to take into account. Therefore, the method and the proposed limits could help to reduce difficulties in checking compliance of measured magnetic field levels with the provisions of standards.

References:
1. International Commission on Non-Ionizing Radiation Protection, "Guidelines on limits of exposure to static magnetic fields", Health Physics, vol. 66, 1994.
2. International Commission on Non-Ionizing Radiation Protection, "Guidelines for limiting exposure to time-varying electric, magnetic and electromagnetic fields (up to 300 GHz)", Health Physics, vol. 74, 1998.

Radiofrequency Multielectrode Ablation Catheter with Temperature Controlled Gain and Phase for each Electrode

B. M. Hakim, M. S. Mirotznik, and B. L. Good

Catholic University of America, Department of Electrical Engineering and Computer Science, Washington, DC, USA

Email: hakim@umd.edu

Radiofrequency (RF) catheter ablation therapy has been recognized as an effective treatment for cancer and a variety of cardiac arrthythmias [1]. A Novel RF multielectrode ablation catheter is presented where the heating pattern, and hence the lesion size and relative location, is controlled by temperature sensors at pre-selected locations. The amplitude (gain) and phase of the RF input signal to each electrode is independently controlled. Temperature measurements are fed to a microcontroller that adjusts the gain and phase to each electrode independently to change the heating pattern. Figure 1 shows a general block diagram of a temperature-controlled multielectrode ablation catheter. Finite Element Method (FEM) analyses are utilized as a numerical tool to determine the temperature-controlled heating pattern of the RF multielectrode ablation catheter [2]. FEM models and current density measurements are used for input parameter design namely gain and phase of the RF input signal at each electrode. The change in temperature (T), measured in kelvin (K), during ablation at any point in the body is given by the bioheat transfer equation (1)

$$\rho c \frac{\partial T}{\partial t} = \nabla . k \nabla T + \mathbf{J}.\mathbf{E} - h_{bl}\left(T - T_{bl}\right) - Q_{el} \qquad h_{bl} = \rho_{bl} c_{bl} \omega_{bl} \tag{1}$$

where ρ is density (kg/m^3), c is specific heat ($J/(kg.K)$), k is thermal conductivity ($W/(m.K)$), $\mathbf{J}$ is the current density (A/m^2), $\mathbf{E}$ is the electric field intensity (V/m) calculated using the Laplace equation, ρ_{bl} is the blood density (kg/m^3), c_{bl} is the blood heat capacity ($J/(kg.K)$), ω_{bl} is the blood perfusion (s^{-1}), T_{bl} is the blood temperature (K), and Q_{el} is the heat exchange between the tissue and the electrode (W/m^3), usually negligible. The Specific Absorption Rate (SAR), measured in (W/kg), is defined as in (2). SAR is an important parameter in defining the tissue-heating profiles.

$$\mathrm{SAR} = \left(\rho^{-1}\right) \mathbf{J}.\mathbf{E} \tag{2}$$
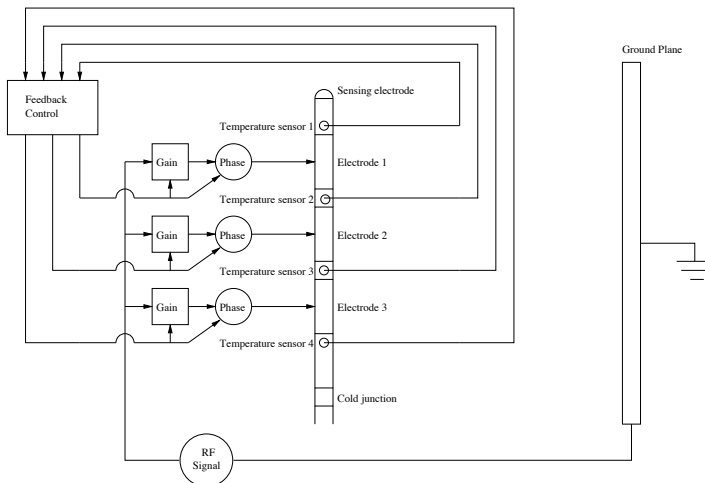
Fig. 1 – Block diagram of an RF Multielectrode Ablation Catheter

References

1. D. Panescu, S. Fleischman, J. Whayne, D. Swanson, M. Mirotznik, I. McRury, and D. Haines, "Radiofrequency Multielectrode Catheter Ablation in the Atrium," *Physics in Medicine and Biology*, vol. 44, pp. 899–915, 1999.
2. S. Tungjitkusolmun, D. Haemmerich, H. Cao, J. Tsai, Y. Choy, V. Vorperian, and J. Webster, "Modeling Bipolar Phase-Shifted Multielectrode Catheter Ablation," *IEEE Transactions on Biomedical Engineering*, vol. 49, no. 1, 2002.

Oral Presentations

Theoretical and Experimental Results for an Electric Field Applicator Used in Oncology Hyperthermia

C.J. Trujillo, L. Leija, A. Vera.

Department of Electrical Engineering, CINVESTAV-IPN, Mexico D.F., México

E-mail: ctrujillo@cinvestav.mx

Electromagnetic hyperthermia equipment consists of one system for radiation and another for thermometry. One of the most important parts of the equipment is the applicator since it determines the area of heating and the depth of penetration, among other parameters. In this paper, we present a rectangular waveguide as applicator. The waveguides used in applications of communications are filled with air and their dimensions are large, for this reason it is not possible to use them in medical applications; therefore, it is necessary to introduce another dielectric inside of waveguide in order to reduce dimensions.

This paper describes a process for modeling and for validation of an applicator of electric field for its use in oncology hyperthermia in order to obtain the necessary characteristics for this kind of therapy like dimensions, focused energy, and applicator capability of achieving increases of temperature in phantom (substitute of tissue). In the model carried out by the finite element method and the experimental characterization, we showed distributions of temperature and electric field inside the phantom.

The first part of the paper describes the mathematical design of applicator; in this process, different dielectrics were studied for their use inside the applicator in order to reduce the dimensions and obtain focusing of energy in the tumor region. It was necessary to choose the ideal frequency to achieve a penetration depth approximately of 6 cm. The material chosen for this intention was deionized water and the frequency was 200MHz. The final waveguide dimensions were 8.5 cm x 4.2 cm x 16.9 cm.

In the second part, it was carried out a model by using the finite element method. The modeled is based in Maxwell's and Bioheat equations because these govern the radiation of electromagnetic systems and the Bioheat equation relates directly the generation of electric field generated by RF with the heating of tissue. The parts of the modeled system were defined (applicator, antenna, container of the Phantom and phantom). Taking advantage of the symmetry of the problem, a simplification was realized and a model was carried out in 2D and axial symmetry. The Maxwell equations, boundary and subdomain conditions that govern the system were defined. Finally, distributions of electric field and temperature were obtained.

This paper also describes the construction and characterization of the applicator. After designing and construction the applicator, it is important to know its characteristics, so it can be used in oncology hyperthermia. Calorimetric measurements have to be done to determine the increases of temperature obtained when the waveguide is radiating. Finally, an electric distribution has to be determined, so it can be used to calculate some important parameters for physicians, as for example penetration depth, effective field size, and radiation pattern. Finally, we present the comparative study of the obtained results, theoretical and experimental.

The importance of the treatment modelling as a tool in oncology hyperthermia comes from the impracticability to obtain detailed temperature measurements throughout treatment region, particularly from depth seated tumors and due to the degree of variability among patients; also, it is important because is not necessary a lot of time, a big effort or an expensive laboratory.

References

1. Van Der Zee J., Koper P.C.M, and Van Rhoon G.C., "Re-irradiation and hyperthermia for recurrent breast cancer in the orbital region: a case report", *Int. J. Hyperthermia,*, vol. 20, No.1, pp. 1-6, 2004.
2. Blake, Lamont V., "Transmission lineas and waveguides", USA. John Wiley & Sons, Inc. 1969, Pag. 99-141.
3. Collin, Robert E., "Field theory of guided waves", New York. IEEE Press. 1991.
4. P.R. Stauffer, F. Rossetto, M. Prakas , D.G. Neuman and T: Lee, "Phantom and Animal Tissues for Modelling the Electrical Properties' of Human liver", *Int. J. Hyperthermia*, vol. 19, No. 1, pp. 89-101, 2003.

Millimetre-Wave Extra Low Radiation Measuring System for Environment and Biomedical Applications

Y. Savenko [1], V. Vodotovka [2], Y. Skrypnik [2] and F. Repa [1]

[1] *National Technical University of Ukraine "Kyiv Polytechnic Institute", Kyiv, Ukraine*
[2] *Kyiv National University of Technology and Design, Kyiv, Ukraine*

E-mail: yaroslav_savenko@ieee.org

This paper reports results of the research work on development of techniques and devices for measuring of extra low radiation in mm-range. This radiation is widely used for investigation of environment and medical diagnostics of human physiological state. There are considered basic engineering aspects of measuring extra low mm-range radiation in the paper. It is also described an original measurer that helps researchers to get more clear understanding about environment physics and biomedical physiology, how low energy mm-range radiation interacts with human organism. Certain applications have been proposed for the measurer as for testing calibrating and diagnostic devices.

This paper should be considered as a current completed step in the research process of a role of extra low mm-range radiation on environment and human being as well. At this step a previous mm-range extra low radiation measuring and medical experience had been analytically summarised. This analysis made possible to accept an assumption how we are able to measure (investigate) mm-wave influence on objects and human organism as well. It should be noticed that only extra low radiation was taking into account.

There was the main problem, that it was required to measure radiation at the noise level and even lower him. That is why the main task had been decided how these measurements must be provided. An original measurer has been developed for investigations above mentioned. For example spectral density of impact avalanche transit time (IMPATT) diodes amounts 10^{-12}-10^{-18} W/Hz at 4.8-5.7 mm wavelength range. Self-radiation of human organism amounts 10^{-21}-10^{-22} W/Hz. Measuring of this level of radiation requires the development of special techniques and devices. It has been measured noise powers for used IMPATT diodes by original device. It should be noticed that noise spectral power density is different for these IMPATT diodes. This difference is not essential and all of them have the same order of noise spectral power density in 10^{-19} W/Hz.

Proposed measuring system consists of subsystem of reflected or/and self radiation scanning and subsystem of hardware-software processing scanned data from the object. Subsystem of hardware-software scanned data processing consists of multichannel correlation receiver, receiver to PC junction and program of analyzing and indication of scanning results. Main part of hardware system is multichannel correlation receiver, where it is operated correlation comparison of test signals and signals obtained during scanning process. Test signals are obtained previously for certain conditions of certain object and they are saved as special test data.

The measurer helps researchers to get more clear understanding about environment and biomedical physics, in particular, how low energy mm-range radiation interacts with human organism. In medical practice it could be used as diagnostic device and calibrating unit of therapeutic low energy mm-range device as well

In conclusion we must determine that getting of regulate statistic data of medical engineering investigations at different levels of complexity from a cell to a whole organism will be the next step in the way to make clear understanding about the role of low energy mm-range EMW in human life.

References

1. Savenko Y.V., Bogomolov N.F., Zinkovsky U.F. The Using of Laser and mm-range Radiation in Biomedical Diagnostics and Therapy // Proc. Euro Electromagnetics. – Edinburgh (Scotland). – 2000. – P.100.
2. Savenko Y.V., Pravda V.I., Bogomolov N.F. Investigation of Positive Effects on Human Organism with Action of Noise Radiation of IMPATT Diode and Low Energy He-Ne Laser // Proc. International Symposium on Electromagnetic Compatibility. – Montreal (Canada). – 2001. – P.1058-1060.
3. Vodotovka V., Kashtanov S., Repa F. Device for diagnostic internal organs of living being // Proc. Measuring and computing engineering in technological processes. – 1999. - ¹3. – PP 181-186.

HPEM - 35
Biological Standards and Medical Applications

Oral Presentations

Experimental Analysis of Corn Seed Germination Enhancement under the Application of Electromagnetic and Magnetic Fields

D. Sleper[1], M. S. Pathan[1], B. Camps-Raga[2], N. Boriraksantikul[2], S. Tantong[2], S. R. Gyawali[2], P. Kirawanich[2], and N. E. Islam[2]

[1]*Division of Plant Sciences, University of Missouri*
Columbia, Missouri, USA 65211
[2]*Department of Electrical and Computer Engineering, University of Missouri*
University of Missouri, Columbia, Missouri, USA
Email: IslamN@missouri.edu

Nowadays, there is an increasing interest in developing new techniques to improve the production of biofuels such as ethanol, not only as a renewable and inexhaustible source of fuel but also because it has a very low emission rate per gram, which makes it environment-friendly. Ethanol production from *maize*, also know as corn, is a widely used source for bioethanol, and is obtained by processing the product resulting from corn biomass fermentation.

Seed germination is already known to be affected by both the electric and magnetic fields from the earth itself, without the application of external electromagnetic radiation. Biological stimulation also plays an important role in optimizing corn crops in terms of the maximization of yield, promotion of plant growth, and protection against exogenous agents that cause plant disease, among others. Biostimulation can be accomplished by applying different techniques such as electromagnetic stimulation, magnetic stimulation, laser, ultraviolet (UV), gamma-rays, ultrasound or ionized radiation, application of the effect of "gold crossing" of electromagnetic fields and the principle of the "Keops pyramid", among others. The main advantage of using electromagnetic stimulation methods over traditional chemical processes is the absence of toxic residues. Previous research has been done in this field of study, with positive results in tomato [1], rice [2], barley [3], and lettuce [4] seed germination enhancement.

Three different methods are proposed here to analyze the effects of electromagnetic radiation techniques on corn seed germination, in an effort to prove the results from previous research. These techniques include seed exposure to i) moderately high frequency in a semi-anechoic chamber, ii) high frequency in a custom-designed transverse electromagnetic (TEM) cell, and iii) low-frequency magnetic field through the use of an in-house built single-axis Helmholtz coil system. These methods focus on the effects observed in seed germination after the application of an electromagnetic (first two techniques) or magnetic (last technique) field. The protocols followed during the experiments are based on the optimization of three parameters: frequency of operation, time of exposure and irradiating power. The purpose of the experiments was to organize the results in a 3D space (time, frequency, power) in order to compare and find the most efficient area of application to enhance corn seed germination.

Fig 1 – Helmholtz coil used for magnetic field analysis
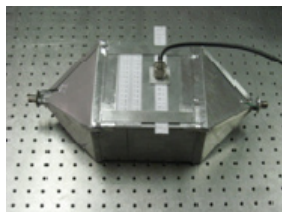
Fig 2 – TEM cell used for high-frequency analysis

References
1. A. De Souza, D. Garcí, L. Sueiro, F. Gilart, E. Porras, and L. Licea, "Pre-sowing magnetic treatments of tomato seeds increase the growth and yield of plants," Bioelectromagnetics, vol. 27, no. 4, 2006, pp. 247-257.
2. M. V. Carbonell, E. Martinez, and J. M. Amaya, "Stimulation of germination in rice (oryza sativa l.) by a static magnetic field," Electroand Magnetobiology, vol.. 19, no. 1, 2000, pp. 121-128.
3. S. Lynikiene and A. Pozeliene, "Effect of Electrical Field on Barley Seed Germination Stimulation", Agricultural Engineering International: the CIGR Journal of Scientific Research and Development, August, 2003.
4. F. G. Reina, L. A. Pascua, and I. A. Fundora, "Influence of a Stationary Magnetic Field on Water Relations in Lettuce Seeds, Part II: Experimental Results", Bioelectromagnetics, vol. 22, 2001, pp. 596-602.

Correction of Frequency-domain Measurements by Hilbert Transform

Lars Ole Fichte, Stefan Dickmann

Chair for Fundamentals of Electric Engineering,
Helmut-Schmidt-Universität - Universität der Bundeswehr Hamburg,
Holstenhofweg 85,D- 22043 Hamburg
E-mail: lars-ole.fichte@hsu-hh.de

The characteristics of a signal (f.i. an electromagnetic pulse) are often described by its spectral function in frequency domain, which is measured using either a spectrum analyser or a vector network analyser. The resulting spectrum is:

$$F(\omega) = R(\omega) + j\,I(\omega) \,\circ\!\!-\!\!\bullet\, f(t), \tag{1}$$

corresponding to the original signal *f(t)*.

If any outside signal is interfering with the correct measurement of the signal, the usual approach is to perform the measurment inside at RF proof environment. In cases where this is not possible (f.i. if a shielded chamber is unavailable), it is possible to reconstruct a segment of the spectrum if both real and imaginary parts are known. This is making use of the fact that the real and the imaginary parts of the spectrum are related to each other for causal signals, i.e. that the imaginary part is the Hilbert transform of the real part and vice versa. Thus, for a causal signals the relations between real and imaginary parts of the transfer function are [1]:

$$R(\omega) = \frac{2}{\pi} \int_0^\infty \frac{\eta\,I(\eta)}{\omega^2 - \eta^2} \, d\eta, \; I(\omega) = -\frac{2\omega}{\pi} \int_0^\infty \frac{R(\eta)}{\omega^2 - \eta^2} \, d\eta \tag{2}$$

if the measured spectrum is corrupted only in the range between the frequencies ω_1 and ω_2, one can derive two coupled integral equations from the relations between real and imaginary parts of the spectrum:

$$R(\omega) - \frac{2}{\pi} \int_{\omega_1}^{\omega_2} \frac{\eta\,I(\eta)}{\omega^2 - \eta^2} \, d\eta = A(\omega), \; I(\omega) = -\frac{2\omega}{\pi} \int_{\omega_1}^{\omega_2} \frac{R(\eta)}{\omega^2 - \eta^2} \, d\eta = B(\omega), \tag{3}$$

with known excitations *A(ω)* and *B(ω)* that can be computed from the non-corrupted part of the spectrum, and which leads to an system of linear equations for a number of discrete frequency inside the corrupted frequency range.

In our paper we will investigate how large the corrupted part of the spectrum may be for the method to give reasonable results.

References

1. F. M. Tesche, "On the Use of the Hilbert Transform for Processing Measured CW Data" IEEE Transactions on Electromagnetic Compatibility, vol. 34, No. 3, 1992.

HPEM - 36
Numerical & Statistical Methods (Invited)

Oral Presentations

Particle Regularization in PIC Simulations: A useful means of reducing numerical noise?

Steinar Børve[1,2] and Jan Trulsen[2]

[1]*Norwegian Defence Research Establishment, Kjeller, Norway*
[2]*University of Oslo, Oslo, Norway*

E-mail: Steinar.Borve@ffi.no

Numerical simulations using the **Particle-in-cell** (**PIC**) method [1] have in the past played a vital role in understanding the fundamental physics of vacuum tubes in general, and HPM devices in particular. Today this numerical tool is commonly used in designing new and improved devices [2-3]. The method uses a "first-principle" description where the spatial information is calculated and stored on grid nodes. Information concerning the velocity distribution of the plasma, on the other hand, is stored on nodes which can be viewed as representative macro-particles. The macro-particle description makes **PIC** a statistical method where the inherent noise decreases inversely with the square root of the particle number. In other words, reducing the numerical noise in **PIC** simulations is costly in terms of the number of macro-particles. **PIC** has for this reason been regarded as a computationally demanding technique. To reduce the overall computational cost, it has been suggested to replace the simple **PIC** particles with more complex particles that better can describe the properties of the local distribution function [4], thus removing oneself from the statistical approach. Others have looked into merging and splitting of particles as a means of (a) reducing numerical noise in general, (b) adopting the particle description to a situation where the grid data is non-uniform, and (c) increasing or decreasing the accuracy in regions and specific velocity ranges where this might be desirable [5].

A somewhat related method called **Smoothed Particle Hydrodynamics** (**SPH**) utilizes a particle-only description to simulate the dynamics of neutral fluids [6]. In an attempt to improve the accuracy and reduce the numerical noise of **SPH** simulations, an extension to **SPH** known as **Regularized SPH** (**RSPH**) has been proposed that enables redefining the entire particle distribution at temporal intervals [7]. The **RSPH** techniques make it feasible to use particles with widely different masses in the same simulation. This opens for a numerical description that to a high degree adapts itself to the temporal and spatial variations in the problem being solved. In this work, we explore to what extent **PIC** simulations can benefit from a similar approach incorporating particle regularization. In particular, we consider conservation of the first 3 moments of the particle distribution. We will discuss whether or not a "deterministic" or low-noise **PIC** description can be achieved, in much the same way as **RSPH** can be regarded as a low-noise version of **SPH**. The possibilities of using **SPH** techniques for calculating spatial quantities such as charge density and current density is considered and compared to the standard approach of projecting the charge of the particles directly unto the grid. Finally, we conclude this preliminary investigation by pointing out the future potential of this new approach in simulating HPM sources.

References
1. C. K. Birdsall and A. B. Langdon, Plasma Physics via Computer Simulation. New York: McGraw-Hill, 1985.
2. J. W. Eastwood, K. C. Hawkins, and M. P. Hook, "The Tapered MILO", IEEE Transactions on Plasma Science, vol. 26, 1998.
3. W. Jeon et al., "Output Characteristics of the High-Power Microwave Generated from a Coaxial Vircator With a Bar Reflector in a Drift Region", IEEE Transactions on Plasma Science, vol. 34, 2006.
4. G. G. Coppa et al., "Blob Method for Kinetic Plasma Simulation with Variable-Size Particles", Journal of Computational Physics, vol. 127, 1996.
5. G. Lapenta, "Particle Rezoning for Multidimensional Kinetic Particle-In-Cell Simulations", Journal of Compuational Physics, vol. 181, 2002.
6. J. J. Monaghan, "Smoothed Particle Hydrodynamics", Reports on Progress in Physics, vol. 68, 2005
7. S. Børve, M. Omang, and J. Trulsen, "Regularized smoothed particle hydrodynamics with improved multi-resolution handling", Journal of Computational Physics, vol. 208, 2005.

Finding the best Coupling Incidences with the Reciprocity Theorem

J.-P. Adam[1], J.-C. Joly[2], B. Pecqueux[2], D. Asfaux[1]

[1]*IEEA, Courbevoie, France*
[2]*Centre d'études de Gramat DGA/DET/CEG, Gramat, France*

E-mail: jean-pierre.adam@club-internet.fr

The reciprocity theorem is a powerful simplification tool in electromagnetism. For example, the behavior of a receiving antenna can be deduced from the incident plane wave and the behavior of the antenna when it is transmitting. The reciprocity theorem is often derived in the frequency domain (cf. [1]). A direct application in the time domain with the FDTD software GORF3D is presented in this paper.

The time derivative of the open-circuit voltage in the receiving case is proportional to the radiated field in the transmitting case when the system is fed by a current source. A similar relationship can be established between the short-circuit current in receiving mode and the radiated field when the system is fed by a voltage source. In addition, if a small dipole acting as an electric field sensor is considered, the reciprocity theorem may be used to computed the electric field at a point of the system.

The time domain applications of the reciprocity theorem are usually found in the field of the UWB antennas (cf. [2]). The fig. 1 presents an EMC application : the maximum value of the received open-circuit voltage is considered. The influence of the direction of incidence is investigated. Only one run was used to compute all the directions. Compared to the case of one run per incident plane wave, the required CPU time is almost 300 times lower in that example, despite the time consuming near to far field transformation.
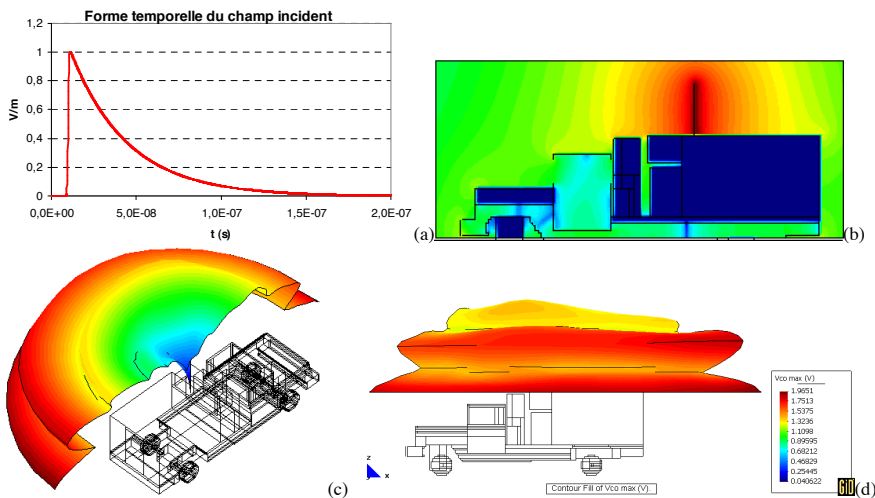
Fig. 1 – (a) waveform of the incident field. (b) electric field (log scale) radiated on a truck by a vertical wire fed with a current source (snapshot of the FDTD simulation). (c) and (d) maximum value of the open circuit voltage at the wire fed point as function of the direction of incidence (vertical polarization). The results (c) and (d) are deduced from (b) by using the reciprocity theorem directly in the time domain.

References

1. S.W. Lee, "Theorems and Formulas", in *Antenna Handbook, Antenna fundamentals and mathematical techniques*, vol. 1, chap. 2, Edited by Lo and Lee, Chapman & Hall, 1993.
2. Glenn S. Smith, "A Direct Derivation of a Single-Antenna Reciprocity Relation for the Time Domain", *IEEE Trans. Antennas Propagat.*, vol. 52, no. 6, pp. 1568- 1577, June 2004

HPEM - 36
Numerical & Statistical Methods (Invited)

Oral Presentations

HPEM - 36
Numerical & Statistical Methods (Invited)

Oral Presentations

Statistical electromagnetic field distribution assessment in a spacecraft cavity by numerical simulation

Y.Herlem[1], A.Schaffar[1], P.Pelissou[2], L.Trougnou[3]

[1]*EADS Astrium Space Transportation, Les Mureaux, France*
[2]*EADS Astrium Satellites, Toulouse, France*
[3]*ESA-ESTEC, Noordwijk, The Netherlands*

E-mail: yannick.herlem@astrium.eads.net

The present paper reports the main results of a basic study dealing with the statistical field distribution assessment in a satellite complex cavity stimulated by high frequency power leakages. It is performed by a set of 3D numerical simulations. The results shall be considered as a reference for the assessment of the oversized cavity theory frequency limits.

The study is based on a generic telecom satellite. Its overall size is $2,30 \times 1,84 \times 1,80 \text{ m}^3$, it is made of aluminium and features 2 coupled cavities limited by a central tube. The computation strategy has led to the use of a Finite Differences in the Time Domain code which solves directly the Maxwell equations in a Cartesian grid. It is the most efficient tool for such a wide band study, at least from the computation time point of view.

The outputs of the code are the 3 components of both electric and magnetic fields on 2000 points randomly distributed in the cavity which is excited by a derivative Gaussian wide band pulse. The frequency analyses require performing a Fourier transform on the time domain rough results, and then a statistical processing of the frequency domain results in order to determine the PDF (probability density function), the standard deviation and the mean value of the spatial electric field distribution.

The meshing comprises about 10^8 cells the dimensions of which being 4,5 mm. This leads to a high frequency limit of about 7 GHz.

The main goals of the numerical study described in this paper are to assess :
- the lower and upper limitations of the frequency range in which the mock-up behaves as an oversized cavity,
- the level of homogeneity and isotropy of the electric field with respect to frequency,
- the effects of apertures surface,
- the effects of cavity geometry by adding metallic boxes simulating the electronic units,
- the spatial limitations w.r.t. frequency,
- the effects of absorbing materials on the homogeneity and the isotropy of the electric field and on the average energy density in the cavity.

The main conclusions of this study are the following ones :
- For all cases the homogeneity of electric field is quite good, particularly beyond 1 GHz.
- On the contrary the results showed in almost all cases a relatively strong anisotropy of electric field on the whole frequency range, except when the mock-up is partially filled with 12 metallic boxes, which increase the geometric complexity of the cavity.
- As far as the frequency limitations of the behaviour as an oversized cavity are concerned the lower limit seems to have been identified near 800 MHz, but the upper limit could not be found because it is certainly out of the computable frequency range of 7 GHz.
- The apertures surface has no sensible effect on the electric field unless they are of the same order as the whole surface of the cavity.
- Near the walls in a thin layer whose thickness is proportional to the wavelength the behaviour of the field does not anymore match with the theoretical statistical behaviour of a complex oversized cavity.
- The behaviour of the mock-up as an oversized cavity gets worse when adding absorbing materials inside.
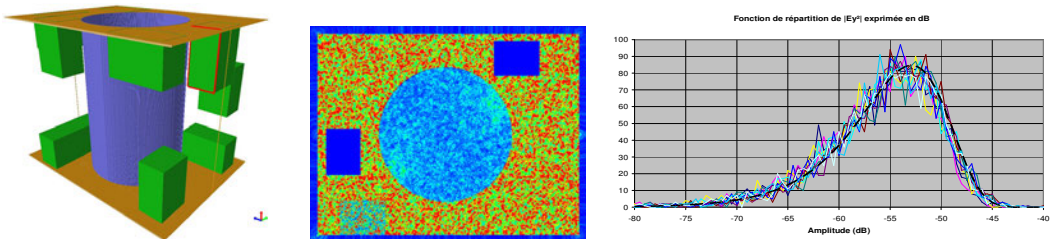
Fig. 1 – Model without walls, field distribution in time domain at 200 ns and PDF of 10 frequencies

Calculation of the input impedance of thin wire antennas

A.Berthon[1], Y. Beniguel[2]

[1]*Admittance, Sceaux, France*
[2]*IEEA, Courbevoie, France*

E-mail: aberthon@)club-internet.fr

Wire antennas are frequent in the HF domain, with radius *b* which may be as small as 10**-5 in terms of wavelength. When computing the input impedance by the method of moments with the usual approximations it is observed that the calculation becomes unstable in this situation, as the results, especially for the imaginary part, strongly fluctuate depending on the discretization of the relevant integral equation. The aim of this paper is to describe the instabilities, explain them and propose better numerical approaches. Commonly the impedance is obtained by solving an EFIE along the wire, the unknown current being expanded on a set of basis functions and the voltage at the right-hand side taken as 1 on the excitation gap and zero elsewhere. The basis functions are generally translated copies of a given function with compact support; the number of patches gives the size of the impedance matrix Z which relates the electric field along the wire to the current density. The input admittance is the diagonal element of the inverse of Z corresponding to the patch at the excitation point. Using Galerkin expansions, the matrix elements are given by

$$Z_{mn} = -ika \int \exp(-ikr)/4\pi r \left[f_m(s') f_n(s) - df_m/ds(s') df_n/ds(s)/k^2 \right] ds ds' d\alpha \qquad (1)$$

With $r = \sqrt{(s-s')^2 + 4a^2 \sin^2(\alpha/2)}$ and *a* is the radius, f_n the basis functions for patch *n*, α the azimut and there is a double integration over the wire. We studied several numerical schemes, including the thin wire approximation $r = \sqrt{(s-s')^2 + a^2}$, and different basis functions; an example of the results is given on Figure 1, where the functions are sinusoidal and their number varies with the abscissa; C0 to C2 denote formulations using different orders of derivative and 'fil' the thin-wire approximation. One reason for the dispersion is that the ratio $|s-s'|/a$, which governs the angular integration, varies from zero to almost infinity and no single approximation is valid on the entire domain. However the main cause is that for all numerical schemes the condition number of the matrix is very poor and deteriorates when the radius decreases. We relate this fact with the non-uniformity of the singularity of the integral equation and we investigate alternative approaches of the modeling of the source at the excitation gap.
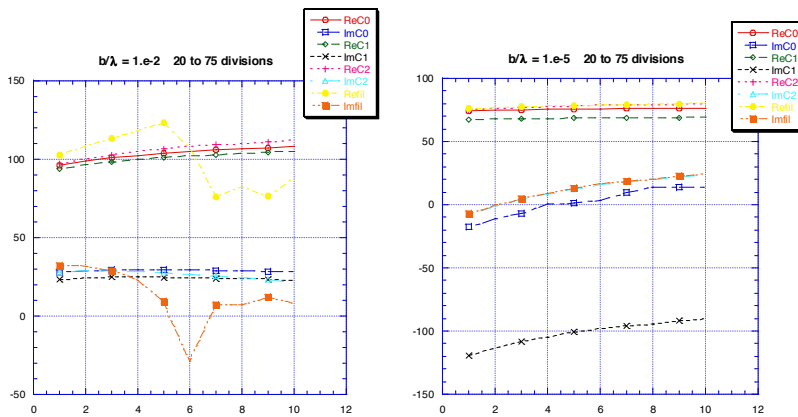
Fig. 1 –Impedances (real and imaginary parts) for different numerical schemes

Fast Computation of Singularity Expansion Method Parameters and the exterior EMC problem of three-dimensional complex scatterers

F. Gronwald and R. Janssen

EADS, Defence & Security, Military Air Systems
OPEM 24 Electromagnetic Effects & Hardening, 85077 Manching, GERMANY
E-mail: Frank.Gronwald@eads.com

For the EMC analysis of complex systems it is often meaningful to distinguish between the exterior and the interior electromagnetic problem [1]. The exterior problem mainly consists of the determination of surface currents and charges on the outermost surface of the complex system under investigation. In this context, it is of major interest to know the natural resonances of the system in order to identify exterior electromagnetic excitations which might lead to resonating surface currents. Mathematically, this problem is best formulated within the framework of the Singularity Expansion Method which defines the notion of exterior natural resonant frequencies, that also are called natural poles, of electromagnetic scatterers [2]. Techniques to determine these natural poles for canonical scatterers already have been investigated for many years and still are a subject of current research [3], [4]. To also investigate scatterers of complex shape it is possible to use frequency domain scattering data which can be obtained from numerical software tools. Then the task is to fit a transfer function to these data in order to obtain the location of the natural poles [5].

In this contribution, we investigate and compare several techniques to numerically determine the natural poles in an efficient way, such as frequency-derivative sampling and multi-frequency sampling. As frequency domain scattering data we will use the results of method of moment calculations that characterize electromagnetic scattering of three-dimensional bodies that are composed from elementary geometric building blocks, such as cylinders or cones. The analysis will be complemented by an inspection of the surface currents and charges that correspond to the natural poles and which might be problematic from an EMC point of view.

References

1. F. M. Tesche, M. Ianoz, and T. Karlsson, EMC Analysis methods and computational models. New York: Wiley Interscience, 1997.
2. C.E. Baum, "The singularity expansion method," in Transient Electromagnetic Field, L.B. Felsen, Ed. New York: Springer Verlag, 1976, pp. 129—179.
3. F.M. Tesche, "On the Analysis of Scattering and Antenna Problems Using the Singularity Expansion Technique," IEEE Transactions on Antennas and Propagation, vol. 21, 1973, p. 53—62.
4. L. Li and C.-H. Liang, "Analysis of resonance and quality factor of antenna and scattering systems using complex frequency method combined with model-based parameter estimation", Progress in Electromagnetics research, PIER 46, 2004, 165—188.
5. J. Chauveau, N. de Beaucoudrey, and Joseph Saillard, "Selection of Contributing Natural Poles for the Characterization of Perfectly Conducting Targest in Resonance Region", IEEE Transactions on Antennas and Propagation, vol. 55, 2007, p. 2610--2617

Influence of the Exhaust Plume on the Lightning Induced Voltage and Current on an Airborne Vehicle

S. K. Nayak and M. Joy Thomas
Department of Electrical Engineering
Indian Institute of Science, Bangalore, India
E-mail: jtm@ee.iisc.ernet.in

Airborne vehicle and its payload are extremely expensive and their loss as a result of a lightning strike is highly undesirable. So in this age of all weather usage of airborne vehicles, it has become necessary to understand the behaviour of an airborne vehicle with its exhaust plume when illuminated with strong electromagnetic fields generated by a nearby lightning stroke as shown in figure 1. When the electromagnetic field gets coupled with the vehicle, current is induced on the skin of the vehicle body which inturn can lead to mission getting aborted. The presence of the ionized exhaust plume can altercate the induced current and voltage on the skin of a perfectly conducting rocket body.

In this paper, an attempt has been made to study the time domain characteristics of the induced voltage (figure 2) and current (figure 3) on an airborne vehicle when the transient field generated by a nearby lightning discharge is incident on it. For the computation, finite difference time domain (FDTD) technique has been used. The distributed electrical parameters in each section of the launch vehicle and its exhaust plume along the axis are computed using method of moments (MoM). The computation has been done for the case when the vehicle has been just lifted off and the end of the exhaust plume is at a height of 10m above the ground. The height of the airborne vehicle is chosen as 10m and its plume length is assumed to be 40m. The conductivity of the plume has been assumed to be exponentially reducing along the plume axis from the exit plane of the vehicle. The results shown are for a peak lightning current of 30 kA with a maximum di/dt of 40kA/μs and the vehicle is at a distance of 250m from the lightning channel. The results show that the presence of exhaust plume will enhance the induced voltage and current on the vehicle body by several factors as shown in the figures 2 and 3. $|\Delta V_{max}|$ and $|I_{max}|$ shown in figures 2 and 3 are for each section of the airborne vehicle and its exhaust plume.
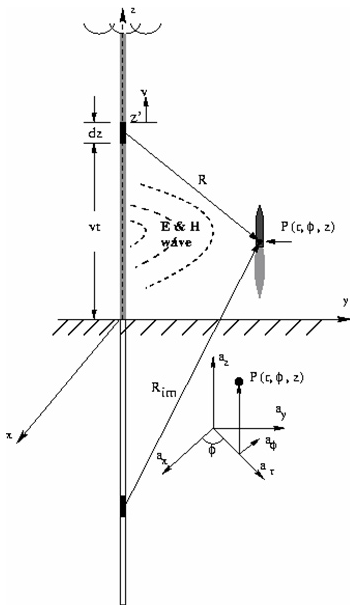
Fig. 1. Geometry of the lightning channel
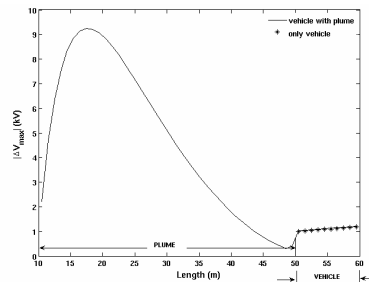
Fig. 2. Variation in induced voltage along the length of the vehicle and its exhaust plume
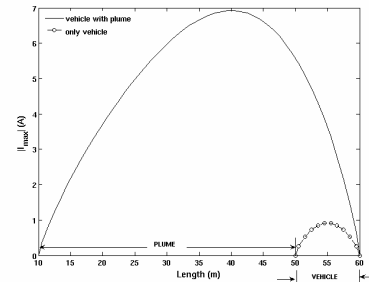
Fig. 3. Variation of the peak magnitude of the induced current along the length of the vehicle and its exhaust plume

HPEM - 37
Coupling to Cables and Structures

Oral Presentations

A New approach for the Analysis of Electromagnetic Coupling between the Lightning and 3D Metallic Structure

B Harrat[1], B Nekhoul[1] , K Kerroum[2] and K EL Khamlichi Drissi[2]
[1]LAMEL Laboratory, University of Jijel, BP N° 98 Ouled Aissa, 18000 Jijel, Algeria.
[2] LASMEA Laboratory, Blaise Pascal University, 24 Avenue des landais, 63177 Aubière, France
E-mail: {Harrat, nek_cem}@mail.univ-jijel.dz

During lightning, the high current intensity of the stroke channel causes intense electromagnetic (EM) emission responsible to many disturbances after coupling between metallic structures and radiation. More frequently, the power network is responsible of the conducted disturbance in case of this indirect effect by EM coupling with power lines and cables. Also, the building realised with metallic structure is target by EM field emitted during lightning stroke. Generally, the electric and electronic devices are located inside the 3D metallic structures, where is developed induced current and voltage under the effect of EM coupling. During lightning stroke near residential area, the EM environment inside the building is significantly influenced by the induced currents distributed in metallic structures. In order to guarantee the immunity of the electric and electronic components it is necessary to characterize the EM environment in the building. For this objective, one of the priorities is the study of the EM transient behaviour of a 3D metallic structure subjected to indirect impact of the lightning strike. In order to evaluate induced voltages and currents in transmission lines, cables, electric towers, … illuminated by an EM wave emitted during lightning strike, different works according to the geometric nature of the metallic structure are proposed in the literature. Traditionally two approaches are used to treat these problems:
- resolution of the integral equation by moment method (antenna theory) [1],
- analytical or numerical resolution of the transmission line equations with second member.
The antenna theory permit to treat the EM coupling problem in frequential [1] with great rigour but it numerical implementation is not easy and require using the Fourier transform for studding in time domain and time consuming.
The purpose of our work is to show that the problem of coupling of the lightning with 3D metallic structure (fig.1) can be treated directly in temporal by numerical tools simpler to implement based on the Agrawal's model [2]. Not that, Agrawal model is developed under transmissions lines assumptions for the study of the coupling between EM wave and lines. Our approach consists in the direct resolution by FDTD (Finite Difference Time Domain) of differential equation in potential spatio-temporal in 3D, while taking into account the semi-infinite environments and the conditions at extremities. Note that, the 3D propagation equation is deducted after some mathematical transformations using the Agrawal's model [2]. For calculating the induced voltage in the structure we deduced and solve matrix equation obtained after the numerical discretization by FDTD of potential propagation equation; the induced current is calculated by numerical integration of the line current equation.
In order to illustrate and validate our approach, we propose to simulate a tree dimensional metallic structure illuminated by lightning channel (fig.1). The 3D metallic structure is realised with an aerial part and a buried part linked by vertical conductors. For this application we compare the results obtained by our development to those realised by NEC4 software based on antenna theory [3].
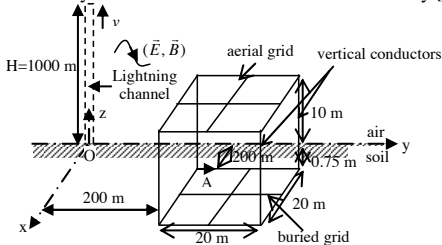
Fig.1. A 3D structure illuminated by lightning channel.
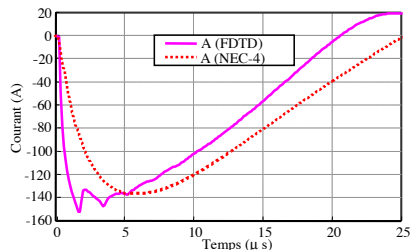
Fig. 2. Transient induced currents in branch A of the grid.

Fig. 2 shows the comparison between the transient induced current in branch A realized by our approach directly in time domain end NEC-4 software [3] in frequency domain and transposed in temporal by Fourier transform.

References
1. F. Dawalibi, and W. Xiong, "Transient performance of substation structures and associated grounding systems", IEEE, Trans. On Industry Applications, Vol.31, No, 3, May/June 1995, pp. 520-526.
2. A. K. Agrawal, H. J. Price, S. H. Gurbaxani, "Transient response of muulticonductor transmission lines excited by a non uniform EM field", IEEE Trans. On EM Compatibility, EMC-22, pp. 119-129, 19803.
3. NEC-4, Numerical Electromagnetic Code, JANUARY 1992.

EMP Transfer Function Measurements and Stress Predictions for Commercial Office Buildings

K.L. Rice, J.I. Lubell

L-3 Jaycor, Colorado Springs, USA

...

jerry.lubell@l-3com.com

The objective of the work reported in this paper was to estimate the HEMP stresses coupled onto wires and conductors inside commercial office buildings. The estimates were based on transfer functions measured using continuous wave immersion test methods, combined with analytical extrapolation using the measured transfer functions to predict EMP response to incident HEMP fields.

Transfer function measurements were made on three different commercial buildings:

> 1. A large warehouse-type structure housing an electromagnetic effects laboratory.
>
> 2. A modern, three-story office building with large windows, and concrete panel and steel frame construction.
>
> 3. An older style glass and concrete, single story office building.

The test approach was continuous wave immersion with transfer functions measured at approximately 800 frequencies spanning the range from 100 kHz to 1 GHz, and with dynamic range in excess of 130 dB over most of the range. This frequency span and dynamic range combination allows the measured transfer functions to be used with various HEMP field specifications to estimate the current coupled to conductors inside the buildings. In all, approximately 130 transfer functions were measured, allowing estimation of approximately 130 currents inside the commercial office structures. The transfer functions were measured for both horizontally and vertically polarized incident fields, and with the transmitting antenna located at several different positions to provide good field coverage and some sensitivity to orientation of the wave relative to the buildings.

A typical time domain current history, and a histogram of peak currents estimated for one of the buildings is shown in Figures 1 and 2 respectively.
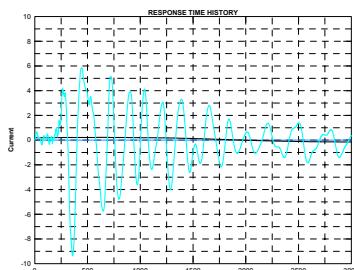
Figure 1. Sample Office Building Transient Response
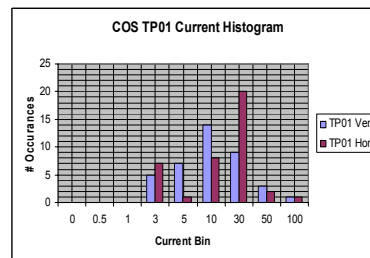
Figure 2. Histogram of Peak HEMP Currents in a Commercial Office Building

HPEM - 37
Coupling to Cables and Structures

Oral Presentations

High-frequency Electromagnetic Field Coupling to Scatterers in Rectangular Resonators

S. Tkachenko[1], H.-G. Krauthäuser[1], J. Nitsch[1], F. Gronwald[1] and G. Vodopianov[2]

[1]*Otto-von-Guericke-University Magdeburg, Germany*
[2]*Radio Research&Development Institute, Moscow, Russia*

E-mail: sergey.tkachenko@ovgu.de

The analysis of high-frequency electromagnetic field coupling to different kind of scatterers, like, e.g., linear structures, equipment and components which might be caused by intentional electromagnetic interference, for example, HPM or UWB – pulses, becomes increasingly important. Usually, related test experiments and corresponding simulation models deal with devices that are located in free space. In reality, however, electronic equipment often is enclosed in different kinds of resonator-like structures, such as cabinets of computers, airframes, frames of cars, etc. These enclosures considerably modify the interaction between electromagnetic fields and scatterers.

Often these scatterers are electrically small but still can have own resonances. For the situation of free space, common-mode currents induced in such objects can be evaluated by the model of a small (near–resonance) linear antenna [1]. In our paper [2] we proposed a method to analyze coupling to electrically small scatterers (dipole antennas) in resonators (Method of Small Antenna, MSA) by consequent use of scattering theory. This method is an electro-dynamical variant of the method of zero (small) radius potential in quantum mechanics [4]. The method of MSA is based on the analysis of the integro-differential equation describing the induced current in the neighborhood of the antenna. The corresponding resonator Green's function is split into two parts: a singular and a regular part. The singular one is connected with electrostatic and magnetic energy saved in the neighborhood of the antenna and coincides with the singular part of the Green's function in free space. The regular part is connected with the far field and contains all information about system's resonances. Of course, there are differences between the free space and resonator Green's functions. However, for both cases the regular part is constant in the neighborhood of the antenna. This circumstance gives the possibility to analytically express the solution for the coupled current in the small antenna from the solution in free space and to investigate the input impedance of the small antenna, the current transfer ratio for two small antennas, the coupling of penetrated radiation to a small antenna, etc.

In this paper, the results of the developed MSA were compared to measurements of the input impedance of a small antenna inside a resonator and the mutual coupling coefficient between two dipole antennas, which were performed in the mode stirred chamber at the University of Magdeburg, where the stirrer was removed. The comparison shows a good agreement for lower resonances where the considered antennas are still electrically small and the MSA is still applicable.

Another important problem is the investigation of the scattering of electromagnetic fields inside chambers with mechanical mode stirrers. In this case the stirrers have to be electrically large to provide a good stirring of electromagnetic fields inside the chamber. However, the developed method of an electrically small antenna advances the calculation technique for electrically large piece-plane scatterers inside resonators. To do that, in a first step, we split one plane scatterer into an equivalent set of small dipoles. The proper values of the polarizability tensor of an elementary dipole and the periods of the grid can be found by comparison of the known analytical solution of the problem for the infinite plane itself and for the periodical grid of dipole scatterers, which substitutes the plane. Next, we begin to build a MOM – like method, with unknown dipole moments of sub-elements. For the calculation of the non-diagonal interaction elements the well known resonator Green's function (in the double sum representation) and for the diagonal elements the results from above for the response function of a small dipole in the cavity are used. As usual, the unknown dipole moments can be found by solving a linear system of algebraic equations. Using the resulting dipole moments we can find and investigate distributions of scattered fields in the resonator. By means of the described algorithm we have developed a computer code and made some investigations of statistical properties of fields in the mode stirred chamber. The results of simulation have shown that the statistical distribution of the electrical field components inside the chamber satisfies the xi-square distributions, which is well known from the general theory of MSC.

References
1. V.I.Kravchenko, E.A.Bolotov, N.I.Letunova, Communication facilities and powerful electromagnetic interferences. Moscow: Radio i sviaz, 1987 (in Russian).
2. S.Tkachenko, G.V.Vodopianov, L.M.Martinov, "Electromagnetic field coupling to an electrically small antenna in a rectangular cavity", 13th Int. Zurich Symp. on EMC, Feb. 1999, pp.379-384.
4. Yu. N. Demkov and V. N. Ostrovskii, Zero-Range Potentials and their Applications in Atomic Physics, Plenum Press, New York (1988).

Numerical Research for the Generation Mechanism and Coupling Effects of HEMP

C. MENG，Y. SH. Chen, J. P. Chen,Y N Liu

Department of Engineering Physics, Tsinghua University , Beijing 100084, China
...
E-mail: mengcui@mail.tsinghua.edu.cn

Enrico Fermi has predicted the generation of electromagnetic field due to nuclear burst before the Trinity explosion[1]. The high altitude electromagnetic pulse (HEMP) will disable the electric equipments, communication system and control systems. In metal shielding objects, electronic equipment may well evade electromagnetic interference, but antenna window or cable channel are inevitably left and the electromagnetic field will be coupled into the shield objects through these holes. Therefore, it is important to understand the high-altitude electromagnetic pulse (HEMP) environment and its physical process coupling into different objects. In this paper, two Fortran softwares MCHII and FDTDM are developed.

MCHII simulates the physical process in which the electromagnetic signal is generated by the interaction of nuclear-explosion-induced Compton currents with the geomagnetic field. The electromagnetic pulse waveforms below the burst point are investigated. The effect of the geomagnetic field is considered and the current results applicable to the gamma rays are:

$$J_r(r,\theta,\varphi,\tau) \approx -\frac{e_q}{c}\varepsilon g(r)\int_0^{R_e/\beta} d\tau \dot{f}_\gamma(\tau - \chi(\tau'))(\cos^2\theta + \sin^2\theta \cdot \cos\omega\tau') \qquad (1)$$

The numerical results show that the early-time nuclear EMP has a sharp rise-time and a slower tail[2]. Its peak value on the ground lies in a region to the south of the ground zero with a distance one or two times of the height of burst (HOB). The region with a minimum peak electric field locates at the north of the ground zero. This is determined by the angle formed by the geomagnetic field and the locus of the electron movement. Half width of the waveform is related to the distance from the target point to the ground zero. The smaller the angel θ is, the narrower the half width becomes. High altitude nuclear EMP has a high electric field strength, ranging from several kV/m to 40kV/m.
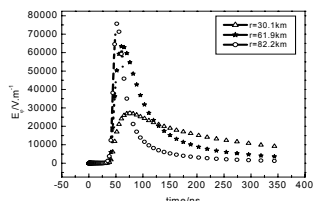
Fig.2 Electric field waveforms at various distances to the burst point

Then FDTDM researches the transient HEMP coupling to the cylinder object which is shielded in another shielding cavity with a hole. Through the calculation , it is found that the electromagnetic field energy, which is coupled into shielding cavity, is related to the frequency spectrum. The smaller the rise time is, the more high frequency content in its frequency spectrum is, then the higher the energy coupled into cavity is. The peak value of the current is the largest in the center of outer shielding object, and the wave oscillation period of the current is consistent with the period electromagnetic wave travels back and forth along the length of cylinder. That fits to the reference result[3].

References
1. W.J.Karzas, R.Latter, "Electromagnetic Radiation from a Nuclear Explosion in Space", Phys. Rew. , Vol.126 No. 6, 1961.
2. IEC 61000-2-9, Description of HEMP Environment -Radiation Disturbance Basic EMC Publication[S] , 1996.
3. C.Meng, "Research on the Value of the Coupling Rules of Transient Electromagnetic Field to Multiple Hole Object", High Power Laser and Particle Beams, vol. 12, No. 6, 2000

HPEM - 37
Coupling to Cables and Structures

Oral Presentations

Modeling of Passive Series Devices on Multiconductor Transmission Lines for Transient Analysis in Power and Railway Systems

Z. Mazloom, N. Theethayi, R. Thottappillil
Uppsala University, Uppsala, Sweden
E-mail: Ziya.Mazloom@angstrom.uu.se

Usually the crosstalk or field to wire coupling mechanisms in multiconductor transmission lines (MTL) are studied considering lumped loads or devices connected at the line terminations (at source and load ends) or as shunt load to ground along the lines, as seen in conventional power system networks e.g. [1-3]. However there are practical systems, e.g. in typical Swedish railway systems, wherein discrete devices exist in series with the line (booster transformers) or in shunt between the lines (auto transformers and track circuits). With lightning transients various parameters that influence crosstalk in MTL systems, such as the ground conductivity, have been analyzed e.g. in [1].

We shall present various cases of crosstalk mechanisms when the devices are connected either in series with the line or in shunt between the lines. The method used for simulating the voltage and current pulse propagation along the MTL systems is the FDTD method [4] in conjunction with the recursive convolution proposed in [5] for inclusion of ground losses. The passive series components connected along the MTL are simulated by the circuit solver ATP/EMTP [6, 7]. Emphasis will be given to present the model that connects the FDTD routine with the circuit solver in a more efficient way. The currents entering or leaving a given type of component at a given position along the lines are modeled as time dependant current sources in the circuit solver and the terminal voltages appearing in the circuit are returned to the FDTD routine as node voltages.

We shall also present the efficacy of the proposed method and mathematically discuss the validity of the present work. The influence of finitely conducting ground on the current pulse propagation is also included in the analysis. From the crosstalk analysis it is also shown that the series connected passive devices cannot be disregarded as they largely influence pulses propagating on the lines in the event of transient phenomena due to lightning or switching. This study could be beneficial for future practical studies of surge protection and insulation coordination.

References
1. N. Theethayi, R. Thottappillil, Y. Liu and R. Montaño, "Important Parameters that Influence Crosstalk in Multiconductor Transmission Lines", Electric Power Research, Vol. 77, No. 8, pp. 896-909, 2007.
2. F. Rachidi, C. A. Nucci and M. Ianoz, "Transient Analysis of Multiconductor Lines Above a Lossy Ground", IEEE Transaction on Power Delivery, Vol. 14, No. 1, pp. 294-302, 1999.
3. M. Paolone, C. A. Nucci, E. Petrache and F. Rachidi, "Mitigation of lightning-induced overvoltages in medium Voltage distribution lines by means of periodical grounding of shielding wires and of surge arresters: modeling and experimental validation", IEEE Transaction on Power Delivery, Vol. 19, No. 1, pp. 423-431, 2004.
4. C. R. Paul, "Analysis of Multiconductor Transmission Lines", John Wiley and Sons Incorporation, 1994.
5. R. Araneo and S. Celozzi, "Direct Time-Domain Analysis of Transmission Lines Above a Lossy Ground", IEE Proceedings: Science, Measurement and Technology, Vol. 148, No. 2, pp. 73-79, 2001.
6. W. S. Meyer and T. Liu, "Alternative Transients Program (ATP) Rule Book", Bonneville Power Administration, Canadian/American EMTP User Group, 1992.
7. H. W. Dommel, "Electromagnetic Transient Program Reference Manual (EMTP Theory Book)", Bonneville Power Administration, 1986.

Review of Research on Lightning Interaction with the Swedish Railway Network

N. Theethayi[1], Z. Mazloom[1], R. Thottappillil[1], P.A. Lindeberg[2], T. Shütte[3]

[1]*Uppsala University, Uppsala, Sweden*
[2]*Banverket HK/BJ, Borlänge, Sweden*
[3]*Rejlers AB, Västerås, Sweden*
E-mail: Ziya.Mazloom@angstrom.uu.se

In the early electrified railway systems, the design of signal and control networks were not always made in accordance with the strict rules of Electromagnetic Compatibility (EMC). This created problems due to Electromagnetic Interference (EMI) when old electro-mechanical signalling, control and communication systems were replaced by modern sensitive electronic circuits. Modern developments in the railway systems have made the system more vulnerable to lightning transients, a natural source of EMI, because the overall network is not designed to reduce the lightning surges to the low levels tolerable to the electronic systems widely being introduced in the railway system. Railway networks are extensive and modernization of signal/control/communication systems are carried out in stages at different times, it is not unusual to find transient related problems in a section of the network on account of inadequate lightning protection design or EMC design of the existing network in which a new module (equipment or system) is introduced. These problems may act as a brake on the upgrading plans of the railways. Also the new railway systems which incorporate advanced signal/control/communication systems sometimes suffers from the effects of lightning transients because many of the standards and guidelines used in the design dates back to the age of electromechanical devices and hence do not include robust transient protection design. There have been many attempts to address EMC issues in railways, but usually these attempts were confined to solving immediate problems of EMI due to introduction of new locomotive drives and EMI due to sparks at the pantograph. A comprehensive review of railway system from the angle of lightning protection and EMC is not yet fully carried out.

The Swedish National Rail Administration (Banverket) reported a delay of about 900-1000 hours in the years 2001-02. Lightning transients were found to damage important devices that control train movements, causing traffic stoppage and delays. This work therefore discusses the EMC problems of large distributed systems, with particular reference to lightning interaction with Swedish rail networks [1]. Lightning induces transient overvoltages in railway conductor systems such as tracks, overhead wires, and underground cables, either due to direct lightning strike to the system or due to the coupling of electromagnetic fields from remote strikes. Models based on multiconductor transmission line theory were developed for calculating the induced voltages and currents [1-3]. Some experiments have also been carried out to better understand the way in which the lighting transients' couple into the systems and also to verify the models used for analysis [4]. From experiments high frequency behavior of different types of transformers used within the railway systems were also derived [1, 6]. Besides, experimental studies on lightning induced transients entering railway systems, failure modes of relay and rectifier units used in the train position/signaling applications for lightning transients are performed. The simulation models are being converted to user friendly software for the practicing engineers of the railway industry [1].

References

1. N. Theethayi, "Electromagnetic Interference in Distributed Outdoor Electrical Systems, with an Emphasis on Lightning Interaction with Electrified Railway Network," Uppsala University, ISBN 91-554-6301-0, 2005.
2. N. Theethayi, R. Thottappillil, Y. Liu and R. Montaño, "Importance of Ground Impedance in the Study of Parameters That Influence Crosstalk in Multiconductor Transmission Lines", Electric Power Systems Research, Vol. 77, No. 8, pp. 896-909, 2007.
3. N. Theethayi, Y. Liu, R. Montaño, R. Thottappillil, M. Zitnik, V. Cooray and V. Scuka, "A theoretical study on the consequence of a direct lightning strike to electrified railway system in Sweden", Electric Power Systems Research, Vol. 74, No. 2, pp. 267-280, 2005.
4. N. Theethayi, R. Thottappillil, T. Yirdaw, Y. Liu, T. Götschl and R. Montaño, "Experimental Investigation of Lightning Transients Entering a Swedish Railway Facility", IEEE Transactions on Power Delivery, Vol. 22, No. 1, pp. 354-363, 2007.
5. "Lightning protection of the Swedish railway network, final technical report", Division for Electricity and Lightning Research, Department of Engineering Sciences, Uppsala University, Banverket project 2001-000282, 2001-03, 2001.
6. Z. Mazloom, N. Theethayi and R. Thottappillil, "Influence of Discrete Series Devices on Crosstalk Phenomena in Multiconductor Transmission Lines", Proceedings of 18th International Zurich Symposium on EMC, pp. 245-248, Munich, Germany, 2007.

Interference with Railway Systems (Invited)

HPEM - 39

Oral Presentations

Susceptibility of Electrified Railway to Intentional Electromagnetic Interference: Research in Sweden

R. Thottappillil[1], D. Månsson[1], M. Bäckström[2]

[1]*Uppsala University, 75121 Uppsala, Sweden*
[2]*Saab Communication, 581 88 Linköping, Sweden*
Email: *Rajeev.Thottappillil@angstrom.uu.se*

A research program is being conducted at Uppsala University, Sweden to investigate the possible susceptibility of civilian systems to intentional electromagnetic interference (IEMI), with emphasis on the Swedish railway network. This paper reviews the details of the research program and some of the results.

There are several possible ports through which intentional EMI can be coupled to the extensive network of electrified railways. Besides, Swedish railways are moving to implement the European Railway Traffic Management System (ERTMS) in different stages. The susceptibility of ERTMS transmission and receiving equipments to IEMI needs investigation. The research started in early 2005, supported by Swedish National Railway Administration (Banverket) and Swedish Emergency Management Agency (KBM).

To have a qualitative understanding of the risks of IEMI to railway systems, a series of EMC audits of several railway facilities were conducted. Some buildings had easily available ports, such as power outlets, on the outside wall. It is conceivable that a portable IEMI source is used to inject a high power pulse into the external power outlet. Therefore, investigations were carried out to determine how far deep an impulse can penetrate into a building. GSM-R antennas were tested in an anechoic chamber to determining its susceptibility levels over a wide band of frequencies and to translate that information into possible risks from radiated IEMI sources. A systematic method for investigating susceptibility of civilian facilities was also proposed.

References

1. R. Thottappillil, D. Månsson, N. Theethayi, M. Bäckström, T. Nilsson, G. Undén, B. Nordström, P. Bohlin, P-A Lindeberg, U. Hellström, P. Lindeberg, G. Bohlin, M. Zitnik, L. Ekenberg, "Response of Civilian Facilities to Intentional Electromagnetic Interference (IEMI), with Emphasis on the Swedish Railway Network", EMC Europe Workshop, Rome, Sept. 19-21, 2005.
2. D. Månsson, T. Nilsson, R. Thottappillil, and M. Bäckström, "Propagation of UWB Transients in Low-voltage Installation Power Cables", IEEE Trans. EMC., Vol. 49, No. 3, Aug. 2007.
3. Daniel Månsson, Rajeev Thottappillil, "Propagation Ability of UWB Transients through Junctions of Low-voltage Power Installation Cable", proc. Of Asia-pacific EMC 2008
4. D. Månsson,, R. Thottappillil, M. Bäckström, O. Lundén, "Vulnerability of European Rail Traffic Management System to Radiated Intentional EMI", IEEE trans. on Electromagnetic Compatibility, Feb. 2008.
5. D. Månsson, O. Lundén, R. Thottappillil and M. Bäckström, "The scenario of intentionally radiated electromagnetic interference to railway systems", Proceeding of the EMC Europe Workshop 2007, Paris, June 14 - 16, 2007.
6. T. Nilsson, R. Jonsson, "Investigation of HPM Front-door Protection Devices and Component Susceptibility", The Swedish Defense Research Agency (FOI) Technical Report, November 2005, FOI-R--1771--SE, ISSN 1650-1942, available for download at www.Foi.se
7. D. Månsson, T. Nilsson, R. Thottappillil and M. Bäckström, "Susceptibility of GPS Receivers and Wireless Cameras to a single Radiated UWB Pulse", Proceedings of EMC Europe, Barcelona, Spain, 2006.
8. D. Månsson, "Investigation of the susceptibility of Facilities to Intentional Electromagnetic Interference (IEMI)", Document prepared for Swedish Emergency Management Agency (KBM), 2007.

Interaction and Interference Between AC and DC in Railway Feeding Systems

S. Midya[1], T. Schütte[2] and R. Thottappillil[3]

[1,3]*Division of Electricity, Ångström Laboratoty, Uppsala University, Uppsala, Sweden*
[2]*Rejlers Ingenjörer AB, Västerås, Sweden*
E-mail: surajit.midya@angstrom.uu.se

AC and DC traction systems can severely disturb each other by all kinds of coupling (galvanic, inductive and capacitive). Often, the AC traction systems have DC fed track circuits and DC traction system have AC fed track circuits to avoid interference and false signalling from the same railway. One kind of current can get a short circuited path, overcoming the blocks for other kind. Especially inductive devices like transformers are easily passed by DC. DC components in AC railway can create interference problems with the track circuits, magnetization and eventually saturation of the transformers, corrosion problems, generate even harmonics etc. The AC component on the DC railway can induce high voltages in the cables and tracks, can create interference problems with the track circuits and other components of the signalling and telecommunication system. After some general overview this presentation focuses on three sources of DC current injected into AC railway systems:

1. Pantograph arcing create asymmetry in current and voltage waveforms in both polarities of the AC supply, resulting in a DC component. Especially icing can result in severe arcing producing DC at levels which can saturate transformers both in the locomotives and in the railway feeding circuits, e g booster- or autotransformers.

2. In many places AC railways, which is mostly the longer distance main lines, run in parallel to DC railways, traditionally shorter distance metro or tramways. Often leakage current from the DC railway creates interference problems with the AC railway.

3. Geomagnetic Induced Current (GIC) is another source of significant DC currents on power systems, single phase systems as the electrified railways are especially sensitive.

Due to climate (winter and icing), geographic position (near the geomagnetically most active region, i.e., around the polar circle), during the active solar cycle or solar maxima, AC-electrified railways in Scandinavia are strongly exposed to these DC sources and more easily saturate different components such as autotransformers, booster transformers, vehicle and substation transformers etc. We will also discuss about different possible ways on how to protect the system against the DC component and mitigate the consequences.

HPEM - 39
Interference with Railway Systems (Invited)

Oral Presentations

Pantograph Arcing and their Consequences to Electromagnetic Interference in Railway Systems

S. Midya[1], D. Bormann[2], A. Larsson[1,3], T. Schütte[4] and R. Thottappillil[1]

[1]*Division of Electricity, Ångström Laboratoty, Uppsala University, Uppsala, Sweden*
[2]*ABB AB - Corporate Research, Västerås, Sweden*
[3]*Swedish Defence Research Agency (FOI), Grindsjön Research Centre, Sweden*
[4]*Rejlers Ingenjörer AB, Västerås, Sweden*
E-mail: surajit.midya@angstrom.uu.se

Arcing in a sliding contact like pantograph-contact wire is a complex phenomenon. It distorts the sinusoidal waveform of current and voltage, creates asymmetry between the two polarities, generates a net DC component and electromagnetic radiation in a wide band. All of these propagate in the entire traction signalling and power system, saturates transformer cores, generate all types of harmonics and create interference problems with traction power, signalling and radio based communication systems.

In order to investigate the arcing phenomenon in the laboratory, an experimental set-up was designed similar to the actual pantograph-wire contact system. The overhead wire, placed at the periphery of a wheel, moves at a certain predefined speed and the pantograph moves back and forth on a carriage, in direction perpendicular to the wire. A small air gap between pantograph and wire is created in which the arc initiates. The variable test conditions, i.e., rms current, relative speed between the electrodes, power factor, pantograph materials and air gap width, were chosen with possible variations. Voltage drop between the pantograph and the contact wire, current, and time varying test parameters were recorded continuously using a transient recorder at 200 kSamples/s for 10 s, the duration of each test run. In addition, all test runs were recorded using an ordinary video camera.

The arc roots on both electrode surfaces are moving, due to the relative motion between the electrodes. However, since the line speed (speed of the contact wire towards the front) is much higher than the pantograph speed sideways, the movement of arc root across the copper conductor is more significant. Depending on the test parameters, these movements either create a short zero current region or just a reduced slope in the current waveform. Correspondingly, the voltage waveform shows either sharp overshoots or minor notches.

The cathode spot requires very high temperature to supply sufficient electrons in order to maintain the high current, which is influenced by the rms current, line velocity and the polarity of the supply. A combined effect of all these three together controls the arc root movement. This can be noticed from the distorted voltage and current waveform: the distortion depends on the current and voltage levels and also on the polarity of the power supply. Higher current and lower line speed enhances the possibility of maintaining the same arc root for a longer period of time. When the pantograph is cathode, it is already hot from the previous half period (when it was anode), and therefore can supply sufficient electrons quicker to maintain the current, which again enhances the possibility of maintaining the same arc root.

The polarity dependant nature of the distorted voltage and current waveforms leads to a net DC component. Different line speed, current and, polarity leads to different patterns of movement of the sliding arc. This causes different types of sharp transients, overshoots, and electromagnetic radiation up to the radio frequency band. The contact wire, the pantograph and other nearby metallic parts and electrical connections work as radiating antennas and create interference with the radio based services, both within and outside the railway system. The traction power and signalling circuits themselves also experience interference problems due to inductive and capacitive coupling from these distorted current and voltage waveforms and field illumination.

Theoretical and practical aspects concerning the electromagnetic disturbancies reducing in an urban electric driving system

P.M. Nicolae, L. Mandache, I.D. Nicolae, I.G. Sirbu, D.G. Stanescu

University of Craiova, Craiova, Romania
E-mail: pnicolae@elth.ucv.ro

The paper presents a series of experimental data and simulation results concerning the operation of equipment based on power electronics. Also one toggles with problems related to electromagnetic disturbances from urban electric driving systems. In some Romanian cities (including Craiova), tram vehicles were imported from Germany. They are endowed with traction motors of 600 V d.c. (two d.c. series motors at rated voltage of 300 V), which must be supplied from a 825 V d.c. network. To fix this mismatch, a first solution was the introduction of a resistance in series with the d.c. motors in the rotor circuit. This technical solution presents a series of drawbacks, among them being a low energetic efficiency. In order to get a compatibility of the Romanian urban travelers transportation with its European counterpart, one must consider the environment requirements, the interference with railway systems, the energetic consumptions reduction and the adaptation of consumption to the travelers flux. Therefore a solution was adopted for the modernization of existing tram vehicles through major changes in the power circuit.

Owing to the chopper's electric circuit where, for short intervals (few µs), currents of hundred of Amperes are switched, the tram that uses chopper can produce disturbancies in the tram systems. The reducing of these perturbancies can be obtained using a radiofrequency filter, in series with the input filter and the smoothing coils from the chopper's force circuit. One performed simulations of the filtering circuits' influence over the operation of a tram's electric energy supplying system. Using a program dedicated to the electric circuit analysis (SPICE), one represents the variations of the voltage when the radiofrequency filter is present or absent. The experimental determinations were performed on a tram submitted to modernization with respect to the driving system-chopper. The voltage at chopper's output and the current absorbed from the electric energy supplying network were been recorded. The numerical recordings were realised for various current steps at acceleration (corresponding to the acceleration treadle pressing by driver) and respectively for the braking regime on a tram that uses chopper. The different steps for current at acceleration and braking were observed. In the same time the numerical records emphasize the choppers efficiency, including the processes for the electric energy recovering (through recovering breakings – when other consumers are present and they absorb energy from the tram d.c. supplying system). Based on this one also notices the efficiency of the input filter, because through the discharging of the capacitor from this filter, the energy transmitted through resistive couplings toward network and inductive couplings (between the motors supplied from the same chopper) has no influence over the supplying line, the recovering braking regime being normal.
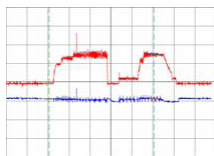
Fig. 1 – Current (red) and voltage (blue) corresponding to chopper 1 for the third running stage
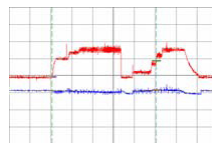
Fig. 2 – Current (red) and voltage (blue) corresponding to chopper 2 for the third running stage

The above waveforms present certain electromagnetic perturbancies owing to the power converter switching processes. These perturbancies might be transmitted through electromagnetic radiation, influencing the operation of other equipment. The RF filter action diminishes a lot these disturbances with visible effects over the telecommunication equipment.

References
1. M.H. Rashid, "Power electronics- Circuits, Devices and Applications,"Prentice-Hall International, Inc., New Jersey, 2003.
2. J.R. Wells, P.L. Chapman, P.T. Krein, "Applications of Ripple Correlation Control of Electric Machinery," Electric Machines and Drives Conference, 2003, IEEE International, vol.3, pp.1498-1503.
3. R. Erbe, J. Reichard, "Drive Technology Alternatives", Proceedings of IEEE International Electric Machines and Drives Conference, Seattle, Washington, USA, 1999, p.710-712.

HPEM - 39
Interference with Railway Systems (Invited)

Oral Presentations

Impedance Matching in EM Lens Design

A. P. Stone, C. E. Baum
University of New Mexico, Albuquerque, NM, USA
E-mail: astone@math.unm.edu

One possible approach to the design of lens waveguide transitions is a differential impedance matching and transit-time conservation method. Ideally one would want to transmit a TEM wave, without distortion or reflection form one transmission line to another. These transitions are usually called EM lenses or transient lenses. This goal is accomplished by specifying the shape and medium of the EM lens by obtaining a solution to an initial value problem. The physical properties of these lenses, given by the permeability and permittivity, may vary from point to point in the lens region, with the assumptions that these parameters are real valued and independent of frequency. It is also assumed that the conductivity of the medium is zero.

While we would like to obtain exact solutions, it may become necessary to make approximations to obtain a practical realization of an EM lens.

In constructing a transition section for a TEM wave propagating from one transmission line to another, two conditions must be imposed for a perfect matching to exist. A plane wavefront in one region should go into a plane wavefront in another region., and hence the travel time for waves following different paths should be equal. The second condition is that impedances must be matched. These requirements give rise to an initial value problem in the case considered here, which is that of finding a transition region between cylindrical coaxial waveguides of different size. This initial value problem can be solved by various methods, one of which involves an Abel type of differential equation, which is a generalization of a Riccati type of equation. A solution to this initial-value problem specifies the lens geometry and medium uniquely.

It should be noted that the physical principles of impedance matching and transit-time conservation led to this type of problem. In the design of reflector antennas, principles such as Snell's law and power conservation must be invoked.

Web-splines for Electromagnetic Theory

G. Apaydin, N. Ari

Applied Research and Development, University of Technology Zürich, Zürich, Switzerland
E-mail: gapaydin@hsz-t.ch

The analyses presented in this study show the suitability of the proposed method to complex electromagnetic (EM) problems. The finite element method (FEM) which uses weighted extended basis-splines (web-splines) is applied to waveguides of arbitrary domain. The eigenvalue analysis is used to compare the proposed method with the standard FEM. Firstly; homogeneous essential boundary conditions can be modeled via weight function, which is zero on the boundary and positive in the domain. Secondly, a well conditioned basis can be obtained by extended b-splines. Combining these two ideas gives the definition of web-splines.

Web-spline method is a new type of meshless finite elements. The resulting web-method does not require any mesh generation and, as a consequence, can be implemented very efficiently. The significance of web-splines is that the contribution of basis functions which are near the boundary is added to the inner basis functions. So, the number of nodes and computing time is reduced. Secondly, instability problem is solved [1-3].

The cutoff wave number analyses of waveguides are determined by solving the Helmholtz equation. With different ratio of radius of coaxial waveguides, the finite element matrices are obtained and then the eigenvalues for different types of waveguides are calculated. Accurate results were obtained by using web-splines; as the relative error for Transverse Magnetic (TM) mode is more accurate than the Transverse Electric (TE) mode according to the error analysis [4].

Using web-splines instead of weighted b-splines for the arbitrary domain shown in Fig. 1, the number of nodes is decreased up to 40 per cent, so the computation time is reduced. Considering the number of nodes used for triangulation, the web-spline method for TM mode analysis with 125, 163, and 198 nodes for linear, quadratic, and cubic web-splines provides same results of 10061 nodes for triangulation.

FEM with web-splines is a successful computational method in electromagnetics, and it is suitable to obtain electromagnetic solution for different frequencies. For high frequencies it is noted that the grid width should be selected as small compared to the wavelength. In addition, the maximum diameter of circle circumscribing domain should be small for higher frequencies in order to provide fast calculation. This new approach for electromagnetics can be applied to various structures and more complex electromagnetic problems such as biomedical modeling and scattering problems.
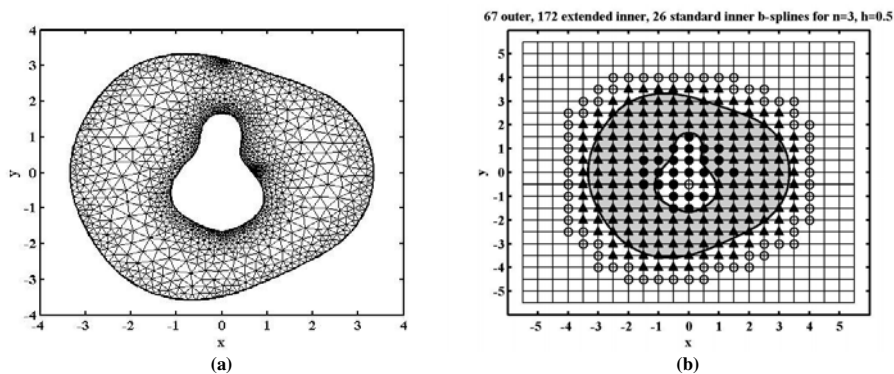
Fig. 1 – a) The triangulation and b) web-spline method for an arbitrary domain

References

1. K. Hollig, U. Reif, and J. Wipper, "Weighted extended b-spline approximation of Dirichlet problems," SIAM J. on Numerical Analysis, vol. 39, 2001.
2. K. Hollig, C. Apprich, and A. Streit, "Introduction to the web-method and its application," Advances in Comp. Math., vol. 23, 2005.
3. K. Hollig, Finite element methods with b-splines. Philadelphia: SIAM, 2003.
4. G. Apaydin, S. Seker, and N. Ari, "Application of web-spline method in electromagnetics," Int. Journal of Electronics and Communications (AEU), doi:10.1016/j.aeue.2007.03.007, 2007.

Infinitesimal Dipole Antenna in the Presence of ENG medium

S. Ghosh and B.Ghosh

Dept of E&ECE,Indian Institute of Technology,Kharagpur,W.B.,India
E-mail: susmita.gh@gmail.com

Here we investigated gain characteristic of an electrically small dipole antenna in the presence of ENG (epsilon negativel.material) [1]. Infinitesimal dipole which is an inefficient radiator in free space [2] was placed along the +z-axis and placed in an ENG medium.
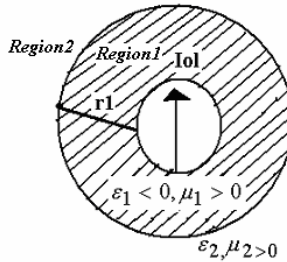
Fig 1.An infinitesimal dipole placed in an EPS medium

The parameters were chosen to be $\mu_{r_1} = 1$ and $\varepsilon_{r2} = 1$ $\mu_{r2} = 1$ with r_1 starting from r_1=0.12mm.Radiated power gain is plotted for different values of radius r_1 and ε_{r1}. An increase in radiated power gain with a moderate thickness of ENG sphere is noticed at r_1=0.54mm and $\varepsilon_{r1} = -2.03$. Though $\varepsilon_{r1} = -2.01$ gives a higher radiated power gain we consider $\varepsilon_{r1} = -2.03$ as it gives a broader bandwidth than $\varepsilon_{r1} = -2.01$. Thus we can consider these parameter values as optimized values.
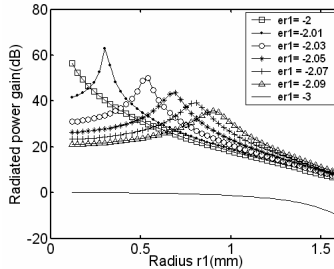
A lossless Drude model was studied to observe the frequency dependency of the infinitesimal dipole antenna. It was seen that a distinct power gain peak was observed at the operating frequency i.e. at 10 GHz. with a very low reactance value. This emphasizes the fact that an electrically small dipole can be used to achieve higher radiated power gain.

References
1. V.G.Veselago, "The Electrodynamic of substances with simultaneously negativen valuesof ε and μ ",
    Sov.phys.Usp.,vol.10,no.4,pp509-514,1968.Russ.Usp.Fiz.Nauk,pp.517-526,vol.92, 1967
2. R.W.Ziolkowaski and A.D.Kipple, "Application of Double Negative Material to Increase the powe radiated by Electrically Small Antennas", in IEEE Transaction on antennas and Propagation, vol.51, Pp2626-2040, October 2003

Testing Target Decomposition Theorems in Radar Polarimetry with the Aid of Electromagnetic Scattering Numerical Simulations

Jose Luis Alvarez-Perez[1], Jose Carlos Nieto-Borge[1]

[1]*University of Alcala, Dept. of Signal Theory and Communications, Alcalá de Henares (Madrid), Spain*

E-mail: joseluis.alvarez@uah.es

Radar polarimetry has been a very active field since the pioneering work of Kennaugh [1] and Huynen [2]. A recent review of the development and current state of the field is given in [3]. The underlying theory of the polarization of electromagnetic waves is still to be found in the work by Stokes and his definition of the four parameters named after him, which predates the introduction of Maxwell's equations. A serious limitation of Stokes' theory is that it describes the information contained in the correlations between the components of the electric field at the same point of space. Therefore it does not include any physical variable that relates two components at two different positions and that can therefore describe the change in the state of polarization and coherence of an electromagnetic wave as it propagates through a random medium. All the tools used in radar polarimetry so far have shared this limitation, including the target decomposition techniques that separate the Mueller or the coherency matrix representing the action of a certain target on an incident wave into different components. A decade ago Cloude and Pottier revised the existing target decomposition schemes in a landmark work [4] in which they proposed a new framework that included the Shannon entropy and other parameters based on the eigenanalysis of the coherency matrix as they defined it. Cloude's decomposition theory includes a physical interpretation consisting in a superposition of independent scattering mechanisms that has gained much acceptance in the field of radar polarimetry. The work presented in this paper comprises two parts. First, a numerical experiment based on the method of moments and the Foldy-Lax equations is performed by creating a scene containing a rough surface and a set of spherical, dielectric scatterers below it. The surface profile has two components: a deterministic, large-scale profile that imitates certain topography and a random, small-scale component that models a fluctuation that is known only through its statistics. The discrete scatterers below the rough surface are included for different values of permittivity, size and concentration. The accuracy of the interpretation of this scattering experiment in terms of its different scattering mechanisms as follows from Cloude's approach is tested here. The second part is dedicated to the study of the propagation of the cross-spectral density matrix as defined by Wolf in [5], which overcomes the difficulties explained above regarding the Stokes' parameters and the associated Mueller or coherency matrices. Namely, it is a physical observable that depends on two different points and two different times and measures the coherence properties of the propagating field. Since its frequency components obey the Helmholtz equation, it can be studied by using the same numerical simulation approach that has been employed in the first part. The importance of this observable is that it makes it possible to describe changes in coherence as the wave is scattered by a random medium. In addition to this, and due to some limitations in Wolf's cross-spectral density matrix, we study the behaviour of the normalized mutual coherence matrix defined by Réfrégier and Goudail in [6] that shows invariance properties that are absent in Wolf's approach. In this second part we compare this extended coherency tensors on pairs of points on the surface with and without the presence of additional scatterers below the surface.

References
1. K. Kennaugh, Polarization properties of radar reflections. M. Sc. Thesis. The Ohio State University, Columbus, Ohio.
2. J. R. Huynen, Phenomenological theory of radar targets. Technical Report. University of Technology, Delft, The Netherlands.
3. R. Touzi, W. M. Boerner, J. S. Lee and E. Lueneburg, "A review of polarimetry in the context of synthetic aperture radar: concepts and information extraction", Canadian Journal of Remote Sensing, vol. 30, pp. 380-4007, 2004.
4. S. R. Cloude and E. Pottier, "A review of target decomposition theorems in radar polarimetry", IEEE Transactions on Geoscience and Remote Sensing, vol. 35, no.2, pp. 498-518
5. E. Wolf, "Unified theory of coherence and polarization of random electromagnetic beams", Physics Letters A, 312, pp. 263-267, 2003.
6. P. Réfrégier and F. Goudail, "Invariant degrees of coherence of partially polarized light", Optics Express, vol. 13, no. 16, pp. 6051-60, 2005.

HPEM - 40
Special Techniques in EM Theory #1

Oral Presentations

Effective Boundary Condition in Problems of Electrodynamics with Near-Surface Sources

A.V. Soldatov

Russian Federal Nuclear Center – All-Russia Scientific Research Institute of Experimental Physics, Sarov, Russia
E-mail: av_soldatov@vniief.ru

Material objects placed in the field of ionizing radiation turn out to be sources of electromagnetic fields. Their appearance is associated with the separation of electric charges when the electron emission occurs from the body's surface under the action of the ionizing radiation and the replacement electric currents flowing along the surface. Effects of secondary electromagnetic radiation in systems generating electromagnetic pulses (SGEMPs) are well known for spacecraft subjected to the action of hard cosmic-ray radiation and x-ray radiation of a nuclear explosion, as well as the results of laboratory experiments with x-ray sources. The traditional method of calculating the electromagnetic environment near an object being irradiated consists in solving the Maxwell equations and the equations for the electron motion. The solution is realized by 2D or 3D computer codes. However, this approach is associated with significant technical difficulties. They occur, first of all, due to the necessity to solve the self-consistent problem often in a complicated geometry. In addition, in this case, we have to deal with quantities of different scales. We mean the sizes of the electric-current layer, of the object, and of the region in which calculations are performed. In the present paper, a method capable of reducing the volume sources of the electromagnetic field to surface ones is suggested. This is attained by introducing effective boundary condition, which allows us to simplify the problem significantly and to reduce it to solving the homogeneous Maxwell equations.

HPEM - 40
Special Techniques in EM Theory #1

Oral Presentations

High Frequency Noises of Explosion Emitted Electron Beam and their Influence on Operation of Relativistic BWO

E. Abubakirov, A. Konyushkov, A. Sergeev
Institute of Applied Physics, Nizhny Novgorod, Russia
E-mail: konyushkov@appl.sci-nnov.ru

The analyses of high frequency noises of electron beam is urgent for microwave devices, employing explosion emitted electron injectors. The problem is actual as for microwave amplifiers, where self noises of electron beam limits the minimum level of input signal and impedes high amplification, as for microwave generators, where these noises serve as initial signal for self excitation of the device and determine the oscillation start up.

According to [1], electrons in explosion emitted beams are injected from separated (different) areas of cathode plasma - cathode flares, and the beam consists of numerous electron packets, called ectons. The duration of the pulse is 5 – 10 ns, and its average charge is about $10^{12}e$. Due to random time of pulse origination and its low duration, the explosion emitted beam has a noise term similar to "shot noise" of conventional electronic tubes. For working current 5 – 10 kA, accelerating voltage about 600 kV the power spectral density of equivalent electromagnetic input signal at 10 GHz frequency can be estimated as 1-2 W/MHz.

A one-dimensional nonlinear model was used to analyze the influence of this effect on relativistic BWO [2]. The existence of shot noise term results in effective density modulation of the electron beam at the input of the electron devise. The process was simulated with modulation of electron phase:

$$\theta = \theta_0 + f(t) \cdot \sin\theta_0, \tag{1}$$

where $\theta_0 \in [0;2\pi)$, and the spectral density of $f(t)$ is equal to the normalized spectral density of the beam noise.

In case of BWO-generator beam noises don't have any significant effect on a steady-state operation of the device, as the relative power fluctuations $\Delta P/P_{av} < 0.01$, but determines the transition process of the generator.

Transition time, found in accordance to this theory is of the same order as experimental results.

At the same time, beam noises produce an essential effect on BWO-amplifiers with low input signal. The report contains the analyses of minimum level of input signal, when the amplification regime is still possible.

References
1. G. A. Mesyats "Ectons", Ekaterinburg, YIF Nayka, (Russian) 1993.
2. N. S. Ginzburg, S. P. Kuznetsov, T. N. Fedoseeva "The theory of transient processes in relativistic BWO", Izv. Vuzov, Radiofizica (Russian), vol.21, no.7, pp.1037-1052, 1978.

HPEM - 41
High-Power Microwaves

Oral Presentations

Oral Presentations   HPEM - 41   High-Power Microwaves

Control over the Radiation Spectra of Broadband Plasma Relativistic HPM Oscillators

O. T. Loza, I. L. Bogdankevich, D. A. Pavlov

A. M. Prokhorov General physics institute RAS, Moscow, Russia

loza@fpl.gpi.ru

HPM oscillators based on the interaction of high-current relativistic electron beams with plasma radiate microwaves with the frequency and spectrum width which may be tuned over a wide range. Such microwave oscillators are known also as relativistic Cherenkov plasma masers (CPM), they generate microwave pulses at the power level of 10^8 W. The method of plasma preformation [1] in these HPM oscillators and the control over its concentration allows tuning the radiation frequencies through several octaves. Moreover, it is possible to "appoint" the radiation frequencies of microwave pulses in a sequence according to any algorithm even for pulses generated with the repetitive rate of ~ 1 kHz. Here we present the results obtained in calculations according to the linear theory and mainly, in numerical modeling. Briefly, the results are as follows.

CPM can generate microwaves at one frequency or concurrently at several frequencies which correspond to longitudinal modes of the beam-plasma resonator. As the plasma concentration varies the radiation frequency changes discretely, the interval depends on the resonator length. The radiation frequency may be tuned continuously, to do this requires the length of the beam-plasma interaction to be modified. To overlap the frequency gaps between neighboring modes the resonator length should be variable within one half of the wavelength.

Almost monochromatic radiation can be obtained if the plasma resonator length exceeds the wavelength not more than a few times. With the further increase of the length new frequencies appear in the spectrum and the interval between them diminishes. The spectrum irradiated in one pulse may be tuned by several means besides the resonator length modification or concurrently with it. As the gap between annular plasma and relativistic electron beam diminishes the amplification rate rises and the radiation spectrum broadens. An increase of partial reflection of microwaves from the outlet unit following from the change of its geometry or magnetic field profile results also in the spectrum broadening. An appropriate choice of magnetic field induction permits to regulate the feedback in the oscillator using the normal Doppler effect [2] for suppressing definite set of frequencies in the spectrum.

A major part of the results has practical confirmations [3, 4], for the other ones simple ways of experimental implementation are proposed, peculiar emphasis was given to this aspect. Particular parameters are described for a microwave oscillator capable to generate frequencies from 3 to 5 GHz with both narrow spectrum and broad frequency set, with tunable intervals and borders. On a basis of these calculation and available technology it is possible to manufacture a source of microwave pulses to irradiate objects with spectral density of ~ 10 W/GHz uniformly within 1-GHz interval during 1 s, first experiments has been recently conducted [5].

References

1. O. T. Loza, A. V. Ponomarev, P. S. Strelkov et al. "Source of an annular controlled-radius plasma for a plasma relativistic microwave oscillator", Plasma Phys. Reports, 1997, vol.23, No.3, pp.201-208.
2. P. S. Strelkov, A. V. Ponomarev, and I. L. Bogdankevich. "Normal Doppler Effect in Experiments on the Interaction of Relativistic Electron Beams with Plasma: Plasma Relativistic Microwave Amplifier", Plasma Phys. Reports, 2007, vol. 33, No. 4, pp. 329-337.
3. P. S. Strelkov and D. K. Ul'yanov, "Emission Spectra of a Cherenkov Plasma Relativistic Maser ", Plasma Phys. Reports, 2000, Vol. 26, No. 4, pp. 303-307.
4. I. L. Bogdankevich, I. E. Ivanov, O. T. Loza, et al. "Fine Structure of the Emission Spectra of a Relativistic Cherenkov Plasma Maser", Plasma Phys. Reports, 2002, vol. 28, No. 8, pp. 690–698.
5. O. T. Loza, I. L. Bogdankevich, D. M. Grishin, et al. "Repetitively-Rated Plasma Relativistic Microwave Oscillator with Tunable Radiation Frequency in Every Pulse", submitted to this Conference

Investigation of a U-shaped Coaxial to Waveguide Transition

Eldar Bahshi[1], Dan Zarobnik[2], Haim Matzner[3], Motti Haridim[4]

[1,2,3,4] *HIT – Holon Institute of Technology, Holon, Israel*
E-mail: e.bahshi@gmail.com

Abstract — An S-band U-shaped coaxial to rectangular waveguide transition component, containing one tuning screw is investigated. Both simulation and measurement show a good matching level in a bandwidth of more than 50%. Good agreement between simulation and measurement was achieved.

Introduction

In this paper we propose a compact wideband, U-shaped coaxial to rectangular waveguide transition. We suggest a setup which is based on a half-ring, made from a conductive wire, which is connected to the inner side of the coaxial cable.

Geometry of the Transition Component

The ring's thickness is e=2mm and the diameter of the central pivot is k=2.6mm. The transmission element is located 33.5mm away from the back wall of the device and is made from a 1.3mm diameter conductor integrated into a 4mm diameter Teflon holder. A special half-ring element made of 1.3mm thick conductor (i.e. brass) which presented in Fig. 1. An additional 2.5mm diameter screw is located 56 mm away from the back wall, penetrating 10mm to the waveguide, and is used for tuning the frequency.

Simulation

During the design stage, simulations using CST-Microwave Studio software were carried out. The range of used frequencies was 2.086 – 3.980 GHz, from which a bandwidth of 1.894 GHz, a mean frequency of 3.033 GHz, and their respective percentage bandwidth ratio of 62% were calculated.

While associating an effectively received power with amplitudes lower than -9.5dB, it can be calculated that the feeding supports a power transmission of f:1.9f.

a=74.6mm
b=37.3mm
h=6mm
k=2.6mm
r=13mm
e=2mm
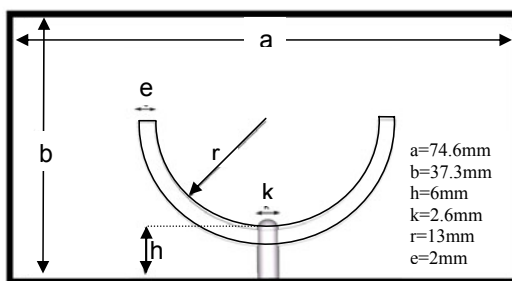
Fig. 1 – The half-ring inner element
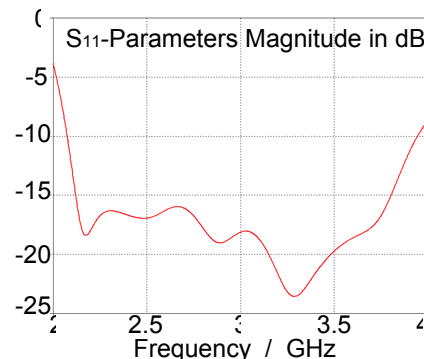
Fig. 2 – Return loss of the transition component.

Conclusions

We have demonstrated a new broad-band transition component from a coaxial line to a waveguide. The device has a miniature design. A high quality matching level has been achieved and it is applicable to both rectangular transmitters as well as to horn antennas. Future studies will involve an optimization process, which hopefully result in a simpler design, excluding the need for a tuning screw.

References

1. R. Tang and N.S. Wong, "Multimode phased array element for wide scan angle impedance matching", Proc. IEEE, vol.56, no. 11, pp. 1951-1959, Nov. 1968.
2. M. D. Desphande, B. N. Das, and G. S. Sanyal, "Analysis of an end launcher for an X-band rectangular waveguide", IEEE Trans. Microw. Theory Tech., vol. MTT-27, no. 8, pp. 731-735, Aug. 1979.

HPEM - 41
High-Power Microwaves

Oral Presentations

Compression of Microwave Pulses in Two Series – Coupled Cavities

S.N.Artemenko[1], A.N.Didenko[2], S.A.Novikov[1], Yu.G.Yushkov[1]

[1]*Nuclear Physics Institute, Tomsk, Ruaaia*
[2]*Russian Academy of Science, Moscow, Russia*
E-mail: novsa@npi.tpu.ru

Compression in series – coupled cavities is put into effect by sequential operation of the resonant cavities along with passing of the microwave pulse. The series compression provides the output pulse power above the single cavity possibility. The report studies the system comprising two storage cavities.

Processes of excitation and transfer were considered for couple of S-band cavities having fixed dimensions and intrinsic Q-factor values, the first cavity having characteristics corresponding to a multimode storage cavity. The system parameters during excitation and energy extraction were defined by different values of transition coefficients of the first and second cavity. The functions of the normalized electric field strength versus time were calculated and plotted for different values of transition coefficients. The optimum and possible working characteristics of processes in question were determined. The calculated envelope and amplitude of the output pulse shows that the total amplification factor over 27 dB and pulsewidth of several nanoseconds could be achieved.

The presented experimental results were obtained at the microwave compressor with the parameters being within the ranges used for calculations. The pulses of maximum peak power 1.1 GW and pulsewidth 2.5 ns at –3 dB level were measured at the second stage cavity output when the input power was 2.5 MW. The compressor was tested at pulse repetition rates up to 100 Hz. The general block diagram, picture of two series coupled cavities and oscillograms for and output microwave pulses are presented.

Frequency Response of Multiple Conductors Buried in a Lossy Ground

D. Poljak[1], V. Doric[1], K. El Khamilici Drissi[2], K. Kerroum[2], D. Cavka[1], S. Sesnic[3]

[1]*Department of Electronics, University of Split, Split, Croatia*
[2]*LASMEA, Blaise Pascal University, Clermont-Ferrand, France*
[3]*Department of Electrical Engineering, University of Split, Split, Croatia*
E-mail: dragan.poljak@fesb.hr

The analysis of electromagnetic field coupling to multiple wires buried in a lossy half-space is of interest in many electromagnetic compatibility (EMC) applications (communications and power cables, geophysical investigations, etc.) and can be carried out by using the thin wire antenna theory, or transmission line model in the frequency and time domain [1]-[3]. In this work both antenna theory and transmission line approach in the frequency domain has been used to study frequency behaviour of multiple buried wires. The formulation arising from the wire antenna theory in the frequency domain is based on the set of coupled Pocklington integro-differential equations for half-space problems [2]. The frequency domain transmission line model is based on the corresponding Telegrapher's equations [1], [3]. The frequency domain coupled integro-differential equations frequency domain, arising from the wire antenna theory are numerically handled via the frequency and time domain Galerkin-Bubnov scheme of the Indirect Boundary Element Method (GB-IBEM) [2], [3]. The frequency domain transmission line equations are treated using chain matrix method [3]. Computational example is related to three conductors buried in a lossy ground with $\sigma=0.001 S/m$, $\varepsilon_r=10$, as shown in Fig 1a. The length and radius of all conductors is 50m and 10.25mm respectively. Distance between neighbouring conductors is 36mm, and the burial depth is 1m.
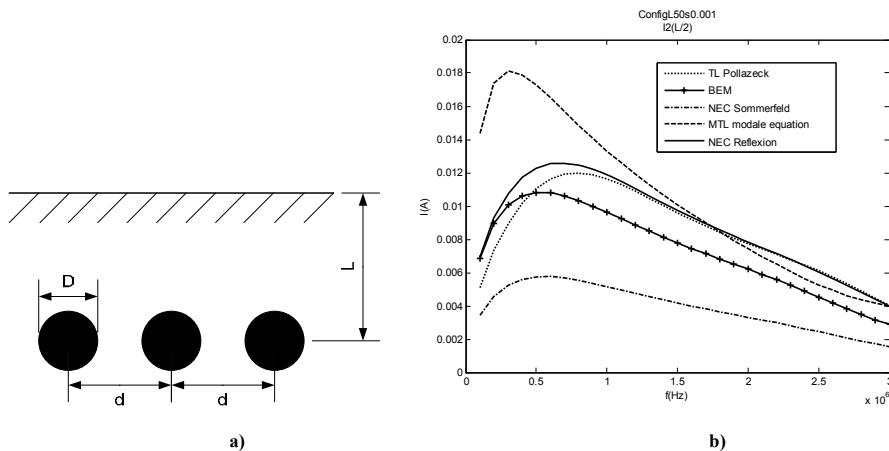
Fig.1 - Frequency response of a three -wire transmission line - comparison between BEM, TL, MTL and NEC

Figure 1b shows the frequency spectrum of the current induced at the centre of wire 2 obtained via GB-IBEM, TL, MTL, NEC2 + reflection coefficient approximation and NEC 2 + Sommerfeld integral approach. The results obtained via different methods vary appreciably.

References

1. F. M. Tesche, M. Ianoz, and T. Karlsson, EMC Analysis methods and computational models. New York: Wiley Interscience, 1997.
2. D. Poljak, EMC Advanced Modelling in Computational electromagnetic Compatibility, John Wiley and Sons, New York 2007.
3. D. Poljak V. Doric, S. Sesnic, K. El Khamlichi Drissi, K. Kerroum, Electromagnetic Field Coupling to Buried Wires: Comparison of Frequency Domain Wire Antenna and Transmission Line Model, ICECom 2007, Conference Proceedings, 19th International Conference on Applied Electromagnetics and Communications, 2007 , pp 123-126.

Oral Presentations

HPEM - 42
Transmission Lines at Low and High Frequencies: Theory, Numerical and Experiments. Part 2: Numerical Methods and Measurements (Invited)

Oral Presentations

Generalized Transmission Line Theory as an Antenna Theory

F. Gronwald, J. Nitsch, and S. Tkachenko

Otto-von-Guericke-University Magdeburg, Germany

E-mail: sergey.tkachenko@ovgu.de

Electromagnetic phenomena along thin-wire antennae and transmission lines play a major role in EMC analysis. While in antenna theory focus is put on the direct solution of appropriate field integral equations, transmission lines, traditionally, have often been modelled within the framework of classical transmission line approximation. It is well known that classical transmission line theory determines a quasi-static approximation of the full dynamics of the electromagnetic field which, in particular, neglects radiation effects. This limitation is not always satisfying since EMC analysis of transmission line structures increasingly often involves high frequencies which do generate radiation effects that need to be taken into account. In order to include radiation effects in a consistent way, a generalized transmission line theory has been developed [1,2] and extended or analyzed [3-5] over the last years. In the derivation of generalized transmission line theory the relevant field integral equations are first transformed into equivalent generalized Telegrapher equations and eventually solved by methods which are tailored to transmission line theory.
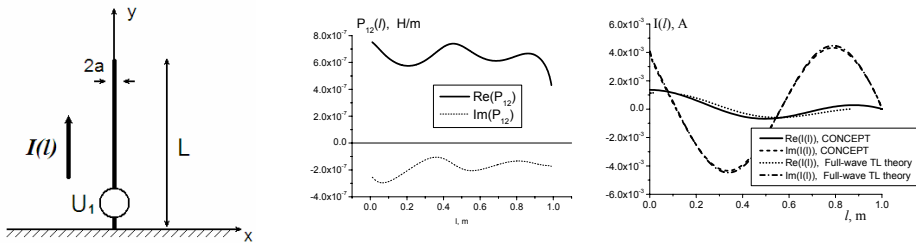
Fig. 1 - Vertical monopole antenna: geometry, parameter $P_{12}(l)$ (generalized inductance) and current distribution
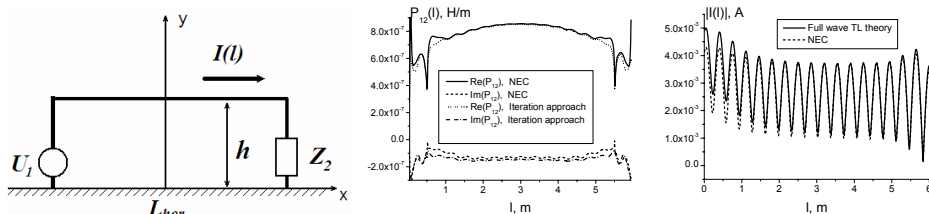
Fig. 2 - Transmission line structure: geometry, parameter $P_{12}(l)$ (generalized inductance) and current distribution

It is the aim of this paper to give a straightforward and compact derivation of this theory and to further point out that a generalized transmission line theory, as it is presented here, comprises the same physical features as antenna theory. This is illustrated by two examples (vertical monopole antenna and horizontal transmission line, see figures) that exemplify the use of generalized transmission line theory in EMC analysis for the investigation of radiating transmission line systems.

References
1. H. Haase, J.Nitsch, "Full-wave transmission line theory (FWTLT) for the analysis of three-dimensional wire-like structures, 14th International Zurich Symp. on EMC, Zurich, Switzerland, pp. 235-240, Feb. 2001
2. H. Haase, J. Nitsch, T. Steinmetz, "Transmission-line super theory: a new approach to an effective calculation of electromagnetic interactions", URSI Radio Science Bulletin, (307), December 2003, pp. 33-60.
3. J. Nitsch, S. Tkachenko, „Global and modal parameters in the generalized transmission line theory and their physical meaning", URSI Radio Science Bulletin (312), March 2005, pp.21-31.
4. J.B. Nitsch, S.V. Tkachenko „Propagation of Current Waves along Quasi-Periodical Thin-Wire Structures: Taking Radiation Losses into Account", Radio Science Bulletin, (322), September 2007, pp. 19-40.
5. Gronwald, F: "On the applicability of conventional transmission line theory within cavities", Advances in Radio Science, vol. 4, (2006), p. 117–123.

Full Wave Transmission Line Theory for a Homogeneous Line with Two Lumped Sources

J. Nitsch, S. Tkachenko

Otto-von-Guericke-University Magdeburg, Germany

E-mail: sergey.tkachenko@ovgu.de

The continuous increase of frequencies of signals which propagate along non-uniform conductors as well as the increase of frequencies of intentional electromagnetic interferences prevent the application of classical transmission line approximation for the analysis of such systems.

For arbitrary frequencies, the current that propagates along non-uniform transmission lines and the potential on the boundaries of the wire (which replaces the voltage in the high – frequency case) are described by a system of integro-differential equations, the so called Mixed Potential Integral Equations (MPIE). In [1-2] it has been shown that the system of MPIE can be reduced to a system of differential equations of the first order, the telegrapher's equations of the Full- Wave-Transmission Line theory (FWTL). The parameters of the corresponding matrix, as in the low-frequency case, depend on a local coordinate. However, in contrast to the low-frequency case, they are complex-valued, frequency-dependent and also contain diagonal elements. The imaginary parts of the non-diagonal elements and the diagonal elements of the parameter matrix are partially responsible for the radiation of the wiring system. In the low-frequency limit the diagonal elements reduce to zero and the non-diagonal elements reduce to the usual length–dependent inductance and capacitance per-unit-length, respectively.

In [3-4] it has been shown that the matrix of FWTL parameters for the wiring system, excited by lumped voltage sources (or loaded by lumped loads) located at the terminals can be found as exact electrodynamics' solutions for currents and potentials for each of the considered source.

For further investigations of the physical properties of the parameter matrix it is interesting to consider the wiring system with known analytical solutions for the lumped voltage sources. In the present paper we deal with an infinite straight wire parallel to the perfect conducting ground, which is excited by two lumped sources (or a lumped source and a lumped load) spaced by a distance L. Besides the pure theoretical interest, the solution of this problem is interesting for the investigation of conducting disturbances caused by faults of the cable shield, and also for the problem of transmission (reception) of telecommunication signals along power lines, which is being discussed at the present time.

For the discussed geometry it can be shown that the region of the wire between the sources can be described by FWTL. The solution for the current of an arbitrary excitation is well known and can be found by a Fourier transformation. For the special case of the excitation by a lumped voltage source the induced current can be represented as a sum of the three kinds of modes: the TEM mode propagating without attenuation; the leaky modes which propagate with exponential attenuation, and the radiation mode propagating with powers attenuation [5-6]. The solution for the induced potential (which coincides with voltage for this system) contains only the TEM mode. The knowledge of the solution for the current and potential allows to derive explicit expressions for the FWTL-parameters using our general theory [3-4] roughly described above. The investigation of the obtained expressions explains earlier numerically calculated oscillations of the FWTL parameters near the terminal regions by oscillations of leaky modes. We compared the obtained exact parameters matrix with approximate results of the perturbation theory for parameters, offered earlier in [2], and have received a good agreement. The solution of the above FWTL system gives an excellent alignment for an exact solution.

References

1. H. Haase, J.Nitsch, "Full-wave transmission line theory (FWTLT) for the analysis of three-dimensional wire-like structures, 14th International Zurich Symp. on EMC, Zurich, Switzerland, pp. 235-240, Feb. 2001
2. H. Haase, J. Nitsch, T. Steinmetz, "Transmission-line super theory: a new approach to an effective calculation of electromagnetic interactions", URSI Radio Science Bulletin, (307), December 2003, pp. 33-60.
3. J. Nitsch, S. Tkachenko, „Global and modal parameters in the generalized transmission line theory and their physical meaning", URSI Radio Science Bulletin, 312, March 2005, pp.21-31.
4. J.B. Nitsch, S.V. Tkachenko „Propagation of Current Waves along Quasi-Periodical Thin-Wire Structures: Taking Radiation Losses into Account", Radio Science Bulletin, No 322, September 2007, pp. 19-40.
5. L.Marin, "Transient Electromagnetic properties of two parallel wires", Sensor and Simulation Notes, Note 173, March 1973 (http://www-e.uni-magdeburg.de/notes/pdf/ssn0173.pdf).
6. Y.Leviatan, A.T. Adams, "The response of two-wire transmission line to incident field and voltage excitation including the effects of higher order modes," *IEEE Trans. Ant. Prop.*, Vol. Ap- 30, No. 5, Sept. 1982, pp.998-1003.

Oral Presentations

HPEM - 42
Transmission Lines at Low and High Frequencies: Theory, Numerical and Experiments. Part 2: Numerical Methods and Measurements (Invited)

Oral Presentations

Propagation of Current Waves along Quasi-Periodical Conductors

J. Nitsch, S. Tkachenko, H.-J. Scheibe

Otto-von-Guericke-University Magdeburg, Germany

E-mail: sergey.tkachenko@ovgu.de

An analysis of the propagation of current waves along periodical structures in different radio-technical and electro-technical applications becomes necessary. These periodical structures show non-trivial electrodynamical properties and sometimes can be used to build filters, antennas and HPM sources. Moreover, they can serve as elements for the design of meta-materials.

In the present paper we outline an analytical method, which describes the propagation of current waves along quasi – periodical wiring structures and takes into account radiation losses.

The homogeneous problem of current propagation along a thin wire of arbitrary geometric form near ground is described by Full-Wave Transmission Line Theory [1] which is transformed into a Schrödinger-like differential equation, with a "potential" depending on both the geometry of the wire and frequency [2, 3]. The "potential" is a complex – valued quantity that corresponds to either radiation losses in the framework of electrodynamics or to the absorption of particles in the framework of quantum mechanics. If the wire structure is quasi periodical, i.e., it consists of a finite number of identical sections (see Fig. 1), the "potential" can be approximately represented as a set of periodically arranged identical potentials. We use the formalism of transfer matrices including some methods of group theory [4] and find an analytical expression for the transmission coefficient of the finite number of periodically located non-uniformities which also contains the scattering data of one non-uniformity.

The analysis of the formulae obtained has shown that for some frequencies the penetration through the chain is practically free, but for some frequencies it is suppressed. A connection is established between the frequency regions with allowed and forbidden zones, which are well known from solid-state physics. The accounting for losses leads to the decrease of propagation in the allowed zones (see Fig. 2).
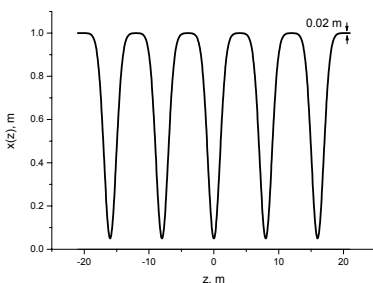
Fig. 1 – An example of the quasi-periodical structure
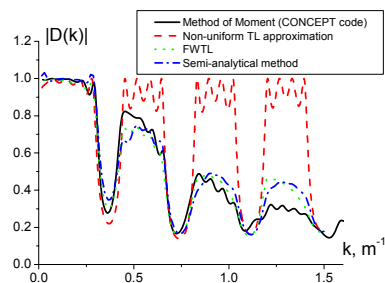
Fig. 2 - Transmission coefficient

Two other effects are noticed. The first effect appears if the potential, which corresponds to one separate non-uniformity, is not easy to penetrate. In this case for allowed zones the current strongly increases inside the structure, what can be a cause, for example, of strong radiation or heating inside the structure. The second effect appears for the infinite periodical chain. In this case it is possible to have opposite directions of phase penetration (direction of the quasi-pulse) and power penetration.

We constructed three different types of quasi-periodical systems and measured the frequency dependency of the transmission and reflection coefficients and the radiated power for current waves. The measurements have demonstrated a good agreement with the results of the developed theory.

References

1.   H. Haase, J.Nitsch, "Full-wave transmission line theory (FWTLT) for the analysis of three-dimensional wire-like structures, 14th International Zurich Symp. on EMC, Zurich, Switzerland, pp. 235-240, Feb. 2001
2.   J.Nitsch and S. Tkachenko, "Propagation of Current Waves along Quasi-Periodical Thin-Wire Structures: Accounting of Radiation Losses", Interaction Notes, Note 601, 23 May 2006.
3.   J.B. Nitsch, S.V. Tkachenko „Propagation of Current Waves along Quasi-Periodical Thin-Wire Structures: Taking Radiation Losses into Account", Radio Science Bulletin, No 322, September 2007, pp. 19-40.
4.   A.M. Peres „Transfer Matrices for One-dimensional Potential", J.Math.Phys., 24(5), May 1983, pp.1110-1119.

Transient Response of Multiple Horizontal Thin Wires Located at Different Heights above a Perfectly Conducting Ground

Dragan Poljak[1], Sinisa Antonijevic[1], Khalil El Khamilici Drissi[2], Kamal Kerroum[2]

[1]*Department of Electronics, University of Split, Split, Croatia*
[2]*LASMEA, Blaise Pascal University, lermont-Ferrand, France*
E-mail: dragan.poljak@fesb.hr

Time domain (TD) modeling of electromagnetic field (EM) coupling to horizontal multiple wires over a perfectly conducting (PEC) half-space finds many applications in the analysis of antenna arrays, transmission lines, printed circuit boards (PCB), etc [1]. In this work, the analysis of EM field coupling to multiple wires located above a PEC ground at different heights has been carried out by using both the wire antenna model (AM) and the transmission line (TL) method. The TD-AM formulation is based on the set of coupling space-time Hallen integral equations while the TD-TL model is based on the corresponding Telegrapher's equations. The set of Hallen integral equations is numerically handled via the TD Galerkin-Bubnov scheme of the Indirect Boundary Element Method (GB-IBEM) [2], while the TD Telegrapher's equations are treated using the Finite Difference Time Domain (FDTD) Method [2]. Computational examples are related to two-wire (a=2cm, L=10m, d=1m, h_1=1m, h_2=2m) and three wire (a=2cm, d=1m, L=10m, h_1 = h_3=1m, h_2=2m) transmission line above a PEC ground, as shown in Fig 1a and Fig 2a, respectively, excited by an electromagnetic pulse (EMP): $E^{inc}(t) = E_0(e^{-\alpha t} - e^{-\beta t})$, with E_0=1V/m, α=4*10^{7}s^{-1}, β=6*10^{8}s^{-1}.

a)   **b)**
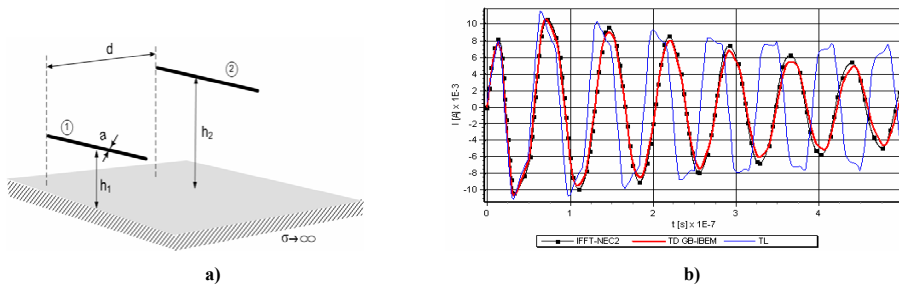
Fig.1 - Transient response of a two -wire transmission line - comparison between IFFT-NEC2, GB-IBEM and TL

a)   **b)**
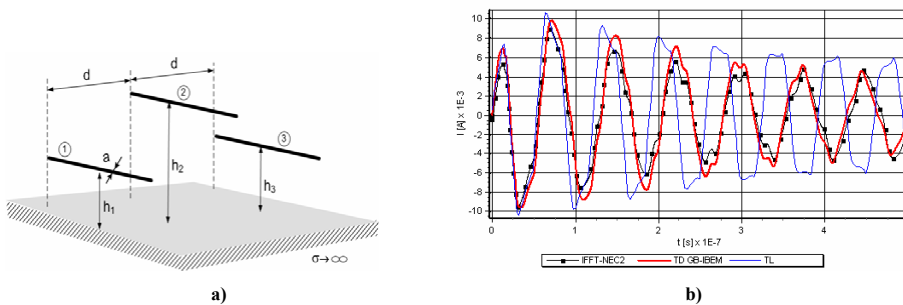
Fig. 2 - Transient response of a three -wire transmission line - comparison between IFFT-NEC2, GB-IBEM and TL

Figures 1b and 2b show the transient current induced at the centre of wire 2 obtained via TD GB-IBEM, TL and NEC2 + Inverse Fast Fourier Transform (IFFT). The results computed via BEM and NEC 2+ IFFT, seem to be in a satisfactory agreement, while TL results are found to be valid only for early time instants.

References
1. F. M. Tesche, M. Ianoz, and T. Karlsson, EMC Analysis methods and computational models. New York: Wiley Interscience, 1997.
2. D.Poljak V.Doric, S. Antonijevic, K. El Khamlichi Drissi, Kamal Kerroum, ICECom 2007, Conference Proceedings, 19th International Conference on Applied Electromagnetics and Communications, 2007 , pp 119-122.

HPEM - 42
Transmission Lines at Low and High Frequencies: Theory, Numerical and Experiments. Part 2: Numerical Methods and Measurements (Invited)

Oral Presentations

HPEM - 42
Transmission Lines at Low and High Frequencies: Theory, Numerical and Experiments. Part 2: Numerical Methods and Measurements (Invited)

Oral Presentations

Full-Wave Analysis of Arbitrary Polygonal Section Coupled Lines

S. Falco[1], M. Lucido[1], G. Panariello[1], F. Schettino[1]
[1]*D.A.E.I.M.I., University of Cassino, Cassino, Italy*

E-mail: simonefalco@sebeto.it

Striplines and microstrips are widely used in microwave integrated circuits, thus making it very important to have an accurate knowledge of their characteristics, such as phase velocity, characteristic impedance and losses, as a function of geometry and frequency. Simple and accurate design formulas and/or plots are of valuable importance to the circuit designers. As a matter of fact there is a trade-off between methods' accuracy and complexity, so that full-wave analyses are usually impractical for design purpose. On the other hand approximate methods often fail to give accurate results, especially for non standard section conductors or strong coupling.

In this contribution we present a full-wave analysis of arbitrary polygonal section coupled lines in a homogeneous medium, taking into account the correct edge behavior of the field [1], thus obtaining a very efficient procedure [2, 3].

The proposed method starts formulating the problem as integral equations in the spectral domain, solved by applying Galerkin method. It is based on the expansion of the unknown current density on each surface of the conductor in a series of Jacobi polynomials, multiplied by their orthogonality weight, thus factorizing the correct singularity of the field at edges, namely a series of functions

$$\varphi_n^{(\alpha,\beta)}\left(\frac{x}{c}\right) = \begin{cases} \frac{1}{c}\left(1-\frac{x}{c}\right)^\alpha \left(1+\frac{x}{c}\right)^\beta \frac{P_n^{(\alpha,\beta)}\left(\frac{x}{c}\right)}{\xi_n^{(\alpha,\beta)}} & \left|\frac{x}{c}\right| \le 1 \\ 0 & \left|\frac{x}{c}\right| > 1 \end{cases} \qquad (1)$$

with $n = 0,1,2,\dots$. In (1) $P_n^{(\alpha,\beta)}(\cdot)$ is the Jacobi polynomial of order n, $\alpha,\beta > $ -1 are parameters to be chosen so as to factorise the right edge behaviour of the unknown function, $2c$ is the width of the generic face and $\xi_n^{(\alpha,\beta)}$ is a suitable normalization quantity. The Fourier transform of (1) can be analytically evaluated as an hypergeometric function [4] and results in a generalization of the Neumann series, effectively applied in the analysis of conductive structures [2, 5, 6]. It can be shown that the elements of the impedance matrix obtained by applying the Galerkin method with functions (1) can be reduced to single integrals. Moreover their computation can be sped up by means of an analytical accelerating procedure [4]. Finally, due to the factorization of the correct singularities of the field, only few terms (usually 2 or 3 terms) are needed in order to achieve accurate results, so that very small matrices have to be dealt with. Moreover, the method can be generalized to non-homogeneous dielectrics, only modifying the Green function of the problem, whilst higher modes can be analyzed by means of the same expansion functions. Finally, the accurate, yet fast, analysis of the problem allows for the evaluation of the p.u.l. parameters of the structure as a function of the geometrical parameters.

References
1. J. Meixner, "The Behaviour of Electromagnetic Fields at Edges," IEEE Trans. on Antennas and Propagation, Vol. AP-20, 1972.
2. M. Lucido, G. Panariello, F. Schettino, "Accurate and efficient analysis of stripline structures," Microwave and Optical Technology Letters, Vol 43(1), 2004.
3. M.H. Burchett, S.R. Pennock, P.R. Shepherd, "Rigorous Analysis of the Higher Order Modes, Impedance and Attenuation Factor of Coupled Striplines", IEE Proc. on Microwave Antennas and Propagation, Vol. 141, 1994.
4. M. Lucido, G. Panariello, F. Schettino, "Analysis of the electromagnetic scattering by perfectly conducting convex polygonal cylinders," IEEE Trans. On Antennas and Propagation, Vol. AP-54, 2006.
5. S. Falco, G. Panariello, F. Schettino, L. Verolino, "Capacitance of a finite Cylinder," Electrical Engineering, Vol. 85(4), 2003.
6. M. Lucido, G. Panariello, F. Schettino, "Electromagnetic scattering by multiple perfectly conducting arbitrary polygonal cylinders," in print on IEEE Trans. On Antennas and Propagation.

Reverberation Chamber Measurements of Transmission Line Radiated Susceptibility

David A. Larrabee[1], Michael T. Franck[2]
[1]*East Stroudsburg University, East Stroudsburg, PA, USA*
[2]*East Stroudsburg University,East Stroudsburg, Pa, USA*

E-mail: dlarrabee@po-box.esu.edu

East Stroudsburg University has just finished building a reverberation chamber of dimensions 1.4 meters by 2.0 meters by 2.1 meters. Initial data suggests that this chamber initializes its "over-moded behavior" between 300 and 400 MHz. Above 400 MHz the orientation of the fields inside the chamber at a given point are highly dependent on the position of the "mode-stirrer", a set of paddles that rotate and alter the nature of the resonances inside the chamber. A transmission line placed in this environment will have a response that changes with the "mode-stirrer" orientation. Consequently the amplitudes of the various harmonic resonances on the transmission line are dependent on the field geometry, as determined by the paddle location. This reverberation chamber environment provides a way to determine the susceptibility of transmission lines to electromagnetic waves in environments where the orientation, polarization and spatial distribution of the interfering signal are unknown.

Traditional theory assumes that the nature of the interfering signal is known and uses modified transmission line equations to determine the response of the transmission line. Work in the field has shown that above the first resonance of the transmission lines the responses are dependent on the orientation of the field to the transmission line. This makes traditional plane wave testing difficult at best, since many different field orientations are required to determine the peak response of the transmission line.

The response of the transmission line to the fields in a reverberation chamber can be modeled as a pseudo statistical process where the random variable is the paddle orientation. The paddle changes all aspects of the field (including the magnitude). Ideally, the magnitudes of the fields in the reverberation chamber obey a truncated Raleigh distribution. The resulting statistical response can easily mask resonances on the line that do not have a large Q and typically results in a difference between the average response and the peak response of between 6 and 12 dB.

We will describe this effort in detail, present some of the early data and compare this data to the modified transmission line equations that have been used by many authors.

HPEM - 42
Transmission Lines at Low and High Frequencies: Theory, Numerical and Experiments. Part 2: Numerical Methods and Measurements (Invited)

Oral Presentations

HPEM - 42
Transmission Lines at Low and High Frequencies: Theory, Numerical and Experiments. Part 2: Numerical Methods and Measurements (Invited)

Oral Presentations

Modeling of the grounding electrodes of power transmission towers

N.V.Korovkin[1], M.Hayakawa[2], S.L.Shishigin[3]
Y.N.Bocharov[1], S.I.Krivosheev[1]

[1]Saint-Petersburg State Polytechnic University, Saint-Petersburg, Russia
[2]The University of Electro-Communications, Tokyo, Japan
[3] State Technical University, Vologda, Russia

E-mail: Nikolay.Korovkin@gmail.com

The reliability of the analysis of the lightning current spread processes in the power line substantially depends on the adequacy of the mathematical model of grounding electrode of transmission tower. So called "impulse resistance" R_i is currently used for the description of the spread processes in the earth. R_i is defined as the ratio of the maximal voltage to the maximal test impulse of current:

$$R_i = \max_t u(t) \Big/ \max_t i(t) .$$

Involving of the impulse resistance R_i is convenient for measurements because it allows to use peak voltmeters. But application of this notion does not guarantee the results accuracy for the short time processes. In our full-scale experiments we have obtained the oscillatory voltage and current on the grounding electrode of transmission tower. The notion of impulse resistance R_i is unacceptable for modeling in this case. In this report we present a new modelling technique of the grounding electrode with the use of its transitive resistance $z(t)$ (response on the unit-step function), which is determined from the oscillogram of the test impulse of the current.

Let's split a time interval, where we measure the current $i(t)$, into the N segments with length $"h"$ by the nodes $t_n=(n-1) h$, $n=1\ldots N+1$. Next we approximate the transitive resistance $z(t)$ by a piecewise-constant function z_n $n=1\ldots N+1$ (where z_n are unknown constants) and the observed current by a piecewise-linear function (i'_n=const). Using the discrete form of Duamel's integral [1] with the zero initial conditions we receive recursive equations for z_n:

$$z_1 = u_2 / i_2, \qquad z_n = \frac{\left[u_{n+1} - \sum_{m=2}^{m=n} z_{n-m+1}(i_{m+1}-i_m) \right]}{i_2}, \qquad n = 2..N, \qquad i_1 = u_1 = 0 .$$

Then, we can obtain the approximate expression of $z(t)$ by the regression analysis. Now the voltage of grounding electrode under influence of arbitrary current pulse can be defined by the Duamel's integral. We can also find the electrical circuit with the transient resistivity $z(t)$. In our applications the circuit contains in-series resistor R_s and parallel GLC circuit where R_s is resistivity of grounding electrode in the steady-state mode.

The considered technique was verified both on model problems and on experimental data of the real grounding electrodes of a transmission tower. It was shown that our simulation results are very close to the voltages measured in the experiments.

References

1. K. S. Demirchjan, L. R. Neiman, N. V. Korovkin, V. L. Chechurin, Theoretical bases of the electrical engineering. St.-Petersburg: "Piter", 2003, vol. 2, 575 p.

Analysis of Electromagnetic Transients in HV Substations: Main Issues and Investigation Methodologies and Tools

F. Delfino, R. Procopio, M. Rossi and P. Girdinio

Department of Electrical Engineering, University of Genoa
Via Opera Pia 11a, I-16145 Genova

E-mail: mansueto@die.unige.it (Corresponding Author: Mansueto Rossi)

This paper addresses the issue of the analysis of the effects of lightning flashes (direct and indirect) on power grid HV substations, in terms of the evaluation of overvoltage/overcurrent waveforms reaching the devices which could be potentially more afflicted by such disturbances, namely the power transformers (or autotransformers). The study is mainly devoted to identify the more suitable models, methodologies and investigation tools to carry out transient evaluations on HV substations [1] with the final aim to define a calculation platform into the PSCAD-EMTDC electromagnetic environment [2] for the simulation of real power grid configurations.

To investigate the cause of lightning failures of interconnection (auto)transformers, the first issue to be considered is the definition of suitable high frequency (HF) models for all the components of the power system under analysis (Fig. 1) and the development of techniques for fitting the model parameters with rated characteristics and experimental tests available for real devices. It should be highlighted that the scientific literature is plenty of models to simulate the power transformer HF behavior (see e.g. [3]) as well as the metal oxide surge arrester response to voltage pulses of atmospheric origin (well-established circuital blocks have already been implemented into the PSCAD-EMTDC environment), whereas, on the contrary, there is a certain lack of information on how to represent the other classical component of the protection system against overvoltages, namely the spark gap, which is often placed at the beginning of the transmission line (see Fig. 1) and whose use (also as back-up) is debatable, in view of the reliability and low price of modern surge arresters, and the behavior of the spark gap, inherently stochastic and leading to short circuit when sparkover occurs.

Physical models of the spark gap [4] are quite complex and not suited for an easy implementation in a circuit simulator; to overcome such difficulty, we opted for simpler integral methods [5], whose parameters have been tuned to fit computed and measured breakdown characteristics presented in [4].

Once the HF models of the power system under study have been defined and assessed, one has to face the problem of the choice of the line representation [6, 7]. Finally, a further investigation has been conducted in order to assess the dependence of the results provided by the power system model on the model itself level of complexity, that is to say that higher details have been introduced in some components (e.g.: modeling of the interconnections in the substation) and several comparative simulations have been performed in order to compare the basic model and the complex one.
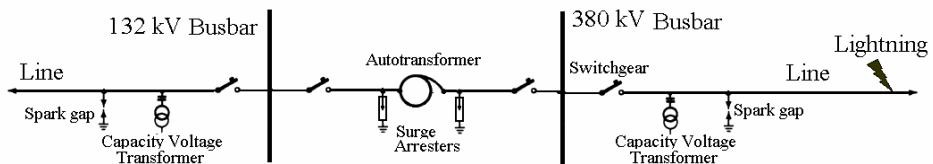
Fig. 1 – One-line diagram of a two-line 380/132 kV substation.

References
1. A. Greenwood, Electrical Transients in Power Systems. New York: Wiley, 2nd Edition, 1991.
2. PSCAD-EMTDC version 3.0, The Professional's Tool for Electromagnetic Transients Simulation, Manitoba HVDC Research Centre Inc., 2001.
3. A. Morched, L. Marti, J. Ottevangers, "A High Frequency Transformer Model for the EMTP," IEEE Transactions on Power Delivery, vol. 8, no. 3, pp. 1615-26, 1993.
4. A. Pigini, G. Rizzi, E. Garbagnati, A. Porrino, G. Baldo, G. Pesavento, "Performance of large air gaps under lightning overvoltages: experimental study and analysis of accuracy predetermination methods," IEEE Transactions on Power Delivery, vol. 4, no. 2, pp. 1379 - 1392, 1989.
5. A. Ancajima, A. Carrus, E. Cinieri, C. Mazzetti, "Breakdown characteristics of air spark-gaps stressed by standard and short-tail lightning impulses: Experimental results and comparison with time to sparkover models," Journal of Electrostatics, vol. 65, no. 5-6, pp. 282–288, 2007.
6. C. R. Paul, Analysis of Multiconductor Transmission Line. New York: Wiley, 1994.
7. F. Delfino, M. Nervi, R. Procopio, M. Rossi, "A Full-Maxwell Algorithm For the Field-to-Multiconductor Line-Coupling Problem", COMPEL, 22, 3 (2003), pp. 789-805.

HPEM - 42
Transmission Lines at Low and High Frequencies: Theory, Numerical and Experiments. Part 2: Numerical Methods and Measurements (Invited)

Oral Presentations

HPEM - 42
Transmission Lines at Low and High Frequencies: Theory, Numerical
and Experiments. Part 2: Numerical Methods and Measurements
(Invited)

Oral Presentations

Lightning Induced Disturbances in Complex Network of Lines or Cables

S Mezoued[1], B Nekhoul[1], K Kerroum[2], K El Khamlichi Drissi[2]
[1]*LAMEL Laboratory, Jijel University, Jijel, Algeria*
[2] *LASMEA Laboratory, Blaise Pascal University, Clermont Ferrand, France*
E-mail: Mezoued@mail.univ-jijel.dz

The coupling phenomenon for a complex network of lines or cables, excited by external electromagnetic fields is one of the most important issues in electromagnetic compatibility research. For this reason, C. R. Paul [1] proposed two frequential concepts (by [Φ] matrix or [S] matrix) to study this problem which allows only the determination of the induced currents or voltages.

In order to avoid the numeric heaviness while taking into consideration the electromagnetic aggression distributed along the transmission line, some authors [1-2] propose to replace it by current generators deducted after some mathematical manipulations. The choice of this representation of the electromagnetic wave emitted by lightning facilitates the modelling; the electromagnetic coupling problem becomes the study of a line directly powered by a generator. Unfortunately, this approach finds its limit in the non possibility of a network treatment. In our work we propose a new approach permitting to palliate such a difficulty and also to interface the results of the electromagnetic coupling with other software which allows the modelling of the circuits with generators well-defined.

For network, we translate the aggression in several current generators located at the nodes, by using an appropriate mathematical treatment. Using a topological representation for a network (containing lines, junctions and extremities) excited by the equivalent generators (representation of the electromagnetic wave), we deduct directly induced currents and voltages on the set of its extremities.

The principle of the concept which we propose to treat the electromagnetic coupling between the lightning and a complex network is based to translating the propagation relations expressed by [Φ] matrix [1] for all tubes (lines or cables) and the electric relations in the all nodes (Kirchhoff laws) to a matrix equation system: $[A][X] = [B]$; Where the matrix $[A]$ is made up of two submatrices $[A_1]$ and $[A_2]$ which is deducted from the representation by Φ matrix and the Kirchhoff laws for terminal and interconnection nodes, respectively. The vector $[B]$ includes the external field effects in form of localized generators. The vector $[X]$ contains the unknowns of the problem, i.e. the terminal total voltages and currents.

The results shown in Figure 1 and 2 represent respectively the computed and measured (realised by France-Telecom) induced currents at the last extremity of a radial network composed of nine multi - core shielded cables (3 cores). The total length is 2588m and it is at 4m above the ground. The shield of the cable is ended at the extremities by two resistances of 40 and 228Ω respectively and grounded at the first extremity of the segment 4 [3].
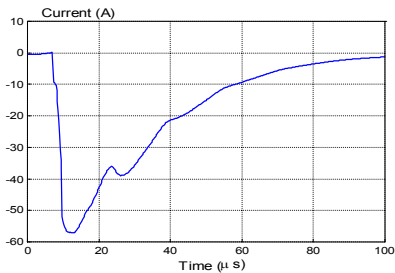
Fig. 1 Computed total current at the second extremity of the 9th cable shield using the generators model.
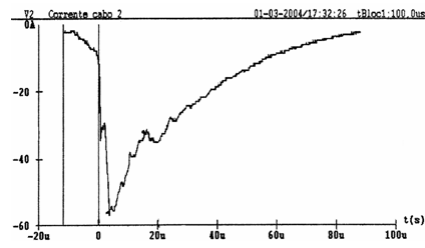
Fig.2 Measured total current at the second extremity of the 9th cable shield [3].

References
1. Analysis of Multiconductor Transmission Lines, New York: Wiley, 1992.
2. S. Mezoued, S. Kaouche, B. Nekhoul, K. Kerroum, K. El Khamlichi Drissi, F. Paladiane "Illumination d'un réseau de lignes ou de câbles par une onde de foudre : Modélisation par des générateurs de courant ", Annales de Télécommunications, Vol. 61, n° 5-6, pp. 721-747, 2006.
3. E. F. Gastaldi, F. José Pissolato, J. A. Rossi, "*Computer Simulation of some Lightning Effects on a Telecommunication Network"*, in Proc, International Symposuim on Electromagnetic Compatibility, EMC 2004, Vol. 2, pp 452, 457, Aug. 2004.

Transmission-Line Modeling of Materials with Nonlinear Properties in an Unstructured Triangular Grid

J. G. Wykes, P. Sewell, A. Vukovic, C. Christopoulos, T. M. Benson, D. W. P. Thomas
George Green Institute for Electromagnetics Research, University of Nottingham, Nottingham, UK

E-mail: jim.wykes@nottingham.ac.uk

The Transmission-Line Modeling (TLM) method formulated for unstructured triangular grids is extended to model materials exhibiting instantaneous dielectric nonlinearity. This has applications in modeling various optical devices—e.g. switches, limiters, and all-optical photonic circuits—whose operation is based upon the nonlinear material properties. The time-domain formulation of TLM makes it an effective method for modeling nonlinear phenomena. In addition, unstructured meshes facilitate the accurate description of oblique or curved material interfaces and allow mesh grading to be applied around fine-features and complex structures.

The unstructured triangular TLM scattering algorithm is derived via a modal approach which is detailed in [1]. The equivalent circuit for the triangular node consists of three transmission lines connected at the node centre. A time-domain model of the circuit is obtained via a transmission line equivalent circuit which models the inductors as series links and adds stub capacitors at the connection ports to model any excess capacitance required on each line. The dielectric behavior is localized to the stub capacitors, hence the nonlinear stub admittance is modeled using a discrete time transform which explicitly factors out the capacitance from the scattered state voltages in the stub. This allows an instantaneous capacitance value to be used to retrieve the stub voltage [2,3]. A Newton-Raphson iteration is used to solve for the port voltage V_p, since in the nonlinear case the capacitance is a function of V_p.

The propagation of a 1.2µm FWHM Gaussian beam in linear and nonlinear media is shown in Fig. 1 to demonstrate the operation of the model. An unstructured triangular mesh was used with minimum, maximum and average link lengths of 0.006µm, 0.034µm and 0.015µm respectively. The operating free-space wavelength is 1.55µm and the linear refractive index is $n_0 = 3$. The functional form of the nonlinear refractive index is $n = n_0 + \Delta n_s(1-\exp(-n_{ni}I))$ where I is field intensity. Self-guiding behavior is clearly observable in the nonlinear medium. Further results will be reported on other structures which benefit from the advantages offered by unstructured meshes. Finally, discussion will be made about the constraints placed upon the time step of the algorithm when integrating the unstructured mesh formulation with negative nonlinearity.
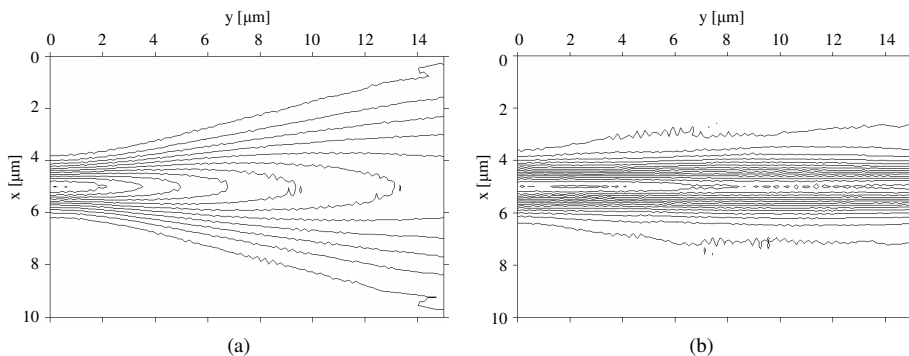
Fig. 1 –Propagation of a Gaussian beam in (a) linear and (b) nonlinear media.

References
1.   P. Sewell, J. G. Wykes, T. M. Benson, C. Christopoulos, D. W. P. Thomas, A. Vukovic, "Transmission-line modeling using unstructured triangular meshes", IEEE Trans. Microwave Theory and Techniques, vol. 52, no 5, 2004.
2.   C. Christopoulos, The Transmission-Line Modeling Method: TLM. New Jersey: IEEE Press, 1995
3.   S. Y. R. Hui and C. Christopoulos, "Discrete transform techniques for solving nonlinear circuits and equations", IEE Proceedings-A, Vol. 139, No. 6, 1992.

Investigation on the transmission of a DC current through a space gap

F. Roman[1] , N. Peña[2], L. Arevalo[1], F Santamaria[1], J. Herrera[1] A. Alarcón[2], F. Vega[1]
[1]*Grupo de Compatibilidad Electromagnética, Universidad Nacional de Colombia, Bogotá, Colombia*
[2]*Grupo de Electrónica y Sistemas de Telecomunicaciones, Universidad de los Andes, Bogotá, Colombia*

E-mail: fjromanc@unal.edu.co

Oral Presentations

It is well known that when a relative high-voltage is applied to a needle or group of needles placed in a plate electrode, corona discharge appear on the needles tip. Corona discharges are associated with the generation of current impulses such as Trichel or streamer impulses (see Fig. 1). Such impulses have a short rise time, in the order of a few nano-seconds. Some are regular such as the Trichel pulses in the negative polarity. Others, like the streamer impulses in positive polarity are more chaotic.

In several floating electrode experiments, it has been observed that a DC Corona source can charge a floating electrode. However, by extending these experiments to a high impedance current source, it has been observed that Corona discharge can bridge gaps of certain length –circa 500 mm-.

 Observations in well controlled gap-experiments have shown that the current flowing in the high voltage electrode side is the same as the current measured in the earth side. These gap-experiments have shown that it is possible to transfer a DC current through the air. This indicates that a DC current is transformed into an ionic current that bridges the gap. However, it is interesting to investigate if displacement or currents are also produced in the interelectrodical gap space.

In this paper we investigate if there are important displacement currents responsible for the measured current in the earth side. Obtained results are presented and discussed.
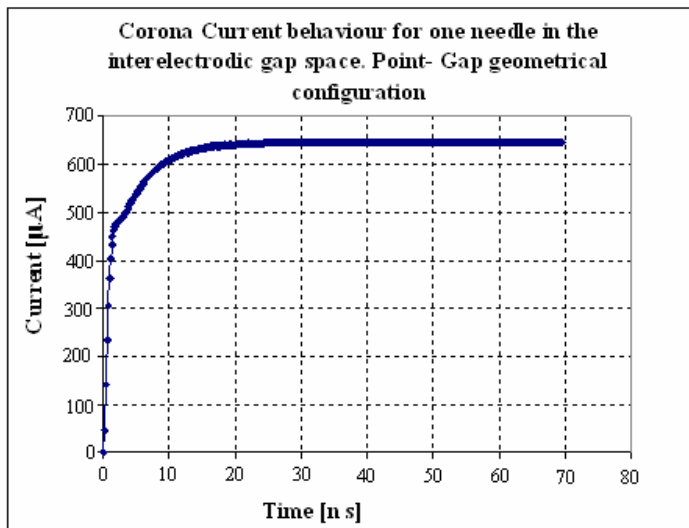
Fig. 1 –Corona Current behaviour in the interelectrodical gap space for a needle-to-point configuration. Notice the calculated first nanoseconds of a Trichel pulse

Microwave Pulse Compression Experiments at Low Power

E. G. Farr[1], L. H. Bowen[1], C. E. Baum[2] and W. D. Prather[3]
[1]Farr Research, Inc., Albuquerque, U.S.A.
[2]University of New Mexico, Albuquerque, U.S.A.
[3]Air Force Research Laboratory, Kirtland AFB, U.S.A.
E-mail: efarr@farr-research.com

Microwave Pulse Compression is a technique for converting a long-duration pulse of microwave power into a pulse with shorter duration and higher amplitude. This is normally implemented by filling a resonant cavity with microwave power, and firing a switch that makes the cavity no longer resonant, thereby dumping the power.

The advantage of pulse compression is that it allows one to use a source with only modest power to realize a source with significantly higher power. Such considerations become important in operational HPM systems, because they otherwise can be quite massive, making them impractical for field use.

In this paper, we demonstrate pulse compression at low power levels. Most of our experiments were carried out at L-band, at a frequency of 1.3 GHz. We drove the cavity with either a 100 W or 1 kW amplifier, and realized a gain of around 20 dB within the cavity, and 12 dB at the output.

We experimented with a variety of switches, including triggered and untriggered gas discharge tubes (GDTs) filled with low-pressure air. Our trigger was either a 30 kV FID pulser, with pulse width of 3 ns, or a homemade pulser built from an automotive ignition coil. We found that if we controlled the pressure carefully, the switch would self-break with acceptable reliability, so a trigger was not necessary. Typical operating pressures were around 100 mTorr, which was near the bottom of the Paschen curve for breakdown of gases.

The resonant cavity was a length of WR-650 rectangular waveguide, $3\lambda_g$ in length, where λ_g is the guide wavelength. Our cavity was constrained on the input end by an inductive iris centered in the waveguide, with a slot width of one-quarter the waveguide width. On the output end, the cavity was constrained by an H-plane tee, with a sliding short tuned to provide an optimal resonance. The GDT containing the switch was positioned $\lambda_g/4$ from the sliding short.

An example of our data is shown in Figure 1. Data were measured with B-dot sensors positioned in the side of the waveguide, at the location of maximum field, in both the input and output sections of the WR-650 waveguide. The probes were calibrated to provide the same output. Based on these results, we find a gain of 12 dB at the output, and a pulse width of 50 ns.

We will be testing a higher power input source this spring, and we hope to report on those results as well.
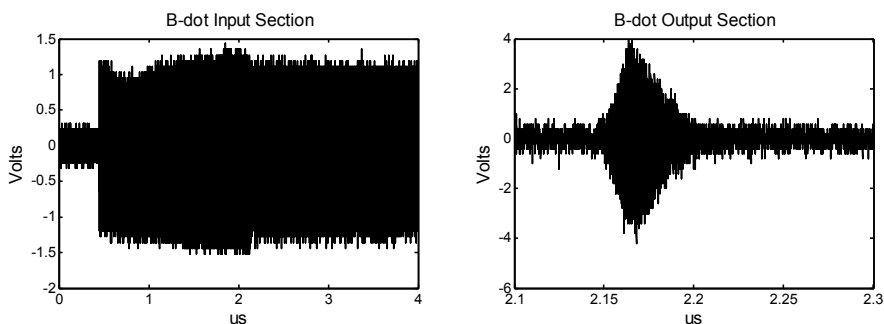
Fig. 1 – Pulse Compression, input (left), and output (right).

HPEM - 43
Pulsed Power

Oral Presentations

Broadband Antenna SWR Improvement Using Parallel RLC Loads

T. T. Gazizov, T. R. Gazizov

Television and Control Department, Tomsk State University of Control Systems and Radioelectronics
634050, Lenin Ave., 40, Tomsk, Russia
timur@tomline.ru

The antenna SWR (Standing Wave Ratio) shows how much of radio's transmitting power is reflected from the antenna back to the antenna cable and is very important antenna characteristic. Thus, engineers are often interested in SWR decrease. Unfortunately, it is hard to achieve this aim in wide frequency band and with various limitations, for example, on structure and form of antenna.

Main object of this work was to design broadband antenna with SWR < 5 in frequency band from 1 to 30 MHz. One of the SWR decrease methods is using parallel RLC loads in antenna structure. Parallel RLC circuit is the most common trap, which anti-resonates at $f = 1/2\pi\sqrt{(LC)}$. By properly integrating one or more of these traps into a wire antenna, it is possible to strongly modify the current distribution in wires at different frequencies and therefore electromagnetic features of antenna.

First, simulations of antenna structure were done to design the antenna geometry (Fig. 1*a*). Then, genetic algorithm (GA) was used to optimize parameters and location of parallel RLC loads in antenna. (Genetic algorithms are stochastic search techniques that guide a population of solutions using the principles of evolution and natural genetics. In recent years, genetic algorithms have become a popular optimization tool for many areas of research, including the antenna design [1].) Each of four antenna wires was parted with 100 segments and the number of segment in which parallel RLC load have to be included was optimized. After this, R, L, and C values for load groups in wires were optimized with the same aim: to decrease SWR.
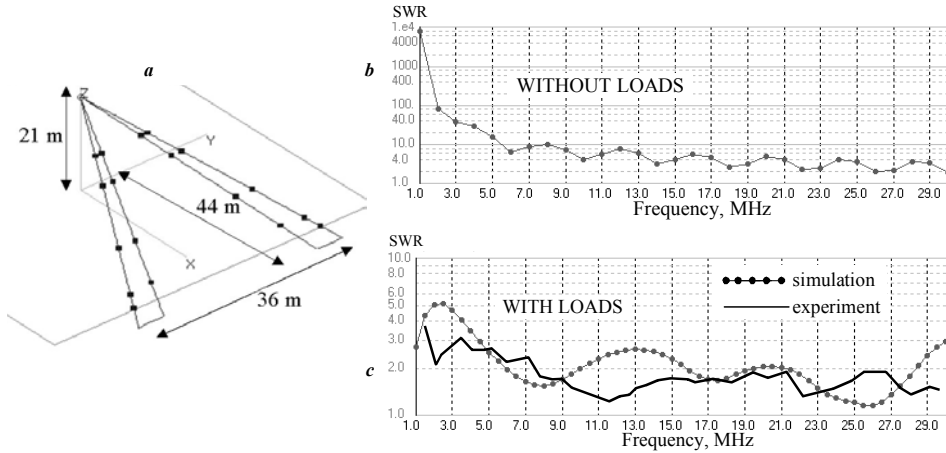
Fig. 1 – Antenna structure (*a*) and SWR frequency dependances without (*b*) and with (*c*) loads

The real antenna was made according to simulations and its SWR was measured. Simulated SWR for antenna without loads is shown in fig. 1*b*. It is seen that antenna SWR < 5 from 13 to 30 MHz. Simulated and measured SWR for antenna with parallel RLC loads are shown in fig. 1*c*. It is seen that antenna SWR < 5 from 1 to 30 MHz, according to assigned design specifications. The similarity between the simulated and experimental data is satisfactory. Difference found in fig. 1c between simulated and measured SWR can be explained through the presence of the matching transformer (50 to 200 Ohms) in the experiment, while the absence in simulation (SWR for 200 Ohms). Moreover, some differences between real parameters and parameters used in simulation have contributed to SWR difference. Thus, the arrangement of parallel RLC loads and the GA optimization of their technical parameters allow improving SWR of antenna without changing its structure or shape.

References

1.   J.M. Johnson, Y. Rahmat-Samii. Genetic algorithms in engineering electromagnetics. IEEE Antennas and Propagation Magazine, vol. 39, no. 4, August 1997.

HPEM - 43
Pulsed Power

Oral Presentations

Study of High Power Terahertz Generation Using Integrated Wide-bandgap Semiconductor Photoconductive Switches

P. Kirawanich[1], S. J. Yakura[2], C. E. Baum[3], W. C. Nunnally[1], and N. E. Islam[1]

[1]*Electrical and Computer Engineering Department, University of Missouri, Columbia, MO, USA*
[2]*Air Force Research Laboratory, Directed Energy Directorate, Kirtland Air Force Base, NM 87117 USA*
[3]*Electrical and Computer Engineering Department, University of New Mexico, Albuquerque, NM 87131 USA*

E-mail: IslamN@missouri.edu

High power terahertz (THz) devices, which operate in the sub-millimeter wavelengths, offer the possibility of high resolution imaging of objects at relatively far distances (e.g.., relative to the capabilities of infrared devices) and provide undetectable THz communication links between troops in the battlefield. These devices provide superior performance when operated at high switch voltages for wideband THz applications.

Although many different schemes for THz generation have been demonstrated thus far, one of the most promising techniques for the creation of intense THz fields is through photo excitation of biased semiconductor antennas. The figure below shows the three-dimensional models of the standard Auston photoconductive (PC) antenna and the power-enhanced wideband PC antenna integrated with wide-bandgap semiconductors, such as GaN and SiC [1], investigated under this study. The two interdigitated finger electrodes accompany the large-aperture antenna structure to overcome the limitation of high bias voltage or pulsed voltage supplies [2]. Shadow masks were deposited on the top layer to allow radiation only at every other electrode spacing. This design forces the THz radiation, emitted through the substrate, to constructively interfere in the far field. The simulation method used in the preliminary simulation study is the finite-difference time-domain (FDTD) technique, which provides a discrete formulation of Maxwell's equations for computer programs applied towards electromagnetic field problems with complex geometries. Preliminary simulation analyses, using an in-house FDTD code, show encouraging results on a proposed antenna system as compared with the standard antenna system in terms of increasing the field strength at a specified target location.

In this presentation, we report on the simulation results from which we have obtained through coupling of the carrier transport equations in the semiconductor material with Maxwell's equations for THz radiation from an antenna. We also expect to present our fabrication techniques and the testing of wide-bandgap semiconductor materials, used in the photoconductive, semiconductor-switch (PCSS)-based THz antenna system.
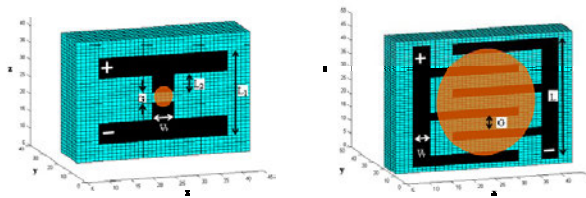
Fig. 1 – Schematics of the standard and power-enhanced wideband PC antennas.

References
1. R. Gunda, D. S. Gleason, K. Kelkar, P. Kirawanich, W. C. Nunnally, and N. E. Islam, "Radio-frequency heating of GaAs and SiC photoconductive switch for high-power applications", IEEE Trans. Plasma Sci., vol. 34, no. 5, pp. 1697–1701, Oct. 2006.
2. H. Yoneda, K. Tokuyama, H. Nagata, S. Ohta, R. Nakamura, K. Ueda, H. Yamamoto, K. Baba, "Generation of high-peak-power THz radiation by using diamond photoconductive antenna array," pp. 644-645, Vol. 2, LEOS 2001: The 14th Annual IEEE Meeting, 12-13 Nov. 2001.

HPEM - 43
Pulsed Power

Oral Presentations

Radiating broad-band pulse generator with corona charging mechanism

F. Roman[1], N. Peña[2], J. Herrera[1], F. Santamaría[1], N. Mora[1], E. Aguilera[2], O. Díaz[1], F. Vega[1]

[1]*Grupo de Compatibilidad Electromagnética, Universidad Nacional de Colombia, Bogotá, Colombia*
[2]*Grupo de Electrónica y Sistemas de Telecomunicaciones, Universidad de los Andes, Bogotá, Colombia*

E-mail: fjromanc@unal.edu.co

A radiating pulse generator conformed by a discone antenna fed by a corona source is proposed. The electromagnetic pulse generator consists of a broad-band impulse radiating antenna (IRA) connected to a gas-discharge switch. The antenna behaves as the charge-holding element avoiding the need of an external capacitor. The discone antenna is connected to a switch, as indicated in Fig. 1. The cone element of the antenna is grounded, while the disc element is a floating electrode: the switch isolates it from the ground. The floating disc element is charged by the corona-needles source. The deposited electrical charge on the floating disc electrode raises its potential to several kilovolts. Once the voltage across the switch reaches its breakdown threshold, the floating disc element will discharge to ground radiating in the process a clean, broad-band damped-sinusoidal pulse. Corona charging mechanism provides independence of the radiating system from the primary source because they are DC isolated. One of the main advantages of this device is the low inductance of the discharge path. For this reason, extremely fast impulses can be produced [2].Thus, repetition rates around hundreds of Hz can be achieved. This novel charging mechanism is a simple alternative to inductor or transformer-based charging systems that require special precautions to prevent arc-breakdown between adjacent loops in the coils [1]. A prototype of the proposed pulse generator was constructed using a pressurized-air switch. Measurements with a B-dot sensor show that the generator is able to produce pulses in the tens of volts per meter at 20 m with a repetition rate around of Hz when charged with a high-voltage DC source.
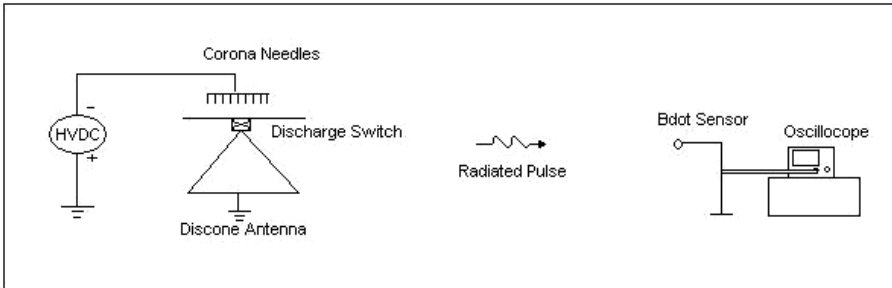
Fig. 1 – Schematic representation of the experimental set-up. Notice the discharge switch between the two elements of the discone antenna. The antenna disc is fed by a corona source. A B-dot sensor registers the radiated emission of the radiating broad-band pulse generator.

References
1. K. D. Hong, S.W. Braidwood, "Resonant Antenna-Source System for Generation of High-Power Wideband Pulses," IEEE Transactions on Plasma Science, vol. 30, 2002.
2. F.J. Roman, "Effects of Electric Field Impulses Produced by Electrically Floating Electrodes on the Corona Space Charge Generation and on the Breakdown Voltage of Complex Gaps," Comprehensive Summaries of Uppsala Dissertations form the Faculty of Science and Technology 246, ACTA UNIVERSITATIS UPSALIENSIS, UPPSALA 1996.

New Possibilities of FID Technology of Forming of Nano- and Picosecond Voltage Pulses with Gigawatt Peak Power

M. V. Efanov[1] and V. M. Efanov[1]
[1]*FID GmbH, Burbach, Germany*
E-mail: vlad@fidtechnology.com

Forming of voltage pulses with amplitude of tens of kilovolts and rise time of about 100 ps remains a complex technical task and at pulse repetition rate of tens and hundreds of kilohertz is possible only using FID technology. When amplitude of pulses is increased to 100-200 kV it was possible to obtain rise time of 100-200 ps but only at PRF of up to 1 kHz.

Further increase of amplitude to 500-1000 kV has been making the task of forming of pulses with rise time of 300-500 ps almost impossible in repetitive mode.

FID GmbH has solved several principal problems and obtained a qualitative jump increasing peak power of nano and picosecond pulse generators.

1. Solid state FID switches with peak power of more than 1 gigawatt and transition time from hundreds to tens of picoseconds have been developed;
2. New principles of forming voltage pulses of nano- and picosecond range with amplitude from several hundreds of kilovolts to several megavolts have been researched;
3. New methods of generation of picosecond and nanosecond voltage pulses with extremely low timing jitter of less than several tens of picoseconds have been found.

New principles of generation allow simultaneously achieve high amplitude, short rise time, compact size and high efficiency. The ongoing development work and experimental testing of pulses with rise time of 500 ps and amplitude of 1 megavolt into 50 Ohm with peak power of 20 GW and pulse repetition rate of several hundreds of hertz.

At the same time a pulse generator is being developed with amplitude of 30-50 kV, rise time of 100 ps, pulse duration of about 1 ns and pulse repetition rate of up to 100 kHz.

HPEM - 43
Pulsed Power

Oral Presentations

Solid State Pulse Generators with Picosecond Pulse Duration and Megawatt Peak Power

V. M. Efanov[1], M. V. Efanov[1], A. V. Komashko[1], P. M. Yarin[1]

[1]*FID GmbH, Burbach, Germany*

E-mail: vlad@fidtechnology.com

At the present days the pulse terahertz range pulse technology is experiencing a rapid growth. In this case it is necessary to generate voltage pulses with duration from tens of picoseconds to several picoseconds. The known methods of generation of such pulses allow forming of pulses with amplitude from several volts to tens of volts which corresponds to peak power of not more than few watts.

FID GmbH has performed a large volume of theoretical and experimental studies which allowed foundation of a new class of FID switches with turn on time of 10-20 ps and operating voltage of from 1 to 10 kilovolts.

On the basis of these devices pulsers which output voltage pulse with amplitude of up to 10 kV, rise time of about 20 ps and pulse duration of 50-100 ps have been developed.

Research of operating specifications of pulse generators at pulse repetition rate of 1-20 kHz has been performed.

As a result high stability of all parameters was reached. Jitter of delay time between a triggering pulse and output pulse has been estimated as 5 ps.

A method and testing plant for measuring high voltage pulse with rise time of 10-20 ps has been developed.

High voltage attenuators manufactured by FID GmbH and Barth Electronics Inc. with bandwidth of up to 30 GHz were used for measurements. Effects of feeding picosecond high voltage pulses through different types of cables and strip lines were researched.

Pulse generators have compact size, high efficiency and reliability.

HPEM - 43
Pulsed Power

Oral Presentations

A New Approach In Miniaturization Of Printed Circuit Antenna Using ARL For SB, DB & Wideband Applications

S. V. Pandey[1], B. K. Sarkar[2], S. Ghosh[3]

[1,3]*PG Student, M.Tech (RF & Microwave Engg-4),E & EC Engg. Deptt., Indian Institute of Technology, Kharagpur- 721302, (W. B.) INDIA*
[2]*ISRO Chair Professor,E & EC Engg. Deptt., Indian Institute of Technology, Kharagpur,(W. B.) INDIA*
E-mail: svpandey@ece.iitkgp.ernet.in, shailesh_pandey@yahoo.com

A miniaturized printed circuit antenna is finding increasing usage in mobile-communication handsets. Thus, reduction of antenna size is required for practical use. Several methods for size reduction have already been examined through simulation and experiment. But all these techniques are able to reduce the antenna size more or less by 50%. Since the resonant frequency of a patch antenna is inversely proportional to √permittivity, it is possible to reduce the resonant frequency by using a substrate with high dielectric constant. However, high-permittivity material entraps the EM energy within the near-field region due to existence of impedance contrast between the dielectric material and the surrounding air region and, as a result, the impedance bandwidth becomes very narrow.

Here is a approach of low-profile miniature design using an annular-ring loaded circular patch antenna, which has a smaller size when compared to a circular patch antenna without annular-ring for a given frequency. An annular-ring patch antenna, which comprises of an inner radius and outer radius, is resonant at a lower frequency when inner radius is smaller, when inner radius becomes much smaller, the impedance of feed point becomes large and it is difficult to match the impedance using coaxial probe. A cross-slot in the ground plane can achieve much more reduction of patch size and the introduction of a concentric slot-ring provides the broadband characteristics.

A circular patch of radius is centered in the narrow annular-ring, of outer radius and inner radius. These patches are printed on substrate, of different permittivity and different thickness for getting the desired & ideal result. The crossed slot in the ground plane has unequal lateral lengths, with a certain slot width. This structure excites two different orthogonal modes with equal amplitude and out of phase difference. The optimized dimensions are selected and certain simulations are done according to which results are selected. For better matching of input impedance, a circular slot of certain radius is selected at the centre of the cross slot. This antenna provides circular polarization and is significantly smaller than the conventional annular-ring patch antennas with a strip. The proposed structure is shown as below in Fig.1. In this proposed structure 10 dB Return loss bandwidth is improved upto 6.6% compare to conventional Circular, & shorted circular patch antenna. The designed miniaturized printed circuit antenna is reduced in size by over 55% & has enough antenna gain for practical applications. The relatively wide bandwidth and centre-frequency are not heavily dependent on the feed point position, as antenna provides a convenient match to 50Ω.
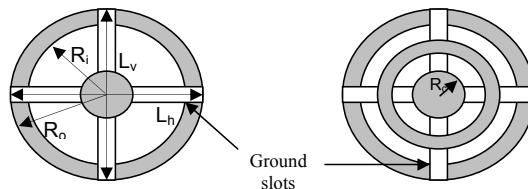
Fig. 1 – Proposed ARL Antenna

References
1. Shen, L., Long, S., Allerding, M., Walton, M., "Resonant frequency of a circular disc, printed-circuit antenna", Antennas and Propagation, IEEE Transactions, Vol. 25, pp. 595–596, July 1977.
2. Weng Chew, Jin Kong, "Analysis of a circular microstrip disk antenna with a thick dielectric substrate", Antennas and Propagation, IEEE Transactions, Vol. 29, Issue 1, pp. 68 – 76., January 1981.
3. R. Garg, P.Bhartia, Inder. Bahl, A. Ittipiboon, Microstrip Antenna Design Handbook, Artech House, Nov. 01, 2000.
4. Tzung-Wern Chiou; Kin-Lu Wong, "Designs of compact microstrip antennas with a slotted ground plane", Antennas and Propagation Society International Symposium, 2001 IEEE, vol. 2, pp. 732 – 735, July 2001.
5. Jeen-Sheen Row and Kuang-Woei Lin, "Design of an Annular-Ring Microstrip Antenna for Circular Polarization", Microwave And Optical Technology Letters, vol. 42, No. 2, pp. 156-157, July 2004.

HPEM - 44
Microstrip and Patch Antennas

Oral Presentations

Optimization of Helical Microstrip Antenna for Space Applications by Means of Genetic Algorithm

Elham Sharifi Moghaddam[1], S. M. Nematollahzadeh[2], S. Amiri[3]

[1]Iranian Space Agency, Tehran, Iran
[2]Iran Telecom Research Center, Tehran, Iran
[3]Iranian Research Organization of Science and Technology, Tehran, Iran
[1]esharifi@itrc.ac.ir, [2]nematz@itrc.ac.ir, [3]amiri@irost.org

Helical microstrip antenna has conformal nature and unique radiation characteristics which have made it suitable for space applications. This antenna consists of a tape helix around a dielectric cylinder with a conducting core (Fig.1). In this article a microstrip helix antenna is designed and optimized for a LEO satellite in X-band. The aim of optimization is obtaining saddle-shape pattern for compensating free space loss variations in the coverage area. Satellite altitude and minimum elevation angle of user terminals are the parameters which determine the radiation pattern shape.

Radiation pattern of microstrip helix antenna depends on helix radius, number of turns, pitch height and relative permittivity of substrate. In special physical states microstrip helix is a leaky wave antenna and could have a saddle-shape pattern which is proper for LEO satellites. A leaky wave is a traveling wave progressively leaking out power as it propagates along a wave guiding structure. Solutions for the complex-valued propagation constant $\square$ provide information about the excitation of fast waves [1-2].

For the antenna analysis and optimization, we have used CST MWS (Computer Simulation Technology, Microwave Studio), the powerful electromagnetic field simulation software which uses FIT (Finite Integration Technique) method. The validity of the analysis results is approved by comparing them with the results which have been derived from an analytical method based on reciprocity theory. [3]

We applied a Genetic Algorithm (GA) optimization technique in CST MWS's VBA (Visual Basic for Applications) compatible macro language. In this optimization the steady-state GA is used and elitist strategy is implemented. The stochastic selection strategy for selecting parents is proportionate selection (Roulette wheel selection). The method for selecting the individuals to be replaced by temporary population is also proportionate selection. Fitness function in this optimization is defined for the aim of obtaining arbitrary saddle-shaped pattern. In this problem the real-valued chromosomes have been used and each chromosome has six genes: b (helix radius), a (conducting core radius), n (number of turns), p (pitch length), w (tape width) and ε_r (relative permittivity of substrate) [4-5].

Effects of ε_r and the radius of conducting core on the radiation pattern have be studied in the article. Results show that, when ε_r increases, the portion of leaky-wave radiation

Fig. 1: A microstrip helix antenna with conducting core

decreases and radiation pattern tends to the axial mode. When radius of conducting core decreases, leaky-wave increases and the saddle-shape pattern comes near to the pattern of normal mode.

References

1. Andrew F. Peterson, Bruce S. Greene, Raj Mittra, "Propagation and Radiation Characteristics of a Tape Helix with a Conducting Core and Dielectric Substrate," IEEE Transactions on Antennas and Propagation, Vol. 38, No. 4, April 1990.
2. E. A. F. Abdallah, A. A. Mitkees, S. A. Hamdy, A. A. Elsohly, "Propagation Constant of Microstrip Leaky-Wave Antennas", Microwave and Optical Technology Letters/ Vol. 3, No. 12, Dec. 1990.
3. Rodney. A. Martin, Douglas. H. Werner, "A Reciprocity Approach for Calculating the Far-field Radiation patterns of a Center-Fed helical on a Dielectric-Coated Circular Cylinder," IEEE Transactions on Antennas and Propagation, Vol. 49, No. 12, dec.2001.
4. Y.Rahmat-Samii and Eric Michielssen, Electromagnetic optimization by genetic algorithms, John Wiley Inc., 1999.
5. J.M.Johnson and Y. Rahmat-Samii, "Genetic algorithms and method of moments (GA/Mom) for design of integrated antenna," IEEE Trans. Ant\\0ennas and propagation, vol.47, p.1606, Oct.1999.

Empirically Comparing Computational Optimisation Techniques for Microstrip Antennas

R. A. Woodhouse, S. J. Porter and J. F. Miller
University of York, York, U.K.
Email: raw113@ohm.york.ac.uk

Evolving antennas using various computational techniques, as opposed to using conventional design techniques, is an established and successful method of antenna creation. One of the best examples is the evolution of wire antennas for a NASA satellite [1].

Microstrip antennas are becoming increasingly used in personal mobile communications devices such as mobile phones and personal digital assistants. The main reasons for this are their low profile and low cost. Modern mobile communications systems typically require that not only should the antennas be electrically small but also that they should be able to operate in several different frequency bands that are not necessarily harmonically related.

Only a very limited number of techniques have been applied to the optimisation of microstrip antennas. This study aims to empirically compare the efficiencies of various techniques when evolving multi-band microstrip antennas. The goal was to produce a dual-band probe fed antenna with bands centered at 3.5 and 4 GHz, each with a -10 dB, or less, return loss bandwidth of 100 MHz. Existing theory and studies at The University of York showed that optimising for directivity and polarisation was not necessary, thus making the problem considerably simpler.

The top surface of the microstrip antennas in this study consisted of a 12 x 12 grid of squares. Each square was approximately 2mm x 2mm, and could be metalised or not. Meandered current paths and parasitic patches are some of the structures that result in one or more of the following beneficial features of microstrip antennas: electrically small size, broad-band and multi-band operation. The grid representation should enable various optimisation algorithms to generate structures that result in these desirable characteristics.

Various techniques have been used in this study including a relatively new one called Cartesian Genetic Programming (CGP) [2] which has never before been used in any electromagnetic optimisation problems. Results so far indicate that steady-state genetic algorithms are the most efficient optimisation techniques.

The study has yielded several antennas that either fully meet the specification or come very close to it. One such antenna can be seen below (Fig 1).
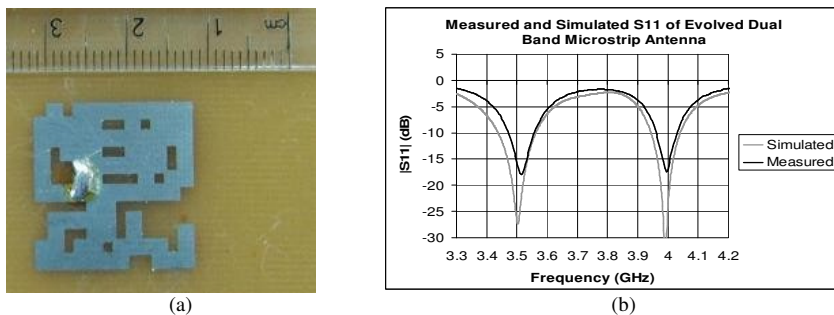
(a)   (b)
Fig. 1 – (a) Evolved antenna and (b) S11 of evolved antenna.

References

1.   J. D. Lohn, G. S. Hornby, D. S. Linden, "An Evolved Antenna for Deployment on NASA's Space Technology 5 Mission," Genetic Programming Theory Practice 2004 Workshop (GPTP-2004), May 2004.

2.   Miller, J., "What bloat? Cartesian Genetic Programming on Boolean problems", In: Late Breaking Papers, Proceedings of the 3rd Genetic and Evolutionary Computation Conference (GECCO'01), pp. 295 -302.

On the behavior of short-circuit, permittivity and arms in planar antennas miniaturization

C. M. Costa Jr[1]., G. Fontgalland[1], M. A. B. de Melo[1], T.P. Vuong[2], R. C. S. Freire[1]

[1]*UFCG/CEEI/DEE/LEMA, Av. Aprígio Veloso, 882, Campina Grande, PB, 58109-970, Brazil*
[2]*LCIS/ESISAR-INPG, 50,* rue Barthélémy de Laffemas, Valence, 26902, France

Crezo.jr@yahoo.com.br, fontgalland@dee.ufcg.edu.br, marcos@dee.ufcg.edu.br, Tan-Phu.Vuong@esisar.inpg.fr, rcsfreire@dee.ufcg.edu.br

The miniaturization is one of the main goals of research and applications in electrical engineering. In applications such as: embedded systems, biomedical and systems for radio-frequency identification (RFID), the physical size of the antenna becomes a limiting to the reduction these systems. In this paper some parameters was studied to reduce the physical size of the antenna, such as: short-circuit, permittivity and a particular geometry of the E-shape patch antenna. The influence on the antennas radiation characteristics of short-circuits position and diameter, permittivity value and thickness, as well as, tangent loss, the numbers and length of arms are presented. In the analysis of antenna's sensitivity, the geometry used is of the electrically small rectangular patch antenna (Figure 1.a). The resonance frequency is 2.45 GHz, dielectric substrate is the FR4 (ε_r = 4.6, $tan\delta$ = 0.02 and h = 1.6 mm) and the other parameters are: a = 13.5 mm, b = 9.6 mm, r_s = 0.3 mm, r_s = 0.3 mm, d_f = 1.7 mm and d_s = 0.4 mm, figure 1.a. The metal surface of the rectangular patch antenna is 0.2 mm less than the surface of the substrate in each edge. To analyze the short-circuit position effects, the previous parameters simulated were maintained constant and the position of the short (d_s) were modified for two others positions: 0.5 mm and 0.6 mm. The results were simulated using the CST-Microwave Studios software and to show the return loss and others parameters (figure 1.b).
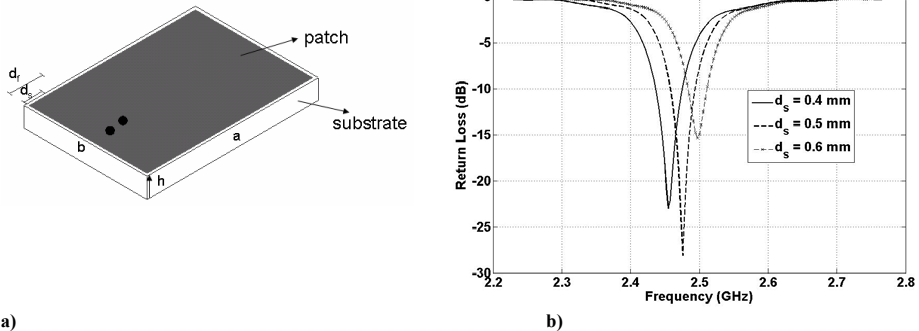
Figure 1. a) Geometry of the rectangular patch antenna and b) results of the return loss for variation in the position of the short-circuit.

In this work **t**he equivalent circuit models geometry and current distribution on patch antenna, as well as, the sensitivity to permittivity, thickness and tangent loss of substrate were obtained. Finally, in this work we can show the behavior of the antenna's response to the introduction of arms to reduce the physical size of the antenna. The results can be used as a first step guide to design miniaturized patch antennas. The comparisons with literature results are in good agreement and it suggest the design of new types of structures.

References

1. Ramesh G., Prakash B., Inder B., Apisak I., "Microstrip antenna designe handbook", Artech House, Inc., 2001.
2. Kin-Lu Wong, "Compact and Broadband Microstrip antennas", John Wiley & Sons, inc, 2002.
3. G. Kumar, K.P. Ray, "BroadBand Microstrip Antenna", Artech House, Inc, 2003.

HPEM - 44
Microstrip and Patch Antennas

Oral Presentations

Integrated GPS-DSRC Antenna and Radio Front-End for Car Communications

GH. Z. Rafi*, S. Safavi-Naeini*, Alastair Malarky**, S. K. Chaudhuri*, and
Kai Wai-Cheung
*RF Microwave & Photonics Group,
Department of Electrical and Computer Engineering
University of Waterloo, Waterloo, CANADA
** MARK IV, Mississauga,, CANADA
ghrafi@maxwell.uwaterloo.ca

Adaptive, multi-band, low profile antennas are on high demand for many wireless communication and sensor network applications. In the U.S.A. the frequency band 5.850-5.925 GHz has been allocated for Intelligent Transportation Systems (ITS) Dedicated Short-Range Communication Service (DSRCS) and is intended for communications that generally occur in medium to short range between vehicles and roadside units and between moving vehicles.

This paper describes the design and measurement of a low profile microstrip antenna for GPS-DSRC application. The antenna operates at both the L1 frequency of 1.5745 GHz (GPS) with circular polarization and 5.88 GHz (DSRC) with vertically linear polarization. The proposed antenna consists of a corner cut patch for GPS (at the bottom layer) and circular patch with ring slot on the top layer for DSRC patch (Fig. 1), in a multi-layer configuration. The antenna pattern performance at both frequency bands, taking into consideration the effect of the roof of car as well as the antenna package, has been measured and will be presented (Table 1).
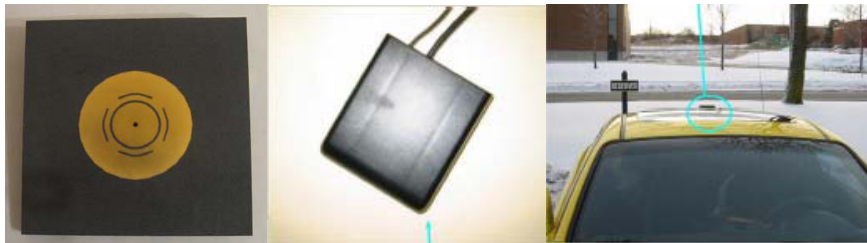
Fig.1 Antenna Geometry, package and location on the car roof

Theta	0	45	90
Simulated Antenna gain	2.8	5	3.1
Measured Antenna gain	2.3	4.5	3

Table 1. Antenna maximum gain at DSRC frequency at different Theta cuts, (measured and simulated)

HPEM - 44
Microstrip and Patch Antennas

Oral Presentations

Near Field Estimation of Patch Antennas from the Fringing Fields

John Rajeev Ojha[1], Marc Peters[2]
[1]*EM Sofware and Systems, Böblingen, Germany*
[2]*Technical University of Hamburg Harburg, Hamburg , Germany*
E-mail: j.ojha@emss.de

Determination of far fields using magnetic line currents [1] has been found to be accurate. However, this approach fails when near fields are determined. The magnetic line currents determined from the Eigen functions [2] were earlier determined along the periphery of a patch antenna. This approach was found to be sufficiently accurate only for the far fields. The accuracy of the near fields using this approach is found to deviate when compared to the full-wave model. This problem is overcome by modelling the fringing fields and incorporating this to analytical approach by which the Eigen functions are determined. Accurate modelling of near fields is a must especially for determining the magnetic interactive currents for patch antenna arrays. The fringing fields are modelled as magnetic line currents projected along the outer periphery shown in figure 1.
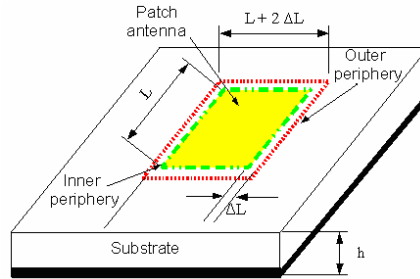
Fig. 1 – Magnetic line currents along an equivalent periphery of a patch antenna.

The incremental length ΔL is

$$\Delta L = 0.412 \cdot h \cdot \frac{\left(\varepsilon_{reff} + 0.300\right)\left(\frac{L}{h} + 0.264\right)}{\left(\varepsilon_{reff} - 0.258\right)\left(\frac{L}{h} + 0.813\right)}, \tag{1}$$

As an example the near field is determined for a 4 x 4 cm antenna in frequency domain at a few observation points at distances ranging from 0.2 cm to 1 cm with respect to the patch antenna. The dielectric constant, loss angle and substrate thickness are 2.32, 0.02 and 0.5 mm respectively. The patch is fed by a normalised current source with a feeding pin at (1, 1) cm. The observation points are on the same plane, z = h, as the metallic patch. The near fields are determined as

$$E_z = -\frac{1}{4 \cdot \pi} \int \left[(y-y')M_x - (x-x')M_y\right] \cdot \frac{1 + jk_{eff} \cdot R}{R^3} \cdot h \cdot e^{-j \cdot k_{eff} \cdot R} dl', \tag{2}$$

in terms of the x and y components of the magnetic line currents.

References

1.   W. L. Stutzman, G. A. Thiele, Antenna Theory and Design, New York : John Wiley & Sons, 1981.
2.   G. T. Lei, R. W. Techentin and B. K. Gilbert, "High-Frequency Characterization of Power/Ground-Plane Structures", IEEE Transactions on Microwave Theory and Techniques, vol. 47, pp. 562 - 569, May 1999.

A High Gain Rectangular Patch Radiator with Square Holes in the Ground Plane

Amol Choudhary, N. S. Raghava and Asok De

Department of Electronics and Communication Engineering,
Delhi College of Engineering University of Delhi, Delhi-42.,India

E-mail: amolchoudhary.86@gmail.com and nsraghava@gmail.com

A rectangular microstrip antenna (RMSA) or radiator is designed with infinite ground as shown in Fig. 1. The permittivity of the dielectric material is 2.65 and the height of the substrate is 1.5mm. The length of the patch is 13mm and the breadth is 16mm. The structure of RMSA is modified as shown in Fig. 2. On the bottom side of the dielectric substrate a rectangular metallic plane of 56mm x 100mm is constructed with three columns of square holes, which acts as a ground plane. These square slots are 7.05mm x 7.05mm in dimension and the distance between centers is 14.1mm. This lattice of square holes acts as an electromagnetic band gap (EBG) structure [1-5]. These structures consists of an uniformly distributed periodic metallic pattern on one side of a dielectric slab which is capable of prohibiting the propagation of all the electromagnetic waves of certain band of frequencies. The whole structure is backed by a plane ground at a distance of 8.5mm. This structure is named as EBGRMSA.

This electromagnetic band gap structure suppresses surface waves excited and thus improves the efficiency and the directivity of the radiator. IE3D software [6] is used to simulate both antennas RMSA and EBGRMSA and the various parameters of these antennas are tabulated in Table 1. As seen from the table, the resonant frequency of the EBGRMSA has been increased when compared to the RMSA's resonant frequency which shows that the size of the EBGRMSA has been reduced. Hence compactness is achieved. Even though VSWR has increased slightly it is well within the acceptable range. The radiation efficiency of the EBGRMSA is increased by 36% whereas its antenna efficiency has been increased by 70 %. The gain of EBGRMSA is increased by nearly 9 dB and its directivity was found to have increased by 1.2 dB.
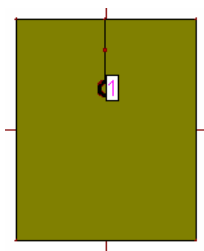
Fig. 1 Front view of the RMSA   **Fig. 2. Front view of the EBGRMSA**
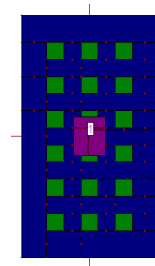
Table 1-Comparison of RMSA and EBGRMSA

Design	Frequency	VSWR	S11	Rad Eff	Ant. Eff	Gain	Directivity
RMSA	4.818	1.56	-13.21	63.39	12.98	-2.56	6.3
EBGRMSA	5.667	1.662	-12.09	100	83.8	6.74	7.55

References
1. V. Radisic,Y.Qian,R.Coccioli,and T.Itoh, "Novel 2-D photonic bandgap structure for microstrip lines" ,IEEE Microwave and Guided Wave Letters, vol 8, No.2, pp.69-71, Feb, 1998.
2. V. Radisic,Y.Qian,R.Coccioli,and T.Itoh, "Broadband power amplifier using dielectric photonic bandgap structure", IEEE Microwave and Guided Wave Letters, vol 8, No.1, pp.13-14, Jan, 1998.
3. T. Lopetegi,F.Falcone,B.Martinez,I.Edarra,R.Gonzalo and M.Sorolla, "Photonic bandgap resonator structures in microstrip" , 1998 Asia-Pacific Microwave Conference, pp. 597-600.
4. Hu Rong , Zhang Xue Xia and Gao Bao Xin , "2-D PBG Structure in Microstrip Line and Symmetrical Microstrip Line" 2000 Asia-Pacific Microwave Conference, pp. 1218-1221.
5. N. S. Raghava and Asok De, "Photonic Bandgap Stacked Rectangular Microstrip Antenna for Road Vehicle Communication," IEEE Trans. Antennas and Wireless Propagation Letters, vol. 5, pp. 421-423, Dec. 2006.
6. IE3D User's Manual, Dec. 1999. Zeland Software, Inc.

FDTD Thin Strut Coding

E. B. Savage, J. L. Gilbert

Metatech Corporation, Goleta, California, USA

E-mail: savagee@cox.net

The beauty of Yee's 3D FDTD[1] (finite-difference time domain) approach is its simplicity, while it is also very versatile. There we present a similarly simple and versatile approach, represented by the table below, for modeling thin conductors (wires) within a 3D FDTD simulation. Normally a 3D FDTD would have prohibitively small cells if the cell size was set according to the thickness of any thin wires – so "subcell" approaches have been developed (Chapter 10 of Ref. 1). The wire model approach presented here uses a 1D (TEM transmission line) Yee FDTD approach for the wire, with voltage and current for the "fields", and with easily understood coupling between the 3D and 1D models. This approach was initially developed by Gilbert et al.[2] Here we present this approach, and new material[3] on the "in-cell inductance", and on the effect on stability of the wire coding.

Implementation is very simple – usual 3D and 1D FDTD coding is used, except with the addition of coupling between the two systems provided by:

   1D current (I) is feed into the 3D as a current source (J_{Source})

   3D electric field (E) is feed into the 1D as a voltage source (V_{Source}).

However, there is one uncertainty in this approach: normally there should be two conductors associated with a 1D transmission line, yet here there is only a single wire. The basis of this issue is the determination of the capacitance (C), inductance (L), and conductance (G) values for the 1D equations, and the definition of what "voltage" means. Often this coding approach is thought of as having an imaginary coaxial outer conductor around the wire, and the distance to that conductor then defines the C, L, G values according to the usual coaxial line formulas. Various solutions have been proposed for this "in-cell inductance" issue. In our approach we used the 3D-1D system to simulate a rectangular coaxial line, and adjusted the in-cell inductance so that the simulation results matched the analytical inductance for the rectangular coax structure. Furthermore, we have determined this value for non-square cells also, with a wide range of aspect ratios.

We also derived a stability criterion for this approach. If the wire is small enough, then the stability criterion is no different than given by the normal 3D Courant time step limit. If the wire gets too big, then the time step limit decreases; and stability requirements sets a maximum limit on how thick the wire can be.

3D	1D
$$\varepsilon \frac{\partial \overline{E}}{\partial t} + \sigma \overline{E} + \overline{J}_{Source} = \nabla \times \frac{\overline{B}}{\mu}$$ $$\frac{\partial \overline{B}}{\partial t} = -\nabla \times \overline{E}$$	$$I = C \frac{dV}{dt} - G V$$ $$V = L \frac{dI}{dt} - V_{Source}$$

References
1. Allen Taflove and Susan C. Hagness, "Computational Electrodynamics: The Finite-Difference Time-Domain Method", 3rd edition, Artech House, Inc., Norwood, Massachusetts, 2005.
2. R. Holland and L. Simpson, "Finite-Difference Analysis of EMP Coupling to Thin Struts and Wires" IEEE Trans. Electromagnetic Compatibility, Vol. EMC-23, No. 2, pp. 88-97, May 1981.
3. Ed Savage and Jim Gilbert, "FDTD Wire Coding", Meta-N-047, Metatech Corporation, Goleta, California, January 2008.

Semi-analytical scattering matrix of one-dimensional periodic Electromagnetic Band Gap structures lighted in conical mounting

P. Boyer[1], M. Thévenot[2] and T. Monédière[2].

[1] *IMEP Minatec – INPG, 3 Parvis Louis Néel BP 257, 38016 Grenoble Cedex 1, France*
[2] *XLIM, Ester BP 6912, 87069 Limoges Cedex, France*

E-mail : philippe.boyer@minatec.inpg.fr

We present a semi-analytical and rigorous theory for modeling Electromagnetic Band Gap (EBG) devices. The formulation consists in computation of its scattering matrix (*S*-matrix) by coupling the Modal Method (MM) with the Scattering Matrix Propagation Algorithm (SMPA). The numerical implementation requires few computation times and memory sizes, and permits to achieve very high accuracies.

In Cartesian coordinate system, we interest particularly in a planar multilayer scattering object periodic with respect to *y* and invariant with respect to *x*. Each parallel layer to the *Oxy* plane can be a perfectly conducting lamellar grating as depicted in figure 1 or a homogeneous layer. In whole space, invariance and periodicity permit to write the electromagnetic fields as Fourier developments truncated to the Nth order in view of numerical implementation. The region containing the stack of scattering objects is called modulated area and is surrounded by two homogeneous and isotropic regions in which the fields are expressed by the well-known Rayleigh development. We assume that all electromagnetic components have a harmonic time dependence.

We first extend the MM [1] to the conical and transmission diffracting problem in order to express the scattering matrix of one metallic cylinder layer. Its principle consists in finding explicit expression of the fields from resonant modes liable to propagate in each homogeneous slot of the grating. Knowing the transmission matrix of a homogeneous layer placed between gratings, an iterative process (SMPA) [2] is secondly applied along the *z*-axis to compute the *S*-matrix of the entire device. Thanks to the SMPA, the modulated area can be automatic split into several slices in order to avoid numerical instabilities due to growing exponential terms of the electromagnetic fields in important deep gratings. Besides, the Staircase Approximation [3] can be applied to modelize metallic cylinders with arbitrary cross-section.

Many numerical results have permit to validate the theory by comparison with the ones stated in references [4,5]. For instance, Figure 2 shows the transmittance versus the frequency for EBG objects with several lamellar metallic gratings. In the case of five metallic cylinder layers, the numerical accuracy reaches 10^{-13} (relative error with the energy criterion) for a development order (*N*) equal to 5. The computation time of one iteration (one point in figure 2) is less than 1 second for *N*=15 on personal computer.

Our future work will deal with the addition of a transverse modal searching algorithm in order to design ultra-compact and directive EBG antennas. Then, the theory will be generalized to bi-dimensional periodic EBG objects as a stack of metallic grids (crossed gratings) and woodpile structures.
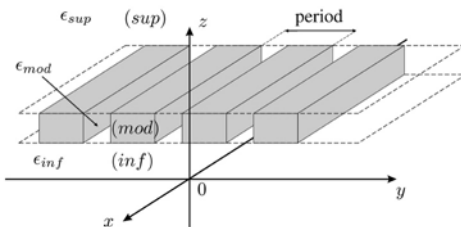
Fig. 1. Perfectly conducting lamellar grating
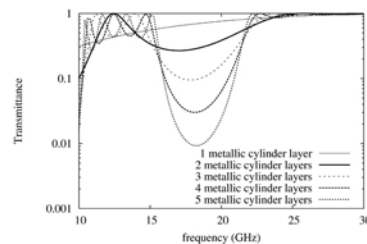
Fig. 2. Transmittance for EBG objects with several layers

References

1. D. Maystre and R. Petit, "Diffraction par un réseau lamellaire infiniment conducteur", Optics Communications, vol. 5, number 2, 1972.
2. L. Li, "Formulation and comparison of two recursive matrix algorithms for modeling of diffraction gratings", Journal of Optical Society of America A, vol. 11, 1994.
3. M. G. Moharam and T. K. Gaylord, "Diffraction analysis of dielectric surface–relief gratings", Journal of Optical Society of America, vol. 72, 1982.
4. G. Guida, D. Maystre, G. Tayeb and P. Vincent, "Mean-field theory of two-dimensional metallic photonic crystals", Journal of Optical Society of America B, vol. 15, number 8, 1998.
5. J. Y. Suratteau, M. Cadilhac and R. Petit, "The perfectly conducting wire grating: Computation of the diffracted field from Maxwell's equations and Hamilton's canonical system", IEEE Transactions on Antennas and Propagation, vol. AP-33, number 4, 1985.

Model of Electromagnetic Wave Propagation in the Stratified Random Media Inclusive the Semitransparent Objects

V.G. Spitsyn

Tomsk Polytechnic University, Tomsk, Russia
E-mail: spvg@tpu.ru

The purpose of this work is a numerical investigations of the process of electromagnetic wave multiple interactions with random discrete inhomogeneities disposed in the stratified media. This media includes the semitransparent objects in a view of sphere, disk and plate. In this work we consider the numerical method of computation electromagnetic wave multiple interactions with discrete random scatterers in the stratified media. The method of solving this problem is based on the stochastic modelling of wave interaction with random discrete media [1, 2].

Here is assumed that the wavelength of the wave is less than the sizes of the layers and objects and scattering occurs incoherently by an image on statistically independent discrete inhomogeneities. The oscillator of electromagnetic signal is presented as a source of photons with corresponding diagram of radiation. The initial coordinates of photons get out in the point of oscillator disposition. The type of wave interaction with discrete inhomogeneity is determined according to set cross sections of absorption and scattering. In case of fulfillment of a wave scattering condition the direction of photon propagation changes according to set indicatrix of discrete inhomogeneity over-radiation (isotropic, Lambert and quasi-mirror types). Solving the problem of linear and nonlinear wave propagation in the random discrete media is reduced to definition of photon distribution function in space of coordinates and time.

There is supposed that the interaction of wave with random discrete inhomogeneous take place in according to the isotropic scattering indicatrix. Here is considered the source of electromagnetic signal, which disposed in the centre of Cartesian coordinates system on the surface of media. In this paper is supposed that all distances measured in the relative units. In Fig. 1 is presented the distribution of scattering signal energy in stratified media inclusive the semitransparent spherical object. In this picture we can see such as the distribution of scattering signal energy is represented the contours of spherical object and layers in media. The semitransparent disks (Fig. 2, 3) and holes in barrier (Fig. 4) with radius *R=1.5* and *R=2.5* are disposed inside media in plane *z=2.3*. In Fig. 2-4 are presented the results of computation of energy scattering signal in cross-section plane *z=2.5* (Fig. 2) and z=*4.5* (Fig. 3, 4). Here we can see the well-defined projection of disks in Fig 2 in comparison with Fig. 3. The analysis of results shows that with increase of distance to disks and the coefficient transparency of disks is take place the edge smearing of disks on the images.

Thus in this work the numerical model concerning linear and nonlinear electromagnetic wave propagation in the three-dimensional random discrete media, inclusive the semitransparent objects is developed. Dependencies of energies scattering and absorption signals from the parameters, describing the nonuniform structure of random discrete media and objects are investigated.
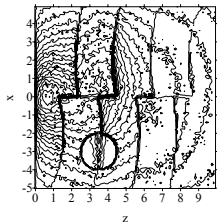
Fig. 1 — **The distribution of scattering signal energy in stratified media inclusive the spherical object**
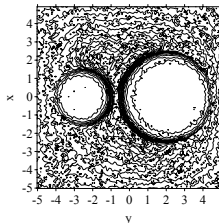
Fig. 2 — **The distribution of scattering signal energy in the plane *z=2.5* for the presence of two disks**
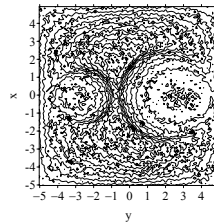
Fig. 3 — **The distribution of scattering signal energy in the plane *z=4.5* for the presence of two disks**
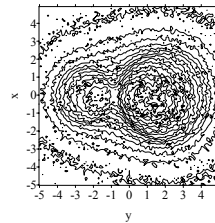
Fig. 4 — **The distribution of scattering signal energy in the plane *z=4.5* for the presence of two holes**

References

1. V.G. Spitsyn, Modelling of radiowave scattering on the ionospheric plasma disturbances created of spacecraft. Moscow: Physmatlit, 2003.
2. V.G. Spitsyn, "Development of a numerical model concerning electromagnetic wave propagation in turbulent flows," Journal of Applied Electromagnetism, vol. 1, 1997.

Characterization of Plane Wave Penetration through Multilayered Cylindrical Apertures by a Transverse Wave Method

T.Bdour[1], N.Ammar [1], T.Aguili [1], and H.Baudrand[2]

(1) Communications Systems Laboratory in Tunis Engineering School, Belvedere, BP 37 Tunis, 1002 Tunisia
(2) Electronics laboratory LEN7, ENSEEIHT, 2 rue Camichel, 31071, Toulouse, France

E-mail: bdour_tarek@yahoo.com

Electromagnetic wave penetration through slots or apertures on cylindrical structures is an important subject in electromagnetic compatibility (EMC).In fact, the coupling of EM energy with small apertures of an embedded system can seriously damage the performance of electronic circuits installed inside the embedding enclosure. Then, the estimation of the penetrated field into the aperture is important to evaluate the performance of the studied electronic system.

Many techniques have been proposed to solve the problem of EM wave penetration into circular slotted cylinders due to their wide use in engineering applications. The most important approach which treated such problem is the method of moments MoM [1-3]. Although its performance, the investigation of EM energy penetration into multilayered slotted cylinders is not obviously solved by the MoM technique. In fact, for multilayered geometries, the problem cannot be easily characterized due to the difficulty to extract the Green singularity. Recently, a numerical method based on integral equation technique combined with the Galerkin's procedure has been advanced by [4] to solve the resulting multiple coupling system. In this paper, another, original method [5-6] is developed to characterize multiple wave penetration in multilayered slotted cylinders. It has been successfully applied to solve the problem of EM energy coupling with cylindrical slots [5].Our full wave approach is based on transverse wave formulation of the electromagnetic problem.

The coupling of electromagnetic (EM) wave through multilayered cylindrical apertures is analyzed by a transverse wave method called Wave Concept Iterative Process (WCIP). The efficiency and accuracy of the proposed technique are validated by illustrative examples in both TE and TM polarizations [7].

References

1. El-Hajj, A., K. Y. Kabalan, and R. F. Harrington, "Characteristic modes of a slot in a conducting cylinder and their use for penetration and scattering, TE case," IEEE Trans. Antennas Propagat., Vol. AP-40, pp 156–161, February 1992.
2. Mautz, J. R., and R. F. Harrington, "Electromagnetic penetration into a conducting circular cylinder through a narrow slot, TE case," J. Electromagn. Waves Applicat., Vol. 3, pp 307–336, April 1989.
3. Mautz, J. R., and R. F. Harrington, "Electromagnetic penetration into a conducting circular cylinder through a narrow slot, TE case," J. Electromagn. Waves Applicat., Vol. 2, pp 269–293, April 1988 .
4. W. Yin,L.Li, T.Yeo,:" Multiple Penetration of a TEz-Polarized Plane Wave into Multilayered Cylindrical Cavity-Backed Apertures", IEEE Trans. electromagn compat, vol.42,No .4, pp 330-338, November 2000.
5. T.Bdour,N.Ammar,T.Aguili and H. Baudrand:" Modeling of Wave Penetration through Cylindrical Aperture using an Iterative Method Based on Transverse Wave Concept", IEEE Microwave Conference KJMW, pp 45-48 , November 2007.
6. S. Wane, D. Bajon, H. Baudrand, and P. Gamand, ""A new full-wave hybrid differential–integral approach for the investigation of multilayer structures including non uniformly doped diffusions", IEEE Trans .MTT, vol.53, No.1, pp.200–214,Jan. 2005.
7. Wen-Yan Yin, Le-Wei Li, Tat-Soon ,Mook-,Seng Leong, and Pang-shyan Kooi, "The near-zone field characteristics of an e-polarization plane wave penetrating through cylindrical multiple aperturescoated with lossy and lossless media", IEEE Trans. electromagn compat, vol.44, pp.329-337,May 2002.

Specifying and Measuring Electromagnetic Shielding on Aircraft

W. D. Prather[1], R. J. Torres[1], and T. C. Tran[1]

[1]*Air Force Research Laboratory, Kirtland AFB, NM, USA*

E-mail: william.prather@ieee.org

Many modern aircraft use some combination of primary structure and shielded cables to provide electromagnetic protection for the system electronics. However, unlike a ground-based screen room, an aircraft fuselage requires a very large number of penetrations through the shield because of antennas, wiring, and control cables as well as pneumatic and hydraulic lines. An aircraft also has to have numerous windows, doors, and hatches for access and maintenance. In every case, the penetration through the shield must be hardened, and that requires hardening specifications and some method of measuring the shielding to assure that the hardening is adequate. Thus, the first step in the implementation of a shielded system is to create a properly written set of specifications in measurable engineering units. If this is done, there exist a number of measurement methods and tools that can be used to measure the shielding. As a result, the verification and maintenance can be accomplished in a straightforward manner.

Laboratory measurements of hardening element performance can be used to verify the design approach, but in order to assure in-flight performance, the hardening must be measured on board the aircraft in its actual installation. This is often more difficult than making a measurement in a laboratory fixture.

This paper discusses the shielding design of a typical aircraft system and describes both CW and time domain methods for measuring the effectiveness of the shielding elements and the overall shielding of the whole aircraft. Illustrative examples are presented..

References

1. W.D. Prather, "Shielding Specification Techniques and Measurement Methods for Aircraft," Proceedings IEEE/EMC International Symposium, Honolulu HI, July 2007.
2. W.D. Prather, "Shielding Specification Techniques and Measurement Methods," Proceedings Joint Spectrum E3 Conference, Orlando FL, April 2006.

Coordination of Varistors in Low Voltage System by use of Electrical Charge

C. A. Avendaño Avendaño[1], H. F. Ibáñez Olaya[2], H. E. Ortiz Suárez[3]

[1]*Distrital University Francisco José de Caldas, Bogotá, Colombia*
[2]*Distrital University Francisco José de Caldas, Bogotá, Colombia*
[3]*Distrital University Francisco José de Caldas, Bogotá, Colombia*

...
E-mail: hfibanezo@udistrital.edu.co

Previously the coordination of protections against electrical surges because of lightning in electrical systems of low voltage was made using devices with gap and varistores, due to the great handling of electrical charge of first. Nowadays they exist varistores of ZnO that can handle to discharge energy and therefore it allows to make coordination of protections among them in the different zones from protection.

The present article shows a procedure to select and to coordinate surge protective devices type varistors in electrical systems of low voltage highly exposed to direct lightning currents. The selection procedure considers parameters like: Handling of the electrical charge, Curve voltage - current of the devices, Voltage protection level, decoupling inductive natural of the installation

The article in addition shows a comparison between standard IEC 61312[1] and method used for the calculation of electrical charge present by each one of the incoming of electrical services of the installation, and whose results are very important at the time of select and coordinate surge protective devices type varistors.

Between some of the reached results it is necessary that the surge protective device in the more sensitive protective zone it has a higher voltage protective level than a surge protective device located in a previous zone of internal Lightning Protection System, in order to obtain waveform of current with smaller content of electrical charge. The before condition would work in low voltage electrical installation where is not adequate to use decoupling net type resistor because the regulation of voltage and efficiency of the system not permit to use it. So, the use of decoupling inductive is enough due to that there is a natural inductance in the circuit of the low voltage power distribution system. This would seem a contradiction with respect to the generally accepted philosophy, in which the best levels of protection (lowest) are in the more sensible zones of protection, so for these conditions there would not be a reduction in the levels of electrical charge when a surge is going through of a zone of protection to the following one.

If is required a better voltage protection level on a sensible equipment, it does necessary the design of a protective device with decoupling element type resistor. In this way a protection device closer to sensible equipment will have the lowest voltage level protection [2], [3].

References

1. International Electrotechnical Commission (1997). Standard IEC 61312 "Protection against Lightning Electromagnetic Impulse".
2. International Electrotechnical Commission Standard IEC 62305-4 "Protection against Lightning. Part 4: Electrical and electronic system within structures.
3. International Standard IEC 61643-12: Surge protection Devices connected to low voltage power distribution systems. Selection and application principles.

HPEM - 47   Hardening: Protection, Assurance and Maintenance

Oral Presentations

Design of SPDs Class I for Low Voltage Electric Systems, using Combination of Metal Oxide Varistors

C. A. Avendaño Avendaño[1], H. F. Ibáñez Olaya[2], H. E. Ortiz Suárez[3]
[1]*Distrital University Francisco José de Caldas, Bogotá, Colombia*
[2]*Distrital University Francisco José de Caldas, Bogotá, Colombia*
[3]*Distrital University Francisco José de Caldas, Bogotá, Colombia*

...
E-mail: hfibanezo@udistrital.edu.co

This paper describes the methodology used in the design of a Surge Protection Device Class I (SPDs I) required for the protection of low voltage electric systems, highly exposed to direct impacts of lightning. The SPD was developed by means of the combination of metal oxide varistors of same nominal voltage and current, with non homogeneous characteristics voltage-current. The presented designs satisfy the conditions required by the international standard of insulation coordination for low voltage electric systems IEC 60664[1], and parameters required by the standard IEC 62305[2]. An equation that allows estimating the number of required varistors is presented. This equation is function of both, the electric charge of the lightning partial current and the tolerance given by the manufacturers of the used varistors.

The validation of the equation is carried out by means of the comparison with simulations in PSpice, analyzing parameters of each one of the elements as charge, as well as the same parameters for the group. Finally the application of the methodology proposed in the design of a SPD class I with capacity of supporting 10kA with waveform 10/350μs with a protection level not bigger than 1.5kV, is shown with the purpose to make a coordination of protection using only varistors.

References
1. International Electrotechnical Commission. Standard IEC 61312 "Protection against Lightning Electromagnetic Impulse" (1997).
2. International Electrotechnical Commission Standard IEC 62305 – 1 "Protection against Lightning. General Principles" (2004).

Polarimetric Suppression of Early-Time Scattering
for Late-Time Target Identification

C. E. Baum
University of New Mexico
Department of Electrical and Computer Engineering
Albuquerque New Mexico 87131
E-mail: cebaum@ece.unm.edu

To recognize the target by its complex natural frequencies s_α , one sometimes encounters a problem with a large early-time transient signal in the presence of a low-level late-time resonant signature. This introduces a dynamic range problem in the transient-signal recording devices (such as digitizers). One would then like to avoid the earlytime signal in the recording to accurately measure the late-time waveform.

One can approach the problem of early-time suppression in various ways. One can use limiters to chop off the early-time peak(s). This raises practical questions concerning the response time of the limiter (early-time feed through) and the recovery time (hopefully before the beginning of the late-time signal). Another possibility would have linear (passive and/or active) analog filters. If the early-time signal is sufficiently narrow in time, then special low-pass filters (i.e., integrators) can reduce the early-time amplitude relative to the late-time amplitude. One can also use an incident (interrogating) wave which is designed by its frequency content to maximize the return of the late-time resonances.

The present paper considers the use of the polarization properties of the scattering. If the early-time polarization is sufficiently different from the late-time polarization, then one can in effect "cross polarize" (in a general sense) the radar to the early-time scattering, while letting the late-time scattering (or useful portions of this) through to the recorder.

Continuing the discussion, this paper considers various possibilities for cancelling of early-time scattering signals for better recording of the late-time resonances for target identification. Topics include rotation of the polarization basis (antenna rotation), and including of various gains (filters) in the radar channels. Of special interest is the possibility of using an inverter in one of the radar channels. The case of polarization-independent early time scattering, provided that the resonance(s) of interest are approximately characterized by a single polarization. This leads to schematic system designs for one or two dual-pol antennas.

HPEM - 48
Special Techniques in EM Theory #2

Oral Presentations

Constitutive Parameters of Left-Handed Materials
for UWB Passive Devices

M. G. Banciu[1], N. Militaru[2], G. Lojewski[2],

[1]*National Institute of Materials Physics, Microwave Group, Magurele, Romania*
[2]*POLITEHNICA University of Bucharest, Faculty of Electronics, Telecommunications and Information Technology, Bucharest, Romania*

E-mail: gbanciu@infim.ro

Microwave investigations on a new metamaterial are presented in this paper. A new resonator for the unit cell of the metamaterial is proposed. The dispersion relations and the Bloch impedance were directly obtained from the scattering parameters. The structures were designed by using a Finite Difference Time-Domain (FDTD) method employing periodic boundary conditions. The in-house developed FDTD method (Fig. 1a) was previously successfully applied to cross –coupled planar filters [2].
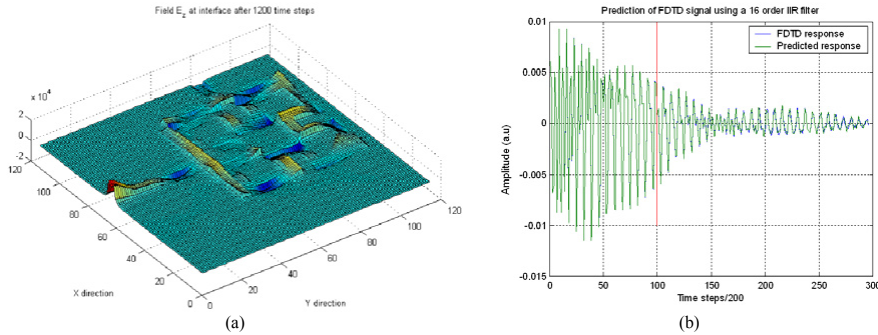
Fig. 1. FDTD simulations on a meander structure.

Estimation techniques were developed and the FDTD signal was processed in order to reduce the computation time, as shown in Fig. 1b. The scattering parameters are in good agreement with the simulated responses.

An effective medium theory in the long wavelength approximation is presented. In this theory, the structure is considered as a two-port with the scattering parameters S_{11}, S_{21}, and the propagation factor τ given by

$$S_{11} = \frac{\Gamma\left(1 - \tau^2\right)}{1 - \Gamma^2 \tau^2}, \; S_{21} = \frac{\tau\left(1 - \Gamma^2\right)}{1 - \Gamma^2 \tau^2}, \; \tau = e^{-\gamma l}, \tag{1}$$

respectively, where Γ is the reflection coefficient γ is the propagation constant. In this case, the effective refraction index can be expressed as

$$n = \mp j \frac{c}{2\pi f l} \cosh^{-1} \frac{1 + S_{21}^2 - S_{11}^2}{2 S_{11}}. \tag{2}$$

Moreover, theoretical models were developed for double- and single-negative media in order to deduce the effective permittivity ε and permeability μ.

In this paper, investigations on the utilization of the proposed metamaterial to an UWB antenna in order to obtain a rejection of the interferences due to such source as the WLAN systems, are presented. On the other hand, it is shown that the use of the proposed can improve the devices dispersion characteristics and the group delay.

References
1.   M. Stupf, R. Mittra, J. Yeo and J. R. Mosig, "Some novel design for RFID antennas and their performance enhancement with metamaterials", Microwave and Optical Technology Letters, Vol. 49, Nr. 4, pp. 858-867, 2007.
2.   M. G. Banciu, R. Ramer, A. Ioachim, "Compact microstrip resonators for 900 MHz frequency band", IEEE Microwave and Wireless Components Letters, Vol. 13, Nr. 5, pp. 175-177, 2003.

Determining Complex Permittivity, Permeability, and Thickness of a PEC-Backed Material Using a Dual Waveguide Probe

M. W. Hyde IV, M. J. Havrilla †

Air Force Institute of Technology, Dayton, OH 45433-7765, USA

E-mail: milo.hyde@afit.edu

Coaxial and waveguide probes have been studied for the past 30 years. Their uses include nondestructive material evaluation, subsurface crack detection, and even hyperthermia treatment [1-3]. Existing research has focused on obtaining the reflection coefficient, using a single probe, of an unknown material backed by a dielectric half-space or a PEC. While this scenario is ideal for determining the dielectric constant of an unknown material, it suffers when one wants to determine permeability or thickness because it lacks two (or more) independent measurements. Several authors have developed techniques—most notably, two-thickness method, sample added method, and frequency varying method—to fill this single waveguide probe shortfall. The two-thickness method, being the most popular because of its simple implementation, requires two separate measurements: one measurement with the material under test (MUT) (of thickness 1) backed by a dielectric half-space or PEC and another measurement with the MUT (of thickness 2) backed by a dielectric half-space or PEC [4]. These two measurements allow for the determination of complex permittivity and permeability; however, one must know the thickness of the MUT to use the technique. The research presented in this paper introduces a method to determine the permittivity, permeability, and thickness of an unknown material backed by a PEC, using a variation of the two-thickness method and a dual waveguide probe. The dual waveguide probe, shown in Fig. 1, allows for the simultaneous measurement of reflection and transmission coefficients allowing one to obtain complex permittivity and permeability with a single measurement [5]. A second measurement is required to determine the thickness of the MUT. The paper will include theoretical development of the method, mainly application of Love's Equivalence Principle and the Method of Moments. Lastly, measurement results will be shown, comparing the results of the technique to standard waveguide methods, to verify its accuracy.
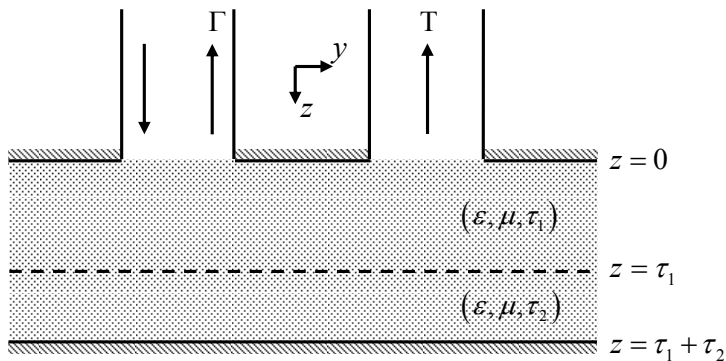
Fig. 1 — Measurement Geometry

References

1. C. Chang, K. Chen, and J. Qian, "Nondestructive determination of electromagnetic parameters of dielectric materials at X-band frequencies using a waveguide probe system," *IEEE Trans. Instrum. Meas.*, vol. 46, no. 5, pp. 1084-1092, Oct. 1997.
2. F. Mazlumi, S. Sadeghi, and R. Moini, "Interaction of rectangular open-ended waveguides with surface tilted long cracks in metals," *IEEE Trans. Instrum. Meas.*, vol. 55, no. 6, pp. 2191-2197, Dec. 2006.
3. D. Popovic *et al*, "Precision open-ended coaxial probes in *in vivo* and *ex vivo* dielectric spectroscopy of biological tissues at microwave frequencies," *IEEE Trans. Microwave Theory Tech.*, vol. 53, no. 5, pp. 1713-1722, May 2005.
4. J. W. Stewart and M. J. Havrilla, "Electromagnetic characterization of a magnetic material using an open-ended waveguide probe and a rigorous full-wave multimode model," *Journal of Electromagnetic Waves and Applications*, vol. 20, no. 14, pp. 2037-2052, 2006.
5. J. W. Stewart and M. J. Havrilla, "A novel method for simultaneously extracting electric and magnetic properties of shielding materials using two coupled collinear open-ended waveguides," in *23rd Annual Review of Progress in Applied Computational Electromagnetics*, Verona, Italy, Mar. 19-23, 2007.

Computational Techniques for the Electric Characterization of Dispersive Materials Using Open-Ended Coaxial Probes

L. Sandrolini, U. Reggiani, M. Artioli

Department of Electrical Engineering, University of Bologna, Bologna, Italy

E-mail: leonardo.sandrolini@mail.ing.unibo.it

Open-ended coaxial probes are widely used for the nondestructive electrical characterization of dispersive materials over a broad band of frequencies [1]. Although the method of measurement is simple in principle, the determination of the electrical properties of the material requires an inverse problem to be solved. In fact, the complex permittivity of the material has to be calculated from the measured reflection coefficient as a function of frequency at the probe aperture which can be converted into the aperture admittance. Several formulas for the aperture admittance have been presented, some approximate and others derived from a full-wave analysis of the field at the probe opening [2]. However, an explicit form of the complex permittivity as a function of the admittance cannot be obtained. In this paper two numerical procedures to obtain the electrical properties are examined, both based on a particle swarm optimization algorithm. The former procedure consists in fitting the chosen analytical expression of the aperture admittance to the experimental admittance at each measured frequency, in order to obtain the corresponding complex permittivity values. In the latter, a model for the complex permittivity as a function of frequency such as Cole-Cole is fitted to the measured aperture admittance in the whole frequency range (300 kHz-3.6 GHz).

The analytical expression chosen for the aperture admittance is [2]

$$Y(\omega) = \frac{jk\varepsilon Y_0}{\pi \ln(b/a)\sqrt{\varepsilon_i}} \int_a^b \int_a^b \int_0^\pi \cos\phi' \frac{\exp(-jk\sqrt{\varepsilon}r)}{r} d\phi' d\rho' d\rho \tag{1}$$

whereas the complex permittivity according to the Cole-Cole model is [3]

$$\varepsilon(\omega) = \varepsilon_\infty + \frac{\varepsilon_s - \varepsilon_\infty}{1 + (j\omega\tau)^{1-\alpha}} - j\frac{\sigma(0)}{\omega\varepsilon_0} \tag{2}$$

The method of the electrical characterization will be applied to conductive plastic materials for electromagnetic shielding. The two procedures mentioned above will be compared considering calculation time and reliability of the results. The aim of the paper is to develop a fast procedure to obtain in real time the electrical parameters from the reflection coefficient measurement. The results of the electrical characterization of a few material samples will be presented in details in the final manuscript.

References
1. S. Van Damme, A. Franchois, D. De Zutter, L. Taerwe, "Nondestructive determination of the steel fiber content in concrete slabs with an open-ended coaxial probe," IEEE Transactions on Geoscience and Remote Sensing, vol. 42, 2004.
2. Y. Xu, R.G. Bosisio, T.K. Bose, "Some calculation methods and universal diagrams for measurement of dielectric constants using open-ended coaxial probes," IEE Proc. Part H Microwaves Antennas Propag., v. 138, 1991.
3. A. Robert, "Dielectric permittivity of concrete between 50 MHz and 1 GHz and GPR measurements for building materials evaluation," Journal of Applied Geophysics, v. 40, 1998.

Characterization of Rubber Composites Using Microwave Non-Destructive Technique and Electromagnetic Modeling

Z. Awang and K. Ismail

Microwave Technology Centre, Faculty of Electrical Engineering, Universiti Teknologi MARA, 40450 Shah Alam, Malaysia
E-mail: zaiki437@salam.uitm.edu.my, qamariah79@yahoo.com

This paper reports on a novel method of detecting the types and particle sizes of fillers used in rubber composites using a free space microwave non-destructive testing technique. The samples were measured at X-band using a rectangular dielectric waveguide (RDWG) system which offers the advantage of minimal sample damage, and thus more accurate de-embedding, convenience and good repeatability.

In addition to comparing with the reference standards [1-3], our results are validated by carrying out a full three-dimensional electromagnetic simulation of the measurement set-up using *CST Microwave Studio*. This allowed the physical properties of computed fields to be analyzed accurately and generated exact analogues to Maxwell's equations, thus leading to a unique solution. The electromagnetic modeling enabled an accurate de-embedding of the RDWG set-up, thus enhancing the accuracy of our data. The simulation results agree well with the data obtained from the measurement.

We found that the dielectric constants of both aluminium silicate-and china clay-filled rubbers do not depend so much on the filler content, while those filled with carbon black (CB) show a pronounced dependence. The dependence levels off, however, for higher filler contents. This differing trend between different filler types are partly due to the fact that carbon black is a conductor and hence electromagnetic waves are absorbed and stored whereas both china clay and aluminum are insulators. The complex permittivity values differ significantly for different particle sizes of the CB -they increased as the particle size of the CB decreases. Finer-sized CBs increase both the permittivity and the losses, but their behaviours are almost constant throughout the frequency range. This may be due to the fact that finer-sized fillers will result in more particles in the rubber composites, and this creates more propagation paths for the waves.

Owing to its simplicity and ease of sample-mounting, the approach can be applied to other industrial materials in both solid and liquid form. The measurement can also be extended to hazardous liquids, and the set-up is easily modified for other frequency ranges. We have also demonstrated the use of electromagnetic modeling as an alternative to verify microwave non-destructive testing technique.

References
1. A. von Hippel, Dielectric and waves. Boston: Artech House, 1995.
2. C. M. Alabaster, The microwave properties of tissue and other lossy dielectrics. University of Cranfield, Cranfield, U. K., PhD thesis, 2004.
3. E. Krantzenberg, M. N Afsar, Y. Wang, "Complex Permittivity of Chicken Blood," Microwave and Optical Technology Letters, vol. 39, p. 54, Oct. 2003..

HPEM - 48
Special Techniques in EM Theory #2

Oral Presentations

Accurate Modeling of Ultra-Short Electromagnetic Pulse Scattering using a Locally Conformal Finite-Difference Time-Domain Scheme

D. Caratelli[1], R. Cicchetti[2], M. Simeoni[1], and A. Yarovoy[1]

[1]*Delft University of Technology, IRCTR, Delft, the Netherlands*
[2]*Sapienza University of Rome, Department of Electronic Engineering, Rome, Italy*
E-mail: d.caratelli@tudelft.nl

The computation of the transient responses of complex metal-dielectric structures (radar targets, antennas, etc.) to ultra-short electromagnetic pulses requires accurate and fast numerical schemes. One of such widely used techniques is the finite-difference time-domain (*FDTD*) algorithm. However, in the conventional formulation proposed by Yee [1], each cell in the computational grid is implicitly supposed to be filled by a homogeneous material. For this reason, the adoption of well-posed orthogonal Cartesian meshes could be responsible for reduced numerical accuracy when complex electromagnetic structures having curved boundaries are to be modeled. In such cases, locally conformal *FDTD* schemes [2] provide clear advantages over the use of the stair-casing approach or unstructured and stretched space lattices [1], potentially suffering from significant numerical dispersion and/or instability.

In this communication, a novel locally conformal *FDTD* scheme, based on the effective electrical parameters concept, is proposed. In particular, a static finite-difference approach is adopted to rigorously evaluate the intrinsic capacitance C_{eff}, and conductance G_{eff} of each non-uniformly filled cell in the computational grid. Then, using simple algebra, the effective permittivity ε_{eff}, and electrical conductivity σ_{eff} of the generic cell is easily derived. In this way, the information regarding the physical and geometrical characteristics of the electromagnetic structure under consideration is transferred to the position-dependent effective electrical parameters ε_{eff}, and σ_{eff}. The computation of such quantities is carried out before the *FDTD*-method time marching starts, hence, unlike in conformal techniques based on stretched space lattices, no additional correction is required in the numerical algorithm. Therefore, the proposed scheme has the same stability properties as the conventional *FDTD* formulation.

In order to assess the numerical accuracy and effectiveness of the proposed technique, several test cases have been performed. In particular, for the sake of brevity, only the computation of the fundamental resonant frequency f_r of a rectangular metallic cavity loaded with a dielectric rod resonator (see Fig. 1*a*) is presented in this contribution. To this end, a cubic *FDTD* mesh having fixed spatial increment Δh has been adopted to analyze the structure. As it appears in Fig. 1*b*, this example clearly demonstrates the suitability of the proposed approach to efficiently handle complex structures with curved boundaries, achieving dramatic improvement in accuracy over the stair-casing approximation. Further analyses showing the numerical performances of the proposed scheme, are in progress, and will be presented at the symposium.
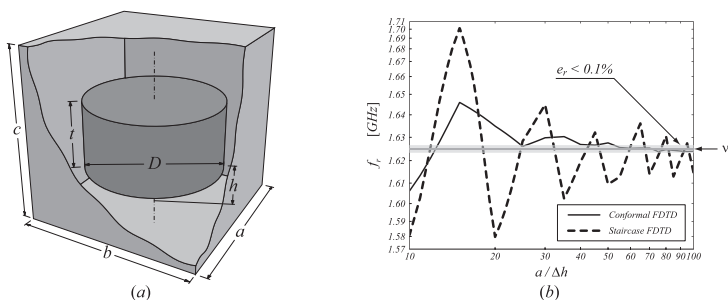
Fig. 1 – Geometry of a dielectric loaded rectangular cavity (*a*) **and behavior of the fundamental resonant frequency** f_r **for different *FDTD* mesh sizes** (*b*)**. Structure characteristics:** $a=b=50$ *mm*, $c=30$ *mm*, $D=36$ *mm*, $t=16$ *mm*, $h=7$ *mm*, $\varepsilon_r=37$**. The reference value** v_r **has been obtained using a commercially available *TLM* technique [3].**

References

1. A. Taflove and S. C. Hagness, *Computational Electrodynamics: The Finite-Difference Time-Domain Method*. Norwood: Artech House, 2000.
2. D. Caratelli and R. Cicchetti, "A full-wave analysis of interdigital capacitors for planar integrated circuits," *IEEE Trans. Magnetics*, Vol. 39, No. ,3 pp. 1598–1601, May 2003.
3. J. Chuma, C. W. Sim, and D. Mirshekar-Syahkal, "Computation of resonant frequencies of dielectric loaded rectangular cavity using TLM method," *Electron. Lett.*, Vol. 35, No. 20, pp. 1712–1713, Sept. 1999.

Applicability of Multiple Signal Classification Algorithm for Imaging Two-Dimensional Scatterers in Special Scenarios

K. Agarwal, X. Chen

National University of Singapore, Singapore

E-mail: g0600069@nus.edu.sg

In this paper, we study the MUSIC (Multiple Signal Classification) algorithm for imaging two-dimensional scatterers [1]. We present three aspects of MUSIC imaging here. First, some properties of MUSIC imaging of small dielectric cylinders under TE illumination, which have not been investigated earlier, are studied. Detailed analysis of the sources induced on the small dielectric cylinders and their linear dependency on each other gives a distinct insight into the use of MUSIC to locate them. It is observed that:

(1) if the signal subspace is chosen appropriately, MUSIC can detect a cylinder by employing a test function corresponding to a non-prominent induced source as well. As an example, we show that for small isotropic dielectric cylinder, though the line source is not a prominent induced source, we can detect the cylinder using a test line source as in **Fig. 1**;

(2) the geometry or material properties of a cylinder may result in a feeble or null strength of the induced source along one of the principal axes, and in such a case (called degenerate case) the knowledge of the direction, in which the sole independent source is induced, becomes mandatory to detect the cylinder (**Fig. 2**). The authors have recently proposed an algorithm to image such scatterers using a modified MUSIC approach [2].

Next, we attempt to use MUSIC for imaging large scatterers under the TM incidence [3]. It is noticed that:

(3) the use of antenna arrangement providing full aspect to the cylinders can indeed generate information about the presence and approximate locations of the cylinders, which can be used as an initial guess for contour optimization algorithms [4]. We show that the method can generate a reasonable initial guess even in presence of multiple large scatterers with separation of less than one wavelength between them (**Fig. 3**).
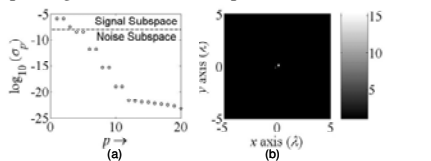
Fig. 1: Implication of choice of signal subspace. (a) Singular values' plot. Signal subspace is formed using singular vectors corresponding to the first three singular values (third one not being prominent). (b) Pseudospectrum using line test source can detect the cylinder when signal subspace is as in (a).
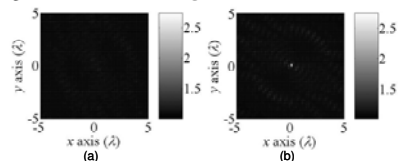
Fig. 2: MUSIC result for anisotropic degenerate cylinder. (a) Pseudospectrum using *x*-directed test dipole cannot detect the cylinder. (b) Pseudospectrum using test dipole along the optic axis can detect the cylinder.
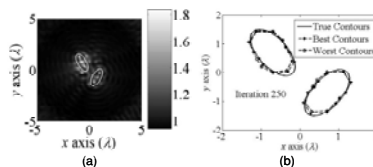
Fig. 3: Use of MUSIC to image large elliptic cylinders and the result of DES with initial guess as generated using MUSIC. (a) Result of MUSIC for two large elliptic cylinders being investigated under full aspect arrangement and TM illumination. (b) Contour optimization result of 250th iteration of Differential Evolution Strategy.

References
1. H. Ammari, E. Iakovleva, and D. Lesselier, "A MUSIC algorithm for locating small inclusions buried in a half-space from the scattering amplitude at a fixed frequency," SIAM Journal on Scientific Computing, vol. 3, 2005, pp. 597–628.
2. X. Chen and K. Agarwal, "MUSIC algorithm for two-dimensional inverse problems with special characteristics of cylinders," IEEE Trans. Antennas Propagat., accepted.
3. S. M. Hou, K. Solna, and H. K. Zhao, "A direct imaging algorithm for extended targets," Inverse Problems, vol. 22, 2006, pp. 1151–1178.
4. A. Qing, "Electromagnetic inverse scattering of multiple two-dimensional perfectly conducting objects by the differential evolution strategy," IEEE Trans. Antennas Propagat., vol. 51, pp. 1251–1262, Jun. 2003.

Rigorous Numerical Simulation Technique for Electromagnetic Wave Propagation through Large Systems of Discrete Scatterers

E. H. Bleszynski, M. Bleszynski, and T. Jaroszewicz

Monopole Research, Thousand Oaks, CA 91360, USA

E-mail: elizabeth@monopoleresearch.com

An accurate and efficient technique for simulation of electromagnetic (EM) wave penetration through large systems of discrete scatterers is of interest in many practical applications, such as imaging through cluttered media (e.g., clouds or foliage), or designing materials with suitable transmission and reflection properties for ultra wide-band (UWB) antenna applications.

The purpose of this contribution is to present the underlying formulation and applications of an algorithm suited for an efficient and rigorous modeling of propagation of EM waves through large collections of discrete, strongly interacting, scatterers. The scatterers may form ordered, partially disordered or random systems.

We model the system of scatterers as a doubly ("laterally") periodic set of cells. Each cell may contain a large number of scatterers (from thousands to hundreds of thousands), where each scatterer is usually described by several hundred of unknowns. The total number of unknowns per cell may be in millions.

The approach is based on solving Maxwell equations in the integral form and utilizing a rigorous, non-lossy impedance matrix compression. The near-field part of the impedance matrix is evaluated by means of the usual method-of-moments, modified by contributions due to the Green function (quasi-)periodicity (i.e., allowing for phases arising from propagation of waves with wave vectors of non-zero lateral components). The far-field part of the impedance matrix is efficiently compressed with a suitably constructed version of the Adaptive Integral Method (AIM) (Fast Fourier Transform-based) acceleration technique, utilizing the periodic Green function. Our approach is applicable to scatterers of arbitrary shapes, sizes, and material properties (including magnetic materials), packed with an arbitrary density. There is no restriction on the scatterer size relative to the wavelength; in particular, the method is not limited to the dipole approximation for the scattering amplitudes. The computational cost of the solution is approximately proportional to the number of unknowns per periodicity cell.

The method allows us to rigorously solve scattering and propagation problems for large systems of scatterers, i.e., large samples of a spatially extensive medium, while minimizing (through periodicity) the effects of the sample boundaries. It also allows high precision simulation of periodic and nearly periodic systems, and analysis of the band-gap structure of complex materials. As an example of such an application, Fig. 1 shows the band-gap structure of the reflection coefficient computed for a periodic slab of densely packed dielectric spheres.

Due of its competitive performance and accuracy, our algorithm may be considered as an alternative to such simulation techniques as finite-difference time-domain (FDTD) or multiple scattering (T-matrix) approach.
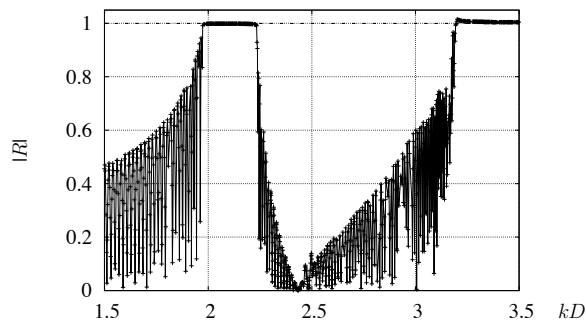
Fig. 1: Reflection coefficient for a periodic slab of 100 layers of densely packed dielectric spheres of permittivity $\epsilon = 5.84$ and radius to center-to-center distance $a/D = 0.45$, plotted as a function of kD, where k is the incident wavenumber.

A Hybrid Method for Solving 2-D Inverse Scattering Problems

A. Semnani, M. Kamyab

K. N. Toosi University of Technology, Tehran, Iran

a_semnani@eetd.kntu.ac.ir

Inverse problems are inherently nonlinear, ill-posed and non-unique. Therefore, these problems are usually considered in global optimization-based procedures and several types of regularizations are used to overcome the ill-posedness [1]. The general form of cost function for optimization routine can be considered as

$$F = \sum_{i=1}^{I} \sum_{j=1}^{J} \int_{0}^{T} \left(\left\| \vec{E}_{ij}^{\,sim} - \vec{E}_{ij}^{\,meas} \right\|^2 + \eta_0^2 \left\| \vec{H}_{ij}^{\,sim} - \vec{H}_{ij}^{\,meas} \right\|^2 \right) dt + \lambda \times R\left(\varepsilon_r, \sigma, \mu \right) \tag{1}$$

where $\vec{E}_{ij}^{\,sim}, \vec{H}_{ij}^{\,sim}$ are the simulated fields, $\vec{E}_{ij}^{\,meas}, \vec{H}_{ij}^{\,meas}$ are measured fields, $R\left(\varepsilon_r, \sigma, \mu \right)$ is the regularization term and λ is the regularization factor. I and J are the number of transmitters and receivers, respectively and T is the total time of measurement. Unfortunately, these methods have two main drawbacks. The first is the huge number of the unknowns especially in 2-D and 3-D structures which increases not only the amount of computations, but also the degree of ill-posedness. The other disadvantage is the determination of regularization factor which is not straightforward at all. It has been shown that by expansion method, instead of direct optimization of the unknowns, it is possible to expand them in terms of a complete set of orthogonal basis functions and optimize the coefficients of this expansion [2]. The problem here is the imperfect accuracy due to limited number of expansion terms, have been used. In this paper, a new hybrid algorithm for fast and accurate solving of 2-D inverse scattering problems is proposed using a two-step optimization-based method. In the proposed algorithm, a coarse solution is obtained by choosing relatively small number of terms in an expansion routine in the first step [2]. Then, based on this answer as the initial guess of the direct optimization problem, a more accurate solution is obtained in the second step. In both steps, finite difference time domain (FDTD) and particle swarm optimization (PSO) are used as electromagnetic solver and global optimization routine, respectively. The most important advantage of this method is that because of a suitable initial guess in direct optimization routine, sensitivity of the algorithm to the regularization parameter is decreased and convergence of the algorithm is completely guaranteed.

Performance of the method is studied for several 2-D case studies. Fig. 1 shows the results of a sample permittivity profile reconstruction. The results show that the hybrid method is able to reconstruct unknown media more precisely in comparison with conventional direct and expansion reconstruction methods.
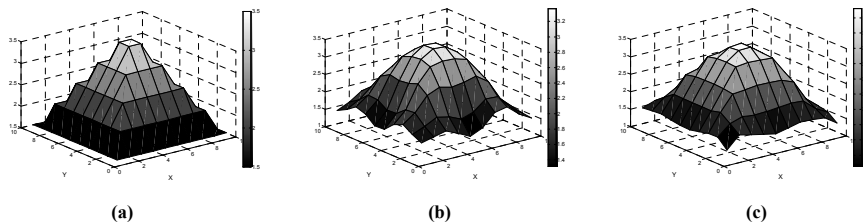
Fig. 1 – Permittivity profile reconstruction. (a) Original profile, (b) by expansion method after 200 iterations (step 1), (c) by hybrid method after 400 iterations (step 2).

References
1. I. T. Rekanos and A. Raisanen, "Microwave imaging in the time domain of buried multiple scatterers by using an FDTD-based optimization technique," IEEE Transactions on Magnetics, vol. 39, no. 3, pp. 1381-1384, May 2003.
2. A. Semnani and M. Kamyab, "Truncated cosine Fourier series expansion method for solving 2-D inverse scattering problems," Progress In Electromagnetics Research, PIER. 81, pp. 73-97, 2008.

UWB - 01
UWB - Scattering

Oral Presentations

Electromagnetic Investigation of Scattering by Arbitrarily Shaped Structures in Free Space Using a Full Wave Transverse Formulation (TWF)

T.Bdour[1], N.Ammar [1], T.Aguili [1], and H.Baudrand[2]

(1) Communications Systems Laboratory in Tunis Engineering School, Belvedere, BP 37 Tunis, 1002 Tunisia
(2) Electronics laboratory LEN7, ENSEEIHT, 2 rue Camichel, 31071, Toulouse, France

E-mail: bdour_tarek@yahoo.com

In this paper, a new approach of the Wave Concept iterative Process (WCIP) [1]-[4] method is presented to study the electromagnetic scattering problem by arbitrarily shaped structures in the free space. This iterative integral approach is based on transverse wave formulation TWF. The WCIP principle consists in expressing the boundary and the closing conditions in term of incident and scattered waves related by bounded diffraction operators. A system of equations is deduced from these conditions: The integral relations are described in the spectral domain and the continuity conditions are formulated in the spatial domain. The iterative process is ensured between the two domains in order to compute the unknown electromagnetic fields. The iterations are stopped when a desired precision is reached on the problem value. In the case of embedded circuits, the toggling between the spatial and the spectral domains is accelerated by the fast modal transform FMT. Unlike the MoM method, the WCIP handles bounded and usually convergent integral operator avoiding to treat possible singularities involving the Green operator. It also dissociates its two basic equations which enhances its real-time optimization technique. It has been proven that the iterative process of our full-wave approach is always convergent [3] and a considerable reduction of the computational CPU time can be achieved regarding the MoM simulation time. Despite its performance, the use of WCIP method is limited to closed structures.

The main motivation of this paper is to extend the use of our full wave approach to the electromagnetic investigation of more general class of open geometries, and in consequence to explore the capability of this method in predicting their scattering features in free space. In this approach, the cylindrical coordinate system is adopted to the formulation of the problem [5]. Diffraction operators describing the coupling between the studied structure and the free space are defined and expanded in an appropriate cylindrical local-domain functions basis. The two basic equations are fully reformulated in the spatial domain. A comparative study of the simulation computational time of the present method and the MoM method is proposed. Numerical results which illustrate the efficiency of our approach are presented for two scattering problems involving structures with sharp edges and wedges (corner reflector [6] and L-shape [7]). The computed currents density and the normalized scattering coefficient present a very good agreement with the literature.

References
1. S. Wane, D. Bajon, H. Baudrand, and P. Gamand, ""A new full-wave hybrid differential–integral approach for the investigation of multilayer structures including non uniformly doped diffusions", IEEE Trans .MTT, vol.53, No.1, pp.200–214,Jan. 2005.
2. S. Wane, D. Bajon, H. Baudrand, and P. Gamand, ""Full wave analysis of isolated pockets to improve isolation performances in silicon based technology", IEEE MTT-S Int. Microwave Symp. Dig., Jun. 2002, pp.987–990.
3. R.S. N'Gongo and H. Baudrand, "Application of Wave Concept Iterative Procedure in Planar Circuits," Recent Res. Devel. Microwave Theory and Technique, vol. 1,pp. 187-197, 1999.
4. N. Raveu , T. P. Vuong , I. Terrasse , G.-P. Piau and H. Baudrand, "Near fields evaluated with the wav e concept iterative procedure method for an E-polarisation plane wave scattered by cylindrical strips", *Microwave and optical technology letters*, vol. 33,no.1,pp.57-61, April 2002
5. T.Bdour,N.Ammar,T.Aguili and H. Baudrand:" Modeling of Wave Penetration through CylindricalAperture using an Iterative Method Based on Transverse Wave Concept", *IEEE Microwave Conference KJMW*, pp.45-48 , November 2007.
6. T.Shijo ,T.Harino and M.Ando " Large –Size Local- Domain basis functions with phase detour and fresnel Zone Threshold for Sparse Reaction matrix in the Method of Moments" ,*IECE trans.Electron*,E88-C,pp .2208-2215,Dec2005
7. George W.Pan, Youri V and Barry Gilbert " Smooth local cosine based Galerkin method for scattering problems " *IEEE Tansactions on Antennas and propagation*,Vol.51,NO,6,june 2003

UWB - 01
UWB - Scattering

Oral Presentations

Scattering of Electromagnetic Waves by Periodic Rough Surfaces

S Yildiz[1], Y Altuncu[1], O Ozdemir[2]

[1]*Istanbul Technical University Electrical and Electronics Engineering Faculty*
Maslak 34469, Istanbul,Turkey
[2]*INRIA Rocquencourt, BP 105,78153, Le Chesnay Cedex, France*

yildizselda@gmail.com

Abstract - Periodic structures often appear in the applications such as antenna design, microwave systems, metamaterials etc. and the analysis of electromagnetic wave propagation in such structures has an important place in the electromagnetic theory. Among them scattering of electromagnetic waves from rough surfaces is important due to both theoretical and practical points of view. For the periodic surfaces having a slow variation, one can obtain the solution under the Rayleigh hypothesis in terms of Floquet modes. On the other hand, for surfaces which does not satisfy the Rayleigh condition it is required to develop new methodologies.

In this paper, it is aimed to give two methodologies for the solution of scattering problems related to periodic dielectric rough surfaces which are valid beyond the limits of the Rayleigh Hypothesis. The first method is the extension of buried object approach (BOA) given in [4] to the present problem. The basic idea here is that the irregularities of the rough surface are considered as buried objects in a two half-spaces medium with planar interface, that allows us to formulate the problem as a scattering of electromagnetic waves from cylindrical bodies located periodically in a two half-spaces medium. By considering that the number of irregularities in a period is finite and using the periodic Green's function of two half-spaces medium with planar interface, the problem is reduced to the solution of a Fredholm integral equation of second kind that can be treated by using one of the known techniques. In this approach, we solved the integral equation via an application of Method of Moments (MoM) by reducing it to a linear system of equations. Since the Periodic Green's function can be obtained in terms of Floquet modes, the computational cost of the method is very low. This approach can also be used for solving scattering problems related to surfaces of infinite extend and having a local roughness. In such a case, it is assumed that the local rough surface is periodically repeated in one direction which allows us to formulate the problem as a scattering from a periodic rough surface. In order to have an accurate model the period should be chosen large enough as compared to length of the rough part. The second method is an analytical continutaion method through Taylor Expansion in which the layers just above and below the rough surface are separated into two parts by fictitious planes. While the scattered field is represented in terms of Floquet Modes above and under of these fictitious planes, the scattered field in the region between these fictitious planes is expressed as a Taylor series. Both methods are compared with existing methods and yield quite satisfactory results.

References

1. Hastings, F. D., J. B. Schneider, and S. L. Broschat, "A Monte-Carlo FDTD technique for rough surface scattering," *IEEE Trans. on Anten. and Prop.*, Vol. 43, No. 11, 1183-1191, 1995.
2. Demir, M. A. and J. T. Johnson, "Fourth-and higher-order small-perturbation solution for scattering from dielectric rough surfaces," *Journal of the Optical Society of America A-optics Image Science and Vision*, Vol. 20, No. 12, 2330-2337, 2003.
3. A. Ishimaru, *Electromagnetic Wave Propagation, Radiation and Scattering*, Prentice Hall, New Jersey, 1991.
4. Altuncu, Y., A. Yapar, and I. Akduman, On the scattering of electromagnetic waves by bodies buried in a half-space with locally rough interface," *IEEE Trans.on Geoscience and Remote Sensing*, Vol. 44, No. 6, 1435-1443, 2006

UWB - 01
UWB - Scattering

Oral Presentations

Benchmark Problems for Coupling and Scattering with Cavity Structures of General Form

P. D. Smith[1], E. D. Vinogradova[1], S. B. Panin[1], Y. A. Tuchkin[2] and S. V. Vinogradov[3]

[1]*Department of Mathematics, Macquarie University, Sydney, Australia*
[2]*Electronics Department, Gebze Institute of Technology, Gebze-Kocaeli, Turkey*
[3]*Department of Mathematics, Macquarie University, Sydney, Australia*
E-mail: pdsmith@maths.mq.edu.au

The need for reliable and accurate prediction of electromagnetic wave coupling to, or scattering from, structures arises in many contexts including target identification, antenna design and system vulnerability. General purpose computational codes have been extensively developed in the last few decades as computing power and resources have become widely available; they have had a significant impact in providing numerical solutions and insight into important coupling and scattering mechanisms. However the accuracy of present-day purely numerical methods can be difficult to assess, particularly for objects of some complexity, incorporating edges, re-entrant structures and partially enclosed scatterers (metallic or dielectric). The classic text [1] provides rigorous solutions for closed canonical bodies of simple geometric shape. We describe an equally rigorous treatment for structures possessing edges, cavities and inclusions that greatly expands the set of benchmark solutions available for the validation of numerical solutions obtained from more general purpose numerical codes; moreover the analysis of such a canonical problem, judiciously chosen, can provide great insight into the relative importance of the various scattering and coupling mechanisms encountered in complex structures.

Cavity and edge structures often pose difficulties of accuracy and convergence for standard numerical techniques applied to Maxwell's equations becoming pronounced for structures of moderate or large size (in wavelengths). The conversion to an equivalent integral equation formulation usually does little to ameliorate the difficulty, because most customary approaches rely on the numerical solution of a first kind Fredholm integral equation, which is ill-posed, and therefore the computational scheme is not stable and its convergence is questionable. Thus, it is highly desirable to transform this type of equation into a second kind Fredholm equation; stable and fast converging computational algorithms can then be readily devised, enabling us to reach any pre-specified accuracy. This paper surveys recent progress in techniques that address these difficulties for a variety of structures, some canonical and some of more general shape.

For cavities of spherical and other canonical shapes, a process of analytical regularisation [2,3] may be used to transform the basic equations to a second kind Fredholm matrix equation. This approach has been adapted to the study of two-dimensional scattering problems, including arbitrarily shaped cavity structures, for both E- and H-polarizations.

This technique has recently been extended to three-dimensional cavity structures that are axisymmetric, and provides a rigorous analysis of diffraction from an arbitrarily shaped open shell of revolution under excitation by an axially located vertical electric dipole or scalar wave illumination. It relies on decomposing the kernel in the integral equation formulation into a singular part, which may be analytically inverted by exploiting the solution for the canonical problem of the punctured sphere, and a smooth remainder.

Varying the geometric parameters provides a large number of physically interesting benchmark solutions of guaranteed accuracy. Prospects for further progress with this method will be discussed.

References
1. J. J. Bowman, T.B.A. Senior, and P.L.E. Uslenghi, Electromagnetic and Acoustic Scattering by Simple Shapes. New York: Hemisphere Publishing Corporation, 1987.
2. S. S. Vinogradov, P.D. Smith, and E.D. Vinogradova, Canonical Problems in Scattering and Potential Theory, Part I: Canonical Structures in Potential Theory. Boca Raton: Chapman & Hall/CRC Press, 2001.
3. S. S. Vinogradov, P.D. Smith, and E.D. Vinogradova, Canonical Problems in Scattering and Potential Theory, Part II: Acoustic and Electromagnetic Diffraction by Canonical Structures. Boca Raton: Chapman & Hall/CRC Press, 2002.

A Metallic Wire Electromagnetic Crystal structure for Radar Applications

F. Ghanem[1], G.Y. Delisle[2], T.A. Denidni[2], K. Ghanem[3] and P.S. Hall[1]

[1]*Funiversity of Birmingham, Birmingham, UK*
[2]*INRS-EMT, Montreal, Canada*
[3]*USTHB, Algiers, Algeria*
E-mail: f.ghanem@bham.ac.uk

In this paper, an electromagnetic crystal structure, composed of parallel metallic wire rows and excited by a monopole disposed in the middle of the structure, is proposed for radar applications.

The proposed approach exploits the high frequency dispersion of the radiation patterns of these structures. Indeed, it has been shown in [1] and [2] that the radiation pattern steering angle can be changed by varying the operating frequency of the structure, which allows scanning the space by varying the frequency of the excitation signal as shown in Fig. 1-a.
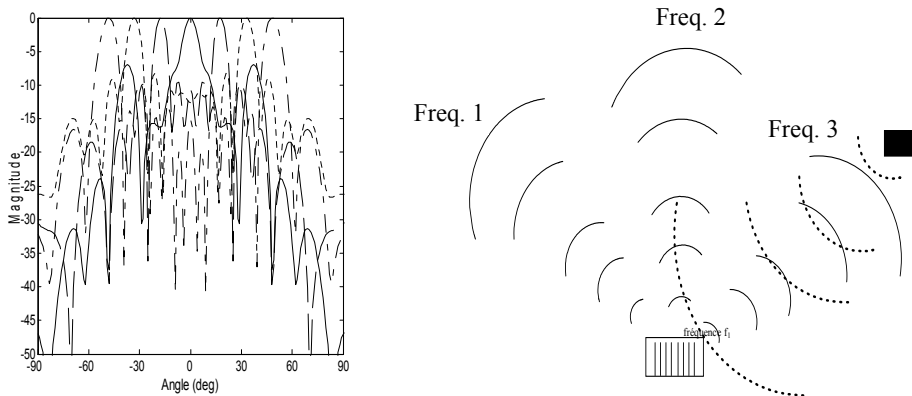
Fig. 1 – Functioning principle. a) Variation of the steering angle with frequency. b) Simplified positioning principal

Based on this property, a new algorithm has been proposed to perform target positioning and tracking. The new radar starts by transmitting an UWB signal that contains all frequencies needed to scan the space. Due to the frequency dispersion of the radiation patterns, the different signal frequencies will be transmitted in different space directions as shown in Fig. 1-b. If a target is present, then only the signal having the frequency that goes in its direction (Freq. 3) is reflected. The other components (Freq. 1and Freq. 2) propagate in different directions and will not be reflected to the radar. The radar receptor is composed of frequency detectors that detect selected frequencies (Freq. 1, Freq. 2 and Freq. 3). The detected frequency determines the angle of the target and the time propagation determines its distance. For the tracking, as the target moves, it will be detected at different frequency.

Finally it is important to mention that since the target position is determined by the detected frequency, the proposed radar needs to be used with a device that compensates for Doppler shifts produced by any movement of the target in the transverse direction.

References
1. R.C. Honey, "A flush-mounted leaky-wave antenna with predictable patterns", IRE Trans. On Antennas and Propagation, vol. 7, Issue 4, pp. 320 – 329, Oct. 1959.
2. F. Ghanem, G. Y. Delisle and T. A. Denidni, "A New Electromagnetic Crystal-Based Antenna for Ultra-fast Radiolocation Applications", IEEE Antenna and Wireless Propagation Letters, vol. 5, pp. 199-203, 2006.

UWB - 02
Applications of UWB Antennas

Oral Presentations

Integrated cm - and mm-Wave UWB Transceiver for M-Sequence Based Sensors

M. Kmec[1], J. Müller[1], P. Rauschenbach[1], S. Rentsch[1], J. Sachs[1], B. Yang[2]

[1]*Technische Universität Ilmenau, Ilmenau, Germany*
[2]*Delft University of Technology, Delft, The Netherlands*

E-mail: martin.kmec@tu-ilmenau.de

Several approaches to extend the operational frequency band of M-Sequence based UWB sensors using frequency up and down converters were presented [1] earlier. To make such sensors affordable for broader application in industry and research, it is necessary to identify inexpensive manufacturing technologies suitable for very broadband circuits. The operational frequency bands of interest cover the baseband (DC to 10 GHz) as well as the cm- and mm-bands. In order to ensure these requirements an IC design program for extended UWB SiGe sensor components has been initiated at our university. On this way a broad scale of SiGe:C chips has been designed, tested and successfully implemented.

It is known, that the break-down voltage of the standard SiGe-transistor is restricted to a relative low voltage. Therefore the signal amplitudes handled with SiGe technology may cover only a few hundred mV. In order to gain sufficient transmit power it is recommended to spread the wideband stimulus over a large time which is well done by modulating the carrier frequency with an M-Sequence. This approach enables the combination of the proven baseband M-Sequence concept with broadband heterodyne or homodyne converters.

An other very important point is that the whole sensor topology may be implemented by balanced circuits, which firstly allows on board integration with the differential broadband radiators (antennas) without introduction of baluns. The second benefit consists in avoiding of the so called "via holes" problem. Unbalanced integrated circuits need a ground plane that lies usually below the substrate, while the active and passive devices are mounted on the top. Therefore, in order to obtain a ground reference for such circuits many via holes must be fabricated to make a proper connection between the top and bottom layers. However vias cause additional inductances which lead to problems at high operational frequencies. Furthermore, extra costs and complexity arise.

Our latest development is a completely balanced broadband transceiver front-end for operation in the cm- and mm-wave range which is compatible to our mother M-Sequence baseband system. The transceiver front-end is based on ICs designed for a commercial 0.25μm SiGe process with f_T = 190 GHz. The design of such front-end is a challenging task since not only due to the high carrier frequency but also the large bandwidth. For example, every transition between the chip and the chip carrier or between different types of RF-lines can cause discontinuities which disturb the broadband sensor signal. With an one-chip solution, one could avoid many interface problems of such kind, but parasitic signal coupling on chip would provoke other difficulties. To achieve the optimum compromise, we decided to design three different front-end ICs, up-converter, down-converter and LO-unit, mounted on a LTCC (Low Temperature Cofired Ceramics) RF-board in order to minimize the cable interconnections between the RF components. The front-end ICs will be flip-chipped directly in the feed-point of the radiators (Rx and Tx antennas).

The proposed circuit topologies for up- and down- converter ICs are based on differential pairs with emitter degradation as buffers and Gilbert cells as mixer cores. The first version of up- and down- converter ICs is already manufactured, partly on wafer tested and ready to be mounted into the LTCC test board. The LO-unit is buffered with appropriate differential buffers and consists of a tripler and doubler, where both can operate separately or cascaded. The frequency multipliers will be driven from the system master clock which typically lies in the 10 GHz range.

In the final paper we will present the broadband M-sequence based sensor demonstrator for operation in cm- and mm-wave range in more details. We will discuss measured results of the fabricated ICs and demonstrate the feasibility of our approach for broadband sensing in such high frequency ranges.

References
1. M. Kmec, R. Herrmann, J. Sachs, P. Peyerl, P. Rauschenbach, "Extended Approaches for Integrated M-Sequence Based UWB Sensors" 2006 IEEE AP-S International Symposium with Radio Science and AMEREM Meetings, Albuquerque, NM USA, 2006.
2. S. Rentsch, J. Müller: "Design and Implementation of Baluns at 60GHz on LTCC"; Invited Paper, Journal of Microelectronics and Electronic Packaging, JMEP, Vol.4 No. 4, 4th QTR, 2007 (ISSN 1551-4897)

Radar Observation of Objects, which Fulfill Back-and-Forth Motion

Igor Immoreev

Moscow Aviation Institute, Moscow, Russia

E-mail: immoreev@aha.ru

In medical radars the main objects - the thorax and heart - have back-and-forth motion. In result, radar observation of such objects becomes unusual. Let's consider model shown on Fig. 1. The object makes back-and-forth motion under the harmonious law with frequency Ω: $R(t)=R+\Delta R sin(\Omega t+\theta)$.

Fig.1 Back-and-forth motion of the object

Fig. 2 Correlator

Fig. 3 The form of a signal when $\Delta R \gg \lambda_0$
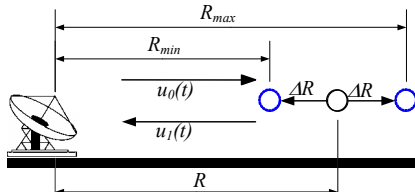
The radar radiates a signal: $u_0(t)= E_0 sin\ \omega_0 t$. The signal, reflected from object, is equal:

$$u_1(t)=E_1 sin \omega_0 \left[t - \frac{2R(t)}{c} \right] = E_1 sin \left[\omega_0 \left(t - 2 \left(\frac{R + \Delta R sin(\Omega t + \theta)}{c} \right) \right) \right] (1)$$

The receiver is the correlator with an output signal z_c (Fig. 2).

We believe object is motionless during time of integration. Then the output signal of the correlator:

$$z_c(t) = \frac{E_0 E_1}{2} n T_0 cos \left[2\omega_0 \left(\frac{R + \Delta R sin(\Omega t + \theta)}{c} \right) \right] =$$
$$= \frac{E_0 E_1}{2} n T_0 cos \left(\frac{4\pi R}{\lambda_0} \right) cos \left[\frac{4\pi \Delta R}{\lambda_0} sin(\Omega t + \theta) \right] -$$
$$- \frac{E_0 E_1}{2} n T_0 sin \left(\frac{4\pi R}{\lambda_0} \right) sin \left[\frac{4\pi \Delta R}{\lambda_0} sin(\Omega t + \theta) \right] \quad (2)$$

At $\Delta R \ll \lambda_0$, function $z_c(t)$ is close to harmonious function. When the amplitude of movement of object ΔR increases and approaches to length of wave λ_0, the function $z_c(t)$ appreciably changes and gets the complex form (see example at Fig. 3) and a complex spectrum.

In this case is necessary restoration the form of the signal corresponding to true movement of object. For this purpose the receiver has two quadrature channel $z_s(t)$ and $z_c(t)$. The true trajectory of movement of object is described by the formula:

$$R(t) = \frac{\lambda_0}{4\pi} arg\ [z_c(t) + jz_s(t)] \quad (3)$$

To find argument we should calculate function of arc tangent:

$$arg\ [z_c(t) + jz_s(t)] = arctg \left(\frac{sin \left(4\pi \frac{R}{\lambda_0} + 4\pi \frac{\Delta R}{\lambda_0} sin(\Omega t + \theta) \right)}{cos \left(4\pi \frac{R}{\lambda_0} + 4\pi \frac{\Delta R}{\lambda_0} sin(\Omega t + \theta) \right)} \right) = \frac{4\pi}{\lambda_0} [R + \Delta R\ sin(\Omega t + \theta)] \quad (4)$$

Then the law of movement of object $R(t)$ will be equal:

$$R(t)=R+\Delta R sin(\Omega t+\theta). \quad (5)$$

If the equipment of a radar allows to define distance up to object R, that, subtracting her from $R(t)$, it is possible to define the law of movement of object precisely: $\Delta R\ sin(\Omega t + \theta)$.

In a paper the circuit of processing of a signal of radar will be given and the algorithm of signal processing for restoration of a trajectory will be described at back-and-forth motion of the object.

Experimental Focal Waveforms of a Prolate-Spheroidal Impulse-Radiating Antenna (IRA)

S. Altunc[1], C. E. Baum[2], C. G. Christodoulou[3] and E. Schamiloglu[4]
University of New Mexico Department of Electrical and Computer Engineering
Albuquerque New Mexico 87131, USA
E-mail: saltunc@ece.unm.edu

Experiments using two-arm and 60^0 four-arm prolate-spheroidal IRAs are used to obtain better focusing for a prolate-spheroidal IRA and these results are compared with analytical results in [1] for comparison. This paper presents a summary of the experimental setup and the dimensions of these experiments are based on [1, 2]. These setups were motivated by a biological application [3].

Experiments were performed at the University of New Mexico (UNM) Transient Antenna Laboratory. We feed our IRA using a $V_0 = 0.5$ V (peak-peak 1 V) and $t_\delta = 100\, ps$, rise time ramp-rising step. The experimental setup basically includes three components: a prolate-spheroidal reflector with feed arms, a sampling-oscilloscope, and a pulse generator. Analytical, numerical and experimental prepulses' amplitudes agree very well. The analytical and numerical impulses' amplitudes agree. However, the experimental impulse amplitude was smaller than the others. It was also broader near the base. We have also a feed arm blockage effect that decreases the amplitude of the experimental impulse; however, we did not see this effect in our numerical results. Our analytical result was based on an idealized assumption and it did not account for the feed arms. For all cases the postpulse behaviors were different. However, this part of the pulse was less important for our biological application. Our concern was obtaining the largest possible impulse amplitudes at the focal point to kill skin cancer. The analytical waveform, while simple, is still good, albeit not perfect. The geometric shape or alignment of the prolate-spheroidal reflector may also causes some errors. The misshape of the reflector will lead to a broader focus and smaller amplitude. The prolate-spheroidal reflector was manufactured from fiber and the inside of the reflector is painted with copper conductive paint. We checked the reflection from the conductive paint on the reflector and measured about 99% reflection; however, there might be some hot spots that do not reflect very well and this can cause some errors.

Finally, experimental setups and problems related with measurements or devices were discussed. Experimental and analytical results were compared. Differences between these results were discussed and the differences were analyzed.

References
1. Baum, C.E. (2007), Focal Waveform of a Prolate-Spheroidal Impulse-Radiating Antenna (IRA), Radio Sci. , Vol. 42, RS6S27.
2. S. Altunc and C.E. Baum. "Extension of the analytic results for the focal waveform of a two-arm prolate-spheroidal impulse-radiating antenna (IRA)," Sensor and Simulation Note 518, Nov. 2006.
3. K.H. Schoenbach, R. Nuccitelli and S.J. Beebe, "ZAP," IEEE Spectrum, Aug 2006, pp. 20-26.

Development of a Resonant Chamber Microwave Tomography System

C.J. Kaye, C. Gilmore, P. Mojabi, D. Firsov and J. LoVetri
Department of Computer and Electrical Engineering, University of Manitoba, Winnipeg, Canada
E-mail: Joe_LoVetri@UManitoba.Ca

In this work, progress in the development of a resonant chamber microwave tomography system is reported. This includes mainly the system design and calibration, but imaging results using various inverse scattering algorithms will also be presented.

Relatively recent advancements in mathematical techniques for solving inverse scattering problems have allowed microwave tomography (MWT) to emerge as a promising technology for medical imaging. MWT exploits the differences in dielectric properties among various biological tissues in the body to create an image of the contrast in such properties throughout the imaging region. Furthermore, MWT boasts the use of safe, non-ionizing radiation as well as being potentially drastically less expensive than existing X-ray-based or Magnetic Resonance Imaging modalities. Despite these advantages, reliable image reconstruction of acceptable resolution remains a difficult hurdle, and consequently, only a handful of functional microwave tomography systems have been designed, assembled and tested within the past twenty years [1].

Our group is currently developing several MWT experimental prototypes with the aim of studying several design features and inverse scattering algorithms. One system design, reported here, incorporates a resonant imaging chamber that, using synthetic scattering data, has been shown to produce enhanced images as compared to open imaging systems. It is theorized that the enhanced imaging is due to two factors: 1) the greater amount of useful electromagnetic energy that interrogates the object of interest (OOI) and 2) the mathematical features of the resonant Green's function that is used in such sytems. This has been reported elsewhere [2]. Images have been generated via two suitably modified non-linear inversion algorithms: the Contrast Source Inversion (CSI) method [3], and the Distorted Born Iterative Method (DBIM) [4].

Our prototype system consists of a circular array of twenty-four dipole antennas (evenly distributed at fifteen-degree intervals) inside a cylindrical metallic chamber approximately forty centimeters in diameter and fifty centimeters in height. Various wideband antennas have been designed for the system including resistively-loaded dipoles, the design of which is based on the well-known Wu-King profile [5]. The nominal frequency range of the prototype is from 1 GHz to 8 GHz. In order to calibrate the system, the electromagnetic field without the OOI (*i.e.*, the incident field) is accurately modelled using a Finite-Volume Time-Domain software package that we've developed [6]. Obtaining good imaging results depends on the accuracy with which the actual incident field can be modelled. Incorporating this information into the DBIM and the CSI method will be discussed. The chamber itself is filled with a matching medium and imaging results obtained with matching media of different dielectric constants will be presented.

References
1. T. Gunnarsson, "Microwave Imaging of Biological Tissues: the current status in the research area," Mälardalen Research and Technology Centre, Mälardalen University, Västerås, Sweden, *Technical Report*, Dec. 2006.
2. C. Gilmore, J. LoVetri, "Improved Microwave Tomography using Resonant Enclosures," to be presented at the *2008 URSI General Assembly*, Chicago, Il., Aug. 7-16, 2008
3. P. M. van den Berg, R. Kleinman, "Contrast source inversion method," *Inverse Problems*, vol. 13, pp.1607-1620, 1997.
4. W. C. Chew, Y. M. Wang, "Reconstruction of two-dimensional permittivity distribution using the distorted Born iterative method," *IEEE Transactions on Medical Imaging*, vol. 9, 1990.
5. T. T. Wu, R. W. P. King, "The cylindrical antenna with nonreflecting resistive loading," *IEEE Transactions on Antennas and Propagation*, vol. 13, no. 3, pp.369-373, May 1965: Corrections, vol. 13, no. 6, p.998, Nov. 1965.
6. D. Firsov, C. Kaye, J. LoVetri, "FVTD Thin-Wire Modelling of a Mircrowave Tomography System," presented at the 24th *International Review of Progress in Applied Computational Electromagnetics (ACES 2008)*, Niagara Falls, Canada, March 30- April 4, 2008

A New Trimmed Notch-Cut Printed Antenna for UWB wireless application

A. A. Alshehri, A. R. Sebak

Electrical and Computer Engineering Department
Concordia University, Montreal, Canada
E-mail: a_alshe@ece.concordia.ca

Since the Federal Communications Commission (FCC) has released the unlicensed frequency band of 3.1 - 10.6 GHz in 2002 for ultra wideband (UWB) technology and applications, it has received high worldwide interest because it is a promising solution for short range high speed indoor mobile communications and the emerging reconfigurable and software-defined wireless networks. Consequently, several shapes and designs of UWB antennas such as square, circular, pentagonal, hexagonal, elliptical and trapezoidal shape have been proposed to satisfy UWB specifications [1]. However, some shapes like the square and circular planar monopole antenna have a drawback of a relatively small impedance bandwidth [2].To enhance the impedance bandwidth, several bandwidth enhancement techniques have been proposed such as the use of an asymmetrical feed arrangement [2], a partial ground, adjusting the gap between radiating element and ground plane [3] and cutting two notches in the radiating element or using steps to control the impedance stability [2]. In this paper, a new UWB planar patch antenna is proposed as depicted in Fig. 1. We use various bandwidth enhancement techniques including adjusting the gap between radiating element and ground plane, partial ground plane, using a step to control the impedance stability and notch cut technique which is also used to reduced the size of the planar antenna [3]. The proposed antenna is composed of a planar rectangular patch with notch cut and a transition step fed by a microstrip line with a partial ground plane. The antenna and the partial ground plane are etched on the opposite sides of Rogers RT/Duroid 5880 substrate with a thickness of 1.575 mm, dimensions of 40×32 mm^2 and a relative permittivity ε_r=2.2. The dimensions of rectangular patch are w=22 mm and h=16.33 mm. The transition step of $w_1 \times h_1$ = 17 mm $\times$ 2.5 mm is attached to the rectangular patch. To reduce the overall size of the antenna and get better impedance matching, a rectangular-shaped notch with dimensions of $l_s \times w_s$ = 5.6 mm $\times$ 13 mm is symmetrically cut in the top middle of the radiator and both top edges of the patch are trimmed. The shape of the partial ground plane is rectangular with dimensions of 9.5×40 mm^2. The radiator is fed through a microstrip line having a length of 10.5 mm and width w_f =3.6 mm to ensure 50-Ω input impedance with a feed gap g = 1.0 mm. HFSS simulation software is used to design and optimize the antenna. The proposed antenna is successfully implemented. A measured -10 dB bandwidth of 7.5 GHz (3.1-10.6 GHz) is obtained as shown in Fig. 2. The proposed antenna provides an acceptable radiation pattern and a relatively flat gain over the UWB frequency band. In addition, a parametric study is carried out to optimize the antenna and provide more information about the effects of its geometrical parameters such as the notch cut, the transition step and feed gap.
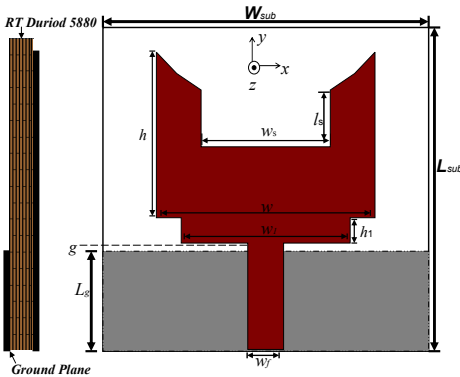
Fig. 1 – Geometry of the proposed antenna
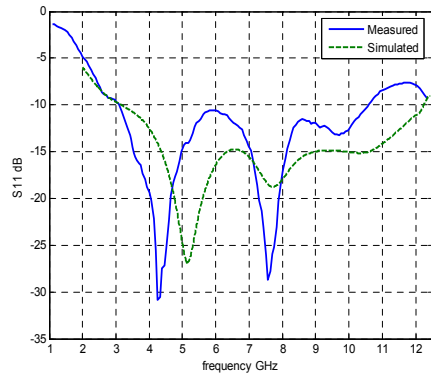
Fig. 2 – Simulated & measured Return loss

References

1. S. W. Su, K. L. Wong & C. L. Tang, "Ultra-wideband square planar monopole antenna for IEEE 802.16a operation in the 2–11GHz band," Microwave Optical Technology Letters, vol. 42(6), pp. 463-466, 2004.
2. M. J. Ammann, & Z. N. Chen, "An asymmetrical feed arrangement for improved impedance bandwidth of planar monopole antennas," Microwave Optical Technology Letters, vol. 40(2), pp. 156–158, 2004.
3. Z. N. Chen, T. S. See & X. Qing, "Small printed ultrawideband antenna with reduced ground plane effect," IEEE Transactions on Antennas and Propagation, vol. 55(2), pp. 383-388, 2007.

Ultra Wideband 4x4 Phased Array containing Exponentially Tapered Slot Antennas and a True-Time Delay Phase Shifter at UHF

J. Schmitz[1], M. Jung[1], J. Bonney[2], R. Caspary[2], J. Schueuer[3], J. Schoebel[2]

[1]*Rheinmetall Waffe Munition GmbH, Heinrich-Erhardt-Strasse 2, D-29345 Unterluess, Germany*
[2]*Institut fuer Hochfrequenztechnik, Technische Universitaet Braunschweig, Schleinitzstrasse 22, D-38106 Braunschweig, Germany*
[3]*Institut fuer Elektromagnetische Vertraeglichkeit, Technische Universitaet Braunschweig, Schleinitzstrasse 23, D-38106 Braunschweig, Germany*

E-mail: juergen.schmitz@rheinmetall.com

For angular scanning a true time array is developed for UHF ultra wideband (UWB) applications in time and/or frequency domain. It is based on a 4x4 array with antipodal exponentially tapered slot antennas (ETSA, Vivaldi, see Fig. 1 (b)) similar to [1] and a 3 bit phase shifter acc. to Fig. 1 (a) [2]. Distances of antenna elements are designed to be compromise between gain, scanning angle, side/grating lobe levels. The uniform spaced and fed array maximizes the overall gain. After defining the antenna shape, corrugations are introduced to improve antenna matching and gain pattern. Nine equally spaced beam positions for a 90 degree scanning angle are induced by an optimized 3 bit phase shifter on high permittivity substrate while 4 bits are usually needed. Parasitic resonances are avoided by using PIN diodes in single pole double throw configuration.

All components and the complete array system are simulated and verified in frequency domain with good agreement (see Fig. 2). Adaption to UWB pulses is possible.

(a) Phase shifter system   **(b) Antenna array**

Fig. 1 – Components
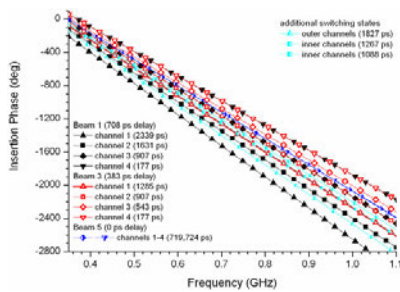
(a) Insertion phase of the phase shifter   **(b) Beam rosette at 850 MHz in H plane**
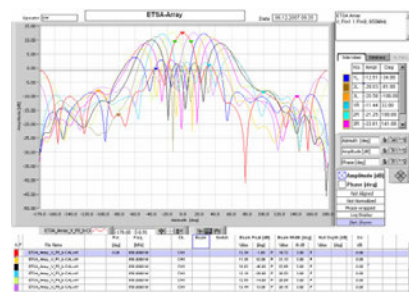
Fig. 2 – Measurements

References
1. W. Soergel, J. Schmitz, M. Jung, G. Wollmann, W. Wiesbeck, "Design and Integration of Antipodal Vivaldi Antennas for High Power Microwave Applications in Mobile Systems", 2006 IEEE AP-S International Symposium with USNC/URSI National Radio Science and AMEREM Meetings, ISBN 1-4244-0123-2, p. 813, Albuquerque.
2. J. Schoebel, J. Schueuer, R. Caspary, J. Schmitz, M. Jung, "A true-time-delay phase shifter system for ultra wideband applications", will be presented at the German Microwave Conference 2008.

UWB - 04
UWB Microstrip and Array Antennas

Oral Presentations

Planar Elliptical Differential Antenna for UWB Applications

G. Quintero, J. F. Zurcher, A. K. Skrivervik

Laboratoire d'Electromagnétisme et d'Acoustique (LEMA),
Ecole Polytechnique Fédérale de Lausanne (EPFL)
E-mail: gabriela.quintero@epfl.ch

Differential antennas are becoming of great interest for UWB systems because of their simplicity to be connected to an input amplifier. The antenna can be connected directly to the system without using an external balun, or balanced to unbalanced transition; thus reducing the size and complexity of the UWB system. Most of differential antennas reported in the literature are fed with coaxial cables perpendicular to the antenna plane [1,2]. This could be of use for some applications, but it may be space consuming in other cases.

In this work we investigate a differential elliptical UWB antenna fed by coplanar striplines. This allows the antenna to be in the same plane as the circuit board, reducing the size of the system, and facilitating the connection to the input amplifier or LNA. An example of this type of implementation is given in [3], where the UWB antenna is included in a USB stick.

The proposed antenna is shown in Figure 1 and has a total size of 5.0 x 3.4 cm. Simulations were done using CST Microwave Studio and Ansoft HFSS. Figure 2 shows the simulated return loss, which is below -10dB over all the band of interest (3.1 – 10.6 GHz). The transfer function (Figure 3) shows the performance of the antenna system in the frequency domain. The fidelity factor measures the pulse distortion produced by an antenna. It is obtained by the correlation between the input and transmitted pulses, and is shown in Figure 4.

Results revealed a good performance of the studied UWB antenna. Its peak radiation is in the *y* direction; therefore it can be connected directly to the system as it exhibits low radiation in the direction of the circuit. Its reduced size and totally flat characteristics make it a good candidate for use in UWB Systems.
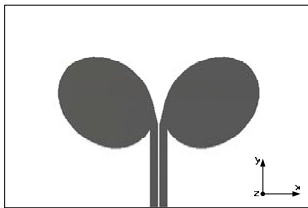
Figure 1. Antenna structure
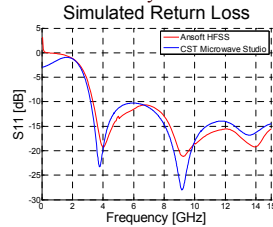
Figure 2. Simulated return loss
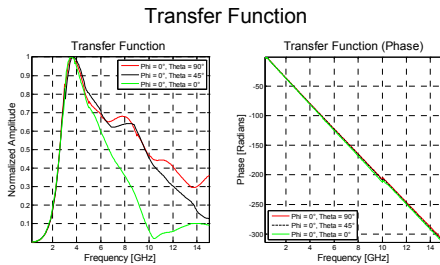
Figure 3. Transfer function of a 2 antenna system
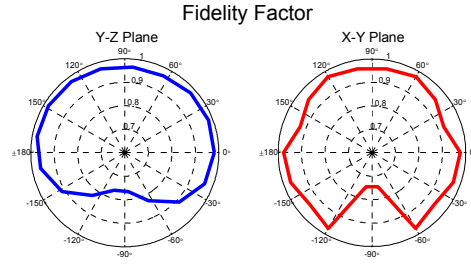
Figure 4. Fidelity factor in Y-Z and X-Y planes.

References
[1] J. Powell and A. Chandrakasan, "Differential and Single Ended Elliptical Antennas for 3.1-10.6 GHz Ultra Wideband Communication", *IEEE Antennas Propagation Society Int. Symp.*, Jun. 2004, pp. 2935 – 2938.
[2] Ch. Zhang, J. H. Wang and Y. Han, "Coupled Planar Dipole UWB Antenna Design For Wearable Computer", *IEEE Int. Conference in Microwave and Millimeter Wave Technology*, April 2007, pp. 1 – 4.
[3] R. Bourtoutian, C. Delaveaud and S. Toutain, "Differential, Shorted Dipole Antenna for European UWB Applications", *EuCAP 2007*, Nov. 2007.

Characterization and Phase Compensation of a Coplanar-waveguide to Coplanar-strip Balun

Johan B. du Toit[1], Johann W. Odendaal[2] and Johan Joubert[2]
[1]*Saab Grintek Avitronics, Pretoria, South Africa*
[2]*University of Pretoria, Pretoria, South Africa*
E-mail: wimpie.odendaal@up.ac.za

Antennas that can be manufactured using photo-etching techniques are attractive for a variety of applications because they are planar, light-weight, low cost, and can easily be integrated with monolithic microwave integrated circuits. For many of these antennas a balanced-to-unbalanced transition is needed from the etched transmission line (e.g. a coplanar-waveguide) to the two feeding points of the antenna structure (e.g. a Vivaldi or etched dipole). The principle of operation of such a relatively compact and wideband uniplanar coplanar-waveguide (CPW) to coplanar-strip (CPS) balun was described in [1, 2]. This type of balun was previously characterized using a two element back-to-back configuration. In this presentation results of a more comprehensive characterization of this balun type will be presented. The reflection coefficient of the balun as a single element terminated in a load is investigated, and the magnitude and phase balance as function of frequency are also determined using a test circuit, based on a characterization technique described in [3] for a double-Y balun. Simulated as well as measured results will be presented for a designed CPW-to-CPS balun on FR4 substrate with an operating bandwidth from DC to 2 GHz. An important characteristic of the newly designed balun is the implementation of etched bond wires, which is very desirable for manufacture repeatability. A relatively simple phase compensation technique and the resulting improvement in phase balance results will also be presented (see Fig. 1 for the simulated phase balance between the output ports). As a final validation of the balun performance radiation pattern results of an etched dipole fed through the balun will be shown, with and without the additional phase compensation.
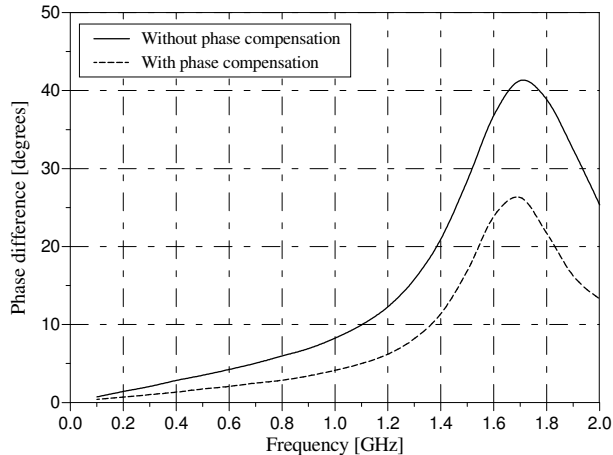
Fig. 1 – Simulated phase balance between output ports.

References
1. J. Thaysen, K. B. Jakobsen and J. Appel-Hansen, "A wideband balun – how does it work?," Applied Microwave and Wireless, vol. 12, 2002.
2. K. Tilley, X.-D. Wu and K. Chang, "Coplanar waveguide fed coplanar strip dipole antenna," Electronics Letters, 30, (3), 1994.
3. B. Jokanović, V. Trifunović, and B. Reljić, "Balance measurements in double-Y baluns," IEE Proc.-Microw. Antennas Propag., vol. 149, 2002.

UWB - 04
UWB Microstrip and Array Antennas

Oral Presentations

Array Antenna for Directed Radiation of High-Power Ultrawideband Pulses

V. I. Koshelev, V. V. Plisko, and K. N. Sukhushin

Institute of High Current Electronics, SB RAS, 2/3 Akademichesky Ave., Tomsk 634055, Russia
E-mail: koshelev@lhfe.hcei.tsc.ru

One of the promising ways in the development of high-power sources of directed wave beams of UWB radiation with multimegavolt effective potential is excitation of a multielement array antenna from one bipolar voltage pulse generator. In the previously created [1, 2] sources of UWB radiation with 16-element array antennas there were used a series-connected wave impedance transformer and a power divider of the coaxial construction. The array elements were excited via the cable feeder. Such construction had two restrictions: a small number of channels in the power divider and, respectively, elements in the array as well as a low level of the voltage pulse amplitudes or short life time of a source. The latter was conditioned by the cable breakdown.

In this paper, a 64-element array is presented that is intended to be excited by means of high-voltage bipolar pulse of the length 1 ns from a generator with the output impedance of 12.5 Ohm. A combined antenna [2] is used as the array element. The array aperture is 1.41×1.41 m. Fig. 1 presents a physical configuration of the array and feeder system. A new thing in the feeder system is a combination of the wave impedance transformer with the power divider. The feeder system has three stages with division in four in the each stage. The length of one channel from the generator to the antenna input is 1.2 m. Transformer oil is used for electrical insulation. The total output impedance of the feeder system is 0.78 Ohm.

(a)   (b)

Fig. 1 – Physical configuration of the array antenna (a) and feeder system (b)

References
1. V. P. Gubanov, A. M. Efremov, V. I. Koshelev, B. M. Kovalchuk, S. D. Korovin, V. V. Plisko, A. S. Stepchenko, and K. N. Sukhushin, "Sources of high-power ultrawideband radiation pulses with single antenna and a multielement array," Instruments and Experimental Techniques, vol. 48, no. 3, pp. 312 – 320, 2005.
2. M. Efremov, V. I. Koshelev, B. M. Kovalchuk, V. V. Plisko, and K. N. Sukhushin, "Generation and radiation of high-power ultrawideband nanosecond pulses," J. Commun. Technol. Electron., vol. 52, no. 7, pp. 756 – 764, 2007.

Ultrawideband Active Receiving Array Antenna with Dual Polarization

V. I. Koshelev, E. V. Balzovsky, and Yu. I. Buyanov

Institute of High Current Electronics, SB RAS, 2/3 Akademichesky Ave., Tomsk 634055, Russia
E-mail: koshelev@lhfe.hcei.tsc.ru

Transmitting and receiving antennas in high-power UWB radar should be separated in space. When sounding remote objects by UWB pulses with both linear and dual polarizations [1], it is necessary to have array antennas providing a receiving of the reflected signals with a small distortion of the signal waveform and for two polarizations. This is important for the sounding object recognition [2]. To create a receiving array antenna with dual polarization, a dipole active antenna providing a necessary frequency pass band at small dimensions was chosen [3].

This paper presents the results of investigations of an element of a dual-polarized array antenna as well as the first experience on the development of a 2×2 array antenna module. Large multielement arrays are supposed to be created basing on the developed module.

Two crossed dipoles with dual polarization are used as the array element, each of them being loaded to the active FET element with a symmetrical output [3]. The developed balancing unit consists of a phase inverter (providing the phase shifting to 180°) and a two-stage ring summation unit. Fig. 1 presents a physical configuration of the dual-polarized antenna. The dimensions of the crossed dipoles with active elements are equal to 45×45×45 mm. The balancing unit is made at a 162×98×1-mm dimension printed circuit board. The waveforms of the pulses are recorded by two dipoles presented in Fig. 2: orientation of the first dipole coincides with the polarization plane of radiation (curve 1) and the second dipole is orthogonal (curve 2) to the first one. Measurements of the active antenna characteristics were made in the frequency and time domain. A receiving TEM antenna was used for comparison. The active antenna frequency band is 0.3–4 GHz. The effective length of the antenna is 1 cm. The distortion of the pulse waveform at the field strength being less than 10 V/m is not higher than 15% RMS. A dynamic range reaches 50 dB. Polarization isolation between two receiving channels is no less than 25 dB. The antenna breakdown in the incident field with the strength of 6 kV/m takes does not occur. The antenna current consumption is 100 mA at the supply voltage of 3 V.

Fig. 1 - Active receiving antenna with dual polarization
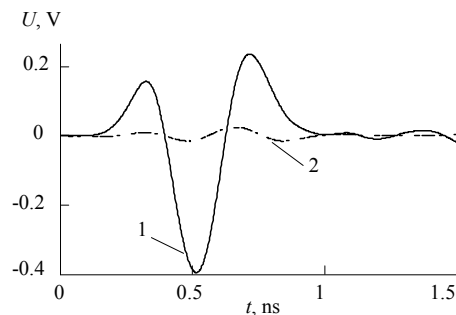
Fig. 2 - Voltage pulses at the antenna output

References
1. M. Efremov, V. I. Koshelev, B. M. Kovalchuk, V. V. Plisko, and K. N. Sukhushin, "Generation and radiation of high-power ultrawideband nanosecond pulses," J. Commun. Technol. Electron., vol. 52, no. 7, pp. 756 – 764, 2007.
2. V. I. Koshelev, "Detection and recognition of radar objects at sounding by high-power ultrawideband pulses", IEEE Inter. Conf. on Ultra-WideBand, Singapore, Sep. 2007.
3. E. V. Balzovsky, Yu. I. Buyanov, and V. I. Koshelev, "An active antenna for measuring pulsed electric fields", Rus. Phys. J., vol. 50, no. 5, pp. 503 – 508, 2007.

UWB - 04
UWB Microstrip and Array Antennas

Oral Presentations

Small Printed Ultrawideband Antennas Combining Electric and Magnetic Type Radiators

D.-H. Kwon[1], E. V. Balzovsky[2], Y. I. Buyanov[2], and V. I. Koshelev[2]

[1]*Department of Electrical Engineering, The Pennsylvania State University, University Park, PA 16802, USA*
[2]*Institute of High Current Electronics, SB RAS, 2/3 Akademichesky Ave., Tomsk 634055, Russia*

E-mail: kwon22@ieee.org

Ultrawideband (UWB) communication antennas require impedance bandwidth over 3.1—10.6 GHz. Considering the small sizes of personal wireless devices, it is highly desirable that the UWB antennas have small form factors and can be manufactured at low cost. Most UWB antennas reported in the literature are planar monopoles and dipoles for omnidirectional radiation patterns, and tapered slot antennas for directive radiation patterns.

Combining the electric- and magnetic-type dipole antennas can extend the pass band to the lower frequency direction [1]. In terms of the spherical vector wave theory, this corresponds to a reduced antenna radiation quality factor for a combined radiation of TM and TE spherical waves compared with a source radiating either the TM or TE modes only [2]. Three-dimensional UWB antennas for high-power electromagnetic pulse radiation applications were reported in [3].

In this paper, two small printed combined UWB antennas having a small dimension of 20 mm×30 mm are presented. One antenna has a horizontal feed and the other has a vertical feed. The antenna is realized by the conductor trace created by selectively etching the top surface of a copper-clad dielectric substrate having a relative permittivity 10.2 (Rogers RO3210). The geometry of the antenna having a vertical feed is shown in Fig. 1(a). The arms 1 and 2 form the electric-type radiator (ER), essentially acting as an electric dipole. The magnetic-type radiator (MR) is realized by the loop, which is formed within the arm 1 of the ER, performs as an equivalent magnetic dipole. Finally, an edge-mount SMA connector is attached from the bottom left, and excites the two radiators via two slotlines forming an asymmetric coplanar waveguide feed. Specific dimensions of the ER and the MR are designed such that the balance between the excess electric energy of the ER and the excess magnetic energy of the MR below the individual resonance frequency shifts the resonance of the combined system into the lower frequency direction. The measured VSWR response is plotted with respect to frequency in Fig. 1(b). The antenna satisfies VSWR≤2 from 2.93 to 10.67 GHz, suitable for entire UWB band operations.

The combined antenna also features directive radiation patterns with a higher maximum directivity than conventional dipole-type UWB antennas. Therefore, the combined antenna simultaneously achieves both a wider bandwidth and a higher gain compared with the conventional dipole-type UWB antennas.

(a)   (b)
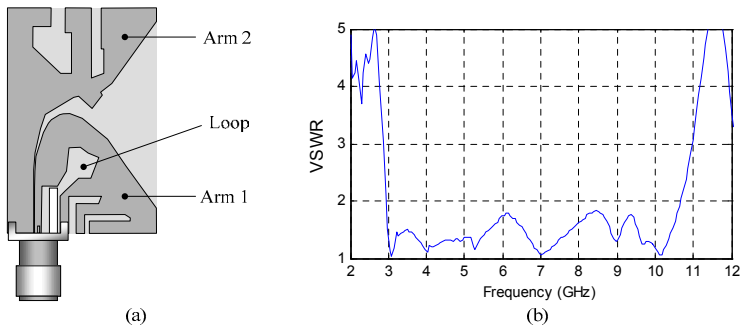
Fig. 1 – The combined antenna geometry and the measured VSWR response

References
1. V. P. Belichenko, Y. I. Buyanov, V. I. Koshelev, and V. V. Plisko, "On the possibility of extending the passband of small-size radiators," *J. Commun. Technol. Electron.*, vol. 44, no. 2, pp. 167—172, 1999.
2. D.-H. Kwon, "On the radiation *Q* and the gain of crossed electric and magnetic dipole moments," *IEEE Trans. Antennas Propag.,* vol. 53, no. 5, pp. 1681—1687, May 2005.
3. V. I. Koshelev, Y. I. Buyanov, Y. A. Andreev, V. V. Plisko, and K. N. Sukhushin, "Ultrawideband radiators of high-power pulses," in *Proc. Pulsed Power Plasma Sci.*, Las Vegas, NV, Jun. 2001, pp. 1661—1664.

Reconfigurable Slot-Filter antenna for cognitive radios

F. Ghanem[1] and P.S. Hall[1]
[1]*University of Birmingham, Birmingham, UK*
E-mail: f.ghanem@bham.ac.uk

In this paper, we present an UWB disk monopole antenna with an integrated slot filter printed in its ground plane for cognitive radios [1]. In cognitive radios, communications can be carried over a very large range of the frequency bands, which necessitates the use of frequency reconfigurable antennas. The reconfiguration scheme can be either a variation of the transmit bandwidth of high Q antennas or an insertion of stopbands in UWB antennas to suppress undesirable bandwidths. The proposed antennas falls in the second category as it is composed of an UWB disk monopole antenna to which we insert stopbands that can be shifted. The schematic of the proposed antenna is shown in Fig. 1.
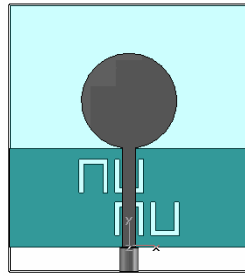
Fig. 1 – Schematic of the designed antenna with its return loss curve.

The insertion of a slot in the ground plane produces notches in the UWB response of the disk monopole antenna. The frequency of the notch can be varied by varying the slot length. Also, by inserting multiple slots in the ground plane and disposing them in the proximity of each other, it is possible to couple them to form a filter in the same manner as with conductor resonators but with the difference that the resonances are for stop band and not pass band.

The disk monopole antenna, without the slots in its ground plane, exhibits a UWB behaviour and is impedance matched from 2 GHz until 12 GHz [2]. The different slots can be inserted to have wide stopbands or multiple stopbands as shown in Fig. 2 representing the frequency responses of a transmission line over slotted ground plane.
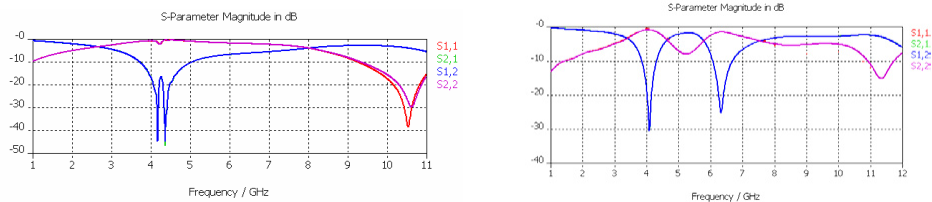
Fig. 2 – Frequency response of a microstrip transmission line with slot printed ground plane

References

1. W.Q. Malik and D.J. Edwards, "COGNITIVE TECHNIQUES FOR ULTRAWIDEBAND COMMUNICATIONS", IET Ultra Wideband Systems, Technologies and Applications Seminar, Apr. 2006.
2. J. Liang, C.C. Chiau, X. Chen, and C.G. Parini, "Printed circular disc monopole antenna for ultra-wideband applications", Electronics Letters, vol. 40, Issue 20, pp. 1246-1247, 2004.

A Compact UWB Antenna with Band Notch Characteristic

S.H. Choi, H.J. Lee, and J.K. Kim

Korea Electronics Technology Institute, Seongnam-si, SouthKorea
E-mail: shchoi@keti.re.kr

The frequency range of UWB system is from 3.1 GHz to 10.6 GHz. However, there are several narrow band services that already occupy some parts of UWB band. In order to solve this problem, UWB antennas had better have a built-in band-pass filter. This structure can reduce interferences from near by WLAN standard 802.11a, which its frequency range is 5.725 - 5.825 GHz. Recently, the Ministry of Information and Communication(MIC) of Korea announces the frequency range of UWB systems that consists of low band(3.1 - 4.8 GHz) and high band(7.2 - 10.2 GHz). In this paper, we propose a compact UWB antenna with band-notch characteristic. To create the band-notch characteristic, the spoon-shaped slots are added in the monopole antenna. Fig.1 shows the geometry of the proposed antenna. This antenna consists of two parts. One part is a radiator made by LTCC and the other part is PCB(ε_r=4.5) feeding to the radiator. CPW line is used for the feed line. In the bottom of the radiator, a pad is located to attach with PCB and this pattern play a role of impedance transformer. The pad and radiator are connected by via-hole. The base of radiator is tapered with shape of a half circle. This tapering of the base results in a smooth transition for wide impedance matching. In order to get the characteristic of band notch, we insert the spoon-shaped slots in the tapering section. These slots resonate at the frequency decided by slot's size. Slots consist of the narrow line part and circle part. The resonant frequency is mainly determined by the length of a line and the diameter of a circle.

Antennas in this paper are simulated by using CST Microwave Studio 2006 and are made by using low temperature co-fired ceramic(LTCC) process. This antenna has the size of 15mm * 15mm and was measured by using the network analyzer HP 8510c. Fig.2 shows the measured VSWRs as the change of slot length. These results are similar to the simulation results. When SR is 1.4 mm and SL is 2.27 mm, the stop band where VSWR is higher than 3 is from 4.8 GHz to 6.3 GHz. The proposed antenna is a good candidate for UWB systems where stop band is needed.
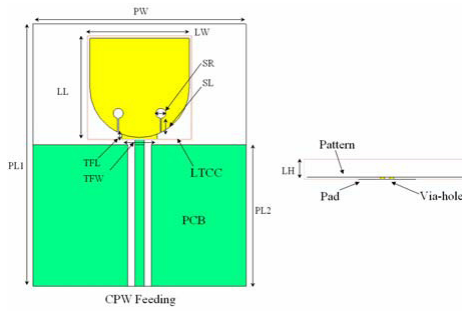
(a) Top view   (b) Side view of LTCC
Fig.1 Geometry of the antenna
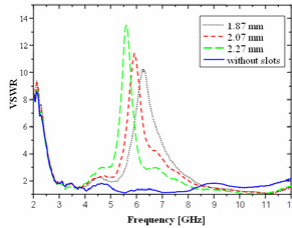
Fig. 2 Measured VSWR for various length of slot

Impulse Signal Mathematical Analysis and Quasi-Rhomboid Antenna Design for Ultra Wideband Communication Systems

S. Thanormsuay[1], P. Thosdee[2] and C. Thongsopa[3]

[1]*College of Industrial Technology, King Mongkut's University of Technology North Bangkok, Thailand*
[2,3]*School of Telecommunication Engineering, Suranaree University of Technology, Thailand*
svl@kmutnb.ac.th, phairat_tosdee@hotmail.com

An ultra wideband radio technology has become an important topic for microwave communication because of its low cost and low power consumption. Therefore, the ultra wideband antenna design and impulse signal analysis is going to the main challenges for ultra wideband system. In ultra wideband applications, antenna must be extremely wide bandwidth. Recently, a lot of ultra wideband antennas have been reported by many research groups. Most of the reported antennas have omni-directional radiation patterns [1-2].

In this paper, *we propose analysis of impulse signal and quasi rhomboid shaped element bowtie antenna design by using a flat reflector for ultra wideband communication systems*. The proposed antenna is designed on FR4 substrate, since **it is small size**, **easily fabricated and low manufacturing cost**. The detailed geometry and parameters of the proposed antenna are illustrated in Fig. 1. Photograph of the antenna prototype and size comparison with a metric ruler are illustrated in Fig. 2. **In measurement, it is found that the propose antenna have impedance bandwidth of 119.83 %** (2:1 VSWR) which covered frequency range 2.85-11.37 GHz. **This antenna has unidirectional radiation patterns** over the frequency range of 3.1-10.6 GHz for ultra wideband technology, and the results are presented in Fig. 3 in the E-plane and H-plane, at frequency 3.1, 5.1, 7.1 and 9.1 GHz, respectively. Fig. 4 shows the gain of the proposed antenna over the operating frequency. For comparison purposes, the average gain of the quasi rhomboid shaped bowtie antenna without the reflector is shown in this figure, which **average gain achieved in the quasi rhomboid shaped bowtie antenna using a flat reflector is much greater than without the reflector about 2 dB**. The advantage of the proposed antenna is that it can be used to design impulse receive transmit system for ultra wideband applications.
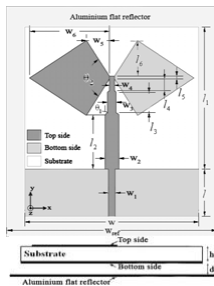
Fig. 1 – **Structure of quasi rhomboid shaped antenna**
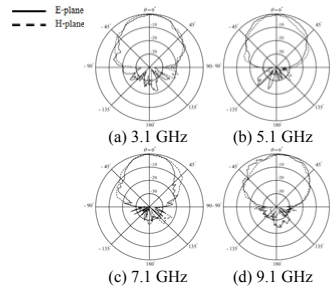
Fig. 3 – **The measured radiation patterns in E-and H planes**
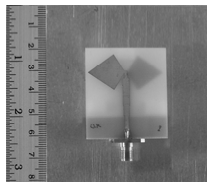
Fig. 2 – **Fabricated prototype of quasi rhomboid antenna**
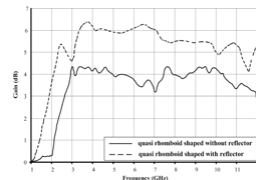
Fig. 4 – **The measured gain of quasi rhomboid antenna**

References
1.   T. Karacolak, and E. Topsakal, "A Double-Sided Rounded Bow-Tie Antenna (DSRBA) for UWB Communication," IEEE Antennas and Wireless Propagation Letters, vol. 5, 2006.
2.   K. Kiminami, A. Hirata, and T. Shiozawa, "Double-Sided Printed Bow-Tie Antenna for UWB Communications," IEEE Antennas and Wireless Propagation Letters, vol. 3, 2004.

UWB - 05
Antennas for UWB Communications

Oral Presentations

100 THz Broadband High Power Antennas – Results of Modeling and Antennas Future Applications

A. S. Podgorski[1], W. D. Prather[1], S. J. Yakura[1], J. T. MacGillivray[1]

[1]*Air Force Research Laboratory, Kirtland AFB, NM, USA*

E-mail: a.podgorski@ieee.org

In this paper, we present the latest achievements in the area of super-computer modeling of broadband antennas operating in the frequency range up to 100 THz. The emphasis of our modeling was directed towards achieving the highest possible antenna gain and peak power, the highest gain uniformity, and the lowest sidelobes, while maintaining the smallest antenna aperture and the lowest multi-antenna coupling.

The modeling efforts were based on earlier achievements in the development of broadband horn antennas operating in the frequency range up to 100 GHz [1]. In our modeling process, the entire THz frequency region extending from 100 GHz to 100 THz was covered using three TEM-Horn antennas - one operating from 100 GHz to 1 THz, the second from 1 THz to 10 THz [2] and the third from 10 THz to 100 THz. To ensure the high power capability of the antennas a high voltage dielectric insert was placed inside of each horn. The low frequency of operation of modeled antennas was limited by the size of the antenna aperture (mouth of the antenna), while the upper frequency was limited by the angular opening of the horn antenna.

The modeling was done using the FDTD and 3D codes. The model grid consisted of 10,000 x 500 x 400 cells for an antenna operating from 100 GHz to 1 THz. An antenna operating from 1 to 10 THz required 32,000 x 500 x 400 cells, and an antenna operating from 10 to 100 THz required 100,000 x 500 x 400 cells. Calculation of gain, size of the radiated beam (E-field plot), rise time of the generated E-field and the E-field derivative resulted in reaching conclusions regarding antenna design, in particular, optimization of antenna dimensions and frequency scaling.

The most important conclusion from our modeling is that for the first time, a broadband high gain (50 dB) antenna operating from 10 to 100 THz, allows reaching a rise time of 5 fs at peak power greater than 100 W. In addition, the results led us to conclude that use of a single high gain and high power broadband antennas will permit achievieng power density of 10 TW/m2. Furthermore, one can only forsee that 100 THz antenna array consisting of 100 x 100 antennas, occupying an area of 3 mm x 3 mm and focused to a single point, would result in reaching peak power density of 100 PW/m2 and peak E-field intensity of 6 GV/m.

Considering our modeling results, an assessment of potential future applications of broadband high power THz antennas permit us to conclude that such antennas could be used for:

• THz radar systems (stratospheric [3] and anti-collision radar),
• THz imaging (IR, Raman and THz spectroscopy, THz microscopy).

References
1. A. S. Podgorski, "100 GHz Broadband High Power Antennas," Chapter 33, Ultra-Wideband Short-Pulse Electromagnetics 7, Springer, Germany 2007.
2. A. S. Podgorski, W. D. Prather, S. J. Yakura, J. T. MacGillivray, "Modeling of THz Broadband High Power Antennas," Proceedings of 2007 North America URSI Meeting, Ottawa, Canada, July 2007.
3. A. S. Podgorski, W. D. Prather, S. J. Yakura, J. T. MacGillivray, "THz Technology in Application to Space Radar Systems," Proceedings of AMEREM 06 Conference, Albuquerque NM, USA, July 2006.

UWB - 06
UWB - Modeling & Simulation #1

Oral Presentations

Modeling of Broadband Antennas for Room Temperature Terahertz Detectors

A. Scheuring[1], I. Türer[1], N. Ribière-Tharaud[2],
A. F. Dégardin[1], A. J. Kreisler[1]

[1]*LGEP-SUPELEC; UMR CNRS 8507; UPMC-Univ. Paris 6; Univ. Paris 11, Gif-sur-Yvette, France*
[2]*DRE-SUPELEC, Gif-sur-Yvette, France*

E-mail: Alexander.Scheuring@supelec.fr

Many terahertz applications in different fields have arisen in the past because of the special behavior of terahertz radiation and its interesting interaction with a multitude of materials. Examples are fusion plasma imaging (renewable energy), radiometry (in medicine) or night vision applications which are used in a wide frequency range, from 500 GHz to 5 THz.

In contrast to superconducting detectors, which require expensive cooling systems, room temperature detectors additionally promise a low priced usage in multi-pixel THz cameras.

As the simplest case, the working principle of a thermal detector of the bolometric type is shown in figure 1. Dependent on its intensity an incident radiation changes the electrical resistivity of the bolometer. By applying an external current source this thermal effect can be detected as a variation of the voltage which can be read out by an electronic circuit.

In our case semiconducting YBaCuO bolometers (figure 2) are used. Because of their small detection area and their low radiation coupling efficiency, planar antenna structures are used to improve the sensor properties [1].

The main challenges at this are on the one hand the requirement of a large bandwidth (1 to 4 THz, typically) and on the other hand the difficult matching of the antenna to the device due to the extremely high detector impedance that is in the MΩ range.

The purpose of this paper is to present modeling investigations dedicated to self-complementary planar broadband antennas because of their frequency-independent characteristics. These structures are attached on thin substrates to avoid losses due to substrate high order modes.

The antenna properties (radiation diagram, reflection coefficient, input impedance) have been investigated by software modeling [2] after which the simulation results were confirmed by experiments. Because of practical reasons, large-scale models were used to test the planar antenna concepts in anechoic chambers (in the 2 to 8 GHz range, typically). In the design process some specific problems have occurred such as the need for a symmetrical source for a large frequency band. Different geometries (among which bow tie, log-periodic, spiral) will be considered.
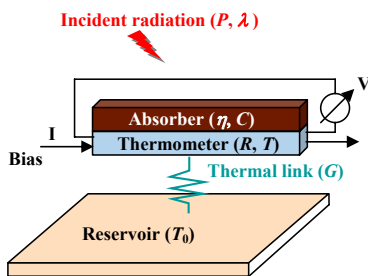
Fig. 1 – Bolometer Principle   **Fig. 2 – 3D Bolometer Assembly**
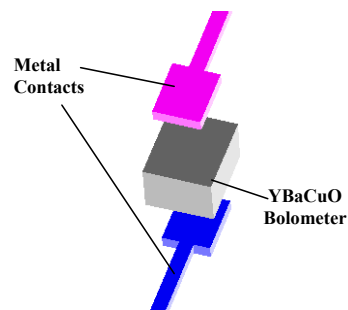
References
1. M. Longhin, A. F. Dégardin and A. J. Kreisler, "Semiconducting YBCO thin films for uncooled terahertz imagers," 4th International Materials Symposium (MATERIAIS 2007), Porto, Portugal (1-4 April 2007), oral presentation.
2. CST Microwave Studio®.

Oral Presentations   UWB - 06   UWB - Modeling & Simulation #1

Modeling Broadband Antennas for Hot Electron Bolometers at Terahertz Frequencies

I. Türer[1], X. Gaztelu[1], N. Ribière-Tharaud[2],
A. F. Dégardin[1], A. J. Kreisler[1]

[1]*LGEP-SUPELEC; UMR CNRS 8507; UPMC-Univ. Paris 6; Univ. Paris 11, Gif-sur-Yvette, France*
[2]*DRE-SUPELEC, Gif-sur-Yvette, France*

E-mail: Ibrahim.Turer@supelec.fr

There is a strong need for wideband and sensitive receivers for radioastronomy and remote sensing applications in the terahertz (THz) region. Superconducting Hot Electron Bolometer (HEB) mixers are a competitive alternative to conventional mixer technologies in the THz range [1].

A HEB THz detector typically consists of an ultra-thin (i.e. a few 10 nm thick) superconducting micro-bridge coupled with a planar antenna. We are developing HEBs for imaging systems at THz frequencies (from 1 to 5 THz, typically) based on high-T_c $YBa_2Cu_3O_{7-\delta}$ (YBCO) materials sputtered on MgO substrates. As the operating conditions of the device are based on heterodyne detection, the unknown electromagnetic input signal is down converted to an intermediate frequency (in the 1 to 40 GHz range, typically) by means of a THz local oscillator.

In the THz range, YBCO materials without any antenna would be totally reflective to the electromagnetic radiation. For optimal device integration, planar antennas should be used. The aim of this work is to investigate broadband THz antennas dedicated to HEBs. A number of different antenna structures (log-periodic, Sierpinski fractal and square-spiral antennas) have been investigated before deciding the final antenna shape. Finally, log-periodic antennas were selected because of the best wideband and quasi-constant impedance behaviour. After designing the THz log-periodic antenna with the help of empirical formulas, we were able to scale it down to the microwave region (from 2 to 18 GHz) for experimental validation purposes. The issues arose from having an electrically thick (~ 10 cm) and MgO-equivalent substrate (ε_r = 10) which was needed and supplied to realize the large-scale model.

In order to get a symmetric antenna feed, a *balun* (<u>bal</u>ance / <u>un</u>balance) device should be used. However, to design a wideband *balun* for a very thick substrate is not an easy task. We have considered a simple solution consisting in feeding the antenna symmetrically through the substrate with two coaxial cables, the inner conductors being connected to the two halves of the antenna. The transition between these cables and the source coaxial cable could then be performed by using a commercially available wideband 180° hybrid power divider. Finally, for confirmation, a large-scale experimental log-periodic antenna on an epoxy substrate (figure 1) was tested by simulation software [2] (figure 2) and measurements which were performed in anechoic chambers (figure 3). We have proven that the simulation results were confirmed by measurements.

This work is going to lead to the final design the linear arrays of HEB detectors.

Fig. 1 – Experimental Antenna   **Fig. 2 – Simulation Model**   **Fig. 3 – Antenna Measurement Setup**
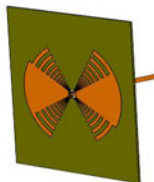
References
1. A. J. Kreisler, A. F. Dégardin, M. Aurino *et al.*, "New trend in terahertz detection: high Tc superconducting hot electron bolometer technology may exhibit advantages vs. low Tc devices," IEEE International Microwave Symposium (IMS 2007), Honolulu, Hawaii, USA (June 2007). Proceedings pp. 345-348.
2. CST Microwave Studio®.

TLM Simulation of Wave Envelopes using Dynamic Phasors

D. W. P. Thomas[1], J. D. Paul[1] and C. Christopoulos[1]

[1]*The George Green Institute for Electromagnetics Research, TheUniversity of Nottingham, UK*

...
E-mail: Dave.Thomas@nottingham.ac.uk

A novel technique is described for the TLM simulation of the slow-varying envelope of a carrier wave using the principle of dynamic phasors which enables the computational element size to greatly exceed the normal $\lambda/10$ restriction. Many electromagnetic problems such as radio propagation, RADAR or optical devices have time dependent or non-linear behavior which can best be simulated using time domain differential techniques such as TLM or FDTD. However, in many practical cases the problem size is often many wavelengths which makes it computationally too expensive to solve directly using time domain differential techniques. On the other hand, by using a dynamic phasor representation of the waveforms, simulation of the dynamic phasor amplitude and phase variation is only restricted by the carrier wave envelope bandwidth and the system time constants. The simulation in the time domain of electrically large problems then becomes more manageable. The principle of dynamic phasors was first described in [1]. The carrier wave is represented by a phasor with a time dependent amplitude and phase and it is this which is then applied to the simulation algorithm.   Dynamic phasor propagation can be represented by propagation along a transmission line with complex conductivity and resistivity :

$$\mathbf{G} = G + j\omega C, \quad \mathbf{R} = R + j\omega L \tag{1}$$

where C and L are the per unit length capacitance and inductance. The TLM [2] implementation of dynamic phasor simulation therefore is achieved with a node that has complex conductivity and resistivity as given by (1). Care must be taken to note that the terms are distributed and for large cell sizes the lumped equivalent circuits will not be valid. A formulation for the cell using distributed parameters has to be used as given by the Norton equivalent circuit in Fig. 1. where $v_L{}^i$ and $v_R{}^i$ are the incident voltage pulses from the left and right respectively $Z_0 = \sqrt{L/C}$, $Z_{tl} = \sqrt{\mathbf{R}/\mathbf{G}}$ and the other quantities are calculated   at each time step. To illustrate the TLM simulation of dynamic phasors, the propagation of a pulse with a 1 GHz carrier frequency and modulated by a Gaussian envelope along a lossy transmission line with a capacitive stub that halves the characteristic impedance and propagation velocity is given in Fig. 2. The complete waveform was simulated using standard TLM cells of length Δz=1.5cm ($\lambda/20$) and is compared with the dynamic phasor simulation of the waveform using cells of length Δz=30cm (λ). Two profiles are shown. One is after propagation for 10ns and the other after 20ns. The dynamic phasor simulation reproduces the same attenuation as for the normal TLM simulation (-3.6dB/m).
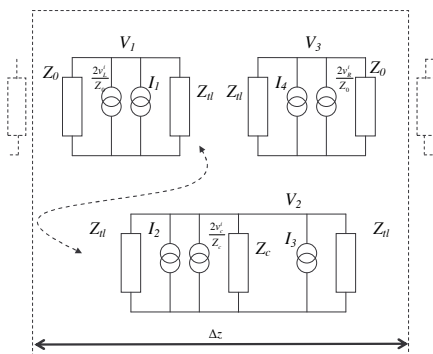
Fig. 1 – Norton equivalent circuit of a dynamic phasor TLM cell with capacitive stub added
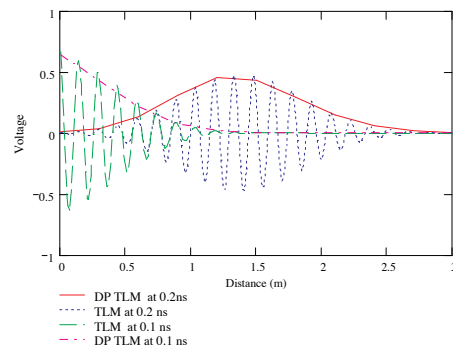
Fig. 2. Simulated propagation with capacitive stubs representing a relative permittivity = 4 using both normal TLM and TLM with dynamic phasors

References
1. A M Stanković "Analysis of asymmetrical faults in power systems using dynamic phasors" *IEEE Trans. on Power Systems*, Vol. 15, No. 3 August 2000, pp1062-1068.

2.   C Christopoulos "The Transmission-Line Modeling Method TLM" *IEEE Press*, 1995. ISBN 0-7803-1017-9

UWB - 06
UWB - Modeling & Simulation #1

Oral Presentations

Enhancing the Resolution of MUSIC Imaging Method by Choosing an Optimal Test Dipole Polarization

Yu Zhong and Xudong Chen

Department of Electrical and Computer Engineering, National University of Singapore, Singapore, 117576
E-mail: zhongyu@nus.edu.sg

The multiple signal classification (MUSIC) algorithm has been of great interest in the inverse scattering community since it was proposed to locate point-like scatterers from the multi-static response (MSR) matrix generated by an array of transceivers [1-5]. MUSIC imaging was first applied to acoustic imaging, where scalar field is involved [2,3,5]. Recently, MUSIC algorithm was generalized to electromagnetic imaging of small three-dimensional targets [4,6].

This paper focuses on two phenomena in electromagnetic MUSIC imaging that are different from the ones in acoustic MUSIC imaging. The first is regarding the spatial resolution in the presence of noise. In acoustic imaging, the test function used to generate MUSIC pseudo-spectrum is the Green's function of the background medium associated with a monopole source. In electromagnetic imaging, the test function that is used to generate the MUSIC pseudo-spectrum is chosen to be the Green's function of the background medium associated with an electric or magnetic dipole. Although the test dipole can be oriented in any direction in the noise free case for the non-degenerate scatterers [4,6], the MUSIC pseudo-spectrum depends noticeably on the orientation the test dipole in the noisy scenario. The second phenomena is regarding degenerate scatterers in which only one or two independent components of an electric or magnetic dipole are induced inside some small scatterers due to special shape or composing material of the scatterers. For example, a needle-like or disk-like small object may present only one or two dominant components of induced electric dipoles. For an anisotropic small sphere, when some components in the principal axes of the permittivity tensor are equal to the permittivity of the background medium, the number of independent electric dipole components is less than three. In degenerate cases, standard MUSIC algorithms [4,6] do not work because the arbitrarily chosen direction of test dipole is not necessarily located in the space spanned by actually induced independent dipole components.

The choice of the test dipole direction has been investigated in [7,8] in two and three dimensional degenerate cases, respectively. However, to the best of our knowledge, the effect of the choosing test dipole direction on the resolution of imaging has not been investigated in electromagnetic imaging. In this paper, we propose an algorithm to obtain the direction of the test dipole that yields optimal resolution, and it can also deal with degenerate cases. Compared with the previous MUSIC algorithms [4,6-8] that search for the test dipole direction so that the corresponding Green's function vector is orthogonal to the noise space, the proposed algorithm determines the test dipole direction so that the corresponding Green's function vector is in the space spanned by the dominant eigenvectors of the MSR matrix. The analysis of the induced electric dipoles in eigenstates provides the physical insight of the proposed method. The theoretical and numerical results show that the amplitudes in three directions of the optimal test dipole direction are not necessarily in phase, i.e., the optimal test dipole may be not corresponding to a physical direction in the real three-dimensional space. The proposed algorithm was tested through numerical simulations and was found to not only provide better resolution than the standard MUSIC algorithm but also work well in the presence of degenerate objects.

References
1. A. J. Devaney, "Time reversal imaging of obscured targets from multistatic data," IEEE Trans. Antennas Propag., vol. 53, no. 5, pp. 1600–1610, 2005.
2. A. J. Devaney, E. A. Marengo, and F. K. Gruber, "Time-reversal-based imaging and inverse scattering of multiply scattering point targets," J. Acoust. Soc. Am., vol. 118, pp. 3129–3138, 2005.
3. A. Kirsch, "The MUSIC-algorithm and the factorization method in inverse scattering theory for inhomogeneous media," Inverse Problems, vol. 18, pp. 1025–1040, 2002.
4. H. Ammari, E. Iakovleva, D. Lesselier, and G. Perruson, "MUSIC-type electromagnetic imaging of a collection of small three-dimensional bounded inclusions," SIAM Sci. Comput., vol. 29, pp. 674–709, 2007.
5. M. Cheney, "The linear sampling method and the MUSIC algorithm," Inverse Problem, vol. 17, pp. 591–595, 2001.
6. Y. Zhong and X. Chen, "MUSIC imaging and electromagnetic inverse scattering of multiply-scattering small anisotropic spheres", IEEE Trans. Antennas Propag., vol. 55, pp. 3542-3549, 2007.
7. X. Chen and K. Agarwal, accepted by IEEE Trans. Antennas Propag., 2007.
8. X. Chen and Y. Zhong, Inverse Problem submitted, 2007.

Numerical Evaluation of Energy Conservation of the Meshless Radial Point Interpolation Method for Time-Domain Electromagnetics

T. Kaufmann, C. Fumeaux and R. Vahldieck

Laboratory for Electromagnetic Fields and Microwave Electronics (IFH), ETH Zurich, Zurich, Switzerland

thomas.kaufmann@ifh.ee.ethz.ch

Meshless methods build an emerging class of methods in the field of numerical electromagnetic modeling. Instead of using an explicit mesh, only a distribution of nodes is required to describe a physical model. A relevant advantage is that the node distribution can be adapted dynamically, i.e. nodes can be added, removed or moved during simulation. Meshless methods are based on the assumption that a particular node is only influenced by a certain number of surrounding points within a *support domain.* Properties of the interpolation of these points are used to solve the partial differential equations. Even though meshless methods have been successfully applied in astrophysics and hydrodynamics [1], efforts started only recently towards an adaptation for time-domain electromagnetics using Smoothed Particle Hydrodynamics (SPH) [2]. Another meshless method, the Radial Point Interpolation Method (RPIM) [3], has been introduced to electrostatic and magnetostatic problems in the recent years. RPIM provides several advantages over SPH. Firstly, it uses a local interpolation scheme which facilitates large scale modeling; secondly, it possesses the intrinsic property to accurately interpolate arbitrarily scattered data points, and therefore it does not require costly consistency restoring techniques for conformal models; thirdly, RPIM does not require any information about the volume associated to a particular node for interpolation, and hence this makes it a true mesh-free method.

The adaptation of RPIM used in this paper solves the Maxwell equations by applying the approximate spatial derivation of the interpolation functions for the nodes in the support domain and a leap-frog finite difference scheme. Numerical experiments have been performed in a two-dimensional TE implementation using H_x, H_y and E_z fields with propagation in the xy-plane. Eqn (1) shows the update equation for the E_z-component.

$$E_{z,i}^{n+1} = E_{z,i}^n + \frac{\Delta t}{\varepsilon}\left[\langle \partial_x H_{y,i}^{n+1/2}\rangle - \langle \partial_y H_{x,i}^{n+1/2}\rangle\right] \tag{1}$$

The angular brackets $\langle\circ\rangle$ denote the interpolation of the spatial derivations of the H-fields. The present RPIM implementation uses radial basis functions of Gaussian type and monomial basis functions of first order.

To numerically check energy conservation in this RPIM algorithm, the total energy was approximated using the energy density discretely integrated over the computational domain. The volumes associated to the nodes necessary for the integration, were taken from a Voronoi tessellation. The experiment was conducted within a lossless cylindrical metallic cavity with radius 241.3 mm, discretized using an evenly spaced cylindrical node distribution. The source was a band-limited pulse of center frequency 4.2 GHz and bandwidth of 1 GHz. The support domain was chosen to contain at least 4 nodes. Fig. 1 shows that energy is conserved over 4000 time steps or a simulation time of 41.2 ns. Energy is transferred between the E- and H-field. Fast oscillations are likely caused by the uncertainty of the volume attributed to the nodes.

This numerical example illustrates the potential of the novel radial point interpolation method for electromagnetics.
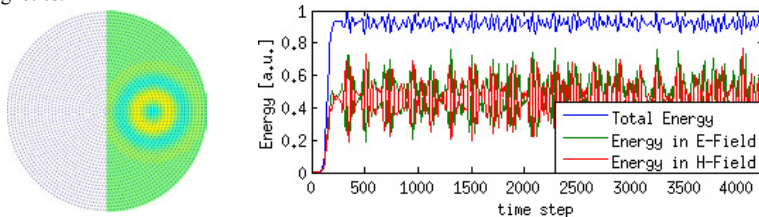
Fig. 1 – Model, field distribution and energy conservation within a metallic cavity

References
1. J. J. Monaghan, "Smoothed particle hydrodynamics," Annual review of astronomy and astrophysics, vol. 30, pp. 543–574, 1992.
2. J. G. Wang and G. R. Liu, "A point interpolation meshless method based on radial basis functions," International Journal for Numerical Methods in Engineering, vol. 54, no. 11, pp. 1623–1648, 2002.
3. G. Ala, E. Francomano, A. Tortorici, E. Toscano, and F. Viola, "Smoothed particle electromagnetics: A mesh-free solver for transients," Journal of Computational and Applied Mathematics, vol. 191, no. 2, pp. 194–205, 2006.

UWB - 07
Conformal Time Domain Numerical Methods (Invited)

Oral Presentations

Conformal Treatment of Finite-Volume Absorbing Boundaries for Time-Domain Simulations

Dirk Baumann[2], Christophe Fumeaux[1], Thomas Kaufmann[1], Rüdiger Vahldieck[1], ErPing Li[2],

[1]*Laboratory for Electromagnetic Fields and Microwave Electronics (IFH), ETH Zurich, Zurich, Switzerland*
[2]*Institute of High Performance Computing (IHPC), A*STAR, Singapore*
dirk@ihpc.a-star.edu.sg, fumeaux@ifh.ee.ethz.ch

The truncation of the computational domain for Finite-Volume Time-Domain (FVTD) simulations has traditionally been realized using either absorbing boundary condition (ABC) such as the Silver-Müller ABC [1], or finite-volume absorbers derived from perfectly-matched layers (PML) [2]. The flexibility offered by the FVTD method when applied in an unstructured polyhedral (e.g. tetrahedral) mesh allows shaping the outer boundary for an optimum balance between accuracy and computational cost.

The performance of the Silver-Müller ABC is described first. This truncation technique is characterized by an extreme simplicity of implementation in FVTD, since it only requires setting incoming fluxes at the outer boundary to zero. However, as a result, only first-order accuracy is achieved, which translates into an absorbing performance degrading rapidly as the angle of incidence deviates from normal. Therefore, to achieve a near-normal incidence condition, the Silver-Müller outer boundary of a FVTD computational domain is usually shaped to match expected wave-fronts. Reflection coefficients realized in practice using a sphere as outer domain boundary for scattering and radiation problem can be as low as -40 to -50 dB. For many radiation problems, this performance yields sufficient accuracy for engineering purposes. There are, however, large classes of problems where low-level scattered fields or small coupling coefficients need to be accurately modeled. In those cases, PML-type absorbers can be used as a domain truncation for superior performances, typically resulting in reflection coefficients down to -70 to -80 dB. The traditional PML implementations of uniaxial PML [4] in the Finite-Difference Time-Domain (FDTD) method consider rectangular box-shaped computational domains. The PML layers are arranged as uniaxial media with an appropriate direction of anisotropy, dependent on the location of the truncating layer. In FVTD models, there are no restrictions or principal axis for the definition of the domain truncation. Therefore, spherical [2] and ellipsoidal [3] absorber configurations with excellent performances have been demonstrated using approximate PML formulations: The principle presented in those two papers can be extended to more general (i.e. "conformal") convex computational domain truncation. The main advantage of arbitrary shapes is to minimize the volume of computed space through adaptation to the structural shape, while preserving the accuracy of the results. In the example presented in Fig. 1, different shapes of the computational domains are computed, delivering transmission coefficient between two dielectric resonator antennas (DRA) with negligible differences. Those absorbing layers can be placed much closer to the simulated structure as a Silver-Müller ABC, and therefore result in a lower computational effort. This demonstrates how the efficiency of the computation can be enhanced through the use of conformal absorber models.
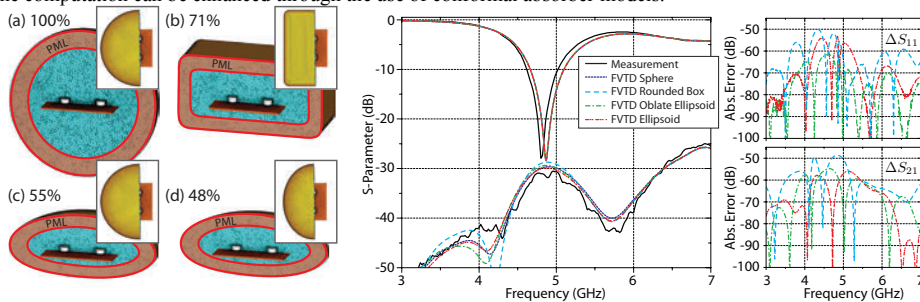
Fig. 1 – LHS: Different shapes of computational domain: (a) sphere, (b) rounded box, (c) oblate ellipsoid, (d) ellipsoid, with indication of size reduction relative to the sphere. RHS: S-parameters of two DRAs on a common ground plane and absolute error between the spherical PML formulation and the simulation results obtained in the rounded box and ellipsoidal computational domains.

References
1. P. Bonnet, X. Ferrieres, B. Michielsen, P. Klotz, and J. Roumiguieres, "Finite-Volume Time-Domain Method," ch. 9 in Time Domain Electromagnetics, Academic Press, 1999.
2. C. Fumeaux, K. Sankaran, R. Vahldieck, "Spherical perfectly matched absorber for finite-volume 3-D domain truncation," IEEE Transactions on Microwave Theory and Techniques, vol. MTT-55, no.12, pp. 2773-2781, 2007.
3. D. Baumann, C. Fumeaux, R. Vahldieck, E. Li, "Conformal perfectly matched absorber for finite-volume time-domain simulations," 2008 Asia-Pacific Symposium on Electromagnetic Compatibility, Singapore, May 19-23, 2008
4. S. Gedney, "An anisotropic perfectly matched layer-absorbing medium for the truncation of FDTD lattices," IEEE Trans. Antennas Propag., vol. 44, no. 12, pp. 1630–1639, December 1996.

Time Domain Eigenmodal Analysis with the Finite Element Method Including a Surface Impedance Boundary Condition

Benedikt Oswald[1] and Patrick Leidenberger[2]

[1] Paul Scherrer Institut, GFA, CH-5232 Villigen, Switzerland, Corresponding Author
[2] Swiss Federal Institute of Technology, IFH, CH-8092 Zurich, Switzerland
Email: benedikt.oswald@psi.ch,

Abstract   Resonant cavities are essential building blocks in almost all types of particle accelerators. Considerable effort has therefore be invested into theoretical and numerical models for computing their eigenmodal properties. We present a time domain approach using a finite element (FE) discretization for extracting resonance frequencies (2; 4; 3) The finite element approach is efficient in modeling delicate geometrical features with a variable level of detail (LoD). The cavities are modeled as devices with ohmic loss where both the boundary wall and filling material can be lossy. For cavity walls with finite ohmic conductivity σ we use a surface impedance boundary condition (SIBC) for efficiently modeling surface resistivity (1). The inclusion of a SIBC implicitly models boundary losses and their influence on the eigenmodal solution. We present numerical results for increasingly complicated geometries, modeled with and without loss.
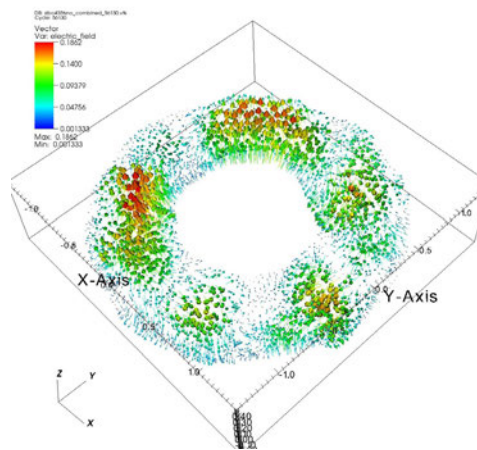
References

[1] J. D. Jackson. *Classical Electrodynamics*. Wiley, 111 River Street, Hoboken, NJ 07030, 3rd edition, 1999.

[2] J. Jin. *The Finite Element Method in Electromagnetics*. Wiley-Interscience, 2nd edition, 2002.

[3] B. Oswald, P. Leidenberger, and C. Hafner. 3-dimensional finite element time domain analysis of an asymmetric near field optical probe. *Journal of Computational and Theoretical Nanoscience*. accepted for publication.

[4] B. Oswald and K. Roth. Electromagnetic full wave analysis of sub-wavelength sized objects in ground penetrating radar (GPR). In *Geophysical Research Abstracts*, volume 7, page 04437, Vienna, 2005. European Geosciences Union, EGU.

UWB - 07
Conformal Time Domain Numerical Methods (Invited)

Oral Presentations

Imaging of distributed objects in UWB sensor networks

R. Zetik, R. S. Thomä

Electronic Measurement Research Lab, Ilmenau University of Technology, Ilmenau, Germany

E-mail: rudolf.zetik@tu-ilmenau.de

Ultra-wideband (UWB) radio sensors promise interesting perspectives for localisation, object detection and identification in short range environments [1]. In [2] we gave an overview on their application in UWB sensor networks. We presented measurement examples showing the potential of the sensor networks for imaging of its environment. These examples were based on migration algorithms [3], [4] known from remote sensing e.g. ground penetrating radar, or through-wall applications. In this article we describe drawbacks of these migration algorithms for the imaging of distributed objects by a sensor network and propose a new imaging algorithm. We compare performance of both imaging algorithms by a simulated example.

Our envisaged scenario assumes a number of sensor nodes that are static or roaming through the unknown environment. The nodes illuminate the environment from different positions and acquire so information necessary for the imaging algorithm. In contrast to the migration algorithms where a sensor is moved usually along a linear track, the static nodes are distributed in the network in a random way and the track of moving nodes is flexible and can be even changed by purpose. Thus, the environment is observed by the sensor nodes non-uniformly. The traditional range migration algorithms are not capable to properly fuse these non-uniform observations (impulse responses) together. Especially distributed objects are improperly mapped in the fused images. Their intensity in the image varies according to the topology of the sensor network. We can actually observe a projection of the nodes distribution in the environment on objects. Fig 1 shows this effect on a focused image of an environment inspected by a sensor node moving along oval track (black dots). The simulated environment contains 3 walls and one point like scatterer. The over-illumination of some parts of the walls (see Fig. 1 left) is due to neglecting the spatial information of the network by the range migration algorithms. Besides the over-illumination, the focused image is further corrupted by disturbing artifacts produced by the range migration algorithm. Thus, the correct interpretation of this focused image is almost impossible.

In this article, we propose a new algorithm which will take the networks topology into account. It is based on the cross-correlated imaging algorithm [5]. Thus, it inherently reduces number of disturbing artifacts as described in [5] and moreover it removes the varying intensity of distributed objects (Fig. 1 right) by the proper data fusion.
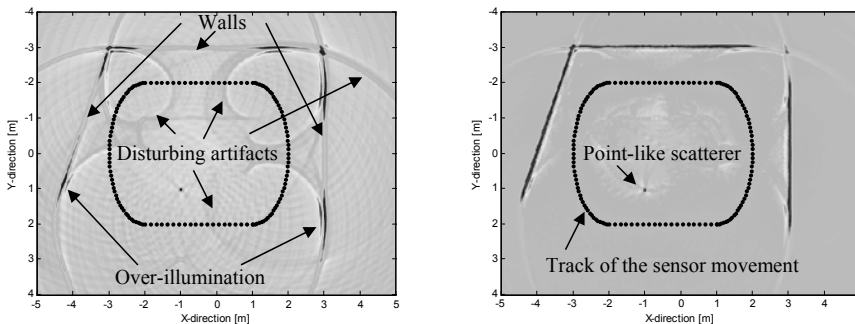
Fig. 1 – Focused image of the environment (left - range migration algorithm, right - proposed algorithm)

References
1. R. Zetik, J. Sachs, R.S. Thomä, "UWB Short-Range Radar Sensing", IEEE Instrumentation & Measurement Magazine, vol. 10, no. 2, 2007
2. R.S. Thomä, O. Hirsch, J. Sachs, R. Zetik, "UWB sensor networks fot position location and imaging of objects and environments," EuCAP 2007 The Second European Conference on Antennas and Propagation, Edinburgh, UK, November 2007
3. D.J. Daniels, "Ground penetrating radar - 2nd edition", IEE, London, 2004
4. J. M. Lopez-Sanchez, J. Fortuny-Guasch, "3-D Radar Imaging Using Range Migration Techniques," IEEE Transactions on Antennas and Propagation, vol. 48, no. 5, 2000
5. R. Zetik, J. Sachs, R.S. Thomä, "Modified Cross-Correlation Back Projection for UWB Imaging: Numerical Examples", ICU 2005 IEEE Int. Conference on Ultra-Wideband, Switzerland, September 2005

Time Domain Characterization of Asymptotic Conical Monopole

D. K. Singh and D. C. Pande

Electronics & Radar Development Establishment, Bangalore, India
E-mail: dhiraj_lrde@rediffmail.com

Considering the problem of estimating the impulse response of a system, wherein the stimuli and the responses of the system can be acquired Experimentally. The instrumentation inaccuracies add errors during deconvolution. The errors being such that the correct dimension of the impulse response of the system where the system is represented as a vector might not be estimated accurately.

The problem with data acquisition cannot be totally averted. A possible solution to the above problem, without delving into optimizing the methods of acquiring data is a feasible solution. A fair estimate of the system under consideration can thus be obtained by using the cross correlation among the system responses obtained for the various input-output pairs. An acceptable estimate of such is presumed on the premise that optimal techniques are employed when system responses are individually estimated. In the present work, an asymptotic conical monopole is used as test object placed in TEM cell, its impulse response is estimated using a set of input and output data using deconvolution technique in time domain. The instrumentation used in the experiment is Solar Electronics Pulse generator Model 9355-1, a TEM cell (cut-off frequency 500 MHz) and a 500 MHz oscilloscope from Agilent.

Fig. 1 – Measurement Setup
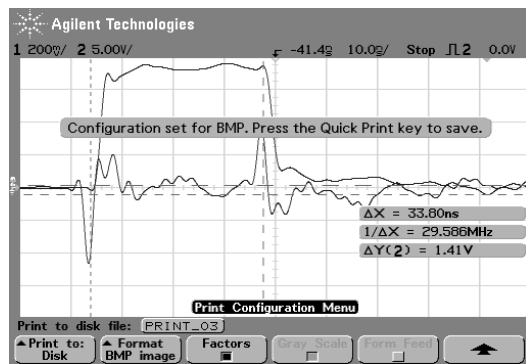
Fig. 2 – Input/Output waveforms for Impulse Response estimation

References

1. T.K. Sarkar, D.D Weiner et.al, "Impulse Response Determination in the Time Domain-Theory", IEEE Transactions on Antenna & propagation, Vol.AP-30, N0.4, July1982.
2. T.K. Sarkar, D.D Weiner et.al, "*Some Mathematical Considerations in dealing with the Inverse Problem,*" IEEE Transactions on Antenna & propagation, Vol.AP-29, N0.2, March1981.

UWB - 07
Conformal Time Domain Numerical Methods (Invited)

Oral Presentations

UWB - 07
Conformal Time Domain Numerical Methods (Invited)

Oral Presentations

A TDFEM Employed Temporal Second Order Lagrange Interpolation for Three-Dimensional EM Radiation Problems

Xia Wu[1], Lezhu Zhou[1]

[1]*School of Electronic Engineering and Computer Science,Peking University, Beijing, P.R.China*
E-mail: wuxiaeecs00@gmail.com

In this paper we investigated a new time-domain finite element method (TDFEM) based on Lagrange interpolation and high-order Whitney elements for temporal and spatial expansion, respectively. This approach is motivated by goals of achieving computational efficiency and further applying on UWB antenna's simulation. Compared with the reported TDFEM scheme[1], which is based on Galerkin's method with a piecewise linear temporal expansion of electric field, in our scheme, the electric field is expanded in terms of second-order Lagrange interpolation polynomial, namely multistep interpolation, both for a more robust interpolation and a more efficient approximation[2]. Moreover, this method allows for a consistent time discretization of the electric field vector wave equation with the augmented PML regions. The formula will be briefly described as follows.

On one hand, in frequent domain, we employ the Laplace transform to the second-order vector wave equation. By letting $s=j\omega$, in the PML region, with a testing function $\vec{N}_i$ (second-order Whitney edge elements) and applying Green's first vector identity, the electric field will satisfy the following equation:

$$\iiint_\Omega \left(\left(\nabla \times \vec{N}_i \right) \cdot \vec{\Lambda}_M^{-1} \left(\nabla \times \vec{E} \right) + \vec{N}_i \cdot \frac{s^2 \vec{\Lambda}_E}{c_0^2} \vec{E} \right) dV = \iiint_\Omega \left(-s\mu_0 \vec{N}_i \cdot \vec{J}_0 \right) dV \tag{1}$$

where, $\vec{\Lambda}_M = \mu_r + \sigma_M/s\mu_0$, $\vec{\Lambda}_E = \varepsilon_r + \sigma/s\varepsilon_0$ and $\vec{J}_0$ is the electric current source and the electric current in PEC.

On the other hand, in time domain, it is useful to introduce the appropriate mechanism which will enable us to express discrete sequences in a matrix system (1). In order to do that, first we employ the inverse Laplace transform to obtain a semi-discretized matrix system, secondly, we use a discretization with respect to time:

$$\vec{E}(\vec{r},t) = \sum_j e_j(t)\vec{N}_j(\vec{r}) \quad (2); \qquad W_n(t) = 40|t/\Delta t|^3 - 45(t/\Delta t)^2 + 9|t/\Delta t| + 1 \qquad -\Delta t < t < \Delta t \tag{3}$$

where the electric field $e_j(t)$ are expressed in terms of 2-order Lagrange interpolation polynomial. Following a procedure analogous to that for Galerkin method, the time step scheme can be easily derived. It is of interest to note the testing function is shown in (3), which is found to appropriately match the Newmark-β unconditional stable scheme in the non-PML region.

Finally, the numerical results are exhibited. The typical case is a dipole antenna. For the source impulse as a function of time, we use Gaussian pulse with the frequency equivalent to 294.6MHz. Fig.1 demonstrated the features of electric field value (hereby we show Ey) with respect to time and θ. Fig.2 illustrates the radiation pattern of E-plane and comparison to control group using the approach given by [1] shows good agreement.
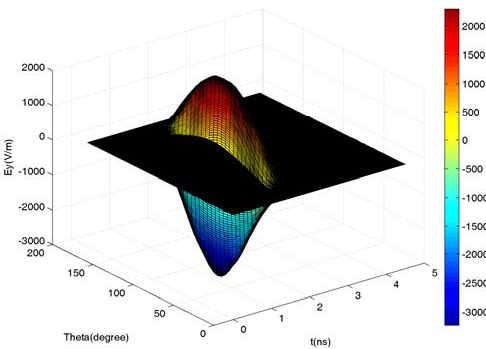
Fig. 1 – TD Radiation Pattern of Dipole Antenna (Ey)
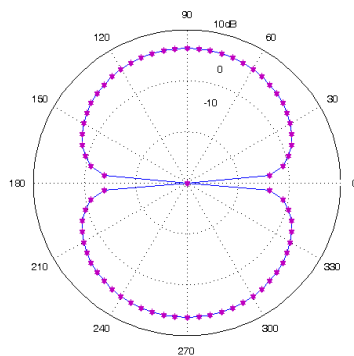
Fig. 2 –E-plane Radiation Pattern(dB) Comparison

References
1.   T. Rylander and J. M. Jin, "Perfectly matched layers in three dimensions for the time-domain finite element method," in IEEE APS Int. Symp.Dig., vol. 4, Monterey, CA, June 2004.
2.   Raman, S. and Bai, E.-W., "A linear, robust and convergent interpolatory algorithm for quantifying model uncertainties," Decision and Control, Proceedings of the 30th IEEE Conference on vol.1.1, Dec. 1991.

The GIMLI: a compact High-power UWB radiation source

Benoît Martin, Philippe Delmote

French-German Research Institute of Saint-Louis, Saint-Louis, France
E-mail: benoit.martin@isl.eu

This paper presents the first results of the tests carried out on a compact general-purpose high-power ultra-wide band source named the GIMLI. The system was designed for dual use field and lab applications. The GIMLI is powered by a compact, coaxial 12-stage ISL Marx generator with a rise time lower than 25 ns and an operating voltage up to 360 kV. A fast monocycle pulse is sharpened thanks to a pulse former. The former is made of a switching assembly with a peaking and a grounding multi channel spark gap under a N_2 pressure of 6 MPa. The spark gaps are followed by a monopulse-to-monocycle converter based on a coaxial Blumlein pulse forming line (Fig. 1). The bipolar signal measured at the output of the MPF has duration shorter than 2 ns with a rise time of 250 ps. The peak-to-peak output voltage is 250 kV measured on a 50 Ω resistive load. Electromagnetic energy is focused by a dedicated TEM horn-antenna (Fig. 2). High-power radiation tests performed in the ISL anechoic chamber show that the field measured at a distance of 9 m from the TEM Horn-antenna is higher than 120 kV/m. Susceptibility tests were carried out on PC and commercial electronics.
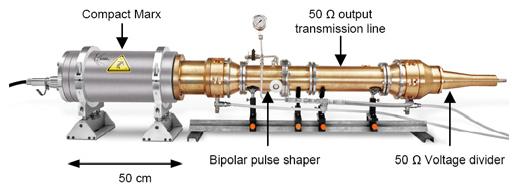
Fig. 1 – The 360 kV Marx generator with the bipolar pulse former connected to a 50 wideband voltage divider during characterization experiments.
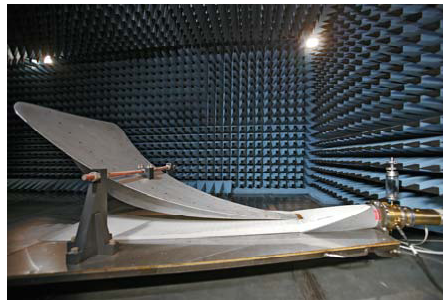
Fig. 2 – The half TEM horn-antenna of the GIMLI on its 2.5 m long ground plane.

UWB - 08
UWB - Pulsed Power

Oral Presentations

Pulsed Power Design Considerations for a Prolate Spheroidal Impulse Radiating Antenna Intended for Biological Applications

J. A. Gaudet[1], W. D. Prather[1], C. E. Baum[2], R. P. Joshi[3], Shu Xiao[4], and K. H. Schoenbach[4]

[1]*Air Force Research Laboratory, Directed Energy Directorate, Kirtland AFB,USA*
[2]*The University of New Mexico, Electrical & Computer Engineering Department, Albuquerque, USA*
[3]*Old Domion University, Electrical & Computer Engineering Department, Norfolk, USA*
[4]*Frank Reidy Research Center for Bioelectrics, Old Dominon University, Norfolk, USA*

...
E-mail: john.gaudet@kirtland.af.mil

Recent developments in bioelectric experiments have indicated that short electromagnetic pulses can be used to treat cancerous cells while not having a deleterious effect on adjacent healthy cells [1]. This effect has led to the design and testing of an impulse radiating antenna (IRA) laboratory model which focuses a large electromagnetic pulse generated at one of the foci of the ellipsoid of revolution at a point (small volume) located at the second focus [2]. The Prolate Spheroidal Impulse Radiating Antenna (PSIRA) has many of the features of the original IRA design and, therefore, many of the analysis techniques developed for the IRA can be used for this antenna with only slight modifications to take into account the different shape of the reflector. It is anticipated that in order to achieve the extreme fields necessary to treat cells with subnanosecond electrical pulses, faster rise times will be required.

The pulsed power used for the original reflector IRAs consists of a hydrogen spark gap switch under high pressure (1500 psi) using a thyratron which charges up ceramic capacitors and are discharged into the spark gap. For this original IRA design, it was believed that the rise time of the pulse was determined by the resistive phase of this gas switch, about 100 ps [3]. However, the theoretical limit of switch operation for this type of IRA (driven by a gas switch), and presumably the PSIRA, is given by the inductive phase of the spark channel, about 20 ps for a 1 mm single gap. However, there is a voltage dependency on this limitation and for 1 MV switching voltage it is about 100 ps [4]. Obviously, the PSIRA design that achieves the closest to the optimum value will also obtain the highest peak power necessary for the medical application.

This paper will review various techniques for the PSIRA to achieve this ideal rise time to the maximum extent possible. The following approaches to peak-up the voltage rise time to near ideal behavior have been evaluated: (1) different spark gap switch designs, (2) solid state switching using GaAs photoconductive semiconductor switches (PCSS) or silicon carbide (SiC) or silicon (Si) fast ionization dinisters [5], and (3) the use of nonlinear transmission lines [6]. Recommendations will be made for a working PSIRA pulsed power design for medical applications that will achieve a specified level of field intensity. In addition, the critical issue of repetition rate and total pulses for this system must be addressed in detail. It has already been established that a large number of pulses must be delivered to the cancer cell in order to obtain a good probability for cell death [1]. This study will allow the medical community to evaluate the practical implications of implementing a PSIRA for cancer treatment.

References
1. K. S. Schoenbach, et al., "Bioelectric Effects of Intense Nanosecond Pulses," IEEE Transactions on Dielectrics and Electrical Insulation, vol. 14, no. 5, pp. 1088-1109, 2007.
2. C. E. Baum, "Focal waveform of a prolate-spheroidal impulse-radiating antenna," Radio Science, Vol. 42, RS6S27, doi:10.1029/2006RS003556, 2007.
3. D. V. Giri, H. Lackner, I. D. Smith, D. W. Morton, C. E. Baum, J. R. Marek, W. D. Prather, and D. W. Scholfield, "Design, Fabrication and Testing of a Paraboloidal Reflector Antenna and Pulser System for Impulse-Like Waveforms," IEEE Transactions on Plasma Science, Vol. 25, No. 2, April 1997, pp. 318-326.
4. J. Lehr, C. E. Baum, W. D. Prather, and R. Torres, "Fundamental Physical Considerations for Ultrafast Spark Gap Switching," in **Ultra-Wideband, Short-Pulse Electromagnetics 4**, E. Heyman, B. Mandelbaum, and J. Shiloh (eds.), Kluher/Plenum: New York, 1999.
5. I. V. Grekhov, "Research and Development of Silicon Carbide (SiC) Avalanche Sharpeners for Picosecond Range, High Power Switches," Final Report on EOARD-CRDF Project REO-1381-ST-03, December 2005.
6. G. Zhao, R. P. Joshi, S. Rogers, E. Schamiloglu, and H. P. Hjalmarson, "Simulation Studies for Non-Linear Transmission Line Based Ultra-Fast Rise Times and Waveform Shaping for Pulsed Power Applications," unpublished.

UWB - 08
UWB - Pulsed Power

Oral Presentations

Traveling-Wave Switches and Marx Generators

C. E. Baum

University of New Mexico
Department of Electrical and Computer Engineering
Albuquerque New Mexico 87131
E-mail: cebaum@ece.unm.edu

This paper considers a possible technique for reducing the rise time of high-voltage switches by placing an array of smaller-voltage switches in a traveling-wave geometry. This same technique can also be incorporated in a Marx generator.

Fundamental limits for switching speed are based on the arc inductance for the shortest switch-electrode spacing for a given voltage across the switch. This in turn requires the highest dielectric-strength switching medium, this also being influenced by any requirement for repetitive switching, requiring switch recovery before the next pulse. By rapidly charging the switch some improvement can be gained, but this has its limits.

By analogy to traveling-wave or distributed amplifiers, let us have a switch-closure propagate along a line array of switches. With differential charging voltages $\pm V_{ch}$ across the whole array of N switches, each switch initially has a voltage of $2V_{ch}/N$ across it. This is accomplished by some high-impedance resistive grading network, say N resistors, each of resistance R across each switch.

One then triggers switch 1, which, in turn, overvolts switch 2, and on to switch N. The switches and associated electrical connections form the center conductor of a transmission line along which waves can propagate. As each switch closes it sends out two waves which can be designated as forward and backward. Each wave has amplitude V_{ch}/N, adding up to V_{ch} for the whole array. Ideally the wave speed approaches the speed of electromagnetic propagation in the surrounding dielectric medium (near c in the case of various gases). In this case the forward wave has a rise time limited approximately by that of a single switch, each switch contributing to the sharpening of the wavefront. The backward wave is, of course, highly dispersed and appropriately terminated for negligible reflection.

Now let us substitute for each switch section a Marx-generator section. The connections between successive switches are replaced by two high-ε dielectric blocks. As such, these dielectric pieces act like conductors at high frequencies, thereby becoming part of the waveguide structure. The traveling-wave Marx generator is then quite similar to the traveling-wave switch. The difference lies in how the switches are changed.

UWB - 08
UWB - Pulsed Power

Oral Presentations

The High Intensity Radiated Field Synthetic Environment Research Programme

Ian Flintoft[1], Peggy Favier[2], Ilario Bertino[3], Hristos Anastassiu[4], J-Philippe Parmantier[5], Christophe Girard[6], Sabrina Sarto[7], Marco Bozzetti[3], J-Patrick Moreau[8] and Andrew Marvin[1]

[1]*University or York; UK , *[2]*L-up SAS, France; *[3]*Alenia Aeronautica, Italy ;*
[4]*Hellenic Aerospace Industry SA, Greece; *[5]*Office National D'Etudes et de Recherches, France ;*
[6]*Ginkgo Solutions SAS, France;*[7]*Università di Roma "Sapienza"; Italy, *[8]*Dassault Aviation, France*

E-mail: idf@ohm.york.ac.uk

The Electromagnetic environment in which air vehicles have to operate is becoming increasingly complex with developing threats arising outside the air vehicle and the demand from passengers to operate increasing numbers of diverse personal electronic devices within the cabin in flight. Modern airframe design is also exploiting new developments in materials and structures to construct ever more efficient air vehicles that impacts on the electromagnetic performance of the vehicle.

The recently started High Intensity Radiated Field Synthetic Environment (HIRF SE) project has the goal of providing the European aeronautics industry with a computational framework which can be used in the development phase to enable electromagnetic aspects of the airframe design to be accounted for at an early stage of the design process. Currently much of this work has to be done at the test phase, risking considerable re-work costs if problems arise. It is expected that the application of the HIRF SE framework will thus confer a substantial economic benefit and in addition it will provide a considerable reduction in the certification and qualification tests required on an air vehicle. The HIRF SE programme's main objectives can be summarized as:

1. Full validated and integrated solutions to model, simulate and test air vehicles for electromagnetic aspects during the whole life cycle;
2. To build, from both past and ongoing works, an integrated approach to electromagnetic modelling of air vehicles with an open and evolutionary architecture.

The first objective addresses the current drawbacks of the actual design, certification and modification approach with the assistance of computational electromagnetics techniques. The second objective addresses the gathering together of the whole currently available numerical simulation competence to cooperate in the solution of complex electromagnetic problems. HIRF SE proposes to overcome the difficulties of this hybridisation process using an innovative and systematic solution based on a high level of software integration, offering an open and evolutionary architecture: a computer framework. The framework will incorporate a number of already existing elementary codes for the simulation of physical processes of electromagnetic field penetration and scattering and will have the capability to deal with the complete foreseen internal and external electromagnetic environment.
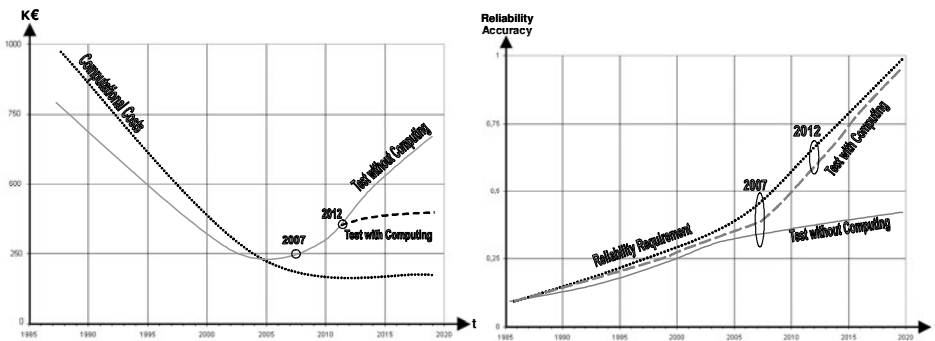

Figure 1 Testing cost versus increasing complexity of air vehicles. Figure 2 -Reliability and accuracy versus increasing of air vehicles.

The HIRF SE project will be validated on small and medium air vehicles by real tests. The expected technical and economic benefits of the programme are illustrated in Figures 1 and 2. The HIRF SE project will increase the confidence in the EMC assessment process as shown on Figure 2, fulfilling the current and future reliability requirement that increases as a function of the number of safety critical functions performed by electronics.

We will report on the initial phases of this EU Framework 7 research programme, which brings together a community of forty-four airframe manufacturers, research institutes and universities.

High Voltage and High PRF FID Pulse Generators of Nano- and Picosecond Range

V. M. Efanov[1], M.V. Efanov[1], A. V. Komashko[1], A.V. Kriklenko[1],
P.M. Yarin[1], and S. V, Zazoulin[1]

[1]*FID GmbH, Burbach, Germany*
E-mail: vlad@fidtechnology.com

Several types of pulse generators with amplitude from 200 kV to 10 kV, rise time from 200 ps to 50 ps, pulse duration from several nanoseconds to 100 picoseconds have been developed. At amplitude of 100-200 kV maximum pulse repetition rate in continuous operation can be 2-5 kHz. Testing of such pulse generators has been performed which shown that total efficiency can reach more than 60% at pulse duration of 1-2 ns. Tests have also revealed that electric strength of connectors and transmitting cables is rapidly decreased at pulse repetition frequency of 1 kHz and higher.

At PRF of up to 10 kHz amplitude of voltage pulses can reach 30-50 kV with rise time of 100-150 ps. In such pulse generators transformer oil used for insulation and cooling purposes allow reaching of compact dimensions and high efficiency.

At amplitude of 10 kV, rise time of about 100 ps and pulse duration of 0,5 ns an operating frequency of 200 kHz in continuous mode has been reached. Jitter of delay time between an external triggering pulse and output high voltage pulse from the generator is about 10-20 ps.

A new type of pulsers which form voltage pulses with amplitude of 5-10 kV, rise time of 0,5-1 ns, pulse duration of 1-2 ns, operating at pulse repetition rate of 3-6 MHz has been developed.

All pulsers have high stability of specifications and can be used in multichannel systems to reach high peak power.

UWB - 08
UWB - Pulsed Power

Oral Presentations

Experimental and Theoretical Investigation of Directional Wideband Electromagnetic Pulse Photoemission Generator

P.V.Petrov[1], V.I.Afonin[1], D.O. Zamuraev[1], E.V.Zavolokov[1], N.V.Kupyrin[1], Yu.N.Lazarev[1], Yu.O.Romanov[1], Yu.G.Syrtsova[1], I.A.Sorokin[1], A.S.Tischenko[1], G.I.Brukhnevich[2], N.P.Voronkova[2], L.Z.Pekarskaya[2], V.S.Belolipetskiy[2]

[1] *Russian Federal Nuclear Centre - Institute of Technical Physics, Snezhinsk, Russia*
[2]*Institute of Optical-Physical Measurements, Moscow, Russia*

...
E-mail: pvpetrov@mail.ru

The effect of electromagnetic wave generation by the electric current pulse propagating at the superluminal velocity along a conducting surface may be promising to create high-power wideband microwave generator [1]. The oblique irradiation of the electron photoemission-ability surface by the plane front of pumping radiation can be employed to produce the superluminal current pulse [2].

One variant to realize this scheme of electromagnetic pulse generation is the system comprising a plane vacuum photodiode with a transparent anode and using laser radiation to initialize electron emission [3].

This report presents results of experimental researches in characteristics of such radiating element with the cesium-antimonide cathode of $\varnothing 50$ mm and the anode of the optical transparency 0.7 (Fig.1). The anode-cathode gap varied from 1 to 4 mm. The electron emission was initialized by the pulse of laser radiation of the wavelength 527 nm and the duration 1 ps that incident at the angle 45° on the photocathode. Photoelectron acceleration was induced by applying voltage from 20 to 60 kV to the anode-cathode gap.

The time dependence of the electric field strength, the photoemission current, the photodiode pulse voltage and laser pulse parameters have been measured in experiments. The dependence of the generated electromagnetic field on the laser radiation intensity, the anode-cathode gap size and the accelerating voltage have been studied. The far-field radiator spatial-angular distribution of the microwave radiation electric component has been measured.

The performed researches have shown that the generated wideband pulse ($f_0 \approx 3.3$ *GHz*, $\Delta f / f_o \sim 1$) is directed at the angle specular to the laser radiation angle of incident, the electric field amplitude increases with the increasing of the accelerating voltage.

Under the voltage of about 50 kV the electric field strength of 44 kV/m at the distance of 1.3 m has been recorded that corresponds to the generator power ~10 MW.
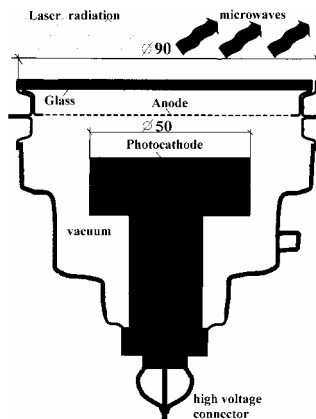

Fig. 1 – Scheme of photoemission radiating element

References
1. V.L. Ginzburg, Theoretical Physics and Astrophysics, Moscow, Nauka, 1975.
2. N.J., Carron, C.L., Longmire," Electromagnetic Pulse Produced by Obliquely Incident X-Rays," IEEE Trans. On Nucl. Sci., Vol. NS-23, p.1897-1902, 1976.
3. Yu. N. Lazarev, P.V. Petrov, "Microwave electromagnetic radiation generator based on the superluminal source", J. Of Exper. And Techn. Physics, Vol. 115, pp..1689-1707, 1999.

Dynamic Parameters of the Dipole Layer Formed during Pulsed Photoemission Discharging of a Plane Vacuum Diode

S.P. Martynenko, A.V. Bessarab, A.V. Soldatov, A.A. Solov'ev,
V.A. Terekhin, and M.S. Terekhina

Russian Federal Nuclear Center – All-Russia Scientific Research Institute of Experimental Physics,
Sarov, Russia
E-mail: terekhin@vniief.ru

The parameters of the current and dipole moment that arise during the discharging of a plane vacuum diode by a short photoemission pulse are studied analytically and numerically. Electron emission is induced by the ionizing radiation incident obliquely on the cathode. An approximate analytic model is developed that, under certain conditions, makes it possible to reduce the problem to that having a known solution for the normally incident ionizing radiation. In the case of a short pulse, scaling relationships for the parameters of the dipole layer are obtained as functions of the diode parameters (the interelectrode gap and applied voltage) and the angle of incidence of the ionizing radiation. So, experimentally, a planar accelerating diode comprising a metallic cathode and grid anode was initiated by an oblique short soft X-ray pulse from a point laser plasma source. The plasma was formed when a short-pulse (~0.3 ns) radiation from laser facility was focused onto a plane Au target. The parameters of the photo-emission current and accelerated electron current are measured. Comparison between the theoretical and experimental parameters of the currents arising in the vacuum diode discharge is carried out.

Modeling for Interaction of the Rarefied Plasma Streams with a Surface of the Sensitive Elements in the Fiber-Optic Cables

E.L. Stupitsky[1], A.S. Kholodov

[1]*Moscow Institute of Phycics and Technology, Moscow, Russia*

e-mail: stup@bk.ru

Now the question on long influence (more than 1 s) strongly rarefied streams of relativistic electrons and plasmas (more than 10^{11} 1/cm^2·s) on dielectric and conductive surfaces which, not leading to thermomechanical effects, can essentially change optic-electronic properties and functionalities of such surfaces is practically not investigated.

The practical importance of job is very great, as its performance will allow to answer a question on a status of optic-electronic and navigating systems which job can occur in conditions of the artificial radiating belt formed at large-scale space experiments.

In the given work it is analyzed interaction of an ionic stream with a superficial layer of a solid-state target and the preliminary physical model of such interaction in view of that streams are rather rarefied is developed. At characteristic energy of ions E=1,3 keV depth of their implantation in a target from aluminum l=2,1·10^{-6} sm ($l \approx 1,5 \cdot 10^{-6} E^{3/2}$(keV), sm), characteristic concentration after end of action of a stream n =(0,3–8)·10^{18} sm^{-3} and accordingly average distance between ions 0,5·10^{-6}–1,5·10^{-6} sm, i.e. compared with thickness l. After a temperature relaxation its increase is equal ΔT=730°, that in itself can lead to thermal decomposition of some materials. However the greatest interest that system of individual microeffects, which form ions in the surface layer, changing its optical and represents electrophysical properties. The nature of defects is caused by education of vacancies and introduction of the beaten out atoms in next between knots. Calculations of stochastic movement of ions in a superficial layer have shown, that defects have the form of the wedge structures. Concentration of the displaced atoms does not depend on energy of flying particles and causes constant linear density of the displaced atoms along a wedge of displacement. Density of streams of plasma at which accumulation of microeffects leads to their merge and education of a superficial layer to others optical and electrophysical properties are certain. Influence of this layer on functionalities of some optical and electronic devices is estimated.

A Chopping-Peaking High Power Bipolar Pulse Former

l shi, y j fan, g z liu,s t zhu,j s zhou,y f zhu,s liu,w f xia
Northwest Institute of Nuclear Technology, P.O.Box 69-13, Xi'an. 710024, China
E-mail: Zhu_sitao@sina.com

The ultra-widespectrum(UWS) electro-magnetic pulse is very useful in many applications, such as radar target identification, underground and hidden objects detection and remote sensing. The high power UWS pulse source generates a single-polar pulse, a bipolar pulse will be formed when the single-polar pulse goes through the combined the Chopping-Peaking switches, the Chopping switch is on the side near the pulse source and there is a transmission line of a certain distance from the Peaking switch. A high power bipolar pulse generator with combined Chopping-Peaking switches is designed and developed. Operating principle is studied and the circuit analysis is performed. The peak-to-peak voltage of the forming bipolar pulse is double of the impulse peak level in ideal，the duration of the bipolar pulse can be changed by adjusting the gaps of the Chopping-Peaking switches. Experimental study on the bipolar pulse generation with Chopping-Peaking switches is discussed in this paper. The single-polar impulse voltage is 205kV in the experiment. A bipolar pulse with maximum peak-to-peak voltage of 360kV is gained, which in rate is 1.76 of the input pulse. The duration of the bipolar pulse can be changed and the maximum equals to the input single-polar pulse. The steeper the input pulse, the higher the peak-to-peak voltage of the generated bipolar pulse.

UWB - 08
UWB - Pulsed Power

Oral Presentations

Model Synthesis of Resonant Units for Radiators of High-Power Short Radio Pulses

O. S. Shafalyuk[1], L. G. Velychko[2]

[1] *AmberCore Software, Inc., Ukrainian Office, Kharkiv, Ukraine*
[2] *Institute of Radiophysics and Electronics, National Academy of Sciences, Kharkiv, Ukraine*
E-mail: lgv@ire.kharkov.ua

The paper deals with the theoretical problems associated with simulation of transient and steady-state processes in radiators of high-power short radio pulses. We present the results of analysis and synthesis of principal resonant and non-resonant units of these systems, namely, coupling windows with supplying waveguides, energy storage systems (compressors), switches locking the pulse output line during the charging phase, and radiating units.

The algorithm of model synthesis has been developed for the systems, in which the energy is compressed in a section of supplying waveguide, while for the energy radiation a standard antenna possessing suitable electrodynamic characteristics (radiation efficiency, directional pattern, etc.) is used (Fig.1). The following problems have been solved:

–   synthesis of the energy-storage resonator (optimization of the coupling window, selection of the working oscillation and estimation of its spectral characteristics, analysis of spectral characteristics of the energy-storage resonator in discharging phase and additional spectrum sparseness);
–   synthesis of the switching system (lock), correlation of its operating frequency with the resonator's operating frequency;
–   a complete electrodynamic analysis of the system 'storage resonator + unlocked switching system', refinement of all compressor's parameters during the charging phase;
–   simulation of the transition into the discharging phase, computation of basic compressor's parameters;
–   analysis and synthesis of the radiating unit.

We have considered the structure, in which an open resonator acts as a compressor and a radiator simultaneously, while resonator's mirror possesses different transparency during the charging and discharging phases (Fig.2).

All the problems are solved in the context of the rigorous time-domain approach based on the finite-difference algorithm with the 'fully-absorbing' conditions [1]. This technique allows us to study long-term transient processes obtaining reliable results. To study spectral characteristics of open resonant systems, a computational procedure based on the analytic connection between space-time and space-frequency characteristics of the forced and free electromagnetic oscillations in these structures has been developed [2].
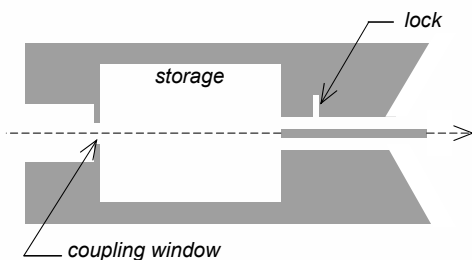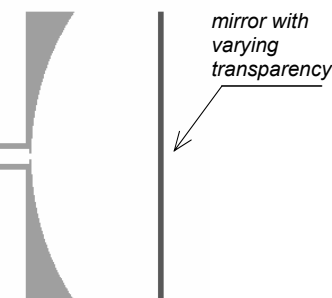

Fig. 1.   Fig. 2.

References
1.   Y. K. Sirenko, S. Strom, and N. P. Yashina, Modeling and Analysis of Transient Processes in Open Resonant Structures. New York: Springer, 2007.
2.   Y. K. Sirenko, L. G. Velychko, and O. S. Velychko, "Time-domain analysis of open resonators. Analytical grounds," Progress in Electromagnetics Research, vol.61, 2006.

A Long Range UWB Channel Sounding System Exploiting UWB over Fibre Technology

Athanasios Kavatjikidis, David J. Edwards, Christopher J. Stevens

Department of Engineering Science, University of Oxford, Parks Road, Oxford, OX1 3PJ, U.K.

{Thanasis.Kavatjikidis, David.Edwards, Christopher.Stevens}@eng.ox.ac.uk

The demand for bandwidth for long haul networks is relatively static, current and future developments in short range data applications will require larger data capacity for audio/video streaming. UWB systems offer a technology that can achieve good performance for short-range wireless high-throughput applications. However UWB signals are only limited to short distances of a few meters, due to the combination of very low transmitted power and the poor performance of long RF cables at high frequencies. A typical UWB cable has a loss of 4 dB/m at the UWB bandwidth. In a typical indoor scenario with antenna separation of 2-3 m a total length of 5 m UWB cables is needed. With this length of cables a loss of 20 dB will be introduced and the system's performance will be reduced substantially. This poor performance limits the distribution of data over wired UWB links or wide wireless networks, remote UWB antenna systems and even within instruments.

An efficient solution can be achieved using UWB over optical fibre technology. The combination of very low loss of optical fibres 0.5 dB/Km at modulation frequencies up to 100 GHz with the immunity to electrical interference, which prevents cross-talk between signals in different cables and pickup of environmental noise, makes transmission of UWB over fibre a reliable technology for UWB transmissions. With optical fibre systems an effective approach is proposed to achieve extremely high data rate transmissions. Thus, real time indoor environment applications such as sharing images, music, video streaming, data, and voice among networked fixed and mobile devices can be realised with undisrupted transmissions [1-2].

This work presents a novel UWB over fibre system, illustrated in Fig.1. This point to point UWB over fibre connection is experimentally implemented with a tunable laser source to emit through a Single Mode Fibre between 1530-1615 nm. The concept of the characterisation system is based upon the classic vector network analyzer (VNA) technique [3]. The results confirm that an improvement of 20 dB can be achieved with the proposed system in comparison with conventional 5 m UWB cables. Due to the very low attenuation of single mode fibres, only 0.5 dB/Km, distribution of UWB signals up to 60 Km can be achieved with our system before the noise floor is reached. This enables longer range UWB systems than has hitherto been reported. The frequency is limited at 12 GHz, but can be extended upwards in frequency with the use of an appropriate LNA with very small degradation in performance. This technology can be used to distribute UWB signals around buildings or medium range networks. Thus, this approach can provide bandwidths of several GHz for high-throughput wireless communication and sensor networks services.
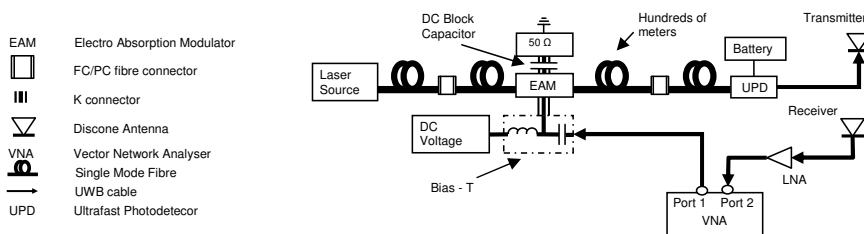

Fig.1 - Schematic diagram of the designed UWB channel sounding system.

References
1. "Revision of Part 15 of the Commission's Rules Regarding Ultra-Wideband Transmission Systems, FIRST REPORT AND ORDER.", Federal Communications Commission, ET Docket 98–153, FCC –2–48, April 2002.
2. Zeng F., Yao J.P., "An approach to ultrawideband pulse generation and distribution over optical fiber", IEEE Photonics Technology Letters, vol. 18, Issue 7, April 1, 2006.
3. Street, A.M., Lukama, L., Edwards, D.J.,"Use of VNAs for wideband propagation measurements," IEE Proc.- Communications, vol. 148, Dec 2001.

UWB Antennas Integration Effects for Wireless Communications Applications

M.A Mellah , Ch. Roblin and A. Sibille

ENSTA, 32 Bd Victor 75739, Paris, France
Tel: +33145525434 / Fax: +33145522783

E-mail: mohammed-amine.mellah@ensta.fr

Nowadays, the interconnection and communication between different devices in a given environment is becoming an important aspect of the wireless applications. The rising interest in the UWB technology as a solution for such wireless systems is confirmed by the high number of UWB antennas designed these last years. In this paper, we investigate the disturbing of UWB antennas characteristics when mounted on common used devices. To analyze the effect of the UWB antennas integration, four UWB antennas (named: Cir, DFMM, MSS, and Fractus) were studied in close proximity of various devices: Screen, two different Laptops, two different boxes (Internet, DVD player) and a keyboard. For each device, the antennas return losses were measured in several positions. The bandwidths - defined for: $S_{11} < -10$ dB – of the antennas on devices were extracted and compared with the case of isolated antennas. The comparison was illustrated by the Bandwidth Ratio BR defined as follow:

BR (a,d,i) = Bandwidth of antenna "a" on device "d" in position "i" / Bandwidth of antenna "a" isolated   (1)

Depending on the position and the device under test, the antenna's bandwidth can be enhanced or reduced. However, for some positions the bandwidths were divided into different separated parts, in this case, the cumulative bandwidths were considered.

General similarities in the bandwidth behavior were noticed for the antennas when mounted on the same device in the same positions as illustrated in figure (1b). In a purpose of modelling, a statistical study was carried out to extract mean values and variances of BR on each device in one hand and to define the approaching statistical law that best describes the distribution of the UWB antennas BR values in the other hand. Finally, the results give the best positions to choose when integrating UWB antennas in the cited devices. More details about the antennas and the statistical study will be given in the final version.
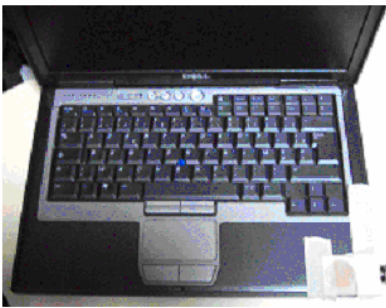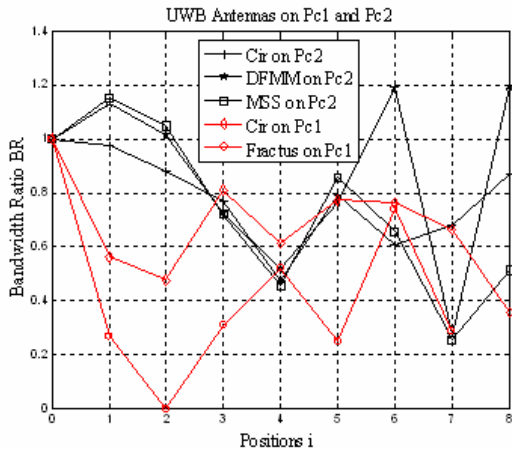
(a)   (b)

Fig. 1 – (a) Cir Antenna on Pc2 in position 2. (b) BR vs Position on Pc1 and Pc2 for all UWB antennas
(**Position 0 refers to the case of antenna isolated)**

Bit Error Rate of a Non-ideal Impulse Radio System

J. Timmermann[1], E. Pancera[2], P. Walk[3], W. Wiesbeck[4], and T. Zwick[5]

[1,2,4,5] *Institut fuer Hoechstfrequenztechnik und Elektronik, Universitaet Karlsruhe,*
Kaiserstr. 12, 76131 Karlsruhe, Germany
[2]*Lehrstuhl fuer Mobilkommunikation, Technische Universitaet Berlin,*
Einsteinufer 25, 10587 Berlin, Germany

E-mail: jens.timmermann@ihe.uka.de

Carrierless ultrawideband transmission (called impulse radio, IR) is a promising wireless technique to realize high data rates. Without carrier, the frontend architecture is simplified in comparison with conventional systems. Therefore, IR has also the potential to be a low-cost technique. On the other hand, UWB devices demand for components that have constant characteristics over an ultrawide bandwidth in the range of GHz. This is difficult to realize and leads to an increase of costs. So in practice, a trade-off between system behavior and economic aspects must be made. This means that non-ideal behavior versus frequency cannot be completely neglected. The question is which performance can be achieved using non-ideal components in an UWB impulse radio system. To answer this question before constructing a prototype, suited component modeling and simulation techniques must be applied. In literature, many proposals have been presented how single elements can be modeled [1], but to our knowledge, a full description of the non-ideal transmission chain including all critical elements and effects for IR has not been presented before. This paper starts with finding the critical components and effetcs. Critical is the oscillator due to jitter, antennas because of their frequency dependent patterns, the multipath channel, interference and the frequency dependent low noise amplifier. Then component modeling is performed as an extended version of [2]. Finally, the interfaces between the components are realized and implemented into Advanced Design System (ADS). To estimate the system performance, system simulation is performed, and the bit error rate of a non-ideal impulse radio system based on pulses for the FCC regulation is determined.

First, the distance between transmitter (Tx) and receiver (Rx) is fixed while sweeping the UWB interference power: The power spectral density of the interference power is supposed to tremble around a constant level inside the FCC mask. Since different interference power can be expressed in terms of different receiver SNR, it is possible to determine the dependency between BER and SNR. The result can be seen in Fig. 1: For the shown indoor scenario (Line of Sight) with a distance of 2.4 m between Tx and Rx, the BER increases with worse SNR. The simulated BER is only then a good estimate of the actual BER if the number of simulated bits is at least factor 10 of the inverse simulated BER. This is respected by the fact that the number of simulated bits is 10^4.
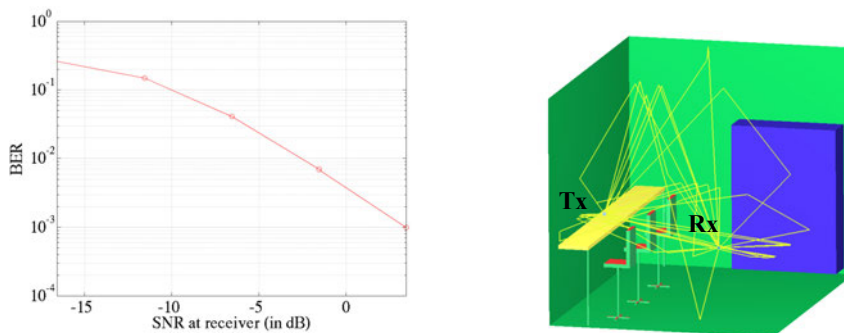

Fig. 1 – Bit error rate versus SNR for non-ideal UWB transmission based on the shown scenario

Second, the bit error rate is calculated for several indoor channels to get the distance dependency of the system. The effect of spatial fading will be very small since for UWB signals, it is inprobable that destructive superposition of paths will occur for all frequencies inside a range of GHz.

References
1. A. Sibille, "A Framework for Analysis of Antenna Effects in UWB Communications", Vehicular Technology Conference, Stockholm, Sweden, 2005.
2. J. Timmermann, D. Manteuffel, and W. Wiesbeck, "Simulation of the impact of antennas and indoor channels on UWB transmission by ray tracing and measured antenna patterns", International Conference on Ultrawideband, Singapore, 2007.

UWB - 09
UWB - Communications

Oral Presentations

Requirements of Preselect Filter and Front-End Linearity for Low-Power UWB Systems Operating in a 'Worst Case' Interference Scenario

O. Lauer [1], D. Barras[2], R. Vahldieck[1], H. Jäckel[2] and J. Fröhlich[1]

[1]IFH, ETH Zurich, Switzerland
[2] IFE, ETH Zurich, Switzerland
lauero@ifh.ee.ethz.ch, david.barras@ife.ee.ethz.ch

Ultra-wideband (UWB) communication within the 3-5GHz range operates in the presence of strong signals originating from other wireless services (e.g. ISM, UMTS, W-LAN), some of them just a few MHz away. These wireless technologies feature a much higher transmission power than UWB signals. Through the system specific non-linear characteristic of front-ends these services tend to interfere with UWB signals through their intermodulation products (IMP's), resulting in a loss of sensitivity. Therefore, adding a preselect filter in order to minimize this degradation will allow for robust communication within the UWB band.

In the following a numerical procedure for the derivation of the preselect filter is proposed. The transfer function of the front-end is modeled by a finite polynomial. As out-of-band signals a three-tone excitation:

$$x(t) = A_1 \cos(2\pi f_1 t) + A_2 \cos(2\pi f_2 t) + A_3 \cos(2\pi f_3 t)$$

is applied. The frequency of the IMP's generated by an n-order non-linearity is given by f_{IM}:

$$f_{IM[l,k]} = \pm k \cdot f_1 \pm l \cdot f_2, k + l = m \wedge m = 2,3,...n$$

The corresponding amplitudes result from the trigonometric terms of the excitation. By setting a level for the maximum acceptable degradation in receiver sensitivity, the minimum filter order can now be numerically evaluated for different front-end characteristics.

The non-linearities of the front-end are mainly characterized by the second- and third-order IMP's. The latter is related to dynamic range and mainly depends on the front-end current consumption. The second order non-linearity reflects the circuit topology. For balanced circuits IMP2 is considerably larger than for unbalanced ones. The order of the preselect filter is directly related to the amplitudes of these two IMP's. Smaller IMP's require a higher order of the filter and vice versa. The order of the preselect filter can be reduced by feedback and offset cancellation techniques [1].

A "worst-case" interference scenario has been used with maximum allowable transmission power for the determination of IMP's. Services such as GSM900, GSM1800, DECT, UMTS, ISM2.4GHz and IEEE802.11a have been identified as the most threatening for UWB applications. To examine a "worst-case" scenario it was assumed that one channel of each of the three considered services are active at the same time and the interference sources are only 10cm away from the UWB receiver. Furthermore the antenna is assumed as isotropic with no reflection, polarization and matching losses for the observed frequency range. As an example of an analog front-end realization the system described in [2] is used. The required signal-to-interference ratio (SIR) is +5.3 dB, which results in an IMP power limit of -67.9 dBm for reliable communication over a distance of one meter characterized by a bit error rate equal to 10^{-3}. In Figure 1 the intermodulation products that potentially fall within the 3-5 GHz UWB band are shown for three different front-end characteristics. In this simulation, the filter order has been determined such that the IMP noise floor stays below the aforementioned power limit. Results show quantitatively how the pre-filter order N has to be traded-off against the receiver linearity. Furthermore it can be seen that a symmetric realization performs better in the presence of a noisy environment. This kind of analysis can also be conducted for 'real-world' interference scenario with considerably lower interference power [3]. Using the proposed framework the corresponding preselect filter with minimal order can be determined for a given specific UWB-receiver structure and near-by interfering sources.

Fig. 1 – Potential IMP in UWB channel for three different second-order front-end non-linearity realizations (IIP3=-12 Bm is assumed).

References

1. A. A. Abidi, "General Relations Between IP2, IP3, and Offsets in Differential Circuits and the Effects of Feedback," IEEE Transactions on Microwave Theory and Techniques, Vol. 51, No. 5, May 2003, pp. 1610-1612.
2. D. Barras, F. Ellinger, H. Jäckel and W. Hirt "A Robust Front-End Architecture for Low-Power UWB Radio Transceivers" IEEE Transactions on Microwave Theory and Techniques, Vol. 54, No.4, April 2006, pp. 1713-1723.
3. O. Lauer, M. Riederer, N. Karoui, R. Vahldieck, E. Keller and J. Fröhlich, "Characterization of the Electromagnetic Environment in a Hospital," accepted for publication at EMC 2008, Singapore.
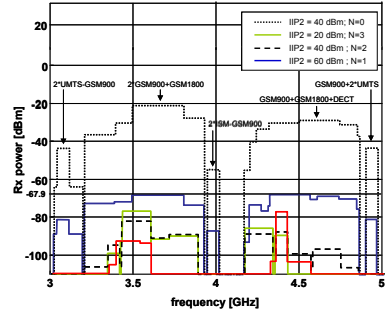
A New Compact Coplanar Defected Ground Structure (DGS) Low-Pass Filter

A. Batmanov [1], A. Boutejdar[2], A. Omar[2], and E. Burte[1]

[1]*Chair of Semiconductor Tech., University of Magdeburg, Germany*
[2]*Chair of Microwave Engineering, University of Magdeburg, Germany*
E-mail: Anatoliy.Batmanov@ovgu.de

Abstract – This paper presents the design of a new compact low-pass defected ground structure filter (DGS LPF). This structure is based on coplanar waveguide (CPW) lines and $\lambda/2$ resonators. The behavior of the structure has been simulated with full wave 2.5D electromagnetic simulator Sonnet 11.54. An equivalent circuit model (Fig. 1 (b)) is used to investigate the DGS characteristics. Both simulations have shown that the proposed filter introduces a very low transition coefficient in the stop-band and is well matched (Fig 1 (c)). The proposed low-pass filter provides the bandwidth of 8.5 GHz, from 3 GHz to 11.5 GHz with the stop-band rejection more than -20 db. The simulated structure is 24×23.4 mm^2 in dimension. The proposed low-pass DGS filter has been fabricated and measured. Good agreement between electromagnetic simulation, equivalent circuit simulation and measurements has been observed.

Fig. 1 (a) shows the schematic diagram of the proposed low-pass DGS filter structure. It consists of the two $\lambda/2$ DGS slot resonators in the ground planes, which are loaded with the open-end stubs. The proposed DGS slots consist of two square heads and a connecting slot with a gap of 1 mm. The DGS units located symmetrically on the both sides of the transmission line. The CPW lines, used for this filter, were designed for characteristic impedance of 50 Ω. This impedance corresponds to G/WG of 0.2/2.8/0.2 mm. The substrate material has a permittivity of 3.38 and a thickness of 0.813 mm. Copper with a thickness of 35 μm has been used as metallization. The slot-head areas basically control the inductance, whereas the width c of the connecting rectangular slot controls the capacitance. The series inductance has been increased by adding the open-end sections of the transmission line between the two DGS heads in the ground plane as shown in Figure 1. In order to investigate the dependence of the filter parameters on the dimensions, the EM simulations were carried out for different values of the parameters a, b and c, see Figure 1 (a).
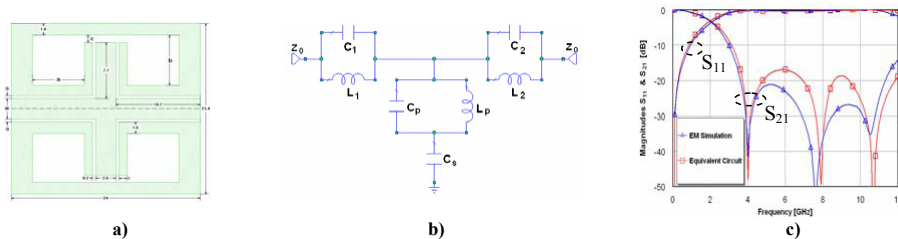

Fig. 1 Proposed DGS LPF : (a) schematic diagram, (b) equivalent circuit, and (c) EM and circuit simulations.
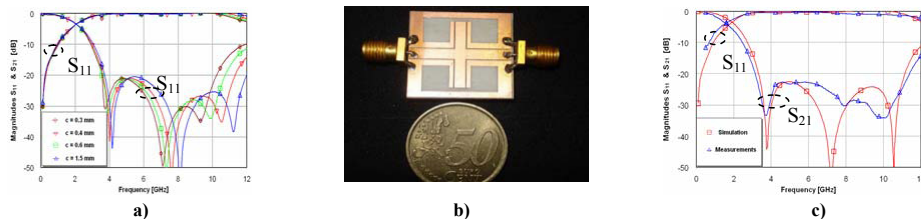

Fig. 2 (a) EM simulation for different values of the gap c, (b) fabricated low-pass DGS filter, and (c) EM simulated and measured results of the proposed low-pass DGS filter.

References
1. A. Batmanov, N. Spiliotis, A. Boutejdar, A. S. Omar and E. P. Burte "Control of Bandwidth and Resonant Frequency of a New Coplanar Bandpass Filter", Proc. Asia-Pacific Microwave Conference, December 11-14, 2007
2. A. Boutejdar, A. Elsherbini and A. S. Omar, "A New Cross-Head Defected Ground Structure (CDGS) for a Compact Lowpass Filter with a Wide Stopband" Proc. 37th European Microwave Conference 2007 (EuMC), München, Germany, October 2007.

A Fast Algorithm to Solve the Half-Space Inverse Scattering Problem Involving Small Scatterers

X. Chen

National University of Singapore, Singapore

E-mail: elechenx@nus.edu.sg

The paper presents a fast algorithm to solve the inverse scattering problem involving discrete small scatterers imbedded in the half space. It can be applied to the detection of subsurface objects and the reconstruction of the image of the sample placed above a flat substrate. This paper is presented in the framework of the total internal reflection tomography (TIRT), a kind of near-field technique, which can be used to improve the resolution [1]. In TIRT, the sample is illuminated with different evanescent waves through a substrate in total internal reflection and then the permittivity of the sample is reconstructed from measurements of scattered fields. The most commonly used methods to solve the TIRT problem are the Born approximation and the numerical optimization method. Although both methods have their merits, the former applies only to weakly scattering samples and the latter is computationally expensive [2].

In this paper, a special case is considered where multiple scattering is included and the computation cost is low. The sample to be studied is discrete scatterers that are much smaller than the wavelength. The small scatterers could be of any shape and their composing materials could be anisotropic. When the multiple scattering effect is taken into account, the inverse scattering problem of locating the scatterers and retrieving their polarization tensors (i.e., scattering strengths) is nonlinear. For the small discrete scatterers, however, the nonlinear inverse scattering problem of the TIRT can be solved by an analytical and noniterative method. The proposed method is fast in the sense that no associated forward problem is iteratively evaluated. In addition, there is no convergence problem involved. The positions of discrete scatterers are determined by the multiple signal classification (MUSIC) method [3]. After the spheres are located by the MUSIC method, the inverse problem of retrieving the polarization tensors is still nonlinear. Despite the nonlinearity, there are noniterative analytical algorithms for the problem [4,5]. The two-step least squares method used in this paper is a modified version of the method proposed in [5].

The orientations of electric dipoles induced in scatterers and their linear dependency are carefully analyzed under various polarizations of the illumination, so that the proposed MUSIC is able to locate correctly the scatterers. The paper also discusses the influences of the propagating and evanescent waves, the substrate, the separation of scatterers from the substrate surface, and the level of noise on the resolution of imaging. Various numerical examples have been carried out to test the effects of the aforementioned factors on the resolution of imaging.

In conclusion, the algorithm presented in this paper can be easily applied to solve other inverse scattering problems involving half-space reflection and transmission. For the inverse scattering problem in the framework of the total internal reflection tomography, the following conclusions are drawn:

1. The locations and polarization tensors of scatterers are obtained by MUSIC and least squares method. Since there is no iterative evaluation of associated forward scattering problems, the proposed method is computationally fast, compared with the numerical optimization approach.

2. Theoretical and numerical analysis indicates that the incidence with a mixture of TE and TM polarization is more effective for the MUSIC to locate the positions of scatterers than using only TE or TM incidence.

3. Compared with propagating waves, evanescent waves that are characterized with large transverse wave vectors help to improve the resolution, whereas they are vulnerable in presence of noise, especially when the scatterers are far from the surface of the substrate.

References
1. P. S. Carney and J. C. Schotland, "Theory of total-internal-reflection tomography, " J. Opt. Soc. Am. A, vol. 20, pp. 542–547, 2003.
2. K. Belkebir, P. C. Chaumet, and A. Sentenac, "Superresolution in total internal reflection tomography, " J. Opt. Soc. Am. A, vol. 22, pp. 1889–1897, 2005.
3. A. J. Devaney, E. A. Marengo, and F. K. Gruber, "Time-reversal-based imaging and inverse scattering of multiply scattering point targets, " J. Acoust. Soc. Am., vol. 118, pp. 3129–3138, 2005.
4. E. A. Marengo and F. K. Gruber, "Noniterative analytical formula for inverse scattering of multiply scattering point targets, "J. Acoust. Soc. Am., vol. 120, pp. 3782–3788, 2006.
5. X. Chen and Y. Zhong, "A robust noniterative method for obtaining scattering strengths of multiply scattering point targets, " J. Acoust. Soc. Am., vol. 122, pp. 1325–1327, 2007.

A Miniature 3.1-GHz Microstrip Band-pass Filter with A Suppression of Spurious Harmonic Using Multilayer-Technik and Defected Ground Structure Open-Loop-Ring (DGS)

A. Boutejdar[1], A. Omar[1], *Fellow IEEE*

[1]*Chair of Microwave Engineering University of Magdeburg, Germany*
E-mail: Ahmed.boutejdar@ovgu.de

Abstract — **H**igh-performance band-pass filter has been studied and exploited extensively as a key circuit block in modern wireless communication systems. The requirements of compact design, low insertion loss in the pass-band and high rejection in the stop band are necessary. To meet the requirements, much effort has been made to develop a variety of compact band-pass filters [1]. One of the most common methods for implementing a planar filter is to use DGS-coupled microstrip filters [1], [2]. In this paper, we design at first a cascaded band-pass filter, which is composed of 3 open-loop $\lambda/2$-resonators. The three elements are electromagnetic coupled as shown in Fig. 2. The simulated results of this cascaded band pass filter show a good result in pass band and in reject band. The Simulation results are depicted in Fig. 3, which show the response of a three-pole band-pass filter and hid dimensions. It can get the 3-dB attenuation pole frequencies f_1 at 0.5 GHz, f_2 at 4.2 GHz and the center frequency f_0 of the filter at 3.1 GHz. In order to develop and to minimize this planar three-pole microstrip band pass filter, two ideas are developed and implemented, the DGS-Technique and the coupling matrix-method [3]. Using DGS resonator on the ground structure, a compact filter with improved response has been realized as shown the Fig. 3. The second process will be done through coupling-matrix procedures [4]. The distance (s) between resonators will be mathematically searched and defined, thus, an improvement in reject band of this filter will be realized and the second harmonic will be suppressed. The new multiplayer-BPF has been fabricated and simulated on a substrate with dimensions of (0.57λg x 0.28λg). The substrate has a relative dielectric constant of 3.38 and a thickness of 0.813mm. The measurements show good consistency with the simulations. Therefore, it is expected that the proposed structure with its characteristics will be a strong candidate for applications in various integrated microwave circuits.
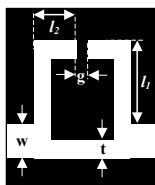
Figure 1. Layout of the open-loop cell.
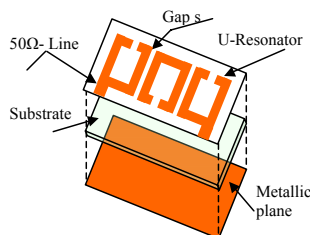
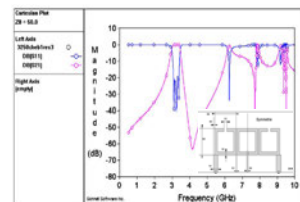Fig. 2. 3D-view of conventional BPF.

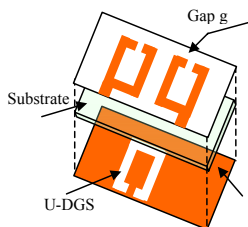Figure 3. Simulation results of the cascaded BPF .

Figure 4. 3-D view of the new BPF.

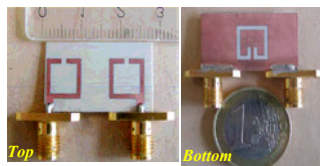

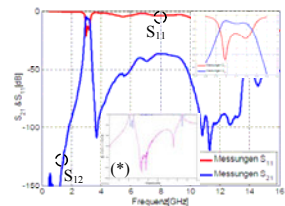Figure 5. Photogtaph of fabricated open-loop band-pass filter.

Figure 6. Mesured results of the proposed compact BPF. (*) Simulation results.

References
1.   Ahmed Boutejdar, Adel Elsherbini, A. Balalem, J. Machac and Abbas Sayed Omar , " Design of New Hairpin Microstrip Bandpass Filter Using Coupling Matrix Method and Defected Ground Structure(DGS) " 2007 Progress in Electromagnetics Research Symposium in Prague PIERS 2007. Prague, Czech Republic.
2.   J.-S. Hong, and M. J. Lancaster, *Microstrip Filters for RF/Microwave Applications*, Wiley, New York, 2001.
3.   A. Boutejdar, A. Elsherbini and A. Omar , "A Compact Microstrip Multi-Layer Lowpass Filter Using Triangle Slots Etched in the Ground Plane" Proc. 36th European Microwave Conference, Manchester, UK, September 2006.
4.   S. Amari, "Synthesis of Cross-Coupled Resonator Filters Using an Analytical Gradiant-Based Optimizatio Technique", *IEEE Trans. Microwave Theory Tech*., vol. 48, No. 9, pp. 1559-1564, Sep. 2000.

A Novel High Miniaturized Semi-Fractal Branch-Line Coupler using Loaded Coupled Transmission-Lines

M. Nosrati, M . Fealy

Department of Electrical and computer Engineering
of Ilam Azad University, Ilam, Iran

E-mail: nosrati_1359@yahoo.com

In this paper, a high-compact model of the loaded coupled transmission lines is introduced using employment of fractal technique on the previous proposed loaded coupled model in [6] for further size reduction in this type BLC. A novel miniaturized BLC is designed and analyzed at 900 MHz on a 0.762-mm-thick substrate with a relative dielectric constant $\varepsilon_r = 3.5$. Increasing of electrical and magnetic coupling and making the best use of the vacant space in the structure of conventional BLC are two important features of the new BLC. The size reduction of this new BLC has been reported about 79% with a comparable performance. The use of connecting lines as a cascade two unit elements instead of the internal series stubs is a useful method for increasing bandwidth in Digital elliptic filters [7]. The implementation of this method is more difficult in practice and needs suspended bars and dielectric shims. In [6], a loaded coupled transmission-line with maximized coupling has been introduced which has a simple structure for implementation and the same performance with a cascade of two unit elements. In this paper has been tried to expand this technique and reduce the size of this type BLC further by increasing of the cascade two unit elements. By this idea, the number of the lumped element in its equivalent circuit will be increase; particularly the negative capacitors and its size reduce. The frequency response of the compact BLC has been simulated by ADS full-wave simulator. Layout of the proposed compact model has been shown in Fig.1.
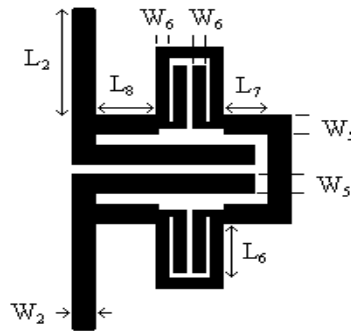
Fig. 1 – A Layout of the Proposed Compact Model

References
1. Kh. Hettak, G. A. Morin, M. G. Stubbs, "Compact MMIC CPW and Asymmetric CPS Branch-Line Couplers and Wilkinson Dividers Using Shunt and Series Stub Loading," *IEEE Trans. Microwave Theory & Tech.,* vol. 53, No. 5, pp. 1624-1635, May 2005.
2. S-S. Liao, P-T. Sun, "A Novel Compact-Size branch Line Coupler," *IEEE Trans. Microwave Theory & Tech.,* vol. 15, no. 9, pp. 588-590, September 2005.
3. R.W. Vogel, "Analysis and design of lumped and lumped-distributed element directional coupler for MIC and MMIC applications," *IEEE Trans. Microwave Theory & Tech.,* vol. 41, No. 9, pp. 2116-2125, December 1993.
4. Hirota, T.A. Minakawa, M. Murauchi, "Reduced-size Branch-Line and Rate-Race Hybrids for Uniplanar MMICs," *IEEE Trans. Microwave Theory & Tech.,* pp. 270-275, Aug. 2002.
5. C.Y. Ng, M. Chongcheawchamnan, M.S. Aftanasar, "Miniature X-band branch-line coupler using photo-imageable thick-film materials," *Electronic letters,*, vol. 37, No. 19, pp. 1167-1168, September 2001.
6. M. Nosrati, S.Karbasy, "A Novel Compact Branch-Line Coupler Using Four Coupled Transmission Lines," Accepted by microwave and optical technology letters, Jan.2007.
7. J. A. G. Malherbe, Ph.D. *Microwave Transmission Line Filters.* Artech House, 1979, pp. 24-26 and 71-79.

Bandwidth Enhancement and Further Size Reduction of a Class of Miniaturized Elliptic-Function Low-Pass Filter

M. Nosrati, S. Abbaspour and A. Najafi

Department of Electrical and computer Engineering
of Ilam Azad University

E-mail: nosrati_1359@yahoo.com

In this paper, a new model for further reducing the size and increasing the bandwidth (BW) of a class miniaturized elliptic-function low-pass filter has been presented. A compact elliptic-function low pass filter using microstrip stepped-impedance semi-hairpin resonators has been developed and a multiple cascaded filter using semi-hairpin resonators has been designed. The overall BW of the proposed low-pass filter has been shown to be increased by more than 40% with a size reduction about 80% compared with the conventional ones. In order to increase BW and reduce size, in this paper a developed model of the stepped-impedance hairpin resonator has been proposed. The layout of this low-pass filter is shown in Fig.1.
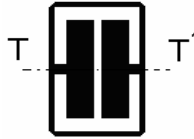
Fig.1- The Stepped-Impedance Hairpin Resonator

The prototype filter has been synthesized from the equivalent-circuit model and is shown this structure provides a wide band-pass with high harmonics suppression in a wide stop-band. To optimize the performance of this filter, electromagnetic simulation is used to tune the dimensions of the prototype filters.

the relationships between lamped and distributed elements have been derived using ABCD matrix and their equivalent-circuit models. Several different microstrip low-pass filters using different stepped-impedance semi-hairpin resonators which were designed at 3-dB cut-off frequencies f_1, f_2 and f_3 GHz respectively. Finaly, a multiple cascaded wide-band low-pass filter has been designed and proposed using these different microstrip filters. The proposed low-pass filter has a 3-dB pass band from dc to 3.26 GHz. The return-loss is better than -12 dB and the rejection greater than 30 dB within stop-band.

References

1. J.T.Ku , M.J.Maa and P.H.Lu , "A microstrip elliptic-function filter with compact miniatorized hairpin resonator" Phil. Trans. Roy. Soc. London, vol. A247, pp. 529–551, IEEE microwave Guided wave lett.vol.10 , PP.94_95 , Mar 2000 .
2. F.Giannini , m.Salerno and R.Sorrentino, "Design of low-pass elliptic filters by mean of cascaded Microstrip rectangular elements, " IEEE Trans.Microwave Theory Tech., vol.30, pp.1348-1353, sept.1982.
3. S.Y.Lee and C.M.Tsai, "New cross-coupled filter design using improved hairpin resonator," IEEE Trans.Microwave Theory Tech., vol.48,pp.2482-2490, Dec. 2000.
4. D.Ahn,J.S.Park,C.S.Kim, J.Kim,Y.Qian and T.Itoh, "A design of the low-pass filter using the novel microstrip defected ground structure," IEEE Trans.Microwave Theory Tech., vol.49,pp.86-92,Jan.2001.
5. L-H. Hsieh, K.Chang, "Compact elliptic-function low-pass filters using microstrip stepped-impedance hairpin resonators, " IEEE Trans.Microwave Theory, vol.51, no.1, pp.193-199, Jan.2003.
6. M.Nosrati, A.Najafi, "A Novel High Compact Elliptic-Function Low-Pass Filter" IEEE Applied Electromagnetics Conference,Dec.2007.

UWB - 10
UWB - Modeling & Simulation #2

Oral Presentations

UWB Detection of a Scattering Object inside a Non-Homogeneous Region

C. Buccella, V. De Santis and M. Feliziani

Department of Electrical and Computer Engineering, University of L'Aquila, 67040 Roio, L'Aquila, Italy
E-mail: buccella@ing.univaq.it, desantis.valerio@ing.univaq.it, felizian@ing.univaq.it

Recently, considerable attention has been given to the ultra-wideband (UWB) technology. There are several areas in which UWB technology can be applied, such as communication systems, automotive collision-detection systems, medical imaging, ground-penetrating radar etc. Here, due to its extremely wide bandwidth suitable to perform accurate imaging of objects, the UWB technology is applied to detect a target object embedded in a non-homogeneous field region. The detection is not trivial, since the field backscattered by the target can be confused with the reflections produced by the discontinuities in the field domain. A numerical approach is therefore proposed to solve this kind of problem by using an approach derived by previous studies on Time Domain Reflectometry (TDR) [1]-[2]. The field is analyzed by a numerical electromagnetic solver and the sensed signal is filtered by the discrete wavelet transform (DWT).

First, a two dimensional configuration of a non-homogeneous region is analyzed by the finite difference time domain (FDTD) method. The computational domain is composed by several regions (Ω_0, Ω_1, Ω_2,...) and by a scattering region Ω_s, whose electrical characteristics differ significantly from those of the other regions, as shown in Fig. 1. The UWB signal has rise times of few picoseconds and pulse durations of hundred picoseconds resulting in a spectral shape smeared out over a wide range of frequencies, from few megahertz to ten gigahertz. The use of the FDTD requires a closed domain where absorbing boundary conditions are applied. The cell size Δ must be less than one tenth of the minimum wavelength λ of the considered signal, $\Delta \le \lambda/10$. The time step Δt must be compliant with the stability criterion: $\Delta t \le \Delta/2c$. Obviously, the computational cost is strongly dependent on the physical dimensions of the considered domain. When an enclosure Ω_s, embedded in the computational domain, is excited by the UWB field, a backscattered field is generated. The signal can be monitored at a given point P, where it appears as the sum of different contributions given by the incident field, the reflected fields by the several regions and the scattered field produced by Ω_s. To detect the target scatterer, it is therefore crucial to discriminate the different reflections. To this aim the DWT can be applied to the captured signal in P in order to extract the approximation coefficients. For many signals, the low-frequency content provides the identity of the signal, while the high-frequency content gives flavour or nuance. Wavelet analysis lets us to capture these two different aspects of a signal, i.e. approximations and details. The approximations and details may be extracted using a discrete sampling or successive filtering techniques. To extract the approximations and details as independent signals, we can pass the signal through a pair of complementary low-pass and high-pass filters to get two different signals [3]-[4]. The low-pass filter yields the first level approximation coefficient and the high-pass filter yields the first level detail coefficient. Repeating the filtering and the downsampling, higher order-level approximation and detail coefficients are extracted, so they clearly allow to estimate the presence and the size of the discontinuities, as shown in Fig. 2.
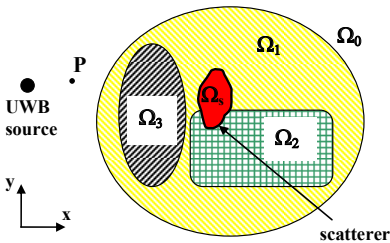

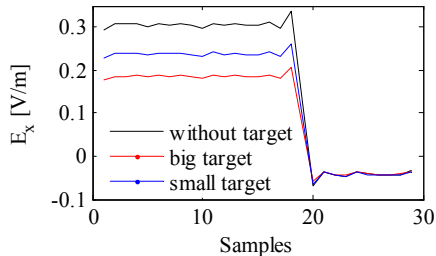**Fig. 1 – Computational domain.**

Fig. 2 – Example of DWT extraction.

References
1. C. Buccella, M. Feliziani and G. Manzi, "Detection and localization of defects in shielded cables by time-domain measurements with UWB pulse injection and clean algorithm postprocessing," *IEEE Trans. on Electromagnetic Compat.*, vol: 46, no. 4, pp. 597- 605, Nov. 2004.
2. C. Buccella, M. Feliziani and G. Manzi, "Accurate detection of low entity cable faults by wavelet transform," *Proc. of the IEEE International Symposium on Electromagnetic Compatibility*, 9-13 Aug. 2004, vol. 3, pp. 936- 941, 2004.
3. C. K. Chui, *An Introduction to Wavelet.* Boston, MA, Academic Press, 1992.
4. G. S. Burrus, R. A. Gopinath and H. Guo, *Introduction to Wavelet and Wavelet Transform. A Primer,* Upper Saddle River, NJ: Prentice-Hall, 1998.

Characterisation of default in Power Network Using Wavelet Transform

H Harrat[1], B Nekhoul[1], S Kaouche[1], K Kerroum[2] and K El Khamlichi Drissi[2]

[1]*LAMEL Laboratory, Jijel University, Jijel, Algeria*
[2] *LASMEA Laboratory, Blaise Pascal University, Clermont Ferrand, France*
E-mail: haroun_harrat@hotmail.com

The quality of the electric power is becoming an important issue for electric utilities and their customers. The quality of the electric power is largely synonymous with the voltage quality and the continuity of the service. The general strategy to assure the continuity of the service of the power supply is based in the detection in real time of the defect affected the power network. Generally the defects appear less often in equipments (transformers) and most of the time in power line. For this reason it's essential to control the state of the power line. Classically, using the TDR (Time Domain Reflectometry) technique it's possible to localize the defect in line or cable. Also, wavelet analysis is used in many areas of engineering and is specifically suited for examining non stationary phenomena. Since a few years, some works devoted to the analysis of signal records (voltages and currents) made on power networks by the wavelet technique are published in the literature [1]. Usually these works are to isolate in time frequency industrial of the frequencies caused by a defect. This allows us to locate in time the appearance of failure and it's rang frequency.

In our work we propose a procedure for localization in space and in time by TDR and discrete wavelet transform (DWT), and identification of the defect nature in power network by traveling wave. Also using continuous wavelet transform (CWT) we deduce the dominant frequency in instant where appears the defect.

For this study we treat and deduce few information's in the power network response without and with defect. At first, it's essential to know the response of the power network excited by impulse voltage. For this objective we use the temporel formalism proposed by S. Kaouche [2]. This formalism consists in translating the nature and the topology of the network in a matrix [A] making appear the lines and the set of the localized networks (nods of extremities and junctions). This procedure allows us to elaborate a system of linear equations: [A] x [X] = [B], where: [X] : unknown vector (currents and nodes' voltage) and [B] : source vector.

The technique of the TDR and the response analysis by wavelet intervene subsequently. The steps of the proposed procedure are described in the following: (1) - localization of a defect in space and in time in an electric network by TDR and discrete wavelet transform (DWT), (2)- identification of defect nature by travelling wave, (3)- the continuous wavelet transform (CWT) is applied to the difference of the responses (without and with defect) of the network in order to obtain a dominant frequency.

In order to illustrate our work we present the first simple application. We consider 3 tri-phase power horizontal lines connected in Y (figure 1.a) with two defects at two different points (E and F) . The double defect is a galvanic contact of 15Ω between the phase 1 of the line 3 and the soil and situated in the F point to 430 m of the interconnection (bus bar) and a short circuit between the phase 1 of the line 2 and soil situated to the point E to 350 m of the node interconnection.
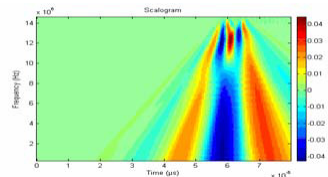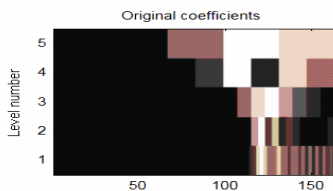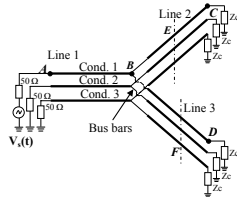

Fig.1.a Power network in Y.   **Fig.1.b. Spectrogram of the coefficients.**   **Fig.1.c. Scalogram wavelet time- frequency.**

Figures 1.b. and 1.c show the analysis by the wavelet transform of the difference network responses in point A (without and with defect) when we use the Gaussian generator voltage Vs (t). These results put in evidence the presence of two reflections due to the changes of the lines impedances in power network. The first reflection in figure 1.b at t=5.66μs (position 116 in spectrogram) traduces the short circuit default; in fact, the calculating of the reflection coefficient at the time of the first oscillation gives value of -1. The second reflection at t=6.2μs (position 127 in spectrogram) traduces galvanic contact where the reflection coefficient gives values of -0.939 and fault resistance of the 14.75Ω. To supplement our analysis we conduct an analysis of the CWT (fig. 1.c). The optimum of the coefficients norm is realized respectively where frequency value is 2.73 MHz for first default and 1.7MHz for second.

1.   C. Buccella, M. Feliziani and G. Manzi, " Accurate Detection of Low Entity Cable Faults by Wavelet transform," International Symposium on Electromagnetic Compatibility : EMC August 9-13 , 2004 Santa Clara, Cuba, pp. 936-941.
2.   S. Kaouche, ''Analyse de Défauts dans un Réseau de Lignes ou de Câbles'', PHD thesis, Université of Jijel, June 2007.

UWB - 11
UWB - Wavelets & Multi Resolution Algorithms

Oral Presentations

UWB - 11
UWB - Wavelets & Multi Resolution Algorithms

Oral Presentations

Artificial Neural Network Application for Digital Image Processing

V.G. Spitsyn[1], Y.R. Tsoy[2]
[1,2]*Tomsk Polytechnic University, Tomsk, Russia*
E-mail: spvg@tpu.ru

The real-time automatic images processing and pattern recognition are very important for many problems in medicine, physics, geology, space research, military applications and so on. For example, it is necessary for pilots and drivers for immediate decision-making in poor visibility conditions. An approach to image enhancement through artificial neural network's (ANN) processing is proposed. The structure and weights of ANN are tuned with use of evolutionary concept [1]. We introduce the method for images enhancement through approximation of image transform function T. This function is approximated with use of ANN which is trained evolutionary in the time of test images processing. Each ANN is genetically encoded as the list of its connections. Truncation selection is used for parental subpopulation formation. Original crossover and mutation operators, which respect structures of the ANNs undergoing recombination and mutation, are used. Nodes with sigmoid activation functions are considered. The population size adapts to the properties of evolution during the algorithm run using simple resizing strategy. In this work we adopt pixel-by-pixel brightness processing with use of ANN paradigm. The topology of ANN is tuned simultaneously with connections weights. The ANN approximating T function should have three input nodes and one output node. During the training we evaluate each ANN with respect to the visual quality of the processed images. For acceleration of image processing is applied the approximate calculation of the local statistics for every pixel [1].

The three-step procedure for image enhancement is proposed: (1) multiplicative adjustment of image brightness; (2) local level processing using ANN; (3) global level auto smoothing algorithm. The artificial neural network training stage with use of single 128x128 pixels image takes about 70 seconds on the Intel Pentium IV 3 GHz processor. After completion of the learning process the obtained artificial neural network is ready to process arbitrary images that were not presented during the training. The processing time for 512x512 pixels image is about 0.25 second. The ANN, as a rule, included 3 input nodes, one or more hidden nodes and one output node. The results of initial images [2] (see Fig. 1, 3, 5, 7) enhancement after applying the three-step processing is presented below (see Fig. 2, 4, 6, 8). It is significant that the three-step method has the small computing complexity in comparison with the algorithm of Multi-Scale Retinex [2], [3]. This method is allows using the trained ANN with acceptable rapidity processed the packets of images. The speed of image processing with used of Intel Pentium IV 3 GHz processor is amount to 1 Megapixel in second.

| Fig. 1 | Fig. 2 | Fig. 3 | Fig. 4 |

| Fig. 5 | Fig. 6 | Fig. 7 | Fig. 8 |

References
1. Y.R. Tsoy, V.G. Spitsyn, "Digital images enhancement with use of evolving neural networks," Lecture Notes in Computer Science, vol. 4193, 2006.
2. Test images: http://dragon.larc.nasa.gov.
3. G.A. Woodell, D.J. Jobson, Z. Rahman, G.D. Hines, "Enhancement of imagery in poor visibility conditions," Proceedings of SPIE, vol. 5778, 2005.

Ultrawideband Electromagnetic Pulse Propagation in a Double-Resonance Lorentz Model Dielectric

K. E. Oughstun

College of Engineering & Mathematical Sciences, University of Vermont, USA
E-mail: oughstun @cems.uvm.edu

The propagation of an ultrawideband electromagnetic pulse through a linear, dispersive attenuative dielectric medium described by the Lorentz model with two isolated resonance frequencies is presented in the context of the classical [1-3] and modern asymptotic theories [4] as generalized by Shen and Oughstun [5]. The analysis is based on the asymptotic approximation as $z \to \infty$ of the exact Fourier-Laplace integral representation of the propagated wave field, given by [4]

$$A(z,t) = \frac{1}{2\pi} \Re\left\{ i e^{-i\psi} \int_C \tilde{u}(\omega - \omega_c) e^{(z/c)\phi(\omega,\theta)} d\omega \right\} \tag{1}$$

for all $z \geq 0$, where

$$\phi(\omega,\theta) \equiv i\frac{c}{z}\left(\tilde{k}(\omega)z - \omega t\right) = i\omega\left(n(\omega) - \theta\right) \tag{2}$$

is the complex phase function describing the dynamical space-time evolution with $\theta \equiv ct/z$ and where $\tilde{k}(\omega) \equiv (\omega/c)n(\omega)$ is the complex wave number. The earlier asymptotic description [5] of dispersive pulse propagation in a double resonance Lorentz model dielectric showed that the inclusion of an additional resonance feature in the dielectric permittivity resulted in the conditional appearance of a new, intermediate frequency precursor field structure $A_m(z,t)$ in the propagated wave field $A(z,t)$ in addition to the high-frequency Sommerfeld $A_s(z,t)$ and low-frequency Brillouin precursor $A_b(z,t)$ fields previously described in the classical and modern theories [1-4]. The propagated wave field structure is then described by the coherent superposition

$$A(z,t) = A_s(z,t) + A_m(z,t) + A_b(z,t) + A_c(z,t), \tag{3}$$

where $A_c(z,t)$ describes the contribition of any poles that may be present in the input pulse spectrum. If the envelope function $u(t)$ of the initial pulsed plane-wave field $A(0,t) = u(t)\sin(\omega_c t + \psi)$ is bounded for all time t, then its frequency spectrum $\tilde{u}(\omega)$ can have poles only if $u(t)$ does not tend to zero too fast as $t \to \infty$. Hence, the implication of nonzero $A_c(z,t)$ is that the total propagated wave field $A(z,t)$ oscillates with angular frequency ω_c for positive time t at $z = 0$ and will tend to do the same for $z > 0$ for large enough t. This contribution then describes the main signal evolution in the dispersive material. The dynamical space-time evolution of each precursor field structure can be traced to the dynamical evolution of the saddle points of the complex phase function $\phi(\omega,\theta)$ and so are a characteristic of the dispersive medium. A sufficient condition for the appearance of this middle precursor was also given there [5] in terms of the energy transport velocity for a time-harmonic wave. These results are extended in this paper through a careful examination of the middle saddle point dynamics and their asymptotic contribution to the middle precursor field. The critical importance of these middle saddle points is fully realized when the input pulse spectrum is centered in the passband between the two resonance frequencies, as typically occurs for optical pulses. In that case, these middle saddle points provide the majority of the observed pulse distortion.

References
1. A. Sommerfeld, "Über die fortpflanzung des lichtes in disperdierenden medien," Ann. Phys., Vol. 44, 177-202, 1914.
2. L. Brillouin, "Über die Fortpflanzung des Licht in disperdierenden Medien," Ann. Phys., Vol. 44, 203-240, 1914.
3. L. Brillouin, Wave Propagation and Group Velocity. New York: Academic Press, 1960.
4. K. E. Oughstun and G. C. Sherman, Electromagnetic Pulse Propagation in Causal Dielectrics, Berlin-Heidelberg: Springer-Verlag, 1994.
5. S. Shen and K. E. Oughstun, "Dispersive pulse propagation in a double-resonance Lorentz medium," J. Opt. Soc. Am.

UWB - 12
UWB - Propagation

Oral Presentations

Analysis of an Ultra Wide and Impulse Radio over Multimode Fiber Ranging System with Experimental Validation

J. George, D. Thelen, A. Chamarti, A. Ng'oma, and M. Sauer

Science and Technology, Corning Incorporated., Corning, NY-14831, USA

E-mail: GeorgeJ@corning.com

Ultra Wide Band-Impulse Radio (UWB-IR) based systems are well known for their inherent capability to provide accurate ranging [1 and 2]. Remote positioning of such systems using radio over multimode fiber technology has been the interest of researchers lately [3 and 4]. The advantages of such systems are two fold: i) the range extension of UWB-IR to greater indoor coverage distances, and ii) cost benefits resulting from the consolidation of head end equipment.

In this paper, we describe the details of a system model for evaluating the performance of a ranging system employing UWB-IR over multimode fiber. Such a system has two distinct parts; i) a wireless section, including antennas and wireless propagation through air, and ii) a Radio over MultiMode Fiber (RoMMF) section, including Electrical to Optical (E/O) conversion, propagation through fiber, and Optical to Electrical (O/E) conversion. This model combines wireless and radio over fiber [5] sections of the system to predict system performance in terms of Bit Error Ratio (BER).

Fig. 1 shows the calculated contours of constant BER of a UWB-IR over a multimode fiber ranging system. The most interesting result is the dominant impact of wireless distance, in comparison to fiber length, on performance. The results shown in the figure are verified by experimental results that demonstrate accurate ranging capability of UWB-IR over 150 m length of multimode fiber. This verification process used the PulsOn 210™ UWB radios from Time Domain Corporation [6]

In the presentation, we will describe the details of the system model and the experimental procedure used for validating the performance evaluation model, and provide some crucial experimental validation data.
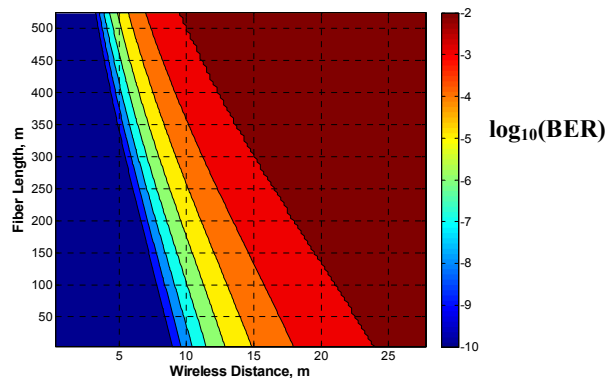
Fig. 1 – Contours of constant BER for a RoMMF based UWB-IR ranging system

References

1. S. Gezici, Z. Tian, G. B. Giannakis, H. Kobayashi, A. F. Molisch, H. V. Poor, and Z. Sainoglu, "Localization via ultra-wideband radios: a look at positioning aspects for future sensor networks," *IEEE Signal Processing Magazine*, vol. 22, no. 4, pp. 70-84, 2005.
2. S. J. Ingram, D. Harmer, and M. Quinlan, "Ultra-wideband indoor positioning systems and their use in emergencies," *Position Location and Navigation Symposium*, pp. 706-715, April 2004.
3. M. Y. Wah, C. Yee, and M. L. Yee, "Wireless ultra wideband communications using radio over fiber," *IEEE Conf. Ultra Wideband Systems Tech.*, pp. 265-269, 2003.
4. B. Luo, L. C. Ong, M. L. Yee, Y. X. Guo, M. Y. W. Chia, "Centralized UWB/WLAN distribution network using low cost radio over multimode fiber technology," *IEEE Veh. Technol. Conf.*, pp. 799-801, 2005.
5. M. Sauer, A. Kobyakov, and J. George, "Radio Over Fiber for Picocellular Network Architectures", *IEEE/OSA J. Lightwave Tech.*, pp. 3301-3320, November 2007.
6. http://timedomain.com/

Impulse Response of the convex objects placed very close to each other.

Piotr Górniak, Wojciech Bandurski
Poznań University of Technology, Poznań, Poland
Poznań University of Technology, Poznań, Poland
E-mail: pgorniak@et.put.poznan.pl

We deal with time domain (TD) modeling of a diffraction caused by convex objects. We do it for the purpose of deterministic UWB channel modeling for the channel with convex objects. Among the examples of such objects are round buildings, round pillars in buildings or rounder corridors in buildings. We consider the diffraction on convex objects for the case, when more than one such object are placed very close to each other in the way that one convex object is in the transition zone of another scattering object. This is the situation when slope diffraction is the key factor and can not be omitted. The model of transition zone diffraction on convex objects was discussed in the frequency domain (FD) in [1]. When the UWB signal propagation is taken into account the time domain modeling is the right choice. In the paper first we derive the closed form of the impulse response of the channel formed by perfectly conducting convex objects situated very close to each other shadowing transmitter and receiver. We do it basing on the Uniform Theory of Diffraction (UTD) formulated in the frequency domain. The frequency response of the channel is transformed into the time domain with the usage of inverse Laplace transform and on-sided inverse Fourier transform. The obtained impulse response is used to examine the UWB pulse distortion caused by the channel, focusing on the influence of the slope diffraction on the shape of the distorted pulse. Then we extend the time domain model of the channel for the case of non perfectly conducting convex objects. The derived time domain formulations is verified by comparing the results of the convolutions of the impulse response of the channel and an exemplary UWB pulse with the results of frequency domain calculations with the usage of Inverse Fast Fourier Transform (IFFT).
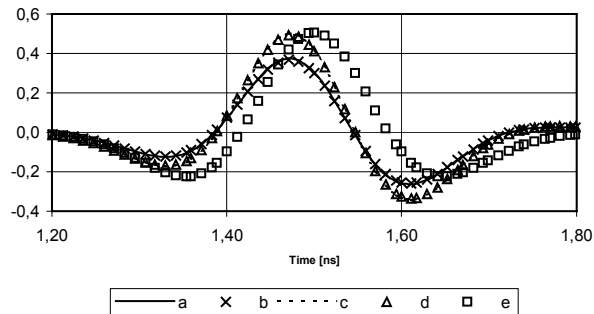
Fig. 1 – UWB pulse distortion on two perfectly conducting convex objects - (the distance from the point where a creeping ray leaves the first convex object to the point where the ray "become attached" to the second convex object is equal $0.08R_{HI}$, where R_{HI} is the radius of the first convex object) : distorted UWB pulse without including slope diffraction, IFFT results – a, convolution results – b, distorted UWB pulse with slope diffraction included, IFFT results – c, convolution results – d, normalized transmitted UWB pulse.

References

[1] G. Koutitas, A UTD Solution for Multiple Rounded Surfaces, IEEE Transactions on Antennas and Propagation, vol. 54, no. 4, April 2006, pp 1277-1283.

UWB - 12
UWB - Propagation

Oral Presentations

Oral Presentations

Adaptive Turbo Equalization Scheme for Wireless ISI Channel

Anindya Kundu[1], Soham Ghosh[2], Binay Kumar Sarkar[1], Ajay Chakrabarty[1]
Kalpana Chawla Space Technology Cell (KCSTC)[1]
Dept. of Electronics & Electrical Communication Engineering
Indian Institute of Technology, Kharagpur – 721 302
Ph: 03222-282298/99; Fax: 03222-282299
Department of Electronics Communication Engineering (ECE)[2]
Netaji Subhash Engineering College, Kolkata-700152, West Bengal
Email: akundu@ece.iitkgp.ernet.in, ghosh_soham@yahoo.co.in

Abstract: From the viewpoint of a communication engineer we find problem arises when the propagation conditions over the transmission channel vary with respect to time. The state of art technology to prevent this effect due to time variation is equalization, a well known method for removing Inter Symbol Interference (ISI) affecting a transmission channel[1,5]. Recent literatures shows a trend to mitigate this effect, decision feedback sequence estimation technique[1,2,5] by truncating the channel memory to a reduced number of terms and by removing the branch matrix tail of the ISI using decision made on the surviving sequence. Here we show a different class of idea from seminal principle of Turbo-Decoding[3-5], which can be applied to equalization.

The basic principle underlying turbo equalization[2] is that an ISI wireless channel can be regarded as convolutional coder & therefore the concatenation of a coder, an interleaver & the transmission channel itself can be considered as a turbo coder. The adaptive equalizer combines a maximum posteriori channel equalizer with a recursive least square algorithm to allow adaptation in the equalization stage. This stage iterates with a soft input, soft output & error correction stage. Here we have tested the adaptive ability of equalizer on unknown time invariant & time varying ISI wireless channel by computer simulation on a Matlab platform.

From the outcome of the simulated result it can be seen that it is one of the best methods for getting the information back from the often heavily scrambled & distorted received signal[2-5]. This scheme tracked unknown wireless channels accurately without a penalty in terms of signal to noise ratio (SNR).

In this paper we will show the implementation of the concepts in a MATLAB platform & measure the performance & display as bit error rate in comparison to SNR.

References

1. S.Ariyavisitakul and L.J. Greenstein, "Reduced Complexity Equalization Techniques for Broadband Wireless Channels", IEEE Journal on Selected Areas in Communications 15(1):5 15, January 1997.
2. S. Ariyavisitakul, N. R. Sollenberger and L.J. Greenstein, "Tap Selectable Decision Feedback Equalization" IEEE Transactions on Communications, 45(12):1497 1500, December 1997.
3. C. Berrou, A. Glavieux, P. Thitimajshima. "Near Shannon Limit Error-Correcting Coding and Decoding: Turbo-Codes." IEEE International Conference on Communications, Geneva, Technical Program, Conference Record,vol. 2, pp.1064-1070, May 1993.
4. C. Berrou, M. Jezequel, C. Douillard, S. Kerouedan. "The Advantages of Non-Binary Turbo Codes." IEEE Information Theory Workshop, Proceedings, pp.61-63, 2001.
5. D.N. Doan, K.R. Narayanan. "Some New Results on the Design of Codes for Inter-Symbol Interference Channels Based on Convergence of Turbo Equalization." IEEE International Conference on Communications, vol. 3, pp.1873-1877, 2002.

Ultra Wideband Propagation Loss Around a Human Body
in Various Surrounding Environments

Hironobu Yamamoto[1,2] and Takehiko Kobayashi[1,2]

[1]*Tokyo Denki University, Tokyo, Japan*
[2]*National Institute of Information and Communications Technology, Yokosuka, Japan*

E-mail: h.yamamoto@grace.c.dendai.ac.jp

Ultra wideband (UWB) technologies have been anticipated for use in wireless body area networks (WBAN) because of their low power consumption and anti-multipath capabilities. A number of measurements have been carried out to characterize UWB propagation in the WBAN scenarios [1]. Most of the previous studies, however, have not evaluated the effects of surrounding environments. In this paper, UWB path losses were measured between on-body antennas (a fixed transmitting antenna and a receiving antenna placed on a grid on a body surface) in three different surrounding environments. The environments included a 7-m radio anechoic chamber (approximately 240 m^3), a classroom (6.6 m wide × 4.3 m depth × 2.5 m height = 71 m^3) and a small room (2.6 m wide × 2.7 m depth × 2.3 m height = 16 m^3). The radio anechoic chamber can be considered as a room extending with an infinite volume in terms of radio propagation. Commercially-available UWB meander line antennas [2] were used for transmission and reception. The transmitting antenna was fixed on the back waist of a volunteer (an adult male, 1.75 m tall, and 60 kg) placed at height of 940 mm from the floor and separated 20 mm apart from the body surface. The receiving antenna was placed at 100-mm intervals on the body. When the receiving antenna was placed on the back of the body, the path was roughly line-of-sight (LOS); and when in the front, it was non-LOS (NLOS). Frequency domain (from 3.1 to 10.6 GHz) path losses were measured with a vector network analyzer between the antennas; and UWB path losses were calculated by integrating the power of the path losses over the occupied bandwidth. The distributions of UWB path losses are shown in Fig. 1. The cases of the small room, particularly NLOS, yielded higher reception power than the cases of larger rooms. This was attributed to the ample multipath from the nearby floor, wall, and ceiling. The maximums, minimums, and medians of the path losses of UWB and CW (6.85 GHz) measured in the three environments were derived, as shown in Fig. 2. The variation ranges in UWB were smaller than ones in CW (in particular, 20-dB smaller in NLOS). This is because nulls caused by interference were cancelled out by the ultrawide bandwidth. The results indicate that UWB technologies are more advantageous than narrowband ones from the viewpoint of reducing fading margins, although frequency selective fading inevitably takes place.
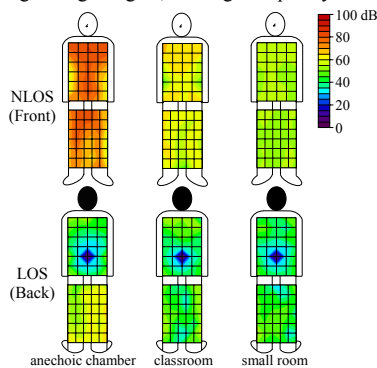
Fig. 1 – The distributions of UWB path losses in three environments.
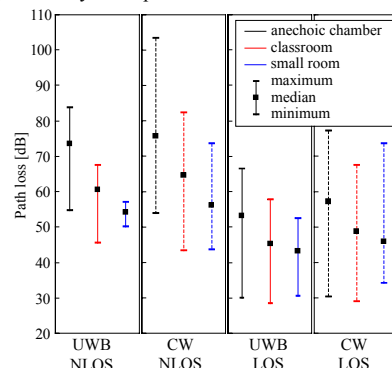
Fig. 2 – The maximums, minimums, and medians of UWB and CW path losses in three environments.

References
1. P. S. Hall and Y. Hao (eds), *Antennas and Propagation for Body-Centric Wireless Communications*, Boston, MA: Artech House, 2006.
2. SkyCross Inc., "3.1 - 10 GHz ultra-wideband antenna," http://www.skycross.com/Products/PDFs/SMT-3TO10M-A.pdf.

UWB - 12
UWB - Propagation

Oral Presentations

Modelling of Electromagnetic Waves Propagation in the Flows of Turbulent Plasma Inhomogeneities

V.G. Spitsyn[1], I.V. Fedotov[2]

[1,2]*Tomsk Polytechnic University, Tomsk, Russia*

E-mail: spvg@tpu.ru

There are considered the numerical models of electromagnetic waves multiple interactions with moving turbulent inhomogeneities in the flows of slightly ionized plasma. We supposed that the turbulent inhomogeneities in a flow of slightly ionized plasma are corresponded to the statistically independent discrete scatterers. To the analysis of this problem a method of stochastic modeling is applied [1], [2]. There are employed the different geometries of the flow: sphere, cylinder, cone and paraboloid. The indicatrix of turbulence over-radiation are supposed by isotropic, Lambert and quasi-mirror types. The waves propagation in the spherical and cylindrical turbulent flows are researched. We modelling of wave propagation in widen spherical cloud of scatterers moving along the radius of sphere. The wave propagation in the cylindrical turbulent flow with inhomogeneous profiles of velocity and concentrations of turbulences is considered. In the results of computations we received the angular and frequency spectrums of multiply scattering signal.

We investigated the scattering of electromagnetic wave on the turbulent plasma inhomogeneities disposed near the body of revolution surface in a view of cone and paraboloid. Here is implemented the modelling of multiply wave scattering on the inner surface of turbulent flow. The turbulent inhomogeneities are moved along the generatrix of body rotation. On the base of computation we received that the increasing of equation order described the scattering surface is reduced to the focusing of signal energy near the axis of body rotation. The comparison of calculated frequency spectrum of scattering signal with the experimental data of radio sounding followed to exhaust plume of space vehicle [3] shoves the good accordance (see Fig. 1, calculated results - dashed and dotted curves, experimental results - full curve). On the base its comparison we do the conclusion about the realized in indicated experiment of the radio wave multiply scattering on the inner surface of the turbulent plasma body of rotation.

There is developed a three-dimensional stochastic model of electromagnetic wave multiply scattering in the stratified random discrete media, including the inhomogeneous flow of scatterers in a view of parallelepiped [4]. Here is considered the source of electromagnetic signal with isotropic indicatrix of radiation, which disposed on the surface of stratified media in the point with coordinates $x = 0, y = 50, z = 50$. In the Fig. 2 shows the results of calculation the distribution of energy absorbing in stratified media, including the semitransparent object. Here we can see the missing of energy wave inside of the object because the coefficient of wave absorption in this area is very small. In the Fig. 3 is presented the result of computation of energy scattering signal in the media. Here we can see that the photons are registered in the area of object shadow. This result is explained by the chaotic direction of moving photons in the media after acts of scattering on the discrete inhomogeneities. We has been received the increasing of width of scattering signal frequency spectrum (see Fig. 4), which is explained by the multiply interaction of wave with moving scatterers of flow.
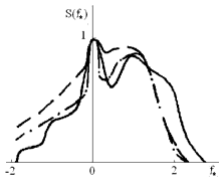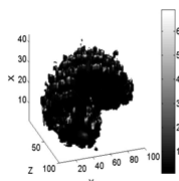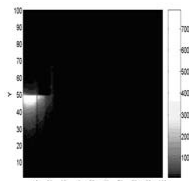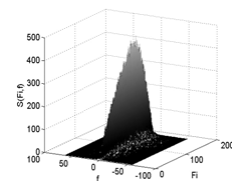
| Fig. 1 | Fig. 2 | Fig. 3 | Fig. 4 |

References
1. V.G. Spitsyn, "Development of a numerical model concerning electromagnetic wave propagation in turbulent flows," Journal of Applied Electromagnetism, vol. 1, 1997.
2. V.G. Spitsyn, Modelling of radiowave scattering on the ionospheric plasma disturbances created of spacecraft. Moscow: Physmatlit, 2003.
3. J.S. Draper, P.O. Jarvinen, T.D. Conley, "Analysis of radar return from turbulent high–altitude rocket exhaust plumes," AIAA Journal, vol. 8, 1970.
4. V.G. Spitsyn, I.V. Fedotov, "Stochastic model of electromagnetic wave propagation in stratified media including the semitransparent object and inhomogeneous flow of scatterers ," Proceedings of SPIE, vol. 6522, 2006.

Ultra - Wide Band Box Shaped Loaded Monopole Antenna

I.D. Zivkovic

HES-SO Valis
Route du Rawyl 47, 1950 Sion, Switzerland

Email: Irena.Zivkovic@hevs.ch

In recent years, there is a high demand for antennas that can operate over a large frequency range. Very popular antennas for using in ultra-wide band (UWB) mobile and wireless communication systems are monopole antennas. UWB monopole antennas are suitable candidates because they are unbalanced and also they are relatively convenient to match to 50 ohm. In this abstract, newly designed monopole antenna for UWB operation is proposed. Presented antenna is of low profile, simple structure and cheap and easy to manufacture.

Proposed antenna is mounted on the ground plane with coax probe feed. All antenna parts are made of 0.5mm thick copper. In Fig. 1. and Fig. 2., geometry of the proposed antenna is presented. The antenna consists of an 'empty' rectangular box that has five sides. The box is placed above ground plane on the piece of foam. The open side of the box is faced toward ground plane, with the top side parallel to the ground plane.

By using the same geometrical concept, broad family of antennas for operation in various frequency bands, can be designed. Antenna model 1 has box dimensions of 20x20x20 [mm] and ground plane size of 80x80 [mm]. In Fig. 3. measured VSWR of the fabricated antenna (antenna model 1) is shown. It is seen from the Fig. 2, that the antenna model 1 has VSWR less than 2.2 from 1.8 to 15GHz, which is 157% bandwidth. In Fig. 4. some simulated results of the antenna which box dimensions are 65x50x45[mm] and ground plane size 140x135 [mm] are presented. This antenna is optimized for multiband operation and has VSWR < 2 for frequencies from 0.6 to 1.2 GHz (67% bandwidth), from 2.05 to 2.75GHz (30% bandwidth), from 3.4 to 4.3 GHz (23% bandwidth) and from 4.8 to 6GHz (22% bandwidth).

In this abstract some measured and simulated results of the new antenna geometry are presented. An extensive parametric study of presented antennas is currently under way.
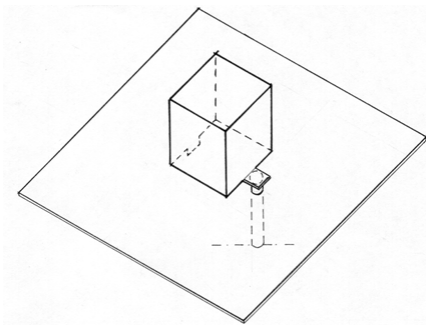
Figure 1: The geometry of the proposed antenna
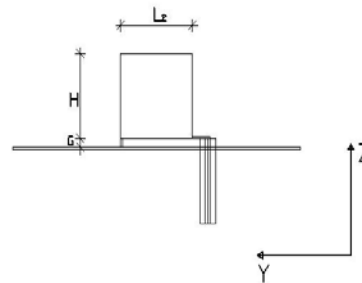
Figure 2: Side view of the proposed antenna
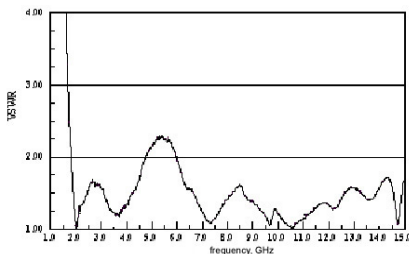
Figure 3: Measured VSWR of the antenna model 1
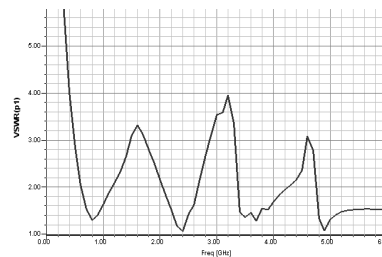
Figure 4: Simulated VSWR of the antenna model 2

UWB - 13
UWB Wire, Plate and Aperture Antennas

Oral Presentations

Investigation on the Phase Centre of Ultra Wideband Monopole Antennas with Band-Stop Functions

Abdelhalim Mohamed and Lotfollah Shafai

Department of Electrical and Computer Engineering,
The University of Manitoba, Winnipeg, Manitoba, Canada R3T 5V6

halim@ee.umanitoba.ca, shafai@ee.umanitoba.ca

To eliminate the interference between the existing and upcoming ultra wideband communication services, Ultra Wideband Antennas with band-stop functions are being investigated [1-3]. A common approach is to implement certain features in the antenna structure, like half wavelength slots at the centre frequency of the required stop-band, to cause resonances and current concentration around the features to eliminate radiation at the required frequencies. This paper investigates the effect of including such features on the phase centre behavior of the ultra wideband antennas. An antenna using a circular monopole of radius 20 mm at 1mm distance from a 120x120 mm^2 square ground plane is studied, as an example. Then, different slot features are included inside the circular antenna to create a stop-band at 5.5 GHz as its centre frequency. HFSS (High Frequency Structure Simulator Based on the Finite Element Method) is used for simulation of the configurations, and computation of the radiated field, and its phase for different θ ranges at φ = 0°, 45° and 90° planes. The antenna phase centre is determined as the origin of spherical waves, over the selected far field angular ranges [4]. It is found that certain feature shapes have small, or even beneficial, effects on the antenna phase centre behavior, while others deteriorate the performance. Examples of Phase centre location behaviors, for the θ range of 80°-90°, and in different φ-planes are shown in Fig. 1, along with their return loss curves. Complete results and other cases will be presented and discussed during the conference.
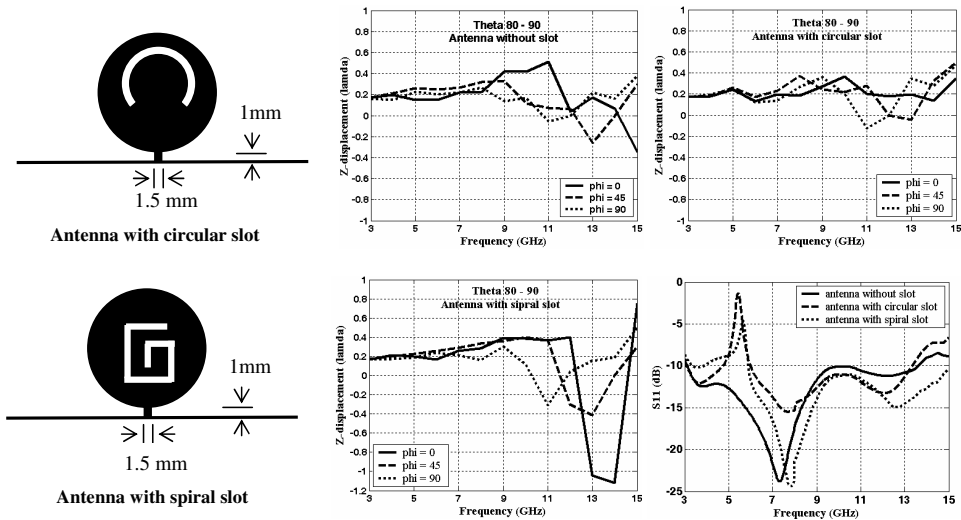
Fig. 1 - Phase centre locations and return losses for a circular monopole antenna without and with slots

References

1. A. Mohamed and L. Shafai, "Ultra wideband circular monopole antenna with spiral-slots for band-notch function", North American Radio Science Meeting (URSI), Ottawa, On, Canada, July 22-26, 2007.
2. A. J. Kerkhoff and H. Ling, "Design of a band-notched planar monopole antenna using genetic algorithm optimization," IEEE Trans. Antenna Propag., vol. 55, no. 3, pp. 604-610, March 2007.
3. J. K. Kim and S. Park, "Analysis of the small band-rejected antenna with the parasitic strip for UWB," IEEE Trans. Antenna Propag., vol. 54, no. 6, pp. 1688-1692, June 2006.
4. H. Moheb, A. Sebak and L. Shafai, "Phase centre analysis of array antennas and its significance for microwave landing system", IEE 7th International Conference on Antennas and Propagation (ICAP), pp. 213–216, April 15-18, 1991.

Low Impedance Bowtie Antenna

Stanley Henriquez[1], Marc Litz[1], Joseph Miletta[2], David Burns[1]
[1]*Army Research Laboratory, Adelphi, MD, USA*
[2]*DE Technologies,Sumerduck, VA, USA*
E-mail: Litz@arl.army.mil

This paper describes the approach taken to match a low impedance pulsed network to a folded bowtie antenna while providing a boresight gain greater than 6 dBi. The output of a 3-ohm transmission-line will be fed into this simple TEM structure, shown in figure 1. A variety of bowtie structures were modeled with FEKO, a commercially available hybrid finite-element and method-of-moments code. A parametric study of plate angle and plate shape (flare angle and length) was performed to optimize the impedance match for ~1.2 GHz frequency regime. An investigation of bowtie shape was performed to adiabatically adapt the pulsed network source impedance to that of free space. Preliminary measurements of system performance in a 50' x 30' x 25' anechoic chamber are described. The results measured compare well with those calculated.
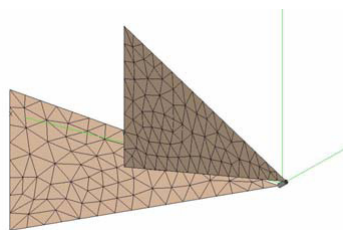
Figure 1. Folded bowtie antenna geometry.

The results of a bowtie, formed from 20-cm-long triangles (forming one-half of the bowtie structure), were compared for gain and impedance. These two parameters are considered the most important in this investigation. Table 1 shows the gain resulting from the parametric study of flare angle and plate separation at 1.2 GHz. The maximum calculated gain occurs when the plate separation angle is 120 degrees and the flare angle is 90 degrees. The load impedance of the antenna on the pulsed forming network is shown in Table 2 as a function of plate separation and flare angle. The acceptable impedance of 70 Ohms occurs when the plate separation is 60 degrees and the flare angle is 90 degrees. These results indicate that further studies and investigation should focus on geometries with characteristics that include the 90 degree flare angle and separation angle of 90 degrees ±60 degrees.

plate separation (deg)	flare angle (deg) 30	60	90
10	-3	-1	-1
60	2	2.5	3.9
120	5.5	5.5	6.1
170	5	5.1	5.1
180	4.5	4.6	4.4

Table 1. Gain calculated at 1.2 GHz as a function of plate angle and flare angle.

plate separation (deg)	flare angle (deg) 30	60	90
10	100	30	30
60	190	160	70
120	270	240	120
170	285	260	140
180	285	260	140

Table 2. Load impedance of bowtie calculated at 1.2 GHz as a function of plate angle and flare angle.

References
1. FEKO, EM Software & Systems (SA) Pty Ltd., 1998-2006.
2. K. Y. A. Lai, A Novel Antenna for Ultra-Wideband Applications, PhD. Dissertation, Ohio State University, 1990.
3. M. Manteghi, Y. Rahmat-Samii, A Novel UWB Feeding Mechanism for the TEM Horn Antenna, *IEEE Antennas and Propagation Magazine*, **vol. 46**, Issue 5, Oct. 2004, pp. 81-87
4. J.D. Kraus, Antennas, McGraw-Hill, 1950.

Development of a Textile Impulse Radiating Antenna

Michael Koch[1], Holger Thye[1] and Frank Sabath
[1]*University of Hannover, Germany*
[2]*Armed Forces Scientific Institute for Protection Technologies, Germany*

...
E-mail: Thye@geml.uni-hannover.de

For military applications it is of interest to affect distant targets with short electromagnetic pulses of high amplitude. Such pulses with and a broad spectral content from 100 MHz to several GHz are known as Ultra Wide Band Pulses (UWB). The standard Impulse Radiating Antenna (IRA) is a reflector type antenna with high directivity. A modified, collapsible textile IRA which can be integrated in a standard parachute was developed as part of a project initiated by the German Armed Forces Institute for Protection Technologies (WIS) in 2001. The design of the antenna and first measurements were presented shortly after.

From these tests emerged major questions demanding further research:

- Electromagnetic considerations. The maximum amplitude of the radiated field is limited by the design of the feeding section. How can the geometry be optimized to minimize reflections and maximize the capability of handling high voltage?
- Aerodynamic considerations. What is the best type of parachute for the application in question. The required loading capacity is about 30 kg. The design should guarantee a stable flight under any conditions.

These questions were subject of subsequent studies from 2003 - 2005. The existing parachute IRA was modified and tests were conducted. In addition, a set of different IRA's exhibiting different aerodynamic properties were developed and tested.

In this contribution, test results and the properties of different electrical and aerodynamic parachute designs will be discussed. The discussion includes measurement results as well as simulations of the electromagnetic fields for different designs of the feeding section and simulations of the static and dynamic behaviour for different parachute designs. The simulations are complemented by videoclips of dropping tests conducted in 2006.
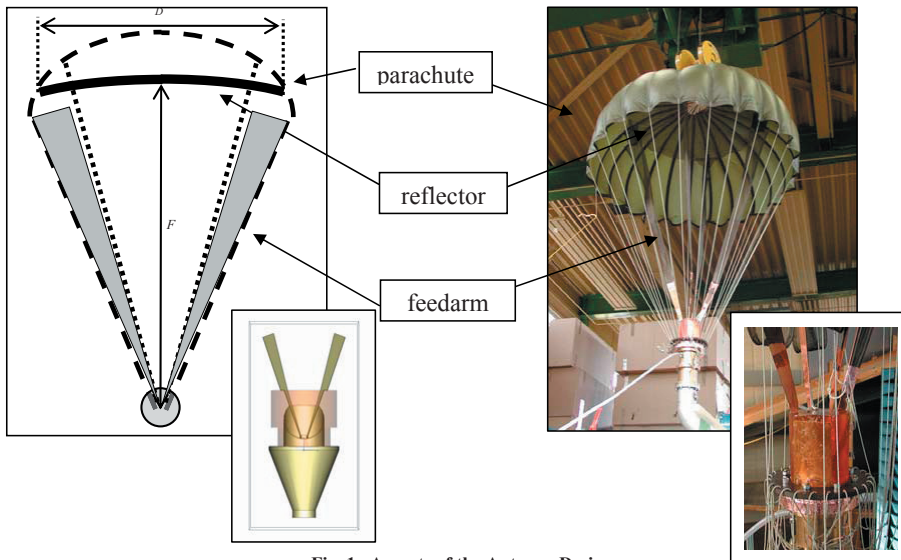
Fig. 1 –Aspects of the Antenna Design

References
1. D. V. Giri, " High Power Electro-Magnetic Radiators,", Harvard University Press, 2004.
2. C. D. Taylor, D. Giri, "High Power Microwave Systems", Taylor and Francis, 1994.
3. H. Herlemann, M. Koch, F. Sabath: "UWB-Antenna for Artillery Applications", EUROEM 2004
4. H. Herlemann, T. Stadtler, M. Koch, J.L. ter Haseborg: "Near-Field Scanning of UWB-Antenna-Footprint in Time Domain", EMC Europe, Barcelona, Spain, 2006, pp.1024-1029

Improvements to the Time-domain Response of the Double-Ridged Horn

James S. McLean[1] and Robert Sutton[1]
[1]*TDK R&D Corp., Cedar Park, TX, USA*
E-mail: jmclean@tdkrf.com

The double-ridged horn is widely used in frequency-domain measurements and can exhibit a nearly 20:1 impedance bandwidth, albeit with substantial and undesirable pattern variations [1]. Aside from high frequency pattern degradation, this antenna also exhibits a deep transmission null in the on-axis response located just above the upper end of the operating frequency range. For the particular design examined here, which is representative of a broad class of commercially available antennas, this notch occurs at about 18.5 GHz as is shown in Fig. 1.
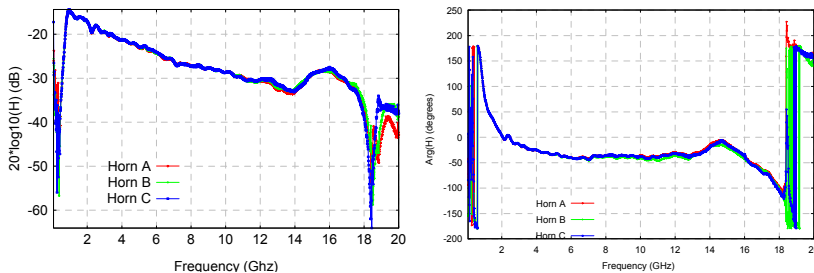
Figure 1: Measured magnitude and phase of the transfer function (as defined in [2]) of the double-ridged horn.

The notch is due to reflection of power at the feed and not splitting of the principal lobe. It is compelling to attribute such a notch to a resonance in the cavity behind the feed region. However, it can be shown conclusively that this is not the case. Instead, the notch is due to coupling in the feed region to high-order trough modes of the ridged waveguide. Removing the two walls of the horn that are perpendicular to the H-plane has been shown to improve its radiation pattern somewhat at the expense of increasing its H-plane beam width at the low end of the operating frequency range. However, the trough modes exist even in the absence of these walls. That is, an open, 3-sided trough can still partially guide electromagnetic energy. Thus, versions of this horn lacking these walls are still susceptible to this problem. Indeed, experiment has shown that removing these walls from the particular horn considered here has practically no effect on the notch in the transfer function or the input impedance of the horn. Even if this notch is considered to be outside the antenna's operating frequency range, the nearly perfect transmission zero causes great variation in the phase of the transfer function at the upper end of the operating frequency range (as can be seen in the figure) as well ringing in the time domain response [2]. This ringing is pronounced and makes the antenna, which is otherwise a very good design, not well suited for time domain measurements. Thus, it would worthwhile to eliminate or at least ameliorate this behavior.

Because of the complexity of such a horn, an analytical solution for the electromagnetic fields is difficult to implement. Thus, a commercial finite element simulation has been used here to model the horn. Nevertheless, analytical techniques can be employed to glean further information from the numerical simulation. The fields in any particular cross section of the horn can be obtained from the finite-element numerical simulation and then expanded in terms of the orthogonal modes of the corresponding uniform ridged waveguide. These are computed from a quasi-analytical eigenvalue analysis [3]. We present results of this analysis indicating coupling to high order trough modes (TE_{6n} modes in notation given in [3]) that reduce the gap field to nearly zero thus resulting in the impedance at the feed point of the horn near 18.5 GHz becoming very low in magnitude and predominantly inductive. Measurements involving de-embedding verify this prediction. Finally, we provide an improved design in which the depth of the notch is greatly diminished while its center frequency is significantly increased thus providing an extended frequency range and very much improved pulse response.

References

1. C. Bruns, P. Leuchtmann, and R. Vahldieck, "Analysis and Simulation of a 1-18 GHz Broadband, Double-ridged Horn Antenna," *IEEE Trans. Electromagnetic Compatibility*, Vol. 45, No. 1, pp. 55-60, Feb. 2003.
2. J. S. McLean, A. Medina, R. Sutton, H. Foltz, and J. Li, "Investigation into the underlying physical mechanisms for high frequency pattern degradation in broadband, double-ridged horns," AMTA Symposium 2006, Austin, TX.
3. J. R. Montgomery, "On the complete eigenvalue solution of ridged waveguide." *IEEE Trans. Microwave Theory and Techniques*, Vol. MTT-19, pp. 547-555, June 1971.

UWB - 13
UWB Wire, Plate and Aperture Antennas

Oral Presentations

A Compact TEM Horn

J. A.G. Malherbe

University of Pretoria, Pretoria, South Africa

jagm@up.ac.za

TEM horns of large bandwidth have been described by a number of authors [1-4]. In order to achieve large bandwidths, these horns are physically large: the horn in [1] measures l = 600mm (length) × h = 750mm (aperture height) × w = 200mm (aperture width); those in [2] and [3] measure 480×733×310mm, and in [4], 450×600×250mm. The TEM horn antenna described in [2] and further developed in [3] was designed to have an elliptic height profile combined with the near-optimal taper described by Hecken. Impedance calculations were based on a microstrip approximation, and a bandwidth of 15:1 was achieved for a VSWR = 2.

In this paper, the effect of variation in horn height (aperture size) and horn length on gain and VSWR was studied with a view to developing a horn with a 6:1 bandwidth ratio but of much smaller size, for specific practical application in the band 2 to 12 GHz. By reducing the height of the aperture, the low frequency cutoff is increased, as described in [3]. It was also shown in [3] that the high frequency performance is determined strongly by the flare shape. For the specific case, the horn width profile was calculated by means of the near optimal taper, but dimensions were obtained using the parallel plate waveguide equation in combination with an elliptic function plate separation. The horn length was varied until the VSWR performance at 12GHz was met.

Figure 1shows the Gain and VSWR performance against frequency for the resulting compact design, as well as the VSWR performance of [3]. Both sets of values were calculated by means of the commercial software FEKO© [5] which had previously been shown to give an excellent approximation to a constructed physical antenna. The VSWR remains below 2:1 from 2 to 12 GHz, while the gain is fairly constant at 15dB. Figure 2(a) compares the cross section of the compact horn with that of [3], while the physical appearance is shown in Figure 2(b), with the compact horn scaled 2.4 times. The compact horn measures 200 x 200 x 101mm.
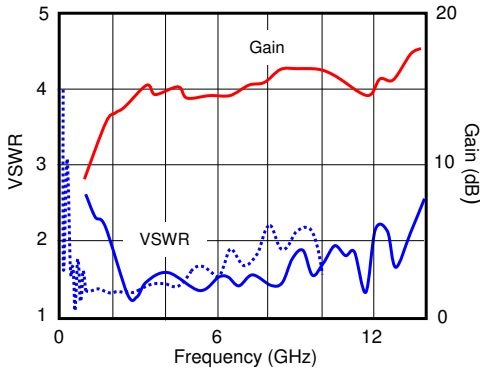
Fig. 1 – Gain and VSWR performance of the compact horn (solid line) *vs* frequency. VSWR of the horn in [3] is also shown (dotted line).
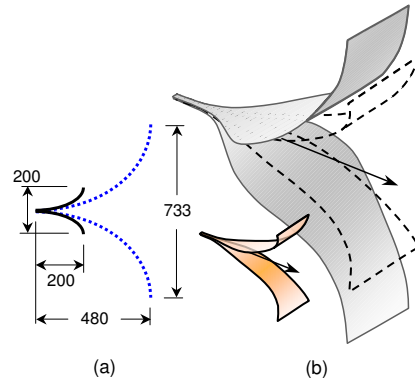
Fig. 2 – Physical shape comparison of the compact horn to that of [3]. (a) Dimensions, (b) enlarged 2.4 times and compared to [3]

References
1. H. Choi and S. Lee, "Design of an exponentially-tapered TEM horn antenna for the wide broadband communication", Microwave and Optical Technology Lett., vol. 40, no. 6, 20 March 2004, pp.531 – 534.
2. J.A.G. Malherbe and N.S. Barnes, "TEM horn antenna with an elliptic profile", Microwave and Optical Technology Lett., vol. 49, no. 7, July 2007, pp. 1548-1551.
3. JAG Malherbe, "Design of Ultra Wideband TEM Horns", 2007 Asia Pacific Microwave Conferenc*e*, APMC 2007, Bangkok, Thailand, 11-15 Dec. 2007, pp. 449-452.
4. A.S. Turk and H Nazli, "Hyper-Wide Band TEM Horn Array Design for Multi Band Ground-Penetrating Impulse Radar", Microwave and Optical Technology Lett., vol. 50, no. 1, Jan 2008, pp. 76 – 81.
5. FEKO©; EM Software & Systems-S.A. (Pty) Ltd. http://www.feko.info/index.html.

The Folded Horn Antenna

E. G. Farr[1], L. H. Bowen[1], C. E. Baum[2] and W. D. Prather[3]

[1]*Farr Research, Inc., Albuquerque, U.S.A.*
[2]*University of New Mexico, Albuquerque, U.S.A.*
[3]*Air Force Research Laboratory, Kirtland AFB, U.S.A.*
E-mail: efarr@farr-research.com

We introduce here a new antenna, the folded horn. This antenna was first proposed by C. E. Baum [1] for radiating high-power mesoband (medium-bandwidth) signals from a very compact package with high efficiency and moderate gain. These antennas were intended to operate at a frequency of a few hundred megahertz, for the application of upsetting electronics at a distance. In this paper we provide the first experimental results for the folded horn.

The advantage of folded horns over other antennas, such as pyramidal horns, is that they have no dimension larger than 2 wavelengths. The requirement to keep the antenna size small becomes apparent at lower frequencies. For example, at 200 MHz, where the wavelength is 1.5 meters, a folded horn with dimensions of 0.5 x 2 x 1.7 wavelengths has a size of 0.75 x 3 x 2.6 meters. An antenna of this size can fit onto the bed of a truck while looking sideways. However, for example, a pyramidal horn would not fit into such a limited space at this frequency.

The folded horn works as follows. The feed point and switch are located in the Feed Section, in which the horn is expanded in the H-plane. A cylindrical wave is launched from the feed point, which is positioned at the focus of the parabolic bend. After reflecting off the parabolic bend, the waves are focused in the H-plane and then proceed into Aperture Section, in which the fields are expanded in the E-plane. The fields in the large dimension of the aperture (H-plane) remain focused, because of the parabolic bend. The fields in the short dimension of the aperture (E plane) are only slightly out of focus, because there is little difference in ray path lengths in this plane.

In this paper, we build and test the first prototype low-power folded horns, operating at a nominal operating frequency of 3 GHz. We describe several iterations, resulting in a realized gain of 10 dB over 3-5 GHz, an aperture efficiency of 80%, and modest return loss. This is quite good performance for such a small antenna. This design could be adapted to high-voltage designs, and it could work well in a dual-antenna configuration, with two antennas positioned back-to-back, driven by a dual-output source.

A number of areas are worth investigating in the future to improve the folded horn. These include investigations on the 180° bend, opening angle, and feed point of the horn. Different configurations may be of use, such as the bi-folded horn, with two folds. This configuration may better accommodate a two-horn array with a single high-power source between them. Ultimately, high-power versions will have to be built and tested.
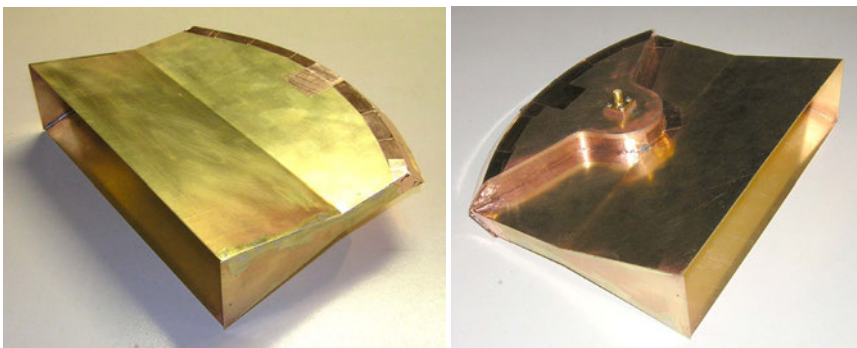
Fig. 1 – The Folded Horn Antenna.

References

1. C. E. Baum, "More Antennas for the Switched Oscillator," Sensor and Simulation Note 493, August 2004.

A Slotline Antenna Using a Taper Based on a Bessel Function

Mohammad Saed

Texas Tech University, Lubbock, Texas, USA

Email: mohammad.saed@tu.edu

This paper presents a slotline antenna with a novel taper. Since the introduction of the exponentially tapered slotline antenna (also known as Vivaldi or notch antenna) in 1974 [1], slotline antennas with various tapers have been very popular as traveling wave antennas capable of operating over multi octave bandwidths with end-fire radiation patterns. In addition to the exponential taper, types of taper shapes investigated in the literature include the linear taper and the constant or stepped width tapers [2-4]. Uniplanar configurations as well as antipodal configurations [5-7] with those tapers were investigated for very broadband continuous-wave applications as well as transmission and reception of ultra wideband pulses. In this paper, we introduce a new taper based on the integral of an expression using a modified Bessel function of the second kind. The goal of introducing this taper is to minimize the antenna length while maintaining similar or better performance than conventional tapers.

The proposed antenna is investigated theoretically using Ansoft HFSS which uses a full-wave finite-element solver as well as the conformal finite difference time domain method (CFDTD). Parametric studies to investigate the effect of taper parameters on antenna performance such as impedance bandwidth, radiation patterns, and gain are carried out. The proposed antenna exhibits an extremely wide 10-dB return loss bandwidth as well as stable radiation characteristics over its entire frequency band of operation. The characteristics of the proposed antenna are compared to the conventional linear and exponential tapers. The design details, theoretical simulations, as well as experimental results will be presented.

References

1. L. R. Lewis, M. Fassett, and J. Hunt, "A broadband stripline array element," IEEE Antennas and Propagation Symposium, Atlanta, GA, digest pp. 335–337, 1974.
2. K. Yngvesson, et al., "Endfire tapered slot antennas on dielectric substrates," IEEE Transactions on Antennas and Propagation, vol. AP-33, pp. 1392–1400, December 1985.
3. J. Shin and D. H. Schaubert, "A Parameter Study of Stripline-Fed Vivaldi Notch-Antenna Arrays," IEEE Transactions on Antennas and Propagation, vol. 47, No. 5, May 1999, pp. 879-886.
4. Homayoon Oraizi and Shahrokh Jam, "Optimum Design of Tapered Slot Antenna Profile," IEEE Transactions on Antennas And Propagation, vol. 51, No. 8, August 2003, pp. 1987-1995.
5. R. N. Simons, R. Q. Lee, and T. D. Perl, "Non-Planar linearly tapered slot antenna with balanced microstrip feed," in IEEE AP-S International Symposium, vol. 4, Chicago, IL, 1992, pp. 2109–2112.
6. J. D. S. Langley, P. S. Hall, and P. Newham, "Novel ultrawide-bandwidth Vivaldi antenna with low cross polarization," Electronics Letters, vol. 29, issue 23, Nov. 1993, pp. 2004 – 2005.
7. J. D. S. Langley, P. S. Hall, and P. Newham, "Balanced antipodal Vivaldi antenna for wide bandwidth phased arrays," Microwaves, Antennas and Propagation, IEE Proceedings, vol. 143, issue 2, April 1996, pp. 97 – 102.

Design And Experiment Of High Power Ultra-wide Band Dual-pulse Radiating Antenna

s t zhu,g z liu,c l yi,x x song,y j fan,l shi,w f xia,y f zhu

Northwest Institute of Nuclear Technology，P.O.Box 69-13,Xi'an 710024 China
E-mail: Zhu_sitao@sina.com

A method to widen the microwave spectrum with radiating two pulses of different FWHM is presented. Based upon this method, a high power ultra-wide band dual-pulse radiating antenna is developed. The antenna is made up of a half-IRA over a ground plane. The diameter of the reflector is 2m with F/D=0.4, and the ground plane is a rectangle of metal with length of 8m and width of 6m. Three TEM horns are adopted to feed two pulses to the reflector. The antenna can radiate two different bipolar pulses with peak-to-peak width of 1.7 ns and 3 ns effectively. The 3 ns bipolar pulse is after 1.7 ns bipolar pulse with a delay of 12.5 ns. Simulation analysis and experiments on the antenna are taken. Good agreements between calculated and measured results are obtained. The radiated spectrum of the 1.7 ns pulse covers from 240 MHz to 400MHz, while the radiated spectrum of the 3 ns pulse covers from 110 MHz to 210MHz. The radiated spectrum of the combined 1.7 ns and 3 ns dual-pulse with 12.5ns delay covers from 100 MHz to 430MHz.Results show that to radiate the combined pulses is a more effective method to widen the microwave spectrum than to radiate a single pulse.

Advanced Imaging by Space-Time Deconvolution in Array GPR

T. G. Savelyev, N. T. van Tol, A. G. Yarovoy, L. P. Ligthart

International Research Centre for Telecommunications-transmission and Radar, Delft University of Technology, The Netherlands

E-mail: T.G.Savelyev@irctr.tudelft.nl

Digital beamforming in array-based UWB radar delivers a high-resolution 3-D image of subsurface in GPR landmine detection while simultaneous data acquisition by elements of the array significantly increases the scanning speed. Such a GPR system with a single transmit antenna and a linear receive array has been developed in the Delft University of Technology [1]. In this system the imaging that combines a weighted near-field focusing of the array with migration in the direction of mechanical scan is done by software means only. Since it needs be as fast as possible for a real-time application we developed an advanced algorithm based on migration by regularized, parametric space-time deconvolution [2]. The algorithm deconvolves a space-time point spread function out of the data volume by means of FFT and inverse Wiener filter controlled automatically with numerical criteria for stability and accuracy [3]. The prior knowledge of GPR impulse response and ground impulse response is used to form a point spread function. Fig. 1 illustrates imaging results for a single array element obtained from the experimental data by classical diffraction stacking and by the developed algorithm. The numerical performance of these algorithms is given in Table 1 for the subsurface case. The comparison shows clearly that the proposed technique provides sharper and much faster focusing.
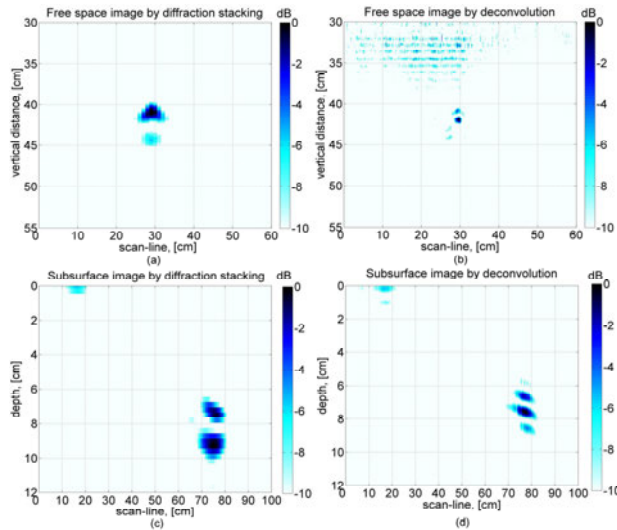
Fig. 1 – Efficiency of radar imaging: (a)-(b) images of metal sphere of 2 cm diameter in free space by diffraction stacking and deconvolution; (c)-(d) images of buried landmine PMN-2 by diffraction stacking and deconvolution

Table 1 – Performance of imaging techniques

Technique	Image resolution, [pixels]	Computational time, [s]
Diffraction stacking	44 x 101	71
Space-time deconvolution	1024 x 410	5

References
1. A. G. Yarovoy, T. G. Savelyev, P. J. Aubry, P. E. Lys, and L. P. Ligthart "UWB array-based sensor for near-field imaging," IEEE Transactions on Microwave Theory and Techniques, vol. 55, pp. 1288-1295, 2006.
2. B. Scheers, and M. Acheroy "Migration technique based on deconvolution," in *Ground Penetrating Radar, 2nd edition,* D. J. Daniels ed., IEE Radar, Sonar, Navigation and Avionics Series 15, pp. 283-293, 2004.
3. T. G. Savelyev, L. van Kempen, and H. Sahli, "Deconvolution techniques," in *Ground Penetrating Radar, 2nd edition,* D. J. Daniels ed., IEE Radar, Sonar, Navigation and Avionics Series 15, pp. 298-310, 2004.

Oral Presentations

UWB for Medical Imaging and Sensing (Invited)

UWB - 14

Human Being Imaging with Low-Frequency UWB Radar

A. Yarovoy[1], X. Zhuge[1], T. Savelyev[1], J. Matuzas[2], B.Levitas[2]

[1]*Delft University of Technology, International Research Centre for Telecommunications and Radar*
Delft, the Netherlands
[2]*GeoZondas Ltd., Vilnius, Lithuania*

...

E-mail: a.yarovoy@ewi.tudelft.nl

Recently, human being imaging by means of active and passive radars became hot research and development area due to concealed weapon detection and search for victims/survivals in buildings on fire or after earthquake. It has been demonstrated that mm-wave radars and radiometers can produce high-quality images [1]. However both require several seconds of time for data acquisition, during which the scene and objects under investigation should be completely still. Furthermore, both system types require expensive mm-wave multi-channel receivers and large antenna arrays (combined with mechanical scanners). Low-frequency UWB radars might be a faster and cost-efficient technological solution for this application. Use of low frequencies has an additional advantage, i.e. possibility to penetrate through skin and human tissues, walls and natural materials which makes it possible to use these radars for medical imaging, victim search after earthquake or for security applications [2]. The major challenge associated with low frequency use is the cross-range resolution of the radar, which believed to be inversely proportional to the central operational frequency of the imaging radar [1]. This paper describes theoretical and experimental study on cross-range resolution of short-range UWB radars and demonstrates principal possibility of high-resolution images (sufficient for human being imaging and concealed weapon detection) produced by low-frequency UWB radar.

The requirement of high cross-range resolution in imaging radars results in a need for an antenna array (at least, at receive part) with a certain aperture. The aperture size L depends on an algorithm to determine an angle of arrival and the operational bandwidth. Assuming utilization of a simple algorithm based on triangulation principle (Fig. 1a) one can derive the cross-range resolution ΔX at the down-range $R >> \Delta R$ (where ΔR is the down-range resolution $\Delta R = c/(2B)$, c is speed of light and B is the operational bandwidth)

$$\Delta X \cong \frac{Rc}{LB}.$$

(1)

This equation proves that the cross-range resolution depends not on central operational frequency but on operational bandwidth and allows for high-resolution images at low operational frequencies. This is proved experimentally by high-resolution imaging four spheres diameter of 3.9cm and separated by 10cm between their centres (Fig 1.b) and 60cm high aluminium foil-covered doll (Fig. 1c, d) at the frequency band from 3GHz till 8GHz. Data acquisition has done in time domain at the distance 50cm and with an imaging aperture of 30cm by 30cm. Kirchhoff migration algorithm has been used for imaging.
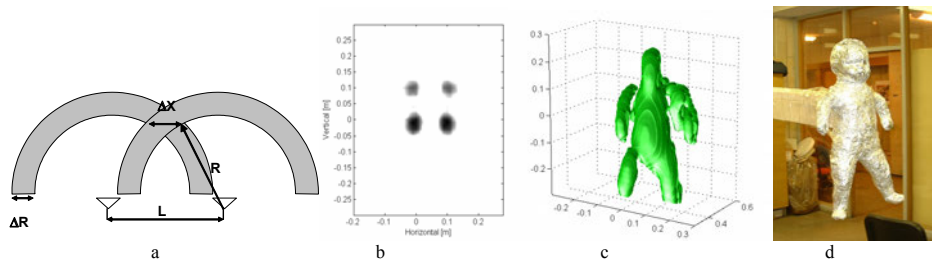
Fig. 1 – Triangulation principle for determining of the cross-range resolution of UWB radar (a); radar images of four metal bolls (b) and a doll (c); photo of the doll (d)

References
1. D. M. Sheen, D. L. McMakin, and Th. E. Hall, "Near Field Imaging at Microwave and Millimeter Wave Frequencies," IEEE Int. Microwave Symp., 2007.
2. T. Dogaru, and Lam Nguyen, "FDTD Models of Electromagnetic Scattering by the Human Body," IEEE Antennas Propagat. Soc. Int. Symp., 2006.

UWB - 14
UWB for Medical Imaging and Sensing (Invited)

Oral Presentations

Measuring the Human Body Impulse Response with UWB Radar

Adrian E.-C. Tan[1], Kevin K.-M. Chan[1], Michael Y.-W. Chia[1]
[1]*Institute for Infocomm Research, Singapore*
E-mail: tanadrian@i2r.a-star.edu.sg

This paper proposes a method of measuring the scattered signal from a human body when illuminated by ultra-wideband (UWB) radar. From the radar received signal, the method computes the impulse response of the human body. This method may be of interest to researchers who seek to use UWB technology to sense and image human body [1]. The proposed method solves the problem of signal distortions caused by the transmitter's component imperfections and the receiver's additive thermal noise. When the first reflection of the air-human body transition is strong, the signal distortions may cause subsequent reflections attributed to signal penetration [2] to be undetectable to the receiver. Finding the impulse response will aid the detection of signal penetration because the method decouples the undesirable signal distortions with the target's scattering characteristics.

The UWB radar used in the measurement transmits 1.8 V, 200 ps pulses, with pulse repetition rate of 1 MHz. The transmitter and receiver share the same Vivaldi antenna [3]. The receiver first amplifies the received signal, and then records the signal with a 50 GS/s sampling oscilloscope. The recorded signal is then processed in a computer to find the impulse response of the target. The targets used for the measurement are human phantom and human body. The human phantom consists of a liquid layer of human tissue simulant that is placed in a transparent plastic container (40cm x 38cm x 28cm). The liquids used are – cooking oil, GSM 1800 solution, saturated glucose solution and water, to simulate the dielectric properties of the human tissues. Measurements are also done at the torso region of a human body, at heart and stomach cross-sections. All the targets are placed at boresight direction, and at far field region of the antenna.

$$h(t) = F^{-1}\left\{ F\left[r(t)\right] \middle/ F\left[r_0(t)\right] \cdot G(\omega) \right\} \tag{1}$$

Eqn. (1) describes the method to compute the human body target's impulse response, $h(t)$. $r(t)$ and $r_0(t)$ are the received scattered signal and the received reference signal (reflection from a large metal plate). However, because both $r(t)$ and $r_0(t)$ are corrupted by thermal noise, at higher frequencies, the signals' spectral ratio results in random values with large variances. A frequency window, $G(\omega)$, is used to filter out the noise contributions. The windowing function, however, will limit the resolution of the impulse response. Hence, given a set of measured signals, a compromise has to be made between maximizing the imaging resolution of the UWB radar and minimizing the noise contribution of the impulse response signal.
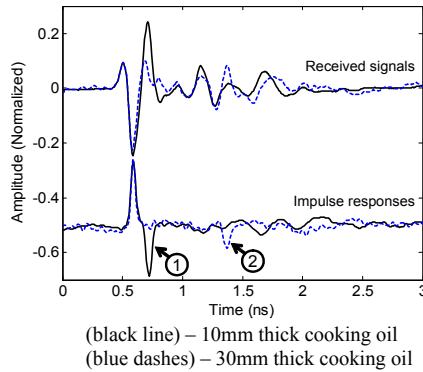
(black line) – 10mm thick cooking oil
(blue dashes) – 30mm thick cooking oil
Fig. 1 Measured received signals and computed impulse responses for two human phantom

Fig. 1 shows the measured scattered signals of two human phantoms, and the computed impulse responses of these signals. The labels "1" and "2" indicate obvious second reflections from the targets in the impulse responses, while these reflections are not obvious in the received signals.

References
1. M. Y. W. Chia, S. W. Leong, C. K. Sim, and K. M. Chan, "Through-wall UWB radar operating within FCC's mask for sensing heart beat and breathing rate," *35th Eur. Microw. Conf.*, Oct. 2005, pp. 1991–1994.
2. E. M. Staderini, "UWB Radars in Medicine", *IEEE AESS Systems Mag.*, vol. 17, pp. 13-18, Jan 2002.
3. Qing X., Chen Z. N., "Antipodal Vivaldi Antenna for UWB Applications", *Book of abstracts EUROEM 2004*, pp 157-158, Jul. 2004.

Ultrawideband Microwave Imaging via MUSIC for Breast Cancer Detection

X. Chen

National University of Singapore, Singapore

E-mail: elechenx@nus.edu.sg

The multiple signal classification (MUSIC) method is well known to detect point-like targets in single (or narrow) frequency domain [1]. Yet, its application in ultrawideband (UWB) is relatively less reported. This paper applies the MUSIC to UWB microwave imaging for breast cancer detection. The main conclusions of the paper are two folds: (1) theoretical and numerical results show that the MUSIC method is an effective and useful tool in detecting small tumors surrounded by randomly distributed clutters; (2) the UWB MUSIC method is more stable than the central frequency MUSIC in the presence of the random inhomogeneous background medium.

The following configurations are investigated. The antenna array is placed above the skin of the flattened breast, and is immersed in the coupling medium whose dielectric property matches the skin permittivity. The dielectric property of breast tissue is described by the first-order Debye dispersion equation [2], and the randomly distributed clutters are modeled as the variation within a prescribed threshold about the nominal value. The UWB (1-11 GHz) multistatic data are collected at the antenna array, which are modeled as the forward scattering data contaminated with the noise [3]. The forward scattering problem at each sample frequency is obtained by solving the three-dimensional Fodly-Lax equation. The MUSIC method applies to each frequency component of the collected multistatic data. The projection of the test half-space Green's function onto the noise space of the multistatic matrix at each sample frequency, and the weighted sum of these projections is defined to be the inverse of the MUSIC pseudospectrum. Therefore, there is a peak in the MUSIC pseudospectrum at the position of the tumor. Theoretical and numerical results show that the UWB MUSIC method is statistically more stable than the central frequency (6GHz) MUSIC in the presence of the randomly distributed clutters [4]. For example, Fig. 1 shows the comparison of the central-frequency and UWB MUSIC imaging results.

As an alternative to the most commonly used beamforming technique, the MUSIC method provides a statistically stable tool in the UWB microwave imaging for the detection of breast cancer.
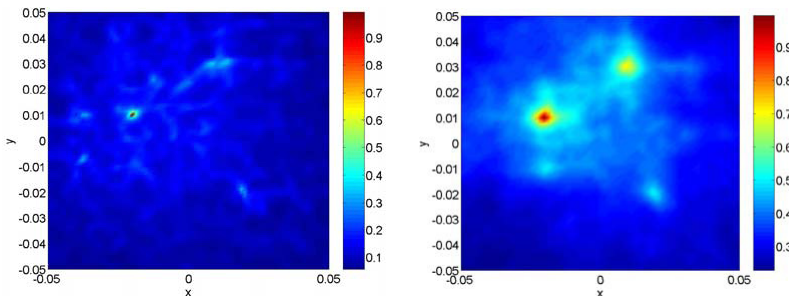
Fig. 1 – MUSIC pseudospectrum in the z = -0.03 m plane for a numerical simulation where two tumors are present together with randomly distributed clutters. The radii of the tumors located at (-0.02, 0.01) m and (0.01, 0.03) m are 3mm and 2mm, respectively. Left figure: Results of central frequency (6GHz) MUSIC, where only the bigger tumor is identified; Right figure: Results of the UWB MUSIC, where both tumors are identified and the bigger tumor shows stronger intensity in the pseudospectrum.

References
1.   A. Kirsch, "The MUSIC-algorithm and the factorization method in inverse scattering theory for inhomogeneous media," Inverse Problems, vol. 18, pp. 1025-1040, 2002.
2.   E. J. Bond, X. Li, S. C. Hagness, and B. D. Van Veen, "Microwave imaging via space-time beamforming for early detection of breast cancer," IEEE Transactions on Antennas and Propagation, vol. 51, pp. 1690-1705, 2003.
3.   Y. Xie, B. Guo, J. Li, and P. Stoica, "Novel Multistatic Adaptive Microwave Imaging Methods for Early Breast Cancer Detection," EURASIP Journal on Applied Signal Processing, vol. 2006, pp. 91961, 2006.
4.   J. Berryman, L. Borcea, G. C. Papanicolaou, and C. Tsogka. "Statistically stable ultrasonic imaging in random media," Journal of Acoustical Society of America, vol. 112, pp. 1509-1522, 2002.

Design of Compact Tunable Band-Pass Filter Using *J*- Inverter and Quasi-Fractal Defected Ground Structure (DGS)

A. Boutejdar[1], A. Batmanov[2], A. Elsherbini[3], A. Omar[1], and E. Burte[2]
[1] *Chair of Microwave Engineering University of Magdeburg, Germany*
[2] *Chair of Semiconductor Tech., University of Magdeburg, Germany*
[3] *Chair of Electrical Engineering University of Ain Shams, Cairo, Egypt*
E-mail: Ahmed.boutejdar@ovgu.de

*Abstract —*This paper presents a new type of reconfigurable compact bandpass microstrip DGS filters employing metal-loaded slots etched in the ground plane and a capacitive gap in the microstrip feed line. With an additional variable capacitor, a new type of tunable band pass filter based on coupled DGS resonators was realized. To get a tunable passband, active devices using Varactor diodes are applied on the DGS section, which is the back side of the microstrip transmission line. One-pole DGS-element has been designed and fabricated. Relying on the proposed one-pole DGS-element, a two-pole (Quasi-fractal) tunable BPF was designed and simulated. The new tunable BPF consists of two similar coupled slots. On each DGS-element, a variable capacitor has been inserted, which allows for shifting the passband. This electromagnetic effect improved the reject band [1, 2]. We also presented the equivalent circuit of the proposed Quasi-fractal BPF based on the equivalent circuit model of the DGS. The circuit parameters are derived from the equivalent inductance and capacitance, that appeared due to the perturbed ground current in the ground plane because of the presence of the slot. The theory is validated using the commercial Microwave Office. Compared with a conventional bandpass filter, the new BPF provides similar Q-factor with very compact size, and provides sharp transition bands, a wide upper stop-band and improved pass-band response symmetry. The BPF without Varactor was simulated and fabricated. The measured and simulated results are agreeing well, as shown Fig. [1-3]. The one-pole DGS element with Varactor was simulated and fabricated. Good agreement between simulated and measured results have been achieved. The quasi-fractal BPF has been simulated on a substrate with dimensions of ($0.52\lambda_g$ x $0.37\lambda_g$) as shown Fig. [4-6]. The substrate has a relative dielectric constant of 3.38 and a thickness of 0.813 mm. The proposed quasi-Fractal tunable structure will be later fabricated and measured. All dimensions are in mm.
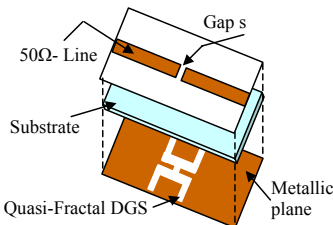
Figure 1. 3-D view of the DGS cell.
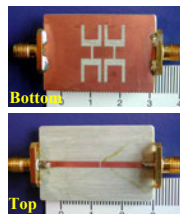
Figure. 2. Fabricated quasi-fractal BPF.
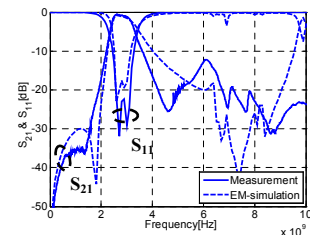
Figure 3. Measured and simulated results of proposed quasi-fractal-BPF
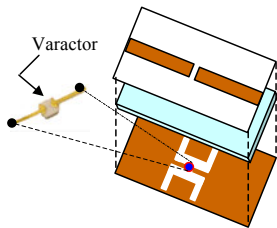
Figure 4. 3-D view of the DGS cell.
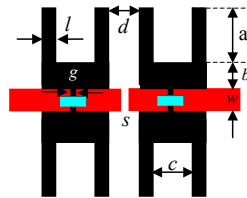
Figure 5. Layout of the new tunable BPF. a=4, b=2, c=3, w=2, s=0.5 d=2, *l*=1 and g=0.5
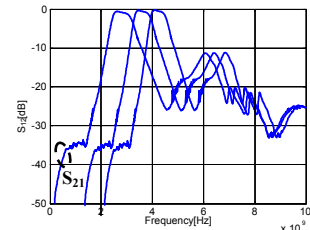
Figure 6. Expected result with tunable effect

References

1. M. Awida, A. Boutejdar, A. Safwat, H. El-Hannawy, and A. Omar, "Multi-bandpass Filters using multi-armed split ring resontors with direct feed," *IEEE MTT-S IMS*, Honolulu, Hawaii, June 2007.
2. J.-S. Hong, and M. J. Lancaster, *Microstrip Filters for RF/Microwave Applications*, Wiley, New York, 2001.
3. A. Boutejdar, A. Elsherbini and A. Omar , "A Compact Microstrip Multi-Layer Lowpass Filter Using Triangle Slots Etched in the Ground Plane" Proc. 36th European Microwave Conference, Manchester, UK, September 2006.

Transient Field Phenomena in a Debye Medium with Static Conductivity

N. A. Cartwright[1], K. E. Oughstun[2]
[1]*State University of New York at New Paltz, New Paltz, NY, USA*
[2]*University of Vermont, Burlington, VT, USA*
E-mail: cartwrin@newpaltz.edu

Ultra-wideband electromagnetic pulses that propagate through dielectric materials have been shown to give rise to specific transients, the so-called Sommerfeld and Brillouin precursors [1], that are a characteristic of the dispersive material. Of particular interest, the Brillouin precursor has a peak amplitude point that only decays algebraically with propagation distance, rather than exponentially [2]. This unusually slow decay rate of the Brillouin precursor is highly desirable in radar applications where the material being interrogated is highly absorptive or in applications that require long interrogation distances. However, many physical applications, such as radar and biomedical imaging, require propagation of electromagnetic signals through conductive material. Thus, a detailed analysis of the transient field structure associated with an ultra-wideband pulse propagating through a conducting material is needed.

Our method of analysis is an asymptotic approximation to the (exact) integral representation of the electric field component of the propagated field on any plane $z > 0$

$$E(z,t) = \frac{1}{2\pi} \Re \left\{ \int_{ia-\infty}^{ia+\infty} E(0,\omega) e^{\frac{z}{c}\phi(\omega,\theta)} d\omega \right\}, \tag{1}$$

where z is the propagation distance into the material. Here, a is greater than the abscissa of absolute convergence for the initial electric field component $E(0,t)$ on the plane $z = 0$ whose spectrum is $E(0,\omega)$, and $\phi(\omega,\theta) = i\omega[n(\omega) - \theta]$ is the complex phase function, where $n(\omega)$ is the complex index of refraction of the conducting material and $\theta = ct/z$ is a dimensionless space-time parameter and c denotes the speed of light in vacuum. In a dielectric material, the complex phase function $\phi(\omega,\theta)$ is analytic at the origin $\omega = 0$. Thus, a saddle point of $\phi(\omega,\theta)$ actually crosses the origin, the very point that provides the slow decay rate of the Brillouin precursor. In a conductive material, $\phi(\omega,\theta)$ possesses a branch point at the origin, which prohibits saddle points of $\phi(\omega,\theta)$ from crossing the origin. The presence of this branch point calls into question the existence and decay rate of the Brillouin precursor.

Here, we study the propagation of a step-function modulated sine wave through a conductive material whose complex dielectric permittivity is given by a Debye model [2] with static conductivity

$$\varepsilon_c(\omega) = \varepsilon_\infty + \frac{\Delta\varepsilon}{1 - i\omega\tau} + i\frac{\sigma_0/\varepsilon_0}{\omega}, \tag{2}$$

where ε_∞ is the high frequency limit of the dielectric permittivity, $\Delta\varepsilon = \varepsilon(0) - \varepsilon_\infty$, and σ_0 is the static conductivity. We have found a non-uniform asymptotic approximation to the propagated field that is valid for low levels of conductivity, $\sigma_0 < 1 \times 10^{-9}$ S/m, which is appropriate for loamy soil. We then study the decay rate of the peak amplitudes of the transients. Our analysis shows that the Brillouin precursor decays exponentially, not algebraically, with propagation distance. When we increase the level of conductivity above 1×10^{-9} S/m, a space-time domain appears about which the non-uniform expansion fails. We will address the issues faced in finding a uniform description of the propagated field that is valid for all levels of conductivity.

References
1. N. A. Cartwright and K. E. Oughstun, "Uniform Asymtotics Applied to Ultrawideband Pulse Propagation," SIAM Review, vol. 49, 2007.
2. K. E. Oughstun, "Noninstantaneous, finite rise-time effects on the precursor field formation in linear dispersive pulse propagation," Journal of the Optical Society of America A, vol. 12, 1995.
3. P. Debye, Polar Molecules. New York: Dover, 1929.

A Robot-Mounted Electromagnetic Induction Sensor for Rapid Identification of an Unexploded Ordnance (UXO)-Free Corridor

Lloyd S. Riggs[1], and Jay H. Bennett[2]
[1]Auburn University, AL, USA
[2]US Army ERDC, Vicksburg, MS, USA
E-mail: riggs@eng.auburn.edu

This paper describes an effort in progress to develop a remotely-operated robot-mounted pulsed electromagnetic induction (EMI) system for rapid identification of a UXO-free corridor. Very often there is a requirement to lay underground utility lines (water, or electric) through an area that is known to contain UXO. Obviously, an ordnance-free corridor must be identified before trenching equipment can be used to prepare the site for underground utility lines.

The EMI system developed consists of a 140 cm X 80 cm transmitter coil and an eight-element array of 28cm X 30 cm receiver coils. Signals from a pair of receiver coils along the short dimension of the array are subtracted yielding four differential data channels across the long dimension of the array. As a target approaches the array from a direction perpendicular to the long side of the array (the direction of forward motion) the response will undergo a phase reversal (sign change). This sign change aids significantly in identifying the exact location of the buried target in the direction of motion. Furthermore, target position perpendicular to the direction of motion can be estimated by comparing the target response amplitude obtained from adjacent differential coil pairs.

To obtain good overall system sensitivity we found that it was necessary to carefully control the transmitter coil current waveform. Our transmitter coil current rises exponentially to a peak value of around 15 amps in approximately 7 ms and afterward attenuates linearly to zero, without significant undershoot, in approximately 80 microseconds. Rapid transmitter current turn off insures that the eddy current response of most UXO targets is of sufficient strength to guarantee detection to a depth of at least 4 ft. Of course the transmitter current is periodic (in our case a repetition rate of approximately 50 Hz) so averaging (stacking) can be used to improve signal-to-noise ratio.

The details of our receiver coil amplifier (or signal condition circuit) will also be addressed. In order to reduce noise it is important to limit the usable bandwidth of the receiver coil amplifier as much as possible but not so much as to distort the target's natural eddy-current response. Good overall dynamic range requires that the receiver coil amplifier have minimal DC offset and drift. Other important design considerations include the parameters of the analogue-to-digital converter including maximum sample rate and resolution (number of bits).

To date, our EMI system has been tested in the laboratory and seems to meet the original sensitivity goal (i.e. have the ability to detect a medium size UXO at a depth of approximately 4 ft.). Furthermore field testing of the EMI system and integration with the remotely operated robot is planned for the near future. Our presentation will elaborate on the topics discussed above and present results from the complete integrated system.

Radar Clutter Modeling And Signal Processing Chain Simulation

S. K. Gour, S. Duvvuri, V. A, R. Paramata.

Signal & Data Processing Group, Electronics & Radar Development Establishment, Bangalore-560093, India
E-mail: g.saroj@yahoo.co.in

The design of complex modern radar systems frequently makes use of computer simulations to predict performance. This is particularly true for multifunction/multimode radars with adaptive modes of operation. The goal of this work has been to develop a generic model, capable of being applied to many different radar systems, thereby avoiding the need to develop a completely new simulation model for the radar under consideration. The simulation makes use of the Signal Processing Work System (SPWS) package, which allow the user to link together functional modules to form the complete simulation model. The modules can be specified at various levels of sophistication. Having developed and verified the interfacing strategy for these modules through the use of a simple radar example, work is focused upon refining the framework and investigating its use for novel modeling techniques.

In this paper, it is proposed to present model for Radar Signal Processing chain of Air-borne Radars. Plot Data Generation includes modules of Signal Processor along with Raw Data Generation for target, clutter and noise. Signal Processor modules consists Platform motion compensation, Moving target indication, Windowing, Doppler filtering, Constant False Alarm Rate (2-D CFAR) and monopulse (d/s) angle Calculation. Radar simulation is rapidly gaining popularity because of several reasons - an important one being the modern radar system are becoming increasingly more complex and less tractable to straightforward analysis. The primary reason for this popularity of simulation is cost factor. A simulation is almost a necessary prerequisite if the radar is designed to operate in remote areas or hostile environment. The objective of simulation is to compare the simulation results with offline data analysis. The several possibilities are component design, algorithm testing and system function evaluation, training, testing radars and integrated system performance analysis..

References
1. M. I. Skolnik, Introduction to Radar Systems, Tata McGraw-Hill Publishing Company Limited, New Delhi
2. Y. Bar-Shalom, Multi-target Multi-sensor Tracking: Applications and Advances Volume II, Artech House, Boston, London.
3. G. Morris, L. Harkness, Air-borne pulsed Doppler radar, Atrech House, Boston, London

UXO-TID - 1
UXO-TID Underground & Subsurface

Oral Presentations

Developments in Electromagnetic Methods for Tripwire Detection

L.J. Carter, S. Jayalath, and R. Edwin

Department of Electrical & Computer Engineering, University of Auckland, Auckland, New Zealand

...
E-mail: lj.carter@auckland.ac.nz

Tripwire-operated bounding fragmentation mines continue to be a significant hazard for deminers.[1,2] A compact and reliable detector of tripwires would be a useful addition to the deminer's toolkit. This paper describes recent work on a detector capable of finding standard military tripwire obscured by vegetation.

Typical military tripwire consists of thin galvanized iron/steel wire, coated with dark green camouflage. It is formidably difficult to detect using conventional metal detectors, since it presents a small target area, and has high electrical resistance, inhibiting the induction of significant current in it. Many modern mine detectors use some form of pulse-induction technology. This enables them to detect quite small buried targets, but even the best will struggle to find vegetation-obscured tripwire. This project builds upon earlier work using pulse-induction, polarization, and acoustic techniques.[3,4,5,6] A detector has been built using a phase-discrimination technique which gives promising results on military tripwire from the former Yugoslavia. The detector can outperform a top-of-the-line commercial mine detector in finding the target. In laboratory tests the prototype detector could detect a stretched tripwire a short distance away, while at the same distance the commercial detector could not. The prototype can also give an indication of the target's nature, i.e., that it is likely to be a tripwire rather than some other metal object. Figure 1 shows the detector output current for targets of different metal and shape. For certain values of phase delay the tripwire can be distinguished from all other targets. Further work is needed to extend the range of the detector, and this is in progress.
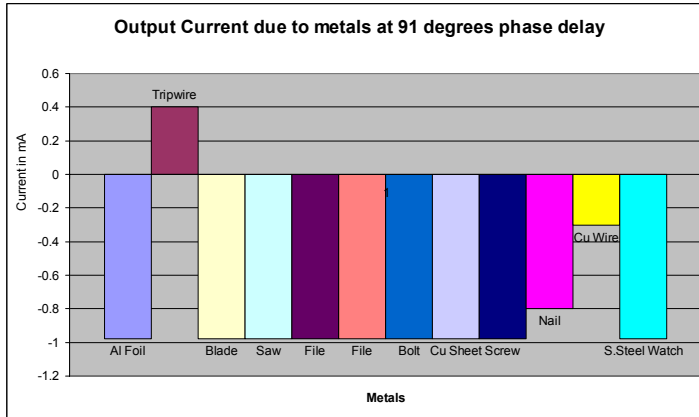
Figure 1 – Detector output showing discrimination between tripwire and other metal targets

References
1.   C. King *Ed.*, Jane's Mines and Mine Clearance, 9th edn., Jane's Information Group, London, 2005.
2.   International Campaign to Ban Landmines, Landmine Monitor Report, Human Rights Watch, Canada, 2005.
3.   L.J. Carter and C.Y. Liao, An optimal technology for detection of vegetation-obscured tripwires, Proc. SPIE: Detection and Remediation Technologies for Mines and Minelike Targets XI, Orlando [USA], April 2006.
4.   L.J. Carter and C.Y. Liao, A new approach to detecting vegetation-obscured tripwires, Proc. IEEE First International Conference on Industrial and Information Systems (ICIIS 2006), Peradeniya [Sri Lanka], August 2006.
5.   L.J. Carter and C.Y. Liao, Sensing technologies for tripwire detection, International Conference on Sensing Technology, Palmerston North, New Zealand, November 2005.
6.   C.Y. Liao, Tripwire Detection Methods, ME Thesis, University of Auckland, New Zealand, 2006.

An Overview of New Technology, Dielectric, Electromagnetic Field Sensors

M. G. Harrison[1], D.H. Wu[2], T. J. Wieting[3], R. Forber[4] and K. Yang[5]
[1]*Air Force Research Laboratory, Directed Energy Directorate, Kirtland AFB,USA*
[2]*Naval Research Laboratory, Code 6362, Washington, DC USA*
[3]*FFA, Inc., Crofton, MD USA*
[4]*Integrated Photonic Technologies, IPITEK, Carlsbad, CA USA*
[5]*Opteos, Inc, Ann Arbor, MI USA*
...
E-mail: michael.harrison@kirtland.af.mil

There have been active efforts to design new electromagnetic (EM) sensors that are largely or entirely constructed of dielectric materials since the 1980s. There is a clear advantage for such sensors in an EM field environment where minimal disturbance of the field being measured is desired. The researchers developing such sensors have found additional advantages such as small size, large bandwidth, wide dynamic range and the ability to replace conducting wires with fiber-optic cables that eliminate any electromagnetic interference that might appear on conducting cables, and allow low-loss remoting of sensor elements from sensor transceiver electronics and signal processing systems.

This presentation presents a survey of three current efforts to develop and improve EM sensors that utilize dielectric materials, either crystals or polymers. The objective of the presentation is to inform the audience of new or near-term capabilities that may be of use for particular applications. The sensors that are currently ready for use or that are being field tested are electric-field sensors. In addition, there are programs aimed at the development of magnetic-field sensors using magneto-optical materials. The sensor programs that will be discussed are being developed by (1) the Naval Research Laboratory (NRL) in cooperation with FFA, Inc., (2) IPITEK, Inc. and (3) Opteos, Inc. The sensor systems developed at NRL and Opteos are based upon dielectric crystals. The sensor system developed by IPITEK is based upon a polymer material. Each of the sensor systems described requires a special laser system to activate the field measurement system and photo-detectors to detect the changes in the laser light properties (polarization or phase) that provide information on field intensity and polarization.

The effort at NRL has extensively addressed the electro-optical (E-O) response of a large number of crystals and investigated the influence of photorefractive effects and dielectric field reduction effects. Much effort has been invested in identifying the properties of crystals that affect their performance in a sensor system. This has allowed the NRL team to determine figures of merit (FOM) for candidate crystals and to identify the type of crystal that should produce the best performance for a specified application. The sensor utilizes the property of the crystal to change the polarization angle of the light passing through the crystal when an EM field is present. There is also a significant amount of work involved in packaging the sensor such that thermal and piezo-electric effects are minimized. These types of instabilities plagued many of the early efforts to develop practical, dielectric-crystal based sensors. Their current work is with Lithium Niobate crystals.

Opteos has developed one very practical E-O sensor system using very small crystals attached directly to a fiber-optic line that can survey the field on a printed circuit board. The initial system could only measure CW fields but Opteos has now developed prototypes for E-O sensors that can measure time-varying electric fields, an electro-optical voltage sensor for detecting voltage levels within an object and a magneto-optical (M-O) sensor for measuring magnetic field levels. The very small size of the Opteos sensors is very attractive for applications where field measurements must be made within confined spaces.

IPITEK in collaboration with BYU has developed and demonstrated bias-stabilized wideband sensors utilizing EO polymer on small glass chip waveguides and also as polymer-in-core sensing fibers. In either case, external E-fields produce instantaneous phase modulation effects detected as intensity modulations in the sensor transceiver. The development is aimed at miniaturized 3-axis vector E-field probes, and fiber-sized embedded probe arrays for HPM test and evaluation.

Oral Presentations

Implementing a Complex Frequency Shifted PML for Finite-Difference Time-Domain Simulation using a simple Recursive Integration approach

Antonios Giannopoulos

The University of Edinburgh, School of Engineering and Electronics, Edinburgh, UK

E-mail: A.Giannopoulos@ed.ac.uk

The perfectly matched layer (PML) is the most efficient and widely used method for the truncation of finite-difference time-domain (FDTD) computational grids. Since the original paper of Berenger [1], that introduced the PML technique in the FDTD numerical solution of Maxwell's equations, a number of different formulations have appeared, as well as, different numerical implementations of it [2]. However, it has been demonstrated that the standard PML stretching function - as introduced by Berenger - does not result in optimum performance for a number of specific problems, especially when waves impinge the PML at small angles or when inhomogeneous waves play an important role [3]. The complex frequency shifted (CFS) stretching function [4] given by (1)

$$\kappa_i + \frac{\sigma_i}{\alpha_i + j\omega t} \qquad i = (x, y, z) \tag{1}$$

allows us to alleviate some of the performance issues associated with PML absorption in such cases [5]. However, the direct implementation of the CFS function into the PML formulation often means an increase in the computational requirements and in algorithmic complexity hence, the CFS PML has not been as widely used. This paper presents a new, simple and efficient implementation of a PML with the CFS stretching function. This new formulation termed Recursive Integration PML (RIPML), by just a simple algebraic manipulation, results in an implementation that does not drastically increase the required computational resources. By using this formulation – which is based on the stretched coordinate PML – there is no need to redevelop or even recode the main FDTD update equations as the RIPML can be applied as a correction – or source - term to the appropriate field components, where is needed, after the main FDTD field update equations. For example, the application of the RIPML to the E_x field component - for a y-directed PML – is given by the following equation:

$$E_{x_{i,j,k}}^{n+1} = E_{x_{i,j,k}}^{n+1} + [CB \times RA] \frac{H_{z_{i+1/2,j+1/2,k}}^{n+1/2} - H_{z_{i+1/2,j-1/2,k}}^{n+1/2}}{\Delta y} + [CB \times RB]\Phi_{zy_{i,j,k}}^{n-1/2} \tag{2}$$

which is then followed by a simple update of the memory variable Φ_{zy} by

$$\Phi_{zy_{i,j,k}}^{n+1/2} = [1 - RC \times RB]\Phi_{zy_{i,j,k}}^{n-1/2} + [RC - RA \times RD] \frac{H_{z_{i+1/2,j+1/2,k}}^{n+1/2} - H_{z_{i+1/2,j-1/2,k}}^{n+1/2}}{\Delta y} + [CB \times RB]\Phi_{zy_{i,j,k}}^{n-1/2} \tag{3}$$

CB is the standard FDTD update multiplier for the magnetic field derivative and **RA**, **RB**, **RC** and **RD** are:

$$RA = \frac{2\varepsilon_0 + \Delta t \alpha_y}{2\varepsilon_0 \kappa_y + \Delta t(\alpha_y \kappa_y + \sigma_y)} - 1 \qquad RB = \frac{2\varepsilon_0 \kappa_y}{2\varepsilon_0 \kappa_y + \Delta t(\alpha_y \kappa_y + \sigma_y)}$$

$$RC = \Delta t \frac{(\alpha_y - \alpha_y \kappa_y - \sigma_y)}{\varepsilon_0 \kappa_y} \qquad RD = \Delta t \frac{(\alpha_y \kappa_y + \sigma_y)}{\varepsilon_0 \kappa_y} \tag{4}$$

The performance of the RIPML is very good and compares favourably with the performance of the convolutional PML [5]. In addition, as it is media agnostic it can be easily applied to inhomogeneous problems.

References
1. J. -P. Berenger, "A perfectly matched layer for the absorption of electromagnetic waves," Journal of Computational Physics, vol. 114, 1994
2. A. Taflove and S.C. Hagness, Computational Electrodynamics: The Finite-Difference Time-Domain method, 3rd Edition, Boston: Artech House, 2005
3. J. -P. Berenger, Perfectly Matched Layer (PML) for Computational Electromagnetics, Synthesis Lectures on Computational Electromagnetics, C. Balanis, Ed., Morgan & Claypool, 2007
4. M. Kuzuoglu and R. Mittra, "Frequency dependence of the constitutive parameters of causal perfectly matched anisotropic absorbers", IEEE Microwave and Guided Wave letters, vol. 6, 1996
5. J. Roden and S. Gedney, "Convolutional PML (CPML): An efficient FDTD implementation of the CFS-PML for arbitrary media", Microwave and Optical Technology Letters, vol. 27, 2000

Success Case Studies & Technology Transfer Bottlenecks in Humanitarian Demining EU-funded Research: Examples from the EC DELVE Project

C. Bruschini[1], H. Sahli[2], L. Van Kempen[2], R. Schleijpen[3], E. den Breejen[3]

[1]*CBR Scientific Consulting, Lausanne, Switzerland*
[2]*Vrije Universiteit Brussel, Dept. of Electronics and Information Processing, Brussels, Belgium*
[3] *TNO Defence, Security and Safety, The Hague, The Netherlands*
E-mail: Claudio.Bruschini@epfl.ch

The EC DELVE Support Action has analyzed the bottlenecks in the transfer of Humanitarian Demining (HD) technology from technology development to the use in the field, basing itself on the assessment of the European HD Research and Technology Development situation from early 1990 until 2006. The situation at the European level was analyzed with emphasis on activities sponsored by the European Commission. This was also done for four European countries and Japan (national activities). Based on this analysis a number of bottlenecks for the transfer of technology from the research to the end user were identified and potential remedies were suggested. Lessons learned and recommendations were established for the benefit of similar future research programs, primarily as an advice to the EC but with a wider application range. Results are provided in full in [1][2].

Notwithstanding the previously mentioned bottlenecks, in some cases it has indeed been possible to bridge, at least partially, the gap to market, bringing new or improved technology all the way to the end users. Four selected success case studies were analyzed [1] in order to identify the enabling factors and the circumstances which actually made this happen.

The first example focused on the MINEHOUND dual sensor detector [3], now in production, which combines a ground penetrating radar (GPR) from ERA Technology Ltd (UK) and a pulsed metal detector (MD) from Vallon GmbH (Germany), to reduce the false alarm rate normally encountered by metal detectors. This results in improved productivity of mine clearing operations. The output to the operator from both the metal detector and GPR is by means of audio signals and LEDs. A number of trials have been completed over the years, including field trials in real minefields in collaboration with several NGOs, alongside the currently used MD and under ITEP invigilation. Trials in live minefields show that the FAR can be reduced by a factor of between two and seven times with respect to a standalone MD, and the GPR also detects zero or minimum metal mines that are difficult for the MD. (Note: For a description of the competing US HSTAMIDS/AMD-14 system, see also [3].)

Success factors include here: (i) the use of a number of funding sources over the years, both civil and military, (ii) constant dedication, (iii) early GPR experience, (iv) continued visibility and readiness to communicate and disseminate information, (v) operational experience with GPR products, (vi) clear vision of end user requirements and acceptance and potential market, (vii) targeting the development of a "simple" acoustic interface, and (viii) commercial awareness and focus on delivering a commercial product.

As a second example we looked at the field tests of sensing equipment carried out within the Japanese three main R&D projects in HD, which ran under three different ministries working in cooperation with each other in the timeframe 2002-2007. We termed the project as a success in the sense that it has been possible, by a concerted effort, to bring a number of systems to the field test phase, to scientifically evaluate their detection performance comparing it with currently used metal detectors, and to publish the results.

The 3rd and 4th examples focused on the development of a polarization camera for the detection of surface laid man-made objects at TNO in the period from 1998 to 2006, and the development of GPR technology at IRCTR (Delft University) in the period from 1997 to 2006, respectively. Full details are provided in [1] and [3].

References
1. DELVE CONSORTIUM, "Humanitarian Demining R&D project funding in Europe", DELVE Deliverable D4.1, v2.2.0, May 2007, 85 pp. http://www.delve.vub.ac.be/
2. DELVE CONSORTIUM, "Humanitarian Demining R&D Lessons Learned", DELVE Deliverable D4.2, v2.3.0, May 2007, 60 pp. http://www.delve.vub.ac.be/
3. C. Bruschini, H. Sahli, and A. Carruthers, Guidebook on Detection Technologies and Systems for Humanitarian Demining. Geneva: Geneva International Centre for Humanitarian Demining, ISBN 2-88487-045-8, 2006. www.gichd.ch and http://www.gichd.ch/1248.0.html

UXO-TID - 2
UXO-TID - Target Detection & Sensor Technologies

Oral Presentations

Information Theory and Electromagnetism: Are They Related?

Sergey Loyka1[1], Juan Mosig[2],

[1]*School of Information Technology and Engineering, University of Ottawa, Ottawa, Canada*
[2]*Swiss Federal Institute of Technology, LEMA-EPFL, Lausanne, Switzerland*

E-mail: sergey.loyka@ieee.org

Multi-antenna (multiple-input multiple-output, or MIMO) system architecture, which promises unprecedentally high spectral efficiency, has recently emerged as a new paradigm of wireless communications in rich multipath channels, and was also enthusiastically welcomed by the industry and has been already incorporated into several popular standards of wireless access (e.g. IEEE 802.11, 802.16, WiFi, WiMAX etc.). However, it is also well recognized that the wireless propagation channel has a profound impact on the MIMO system performance (spectral efficiency, reliability, etc.). In ideal conditions (uncorrelated high rank channel) the MIMO channel capacity (i.e. the ultimate upper bound on the error-free information transmission rate) scales roughly linearly as the number of transmit (Tx)/receive (Rx) antennas. The effect of channel correlation is to decrease the capacity and, at some point, this is the dominant effect. This effect is highly dependent on the scenario considered. Many practically-important scenarios have been studied and some design guidelines have been proposed as well.

In this tutorial, we analyze the effect of the wireless propagation channel from a completely different perspective, by using jointly the techniques of information theory and electromagnetics [1]-[3]. Electromagnetic waves are used as the primary carrier of information. The basic electromagnetism laws, which control the electromagnetic field behaviour, are expressed as Maxwell equations. Hence, we ask a question: What is, if any, the impact of Maxwell equations on the notion of information in general and on the electromagnetic channel capacity in particular? In other words, do the laws of electromagnetism impose any limitations on the achievable channel capacity? Below, we concentrate on this last question and try to answer it. We are not targeting in particular scenarios, rather, we are going to look at fundamental limits that hold in any scenario. Analyzing MIMO channel capacity allows one, in our opinion, to come very close to answering this question.

Our approach is a three-fold one. First, we employ the channel correlation argument and introduce the concept of an ideal scattering to demonstrate that the minimum antenna spacing is limited to about half a wave length for any channel (i.e., locating antennas closer to each other will not result in a capacity increase because of correlation). Secondly, we use the plane wave spectrum expansion of a generic electromagnetic wave and the Nyquist sampling theorem in the spatial domain to show that the laws of electromagnetism in its general form (Maxwell equations) limit the antenna spacing to half a wavelength, for linear antenna arrays, but only asymptotically, when the number of antennas is infinite. For a finite number of antennas, this limit is slightly less than half a wavelength because a slight oversampling is required to reduce the truncation error when using the sampling series. In any case, the existence of the minimum spacing limits the number of antennas and the MIMO capacity for a given aperture size. It should be emphasized that this limitation is scenario-independent. It follows directly from Maxwell equations and is valid in any situation. Thirdly, we consider the MIMO capacity of waveguide and cavity channels [2] and demonstrate that there are final number of degrees of freedom in that environment too, which is dictated directly by Maxwell equations, that can be exploited for MIMO communications. Electromagnetics and information theory can be nicely united in this case to produce insight that is not available by using either of these disciplines separately. In particular, it turns out that the traditional single-mode waveguide transmission, which is so popular in electromagnetics community, is optimal only at small signal-to-noise (SNR) ratio.

References
1. S. Loyka, J. Mosig, Information Theory and Electromagnetism: Are They Related? (Invited), in G. Tsoulos (Ed.), MIMO System Technology for Wireless Communications, CRC & Taylor and Francis, Boca Raton, 2006.
2. S. L. Loyka, Multi-Antenna Capacities of Waveguide and Cavity Channels, IEEE Trans. Vehicular Technology, v. 54, N. 3, 863-872, May 2005.
3. N.U. Ahmed, F. Rezaei, S. Loyka, Control Theoretic Formulation of Capacity of Dynamic Electro Magnetic Channels, SIAM Journal on Control and Optimization, submitted, 2007.

Tutorial #1

High frequency grounding: modeling and design

L. Grcev

Ss. Cyril & Methodius University of Skopje, Faculty of Electrical Engineering, Macedonia
E-mail: Leonid.Grcev@ieee.org

Grounding system (GS) performance is different at low (LF) and at high frequencies (HF); while at LF often the whole area of the grounding system is effective in discharging current to ground (Fig. 1a), at HF only smaller part near the current injection point is effective (Fig. 1b). Latter is also true for fast varying excitation such as, for example, lightning related current pulses. Consequently, GS HF and fast pulse performance might be significantly deteriorated in comparison to the LF performance, for which GS are usually designed. This poses practical problems for safety, EMC and electric system operation, for example, due to excessive voltages between points at GS, high impedance paths to ground for lightning currents and high impedance return current paths for surge protective devices, etc.

This tutorial describes state of the art in modeling grounding systems at HF and transients and presents design guidelines to improve performance of practical grounding arrangements. Short survey is first given on the different approaches to modeling: from the simple circuit models to rigorous electromagnetic models with validation and comparison of the different approaches. The full-wave analysis method based on the rigorous electromagnetic field theory approach, which is considered as the most accurate since it is based on least neglects, is explained in more details [2]. This method enables:

- To analyze possibilities to improve the efficiency of the grounding system in dissipation of the current to earth especially in the beginning of the lightning pulse (or at high frequencies).
- Speaking in circuit terms, to look at possibilities to ensure low impedance path to earth for surge currents, which is important for the operation of protection devices.
- To analyze transient currents, fields, potentials and voltages distributions in order to optimize protection measures.
- To analyze transient grounding behavior in conjunction with the connected electrical or electronic systems, especially including the surge protective devices.

Discussion on the limitations of this analytical method and its validation with comparison with experimental results are also presented. Today this complex approach is utilized by software methods that enable interactive optimization of grounding systems. Software simulation enables parametric analysis in frequency and time domain to identify parameters with dominant influence in practical cases, which lead to simple design guidelines for improved HF and transient performance. In addition to software based analysis, the tutorial focuses on recent advances in analysis based on simple formulas for basic parameters that characterize impulse efficiency of ground electrodes important for practical applications [2].

(a)　　　　　　　　　　　　　　　　　**(b)**
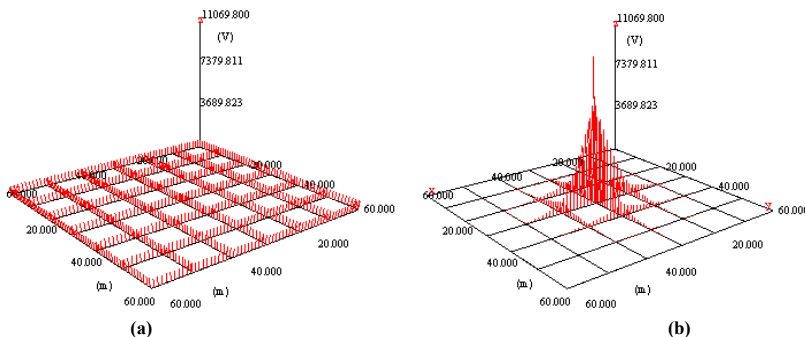
Fig. 1 – Different ground grid performance at low (50-Hz) (a) and high frequency (1-MHz) (b) (Conductor potential distribution in 60-m by 60-m with 6 by 6 meshes ground grid for current injection in the middle point)

References
1. L. Grcev, "Computer analysis of transient voltages in large grounding systems," IEEE Trans. Power Delivery, vol. 11, pp. 815-823, April 1996.
2. L. Grcev, "Impulse efficiency of ground electrodes," IEEE Trans. Power Delivery, 2008, in print.

Tutorial #2

Development of Electron Beam Focusing Magnet in High Power Klystron Amplifier

[1]Y. Sohn, [1]M. S. Hong, [1]S. H. Nam, [1]S. H. Kim, [1]Y. J. Park, [1]S. S. Park, [2]S. D. Park*, [2]J. H. Kim*, [2]J.E. Han, [2]S.Y. Park*, [3]J. W. Shin, [3]J. H. So, [3]W. Jang

[1]*Pohang Accelerator Lab, Pohang, Kyungbuk, Korea*
[2]*POSTECH, Pohang, Kyungbuk, Korea*
[3]*ADD, Daejoen, Korea*

E-mail: younguk@postech.edu

The focusing magnet in a relativistic klystron accelerator (KA) focuses electron beam to intensify beam power and to prevent electron beams colliding to wall of accelerating tube by producing Lorentz force.

We manufactured an electron beam focusing magnet that has 1.2 Tesla peak as DC magnetic field. Magnet was designed as modular type with 10 pan-cake style solenoids. Every module has exact same configuration. The bore of module solenoid is as tight as possible to KA beam tube to increase focusing efficiency, so that all cavities are positioned between modules. 10 modules were integrated as big one solenoid by put spaces between modules same as module height, without loosing flatness of axial field. This configuration makes it possible to save thermal load as much as 228 kW to 120 kW from Joule heating in coils. The magnetic field center of each solenoid was measured with a special measuring system. Then the center of the assembled focusing magnet with respect to the beam center was aligned with the individually measured field data of the pan-cake solenoids. The error of magnetic field center and direction error of magnetic flux line with respect to solenoid axis was less than 200 μm and 3 radians, respectively. The hitting print on circular disk from accelerated electron beam in the klystron beam tube showed perfectness of alignment. This paper is to report design, fabrication, alignment and its performance.

Short Transmission Lines - Lightning Induced Overvoltage

J. Kusala, L. Suchy

VOP-026 Sternberk, s.p., division VTUPV Vyskov,
V. Nejedleho 691, 682 03 Vyskov, Czech Republic,

E-mail: j.kusala@vtupv.cz

The aim of this study is to present some results obtained during simulations of LEMP coupling to transmission and communication lines used in typical military systems caused by nearby (tens to hundreds metres) lightning strike. This lines are typically tens to few hundreds meters long and they are drawn by earth surface. As a worst case were chosen lightning parameters mentioned in [1] for 5 % probability of its occurrence in negative flash to ground: peak current of return stroke 80 kA, time to peak 18 μs, time to half value 200 μs. It was chosen MTLE (Modified method of Transmission Lines with Exponential decay) model for upward moving return stroke current. Figures 1 a) and 1 b) shows both, typical shape and magnitude of LEMP components at distance 100 and 200 metres from strike point as a simulation results for channel length 2500 m, attenuation constant 1000 m, current propagation velocity 1×10^8 ms^{-1} and ground conductivity 1 mS/m. Figures 2 a) and 2 b) shows typical time behavior of induced overvoltage and current at impedance matched termination load for 100 metres long transmission line located in parallel to horizontal component of E vector.

Influence of transmission line height and length, termination impedances, earth conductivity and striking point location upon overvoltage at ends of the line will be presented. All simulations will be carried out in Matlab.
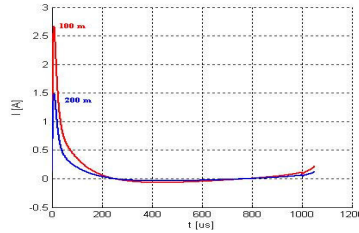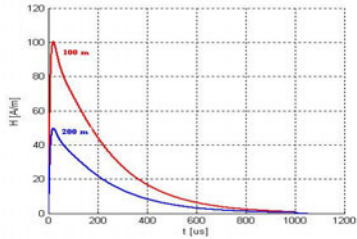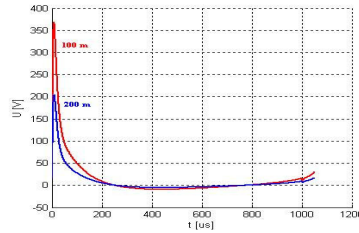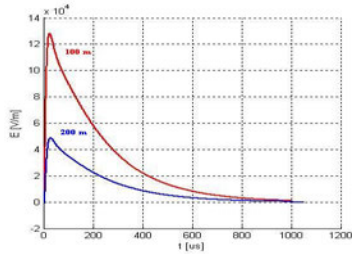
Fig. 1 a) Vertical component of E

b) Azimuthal component of H

Fig. 2 a) Induced overvoltage at termination load

b) Induced current at termination load

References
1. RUPKE E., Lightning direct effects handbook, Lightning Technologies Inc., March 2002

Fabrication of Multi-scale Triangular Patch High Impedance Ground Planes to Improve the Bandwidth of Conformal Bow-Tie Antennas

Bora Cakiroglu[1], Peter J. Collins[1], Michael Havrilla[1], Kubilay Sertel[2], Andrew J. Terzuoli[1]
[1]*Air Force Institute of Technology, Dayton, Ohio 45433 USA*
[2]*ElectroScience Laboratory, The Ohio State University, Columbus, Ohio 43212 USA*

...
E-mail: <peter.collins@ieee.org> *or* <a.j.terzuoli@ieee.org>

Broadband low-profile antennas, such as spirals, log-periodics, and bow-ties, substantially suffer in gain and bandwidth when they are brought close to a conducting surface. Thus, when standard broadband antenna designs are conformally placed on vehicle bodies, they can no longer achieve the high data rates required by modern communication and networking applications. A simple remedy for this has been to place an absorber lined cavity behind the antenna to preserve some bandwidth, at the expense of reduced gain. However, recently introduced high impedance ground planes (HIGPs) have novel electromagnetic features that have been shown to improve conformal antenna performance without the detrimental effects of absorber losses. In [1], thin metamaterial HIGP designs were incorporated into the antenna substrate to replace the lossy absorber layers, maintaining broadband characteristics and avoiding losses.

In this paper, we present a thin triangular-patch mushroom structure HIGP designed as a meta-substrate for a broadband bow-tie antenna. Specifically, two different-scale triangular-patch mushroom HIGP samples were analyzed and optimized using Ansoft's commercial full-wave solver HFSS v.10. The sizes and periodicities were designed such that the two samples have band-gaps that appear successively in frequency. Subsequently, we incorporated both designs into a single, multi-scale periodic HIGP, along with the active bow-tie antenna printed directly onto a RT/Duroid 5880 substrate to form the HIGP-antenna combinations. As seen in Figure 1, these designs were realized using the T-Tech Quick-Circuit system, and were characterized using an Agilent E8362B network analyzer.
We discuss the results of this characterization, and specifically show the advantages of the multi-scale HIGP in increasing the bandwidth of the conformal bow-tie designs.
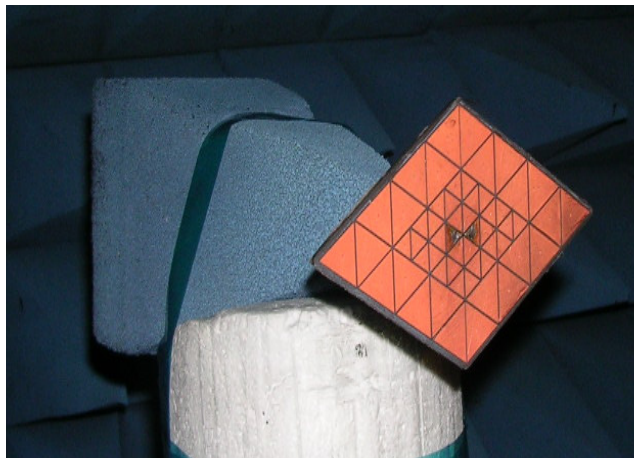
Fig. 1 – Conformal bow-tie antenna on a multi-scale triangular-patch HIGP

References
1. D. F. Sievenpiper, L. Zhang, R. F. J. Broas, N. G. Alexopolus, and E. Yablonovitch. "High-Impedance Electromagnetic Surfaces with a Forbidden Frequency Band," IEEE Transactions on Microwave Theory And Techniques, 47:2059-2074, November 1999.

Electromagnetic Threat for Soldiers – Assessment with Numerical Dosimetry

Lubos Suchy, Libor Palisek

VOP-026 Sternberk, s.p., division VTUPV Vyskov,
V. Nejedleho 691, 682 03 Vyskov, Czech Republic,

E-mail: l.suchy@vtupv.cz

Questions about electromagnetic field influence on health have not been definitely answered. Electromagnetic field levels which can cause health threat by thermal effects can occur in case of accident, in case persons are irradiated by power radiated sources as power transmitters, jamming equipments, radars, electromagnetic (RF) weapons but also personal communication transceivers. People can be unwillingly affected by intensive electromagnetic field during working on RF equipments in case of safety rules break [1].

Subject of presented project are possibilities of assessment of electromagnetic environment risk for soldiers considering electromagnetic irradiation in frequency range 1 MHz – 10 GHz. Specific absorption rate – *SAR* in human body is a typical electromagnetic quantity for threat level assessment in this frequency range. The aim of this project is verification of possibilities and practical use of electromagnetic excitation assessment with use of numerical method (FDTD, software SEMCAD X [2]). 3D structural model of the whole human body – detailed heterogeneous phantom WHPWB-1 [2] and homogenous phantom HWB-1 will be used, compared and evaluated for required averaging over whole body *SAR* as well as spatial peak *SAR*.

In case Specific Absorption Ratio levels absorbed in human tissue are lower than limits given according to ICNIRP (International Commission on Non-Ionizing Radiation Protection) it is possible to consider investigated electromagnetic environment as a safe. Results obtained during solving of this project will be presented in this paper.
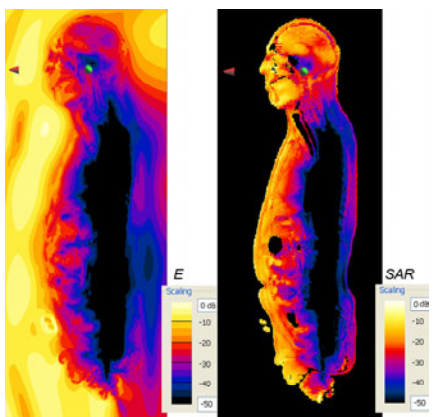
Fig. 1 – Whole Body Adult Male Phantom EMWB-1 [2],
E **and** *SAR* **Distribution,** *f* = 1.25 GHz
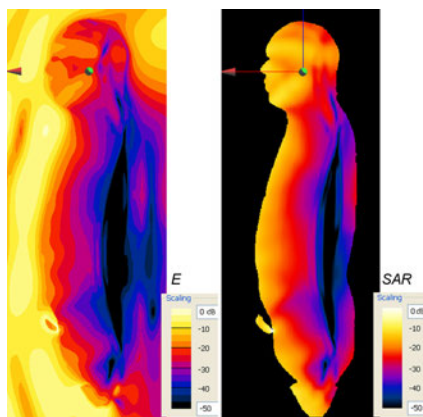
Fig. 2 – Whole Body Adult Male homogenous Phantom HWB-1, *E* **and** *SAR* **Distribution,** *f* = 1.25 GHz

References
1. A. V. Vorst, a. Rosen, Y. Kotsuka, RF/Microwave Interaction with Biological tisues, IEEE Press, Wiley-Interscience, 2006.
2. SEMCAD X, User's Workshop, Zurich, 2005.

The Requirement of Surge Immunity Test in IEC Standard

V. Ngampradit

Center of Excellence in Electrical Power Technology, Faculty of Engineering, Chulalongkorn University, Bangkok, THAILAND.

E-mail: vngampradit@hotmail.com

Nowadays, many IEC standards for household are established the surge immunity test for basic immunity requirement. However, the test waveform and test level that require in the standard are not relative with the installation points. We often found that if the EUT passed the surge immunity test in the laboratory, it may be damage after installation at the working site.

This paper is sought to review the different surge immunity test requirements, test waveform and test level of surge immunity test that require in IEC standard for household uses.

In detail, an author would like to show general basic information of surge overvoltages that can occur on low-voltage a.c. power systems, surge parameter at difference installation points comparing with the specified waveform and test level of surge immunity test requirements in IEC standards i.e. Standard for electricity metering equipment (AC) (IEC62052-11:2003), Standard for residual current operated circuit-breakers with integral overcurrent protection for household and similar uses (RCBOs) (IEC61009-1:2003) and Standard for uninterruptible power systems (UPS) (IEC62040-2:2005).

The above this comparison, the author would like to propose the Technical Committee to review and revise test requirements, test waveform and test levels of surge immunity test that require in IEC standard to relate with the installation points.

References
1. IEC62052-11:2003, "Electricity metering equipment (AC)- General requirements, tests and test conditions- Part 11: Metering equipment".
2. IEC61009-1:2006, "Residual current operated circuit-breakers with integral overcurrent protection for household and similar uses (RCBOs)- Part 1: General rules".
3. IEC62040-2:2005, "Uninterruptible power systems (UPS)- Part 2: Electromagnetic compatibility (EMC) requirements".
4. IEC61000-4-5:1995, " Electromagnetic compatibility (EMC)- Part 4-5: Testing and measurement techniques- Surge immunity test".
5. IEC62305-1:2006, "Protection against lightning- Part 1: General principles".
6. IEC TR62066:2002, "Surge overvoltages and surge protection in low-voltage a.c. power systems- General basic information".

Posters 1

Dielectric properties influence over shielding capability for chiral honeycombs

R.F. Damian[1], R.C. Ciobanu[1], V. David[1]

[1]*"Gh. Asachi" Technical University, Iasi, Romania*
E-mail: rdamian@etc.tuiasi.ro

In the past years, an increasing amount of effort has been invested in the development of new materials, with good mechanical properties, low weight and low cost. In particular auxetic materials benefit from their negative Poisson's ratio and are investigated closely in the last decade. A natural step forward is to investigate the electromagnetic properties of these materials, in order to provide good electromagnetic shielding.

Under test are the chiral panels presented in fig. 1. In this case the chirality is defined by geometry. It's shown in [1], [2] that in the isotropic composite chiral media consisting of chiral microstructures, the electromagnetic properties are those of the equivalent homogenous dielectric material.

In this paper our aim is to investigate the influence of the material properties ($\tan \delta$ and ε) over the transmission and reflective properties. We investigate the interaction between a plane wave and an infinitely large sheet of auxetic material, at normal incidence. Test details can be found in [3]. In this test we have the same geometrical properties (D - Internal cylinder diameter, L - Cylinder separation, h - layers' height, g - ligament width) but we insert variations in material properties: $\tan \delta = [0 , 0.5]$ and $\varepsilon = [1.5 , 10]$. S_{11} (fig. 2) and S_{21} are computed. The parametric curves are plotted in figures 3-6 in order to facilitate shielding design with this improved material. We represent first minimum of the reflectance (fig. 3) and its position (fig. 4). Similar graphs for the first and second maximum (also of interest in shield design) are omitted due to size restrictions in this abstract. Transmittance is plotted at two frequencies: 1GHz (fig. 5, close to GSM band) and 2.4 GHz (fig. 6).
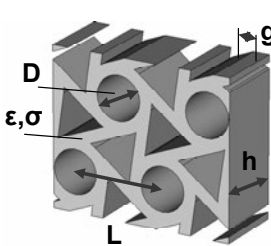
Fig. 1 – Hexachiral honeycomb and dimensions
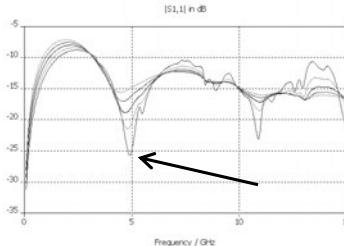
Fig. 2 – S$_{11}$ computed and location of first minimum
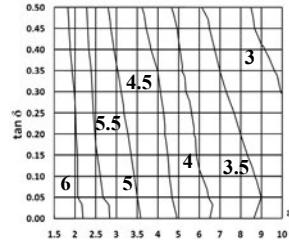
Fig. 3 – First minimum frequency 3-6 GHz
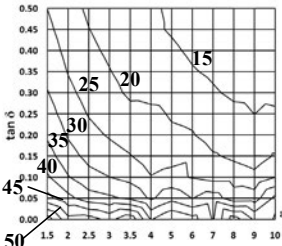
Fig. 4 – First minimum reflectance 15-60 dB
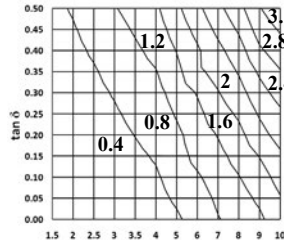
Fig. 5 – Transmittance at 1 GHz 0.4-3.2 dB
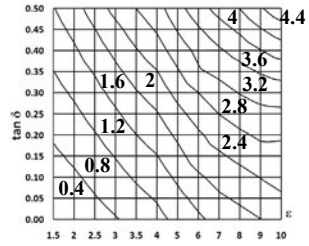
Fig. 6 – Transmittance at 2.4 GHz 0.4-4.4 dB

References
1. Frederic Mariotte, Sergei A. Tretyakov, Bruno Sauviac - Modeling Effective Properties of Chiral Composites, IEEE Antennas and Propagation Magazine, Vol. 38, No. 2, April 1996, pp. 22-32
2. P. Pelet, N. Engheta, The theory of chirowaveguides, IEEE Transactions on Antennas and Propagation, Vol. 38, No. 1, January 1990, pp. 90-98
3. R.F. Damian, R. Ciobanu, C. Schreiner, "*EMC tests and properties vs. microstructure for auxetic materials*", 15th IMEKO TC4 Symposium on Novelties in Electrical Measurements and Instrumentation, Romania, 2007, pp. 105-109

Numerical Computation of Temperature Increase in Pregnant Woman Model Induced by Electromagnetic Absorption of MRI System

Satoru Kikuchi[1], Kazuyuki Saito[1], Masaharu Takahashi[1], Koichi Ito[1], and Hiroo Ikehira[2]

[1]*Chiba Universuty, Chiba, Japan*
[2]*National Institute of Radiological Sciences, Chiba, Japan*

E-mail: kikuchi@graduate.chiba-u.jp

In recent years, there has been increasing concern about adverse health effects of pregnant woman and her fetus exposure to pulsing electromagnetic (EM) waves during magnetic resonance (MR) imaging. However, the safety guideline regarding the SAR for protecting the pregnant woman and her fetus has not been established in various organizations. On the other hand, several studies presented the results that thermal influence of the fetus causes growth-delay and developmental defect [1], [2]. According to ICNIRP (International Commission on Non-Ionizing Radiation Protection) report based on these results [3], it has been suggested that adverse effects on embryonic or fetal development will be avoided if the temperature of the fetus did not exceed 38 ^{o}C, and the body temperature of pregnant woman did not rise by more than 0.5 ^{o}C.

In this study, the temperature rise distribution in a pregnant woman model due to the RF pulse radiation is calculated by use of bio-heat transfer equation. Figure 1 shows the calculation model including the pregnant woman model and the birdcage coil at 64 MHz, which is employed as one of the fundamental RF coils for magnetic resonance imaging (MRI) system. The coil consists of two end rings, eight legs, and RF shield. The diameter and the length of the birdcage coil were set as 600 and 700 mm, respectively, so that the woman model can be inserted. A cylindrical RF shield, with a diameter of 740 mm and a length of 1,260 mm, has been located lateral to the coil. Before the calculation, the capacitors on the birdcage coil were adjusted so that the resonance frequency of the coil is around 64 MHz. Figure 2 shows the calculated temperature rise distribution in the observation plane which is the coronal plane (*xz*-plane) including around the center of the fetus. In this calculation, the SAR values (corresponding to the heating source) are normalized to the whole-body average SAR limit in the IEC standard, which is 2 W/kg for normal operating mode. It is confirmed that the temperature rise of the maternal surface is low, because the temperature rise of the body surface is alleviated by difference of temperature with the ambient air. Moreover, it was found that the maximum temperature in the fetus is 37.5 ^{o}C, therefore, it is confirmed that this result is lower than the threshold dose [3]. As further studies, it is necessary to calculate the SAR and temperature rise by the other RF coils used in conventional MRI systems. In addition, although the SAR and temperature distributions were calculated by a sinusoidal wave excitation in this study, the wave form of RF pluses must be considered for the actual imaging.
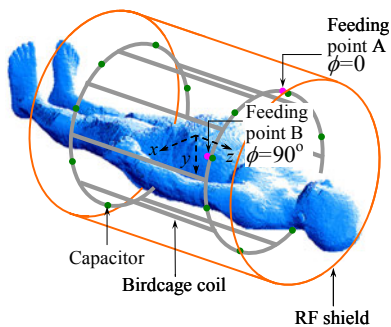
Fig. 1 – Numerical calculation model
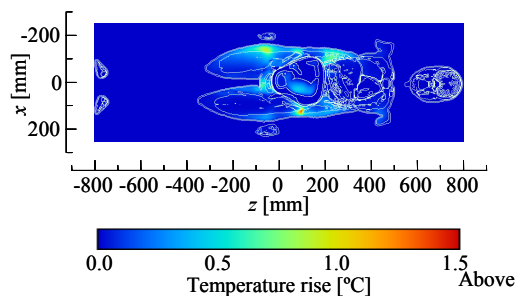
Fig. 2 – Calculated temperature rise distribution

References
1. J. M. Graham *et al.*,"Teratogen update: Gestational effects of maternal hyperthermia due to febrile illnesses and resultant patterns of defects in humans," Teratology, vol. 58, pp. 209-221, 1998.
2. M. J. Edwards, R. D. Saunders, and K. Shiota, "Effects of heat on embryos and foetuses," International Journal of Hyperthermia, vol. 19, no. 3, pp. 295-324, 2003.
3. International Committee on Non-Ionizing Radiation Protection (ICNIRP), Medical Magnetic Resonance (MR) procedures: protection of patients, Health Physics, vol. 87, no. 2, pp. 197-216, Aug. 2004.

Posters 1

Information Communication Security due to High-Power Electromagnetics

H. Sekiguchi, and S. Seto

National Institute of Information and Communications Technolog,, Tokyo, Japan
E-mail: hide@nict.go.jp

Recently, a new threat to information communication infrastructure has emerged due to intentional high-power electromagnetics (HPEM) that may be known as intentional electromagnetic interference (IEMI). The information communication systems are composed of communication cables and equipments such as computers, routers, and hubs constructing the networks. If these equipments are exposed to HPEM environments over their immunity levels, they are physically broken down or their processing powers are dropped away. Since the disruptive interference for information communication terrifies civil society, it is important to examine the security level of information communication against intentional HPEM. Our eventual goal is the development of the evaluation and countermeasure method.

In this paper, the throughput capacity of communications was investigated depending on modulations and exposure levels of HPEM. The equipment under test (EUT) was a commercial 10 Base-T hub with 8 ports. The throughput rate was measured by means of a network performance analyzer (SPIRENT Communications: Smartbits 200) with a personal computer (PC). The HPEM fields were created in a giga-hertz transverse electromagnetic (GTEM) cell (ASTEC: model 5317) with the use of a synthesized signal generator (Hewlett Packard: 8664A) and a high power amplifier (Amplifier Research: 100W1000M1). Our test experimental configuration is shown in Fig. 1. Test measurements were performed turning modulations of HPEM. Then, the amplitude modulation (AM) was adjusted the degree of modulation and the modulated signal frequency, the frequency modulation (FM) was adjusted up its deviation and the modulated signal frequency, and the pulse modulation (PulseM) was adjusted its repetition frequency with duty ratio 1:1, as the operation carrier frequency changed. One example of test measurement results is shown in Fig. 2. The horizontal axis was the operation carrier frequency. The vertical axis was the electric filed strength measured in the same place as the EUT by means of an isotropic electric field probe and its meter (HOLADAY: HI-4422 and HI-4416), from which the throughput capacity began to drop away. Then the EUT was not physically broken down. From Fig. 2, it is found that there is the vulnerability of the EUT depending on each modulations and their parameters. The EUT had most vulnerable level to AM with the degree of modulation of 100 %, although existing immunity tests uses AM with the degree of modulation of 80 %. Also, the EUT has vulnerable wide band to FM.

As shown to experimental results, a new test method should be necessary to evaluate the security of information communication equipments. It has to be discussed the ways and means by many experimental measurement results. These aspects are currently under investigation and will be presented at the symposium.
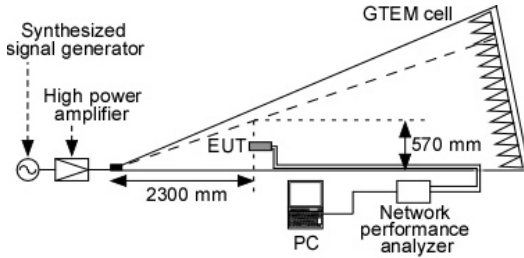
Fig. 1 – Test experimental configration
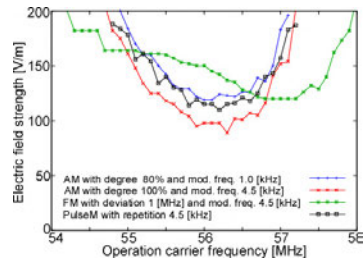
Fig. 2 – Test measurement result

References
1. W. A. Radasky, C. E. Baum, and M. W. Wik, "Introduction to the Special Issue on High-Power ," IEEE Transactions on Electromagnetic Compatibility, vol. 46, 2004.
2. "Electromagnetic compatibility (EMC) - Part 1-5: General - High power electromagnetic (HPEM) effects on civil systems," International Electrotechnical Commission (IEC), IEC/TR 61000-1-5, 2004.
3. T. Tominaga, "Draft text of Recommendation K.hpem ``Application of requirements against HPEM to telecommunication system''," International Telecommunication Union, Telecommunication Standard Secter (ITU-T), Study Group 5, TD613, 2007.

Consideration of the Sensors Gain-Phase Characteristics in High Resolution Image Reconstruction Devices

R. Zaridze[1*], **D. Kakulia**[1], **V. Tabatadze**[1], **D. Mazmanov**[1], **G. Saparishvili**[1], **N. Uzunoglou**[2]

[1]*Tbilisi State University, Laboratory of Applied Electrodynamics, Chavchavadze Ave. 3, 0128, Tbilisi, Georgia*
[2]*Microwave and Fiber Optics Laboratory, Institute of Communication and Computer Systems, National Technical University of Athens, Greece*

rzaridze@laetsu.org

In [1] was presented developed ideas of article [2] - remote sensing methods for buried objects visualization which consist of two parts: first one is determination soil's electrodynamic characteristics (like permittivity and dielectric loss tangent) on the frequency in order to find the best EM monitoring pulse, for deep penetration of its frequency contents waves. Second part dedicated to buried objects image reconstruction by means of reflected field. There are presented results for the holographic/photographical method of immersed body visualization. All researches are dedicated to create software package for of high resolution image recognition devices. For mentioned methodology important condition is to treatment of exact reflected field. The main goal is to get information from the reflected pulse form. In reality, during all kind measurements of the reflected field (especially in case of the pulse detection) we are using some receiving (pickup) antennas, which are very far from ideal one. As an example, in Fig. 1 shows the receiver antenna s11 parameters and as a result of this, we are getting distorted image. It is well known, that the main information of the image contains in the phases of the frequencies spectrum reflected field. The amplitudes of the reflected field are not so responsible for high resolution (in case if the signal is not noisy!) as the phases of the received signals. So, the main problem is to build antennas with minimal pulse-shape and frequency-phase distortion or to consider its distortions. Motivation of this paper is creation of computer program to consider gain-phase characteristics of the receiver antennas to reconstruct real reflected pulse based on measured one. This is important issue in creation of an image recognition system software package for high resolution image reconstruction, target detection and their discrimination system.
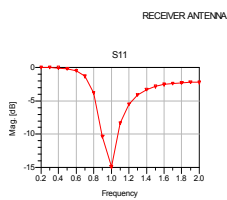
Fig.1
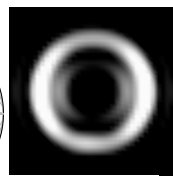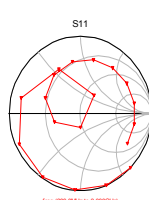
Fig. 2. $V_1 = 1.3$ GHz

Fig. 3. $V_1 = 1.3$ GHz, $\varphi_1 = 0$
$V_2 = 1.13$ GHz, $\varphi_2 = 4.3$
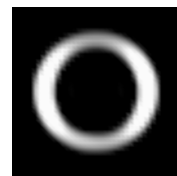
Fig. 4. $V_1 = 1.3$ GHz, $\varphi_1 = 0$
$V_2 = 1.13$ GHz, $\varphi_2 = 4.3$,
$V_3 = 0.88$ GHz, $\varphi_3 = 4.5$.

Fig. 2, 3, 4 corresponds to the torus image reconstruction respectively for one two and three frequencies. These frequencies are in relation 0.69:0.85:1 this is the relation analogical to visible light base colors: red, green, blue. The phases of these frequencies are chosen so that the outer fields of torus for each frequencies liquidates each other and we get comparably good resolvability of reconstruction image. First we reconstruct the torus image for one frequency (Fig.2) in this case the quality of image is not good. Here is seen the other fields out of the torus and it is difficult to distinguish the form of the torus. After that we superpose as complex numbers to the field of first frequency the field of second frequency. We choose the phase difference between these two frequencies for getting better quality of the image which is shown in Fig.3. Here the outer field is apart to torus but it is desirable to avoid this field too. For this reason we superpose to this image the field of third frequency and choose the phase for this frequency too. The phase difference between first two frequencies stays the same. It gives an image represented on the Fig. 4. The change of amplitudes of spectral components do not affect on the result of reconstruction effectively.

References
1.   V. Tabatadze, M. Prishvin, G. Saparishvili, D. Kakulia, R. Zaridze. Soil's characteristics study and buried objects visualization using remote sensing. Proceedings of XII-th International Seminar/Workshop on Direct and Inverse Problems of Electromagnetic and Acoustic Wave Theory (DIPED-2007), September 17-20, 2007, Tbilisi, Georgia. pp. 134-138.
2.   R. Zaridze, G. Bit-Babik, K. Tavzarashvili, N. Uzunoglu, D. Economou. "Wave Field Singularity Aspects Large-Size Scatterers and Inverse Problems." IEEE Transactions on Antennas and Propagation, vol. 50, No. 1, January 2002, p. 50-58.

Posters 1

Microwave Antenna with Thermosensor for Intracavitary Thermal Therapy of Bile Duct Carcinoma

K. Saito[1], T. Kamimura[2], M. Takahashi[1], and K. Ito[2]

[1]*Research Center for Frontier Medical Engineering, Chiba University, Chiba, Japan*
[2]*Graduate School of Engineering, Chiba University, Chiba, Japan*

E-mail: kazuyuki_saito@faculty.chiba-u.jp

Microwave energy is a heating source used for localized hyperthermia, which is one of the thermal treatments for cancer. Depending on position and size of the target tumor, several types of antennas, which radiate micro-wave energy to the target, can be selected. In this study, a microwave antenna for the intracavitary thermal ther-apy was developed and was especially investigated to treatment of bile duct carcinoma. Figure 1 shows scheme of the treatment. A long and flexible microwave antenna is inserted into a forceps channel of endoscope, which is used to insert the tool for treatment. Finally, the antenna is guided to the bile duct through the papilla of Vater, which is placed in the duodenum [1]. The authors have been studying coaxial-slot antenna [2], which is one of the thin microwave antennas for interstitial microwave hyperthermia. This time, based on this technique, a long and flexible coaxial-slot antenna for intracavitary heating shown in Fig. 2 was developed. In addition, in order to prevent overheating the surface of the bile duct, thin thermocouple was equipped around the antenna tip for tem-perature measurement. The thermocouple, which is a thin metallic wire, may affect the electromagnetic distribu-tion around the antenna. In addition, measured temperature by the thermocouple may not be exactly. Therefore, the heating pattern of the antenna and the measured temperature by the thermocouple were evaluated by use of tissue-equivalent solid phantom. As a result, the heating region by the microwave radiation was observed only around the antenna tip. In other words, although thin metallic wire is placed close to the antenna, any undesira-ble hotspots were not observed around the antenna. Moreover, thermocouple placed vicinity of the antenna tip could measure the temperature around the antenna with some ingenuities. From these results, it can be said that the developed antenna is useful for the treatment of bile duct carcinoma. As a further study, the effectiveness of the antenna will be investigated by the animal experiments.
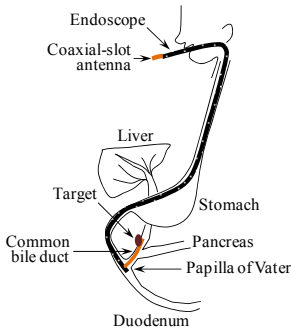
| Fig. 1 – Scheme of the treatment | Fig. 2 – Antenna of trial manufacture for intracavitary heating |
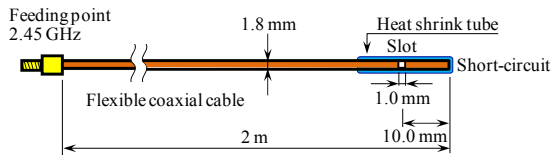
References
1. K. Saito, A. Hiroe, S. Kikuchi, M. Takahashi, and K. Ito, "Estimation of heating performances of a coaxial-slot antenna with endoscope for treatment of bile duct carcinoma," IEEE Transactions on Microwave Theory and Techniques, vol. 54, no. 8, pp. 3443-3449, Aug. 2006.
2. K. Ito, K. Ueno, M. Hyodo, and H. Kasai, "Interstitial applicator composed of coaxial ring slots for microwave hyperthermia," Proceedinf of 1989 International Conference on Antennas and Propagation, pp. 253-256.

Comparative Study Regarding the Accuracy of the Measurements Performed with Frequency Selective Systems in the Case of SDR Emitting Sources

P. Bechet[1], S. Miclăuş[1], I. Bouleanu[2], R. Mitran[1], R. Helbet[2]

[1] *Land Forces Academy, Sibiu, Romania*
[2] *Training Center for Communications and Information Systems, Sibiu, Romania*
E-mail: pbechet@gmail.com

The paper aims to compare the accuracy of the measurements performed by two frequency selective measurement systems, for the analysis of the electromagnetic compatibility (EMC) of Software Defined Radios (SDRs). The EMC measurements are made in Open Area Test Site (OATS) conditions. The compatibility aspects take into account the interferences (INTF) between signals emitted by the SDR sources (the harmonics and the Adjacent Channel Interference levels), their relative spatial positioning and the polarization of the emitted signals, in complex propagation environment. The measurement systems used are the TS-EMF system and the FIELD-NOSE system. They use isotropic antennas but different signal capture techniques. The paper proposes a measurement procedure which allows similar measurement settings of the two systems. Fig. 1 illustrates some results obtained by using the FIELD-NOSE system in the study of the INTFs generated by two SDR emitting sources. The diagram identifies the INTF signals measured at a 10 m distance from the emitting sources, in the following situations: yellow - 3rd harmonic, vertical polarization (VP), 2 m distance inter-sources; blue –INTFs, 2 m distance inter-sources, VP; black –INTFs, 2 m distance inter-sources, orthogonal polarization; red –INTFs, 4 m distance inter-sources,VP. In fig. 2 a comparative example of the measured signal is represented when using the two systems (the power mentioned on the x-axes of the graph is the power of the emitting source). The incident signal has a carrier of 800MHz and the resolution bandwidth (RBW) used was either 10kHz or 30kHz. One observes that dispersion of data sets is sufficiently low, but differences between the two systems results of the measured E-field are significant. This is due to both uncertainty differences between the systems and to different environmental impact on the way the signals are captured (duration between samples, differences in sensor technology, etc.).
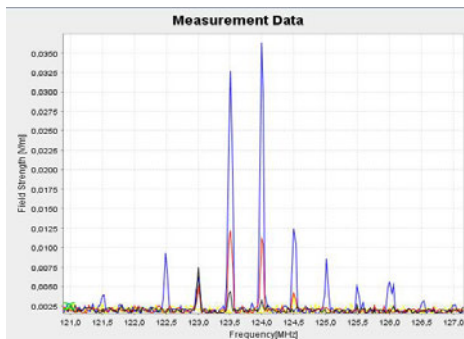
Fig. 1 - Comparative report of the interfering signal levels on the third order harmonic
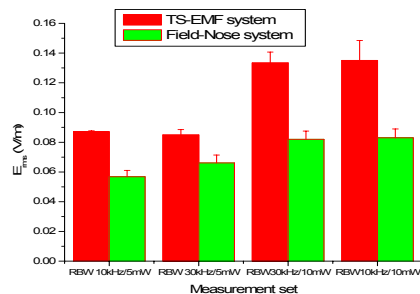
Fig. 2 - Comparison of E-field level measured by the two frequency-selective systems

We followed a comparative study regarding error calculation and uncertainty given by each of the measurement system in the aim of increasing the reliability of the assessment. The results of the study also contribute to the optimization of relative spatial positioning of the emitting systems in different propagation conditions.

Bibliography
1. *** Handbook Spectrum Monitoring, ITU Radiocommunication Bureau, 2002.
2. *** Agilent AN 1328 Making Precompliance Conducted and Radiated Emissions Measurements with EMC Analyzers, 2000.

Posters 1

Lacunarity of rough surfaces from the wavelet analysis of scattering data

J.-R. Poirier [1], H. Aubert [2,3]

[1] *LAME-ENSEEIT, 2 rue Charles Camichel, 31071 Toulouse, France*
[2] *LAAS-CNRS, University of Toulouse, 7 avenue du Colonel Roche 31077 Toulouse, France*
[3] *INPT-ENSEEIHT, 2 rue Charles Camichel, 31071 Toulouse, France*
E-mail: poirier@n7.fr

This research work is placed in the framework of the time-domain analysis of waves reflected by fractal objects and the remote description of their fractal characteristics. The problem consists of determining a direct relationship between the fractal descriptors (dimension, lacunarity, …) of highly irregular surfaces and the characteristics of electromagnetic signals scattered by these surfaces. As it is has been recently reported [1], wavelet analysis is an efficient tool for remotely extracting the self-similar features of fractal objects from their scattering data. . The analysis is extended here to the rough (Weierstrass) surfaces.

The resolution of the direct and inverse scattering problems involving rough surfaces is of crucial interest in practice for predicting, e.g., the ocean electromagnetic echoes or the remote estimation of agricultural ground roughness. The height profile of such natural surfaces may be advantageously described by the Weierstrass function (see, e.g., [2]). In our prevous work [3] the lacunarity descriptor of the Weierstrass surface has been remotely determined from the wavelet analysis of the scattered electromagnetic field in the *near-field region*. In this communication the lacunarity of the rough surface is extracted from the scattered field *in the far-field region*. This result opens the door at multiple applications in the area of remote sensing.

The Figure below illustrates how extracting the lacunarity of a rough surface from the Wavelet Transform Modulus Maxima (skeleton) of scattering data. The lacunarity may be derived from the distance between two particular and detectable bifurcations in time-scale domain. Many other results will be shown and discussed at the conference.
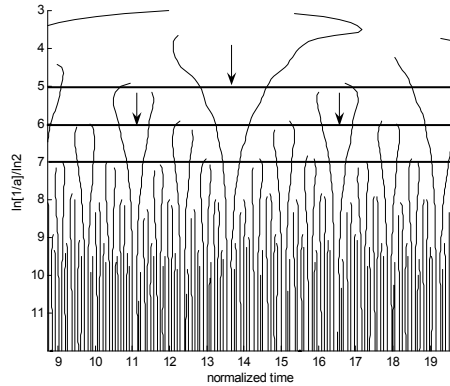
Fig. 1 – Wavelet Transform Modulus Maxima (skeleton) of the far-fied signal scattered by a Weierstrass surface. The arrows indicate the location of bifurcations along the scale axis that allow the remote estimation of the rough surface lacunarity.

References

1. H. Aubert and D. L. Jaggard, Wavelet analysis of transients in fractal supperlatices, IEEE Trans. Antennas Propag., vol 50, no. 3, pp 338-345, Mar. 2002
2. S. Rouvier, P. Borderies and I. Chenerie, "Ultra widebandelectromagnetic scattering of a fractal profile,", *Radio Science*, vol 32, No. 2, pp 285-293, March-April 1997.
3. J.-R Poirier, H. Aubert and D.L. Jaggard,"Wavelet analysis of the electromagnetics cattering from Bandlimited fractal surfaces", EUCAP, Nice, nov. 2006

Posters 1

Controllable broadband Hall element for measuring pulsed and dc magnetic fields in the temperature range from liquid helium to 600 K

M.L. Baranochnikov[1], A.V. Leonov[1], A.D. Mokrushin[1], V.N. Mordkovich[1], D.M. Pazhin[1], N.M. Omelianovskaya[1], and M.M. Filatov[2]

[1]*Institute of microelectronics technology and high purity materials Russian Academia of Sciences, Chernogolovka, Russia*
[2]*Research Institute of Pulse Technique, Moscow, Russia*

E-mail: mord@sci.lebedev.ru

A magnetosensitive element based on the "silicon-on-insulator" structures with a thin (~100 nm) silicon layer is considered.

Its design combines the conventional Hall element and a two-gate field-effect transistor with a control system such as metal--insulator--silicon--insulator--metal. The controllable Hall element has the following experimentally confirmed advantages:

1. Range of measured dc and pulsed magnetic fields $(10^{-6} \ldots 5$ T).
2. Wide range of operating temperatures (1.7 … 600 K).
3. Low energy consumption (operating current 0.1 … 0.4 mA).
4. Range of operating frequencies 0 … 100 kHz.
5. Stability to ionizing (gamma-ray photons) and neutron irradiation no worse than 1 Mrad and 10^{14} cm^{-2}, respectively.

Figure 1 shows the characteristic response of the Hall element to a pulsed magnetic field, Fig. 2 characterizes the linearity of the magnetic sensitivity of the element. The two-gate control system provides new Hall-element circuit capabilities for measuring and processing of magnetically induced signals. In particular variations of gates potential make possible to control the magnitude, dynamic range and temperature dependence of Hall elements magnetosensitivity,
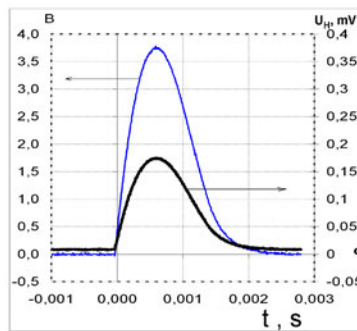
Fig.1 - Characteristic response of the Hall element to a pulsed magnetic field
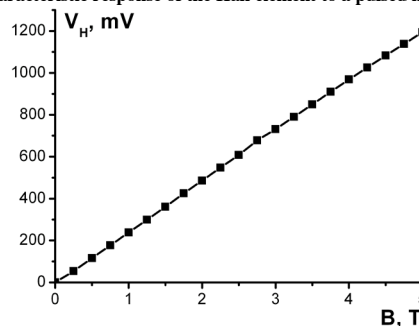
Fig. 2-Magnetic sensitivity of the element

Posters 1

Ultra-wideband pulse generator with radial forming line

V. A. Baldygin, V.P.Lisitsyn, M. G.Nikiforov

Research-and-production enterprise ERA, Moscow region, Russia, http://www.istra.ru/~era
E-mail: lisitsyn@istranet.ru

The paper presents results of development a compact repettitive ultra-wideband pulse generanor [1, 2].

An equivalent circuit of the generator is shown in figure 1. The main elements of this circuit are pulse transformer 5 and pulse forming system, which consist of an accumulative line 7, a commutating switch 8; a radial line 9 with a multi-spark switch 10 on the outer end , an isolating capacity 11 and transmitting line 12. Moreover there are control system 1; charger 2; primary capacity 4, thyristor commutator 3, load 13.
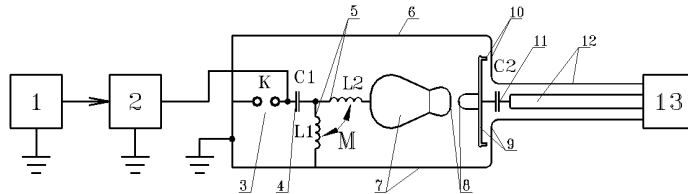
Fig. 1 – Equivalent circuit of the generator

The pulse transformer is autotransformer with ferrite core. The primary winding is made of 200mm – wide copper foil with polyethylene insulation. The copper wire of the secondary winding is wound on polyamide insulation frame. The winding coupling coefficient is 0.8.

The pulse transformer and pulse forming system are installed in 130mm - diameter common metal case filled with hydrogen with overpressure 70 atm. This technical solution permits exclude the isolator, which separates the volumes of pulse transformer and pulse forming system. In consequence, the reliability of the device increases essentially.

Thanks to the original forming system, output impulse amplitude is equals or grater then value of charging voltage. The output impulse has various forms in dependence upon values of isolating capacity and wave impedance of transmission and dimensions of radial line.
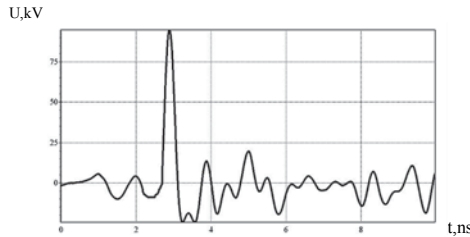
Fig. 2 – Output voltage impulse on equivalent load

The generator tests were carried out in short-term periodic rate with pulse burst time up to 10s, pulse-repetition rate of 1000 Hz, pause between pulse bursts to 10s. According to the results of experiments output power measured in transmitting line is 200 MW. The voltage impulse form on equivalent load of generator is shown in figure 2.The real load of the generator is antenna, for example, the new parabolic antenna [3].

At present time, similar impulse generator with output power near 5 GW is on test.

References
1.   V.A. Baldygin, M. G. Nikiforov A device for forming sub nanosecond pulses, Russia patent №2206175, 2001.
2.   V.A. Baldygin, A. A. Beloshapko, O. V. Davydov, V. P. Lisitsyn, M. G. Nikiforov, High voltage generators of nano and sub nanosecond pulses, Prikladnaja Fizika, №4, 2001., pp.11-14 (in Russian).
3.   V. P. Lisitsyn. A parabolic antenna for radiation power UWB pulses on basis of the satellite dish. Digest of 2006 IEEE AP-S international symposium and UNSC/URSI and AMEREM meetings, p.811.

High Power and Sub-nanosecond Pulsed Power Systems
based on Solid-State Technology for High Power EMC testing

Y.K. Jeong[1], M.Q. Lee[2], D.G. Youn[3]

[1]*Department of Electrical & Computer Engineering, University of Seoul, Seoul, Korea*
[2]*Department of Electrical & Computer Engineering, University of Seoul, Seoul, Korea*
[3]*EMC Research Institute, Cyware, Co., LTD, Seoul, Korea*

E-mail: ripley34@empal.com

In this paper, we developed a solid-state pulsed power system (based on solid-state switch) for the high power EMC testing.

The major advantage of a solid-state pulsed power system is the higher pulse repetition rate than non-solid-state pulsed power system (based on gas switch such as a thyratron, ignitron or spark gap). But its pulse peak power is much lower than non-solid-state pulsed power system [1][2]. In order to solve with this problem, we applied spatial power combining technology by using multi-source/multi-antenna array system.

The designed system is composed of two parts: a solid-state impulse generator and an ultra-wideband antenna. As shown in Fig. 1, a solid-state impulse generator is composed of a power supply, a trigger pulse generator, sub-nanosecond pulsers and power divider. Sub-nanosecond pulser has a capacitor as energy storage and a series-stacked avalanche transistor as a discharging switch. Power divider uses for the time synchronization of the triggering pulse leading to the each sub-nanosecond pulser. A solid-state impulse generator can produce a 10kV pulse with a rise time of 560ps and a pulse repetition rate of up to 1kHz. For the radiation of impulse signals, we designed TEM horn antenna (ultra-wideband antenna) with a center frequency of 400MHz. And it has the frequency band from 200MHz to 1.2GHz with SWR <3.

By using this system, we tested free space impulse radiation at a distance of 3m in the laboratory. Fig. 2 shows configuration of the test bed. We measured E-field strengths in one source/one antenna system and two source/two antenna system, respectively, for the experimental verification of the high power impulse radiating ability using a spatial power combining technology.

In the test results, we obtained 1.4kV/m E-field strengths value in one source/one antenna system and 1.89kV/m E-field strengths value in two source/two antenna. As a result, E-field strengths of the two source/two antenna array system has more upgraded performance by over 35% than the one source/one antenna system, and the spatial power combining efficiency is 67.5%.

In conclusion, we verified the possibility of high power impulse radiating ability using the spatial power combining technology.
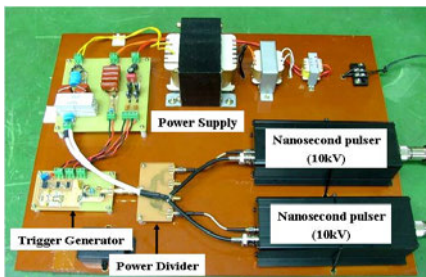
Fig. 1 - Solid-tate impulse generator
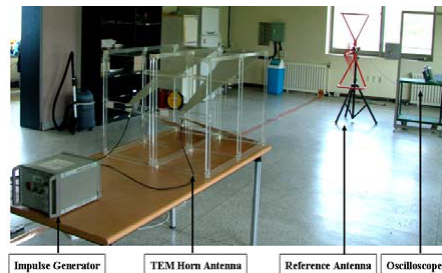
Fig. 2 - Test bed configuration

References
1.   Dr. Stephan Roche, "Solid-state pulsed power systems,"
      http://www.physiqueindustrie.com/Publi/solid_state_pulsed_power.pdf.
2.   John Pasley, "Pulse power switching devices - an overview," 1996 http://home.earthlink.net/~jimlux/hv/pasley1.htm

Posters 1

Axially-Symmetrical Radiators: Widening the Scope of Operation of Structurally Simple Elements and Units

K. Sirenko[1], G. Granet[2]

[1]*A.Ya. Usikov Institute of Radiophysics and Electronics, National Academy of Sciences, Kharkov, Ukraine*
[2]*Laboratoire des Sciences et Matériaux pour l'Electronique et d'Automatique, Université Blaise Pascal, Aubière Cedex, France*
E-mail: kostik13@gmail.com

We present a novel solution of the problem associated with the analysis of transient and steady-state processes in axially-symmetrical ($\partial/\partial\varphi \equiv 0$) radiators of pulsed and monochromatic electromagnetic TE_{0n}- and TM_{0n}-waves. The solution is based on the construction and further usage of original fully absorbing boundary conditions in standard finite-difference algorithms. This approach allows truncate efficiently a computational domain in open initial boundary-value problems [1–3]. The algorithms, being modified by this means, allow one (in contrast to the well-known approaches based on the approximate boundary conditions [4]) to obtain reliable data on space-time transformations of electromagnetic fields under resonant conditions.

The main results are:

- Basic electrodynamic (amplitude-frequency and pulse-response) characteristics for a number of simple axially-symmetrical radiators of TE_{0n}- and TM_{0n}-waves have been obtained, analyzed, and summarized. Structures under study are monopoles, mirror and resonant antennas. Models with a coaxial feeding line and an infinite flange in $z = 0$ plane have been considered. Usually we analyse the directional patterns $D(\theta, \infty, k)$ and the antenna efficiency $\eta(k)$ over a wide range of a frequency parameter k ($k = 2\pi/\lambda$ is the wave number and λ is the wavelength in free space; ρ, φ, z and r, θ, φ are cylindrical and spherical coordinates). Moreover the pulsed patterns $D_p(\theta, r, t)$ [5] in near-field and far-field zones of radiators, pulse-mode power radiation characteristics and field vector distribution in the computational domain Q have been processed.

- We proceeded with the study of slot resonances [6]. The excitation of slot resonances allows one to vary predictably basic characteristics of standard axially-symmetrical radiators of TM_{0n}-waves. New data have been obtained for the dazzled-state antenna phenomena and the effect of maximum growth of the antenna efficiency. Both caused by resonances in narrow radial and longitudinal short-circuited slots in outer and inner conductors of a coaxial feeding line. Furthermore the effects of complete transmission of the input energy into free space through narrow longitudinal slots in the closed end of a coaxial waveguide have been studied.

Some of the results and conclusions can be considered as known or anticipated. However, as a whole, they give a comprehensive data on practically interesting omnidirectional radiators and operating conditions. As an example, we can refer to the radiation mode of the cavity resonator, in which higher modes are excited. Or the radiation mode of a homogeneous disc resonator based on the monopole being an extension of a central conductor of a coaxial feeding line. In the latter case the most interesting effects are the break of the standard half-wave rearrangement of the directional pattern (being typical for monopole antennas) and considerable enhancement of the frequency band, which guides long TM_{0n}-waves practically perpendicularly to the radiator axis.

References
1. Y. K. Sirenko, V. L. Pazynin, A. I. Vyazmitinova, and K. Y. Sirenko, "Compact obstacles in free space: virtual boundaries for scalar and vector 'open' initial boundary-value problems in electromagnetic wave scattering theory," Electromagnetic Waves and Electronic Systems, vol. 8, 2003 (in Russian).
2. K. Y. Sirenko and Y. K. Sirenko, "Exact 'absorbing' conditions in the initial boundary-value problems of the theory of open waveguide resonators," Computational Mathematics and Mathematical Physics, vol. 45, 2005.
3. K. Y. Sirenko, "Transport operators in the axially-symmetrical problems of the electrodynamics of pulsed waves," Electromagnetic Waves and Electronic Systems, vol. 11, 2006 (in Russian).
4. A. Taflove and S. C. Hagness, Computational electrodynamics: the finite-difference time-domain method. Boston: Artech House, 2000.
5. K. Y. Sirenko and V. L. Pazynin, "Axially-symmetrical radiators of pulsed and monochromatic TE_{0n}- and TM_{0n}-waves," Successes of Modern Radioelectronics, no. 4, 2006 (in Russian).
6. K. Y. Sirenko, "Slot resonances in axially symmetric radiators of pulse-modulated and monochromatic TM_{0n}-modes," Telecommunications and Radio Engineering, vol. 66, 2007.

Posters 1

Physical model for effects of microwaves on nucleoids in living cells: role of carrier frequency, modulation and static magnetic field

A. Y. Matronchik[1], I. Y. Belyaev[2,3]

[1]*Department of General Physics, Moscow Engineering Physics Institute, Moscow, Russia*
[2]*Department of Genetics, Microbiology and Toxicology, Stockholm University, Stockholm, Sweden*
[3]*Laboratory of Radiobiology, General Physics Institute, Russian Academy of Science, Moscow, Russia*

E-mail: AYMatronchik@MEPHI.RU

It has previously been shown that microwaves (MWs) and extremely low frequency (ELF) magnetic fields (MF) at low intensities affect conformation of nucleoids in cells of different types [1]. Recent data have shown that MWs from mobile phone affect nucleoids in human lymphocytes [2,3]. Effects of ELF MF depended significantly on collinear static MF. Experimental evidence has indicated that the MW effects have also been dependent on static MF. The physical model has been developed to describe effects of weak static and alternating magnetic fields [4]. Recently, we presented the model of slow nonuniform rotation of the charged DNA domain for combined effects of microwaves, static and alternating magnetic fields [5].

The oscillation of the center of mass x, y, z of the charged nucleoid (DNA domain) in static MF $B = 60\,\mu T$, and high frequency electric modulated fields, $E(t) = E_0 Cos(\tilde{\omega}t) Sin(\omega t)$:

$$m(t)\ddot{x} + kx = Q(t)(B\dot{y} + E(t)), \, m(t)\ddot{y} + ky = -Q(t)B\dot{x}, \, m(t)\ddot{z} + kz = 0,$$

where k is elasticity coefficient, $Q(t)$ - a charge of nucleoid, $m(t)$ -its mass, E_0 -amplitude, ω - high frequency of an electric field and $\tilde{\omega}$ - low frequency of an electric field. The axis z is directed along a vector of a magnetic field and passes through a place of fastening of nucleoid, the axis x is directed along an electric field. The mass and a charge of nucleoid slowly and periodically change in due course as a result of interaction with proteins and ions. In the received solution there is a low-frequency resonance at $\tilde{\omega} = \Omega_0/2 + m\omega_q$,

where $m = 0, \pm 1, \pm 2,...$. In this case the radius of the center of mass increases in time under the law:

$$r_0(t) = (q_0 E_0 / 4\omega_0) J_m(\Omega_1/2\omega_q) tCos(\omega t).$$

Such resonant growth of radius of the center of mass may affect binding of DNA with structural proteins and enzymes resulting in the experimentally observed effects. The predictions of this model are:
1. Amplitude of the electric field should be large enough to induce oscillations of nucleoids.
2. MW effects should be observed only at specific carrier frequencies.
3. Effects of MWs should depend on modulation.
4. Effect should be observed in specific intensity flux densities of static MF.

References
1. I. Y. Belyaev, E. D. Alipov, and M. Harms-Ringdahl, "Effects of weak ELF on E. coli cells and human lymphocytes: role of genetic, physiological and physical parameters," in Electricity and Magnetism in Biology and Medicine, F. Bersani, Ed. NY: Kluwer Academic, 1999, pp. 481-484.
2. R. Sarimov, L. O. G. Malmgren, E. Markova, B. R. R. Persson, and I. Y. Belyaev, "Non-thermal GSM microwaves affect chromatin conformation in human lymphocytes similar to heat shock," IEEE Transactions on Plasma Science, vol. 32, pp. 1600-1608, 2004.
3. I. Y. Belyaev, L. Hillert, M. Protopopova, C. Tamm, L. O. Malmgren, B. R. R. Persson, G. Selivanova, and M. Harms-Ringdahl, "915 MHz microwaves and 50 Hz magnetic field affect chromatin conformation and 53BP1 foci in human lymphocytes from hypersensitive and healthy persons," Bioelectromagnetics, vol. 26, pp. 173-184, 2005.
4. A. Y. Matronchik, E. D. Alipov, and I. I. Beliaev, "A model of phase modulation of high frequency nucleoid oscillations in reactions of E. coli cells to weak static and low-frequency magnetic fields (in Russian)," Biofizika, vol. 41, pp. 642-649, 1996.
5. A.Y. Matronchik, I.Y. Belyaev, "Model of slow nonuniform rotation of the charged DNA domain for effects of microwaves, static and alternating magnetic fields on   conformation of nucleoid in living cells", Frohlich Centenary
 International Symposium "Coherence and Electromagnetic Fields in Biological Systems", Prague, 2005.

Posters 1

UWB Signals with Fractal Spectra

V. N. Bolotov

Karazin National University, Kharkov, 61007, Ukraine

E-mail: bolotov@vl.kharkov.ua

Recent advances in electronic technologies have made it possible to generate and transmit (in air or via cables) short signals with a complicated time dependence of their amplitudes. Thus, the transmission of fractal signals has become a possibility. A fractal signal is a signal whose spectrum or time realization has a fractal structure defined by the Cantor set. In this study, we investigate a sort of the fractal signal, the fractal wavelet. The fractal wavelet (FW) is a pulse with an intricate waveform and spectrum specified by the pre-Cantor set [1]. The FW spectrum is UWB and self-similar; i.e., its parts are similar in shape. The FW time dependence is described by

$$s(t) = \prod_{n=0}^{N} \cos((1-\xi)\xi^n 2\pi f_0 t) \tag{1}$$

where $0 < \xi < 1/2$ and $N \rightarrow \infty$. It will be shown below that the choice of N depends on the electronics capabilities.

The spectrum corresponding to realization (1) has the self-similar structure of a Cantor set and is controlled by parameters ξ and f_0.
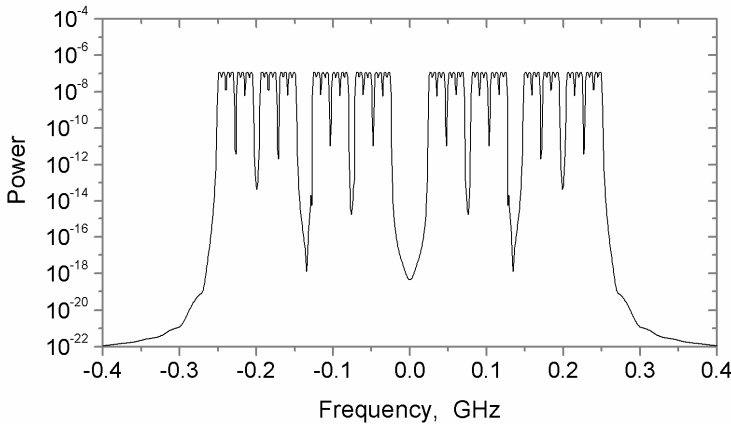
Fig. 1 – Theoretical UWB fractal spectrum

A new fractal ultra wideband (FUWB) signals have been developed for use in communication and radar systems. The basic advantage of fractal communication is the noise-immunity. In this paper, we compare the noise immunities of the FW signal and the Barker signal interfering with Gaussian noise or an electromagnetic pulse (EMP). The efficiency of extracting a fractal wide-band signal from the noisy environment is at least comparable to, and in most cases is much higher than, the extraction efficiency for a Barker signal. It should be noted that this advantage of the FW signal is highlighted in the presence of EMPs.

References
1.   V. N. Bolotov, "The Cantor Distribution and Fractal Transition Scattering", Technical Physics, V. 47, 2002, P. 148.

A Novel Star-shaped Monopole Antenna for UWB Communication

Guo-Luan Huang[1], Jui-Han Lu[1] and Hai-Ming Hsiao[2]

[*1] Department of Electronic Communication Engineering
[2] Department of Marine Engineering
National Kaohsiung Marine University, Kaohsiung, Taiwan 811, R.O.C.
E-mail: jhlu@mail.nkmu.edu.tw

In the recent years, due to rapid development in ultra wideband (UWB) systems, wide-band antenna with the frequency band of 3.1 ~ 10.6 GHz becomes demanding in practical applications for short-distance communication. However, many antenna parameters such as antenna size, bandwidth, and simplicity to manufacture affect the design procedure. Several UWB antennas such as slot antenna [1-2], LTCC antenna [3] and monopole antenna [4] have been introduced. Monopole antenna is one of the most common antennas in UWB systems due to easy design and omni-directional radiation pattern. In this article, a novel star-shaped monopole antenna for IEEE 802.15.3a and IEEE 802.16 application for the USB dongle is proposed. This proposed antenna is composed of the star-shaped monopole with unsymmetrical CPW feeding structure to obtain the ultra-wideband operation. Good impedance matching for the ultra-wideband operation can be achieved with the impedance bandwidths of 11.0 GHz by varying the positions of the embedded slits. To demonstrate the above deduction and guarantee the correctness of simulated results, the electromagnetic simulator HFSS based on the finite element method has been applied for the proposed patch antenna design. Fig. 2 shows the related simulated and experimental results of the VSWR for the proposed patch antenna design of Fig. 1. From the experimental results, the measured impedance bandwidth (VSWR□2) can reach 6.5 (2 ~ 13 GHz) for UWB system which provides much greater bandwidths for the operating band to meet IEEE 802.16 specifications. The measured antenna gain of the proposed UWB antenna is 4.5 dBi across the operating bands.
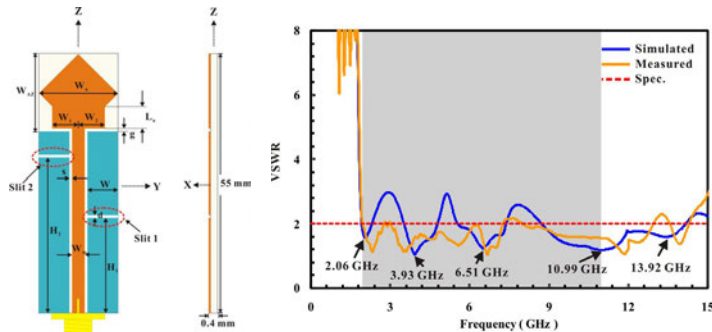
Fig. 1 the proposed star-shaped monopole antenna for UWB communication. (a) geometry, (b) measured and simulated VSWR against frequency.

References
1. T. G. Ma and C. H. Tseng, "An ultra wide-band coplanar waveguide-fed tapered ring slot antenna," *IEEE Trans. Antennas Propaqat.* , vol. 54, pp.1105-1110, April 2006.
2. G. Sorbello, F. Consoli and S. Barbarino, "Numerical and experimental analysis of a circular slot antenna for UWB communications," *Microwave Opt. Technol. Lett.*, vol. 44, pp. 465–470, 2005.
3. C. Ying, G. Y. Li and Y. P. Zhang, "An LTCC planar ultra-wideband antenna," *Microwave Opt. Technol. Lett.,* vol. 42, pp. 220-222, 2004.
4. C. H. Chan, T. K. Lee and W. S. Chan, "Printed UWB pellet-shape microstrip-fed monopolar antenna for 3.1 to 17 GHz" *Microwave Opt. Technol. Lett.,* vol. 50, pp. 490-494, 2008.

Posters 1

Characterization of Effects of Mobile Phone Radiations on the Nematode *Caenorhabditis elegans* as a Model Organism

P. Haldimann[1], M. Muriset[1], P. Zweiacker[2], F. Rachidi[2] and P. Goloubinoff[1]

[1]*University of Lausanne, Department of Plant Molecular Biology, CH-1015 Lausanne, Switzerland*
[2]*Swiss Federal Institute of Technology, Power Systems Laboratory, CH-1015 Lausanne, Switzerland*

...
E-mail: Pierre.Goloubinoff@unil.ch

The popular use of cellular phones and the proliferation of dedicated antenna have generated exposure of living beings to high frequency electromagnetic fields (HF-EMFs), raising public concern about possible effects of HF-EMFs on the environment and to human health. Despite intensive research, it is still unclear what are the biological effects of HF-EMFs and whether exposure is harmful. Organisms have many efficient molecular mechanisms to defend themselves against environmental stresses. In particular, they can accumulate heat-induced chaperones that can prevent heat-damages in native proteins and membranes. Here, we hypothesized that significant biological HF-EMF effects might be more efficiently detected in organisms deficient in chaperone expression or that suffer from a chronic overload of their chaperone network because of the presence in their cells of toxic aggregation-prone, recombinant proteins.

Polyglutamine expansion protein (polyQ) aggregation is the molecular basis for several important neurodegenerative diseases, including Huntington's disease [1]. PolyQ aggregates alter protein-folding homeostasis in cells [2] and render cells sensitive to mild temperature changes. Because HF-EMFs are suspected to have thermal and non-thermal effects on organisms, we analyzed the impact of HF-EMFs on transgenic *Caenorhabditis elegans* nematodes expressing polyQ's with an intrinsic propensity to form toxic aggregates in the muscle cells, resulting in a progressive age-dependent paralysis: the longer the polyQ repeats, the earlier is the onset and the more severe is the paralysis [1].

Here we first characterized, at different culture temperatures and as a function of age, the motility of recombinant *C. elegans* expressing a yellow fluorescent protein (YFP) fused to a polyQ of 35 glutamines (Q35), as compared to a YFP without polyQ (Q0). A detailed analysis of the motility at 22°C revealed that on the third day since hatching, the motility of the Q35 animals was reduced by 50% (± 10%) as compared to the Q0 animals. Thus, in Q35 animals, as little as a 0.5°C difference in culture temperature resulted in a significant and reproducible biological difference of motility. Q35 animals in TEM cells were than exposed to HF-EMFs for 3 days at 22°C for 64-66 hours, continuously or intermittently (2 hours on and 2 hours off). The field was applied at a frequency of 900 MHz and at an intensity of 5 V/m or 500 V/m. The temperature was monitored during the experiment using a highly sensitive temperature probe: whereas the HF-EMF field at 5 V/m did not cause any measurable temperature rise in the culture medium of the nematodes, the field at 500 V/m led to a temperature elevation of about 0.1°C. Motility assays were performed immediately after the different HF-EMFs treatments.

We found that, unlike the significant measurable effect caused by as little as 0.5°C difference in culture temperature, the four tested HF-EMF regimes were <u>significantly ineffective</u> to ameliorate or deteriorate polyQ-dependent paralysis in *C. elegans*. Further studies are therefore necessary to detect and characterize possible potentially hazardous biological effects of mobile phone radiations.

References
1. J.F. Morley, H.R. Brignull, J.J. Weyers and R.I. Morimoto, The threshold for polyglutamine-expansion protein aggregation and cellular toxicity is dynamic and influenced by aging in *Caenorhabditis elegans*. Proc. Natl. Acad. Sci. USA, vol. 16, pp. 10417-10422, 2002.
2. Gidalevitz T., A. Ben-Zvi, K.H. Ho, H.R. Brignull and R.I. Morimoto, Progressive disruption of cellular protein folding in models of polyglutamine diseases, Science, vol. 311, pp. 1471-1474.

UWB Rep-Rate Effectiveness

Libor Palisek, Jiri Kusala

VOP-026 Sternberk, s.p., division VTUPV Vyskov,
V. Nejedleho 691, 682 03 Vyskov, Czech Republic,

E-mail: l.palisek@vtupv.cz

Personal computers (PCs) are one of the most sensitive equipments to electromagnetic irradiation. The criticality of it's reliable function is very important when PCs are used for example in the infrastructures. In this case it is necessary to consider it's vulnerability. There are a lot of possible electromagnetic threats to PCs such as NEMP (Nuclear Electromagnetic Pulse), UWB (Ultra Wide Bandwidth) and HPM (High Power Microwave) [1]. For presented study UWB threat with repetition rate possibility will be considered.

The aim of this study is to present some results obtained during experimental measurements of PCs susceptibility to UWB irradiation when repetition rate signal was used. Repetition rate dependence will be considered for temporary failures as well as for damage levels too. As an equipment under test (EUT) will be chosen regular PCs setups with peripherals like monitors, keyboards and mice and without peripherals too. Setups for Ethernet and USB (Universal Serial Bus) communication will be used too. Moreover simple electronic circuits (as an EUT) will be added for some experiments for possibility to achieve more results related to damage levels without necessity to destroy a lot of PCs. Susceptibility of regular PCs including notebooks to used single pulse UWB and repetition rate UWB signals will be presented as well as susceptibility of Ethernet and USB communications and chosen simple electronic circuits. During presentation suitable simplified circuit models for UWB repetition rate effectiveness for achieving of typical effects on electronics will be mentioned too [2]. At the end of this presentation recommendation for effective UWB rep-rate necessary to achieve typical failures of tested equipments will be carried out.
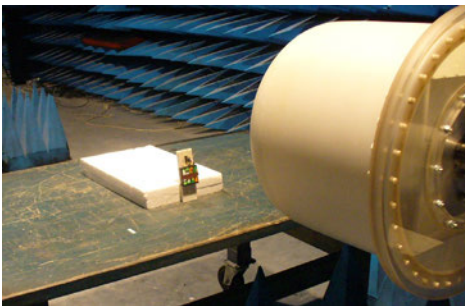
Fig. 1 – UWB Testing of Simple Electronic Circuit Vulnerability (damage level investigations)

Fig. 2 – UWB Testing of Ethernet Communication Vulnerability (temporary failure investigations)

References
1. D. Taylor, D.V. Giri, "High-Power Microwave Systems and Effects", Taylor & Francis, 1994.
2. J. Bohl "HPM Interaction with Electronics, Skript and Presentations" High-Power Electromagnetics Course HPE 201-2007, Bonascre, France, 2007.

Posters 2

Localized thermal effects in electromagnetic shielding applications of auxetic materials

R.F. Damian[1], R.C. Ciobanu[1], V. David[1]

[1]*"Gh. Asachi" Technical University, Iasi, Romania*
E-mail: rdamian@etc.tuiasi.ro

Auxetic materials are investigated closely in the last decade[1], [2]. One of the important proprieties of these metamaterials is the thermal expansion, desired to be zero or negative. In thermal expansion studies the main assumption is a homogenous increase in temperature in the entire volume of the material. In the microwave shielding applications, were high absorption of the electromagnetic energy is desired, we may find ourselves in a certain situation were high power level waves interact rapidly with the structure. The hexachiral honeycomb investigated in this paper, interacts at microscopic level with the incident electromagnetic waves, as a result the power dissipation is not equally distributed inside the structure. One of the advantages of these metamaterials in microwave shielding is their intrinsic sparse nature, giving them good heat dissipation properties but thermal phenomena are slow, so we can expect localized temperature increase.

Electromagnetic simulations were performed in order to prove this concept. In fig. 1 we plot the power loss density inside the ligaments of the hexachiral honeycomb. The two frequencies chosen (3.06GHz /10.69GHz) are those corresponding to a minimum in reflectance/transmittance.

In the case of the hexachiral panel under test, the Salisbury shield configuration will not alter its mechanical properties, but will provide better shielding properties. In fig. 2 the surface current in the resistive sheet is plotted as a indication of the transversal power dissipation distribution (the two frequencies: 2.94GHz/6.01GHz corresponding to a minimum/maximum of the reflectance). Again we find an uneven distribution of the energy.

While other effects (as dramatic increase in temperature with material melting as an effect) cannot be foreseen in these applications (except in the highly improbable case of exceptionally high power levels), microscopic changes in temperature can affect the metamaterial in the direction of the expected thermal expansion.

The aim of this paper is not to address the mechanical/thermal characteristics of the chiral honeycomb but further investigation would be necessary with this new hypothesis: thermal effect can be localized (is even expected to be).
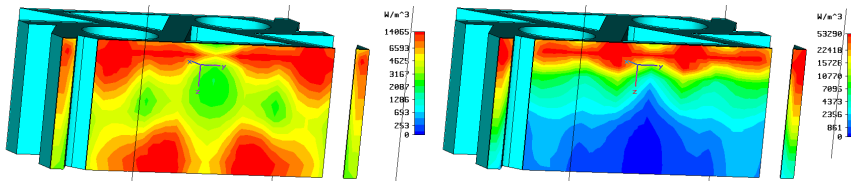
Fig. 1 – Power loss density - hexachiral honeycomb; 3.06GHz (left) and 10.69GHz (right)
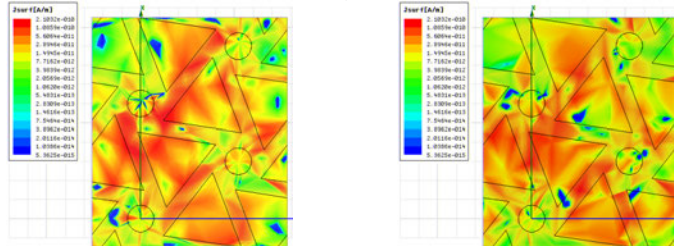
Fig. 2 – Surface current - hexachiral honeycomb in Salisbury shield configuration; 2.94GHz (left) and 6GHz (right)

References
1.   J. Grima, Negative, negative and more negative: systems exhibiting negative Poisson's ratio, negative thermal expansion and/or negative compressibility, 4th International Workshop on Auxetics and Related Systems, Malta, 2007
2.   M.R. Hassan, F. Scarpa, M. Ruzzene, N.A. Mohammedd, Smart shape memory alloy chiral honeycomb, Materials Science and Engineering A, 2007, doi:10.1016/j.msea.2006.10.219

High power microwave studies at CEA/CESTA: from single shot to repetitive devices

J. Gardelle, P. Modin, L. Courtois, A. Sylvestre de Ferron and L. Voisin

CEA/Centre d'Etudes Scientifiques et Techniques d'Aquitaine, BP 2, 33114 Le Barp, France

E-mail: jacques.gardelle@cea.fr

At CEA/CESTA, we developed in the 90's pulsed power technology for high current electron accelerators and we studied microwave free-electron lasers. Then, we started a program on high power microwave (HPM) tubes and we investigated several single shot devices such as Vircators, Relativistic Klystrons, MILOs and, more recently, Reltrons. The latter are well suited for HPM applications between 1 and 3 GHz, they are commercially available HPM tubes which have been studied at TITAN (CA-USA) for about 20 years [1]. The main advantages of Reltrons are their compactness and the absence of any external guiding magnetic field. Nevertheless, they have two drawbacks. First, high repetition rate operation (greater than a few tens of Hz) is difficult to obtain due to cathode outgassing, grid heating and maintaining vacuum (pumping speed). Secondly, the emitted power is limited by the current one can emit and propagate in a given geometry. This limiting current is frequency dependent; the higher the frequency, the smaller the geometry and the current acceptance.

We present in this paper experimental and numerical studies we performed on a commercial S-band (3 GHz) Reltron at repetition rates up to 10 Hz.

Then we describe the test bench which has been developed at CEA/CESTA in order to understand the previously mentioned limitations. A cable transformer capable of delivering 200 kV, 1 kA pulses at a repetition rate of 100 Hz is presented. The first studies using this driver are described.

1.   R. B. Miller *et al*,   "Super Reltron Theory and Experiments", IEEE Transactions on Plasma Science,
       Vol 20, 1992, pp. 332-343.

Posters 2

Powerful Relativistic Microwave Generators based on Backward Wave Oscillator with a Modulating Resonance Reflector

E. M. Totmeninov[1], V. V. Rostov[1], M. I. Yalandin[2]

[1]*Institute of High Current Electronics, Siberian Branch, Russian Academy of Sciences*
2/3 Akademichesky Ave., Tomsk, 634055, Russia
[2]*Institute of Electrophysics, Ural Branch, Russian Academy of Sciences*
106 Amundsen Street, Ekaterinburg, 620016, Russia
E-mail: **totm@lfe.hcei.tsc.ru**

The results of the theoretical and experimental investigations of the relativistic backward wave oscillator with an electrodynamic system of increased cross-section ($D/\lambda > 1$, D is the mean diameter of the slow wave system and λ is the wavelength) and a modulating resonant wave reflector [1] are summarized in this work. The backward TM_{01} wave is reflected from the resonant reflector at the cathode end of the device due to the locked TM_{02} oscillation excited in the reflector. The *z*-component of the electric field at the electron beam radius in the reflector is several times greater than that in the adjacent waveguide. This promotes efficient modulation of the electron energy in the reflector region. The increased cross size of the electrodynamic system decreases the probability of RF breakdown and provides conditions for efficient operation of the device in the low magnetic field range (below the cyclotron resonance region).

The theoretical analysis shows that the preliminary modulation of the electron beam in the reflector influences on the generation start conditions, on the characteristics of the mode selection, on the oscillation frequency and on the efficiency of generation that can reach $40 - 50$ % [2].

The microwave devices listed below were realized in the experiments.

- X-band oscillator with efficiency ~40% and output power ~ 0.8 GW at as strong guiding magnetic field as 2.7 T [3];
- X-band oscillators with efficiency $20 - 24$% and output power $0.5 - 0.8$ GW at as low guiding magnetic field as 0.7 T [1,2];
- S-band oscillator with pulse-to-pulse mechanical frequency tuning in the frequency band ~10% at the multigigawatt output power [4,5] and at as low guiding magnetic field as 0.4 T;
- X-band oscillators with efficiency ~ 31%, output power 4.3 GW and microwave pulse duration 21 ns at as strong guiding magnetic field as 4.5 T [6];
- Q-band oscillator with efficiency ~35% and output power 0.16 GW at as low guiding magnetic field as 2.2 T.

The repetition rate regimes ($10 - 100$ Hz) were realized at low the magnetic field mentioned above that was $1.5 - 2$ times lesser than the magnetic field corresponding to the cyclotron absorption of the back wave condition.

References
1. I. K. Kurkan, V. V. Rostov, E. M. Totmeninov**,** "A possible method of reducing the magnetic field in a relativistic backward-wave tube", Technical Physics Letters, Vol. 24, № 5, pp. 388-389, (1998)..
2. S. D. Korovin, I. K. Kurkan, V. V. Rostov, and E. M. Totmeninov, "Relativistic backward wave oscillator with a discrete resonance reflector", Radiophysics and Quantum Electronics. 1999. V.42 № 12. P. 1047-1054.
3. S. D. Korovin, V. V. Rostov, E. M. Totmeninov, "A relativistic backward wave oscillator with a modulating resonance reflector", Technical Physics Letters, Vol. 31, № 5, pp. 411-413, (2005).
4. S. A. Kitsanov, A. I. Klimov, S. D. Korovin, V. V. Rostov, and E. M. Totmeninov, "Relativistic BWO With Enhanced Frequency Tunability," IEEE Trans. Plasma Science, vol. 33, No. 5, October 2005, p. 1685-1689.
5. A. I. Klimov, I. K. Kurkan, S. D. Polevin, V. V. Rostov, and E. M. Totmeninov, "A periodic pulsed relativistic backward wave oscillator mechanically tunable in an expanded frequency band", Technical Physics Letters, Vol. 33, № 12, pp. 1057-1060, (2007).
6. A. I. Klimov, I. K. Kurkan, S. D. Polevin, V. V. Rostov, and E. M. Totmeninov, "A Multigigawatt X-Band Relativistic Backward Wave Oscillator with a Modulating Resonant Reflector", Technical Physics Letters, Vol. 34, № 3, pp. 235-237, (2008).

Posters 2

Injection of Short Electromagnetic Pulses in Plasma Across the External Magnetic Field

V.B. Krasovitskiy[1], V.A. Turikov[2], V.I. Sotnikov[3]

[1]*Keldish Institute of Applied Mathematics RAS, Moscow, Russia*
[2]*University of Peoples Friendship, Moscow, Russia*
[3]*University of Nevada at Reno, USA*

E-mail: krasovit@mailru

The efficiency of plasma electrons acceleration by a short powerful laser pulse propagating across an external magnetic field is investigated theoretically and numerically. The linearly polarised EM wave created in a vacuum is transformed into the elliptically polarized extraordinary wave at the plasma boundary. Development of the self-modulation instability is accompanied by the deep modulation of the broad wave packet, which results in a transformation of the packet into a chain of solitons with the soliton width of the order of the skin-layer width. Short wave packet injected into in the weak nonlinear plasma is not a soliton and in the process of relaxation it loses fast and slow components due to the dispersion in the group velocity, but the main part of the pulse transforms into the envelope soliton. Initially electron is accelerated on the front edge of the pulse, but later falling into the region of decelerated phases, gives the energy back, to the rear edge of the pulse. The deviation, observed in simulations, of the strongly nonlinear pulse from the soliton is connected with the appearance of relativistic electrons and deviation from the approximation of weakly relativistic plasma, used in the analytical model. The longitudinal component of the electric field of an elliptically polarized resonance electromagnetic wave can be used for an efficient acceleration of plasma electrons across an external magnetic field. The simulation shows that in addition stochastic relativistic electron heating on top of the soliton structure is observed when the threshold of parametric instability is achieved [1,2]. Conditions for the decay of a laser pulse with frequency close to the upper hybrid resonance frequency are analyzed. In the process of parametric instability development electron trajectory is the spiral with the increasing step and increasing period of circulation.
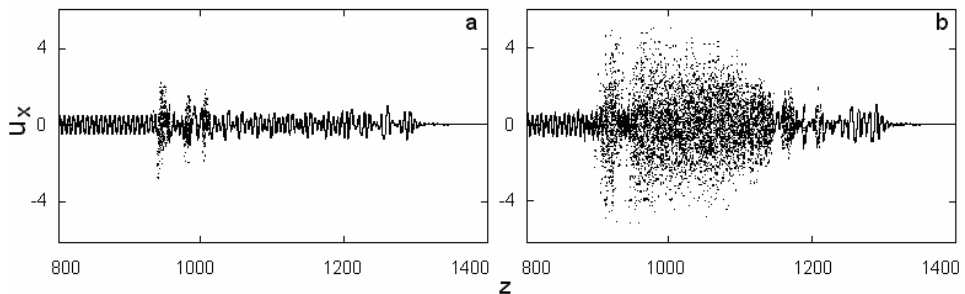
Fig. 1. Stochastic electron heating of plasma electrons with the increase in the field amplitude, $\omega_p / \omega = 0.1$,

$\omega_c / \omega = 0.9$; (a) $\varepsilon = 0.16$;.(b) $\varepsilon = 0.2$ [ω_p and ω_c are the plasma frequency and gyro-frequency,

$\varepsilon = eE_x / mc\omega$, E_x is the wave amplitude, $u_x = p_x / mc$].

References
1. V. B. Krasovitskiy, V. G. Dorofeenko, V. A. Turikov, and V. I. Sotnikov, "Decay instability of a laser pulse propagating in a transverse direction in a magnetized plasma," Plasma Physics Report, vol. 32, 2006.
2. V. B. Krasovitskiy, V. A. Turikov, and V. I. Sotnikov, "Nonlinear dispersion of resonance extraordinary wave in a plasma with strong magnetic field," Physics of Plasmas, vol. 14, 2007.

Posters 2

Rigorous Full-Wave Analysis of Shielding Effect in Assymmetric Unilateral Structures for MMICs Applications

A.Khodja[1], M.L.Tounsi[1], R. Touhami[1], M.C.E.Yagoub[2] and H. Baudrand[3]

[1]*Instrumentation Laboratory, Faculty of Electronics and Informatics, U.S.T.H.B University, Algiers, Algeria*
[2]*School of Information Technology and Engineering, University of Ottawa, 800 King Edward, Ottawa, Ontario, K1N 6N5, Canada*
[3]*ENSEEIHT, 2 rue Charles Camichel 31071, Toulouse Cedex 7, France*

E-mail: hkhodja@yahoo.fr

This article describes the shielding effect of electromagnetic fields appearing in unilateral asymmetric transmission lines (see figure1) which can support two different modes of propagation usually defined by "C" and "π" modes [1]. For this purpose, an integral method, especially transverse resonance method (TRM) is used in conjunction with an adequate choice of trial functions. The mathematical process of this method makes use of operators formalism in electromagnetism which consists to emphasize systematic character in this method [2], this allows to analyze efficiently the dispersion effect of those asymmetric structures

The TRM method is based on the evaluation of the impedance operator $\hat{Z}$ (or admittance operator $\hat{Y}$) [1] to which the Galerkin's technique is applied. So, the full-wave behavior of shielding is analyzed with respect to the dispersion parameters. Cosine trial functions with edge singularities were used [1].

The obtained results have been validated with a good precision compared with those available in the literature.

Coplanar line Coupled microstrip line Suspended coplanar line Suspended coupled microstrip line
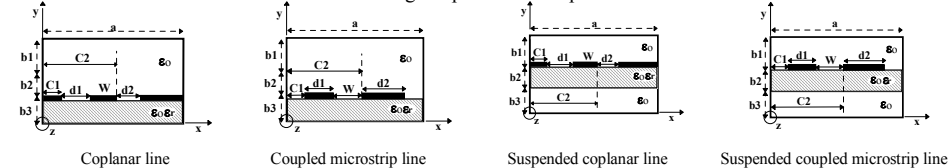
Fig. 1 – Cross sectional view of shielded unilateral asymmetric transmission lines

(d1= d2=0.08mm, b2=0.254 mm, C1=0.1mm, εr=2.22, F=10GHz) *(d1 =0.1mm, b2=0.125mm, C1=0.1mm, εr=2.2, F=33GH)* *(b2=0.254mm, d1 =0.08mm, C1=0.1mm, w=0.45mm, εr=2.22, F=10GHz)* *(b2=0.125mm, d1 =0.1mm, C1=0.1mm, w=0.2mm, εr=2.2, F=33GH)*

(b2=0.254 mm, d1= d2=0.08mm, w=0.45mm, F=10GHz, εr=2.22) *(b2=0.125mm, d1=d2=0.1mm, w=0.2mm, F=33GHz, εr=2.2)* *(b2=0.125mm, d1=0.1mm, εr=2.2)* *(b2=0.125 mm, d1 =0.1mm,εr=2.2)*
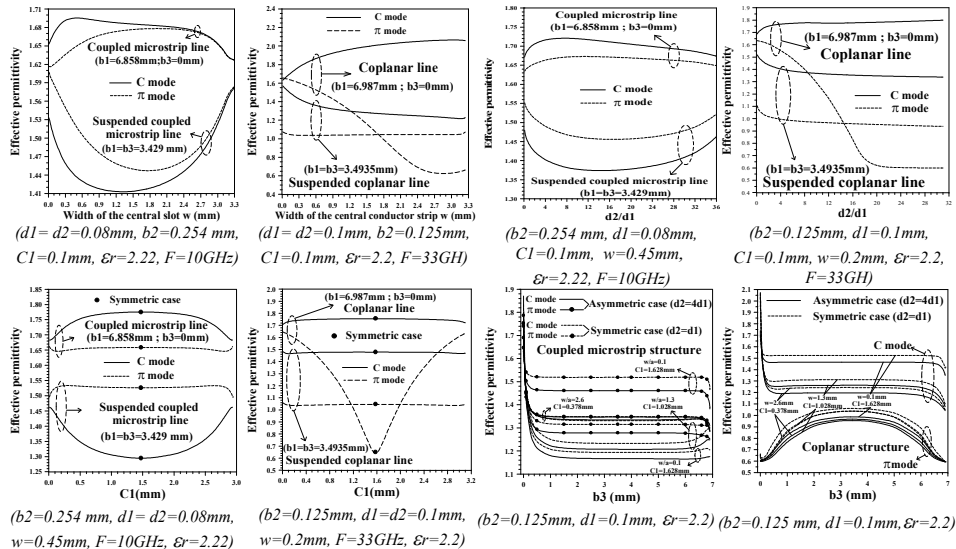
Fig. 2 – Influence of horizontal and vertical metallic sides of shielding on effective permittivity

References

1. A. Khodja, M.L. Tounsi, M.C.E. Yagoub, R.Touhami, K. Idinarene, S.Gaoua "Optimal choice of trial functions in the modeling of unilateral asymmetric microwave structure by integral method", 4th Mediterranean Microwave Symposium (MMS'2004), Marseille, France, 1-3 June 2004.
2. A. Khodja, "Optimisation des Fonctions d'Essai dans la Modélisation de la Ligne à Ailettes Unilatérale par la Méthode de Résonance Transverse", Master Thesis, USTHB, Algiers, Algeria, April 2000.

Posters 2

High-voltage improvement of the Valentine antenna for ultra-wideband applications.

B. Cadilhon[1], L. Pécastaing[1], J. Andrieu[2], S. Vauchamp[2], M. Lalande[2]
[1]Laboratoire de Génie Electrique, Hélioparc 2 av. Angot, 64000 Pau - France
[2]XLIM/IUT GEII, 7 rue Jules Vallès, 19100 Brive – France
E-mail : baptiste.cadilhon@etud.univ-pau.fr

The Valentine antenna was originally designed for an optoelectronic ultra-wideband (UWB) radar demonstrator [1]. The first prototype was built to support high peak voltages of 25kV. Because of its high gain and its capability to radiate short pulses without dispersion in the frequency band 300MHz – 2.5GHz, this antenna was chosen to be the radiating element of a high power, high voltage UWB source [2]. This antenna is made of two curved metallic strips and a copper coaxial-to-strip transition with a N connector. Some modifications were made to improve the dielectric strength of both the antenna and the transition to drive it with a 300kV, few hertz transient source. A 3-D model of the antenna was first performed on a time domain electromagnetic software, to study the influence of these modifications on the main characteristics of the radiating element. Then, tests in frequency and transient domain were realised. Results show that the S_{11} of the antenna remains relatively unchanged and the gain is very closed to the original low voltage design in the frequency band. Furthermore this new antenna is able to take over 300kV-2ns duration impulse. This paper describes this high voltage antenna and its main radiation characteristics.

References
1. J.-C. Diot, P. Delmote, J. Andrieu, M. Lalande, V. Bertrand, B. Jecko, S. Colson, R. Guillerey, M. Brishoual, "A novel antenna for transient applications in the frequency band 300MHz – 3GHz: the Valentine antenna", IEEE Transactions on Antennas and Propagation, vol. 55, n°3, pp 987-990, March 2007.
2. B. Cadilhon, L. Pécastaing, T. Reess, A. Gibert, P. Pignolet, "High power microwave pulser for the electromagnetic radiation", Proceedings of the 20th IET Symposium on Pulsed Power, Didcot, September 2007.

Posters 2

Simulation of Improved Bandwidth Conformal Bow-Tie Antennas Printed on Multi-scale Triangular-Patch High-Impedance Ground Planes

Murat Dogrul[1], Peter J. Collins[1], Michael Saville[1], Kubilay Sertel[2], Andrew J. Terzuoli[1]

[1]*Air Force Institute of Technology, Dayton, Ohio 45433 USA*
[2]*ElectroScience Laboratory, The Ohio State University, Columbus, Ohio 43212 USA*

...
E-mail: <peter.collins@ieee.org> *or* <a.j.terzuoli@ieee.org>

Gain and bandwidth metrics of broad-band low-profile antennas severely deteriorate when they are placed conformally onto the conductive skins of air, sea, and ground platforms. This detrimental effect is primarily due to out-of-phase reflections from the conductive body interfering with the antenna's self radiation. Furthermore, lateral waves launched by the antenna couple into the thin substrate placed between the antenna and the platform, giving rise to surface waves resulting in significant diffraction from the edges of the substrate.

To remedy these two major mechanisms degrading antenna performance, high impedance ground planes (HIGP) were proposed [1]. HIGPs made of a 2-D periodic arrangement of a mushroom structure not only provide perfect-magnetic-conductor (PMC)-like reflection, but also suppress the surface waves within the stop-band of the substrate modes. Thus, when the antenna is conformally placed over the HIGP, its gain is expected to double from the free-space value, due to in-phase reflections. Additionally, its bandwidth is expected to be as large as the band-gap of the mushroom structure, provided the original design has sufficient bandwidth to cover the band-gap of the HIGP.

Previously considered HIGPs were made of square-patch mushroom structures having a single periodicity. Here, we consider a multi-scale triangular-patch HIGP design. Element sizes can be chosen such that the band-gap of each periodic subsection is placed successively in frequency. The final multi-scale composite HIGP structure has increased band-gap, thus providing increased bandwidth for the conformal antenna. Furthermore, triangular mushroom elements provide a natural platform for the particular broadband antenna used in the bow-tie antenna design as shown in Figure 1.

Using Ansoft-HFSS v.10, we simulate the performance of the bow-tie antenna in free-space, on a conducting ground plane, on a PMC, and on the multiscale HIGP. Three HIGPs are considered, two having uniform periodicities with different scales, and one having the multiscale design. We present our simulation results and demonstrate the performance of the broadband, conformal bow-tie antenna placed over the multiscale HIGP.
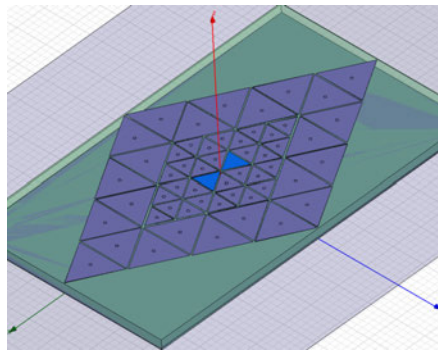
Fig. 1 – Bow-tie antenna inside multi-scale HIGP

References
1.   D. F. Sievenpiper, L. Zhang, R. F. J. Broas, N. G. Alexopolus, and E. Yablonovitch. "High-Impedance Electromagnetic Surfaces with a Forbidden Frequency Band," IEEE Transactions on Microwave Theory And Techniques, 47:2059-2074, November 1999.

Posters 2

Dosimetric-biophysical approach for the assessment of the influence of low-level RF-EMF on plants developed from exposed seeds

S. Miclaus[1], M. Racuciu[2], M. Morega[3]

[1]*Land Forces Academy, Sibiu, Romania*
[2]*»Lucian Blaga» University, Sibiu, Romania*
[3]*Politehnica University, Bucharest, Romania*

E-mail: simo.miclaus@gmail.com

The aim of the present study is the identification of low-level radiofrequency (RF) radiation effects on plantlets developed from exposed seeds of *Zea mays*. A proper investigation of the biological effects requires well-characterized and controlled dosimetric conditions, because nonthermal RF effects are suspected to occur in the exposed biological material. The exposure system is a TEM cell model IFI CC104 SEXX powered by a RF signal generator, while the biological target - cereal seeds enclosed in a Petri dish - is placed inside the cell, in a restricted area, characterized by a quasiuniform electric field distribution. Several samples of 40 seeds were exposed in different exposure conditions. One variable was the exposure duration (chosen between 4 and 72 hours), and the other one was the electromagnetic stimulus waveform. A 900 MHz signal, either in the form of a continuous wave (CW) or as an AM and FM waveform, modulated on the same carrier, was used for the irradiation. Corresponding samples of not-exposed seeds were used as controls, in proper conditions. The incident E-field (rms value) in the TEM cell did not exceed 6V/m, and it was measured by an E-field probe Scan EM-EC (model CTM030) connected to a spectrum analyzer. The dosimetric part of the study was approached by two methods: a) theoretical and b) experimental. A numerical model was built with the finite element method implemented by COMSOL Multiphysics, and it allows the simulation of the experimental situation. The experimental dosimetry approach made use of the differential power method. Numerical modeling was able to provide complementary and accurate information to the experiment, valuable especially when the field distribution inside the sample need to be evaluated, which is almost impossible by experimental means. The uniformity of the field in the unloaded TEM cell was primarily analyzed by using the computational method [1] and then also experimentally assessed, and results converged well. The electric field distribution, the absorbed power, the specific absorption rate (SAR) and the heating of the sample were determined in present work with reliable accuracy. The SAR in our experiments did not exceed 100mW/kg and no thermal shift could be measured by means of the fluoroptic thermal probe Luxtron One.

Biophysical investigations on plantlets developed both from the exposed and not-exposed seeds, followed after 12 days of plant growth. They were focused on the quantification of differences between exposed and control samples, regarding: a) pigment concentration of chlorophyll a, chlorophyll b and carotenoids (by UV-VIS spectrophotometric analysis); b) nucleic acid concentration; c) average water content; d) average length of the plants. Some statistical significant effects were observed in a preliminary study [2] and there are indications that low-level 900MHz exposure may induce changes in *Zea mays* seeds and they may be different for CW and modulated signals. Experiments are underway, and final conclusions will be available soon.

References
1. M. Morega, S. Miclaus, "Electromagnetic Environment generated in a TEM cell for biological dosimetry application", Proceedings of ISEF 2007 - XIII Intl. Symp. on Electromagnetic Fields in Mechatronic, Electrical and Electronic Engineering, Prague, Czech Republic, 13-15 Sept. 2007.
2. M. Racuciu, S. Miclaus, D.E. Creanga "Non-thermal, continuous and modulated RF field effects on vegetal tissues developed from irradiated seeds", International Conference on Electromagnetic Fields, Health and Environment, Wroclaw, Poland, 10-12 September 2007.

Posters 2

Ultra-Low Voltage OpAmp with High EMI Immunity

A. Richelli[1]

[1]*University of Brescia, Dept. of Electronics, Brescia, Italy*

E-mail: anna.richelli@ing.unibs.it

In recent years, EMI were carefully investigated in order to find possible prevention methodologies, in particular in ICs which may include several Operational Amplifiers (OpAmps) [1]-[3]. The most sensitive circuits to EMI are, indeed, the analog ones and, among them, the OpAmps. One of the undesirable effects of EMI is the shift of the output DC mean value (offset) that may force the amplifier to saturation and may cause failures in the (eventually) following circuits. The susceptibility to interferences has been correlated to some special features of the OpAmp transient response. In particular, the asymmetric slew rate and the parasitic capacitances play a significant role, at low-medium frequencies and at high frequencies, respectively [3]. Hence, in order to intrinsically reduce EMI effects a promising approach [2] is based on the design of strongly symmetrical amplifier, as the one shown in Fig.1.
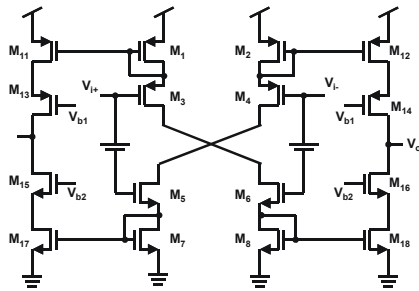
Fig. 1: Symmetric amplifier proposed in [2]

Unfortunately, this architecture is not suitable for the low voltage supply of the current ICs. Therefore, an alternative solution has been investigated and the immunity to electromagnetic interferences of the symmetrical topology in Fig.2 has been demonstrated. The proposed amplifier has been designed in UMC 0.18um standard CMOS process and can be powered at less than 500mV. A lot of simulations were performed also with very large interfering signals (Vp=500mV and frequency ranging from 1MHz up to 4GHz) conveyed to the input pins of the amplifier. The proposed architecture allows the reduction of EMI effects by more than one order of magnitude compared to classical amplifiers suitable for low voltage applications (such as the Miller amplifier). The maximum offset induced by spurious signals (with an amplitude of 500mV, very large compared to the 500mV power supply) is less than 20mV.
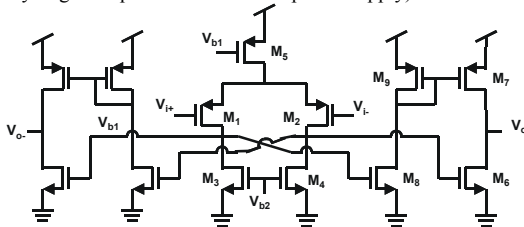
Fig. 2: The proposed amplifier, suitable for low voltgae applications

References
1. F. Fiori, "Design of an Operational Amplifier Input Stage Immune to EMI", IEEE Transactions on Electromagnetic Compatibility, vol. 49, no. 4, November 2007
2. A. Richelli et Al., "Robust design of low EMI susceptibility CMOS OpAmp", IEEE Transactions on Electromagnetic Compatibility, vol. 46, no. 2, May 2004
3. G. Masetti et Al., "On the key role of parasitic capacitances in the determination of susceptibility to EMI of integrated operational amplifiers", Proc. of EMC99, Zurich 1999

Proximity Tolerant, Electrically Small Antenna for Wireless Sensor Networks and Global Positioning Systems

S. Fikar[1,2], R. Bogenberger[1], A. L. Scholtz[2]
[1]*BMW Group Research and Technology, Munich, Germany*
[2]*Vienna University of Technology, Vienna, Austria*

E-mail: stefan.fikar@bmw.de

A small antenna for location aware wireless sensor networks is presented. The antenna is designed to be tolerant to neighboring materials. It can be placed in the proximity of different dielectrics or conductors, while maintaining sufficiently low return loss and stability of resonance frequency. In contrast to readily available, but expensive, antennas based on ceramic materials, our design purely relies on machined metal sheets, which can also be replaced by printed circuit board (PCB) structures and metallization, providing a low cost solution for future wireless sensor designs.

The two operating bands of the antenna are the 868MHz ISM Band as well as the 1575MHz band for reception of GPS signals. As the European 868MHz ISM Band is closely located to the European GSM900 band, the antenna has to offer a narrow resonance at the desired frequency of operation. Remaining exactly matched for this band and still blocking the GSM900 signals, while being directly mounted on and thus extremely closely exposed to varying proximities, was the main challenge for the design of this antenna. The same can be done for US GSM and ISM bands with minor modifications. The distances used for the antennas evaluation are as close as $\lambda/35$ to the bottom of the antenna as well as to its side. In the conductive simulation scenario the antenna is placed in the edge between the sash and the frame of an aluminum window, with 2mm of non-conducting sealing in-between. Figure 1 shows the simulation setup and Figure 2 the results of the reflection coefficient measurement.

Different environmental characteristics are especially found in automobiles, where standardized sensor hardware shall be used on dielectrics like plastics and leather, as well as directly mounted on the car body, which is typically made of steel – a conductor. Another conceivable area of operation is home automation, where sensors are being randomly placed on window frames (made of wood, aluminum or plastics), concrete walls, doors or even furniture without caring for electromagnetic phenomena. The ability to receive GPS signals enables tracking of sensors outside of the car. Sensor readings can be classified by relevance with location information.
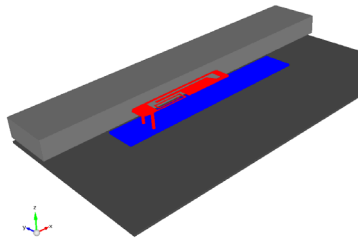
Fig. 1 – Antenna located in the proximity of conductors. The ground-plane of the antenna is depicted in blue, the antenna itself in red, the conductive window frame in dark grey and the windows sash in light grey. The (red) active element is sized 53mm x 9mm, height over ground is 9mm.

| **(a) free-air** | **(b) between sash and frame of an aluminum window** |
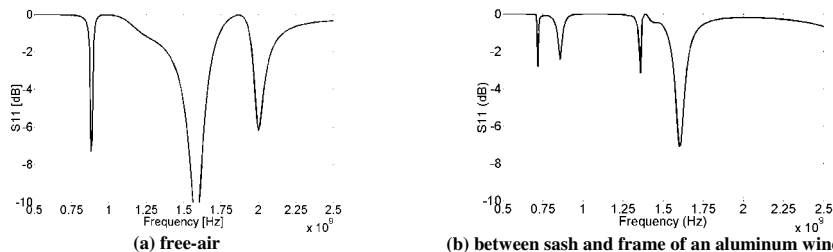
Fig. 2 – Input reflection coefficient of the Antenna for two scenarios. The antenna remains resonant within the required bands. The worse matching in the proximity of a conductor is compensated by higher antenna gain.

Comparison of the computational performances of two numerical methods to compute 2D current distribution in superconductors

F. Sirois[1], F. Roy[2] and B. Dutoit[2]

[1]*École polytechnique de Montréal, Montréal, Canada*
[2]*EPFL, École polytechnique fédérale de Lausanne, Lausanne, Switzerland*

E-mail: francois.roy@epfl.ch

In this work, we compare the computational performances of two promising numerical methods to solve time transient, 2-D current distribution problems in superconductors with transport current and/or applied field, namely the finite element method (FEM) and the semi-analytical method (SAM). The later is a recently published generalization of the so-called "Brandt method". For the purpose of an objective comparison, both problems are solved using the same time integration algorithm, i.e. DASPK, which is a very efficient high order adaptive time step integration method. This algorithm is built-in in the COMSOL Multiphysics package, which served as our benchmark for the FEM, whereas we had to implement it in a compiled version of the SAM based on a C proprietary code. As a first result, the SAM proved to be more efficient than the FEM for small problems, such as the case of a single strip, which is explained by two main factors: 1) the reduced number of elements used with the SAM (no mesh in air regions), and 2) there is no matrix assembly nor linear system resolution to perform at each time step, but only dense matrix products. As the number of element grows in the geometry discretization, the SAM progressively loses its advantage over the FEM. The threshold at which the crossover occurs was evaluated for the case of a simple superconducting strip with different mesh coarseness.

The main limitation of the SAM at this stage of development is the difficulty to include magnetic materials in the model, although this has already been achieved in the past by researchers in computational electromagnetic.

A Tapered Leaky Wave Antennas and its Diverging-Focusing Properties

Onofrio Losito

ITEL Telecommunications Research Laboratory on EM
Via Labriola, 39 - 70037 Ruvo di Puglia, Italy

E-mail: o.losito@itelte.it

Figure 1. A prototype of tapered LWA with holes made in the center line of the antenna

Substantial enhancements were achieved since pioneering studies on microstrip leaky-wave antennas (LWA), and they are now very popular and widely used in applications thanks to their advantages of low-profile, easy matching, narrow beamwidth, fabrication simplicity, and frequency/electrical scanning capability. Nevertheless, in some applications especially with regard to communication applications, the main beam variation of LWA should be as low as possible. Moreover disadvantages of the LWA include the fact that it is usually narrowband. A tapered stepped microstrip LWA (in which each step can irradiate in subsequent ranges of frequency), is a possible first solution studied to obtain a broadband and fixed mainbeam LWA[1]. But the impedance mismatch between subsequent steps, reduces the performance. Furthermore the excitation of a higher order mode without dominant mode perturbation, requires a more elaborate feeding scheme. Consequently, we had studied a curved design of tapered antennas, where the profile of the longitudinal edges was designed, using the reciprocal slope of the cutoff curve, in a symmetrical way respect to the centreline of the antenna, as shown in Fig. 1. The cutoff curve was obtained for different widths of the multisection broadband microstrip LWA.

Figure 2. Return loss of full and half Leaky Wave Antennas (on the left) and The measured and simulated radiation patterns of E field of half tapered LWA (at 8 GHz on the right).

To efficiently suppress of the dominant mode (the bound mode) we have used a physical grounding structure along the length of antenna, which also allows, a reduction of the impedance mismatch, the adoption of a simple feeding, and the reduction of sidelobes. This solution, used to an antenna from 8 to 11 GHz, improves the band, (33% for VSWR<2), the gain (12 dBi) and the efficiency (up to 85%) with reference to conventional uniform microstrip LWAs (which have band of 22% for VSWR<2, peak gain up to 10 dBi and efficiency up to 75%)[2]. Symmetry along this metal wall, invites the application of image theory. In fact, due to the image theory it is also possible to

Figure 3. The normalized phase constant and attenuation constant of tapered LWA frequency and width

design only half of an antenna with the same property of one in its entirety, reducing up to 60% the antenna's dimensions, as shown in Fig. 2 [3]. Nevertheless, we note that a tapered LWA for a fixed frequency, changes the main beam radiation angle. This occurs because the phase constant β and attenuation constant α vary with a cross section along the length of antenna, as shown in Fig. 3. So for a fixed frequency and for ours LWAs profile, we had predicted a corresponding beam radiation range [ϑ_{min} , ϑ_{max}] with respect to endifire direction, and the angle of main beam using a simple equation obtained by geometrical-optical approach.

References

1. O. Losito, "A New Design of Broadband Microstrip Leaky-Wave Antenna" Proceeding of 23rd Applied Computational Electromagnetics, ACES 2007 Int. Conf., Verona, Italy 19-23 March 2007.
2. Y. Qian, B. C. C. Chang, T. Itoh, K. C. Chen and C. K. C. Tzuang, "High Efficiency and Broadband Excitation of Leaky mode in Microstrip Structures", IEEE MTT-S Microwave Symposium Digest, volume 4, pp. 1419-1422, 1999.
3. O. Losito, "A Simple Design of Broadband Tapered Leaky-Wave Antenna" Microwave and Optical Technology Letters, vol. 49, pp.2833-2838, 2007.

Posters 2

3D Inductivity Computation On-Chip

Claudia Răcăşan, V. Ţopa, Adina N. Răcăşan, C. Munteanu, Oana S. Antonescu
Faculty of Electrical Engineering, Technical University of Cluj-Napoca, Cluj-Napoca, Romania
Claudia.Racasan@et.utcluj.ro

Modeling and extraction of inductivity on–chip interconnect has become an issue of great interest for integrated circuit design in recent years. This paper proposes to analyze and extract loop and partial inductivity, magnetic interaction, along with some of the high frequency effects such as skin and proximity effect. We also want to extract self inductivities and mutual inductivities for accurate crosstalk analysis. The paper is an introduction to the problem of modeling, analysis, and extraction of inductivity for integrated circuits.

With technology scaling, on-chip frequencies are increasing as device values exceed 50 GHz. The parasitic inductivity of on-chip interconnect is becoming a concern. The fast and accurate simulation of circuits with on-chip inductivity is a growing problem, and future trends show that the relative contribution of inductive effects on circuit behavior will continue to increase as technologies shrink further and low-k dielectrics are used to diminish capacitive effects. Inductive effects have become important in determining power supply integrity, timing and noise analysis, especially for global clock networks, signal buses and supply grids for high-performance microprocessors.

We want to analyze the basic physical processes which cause inductive effects. Capacitances have very strong geometry dependence. Inductivities, by contrast, have relatively weak geometry dependence, allowing for accurate calculation with relatively simple analytic formulas. Magnetic coupling, however, is dense, leading immediately to circuit-level intractability for large problem sizes. The inductivity matrix is dense physically because magnetic fields induced by a current can spread much further and must be terminated by eddy currents induced in nearby conductors. Furthermore, the partial inductivity formulation is mathematically dense. Partial inductivities are defined by flux areas that extend to infinity. Physically meaningful loop inductivities are only obtained when the more distant flux areas are cancelled out by distant partial mutual inductivities. Small mutual inductivities cannot be discarded without disrupting the passivity of the network.

High-frequency interconnect analysis are relegated to full-wave Maxwell's equations solvers. Q3D Extractor is an interactive software package that electrically characterizes three-dimensional interconnects structures such as those found in connectors, Printed Circuit Boards (PCBs), and Multi-Chip Modules (MCMs). We want to use it to solve the loop and partial inductivity matrices. Parameters extractors, solve the differential form of Maxwell's equations with volume discretization and finite-element techniques.

We want to chose the more important 3D on-chip structures models and analyze them. In figure 1 is presented on of the structure that we want to model and to compute the inductivity matrices.
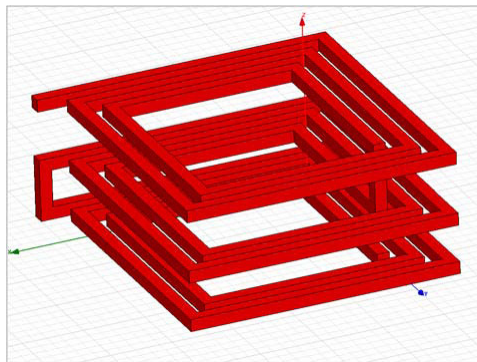
Fig. 1 – Three-layer stack inductor

References
1. H. G. Wang, C. H. Chan, L. Tsang, V. Jandhyala, "On Sampling Algorithms in Multilevel QR Factorization Method for Magnetoquasistatic Analysis of Integrated Circuits Over Multilayered Lossy Substrates", IEEE Transactions on Computer-Aided Design of Integrated Circuits an Sustems, vol.25, no.9. pp.1777-1792, September 2006

Posters 2

Local Impedance Properties in the Near Field of Linear Arrays

D. Wójcik

Silesian University of Technology, Gliwice, Poland

e-mail: dwojcik@polsl.pl

The paper is devoted to local field impedance properties in the near field of linear antenna arrays. The attention is focused on radiating near field region of whole array, where each separated antenna of the array can be treated as point source [1]. Consequently, the fields emitted by every single source can be calculated using far-field equations. The total EM fields in a particular observation point are obtained as a sum of the fields radiated by individual sources [2]. To obtain correct near field morphology, the phase shifts arisen from different distances between particular sources and the observation point must also be taken into account. It has been proved that under these conditions, the local field impedance $\eta_{em} = E / H$ is essentially equal to intrinsic impedance of free space if only the field produced by each unit antenna of the array has both vertical and horizontal component of equal amplitude and the phase shift between these components is constant for every single antenna. In order to verify proposed theorem, the near field of two antenna arrays has been examined by using of method of moments and the value of error function has been determined.

$$err = \frac{|\eta_{em} - \eta_0|}{\eta_0} \cdot 100\% \tag{1}$$

Both arrays contain four half-wave dipoles separated by the distance of one wavelength. For the first array, the dipoles are located collinearly. In the second array, to satisfy conditions mentioned above, the dipoles are rotated by an angle of 45°. In both cases the array are excited with 160^0. Phase progression. Obtained errors in local impedance are presented in Fig. 1. As can be observed, for the second array, satisfying required conditions, the errors are dramatically smaller that for the first array.
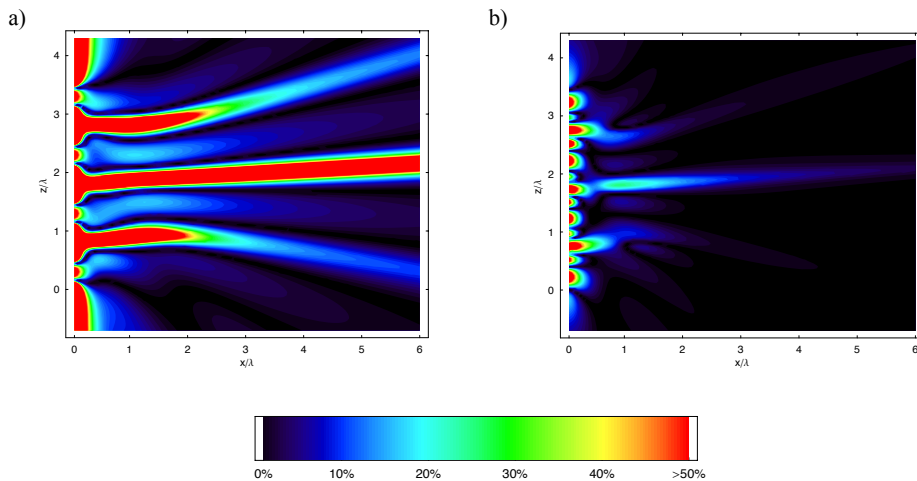
Fig. 1 – Error function (1) in vicinity of a) collinear array, b) rotated dipoles array

References
1. C.A. Balanis, Antenna Theory. Analysis and Design, John Wiley & Sons, 1997.
2. D. Wójcik, Near field of the base-station antennas of the cellular thelephony' (in polish), Ph.D. Thesis, Silesian University of Technology, 2004 Gliwice.

Posters 2

Study of Electromagnetic Interferences
Between AC Systems and Metallic Structures

D. L. Stet[1], D. D. Micu[1], A. Ceclan[1], L. Darabant[1]

[1] Faculty of Electrical Engineering, Technical University of Cluj-Napoca,
G.Baritiu Street Nr. 26-28, 400027, Cluj-Napoca, Romania
E-mail: Denisa.Stet@et.utcluj.ro

A numerical procedure employing the finite-difference method (FDM) is used in order to calculate the induced voltages across points on a underground pipeline, running parallel to a faulted line, and remote earth. We develop a mathematical differential model based on contour integral method to obtain the numerical form of the Helmholtz equation. We determine directly the numerical form of equation for non-homogeneous media, to clearly put in evidence the electromagnetic phenomena. A physical model for experimental calculus of induced voltage in an underground pipeline will be created based on the differential numerical model.

A numerical procedure employing the finite-difference method (FDM) is used in order to calculate the induced voltages across points on a underground pipeline, running parallel to a faulted line, and remote earth. We develop a mathematical differential model based on contour integral method to obtain the numerical form of the Helmholtz equation.

We determine directly the numerical form of equation for non-homogeneous media, to clearly put in evidence the electromagnetic phenomena.
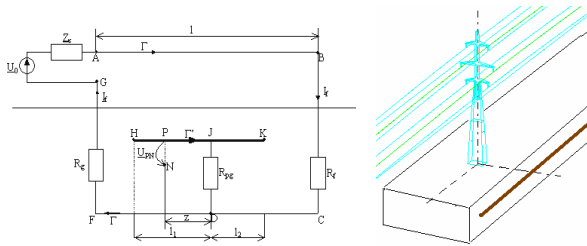
Fig. 1 The system under investigation. The faulted phase
A 3D model for the system under investigation

The numerical and geometrical data for this example is taken from [3], [4], for an objective reference and comparison.

A physical model for experimental calculus of induced voltage in an underground pipeline will be created based on the differential numerical model.

Using the results obtained in literature from applying the finite-element method (FEM) and those obtained with the Technical Recommendation no.7, we made a comparison with our results obtained with the finite-difference method.

References

[1] ***, "*Guide Concerning Influence of High Voltage AC Power Systems on Metallic Pipelines*" CIGRE Working Group 36.02, 1996.

[2] F. Dawalibi, R. D. Southey, "*Software Methods: State of the Art in Power Line/pipelines interference analysis*", Proceedings of the Canadian Association Symposium, Vancouver, Canada, pp.23-38, 1987.

[3] K. Satsios, D. Labridis, P. Dokipoulos, "*Currents and Voltages Induced During Earth Faults in a System consisting of a Transmission Line and parallel Pipeline*", ETEP vol. 8, no. 3, May-June, pp. 193-199, 1998.

[4] ***, "*Arbitration Agency for problems of interference between installations of the German Federal Railways and Power Utilities*", Technical Recommendation No.7, VWEW, Germany, 1982.

[5] Dan D. Micu, "*Numerical algorithm for the accurate evaluation of the induced voltages in a pipeline*", 6th International Conference on Computational Electromagnetics, Aachen, Germany, pp. 230-232, April 4-6, 2006.

[6] Dan D. Micu, I. Lingvay, A. Ceclan, E. Simion, *Computation of the induced AC potential on gas pipelines for complex rights-of-way configurations*, International conference on advancements of medicine and health care through technology, MEDITECH 2007, 27-29 sept. 2007, Acta Electrotehnica, vol. 48, nr. 4, 2007, ISSN 1841-3323, pp. 343-347.

[7] Dan D. Micu, Emil Simion, Dan Micu, Andrei Ceclan, *Numerical Methods for Induced Voltage Evaluation in Electromagnetic Interference Problems*, 9th International Conference, Electric Power Quality and Utilisation, Barcelona, 9-11 October 2007, IEEExplore, Compendex, ISBN 978-84-690-9441-9.

[8] Dan D. Micu, Lucian Man, Denisa Stet, Andrei Ceclan and Emil Simion, *Electromagnetic interferences between ac systems and metallic structures, International Symposium on Electromagnetic Fields in Mechatronics*, Eelectrical and Electronic Engineering, ISEF'2007, 13-15 September, Prague, Czech Republic,ISBN 978-80-01-03784-3, pp. 402-404.

Numerical Analysis of Small Slotted Ultra Wideband Antenna Based on Current Distribution for Bandwidth Enhancement

Y. R. Naumar[1], T. A. Rahman[1], R. Ngah[1], P.S. Hall[2]
[1]*Wireless Communication Centre, Faculty of Electrical Engineering
Universiti Teknologi Malaysia, Johor Bahru, Malaysia*
[2]*Department of Electronic, Electrical and Computer Engineering
University of Birmingham Edgbaston Birmingham, B15 2TT United Kingdom*

E-mail: vannebula2001@yahoo.com

A few years after the early investigation on ultra wideband (UWB) wireless system, considerable research efforts have been put into the design of UWB antennas and systems for communications. These UWB antennas are essential for providing wireless wideband communications based on the use of very narrow pulses on the order of nanoseconds, covering a very wide bandwidth in the frequency domain, and over very short distances at very low power densities. A number of techniques have been developed in past to design antennas with wide band impedance matched characteristics. The use of beveling technique, cutting notches at bottom, and dual feed are some examples of techniques used to improve the impedance bandwidth [1-4]. Slotted on patch radiator is another method that can provide broadband frequency response characteristics [2-3]. In this paper, some examples slotted UWB antennas are designed by studying their current distribution characteristics. The slots cut on the patch radiator means disturbance their current flow thereby wider impedance bandwidth can be achieved. The geometry of the antenna implies the current courses and makes it possible to identify active and neutral zones in the antenna, thus it will be possible to fix which elements will act on each characteristic [1]. The active zone is the matching and radiator zone. Acting on matching and radiating areas allows controlling the bandwidth. To better control an antenna behavior, it is necessary to identify neutral zones where geometry modifications are useless because neither the radiation pattern nor the matching bandwidth is much influenced. For example, the pentagonal antenna has a diamond neutral zone. Indeed, this zone can be removed with no much influence on the matching bandwidth as shown in Fig. 1. The neutral slot size is precisely measured in order not to degrade the antenna performance. Thus, to control antenna characteristics and where to place the slot on the antenna are critically determined by identification of its active and neutral zones.
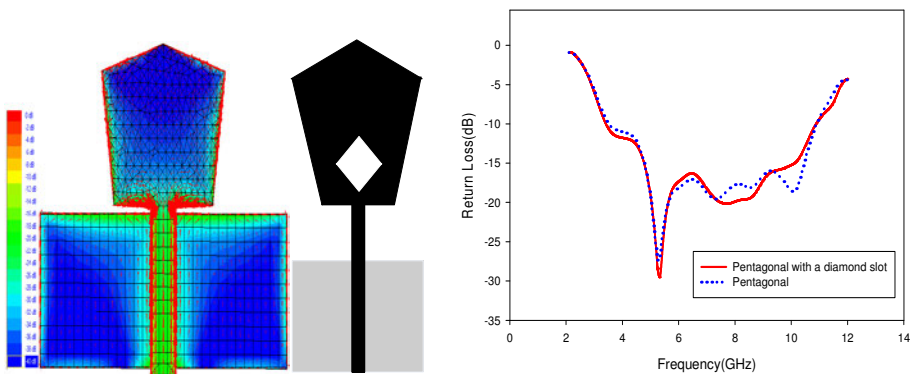
Fig.1 Influence of Neutral Zone to the Matching Bandwidth

References
1. Pele, Y. Mahe, A. Chousseaud, S. Toutain, P. Y. Garel, Ireena, "Antenna design with control of radiation pattern and frequency bandwidth," *IEEE Antenna and Propagation Society International Symposium*, Vol. 1, pp. 783-786, 20-25 June 2004.
2. Zhi Ning Chen, et al, "Planar antennas", *IEEE Microwave Magazine*, Vol. 7, No. 6, Page(s): 63-73, December 2006.
3. Seok H. Choi, et al, "A new ultra-wideband antenna for UWB applications", *Microwave and Optical Technology Letters*, Vol. 40, No.5, pp. 399-401, 5th March 2004.
4. Nader Behdad, Kamal Sarabandi, "A compact antenna for ultra wideband applications", *IEEE Transactions on Antennas and Propagations*, Vol. 53, No. 7, July 2005.

Posters 2

Characteristics of Preliminary Breakdown Pulse Trains in Negative Cloud-to-Ground Discharges

A. Nag and V.A. Rakov

Department of Electrcial and Computer Engineering, University of Florida, Gainesville, USA
E-mail: amitabh@ufl.edu

The first return stroke in a negative cloud-to-ground lightning discharge is thought to be preceded by the initial or preliminary breakdown, which can be defined as the in-cloud process that initiates or leads to the initiation of the downward-moving stepped leader. The amplitude of the preliminary breakdown pulses can be comparable to or even exceed (see Figure 1) that of the first return-stroke pulse. Preliminary breakdown pulses were studied by a number of researchers, including [1-5].

In this study, the characteristics of preliminary breakdown pulse trains in cloud-to-ground lightning discharges were examined and compared to those of similar pulse trains in attempted cloud-to-ground leaders [studied by 6]. The arithmetic mean pulse duration and interpulse interval for preliminary breakdown pulse trains in cloud-to-ground discharges were found to be 4.8 μs and 65 μs, respectively, versus 17 μs and 73 μs for attempted cloud-to-ground leaders. This implies that preliminary breakdown pulse trains in ground discharges contain a larger fraction of "narrow" pulses with durations less than or equal to 4 μs than the pulse trains in attempted cloud-to-ground leaders. Also, submicrosecond-scale pulses are observed as part of pulse trains associated with cloud-to-ground discharges, but not with attempted leaders. If all preliminary breakdown pulses with durations equal to or less than 4 μs in our dataset were excluded, the mean duration of the remaining 108 (out of a total of 655) pulses would be 16 μs, which is closer to, but still outside of the 20-40 μs range for "classical" pulses. We also examined the occurrence of pulses of different duration and amplitude in different parts of the preliminary breakdown pulse train. Pulses with larger durations (>4 μs) tend to occur earlier in a preliminary breakdown pulse train.

We speculate that the preliminary breakdown pulse train occurs as a result of interaction between a descending negative leader and the lower positive charge region in the cloud.
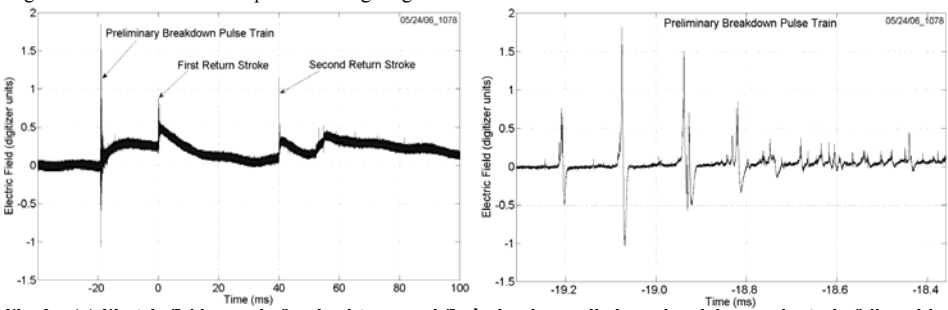
Fig. 1 – (a) Electric field record of a cloud-to-ground flash showing preliminary breakdown pulse train followed by two return strokes and (b) preliminary breakdown pulse train shown in (a), but on an expanded time scale of 0.95 ms.

References
1. N.D. Clarence, and D. J. Malan, "Preliminary discharge processes in lightning flashes to ground," Q. J. R. Meteorol. Soc., 83, 161– 172, 1957.
2. N. Kitagawa, and M. Brook, "A comparison of intracloud and cloud-to-ground lightning discharges," J. Geophys. Res., 65, 1189– 1201, 1960.
3. C.D. Weidman, and E.P. Krider, "The radiation field waveforms produced by intracloud lightning discharge processes," J. Geophys. Res., 84(C6), 3159– 3164, 1979.
4. W.H. Beasley, M. A. Uman, and P. L. Rustan, "Electric fields preceding cloud-to-ground lightning flashes," J. Geophys. Res., 87, 4883– 4902, 1982.
5. C. Gomes, V. Cooray, and C. Jayaratne, "Comparison of preliminary breakdown pulses observed in Sweden and in Sri Lanka," J. Atmos. Solar Terr. Phys., 60, 975–979, 1998.
6. A. Nag, and V. A. Rakov, "Pulse trains that are characteristic of preliminary breakdown in cloud-to-ground lightning but are not followed by return stroke pulses," J. Geophys. Res., 113, D01102, doi:10.1029/2007JD008489, 2008.

Posters 2

Surge Analysis of Twisted Pair in Conducting Tube by Method of Moment

S. Kato.

Toyo University, Kawagoe, Japan

E-mail: s_katoh@toyonet.toyo.ac.jp

Twisted pair transmission line composed of several lines is used widely as data communication signal lines in computer network system. In power distribution line and wiring for control signal, we use also twisted pair wire because of the low inductance, low surge impedance, low coupling and high performance of electromagnetic interference suppression. Twin-lead transmission line with no twist in power distribution line has well been modeled, but it is not clear how the surge characteristic of twisted pair depends on the number of twist or windings[1-2]. We used the Method of Moments (MoM) to study the surge characteristics of twisted pair single phase electric power line. The method used is the frequency domain MoM for transient analysis, and surge response is given by inverse Fourier transform after computation of frequency spectrum.

The work presented in this paper is concerned with the shielded twisted pair transmission line covered with dielectric in metallic tube. For the modeling of the wire with dielectric, we adapted a dielectric coating of wire segments[3] to reduce computing time. Fig. 1 shows the model of twisted wire in MoM. We used about 2000 segments to construct the model of a winding pitch formed by six segments and an insulator with thickness 1mm and a conductor with radius 1mm.

There are two propagation modes in common mode that are fast surge and slow one as shown in Fig.2. Few influences of the number of the strands occur in the fast propagation surge, but the increase of the serge impedance and the decline of the propagation speed are caused by twining in the slow propagation surge.

The relation between surge impedance and number of twist is shown in Fig.3. The result shows that wire stranded less than with several turns/m has almost same surge characteristics as the parallel lines, but the surge impedance decreases in tens of % when the number of the strands increases. According to the result, there are several surge propagation paths and the influence of twine over the surge becomes the decrease of the surge impedance and the decline of the propagation velocities in differential mode. However, the effect of the strand is smaller than that in the free space without the metallic pipe.

We measured the surge characteristics of the model line experimentally, and there are good accordance between simulation results and experimental results. It is possible to simulate the surge in twisted pair covered with polymer dielectric insulator by MoM.

Fig.1 Simulation model of twisted pair in metallic tube
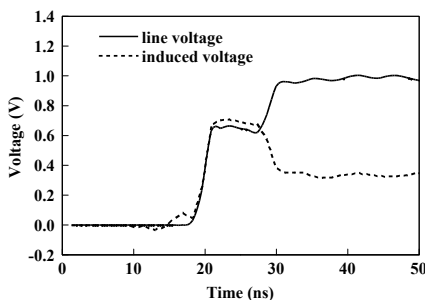
Fig.2 Voltage of the conductor applied voltage and induced voltage at terminal in metal tube at 50 turns/m
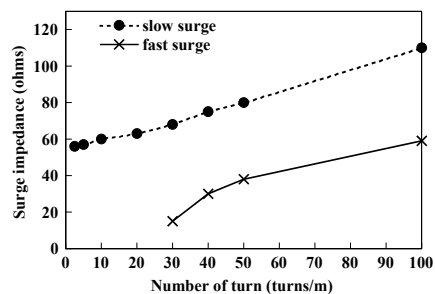
Fig.3 Surge impedance vs. number of twist in common mode

References
1. R.ELARBI, S.KATO, A.MOCHIZUKI, E.ZAIMA, "Transient Electric Field in Winding", 9th International High Voltage Symposium, 83591-83594, 1995
2. K. Chamberlin, K. Komisarek and K Sivaprasad, "A Method of Mometns Solution to The Twisted-Pair Transmission Line", IEEE Trans. On Electromagnetic Compatibility, p121-126, Vol.37, 1995
3. FEKO ver.5.3, EM Software & Sysytem-S.A. (Phy) Ltd, 2007

Magnetic Field Measurement Means for Electromagnetic Environment Control

L. Siny, M. Filatov, V. Goncharov, V. Ksenofontov, V. Molochkov

Research Institute of Pulse Technique, Moscow, Russia

E-mail: cemc@niiit.ru

Testing of technical installations for immunity to impulse magnetic field of Tesla intensity is an important task of electromagnetic compatibility. The lightning discharge is the most typical source of such fields. The current, originating in a discharge channel attains hundreds thousand Ampere. Simulated sources of lightning discharges are widely used for testing of technical installations for immunity. At realization of the experiments, for quantitative determination of immunity of tested equipment it is important to obtain   pattern of a magnetic field distribution near to the lightning discharge. Instrumentations for multipoint recording of the impulse magnetic field are necessary for solution of this problem. The instrumentations should be working at exposure to strong electric fields attacking   electronic circuits of the equipment.

Designed passive loggers are intended for monitoring magnitude of maximum induction of an impulse magnetic field (see Table). They can be used at testing radio- and electro- equipment of different assignment for immunity to impulse electromagnetic attack. Electronic devices, power supplies and transmission lines are absent in the loggers. They ensure a long storage of the recorded information. Overall dimensions and construction of the loggers allow using them in hard-to-reach places, tight volumes, and also in conditions where attack of set of unfavorable factors does not admit presence of staff. The great advantage of these devices is the simplicity of their operation. Application of the loggers simplifies a procedure of data acquisition at multipoint measurements of impulse magnetic fields that is especially important at realization of cost-intensive single experiments.

Table 1 - Brief performances of the storing loggers

Operating range	0,1...1 Tesla
Duration of measured pulses	beyond 0,1 ms
Overall dimensions	$\varnothing$ 5 mm x 5 mm
Storage time of information, over	24 hours
Basic error, under	10 %

Realization of UWB-beamforming with a Rotman-Lens at Low UHF Frequencies

A. Lambrecht[1], T. Zwick[1], W. Wiesbeck[1], J. Schmitz[2], M.Jung[2]

[1] *Institut für Höchfrequenztechnik und Elektronik, Universität Karlsruhe (TH), Engesserstraße 5, D-76131 Karlsruhe, Germany,*
[2] *Rheinmetall Waffe Munition GmbH, Heinrich-Ehrhardt-Str. 2, D-29345 Unterlüß, Germany*

E-mail: andreas.lambrecht@ihe.uka.de

Because it substitutes a whole "switched line length" concept in one passive structure the Rotman lens [1], [2] is investigated here as true-time-delay beamformer. The problem is, that it is a traveling wave structure, which has to be sized in the order of several wavelengths to give proper functionality. The design is hard at lower frequencies and this is the first time this structure was built and measured for the low UHF band. The system concept comprises a 1 x 4 phased array antenna, for which the Rotman lens provides the ultra-wideband phasing of the antenna feeds. The lens is fed by SP9T PIN-switch, which provides the different scan angle positions. The system specifications define a scan angle range of ±45°, a frequency range of 500 MHz – 1000 MHz (67 % bandwidth), desired VSWR of 2:1 and the number of beam directions is 9. The system will be initially used in CW mode. The prototype is etched on an Arlon substrate with a dielectric constant of 10.9 and dimensions of 609.6 mm x 914.4 mm x 3.23 mm. The lens structure has a very small dummyport region compared to wavelength. Further research will concentrate on improvements of the matching and hardware implementation into a whole array and pulse-mode operation. Results are given in Fig. 1 to Fig. 4.
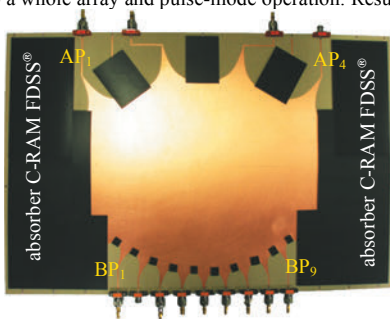
Fig. 1 – Rotman-Lens on Arlon substrate
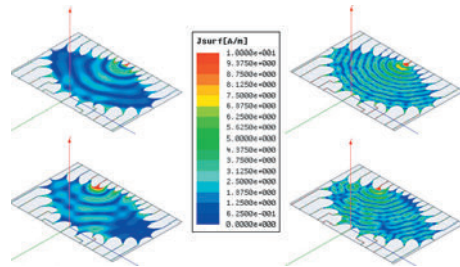
Fig. 2 – left: currents at 450 MHz, right: at 1000 MHz
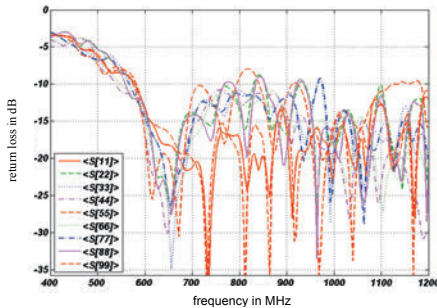
Fig. 3 – Matching of the beamports
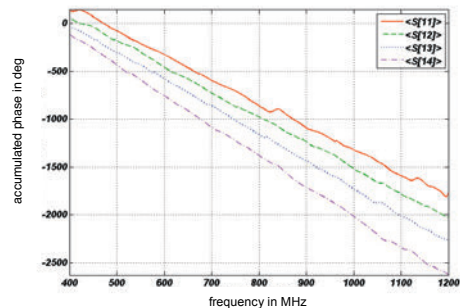
Fig. 4 – accumulated phase for BP$_1$

References

1. Simon P. S., "Analysis and Synthesis of Rotman Lenses", 22nd AIAA International Communications Sattelite Systems Conference & Exhibit, 2004.
2. Rotman W., Turner R.F., "Wide-Angle Microwave Lens for Line Source Applications", IEEE Transactions on Antennas and Propagation, 1963.

Posters 3

Optimizing the Positioning of MIMO & SISO Systems in Indoor Environments

P. Bechet[1], A. Neagu[1], I. Bouleanu[2], R. Helbet[2], A. Hangan[1]

[1] *Land Forces Academy, Sibiu, Romania*
[2]*Training Center for Communications and Information Systems, Sibiu, Romania*
E-mail: pbechet@gmail.com

The paper proposes an analysis for the optimization of information transfer by using Multiple Input Multiple Output (MIMO) and Single Input Single Output (SISO) technologies in indoor environments while taking into account the distance between the emitter and the receiver, the environment characteristics, the wave polarization and the relative spatial positioning of the network elements. Another task is identification of situations when the MIMO systems better fits the technical needs then the SISO systems. For certain network configurations, SISO systems can provide reliable links, thus accomplishing the information exchange with a lesser resource consumption. There is however a limit beyond which this type of system becomes inefficient and where MIMO can offer a significant increase of performances. In the first phase the E-field distribution was mapped in the indoor analyzed environment by the frequency-selective system Rohde&Schwarz. Fig.1 shows the field distribution in a room 4.9x6.3m^2 where the Access Point (AP) was placed. One observes that the minimum E-filed level is sufficient for assuring maximum performances of the SISO system. In this case using of the MIMO system in unjustified. Behind one or more walls (in our case the width of one wall was 60cm, made by bricks), the wave absorption is significant, and these conducts to decreasing of the S/N ratio under the optimum needed by SISO. In this situation MIMO provides a higher transmission rate (almost double). This aspect is revealed also by simulation, as shown in fig.2, where BER is better for MIMO.
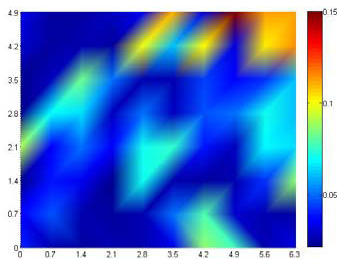
Fig. 1 - The influence of the polarization type on the MIMO signal and the SISO signal strength
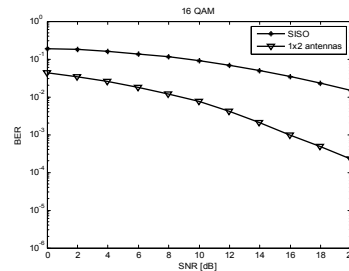
Fig. 2 - Comparison of the BER

The results of the study contribute to the improvement of: a) positioning of the AP in a room; b) selection of the wireless 802.11g technology (MINO/SISO), in order to fulfill the transmission transfer rate need.

References
1. C. N. Chuah, D. Tse, J. M. Kahn, and R.Valenzuela, "Capacity scaling in MIMO wireless systems under correlated fading," *IEEE Trans. Inform. Theory*, vol. 48, pp. 637–650, Mar. 2002.
2. P. J. Smith and M. Shafi, "On a Gaussian approximation to the capacity of wireless MIMO systems," in *Proc. Int. Conf. Communications, ICC 2002*, 2002, pp. 406–410.
3. A. Grant, "Rayleigh fading multiple antenna channels," *EURASIP J. Appl. Signal Processing*, pp. 316–329, 2002.
4. N. Chiurtu, B. Rimoldi, and E. Telatar, "Dense multiple antenna systems," in *Proc. IEEE Information TheoryWorkshop*, 2001, pp. 108–109.

Posters 3

Electromagnetic Fields Radiated by Negative Lightning using an Electrical Network Model

J. H. Rakotonandrasana and A. Beroual

Ecole Centrale de Lyon – AMPERE CNRS UMR 5005,
36 avenue Guy de Collongue, 69134 Ecully, France

E-mail : Abderrahmane.Beroual@ec-lyon.fr

Besides the important damages that can result from the direct lightning hits on the environment (power transmission lines, telecommunications, sub-stations, airports, control centres ...), the electromagnetic fields radiated by these lightning discharges also constitute an important stress to which the electrical systems and their components are exposed. Thus the knowledge of the conducted and radiated electromagnetic fields is very useful to well dimension the protection systems and to attenuate their effects.

This paper presents the simulated electromagnetic fields radiated by negative lightning downward leader using a predictive dynamic model we developed elsewhere [1]. This latter is based on the idea that a substantial similarity exists between the lightning phenomena and the discharge in large air gaps. It takes into account the different phases of the negative discharge propagation (i.e., the initiation of the first corona, the negative and space leaders and the junction of leaders). It uses LCR line electrical network parameters derived from electromagnetic field, physical laws and gas discharge theories. Assuming the discharge channel to a long conductor and taking into account criteria for instabilities and some atmospheric conditions, the mathematical model enables to determine the discharge main macroscopic parameters such as current and propagation velocity. The simulated magnetic and electric fields are found to be in a good accordance with trends of those recorded during natural lightning [2, 3].
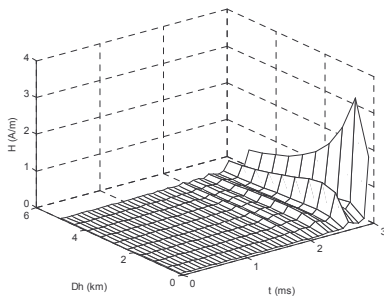
Fig. 1 - Negative leader magnetic field 100 to 5000m from the discharge. Height = 1.2m
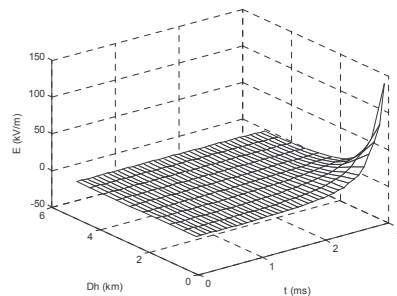
Fig. 2 - Negative leader electric field 100 to 5000m from the discharge. Height = 1.2m

References
1. A. Béroual, J. H. Rakotonandrasana, I. Fofana, "Modelling of the negative lightning discharge with an equivalent electrical network ", IX International Symposium on Lightning Protection (IX SIPDA), Foz do Iguaçu, Brazil, 26th to 30th November, 2007.
2. P. Degauque and J. Hamelin, "La compatibilité électromagnétique" (Edition Dunod, CNET/ENST), 1990.
3. V. Rakov, M. A. Uman, M. I. Fernandez, R. Thottapillil, A. Eybert-Berard, J. P. Berlandin, F. Rachidi, M. Rubinstein, S. Guerrieri and C. A. Nucci, "Observed electromagnetic environment close to the lightning channel", 23rd ICLP, Firenze, Italy, September 1996, pp. 30 - 35.

Radar UWB: Human detection through a wall

C. Lièbe, A. Gaugue, J. Khamlichi, M. Ménard
Laboratoire Image, Informatique, Interaction (L3i)
Université de La Rochelle
La Rochelle, France

E-mail: christophe.liebe@univ-lr.fr

The detection of a target behind an obstruction is a very interesting theme for a wide range of industries. For example, seeing through a wall could be utilized by rescue services, searching for people in rubble and in buildings on fire. The military industry could use this technology for bomb-disposal, neutralization of aggressors, hostage rescue, etc. Many methods exist to see through walls (1), which can be divided into two general groups:

- Passive systems - imaging system types running in millimeter and submillimeter wavelengths

- Active systems - radar system types running in centimeter and millimeter wavelengths and even in X-ray

Nevertheless, most systems are still under development or in pre-research status and they are not ready for manufacturing. A detailed view of the scene under observation is not necessary. Only relevant information i.e. number of people, positions, speed of movement, etc. is required. UWB (Ultra WideBand) radar is very good solution for obtaining this information, because it presents a lot of advantages compared to other systems: a good capability to penetrate wall and floor materials, a good spatial picture resolution (approximately ten centimeters), noise robustness due to a large bandwidth and the possibility to detect and localize a human body.

The main part of our system is composed of UWB communication modules. We re-configured the software and the hardware of these modules to obtain a bistatic UWB radar. The acquisition (fig.1) below left is radar echoes received through a 15cm-thick concrete wall. The pulse marked "E1" corresponds to the direct field between the emitter and the receiver. The echo "E2" is due to the reflection on the wall. The presence of the echo "E3" highlights the human body located behind the wall. The echo "E4" corresponds to a wave reflected by the wall behind the human body. We developed a mechanical scanning system. This system scans the scene, degree by degree, with an opening of 60°.

The picture represented in figure 1 on the right, is obtained by the juxtaposition of the 60 scans, and is rebuilt in polar coordinates. No treatments were used to obtain this result. The development of algorithms has optimized the detection of a human body through a wall and the surrounding environment. The drawback of this system is the slowness of the mechanical scanning. Different solutions will be discussed to improve performance.
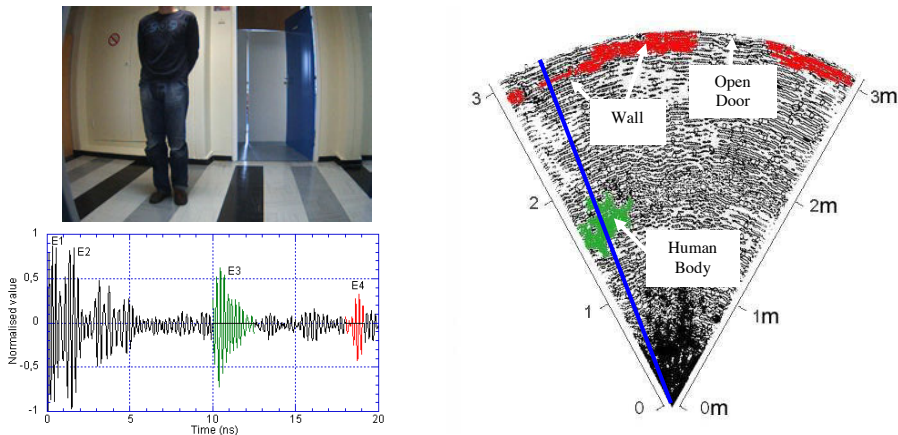
Fig. 1 - Top left: photo of measurement scene. Below left: vertical cut of the radar picture, following the blue line. On the right: results of the measurement scene through a 15 cm-thick concrete wall.

References
1.   A. Gaugue and J.L. Politano "Overview of current technologies for through the wall surveillance", Proceedings of SPIE, Vol 5989, 2005, pp. 1H-1 – 1H-11.
2.   "Ultra-Wideband Radar Technology" J. D. Taylor, 2001, CRC Press.

Ultra Wideband Low Profile Single-Arm Spiral Antenna Using Electromagnetic Bandgap Structures

Mohammad Saed

Texas Tech University, Lubbock, Texas, USA

Email: mohammad.saed@tu.edu

Electromagnetic band-gap (EBG) structures exhibit unique electromagnetic properties that have led to a wide range of applications in electromagnetics. In this paper, electromagnetic bandgap structures are utilized to enhance the bandwidth of a low-profile, unidirectional, one-arm Archimedean spiral antenna built on a thin substrate and backed by a ground plane. It is well known that placing a ground plane (a perfect electric conductor) closely behind a spiral antenna to make the radiation unidirectional severely limits the antenna bandwidth. In order to mitigate the ground plane effect, and therefore increasing the bandwidth significantly, electromagnetic band-gap structures are employed. Specifically, the one-arm spiral is placed over an EBG surface which in turn is backed by a ground plane. Several types of EBG surfaces are investigated for this antenna. These surfaces use a variety of periodic patch shapes. To simplify the construction, the patches are not connected to the ground plane. The EBG surfaces behave as artificial magnetic conductors in the frequency band of operation. The use of EBG structures with planar antennas such as microstrip and printed dipoles was investigated in the literature, primarily, to suppress surface waves resulting in increased antennas efficiency and better radiation patterns. Some attempts to incorporate EBG structures with spiral antennas appeared in the literature. However, they differ greatly from our proposed configurations, both in the EBG structure used as well as the obtained results.

The proposed antenna configurations were investigated theoretically using Ansoft Designer which uses a frequency domain full-wave method based on the method of moments. Furthermore, theoretical simulations in the time domain were carried out using the FDTD technique. Parametric studies to understand the effect of geometrical and substrate parameters on antenna performance (impedance bandwidth and radiation patterns) is carried out. Theoretical results were verified experimentally. It has been shown that the proposed antenna improved the bandwidth greatly. The design details along with simulation and experimental results will be presented.

RF breakdown prediction for microwave passive components in multi-carrier operation

S. Anza[1], M. Mattes[2], J. Armendariz[1], J.Gil[1], C. Vicente[1], B. Gimeno[3], V. E. Boria[4], J. R. Mosig[2], D. Raboso[5]

[1]*Aurora Software and Testing S. L. Parque Científico Universidad de Valencia, 46980 Paterna, Spain*
[2]*Laboratoire d'Electromagnétisme et d'Acoustique, Ecole Polytechnique Fédérale de Lausanne, 1015 Lausanne, Switzerland*
[3]*Departamento de Física Aplicada y Electromagnestimo, Universidad de Valencia, 46100 Valencia, Spain*
[4]*Departamento de Comunicaciones, Universidad Politécnica de Valencia, 46022 Valencia, Spain*
[5]*ESA-ESTEC, Keplerlaan 1, Postbus 299, 2200 AG Noordwijk, The Netherlands*

E-mail: sergio.anza@aurorasat.es, michael.mattes@epfl.ch

The incessantly growth of the telecommunication market led to the development of filter and multiplexer designs with very stringent requirements. Especially the continuously increasing number of channels in multiplexers for satellite applications forces space industry to face the problem of power handling during the design process. In parallel, the output power of amplifiers is increasing, too. This leads to extremely high power levels within the devices and increases the risk of RF breakdown due to corona discharge or multipactor breakdown.

A lot is known about multipactor breakdown for the single carrier case and a homogeneous field distribution, e. g. like in a parallel plate configuration (see for example [1]). More complex geometries, like rectangular waveguide filters have been considered in [2], but, again only for the single carrier case.

However, the prediction of multipactor in multi-carrier operation is much more complex. On the one hand, the standard multipactor criterion for the prediction of multipactor in the multi-carrier case, the "20-gap-crossing" rule [3] may be insufficient when dealing with complicated structures or many carriers [4]. Thus, in order to properly characterize the multipactor process in such systems, the physical effects of the space charge fields, such as detuning, noise and harmonics, need to be considered.

On the other hand, for an accurate prediction of the breakdown threshold, the electromagnetic field distribution inside the component is necessary. Standard simulation tools only offer the possibility to compute the RF response for a single frequency.

This communication addresses the multipactor problem for multi-carrier operation inside rectangular waveguide based devices, e. g. filters, by means of numerical simulations of the electron trajectories and multiplication inside the structure, incorporating accurate field calculation and space charge effects:

- The software permits the excitation of the device under test with several carriers.
- It employs a Particle-In-Cell (PIC) code for tracking the electrons and calculating the space charge fields. The implemented PIC follows a leap-frog algorithm and uses a Finite Differences in Time Domain (FDTD) solver for calculating the space charge fields.

As a result, this novel software offers the possibility of predicting multipactor in multi-carrier systems in a wide variety of situations.

References
1. A. Woode and J. Petit, "Diagnostic investigations into the multipactor effect, susceptibility zone measurements and parameters affecting a discharge", ESA- Working paper No.1556, November 1989.
2. C. Vicente, M. Mattes, D. Wolk, H. L. Hartnagel, J. R. Mosig, and D. Raboso, "Multipactor Breakdown Prediction in Rectangular Waveguide Based Components", Microwave Symposium Digest, 2005 IEEE MTT-S, Long Beach, CA, USA, Vol. 2, pp. 1055-1058.
3. Space Engineering: Multipacting Design and Test, vol. ECSS-20-01A, edited by ESA-ESTEC. ESA Publication Division, The Netherlands, May 2003.
4. S. Anza, C. Vicente, B. Gimeno, V. E. Boria, and J. Armendariz, "Long-term multipactor discharge in multicarrier systems," Physics of Plasmas, vol. 14, pp. 082112–082112–8, Aug. 2007.
5. "*RF Breakdown in Multicarrier Systems*", European Space Agency, Contract No. 19918/06/NL/GLC/RF

A Simple Analytical Model of Metal Foams for EM Shielding Applications

Michele Bozzetti [1], Onofrio Losito [2]

[1]*Department of Electronic and Electrotechnics of Polytechnic of Bari, Bari - Italy*
[2] *ITEL Telecommunications Research Laboratory on EM, Ruvo di Puglia - Italy*
E-mail: o.losito@itelte.it
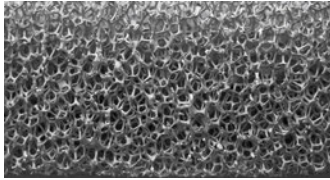
Figure 1. An examples of Duocel® open cell aluminium foam: 9x3x0.5 cm^3 slab (porosity: 10 PPI, actual density: 6.1%)

in literature. Fig. 1, shows an example of an open cell aluminium foam, produced by ERG Aerospace and called Duocel® foam. We can see that its low apparent density, (8%) and its capability to allow both light and air to pass through, can be useful in

Since Metal foams were discovered by the scientific world at the beginning of the last decade, they have been subject to investigation for more than 10 years. Characteristic properties like low apparent (or actual) density guarantees, for example, lightweight and high stiffness/specific-load ratios. Moreover, their porous structure and intrinsic non-homogeneity give good acoustic and thermal isolation properties and also strong impact-absorption and vibration damping capabilities.

Nevertheless, their employment in EM application is new

Table 1 – Esaminated Foam Types

Duocel® Aluminium foam			
Type I	*Type II*	*Type III*	*Type IV*
10 PPI, 6.1% actual density.	20 PPI, 8.5% actual density.	40 PPI, 7.9% actual density.	40 PPI, 8.7% actual density.

Figure 2. Shielding Effectiveness (E field) for single and double wire-mesh screen with single and double thickness.

several applications. The analysis of the shielding properties of different kinds of Duocel® aluminium foams slabs obtained by varying porosity and apparent density, has been investigated and performed through experimental measurements. Their shielding properties have been both discussed and shown. Metal foams are complex and random structures which requiring sophisticated analytical models. Moreover, because of its versatility and its capability to deal with heterogeneous media, the Variable-Mesh Finite Difference Time Domain (VM-FDTD) method, is naturally the most appropriate approach [1], though unfortunately, it is computationally onerous. The 2D laminated wire-mesh screen model, developed by
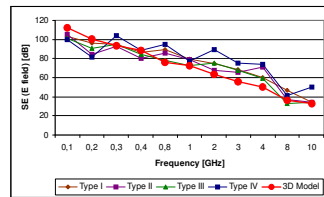
Figure 3. Shielding Effectiveness (E field) for aluminum foam slabs described in Table 1, compared with theoretical values of 3D model.

Casey [2] and compared with commercial aluminium shield perforated periodically with apertures, was a first step to solve the EM problem of the rigorous evaluation of the metal foam's shielding effectiveness [3]. Encouraged by the results, we have improved the previously 2D model, developing a preliminary analytical 3D model. Therefore the electromagnetic shielding behavior of a slab of metal foam, has been investigated considering a model with a double wire-screens mesh, separated by an air space. In fact, from the shielding effectiveness analysis of the double wire-mesh, shown in Fig. 2, it is clear that the shielding effectiveness of a double screen is greater than that of single screens with double thickness. The single screen, whose meshes are assumed to be square, is described by an equivalent sheet impedance operator as mentioned in [3]. The agreement of both experimental and theoretical data, shown in Fig. 3, give us the possibility to optimize this model in 3D.

References

1. Catarinucci, L.; Losito, O.; Tarricone, L.; Pagliara, F, "High Added-Value EM Shielding by Using Metal-foams: Experimental and numerical characterizzation" Electromagnetic Compatibility, EMC 2006, vol. 2, aug. 2006 pp. 285 – 289.
2. K.F.Casey, "Electromagnetic Shielding beavior of wire-mesh screens", IEEE Transactions on Electromagnetic Compatibility, vol.30, august 1988, pp.298-306.
3. L. Catarinucci, O.Losito, L.Tarricone, "On the Use of Metal Foams in EM shielding applications" Proceedings of the Mediterranean Microwave Symposium MMS'2006, Genova, Italy, september 2006, pp. 240-245.

Posters 3

Electromagnetic Modeling of Integrated L-C Structures for EMI Filters Implementation

Adina Racasan, C. Munteanu, V. Topa, Claudia Racasan, Mihaela Plesa

Electrical Engineering Departament, Technical University of Cluj-Napoca,
26-28 Baritiu Street, 400027 Cluj-Napoca, Romania
Adina.Racasan@et.utcluj.ro

The fundamental element of integrated EMI filters is the integrated L-C structure. To understand the HF behavior of integrated EMI filters, HF modeling of integrated L-C structure is essential.

The planar integrated L-C structure consists of alternating layers of conductors, dielectrics, insulation and ferrite materials that produce an integrated structure with similar terminal characteristics as the lumped components [1]. The integrated L-C winding consists of a dielectric substrate with conductor windings directly deposited on both sides, thus resulting in a structure having both sufficient inductance and capacitance. This realizes the equivalent integrated capacitance as well as the inductance. By appropriately terminating the four terminals A, B, C and D of the integrated L-C winding, the same structure could be configured as equivalent L-C series resonator, parallel resonator or low pass filter.

This paper proposes the frequency domain modeling of the basic 2-conductor integrated L-C cell by using the multi-conductor lossy transmission-line theory.

The structure of a 2-conductor planar integrated L-C cell is shown in Figure 1. Figure 2 shows the cross-section at x-y plane. The previous models consider only two conductors and treat them as a four-terminal two-port network [2]. However, if the common ground surrounding the two conductors is considered, as shown in Figure 3, this structure can be treated as two transmission lines (with respect to ground) with magnetic and electric coupling between them. The equivalent circuit of an infinitesimal section is shown in Figure 4.
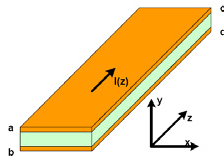
Fig. 1. Planar integrated L-C cell
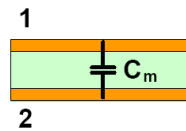
Fig. 2. Cross-section of integrated L-C cell
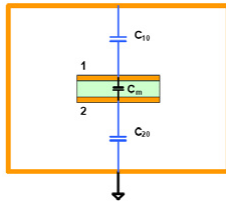
Fig. 3 - Adding the ground plane
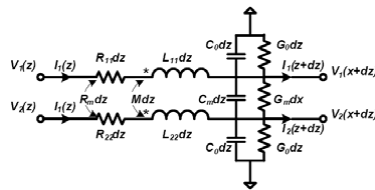
Fig. 4 - Equivalent circuit of a infinitesimal section

The paper will present the results of the analysis of the planar integrated L-C with different terminal configurations. The main conclusions of the studies performed will end the paper.

References
1. J. T. Strydrom and J. D. Van Wyk, "Electromagnetic Modeling for Design and Loss Estimation of Resonant Integrated Spiral Planar Power Passives," IEEE Transactions Power Electronics, vol.19, 2004.
2. P. C. Magnusson, G. C. Alexander, V. K. Tripathi. and A. Weisshaar, Transmission line and wave propagation. 4th edition, CRC Press LLC, 2002.
3. L. N. Dworsky, Modern transmission line theory and applications. J. Wiley and Sons Inc., 1979.
4. C. Rengang, J. D. van Wyk, S. Wang and W. G. Odendal, "Technologies and characteristics of Integrated EMI Filters for Switch Mode Power Supplies," IEEE Power Electronics Specialist Conference, vol. 35, 2004.

Posters 3

Time Response Estimation Algorithm using AWE method and Robust Rational Interpolation Technique

M. Surma

Silesian University of Technology, Gliwice, Poland

e-mail: msurma@polsl.pl

Time response of scattering and radiating objects excited by different kind of sources can be obtained with a few manners. The most obvious approach is to measure parameters of object under investigation but sometimes it could be difficult. In such situation very useful can be computer simulations in time or in frequency domain. Usually, for time domain, Finite Difference Time Domain (FDTD) technique is used. However some problems can be appeared if we take into accounts high-resonant structures because to reach stable state of the results, quite long time of analysis can be required. Other technique consists in analysis of the structure in frequency domain (for example with Method of Moments -MoM) and then using Inverse Discrete Fourier Transform (IDFT) the results can be transformed into time domain. Of course, to obtained good results we need appropriate number of frequency samples. However, in practice, when we analyze electrically large structures over wide frequency range it can be very time consuming process. Additionally, to store all samples for many observation points of interest (it can take place in case of hybrid method MoM-FDTD) big computer memory could be desired.

In this paper, one proposed method that allows to save memory requirement and shorten time of analysis. It consists in combining Asymptotic Waveform Evaluation (AWE) techniques [3] with approach based on robust interpolation technique [4]. The AWE technique is based on rational approximation of current vector over a wide frequency range from relatively small number of discrete frequency and frequency derivative samples. The idea of the second technique is as follows. First, the rational function (obtained by AWE) is expressed in terms of Chebyshev polynomials and then its poles are determined. Afterwards, taking advantage of properties of passive systems the residues are calculated. Finally, the resulting pole-residua model is analytically transform to achieve time domain response.

Advantages of the proposed approach:

1. Unlike the IDFT technique, the proposed approach doesn't require a large number of equally spaced frequency points. Instead of that in computer memory we store coefficients of rational function only.
2. Time of evaluating coefficient of rational function is much shorter that time for obtaining appropriate number of frequency samples necessary for conventional IDFT technique.

These two advantages results in less requirement with respect to time of analysis and computer memory.

To examine efficiency and accuracy of proposed approach the results of the near field E_z component at distance d=1m from dipole excited by Gaussian pulse is presented. As one can see the agreement is quite well. More complex structures were also analyzed.
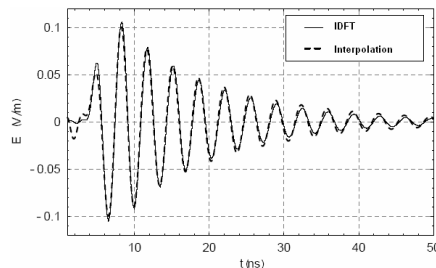
Fig.1. Time response of the near field E_z component at distance d=1m from dipole excited by Gaussian pulse.

References
1. R. F. Harrington, "Field Computation by Moment Methods", MacMillan, 1968.
2. K. S. Kunz, R. J. Luebbers, "The Finite Difference Time Domain Method for Electromagnetics", CRC Press, 1993.
3. C.R. Cockrell, F.B. Beck, "Asymptotic Waveform Evaluation (AWE) Technique for Frequency Domain Electromagnetic Analysis", NASA Technical Memorandum 110292, November 1996.
4. W. T. Beyene, "Improving Time-Domain Measurements with Network Analyzer Using Robust Rational Interpolation Technique", IEEE Transaction on Microwave Theory and Techniques:, vol. 49, pp. 500-508, March 2001.

Posters 3

Transition Radiation of Nonrelativistic Electron Bunches

V. N. Bolotov, S. I. Kononenko, V. I. Muratov, and V. D. Fedorchenko
Karazin National University, Kharkov, 61007, Ukraine

E-mail: bolotov@vl.kharkov.ua

Today, generation of short high-power electromagnetic pulses (EMPs) is of considerable interest. Specifically, EMPs are generated by rapidly reconfiguring the field of a system where a charged electron bunch interacts a conducting solid. A charged particle moving rectilinearly and uniformly either near or through a conducting medium generates time-varying currents in it. The currents induced produce electromagnetic radiation. Thus, electromagnetic radiation arises due to the reconfiguration of the field of a charged particle–medium system.

In this paper the experimental and theoretical results on generating EMPs by using nonrelativistic electron bunches passing through diaphragms of various geometries are described. Results obtained agree with the predictions of the transition radiation theory as applied to nonrelativistic charged particles passing through screens. The influence of apertures of various configurations on transition radiation spectra is studied.

Experiments were carried out with the setup described in [1]. Electron bunches were formed by Bernstein–Green–Kruskal waves (BGK waves). These are stationary nonlinear waves whose profile depends on the initial distribution function of trapped particles. At certain ratios between the velocities and densities of modulated beams, the potential of BGK waves may vary with time in the form of a short pulse. Thus, if the initial distribution function of trapped particles is constant along the particle paths, continuous electron bunches may be generated.

When electron bunch passes through the aperture it excites inductive currents, which are the source of transition radiation. Inductive currents consist of conductivity electrons involved in the motion under the influence of external coulomb field of electron bunch falling upon. The transition radiation spectra were calculated in wave zone. Theoretical results coincide with experimental ones.

Fig. 1 – Experimental transition radiation spectrum

References
1.   V. N. Bolotov, S. I. Kononenko, V. I. Muratov, and V. D. Fedorchenko "Transition Radiation of Nonrelativistic Electron Bunches Passing through Diaphragms" , Technical Physics, Vol. 49, No. 4, 2004, pp. 466–470.

Analysis of anisotropic microwave circuits
with several metallized interfaces

C. Boularak[1], M.L.Tounsi[1], A. Khodja[1], R. Touhami[1] and M.C.E. Yagoub[2]

[1] *Instrumentation Laboratory. Faculty of Electronics and Informatics. USTHB University.*
P.O Box 32 El-Alia, Bab Ezzouar, 16111, Algiers, Algeria.
[2] *SITE, 800 King Edward, University of Ottawa, Ottawa, ON, K1N 6N5, Canada.*

E-mail : boularak_chafik@hotmail.com

Abstract - This paper presents a new theoretical analysis of multilayered anisotropic microwave circuits based on a modified spectral-domain approach (SDA) [1]. The number of conducting strips/slots can be arbitrary set. The proposed technique made the evaluation of Green's functions easier. Figure 1 shows a cross section of the circuit under analysis, printed on biaxial anisotropic substrates with diagonal tensors of permittivity ε and permeability μ. The method uses a transform coordinate system to simplify the calculation of electromagnetic (EM) field components based on Maxwell's equations and boundary conditions applied at all dielectric interfaces. The hybrid-mode EM field is considered as the superposition of LSE and LSM modes. The proposed technique is based on a transfer matrix expression which relay tangential components of EM fields on two consecutive interfaces H_i and H_{i+1}. Such proposed method presents attractive features: (i) the use of Fourier transform allows the conversion of convolution integrals equations into algebraic products, avoiding the necessity of numerical evaluation of complex integrals, (ii) the SDA method is numerically more efficient than others working in space domain since the anisotropic and multilayer problems can be resolved by a simple product of different transfer matrices, (iii) the coupling phenomena between different conducting interfaces can be resolved using superposition theorem., (iv) the solution obtained by this method is stationary by nature. Thus, the solution is insensitive to the first-order error associated with the basis functions. This procedure can then, be generalized to the calculation of the coupling admittances between all arbitrary metallized interfaces. The numerical results were validated with a neural network tool as well as with published data.

Numerical results

Figure 2 illustrates the simulated dispersive characteristics of a three-level microstrip anisotropic coupler (ε_{rx2}=6.64, ε_{ry2}=6.24, ε_{rz2}=5.56; ε_{rx3}=2.35, ε_{ry3}=2, ε_{rz3}=3.5, μ_{rx3}=2.75, μ_{ry3}=2, μ_{rz3}=3.5). These results were compared to those obtained by a neural modeling tool, i.e., *neuromodeler* [2]. The neural models were generated with an average training error of 0.01% and a maximum test error lower than 0.9%, hence confirming the reliability of these models. We can observe that the thickness h_2 influences considerably the effective permittivity ε_{eff} particularly for low values of h_2. The second example is a three-layer bilateral microstrip/coupled-stripline printed on sapphire substrate (ε_{x1}=ε_{x2}=ε_{z1}=ε_{z2}=9, 4, ε_{y1}= ε_{y2}=11.6). Figure 3 shows the frequency dependence of the –odd and –even effective dielectric constant. The computed results agree well with [3] with an average error of 1%.

| Fig. 1 – Cross section of the analyzed multilayer circuit | Fig. 2 Even-mode ε_{eff} versus frequency for several values of h_3 (h_1 =4mm, h_2 =0.5mm, $h_3 + h_4$ =4.5mm) | Fig.3-Variation of ε_{eff} with frequency (2a = 20 mm, b = 6 mm, h_1 = h_2=1 mm, h_3= 2 cm, w/h_1 =1, s/h_1 = 0.5) |

References

[1] T. Itoh, "Spectral domain approach for calculating the dispersion characteristics of generalized printed transmission lines*,", IEEE Trans. Microwave Theory Tech.*, vol. 28, pp.733-736, July 1980.
[2] NeuroModeler v. 1.2, 2000, Q.J. Zhang, Carleton University, Ottawa, Canada.
[3] C. Seo, C. Woong Lee, "Analysis of two-layer three-coupled microstrip lines on anisotropic substrates", *IEEE Trans. Microwave Theory Tech*. vol. MTT-42, pp. 160–162, January. 1994.

A Mesoband Dipole Antenna for High Power Spark Gap Switched Oscillator

S.H. Lee[1], Y.J. Yoon[1], H. Heo[2], S.H. Nam[2], W.S. Lee[3] and D.W. Choi[3]
[1]*Yonsei University, Seoul, Korea*
[2]*Pohang Accelerator Laboratory, Pohang, Korea*
[3]*Agency for Defense Development, Daejeon, Korea*
E-mail: saintfighter@yonsei.ac.kr

Recently, the development of several new types of high power electromagnetic (HPEM) systems has received widespread attention. The HPEM systems can be divided into four types according to the classification based on bandwidth, such as narrowband, mesoband or moderate band, sub-hyperband or ultra-moderate band and hyperband [1]. Among these systems, mesoband systems are appropriate for some applications because of its size, simplicity, operating frequency and bandwidth. Specially, mesoband systems can be compact and portable systems since they have small size and light weight [2]. Mesoband systems designed to generate damped sinusoidal signal which has wide bandwidth use a spark gap switched oscillator. For high directive system, a multirod and a reflector antenna could be used [3-4].

In this paper, we present radiated field of a mesoband dipole antenna and compare the difference between a dipole antenna without multirods and a dipole antenna with multirods. To radiate the high power damped sinusoidal signal, this system is composed of high voltage charger, Marx generator and a dipole antenna with a spark gap switch which uses pressurized dielectric gas or insulating oil to generate high voltage pulse. This system is operated in the VHF band and it can radiate a peak voltage of few hundreds kilovolts. Mesoband dipole antennas with multirods and without multirods are evaluated through simulation via the Finite Integration method (FI-method) and measurement. Simulated radiated field waveforms presented in Fig. 1 shows that the field strength of a dipole with multirods is double the field strength without multirods. These simulated and experimental results will be useful for design of mesoband systems which use a dipole antenna.
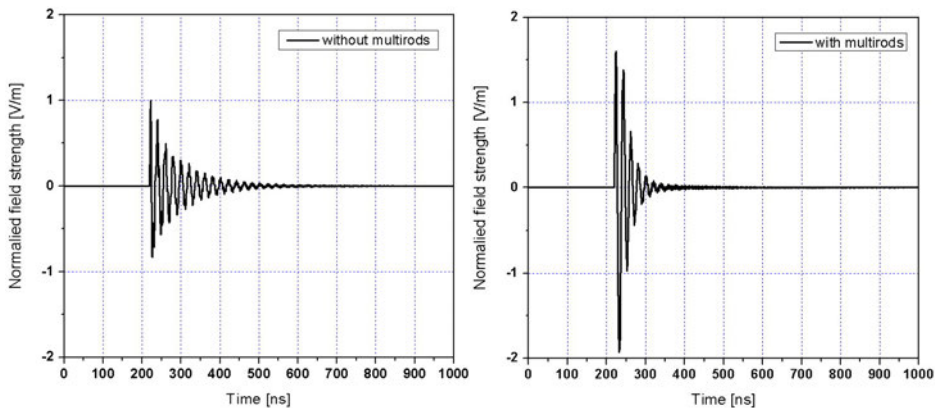
Fig. 1 – Normalized radiated field waveforms of a mesoband antenna at 20 m

References
1. D.V. Giri, F.M. Tesche, "Classification of intentional electromagnetic environments (IEME)," IEEE Transactions on Electromagnetic Compatibility, Volume 46, Issue 3, pp. 322-328, Aug. 2004.
2. P.Sarkar, S.W. Braidwood, I.R. Smith, B.M. Novac, R.A. Miller, R.M. Craven, "A Compact Battery-Powered Half-Megavolt Transformer System for EMP Generation," IEEE Transactions on Plasma Science, Volume 34, Issue 5, Part 1, pp. 1832-1837, Oct. 2006.
3. W.D. Prather, C.E. Baum, R.J. Torres, F. Sabath, D. Nitsch, "Survey of worldwide high-power wideband capabilities," IEEE Transactions on Electromagnetic Compatibility, Volume 46, Issue 3, pp. 335-344, Aug. 2004.
4. L.F. Rinehart, J.F. Aurand, J.M. Lundstrom, C.A. Frost, M.T. Buttram, P.E. Patterson, "DEVELOPMENT OF UHF SPARK-SWITCHED L-C OSCILLATORS," Pulsed Power Conference, 1993. Digest of Technical Papers. Ninth IEEE International, Volume 2, pp. 534-537, Jun. 1993.

Posters 3

Prediction of EMP Effects on IC component Using the BLT Equation

S. M. Han[1], S. M. Hwang[1], C. S. Huh[1], U. Y. Huh[1], J. S. Choi[2]

[1]*Inha University, Inchon, South Korea*
[2]*Agency for Defence Development, Daejeon, South Korea*
E-mail: holyjoyhan@hotmail.com

This paper discusses the computational prediction of effects on IC component due to electromagnetic pulse penetration and coupling on PCB strip lines. The main effect of EMP on IC is 'coupling' on line attached IC and coupled abnormal voltage or current are injected to IC [1]. Analyzing and evaluating the EMP coupling on line is important work to predict IC components from EMP attacks [1]. If the coupled abnormal voltage or current are injected, malfunction or destruction are occurred in IC. The interactions and coupling between the external source and the strip lines of PCB were calculated with computational simulation using the BLT equation [2]. To make the BLT equation suitable for the PCB condition, the characteristic impedance and other characteristic constants are calculated. And the used IC component was modeled as RLC load to set up the BLT equation [3]. To show that the simulation results are reliable, the commercial computer simulation software were used and compared with. Voltages and Currents of each pins of the semiconductor were compared and discussed. The errors between the calculations by commercial computer simulation software and the BLT method are 3%~5%.
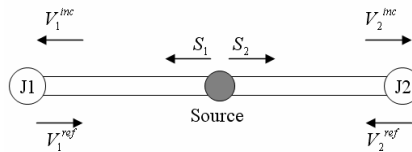
Fig. 1 – BLT equation
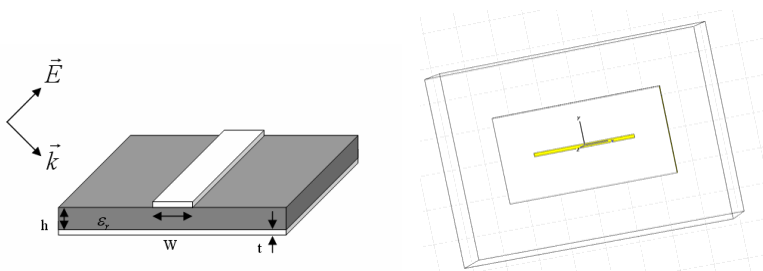
Fig. 2 – Electromagnetic penetration onto PCB strip line (left) and commercial EM alanysis software(right)

References
1. M. Camp, F. Sabath, "Coupling of Transient Ultra Wide Band Electromagnetic Fields to Complex Electronic Systems", 2005 International Symposium on Electromagnetic Compatibility, 2005.
2. F. M. Tesche, M. Ianoz, and T. Karlsson, EMC Analysis methods and computational models. New York: Wiley Interscience, 1997.
3. Marco. Leone, "Radiated Susceptibility on the Printed-Circuit-Board Level: Simulation and Measuremen", *IEEE Trans. Electromagn. Compat.*, vol. 47, no. 3, pp. 471–478, Aug. 2005.

Posters 3

The Susceptibility of CMOS IC Devices to High Power Microwave by Magnetron

J. I. Hong[1], S. M. Hwang[1], C. S. Huh[1], U. Y. Huh[1], J. S. Choi[2]

[1]*Universisty of Inha, Incheon, Korea*
[2]*Agency for Defense Development, Daejeon, Korea*

E-mail: g2051091@inhaian.net

We investigated the malfunction and the destruction characteristics of CMOS IC devices under high power microwave impact by magnetron [1]. High power microwave was rated at a microwave output of 0 to 1,000 W and at a frequency of 2.46 GHz. It was extracted into a standard rectangular WR-340 waveguide and CMOS IC devices were located in the waveguide. CMOS IC devices operated the condition of normal function and standby so that we investigated the influence of CMOS IC devices on the damage effects in the different of conditions by high power microwave. COMS IC devices showed two types of damage, malfunction, which means no physical damage, was done to the system and after a reset the system returned to normal function, and destruction, which means the system incurred physical damage and operation could not be recovered without a hardware repair [2]. The surfaces of the destroyed CMOS IC devices were removed and the chip conditions were analyzed by SEM. The SEM analysis of the damaged devices showed onchipwire and bondwire destruction such as melting due to thermal effects. The obtained results are expected to provide fundamental data for interpreting the combined mechanism of semiconductors in an artificial microwave environment.
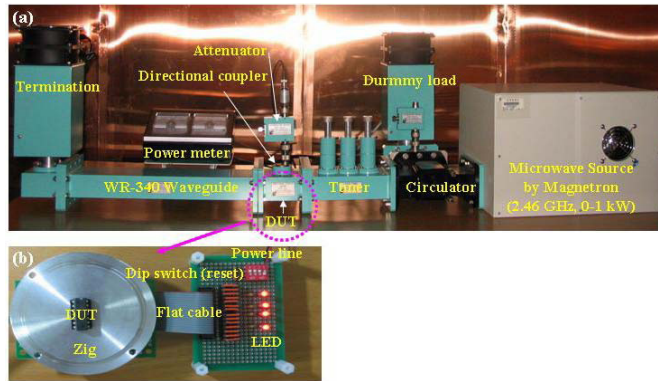
Fig. 1 – Damage effects of digital IC devices by HPM test setup

(a) HPM system setup (b) LED circuit

Table 1 – Tested CMOS NAND devices built in three difference technologies

IC	Logic	Technology	Family	Part Code
CMOS	NAND	High Speed CMOS	HC	74HC00
		High Speed CMOS TTL-Compatible	HCT	74HCT00
		Advanced CMOS	AC	74AC00

References
1.   C. D. Taylor, D. V. Giri, High-Power Microwave Systems and Effects. Washington D. C.: Tayloer & Francis, 1994.
2.   D. Nitsch, M. Camp, F. Sabath, H. Ter, J. L., H. Garbe, "Susceptibility of Some Electronic Equipment to HPEM Threats," IEEE Transactions on Electromagnetic Compatibility, Vol. 46, 2004.

Posters 3

Shields for Special Buildings Based on Chiral-Honeycomb Structures

V. David, I. Nica, R. Ciobanu, R. Damian

Technical University of Iasi, Faculty of Electrical Engineering, Iasi, Romania
E-mail: valdavid@ee.tuiasi.ro

Generally, the electromagnetic compatibility is considered at electronic component level, board level and electrical system level. In view of the electromagnetic protection of the electrical devices and the human beings it is very impotant to consider the electromagnetic compatibility problems and to make a coresponding design at buildings level, such as: hospitals, control rooms of radar or radio transmitters, offices or just houses. This is a very dificult problem, for exemple in the case of hospitals where there are a very large number of electromagnetic field sources and a great diversity of places which must be electromagnetic protected: operating rooms, diagnosis rooms, electrotherapy rooms.

Because of their good mechanical performances [1] and their special electromagnetic proprieties, the chiral-honeycomb structures were considered to obtain the sandwich panels, used as electromagnetic absorbers or/and shields for inside or outside the buildings.

By means of electromagnetic simulation using CST software, we compared the reflectivity of the homogeneous dielectric slab with the reflectivity of the chiral-honeycomb slab, made by the same type of material. For considered dimensions of the unit cell, the chiral-honeycomb slab is an effectively homogeneous structure for frequencies less than 5 GHz.

In order to decrease the absorption frequency for a Salisbury screen, or to decrease their thickness for a given frequency, we used a chiral-honeycomb slab having the permittivity, ε, greater then one. Fig. 1a shows the decrease of the absorption frequency with the increase of the medium permittivity between the resistive sheet and the perfect electrical conductor plane of the Salisbury Screen.

In view of increasing the absorption bandwidth of the Salisbury screen there were used two or more layers, obtaining the multilayer Jaumann absorber, which have two or more minimums in the reflectivity.

Fig. 1b shows the variation of the reflectivity with the dielectric permittivity of the medium, in case of the Jaumann absorber with two layers.

We made an optimization and we propose same panels based on chiral-honeycomb slab, with a view to be used in the electromagnetic protection at the buildings level.
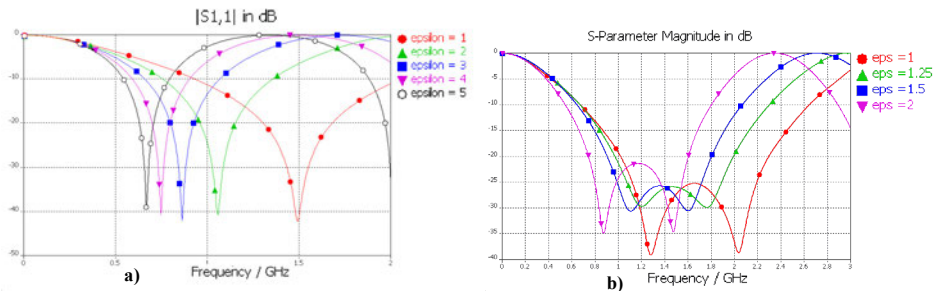
Fig. 1 – Reflectivity versus frequency for various permittivities in case of: a) Salisbury Screen; b) Jaumann absorber

References
1.   F. C. Smith, F. Scarpa, "Design of honeycomb-like composites for electromagnetic and structural applications", IEE Proceedings of Science Measurement Technology, vol. 151, 2004.

Implanted Antenna for Biomedical Sensors

F. Merli[1], L. Bolomey[2], E. Meurville[2] and A. K. Skrivervik[1]

[1]*Laboratory of Electromagnetics and Acoustics, LEMA*
[2]*Laboratory of Microengineering for Manufacturing 2, LPM2*
EPFL, Lausanne, Switzerland
E-mail: francesco.merli@epfl.ch

This work shows the design, realization and measurements of a prototype for an implantable antenna. The complete RF system with insulation, transceiver and power supply has been designed in order to be integrated with an implanted glucose sensor.

Recently some small antenna designs have been proposed for implant uses [1], but today no established solution is yet defined. In fact, several aspects as electrically very small antennas, possible dual band performances, active component placements and shielding, biocompatibility, power supply and constraints due to body's dielectric nature need to be investigated for an implantable system, thus increasing the difficulties of the task. In this work we tried to consider the aforementioned characteristics from the antenna point of view.

Implantable systems can transmit data over the *Medical Implanted Communication System* band (402-405 MHz), that has been chosen to reduce the wave attenuation in the complex human environment but, as a drawback, requires electrically very small antennas. Combining all the performance reductions due to the small antenna size and the effect of the lossy environment, the overall resulting system becomes highly inefficient. Nevertheless, the applications for implanted devices are very promising, especially if indoor communications are considered.

Taking into account the glucose sensor shape [2], the proposed prototype antenna has a hollow cylindrical geometry which allows the maximum use of the available volume and, at the same time, provides the required space for all the active components. Actually a battery, a local processing unit and a transceiver produced by Zarlink Semiconductor [3] could be placed "inside" the antenna. The use of this latter integrated circuit (IC) can reduce the power consumption (thanks to its capability to switch from sleeping to an operational state and vice versa) but requires a dual band antenna, to cover also the wake up signal. In fact data transmission (up to 800kbps) is performed over the MICS band and a signal at 2.45 GHz is necessary to wake the implant up.

Dual frequency properties increase the complexity of the antenna design and in our case the duality feature has been obtained designing some slots. In this first attempt, a very simplified model for the human body was considered, where the device is just immersed in a phantom liquid simulating the muscle tissue. Two different body liquids, one for each working frequency, have been realized following the recipe in [1] and [4] leading to a good concordance between measurements (using the HP dielectric probe kit 85070E) and the desired dielectric properties (as reported in Table 1). The antenna has subsequently been covered with plastic material (1mm thick, PolyEthylEtherKetone), in order to guaranty biocompatibility. Immersing the complete RF system in the body phantom liquids, we performed several range tests in different anechoic chambers (according to the working frequencies) showing very promising results. In fact, the communication between the base station (that remotely controls the unit) and the implant has been found working up to 4 meters (2 meters is the reading distance specified by Zarlink) in the MICS band and almost up to 1 meter for the wake-up signal.

Table 1 – Body phantoms characteristics

Frequency	Recipe	Target values	Measured values
MICS	[1]	ε_r= 57.1, tanδ= 0.622	ε_r= 57.06, tanδ= 0.6573
2.45 GHz	[4]	ε_r= 52.5, tanδ= 0.2488	ε_r= 53.62 tanδ= 0.2563

References
1. P.S. Hall, Yang Hao, Antennas and Propagation for Body-centric Wireless Communications. Artech House 2006.
2. S. Künzi, "Viscosity based implantable glucose sensor", PhD. Thesis, 2007, EPFL.
3. Integrated Circuit ZL70101, .
4. Evaluating Compliance with FCC. Guidelines for Human Exposure to Radiofrequency Electromagnetic Fields. Supplement C. June 2001.

Posters 3

Positive and Bipolar Lightning in Florida

A. Nag, D. Tsalikis, and V.A. Rakov

Department of Electrcial and Computer Engineering, University of Florida, Gainesville, USA
E-mail: amitabh@ufl.edu

Downward positive lightning effectively lowers positive charge to ground and accounts for about 10% of cloud-to-ground discharges [1]. The highest directly measured lightning currents and the largest charge transfers to ground are thought to be associated with positive lightning [2]. Positive lightning has been found to be related to sprites which occur in the middle atmosphere [3]. Positive lightning can be the dominant type of lightning during the cold season.

We acquired electric field records of 20 positive cloud-to-ground lightning discharges consisting of single or multiple strokes in Florida during warmer (May-October) and colder (November-February) seasons. In addition to wideband electric field data, field derivative (dE/dt), as well as HF and VHF radiation signatures associated with positive lightning were also recorded. The wideband electric field measurement system had a useful frequency bandwidth of 16 Hz to 15 MHz. The upper frequency bandwidth of the dE/dt measurement system was 17 MHz. The HF and VHF measurement systems had their center frequencies at 5 MHz (with a bandwidth of 4.7 MHz to 5.4 MHz) and 36 MHz (with a bandwidth of 34 MHz to 38 MHz), respectively. The sampling rate was 100 MHz. Preliminary breakdown pulse trains occurring tens of milliseconds prior to the first positive return stroke were observed. Some positive lightning discharges were preceded by cloud discharges. One flash included in the positive lightning data set was actually a bipolar one. It was composed of three negative strokes followed by a positive stroke and then by a negative one. Various features of positive lightning such as multiplicity, leader stepping, slow front and fast transition in return-stroke waveforms, and continuing currents following return strokes were examined.
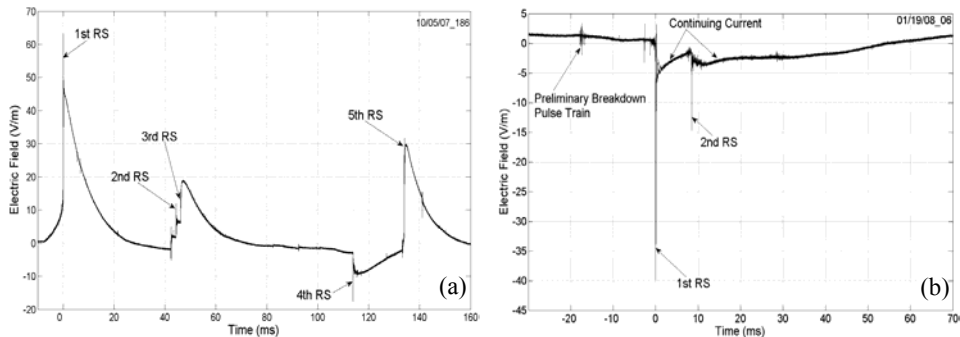
Fig. 1 - Electric field records showing (a) Bipolar flash composed of three negative strokes followed by a positive stroke and then by a negative one, recorded on October 5, 2007 and (b) Two-stroke positive lightning flash with preliminary breakdown pulse train preceding the first stroke, recorded on January 19, 2008. Both records were acquired in Gainesville, Florida.

References
1. V.A. Rakov, "A review of positive and bipolar lightning discharges," Bull. Amer. Meteor. Soc., 84, 767–776, 2003.
2. Y. Goto, and K. Narita, "Electrical characteristics of winter lightning," J. Atmos. Terr. Phys. 57: 449-59, 1995.
3. D.J. Boccippio, E.R. Williams, S.J. Heckman, W.A. Lyons, I.T. Baker, and R. Boldi, "Sprites, ELF transients, and positive ground strokes," Science 269: 1088-91, 1995.

Posters 3

Author Index

A

Abbaspour, Siavash *315*
Abdul Aziz, Mohamad Zoinol Abdin *177*
Abdulla, Parambil *134*
Abubakirov, Edward *223*
Adalev, Alexei *78*
Adam, Jean-Pierre *203*
Afonin, Vasili *302*
Agarwal, Krishna *265*
Aguilera, Ernesto *242*
Aguili, Taoufik *138, 255, 268*
Ait-Amar, Sonia *111*
Aiza, Mahyuni Mozi *177*
Akan, Volkan *173*
Akimoto, Shimpei *167*
Akyuz, Mose *22*
Alarcón, Alexander *188, 238*
Aleksic, Slavoljub *127*
Alshehri, Abdallah *276*
Altgilbers, Larry *150*
Altunc, Serhat *274*
Altuncu, Yasemin *269*
Alvarez-Perez, Jose Luis *221*
Ametani, Akihiro *174*
Amir, Razif Arief Jamil Abdullah *177*
Amiri, Shervin *246*
Ammar, Noemen *138, 255, 268*
Anastassiu, Hristos *300*
Andrieu, Joël *375*
Antonescu, Oana *382*
Antonijevic, Sinisa *231*
Anza, Sergio *394*
Apaydin, Gokhan *219*
Appelgren, Patrik *22*
Aranguren, D. *89*
Arevalo, Liliana *238*
Ari, Niyazi *219*
Ariano, Gaetano Maurizio *48*
Armanious, Miena *184*
Armendariz, Jaime *394*
Arnautovski-Toseva, Vesna *110*
Arnesen, Odd Harry *31*
Artemenko, Sergey *45, 226*
Artioli, Marcello *262*

Asfaux, Didier *203*
Assad Rachid, Elias *128, 142*
Atkinson, Robert *100*
Aubert, Hervé *360*
Avendaño Avendaño, Carlos Alberto *257, 258*
Avgustinovich, Vladimir *45*
Awang, Zaiki *263*
Azremi, Abdullah Al-Hadi *177*

B

Bäckström, Mats *3, 31, 85, 87, 214*
Bahshi, Eldar *225*
Baker, George *33*
Baldygin, Vitaly *362*
Balzovsky, Evgeny *281,282*
Banciu, Gabriel Marian *260*
Bandurski, Wojciech *321*
Barnes, Paul *79, 83*
Barnes, Randy *85*
Barras, David *310*
Baryshevsky, Vladimir *148, 149*
Batista, Emmanuel *36*
Batmanov, Anatoliy *311, 338*
Baudrand, Henry *255, 268, 374*
Baum, Carl E. *2, 146, 168, 183, 218, 239, 241, 259, 274, 298, 299, 331*
Baumann, Dirk *292*
Bayrak, Mehmet *173*
Bdour, Tarek *138, 255, 268*
Bechet, Paul *359, 390*
Belolipetskiy, V. S. *302*
Belyaev, Igor *365*
Béniguel, Yannick *205*
Bennett, Jay *340*
Benson, Trevor M. *237*
Berger, Gérard *111*
Bernier, Maxime *51*
Beroual, Abderrahmane *391*
Bertholet, Pierre *113, 147*
Berthon, André *205*
Bertino, Ilario *48, 300*
Bessarab, Alexander *303*
Bickes , Christian *151*
Bit-Babik, Giorgi *120, 166*

Blake, Roger *24*
Bleszynsk, Elizabeth *266*
Bleszynski, Marek *266*
Bocharov, Yuriy *234*
Boev, Ivan *162*
Bogdankevich, Irina *26, 224*
Bogdanov, Vladimir *28*
Bogenberger, Richard *379*
Bolomey, Léandre *404*
Bolotov, Valeriy *366, 398*
Bonney, Joachim *277*
Bonyadi-ram, Siamak *139*
Bordonos, Alexey K. *118*
Borghetti, Alberto *158*
Boria, V. E. *394*
Boriraksantikul, Nattaphong *126, 200*
Bormann, Dierk *216*
Borve, Steinar *202*
Bouchelouk, Lakdhar *36*
Boudjerda, Nasserdine *65, 69*
Boularak, Chafik *399*
Bouleanu, Iulian *359, 390*
Bourgeois, Yannick *108*
Boutejdar, Ahmed *311, 313, 338*
Bowen, Leland *239, 331*
Boyer, Philippe *253*
Bozzetti, Marco *48, 300*
Brauer, Florian *23*
Braun, Christian *55*
Breejen, Eric den *345*
Bridges, Greg E. *139*
Brukhnevich, Gehhady *302*
Bruschini, Claudio *6, 345*
Buccella, Concettina *316*
Buchenauer, C.Jerald *21*
Burns, David *327*
Burschka, Stefan *119*
Burte, Edmund *311, 338*
Buyanov, Yuri *281, 282*

C

Cadilhon, Baptiste *375*
Cakiroglu, Bora *351*
Camps-Raga, Bruno *126, 200*
Caniggia, Spartaco *14*
Caratelli, Diego *264*
Carboni, Victor *92, 107*